Report on the PHT Scientific Validation for OLP Version 8.4

Ulrich Klaas, Mario Radovich and Karsten Wilke
(PHTNDC at MPIA)

and

Phil Richards
(CCLRC, RAL)

with contributions by:
Huw Morris (CCLRC, RAL)
Rene Laureijs, Bernhard Schulz, Carlos Gabriel (IDC Vilspa)
José Acosta Pulido (IAC)
Peter Ábrahám, Linda Schmidtobreick, Martin Haas (PHTNDC at MPIA)

SAI/1999–041/Rp

Version 2.0

March 10, 2000

Max-Planck-Institut für Astronomie, Heidelberg

Contents

1 Results and Achievements by PHT OLP V8.4 Scientific Validation 4
1.1 Calibration Upgrades from OLP7 to OLP8 4
1.2 Photometric Accuracies of Staring Modes 4
1.3 Re-validation of Staring Mode Photometry and Spectroscopy 8
1.3.1 Flux Dependent Signal Linearization 8
1.3.2 PSF factors for PHT-C arrays 8
1.3.3 Multi-filter Staring Modes 8
1.3.4 Absolute Photometric Modes 8
1.3.5 Spectroscopy in Staring Mode on Extended Sources 8
1.3.6 Spectroscopy in Chopped Mode 8
1.4 Validation 9
1.4.1 Chopped Photometry 9
1.4.2 PHT22 Mapping Mode 10
1.5 General Accuracy Limitations of OLP Processing 13
1.6 Areas of Improved Processing by Interactive Data Analysis 13
1.7 Status of Scientific Validation of PHT AOTs 14

2 Known Limitations and Caveats 17
2.1 Validity Ranges of FCS Calibration Files 17
2.2 Inhomogeneous FCS Illumination of PHT-P Apertures 18
2.3 Non-geometric Aperture Beam Size Scaling 19
2.4 Non-linearity of Detector Responsivity with Flux 19
2.5 Detector Signal Transients 20
2.6 Long Term Detector Drifts 21
2.7 Error Calculation and Propagation 21
2.8 Missing Measurements and Chopper Correction 22
2.9 Limitations in Use of PHT Color Correction Factors 22
2.10 Empirical PPSF Correction Factors for Array Centered C200 Photometry . . 22
2.11 Incomplete Raster Map Appearance in Case of Zero Signal Flag 23
2.12 Application of Point Spread Function Fraction Factors to AAR Data Products 23
2.13 Failure of Chopped Signal Pattern Generator in Case of Data Reduction . . . 24
2.14 Residual Flat-field Structures in PHT22 Raster Maps 25

3 Prerequisites for OLP Scientific Validation 26

4 Overview of Results from SVP1 27

5 Revalidation Tests during SVP1 28
5.1 Upgrade of PHT-S Spectral Response Function for Extended Sources 28
5.1.1 References to Calibration Analysis and Software Change Documentation 28
5.1.2 Summary of Results 28
5.1.3 ISOPHOT-S Spectroscopy of the Extended Reflection Nebula NGC 7023 29
5.2 Dedicated Spectral Response Function for Chopped PHT-S Measurements . . 33
5.2.1 References to Calibration Analysis and Software Change Documentation 33
5.2.2 Summary of Results 33
5.2.3 Consistency Check of Chopped PHT-S Relative Spectral Response Function on Calibration Stars 34
5.2.4 MIR Spectra of Galaxies from Chopped PHT-S Measurements 38

5.2.5 MIR Spectra of a Symbiotic Star and a Nova from Chopped PHT-S Measurements . . . 47
5.3 Verification of Recognition of Varying Aperture Sizes in Multi-filter Raster Maps . . . 49
5.3.1 References to Calibration Analysis and Software Change Documentation 49
5.3.2 Summary of Results . . . 49
5.3.3 Examination of Browse Products of Test Cases . . . 50
5.4 Revalidation of Staring Mode Photometry . . . 61
5.4.1 References to Calibration Analysis and Software Change Documentation 61
5.4.2 Summary of Results . . . 61
5.4.3 General Re-validation of PHT03 and PHT22 Staring Mode: The SED of α Bootes (HR 5340) . . . 62
5.4.4 General Re-validation of Multi-filter Staring Mode (PHT03/PHT22) and Absolute Photometry (PHT05/PHT25): The SED of γ Draconis (HR 6705) . . . 68
5.4.5 General Re-validation of PHT03 and PHT05 Staring Mode: The SED of Sirius (HR 2491) . . . 82
5.4.6 General Re-validation of PHT03 Staring Mode: Photometric Reproducibility Aspects in the Case of the SED of Vega (HR 7001) . . . 86
5.4.7 General Re-validation of PHT03 and PHT22 Staring Mode: The SED of Arp 220 . . . 94

6 Overview of Results from SVP2 101

7 Revalidation Tests during SVP2 103
7.1 Upgrade of PHT-S Spectral Response Function for Extended Sources . . . 103
7.1.1 References to Calibration Analysis and Software Change Documentation 103
7.1.2 Summary of Results . . . 103
7.1.3 ISOPHOT-S Spectroscopy of the Extended HII Region M17 . . . 104
7.1.4 Absolute Surface Brightness Spectrum of the Zodiacal Light . . . 108
7.1.5 Diffuse Emission of the Galactic Disk . . . 110
7.2 Dedicated Spectral Response Function for Chopped PHT-S Measurements . . 112
7.2.1 References to Calibration Analysis and Software Change Documentation 112
7.2.2 Summary of Results . . . 112
7.2.3 MIR Spectra of the Stars HD 23763, HR 7428 and HD 23441 from Chopped PHT-S Measurements . . . 113
7.3 Revalidation of Staring Mode Photometry . . . 116
7.3.1 References to Calibration Analysis and Software Change Documentation 116
7.3.2 Summary of Results . . . 116
7.3.3 General Re-validation of PHT03 and PHT22 Staring Mode: The SED of α Bootes (HR 5340) - Final Assessment . . . 117
7.3.4 General Re-validation of Multi-filter Staring Mode (PHT03/PHT22) and Absolute Photometry (PHT05/PHT25): The SED of γ Draconis (HR 6705) - Final Assessment . . . 124
7.3.5 General Re-validation of PHT03 and PHT05 Staring Mode: The SED of Sirius (HR 2491) - Final Assessment . . . 134
7.3.6 General Re-validation of PHT03 Staring Mode: Photometric Reproducibility Aspects in the Case of the SED of Vega (HR 7001)- Final Assessment . . . 138
7.3.7 General Re-validation of PHT03 and PHT22 Staring Mode: The SED of Arp 220 - Final Assessment . . . 147
7.3.8 Re-validation of C200 Absolute Photometry: The SEDs of Ceres and Uranus - Final Assessment . . . 154
7.3.9 General Re-validation of Point Source Photometry from PHT03 and PHT22 Nodding Mode . . . 158
7.3.10 General Re-validation of Point Source Photometry from PHT22 Mini-Maps . . . 161

8 Validation of the Chopped Point Source Photometry during SVP2 164
8.1 Revalidation of Chopped Photometry Test Cases from OLP 7.0 Validation Program . . . 164
8.1.1 References to Calibration Analysis and Software Change Documentation 164
8.1.2 Summary of Results . . . 164
8.1.3 Validation of PHT03 and PHT22 Chopped Mode: The SED of IRAS 03068-5346 . . . 165
8.1.4 Validation of PHT03 and PHT22 Chopped Mode: The FIR Excess SED of Vega . . . 171
8.1.5 Comparison of Chopped and Staring Mode Photometry of Standard Stars from the Empirical Signal Correction Calibration Program . . . 174
8.1.6 OLP Chopped and Staring Mode Photometric Results for the Faint Point Source Detection Limit Program . . . 183
8.1.7 Comparison of Chopped and Staring Mode Photometry of Stars Observed by the MFAINT and CFAINT Programs . . . 190
8.2 Validation of Additional Chopped Photometry Test Cases for OLP 8.4 Validation Program . . . 195
8.2.1 References to Calibration Analysis and Software Change Documentation 195
8.2.2 Summary of Results . . . 195
8.2.3 Validation of PHT03 and PHT22 Chopped Mode Photometry by Comparison with Staring Mode References on Other Revolutions . . . 196
8.2.4 Validation of PHT03 and PHT22 Chopped Mode Photometry: Fluxes and SEDs of Known Stars . . . 202

9 Validation of the ISOPHOT-C mapping mode PHT22 during SVP2 208
9.1 Verification of Flux Conservation in P22 Raster Maps . . . 208
9.1.1 References to Calibration Analysis and Software Change Documentation 208
9.1.2 Summary of Results . . . 208
9.1.3 Verification of Flux Conservation for Different Raster Step Sizes . . . 209
9.2 Determination of Flat-Field Accuracies . . . 211
9.2.1 References to Calibration Analysis and Software Change Documentation 211
9.2.2 Summary of Results . . . 211
9.2.3 Flat-field Accuracies of C100 Maps . . . 212
9.2.4 Flat-field Accuracies of C200 Maps . . . 247
9.3 Absolute Surface Brightness Values of P22 Maps Compared with COBE/DIRBE Photometry . . . 281
9.3.1 References to Calibration Analysis and Software Change Documentation 281
9.3.2 Summary of Results . . . 281
9.3.3 Absolute Surface Brightness Values of C100 Maps . . . 282
9.3.4 Absolute Surface Brightness Values of C200 Maps . . . 314

10 Conclusions and Outlook 337

Chapter 1

Results and Achievements by PHT OLP V8.4 Scientific Validation

1.1 Calibration Upgrades from OLP7 to OLP8

In Table 1.1 we list the major calibration upgrades which were implemented for OLP8 and describe which AOTs or AOT submodes were affected by the individual upgrades. There are two calibration upgrades which are part of the formal OLP/CALG delivery, but which are standalone and are not used by the OLP processing. They are or can be used in the Interactive Analysis environment.

1.2 Photometric Accuracies of Staring Modes

Global calibration accuracies have been estimated from the investigation of the test cases and the comparison with published reference photometry. (for a dependence on flux, see Table 1.2 below). They can be applied, if not one of the caveats on photometry applies, cf. Sect. 2.
The terms **absolute accuracy**, **relative accuracy** and **reproducibility** have been defined in the following context:

- **absolute accuracy** is the accuracy achieved w.r.t. the reference photometry, if the filter measurement had a corresponding FCS transfer measurement in the same filter. Hence, the quality of the FCS calibration against celestial standards is directly verified. Note that no calibration accuracy of the reference photometry (models, IRAS) has been taken into account, as this is beyond the scope of this report. A typical order of the absolute accuracy of the reference photometry is $2-10\%$. Table 1.2 lists the achieved values per detector and flux range.

- **relative (filter-to-filter) accuracy** is the accuracy achieved w.r.t. the reference photometry, if the filter measurement was not performed in the filter in which the FCS calibration was done. Currently, assumptions about the constancy of the responsivity over the full flux range and for all filters, and, related to that relative filter-to-filter correction factors, apply. It has been proven that this is in general not correct, and it is considered that in future OLP versions corrections for non-linearities of the responsivity with the in-band power will be applied. Hence, the relative uncertainty can be much larger than the absolute one in multi-filter measurements with certain source SEDs. Table 1.2 lists the achieved values per detector and flux range. The number of suitable test cases performed in multi-filter mode is much smaller than the number of test cases in any of the absolute measurement modes (i.e. with an FCS measurement in the respective filter). The relative filter-to-filter accuracy could only be established for a subset of test cases.

Table 1.1: Calibration upgrades from OLP 7 to OLP 8.4 and impact on the different AOT modes

	calibration upgrade	**affects AOT**
1)	flux dependent signal linearization (incl. re-normalization of default responsivities)	all AOTs, except PHT40
2)	FCS characterisation	all AOTs, except PHT40
3)	signal derivation and photometric calibration of chopped measurements	PHT03, PHT22 in chopped mode
4)	PSF factors for PHT-C arrays & pixels	PHT22, PHT25, PHT37/38/39
5)	relative spectral response function for chopped PHT-S measurements	PHT40 in chopped mode
6)	solid angle for PHT-S aperture	PHT40 extended sources
7)	footprint matrixes (not used by OLP, not available for P1)	PHT03, PHT22, PHT32
8)	relative system responses of PHT bandpasses (not used by OLP, for computation of cc factors not covered by color correction tables)	all AOTs except PHT40

- absolute and relative accuracy are assumed to add to the total photometric uncertainty. In multi-filter measurements with one FCS measurement the absolute measurement uncertainty is subtracted from all measurements in non-FCS filters in order to derive the relative measurement accuracy.
- **reproducibility** is the relative consistency of measurements repeated several times with the same measurement set-up. It is a measure of the internal stability of the instrument and describes also the current limitations in signal processing. Table 1.3 lists the achieved values per detector both for a bright secondary standard and a faint source. These values were obtained from special calibration monitoring programs performed during ISO's Routine Phase [18].

In summary, the following calibration accuracies have been achieved per detector (cf. Tables 1.2 and 1.3 for details):

1) **ISOPHOT-P1:**
10 % absolute accuracy and 20 % relative accuracy for bright sources (> 30 Jy). For fainter sources the absolute accuracy is within 40 %. The relative reproducibility accuracy is 5 % for bright sources and 10 % for faint sources.

2) **ISOPHOT-P2:**
Better than 15 % absolute accuracy and 5 % relative accuracy. The relative reproducibility accuracy is 2 % for bright sources and 12 % for faint sources.

3) **ISOPHOT-P3:**
Better than 15 % absolute accuracy and 10 % relative accuarcy down to ~ 0.5 Jy. The relative reproducibility accuracy is 7 % for bright sources and 7 % for faint sources. Under extreme Space Weather conditions and for the very end of the science window the achieved accuracy for faint sources is poorer.

4) **ISOPHOT-C100:**
15 % absolute accuracy and 25 % relative accuracy down to ~ 5 Jy. The absolute accuracy of nodding photometry in the flux range below 1 Jy is 40 %. The absolute accuracy in mini-map mode is ~ 40 %. The relative reproducibility accuracy is 3 % for bright sources and 20 % for faint sources.

5) **ISOPHOT-C200:**
10 % absolute accuracy for fluxes down to 0.5 Jy. At the lowest flux level only absolute photometry and nodding mode achieve this accuracy. The accuracy achieved in mini-map mode is ~ 40 % for the full flux range. Due to the signal linearity correction the multi-filter test case of α Boo indicates that a relative accuracy better than 30 % can be achieved down to fluxes of a few Jy, limited by the accuracy to subtract the then 4 times brighter background. The relative reproducibility accuarcy is around 10 % both for bright and faint sources.

6) **ISOPHOT-S:**
For staring mode observations the standard spectral response function may not work accurately for some flux ranges due to signal transients and therefore the more conservative numbers of better than 30 % absolute and better than 30 % relative still apply. For extended source staring observations the same numbers apply, as the test cases indicate that an additional uncertainty introduced by the amount of the solid angle is now properly corrected for. Thanks to a new calibration method with spectral response functions specific for chopped mode and adjusted to the detector behaviour for a certain flux modulation, 10 % absolute accuracy and 10 % relative accuracy are achieved for chopped point source observations, in the flux range 0.5 to about 500 Jy with the SS detector, and in the flux range 0.2 to about 200 Jy with the SL detector.

Table 1.2: Absolute and relative (filter-to-filter) calibration accuracies per detector achieved for various flux ranges in multi-filter mode with OLP V8.4. Bold values indicate a significant improvement w.r.t. OLP V7.0. For quoted PHT-S accuracies in staring mode refer to Ref. [26].

detector	**AOT mode**	**flux range** [Jy]	**abs. accuracy** [%]	**rel. accuracy** [%]	**standard**
P1	P03 off & on	300 - 6000	$\leq$ **5**	15	α Boo
P1	P03, P05 off & on	70 - 1250	10	25	γ Dra
P1	P03 off & on	50 - 1000	10	10	Sirius
P1	P05 off & on	50 - 1000	**5**	–	Sirius
P1	P03 off & on	30 - 300	**10**	**10**	Vega
P1	P03 nodding	2	$\leq$ **5**	–	HR 5986
P1	P03 nodding	$<$ 0.1	40	–	HD 172323
P2	P03 off & on	100 - 200	$\leq$ 5	5	α Boo
P2	P03, P05 off & on	25 - 40	$<$ 10	**5**	γ Dra
P2	P05 off & on	$\sim$ 25	$\leq$ **15**	–	Sirius
P2	P03 off & on	$\sim$ 25	20	–	Sirius
P2	P03 nodding	0.5	$\leq$ 10	–	HR 5986
P3	P03 off & on	10 - 25	10	**5**	α Boo
P3	P03 nodding	20	$\leq$ **5**	–	α Tau
P3	P03, P05 off & on	$\sim$ 5	10	**10**	γ Dra
P3	P03 nodding	1 - 2	**10**	–	HR 617
P3	P03 nodding	0.6	$\leq$ 15	–	HR 7310
P3	P17/18/19 4 times	$<$ 0.2	**20**	–	HR 5981
C100	P22 off & on	6 - 25	5	10	α Boo
C100	P22, P25 off & on	$\sim$ 5	15	**25**	γ Dra
C100	P22 nodding	$\sim$ 3.5	15	–	Sirius
C100	P22 nodding	0.2 - 0.6	40	–	HR 7310
C200	P25 off & on	500 - 900	**10**	–	Uranus
C200	P25 off & on	40 - 120	**10**	–	Ceres
C200	P22 off & on	2 - 5	$<$ **10**	$<$ **30**	α Boo
C200	P22 nodding	$\sim$ 0.5	$<$ **10**	–	γ Dra
C200	P25 off & on	$\sim$ 0.5	**10**	–	γ Dra
SS	P40 off & on	2 - 5000	$<$ 30	$<$ 30	
SL	P40 off & on	1 - 5000	$<$ 30	$<$ 30	

Table 1.3: Relative Calibration Reproducibility Accuracy per Detector for Bright and Faint Fluxes from Monitoring Programs.

detector	target	**flux** [Jy]	**relative accuracy** **1** σ [%]
P1	NGC 6543	8	5
P1	HD 172323	0.085	10
P2	NGC 6543	100	2
P2	HR 5986	0.67	12
P3	NGC 6543	100	7
P3	HR 7310	0.67	7
C100	NGC 6543	50	3
C100	HR 7310	0.23	20
C200	NGC 6543	11	10
C200	HR 6705	0.67	7

1.3 Re-validation of Staring Mode Photometry and Spectroscopy

1.3.1 Flux Dependent Signal Linearization

This general calibration feature was successfully implemented. A prerequisite for this was a consistent treatment of a significant fraction of the PHT calibration files which were provided for this OLP version. This implementation removes an OLP V7.0 caveat (cf. Sect. 2.4). There are a few areas where fine-tuning is possible.

1.3.2 PSF factors for PHT-C arrays

The upgraded PSF factors for the PHT-C arrays provide consistent photometric results, in particular for all filters of C200. This calibration upgrade removes an OLP V7.0 caveat (cf. Sect. 2.10).

1.3.3 Multi-filter Staring Modes

The PHT staring photometric modes PHT03 and PHT22 OLP processing was successfully re-validated. This includes extended source photometry with PHT-C (PHT22). In general both the absolute and relative calibration are improved by this OLP version, see Sect. 1.2 above.

1.3.4 Absolute Photometric Modes

The PHT absolute photometric modes PHT05 and PHT25 OLP processing was successfully re-validated. The absolute calibration of PHT-P is improved for this version, see Sect. 1.2 above.

1.3.5 Spectroscopy in Staring Mode on Extended Sources

The PHT OLP processing of the spectroscopic mode PHT40 staring on extended sources was successfully re-validated. Spectral shapes and features are maintained. Good matches in absolute level and relative shape with reference spectra and photometry are found.

1.3.6 Spectroscopy in Chopped Mode

The PHT OLP processing of the spectroscopic mode PHT40 OLP chopping was successfully re-validated. Resulting spectral shapes and final accuracies could be improved to an absolute accuracy of 10 % and a relative accuracy of < 10 %.

1.4 Validation

1.4.1 Chopped Photometry

In summary, the following calibration accuracies have been achieved per detector and flux range (cf. Table 1.4 for details):

1) ISOPHOT-P1:
Better than 10 % absolute in the flux range 1 - 10 Jy, better than 50 % absolute down to fluxes of 50 mJy.

2) ISOPHOT-P2:
Better than 40 % absolute in the flux range 0.2 - 6 Jy, albeit it appears that in the flux range 0.5 - 3.5 accuracies in the order of 10 % absolute can be achieved. So far no signal correction is applied to P2 data. This seems, however to be necessary, as general trends can be observed from the test data and signal correction factors should be established for the next OLP version.

3) ISOPHOT-P3:
Better than 40 % absolute in the flux range 1.5 - 20 Jy, with better than 20 % above a flux of 5 Jy.
Relative accuracies are in the order of 20 - 30 %.

4) ISOPHOT-C100:
Better than 60 % absolute in the flux range 0.2 - 15 Jy. Below 0.2 Jy fluxes become less and less reliable, presumably due to an insufficient chopper offset correction which leads to factors 2 - 4 too high fluxes in the flux range 0.03 - 0.15 Jy.
Relative accuracies are in the order of 50 %

5) ISOPHOT-C200:
Better than 20 % absolute in the flux range 2 - 5 Jy. Below 1 Jy, in general negative flux values are derived, presumably due to an insufficient chopper offset correction or due to a non-detection because of sky noise (cirrus confusion).
Relative accuracies are in the order of 20 %.

Based on the results per detector listed above, chopped photometry with ISOPHOT-P and -C can not be declared as scientifically valid because of the too severe restrictions and caveats. These are:

1) In general the accuracy is not better than 40 - 50 %.

2) For C100 and C200 these accuracy values are limited to fluxes above 0.2 Jy and 1 Jy, respectively. For smaller fluxes the current chopper offset correction, being the zero point of the signal correction, is not yet sufficient.

3) For P2 very often an underestimation of the expected flux value is observed. A better accuracy should be achievable by establishment of signal correction factors which are currently not yet available.

Nevertheless the processing of chopped photometry has been significantly improved and for some detectors and flux ranges already reasonable accuracies have been achieved as listed above. It should also be noted that the SPD product contains now the so-called "chop pattern" which is a robust representation of the signal modulation for this measurement. In

case of faint sources the interpretation of this chop pattern is not always straight forward for non-experts due to superimposed instrumental effects.

Table 1.4: Absolute and relative (filter-to-filter) calibration accuracies per detector for chopped photometry achieved for various flux ranges in multi-filter mode with OLP V8.4.

detector	**AOT**	**flux range** [Jy]	**abs. accuracy** [%]	**rel. accuracy** [%]	**standard**
P1	P03	2.5 - 10	**5**	–	HR 6817
P1	P03	1 - 2.6	**5**	**40**	BS 5062
P1	P03	2.2	**10**	–	HR 5986
P1	P03	0.06	**< 50**	–	HD 172323
P2	P03	25	**< 20**	–	Sirius
P2	P03	3.5 - 6	**< 40**	–	HR 6132
P2	P03	5	**< 40**	–	HR 7557
P2	P03	3.5	**10**	–	HR 7310
P2	P03	0.5	**10**	–	HR 5986,HD 185144
P2	P03	0.2 - 0.5	**< 40**	–	BS 5062,HR 5447 HR 5914,HR 4983 HD 185395
P3	P03	7 - 19	**20**	–	HR 1457
P3	P03	6 - 7	**15**	**20**	HR 7001
P3	P03	1.5 - 4.5	**< 40**	**30**	BS 6056
P3	P03	0.6	**< 40**	–	HR 7310
P3	P03	0.15	**< 60**	–	HR 5981
C100	P22	4 - 12	**20**	**60**	HR 8775
C100	P22	1.5 - 2	**< 60**	**30**	HR 6705
C100	P22	0.15 - 1.1	**10**	**10**	HR 7310,HD 203280 HD 12311,HD 187642
C100	P22	0.07 - 0.15	**< 20**	–	HR 5981, SAO248381 HD 142373
C100	P22	0.03 - 0.15	**> +60**[a]	–	HR 5986,HR 7180 BS 5062,HR 5304 HD 142373
C200	P22	2 - 5	**15**	**20**	HR 5340
C200	P22	0.6	– [a]	–	HR 6705
C200	P22	0.02 - 0.15	– [b]	–	HR 7180,HR 7557
SS	P40	0.1 - 20	**10**	**< 10**	
SL	P40	0.1 - 10	**10**	**< 10**	

[a] insufficient chopper offset correction (frequency and pixel dependent)

[b] due to sky noise below detection limit for applied measurement time (best theoretical $1\,\sigma$ value: 64 mJy)

1.4.2 PHT22 Mapping Mode

The PHT22 raster mode is scientifically valid with some caveat on the achieved flat field accuracy in case of no pixel overlap (see summary below and caveat in Section 2.14). This validation is based on the following findings with regard to flux conservation for different raster step sizes, flatfield accuracy, absolute surface brightness accuracy and point source photometry accuracy from maps:

- The flat-field accuracy for C100 maps depends on the pixel overlap, a summary is given in Table 1.6. In general ± 20 % (standard deviation of the mean background surface brightness) are achieved; for proper pixel overlap (shift by half of the array, i.e 1.5 pixels or less) the flat-field accuracy is 4 to 12 %. In case of no oversampling the flat-field accuracy is clearly limited by instrumental flat-field residuals producing

systematic patterns, which need however not to be constant over the whole map area. These patterns are neither wavelength independent nor are they reproduced for the same filter. This points to non-linear drift effects and possibly sometimes temporary spiking of the individual pixels which cannot be corrected for by a linear interpolation between the two bracketing FCS measurements. In case of pixel overlap these flat-field residuals are averaged out.

- The flat-field accuracy for C200 maps depends on the pixel overlap and slightly on the absolute sky brightness, a summary is given in Table 1.6. In general ± 15 % (standard deviation of the mean background surface brightness) are achieved; for proper pixel overlap (shift by one pixel or fraction of one pixel) the flat-field accuracy is 3 to 5 %. In case of no oversampling the flat-field accuracy is clearly limited by instrumental flat-field residuals producing systematic patterns. These patterns are wavelength dependent. In case of pixel overlap by the selected raster step sizes these flat-field residuals are averaged out.

- Flat-field accuracies above 10 %, mainly found for maps with no pixel overlap and low surface brightness levels, and temporal variation of the flat-field residuals, found for C100 maps, mean a restriction of detecting faint sources and a caveat with regard to point source photometry performed on these maps.

- For C100 and C200 filters the consistency of the absolute surface brightness in ISOPHOT maps with COBE/DIRBE photometry is in general < 25 % (for details, see Table 1.5). It should be noted that due to very different beam sizes considerable discrepancies between ISOPHOT photometry and COBE/DIRBE photometry is natural in areas with high dynamic flux range. The comparison is also limited by not yet applying color corrections for the different band pass transmissions and central wavelengths. Note also that the accuracy of COBE annual maps for 140 and 240 μm is typically 20 %. For weekly maps it can be even worse. For wavelengths less equal than 100 μm the quoted accuracy is in general ≤ 1 %.

- Point source photometry from PHT22 raster maps is as accurate as ~ 40 %, independent of the selected raster step size, see Table 1.7.

- The consistency of point source photometry of the same source observed in PHT22 raster mode with different raster parameters is ± 15 %, see Table 1.8. The consistency is very likely limited by the achieved flat-field accuracy (see below). We conclude that the OLP gridding algorithm for maps conserves the flux.

Table 1.5: Calibration Accuracy per Detector for Extended Sources for Various Flux Ranges with OLP V8.4. The range for which both absolute and relative accuracies can be given is covered by multi-filter background measurements, while the larger range is covered by raster maps.

detector	**flux range** [MJy sr^{-1}]	**absolute accuracy** [%]	**relative accuracy** [%]	**standard**
C100	5 - 15	< 25	20	COBE/DIRBE
	5 - 400	< 25	–	COBE/DIRBE
C200	4 - 10	< 25	20	COBE/DIRBE
	3 - 600	< 25	–	COBE/DIRBE

Table 1.6: Flat-field (ff) accuracies for ISOPHOT-C P22 raster maps. The ff accuracies are determined as ratio of the standard deviation of the mean background surface brightness to the mean surface brightness value for a flat sky background field with no sources. They are filter independent. There is some trend that for the same set of raster parameters the ff accuracy improves with increasing absolute surface brightness. For C100 the ff accuracy can vary over the map area.

detector	**flat-field accuracy**	
	no pixel overlap (%)	**with pixel overlap** (%)
C100	8 - 20	4 - 12
C200	7 - 15	3 - 5

Table 1.7: Absolute calibration accuracies achieved for various flux ranges in mini-map mode.

detector	**flux range** [Jy]	**abs. accuracy** [%]	**standard**
C100	$1 - 5$	30	Sirius
C200	$500 - 900$	30	Uranus
C200	$40 - 120$	30	Ceres
C200	0.6	50	γ Dra
C200	0.4	30	HR 1654

Table 1.8: Results from comparison of sets of P22 raster maps with different raster step size. Internal consistency is derived as the ratio of half of the difference in flux to the average flux for a pair of maps on the same target.

target name	**filter** (μm)	**raster parameters**		**flux** (Jy)	**internal consistency** (%)
		MxN	**dMxdN** (arcsec)		
C100 detector					
BD+31 643	60	11 x 11	69 x 69	325.757	+1.0
BD+31 643	60	9 x 9	15 x 15	319.498	-1.0
HR 1457	100	9 x 3	69 x 69	5.464	-13.6
HR 1457	100	7 x 7	15 x 15	7.189	+13.6
C200 detector					
HR 2020	170	2 x 2	90 x 90	2.389	-14.3
HR 2020	170	3 x 3	46 x 46	3.187	+14.3
NGC 6543	170	4 x 4	92 x 92	20.884	-16.0
NGC 6543	170	10 x 10	46 x 46	28.817	+16.0
NGC 6503	170	4 x 4	92 x 92	42.828	-5.6
NGC 6503	170	10 x 10	46 x 46	47.932	+5.6
IC 1228	170	4 x 4	92 x 92	8.421	-25.7
IC 1228	170	10 x 10	46 x 46	14.236	+25.7

1.5 General Accuracy Limitations of OLP Processing

The previous sections provided an overview of the currently achievable average calibration accuracy using OLP products and Sect. 2 lists the conditions of limitations due to yet incomplete corrections or calibrations.
There are, however, a few general accuracy limitations which should be taken into account when using ISOPHOT data products:

- **Accuracy Limitations of Celestial Standards**
  During the course of the ISO project considerable improvements for certain classes of standard sources have been achieved by new observational programmes and refined modelling. One specific case from which ISOPHOT calibration benefited a lot were the new thermophysical models of asteroids [31]. On the other hand, it has to be noted that in the FIR range the stellar spectra a very often extrapolations of measured SEDs up to at most 35 μm. In particular for faint standard stars (< 1 Jy) not much is known about the true SED in the FIR. There are indications that some standard stars do not have good flux predictions. Those will have to be identified by cross-calibration with other stars.

- **Measurement beyond Sensitivity Limit**
  There are measurements in the data base which did not apply the most optimal observing strategy (cf. [27], [28]). Then even the best reduction does not achieve a satisfying result. Sensitivity limits and the corresponding minimum exposure times are given in the above cited reference documents, which have been derived from actual ISOPHOT observations.

- **Confusion by Sky Background Structure**
  In the FIR the sky shows a significant structure, mainly due to IR cirrus (see [32] for a discussion on actual data). This sky confusion limits the ability to adequately determine a sky background and to derive accurate fluxes of faint sources. It can be partly circumvented by an optimized observing strategy (cf. [27], [28]) and by determining the sky background as close as possible to the source.

- **Processing Items which Require User Interaction**
  There are several processing steps from the raw data to the final data products for which interactive processing can provide much better results due to visual inspection of the intermediate data products and optimizing the processing parameters or due to interactive input by the user with regard to special properties of the source (extension, structure, etc.).

1.6 Areas of Improved Processing by Interactive Data Analysis

The provision of a percentage number characterizing which improvements in calibration accuracy can be obtained by careful interactive processing is currently not possible, since so far no comprehensive systematic investigation was performed. Interactive Analysis uses the same set of general calibration files (cal-G) as OLP. The limitations due to photometric bias, e.g. the accuracy of the standard source fluxes, fully apply to interactive calibration, too. One can expect, however, to achieve a higher accuracy with IA for the following cases (cf. [33] for a tutorial):

1) measurements with signal transients which do not stabilise during the measurement time, but which are long enough to perform a reasonable transient fit.

   a) PIA provides already the dynamic spectral response calibration for ISOPHOT-S.

   b) PIA provides several transient correction tools. The most efficient ones are the ones for ISOPHOT-S based on the Fouks-Schubert model (full drift modelling and initial signal jump) and the empirical solution for FIR detectors (P3, C100, and C200) based on exponential functions.

   c) PIA allows to view the transient fitting and to accept or reject it.

2) flat-fielding of maps, depending on the sampling mode and the dynamic range.

   a) In case of pixel overlap the redundancy information in the individual "pixel" maps can be used to do a flat-field correction using the sky measurement itself.

   b) For maps with large areas of flat sky background systematic flat-field residuals can be removed to a certain degree by determining the average and the relative flat-field residual pattern, even for maps with no pixel overlap. The average surface brightness is quite consistent with COBE/DIRBE photometry (cf. Table 1.5).

   c) In case of a sufficient dynamic range in surface brightness a statistical flat-field method can be applied establishing the correlations of the surface brightness per pixel with regard to a reference pixel. This method allows also to correct for additive offsets among the pixels.

3) correction of non-linear signal drifts in maps.

   a) The time sequence of the signals can be interactively inspected and non-linear baseline fits be applied in order to flatten the map.

4) detection of faint sources by refined deglitching and filtering.

   a) PIA offers more refined deglitching methods, like the two-threshold algorithm.

   b) Individual ramps or signal sequences can be inspected by eye and can be deselected or corrected manually.

5) photometry from mini-maps.

   a) The areas for determination of the sky background can be visually checked and selected.

   b) Knowledge of the beam footprint of a point source allows to correct for contamination of the background position by the source beam and to measure closely to the source in order to minimize cirrus confusion.

1.7 Status of Scientific Validation of PHT AOTs

With the finalisation of the OLP8.4 validation the current validation status per AOT submode is given in Table 1.9. With V8.4 the PHT22 raster mode has been scientifically validated. The table also provides an overview of the next steps to further upgrade both validated and non-validated modes and for which OLP version improvements can be expected. There is, however, no warranty for a final implementation of a certain calibration feature, since this needs as a prerequisite a feasibility study including the establishment of the calibration algorithms and parameters.
In Table 1.10 we list the validated modes per detector sub-system. For completeness we have added the polarisation modes which can only be evaluated interactively using PIA and special FORTRAN routines.

Table 1.9: Scientific Validation of OLP AOT Processing, January 2000. non-lin R: refinement of flux dependent signal linearization; FCS aper: correction for use of non-standard apertures in FCS measurement; beam: determination of effective solid angle; chop: chopper signal correction, including correction of chopped FCS measurement; drift: correction of non-linear baseline drifts in maps; flat-field: improvement of flat-field correction using actual sky measurement; map cal: assessment of accuracy of photometry from maps; dyn rsrf: non-static spectral response function correcting for signal transient effects.

AOT	**submode**	**scientifically valid since**	**next upgrades**	**foreseen in OLP Vx.y**
PHT03	staring point source	V6	non-lin R	9.0
			FCS aper	10.0
	staring extended source	no	non-lin R	9.0
			beam	10.0
	nodding	V6	non-lin R	9.0
			FCS aper	10.0
	chopped point source	no	chop & non-lin R	9.0
	raster map	no	map cal	10.0
			drift	10.0
PHT04	staring point source	no	non-lin R	9.0
			beam & FCS aper	10.0
	staring extended source	no	non-lin R	9.0
			beam	10.0
	chopped point source	no	chop & non-lin R	9.0
			beam	10.0
PHT05	staring point source	V6	non-lin R	9.0
			FCS aper	10.0
	staring extended source	no	non-lin R	9.0
			beam	10.0
PHT17/9	staring point source	V6	non-lin R	9.0
			FCS aper	10.0
	staring extended source	no	non-lin R	9.0
			beam	10.0
PHT22	staring point source	V7	non-lin R	9.0
	staring extended source	V7	non-lin R	9.0
	nodding	V7	non-lin R	9.0
	chopped point source	no	chop & non-lin R	9.0
	raster map	**V8.4**	flat-field	10.0
PHT25	staring point source	V7	non-lin R	9.0
	staring extended source	V7	non-lin R	9.0
PHT32	chopped mapping	no	chop & map cal	10.0
PHT37/9	staring point source	V7	non-lin R	9.0
	staring extended source	V7	non-lin R	9.0
PHT40	staring point source	V5	dyn rsrf	9.0
	staring extended source	V6	dyn rsrf	9.0
	chopped point source	V6		
	raster map	V6	TBD	

Table 1.10: Scientifically Validated Observing Modes per Detector, January 2000

detector	**scientifically validated mode**	**AOT**
P1	absolute photometry point sources	PHT05
	staring multi-filter photometry point sources	PHT03
	faint source multi-filter nodding	PHT03
	multi-filter sparse map	PHT17/18/19
P2	absolute photometry point sources	PHT05
	staring multi-filter photometry point sources	PHT03
	faint source multi-filter nodding	PHT03
	multi-filter sparse map	PHT17/18/19
	polarimetry (PIA)	PHT50
P3	absolute photometry point sources	PHT05
	staring multi-filter photometry point sources	PHT03
	faint source multi-filter nodding	PHT03
	multi-filter sparse map	PHT17/18/19
C100	absolute photometry point sources	PHT25
	absolute photometry extended sources	PHT25
	staring multi-filter photometry point sources	PHT22
	staring multi-filter extended sources	PHT22
	faint source multi-filter nodding	PHT22
	staring multi-filter raster maps	PHT22
	multi-filter sparse map	PHT37/38/39
C200	absolute photometry point sources	PHT25
	absolute photometry extended sources	PHT25
	staring multi-filter photometry point sources	PHT22
	staring multi-filter extended sources	PHT22
	faint source multi-filter nodding	PHT22
	staring multi-filter raster maps	PHT22
	multi-filter sparse map	PHT37/38/39
	polarimetry (PIA)	PHT51
SS/SL	staring point source spectroscopy	PHT40
	extended source spectroscopy	PHT40
	chopped point source spectroscopy	PHT40

Chapter 2

Known Limitations and Caveats

This section addresses the limitations and caveats of the PHT calibration file Version 5.4 and the OLP implementation 8.4 which have been identified during the scientific pipeline validation process. It addresses also which caveats from calibration file Version 4.0 and OLP version 7.0 have been closed out by this latest version.

2.1 Validity Ranges of FCS Calibration Files

OLP 7.0 contained the following caveats concerning the validity ranges of the FCS calibration files (cf. Report on the Scientific Validation for PHT OLP 7.0 [1]):

1 *OLP 7.0 Caveat:* A poorer calibration accuracy can be expected for observations for which the headers of the PHT data products indicate that the FCS power settings were outside the validity range given in the header of the P*FCSPOW*.FITS CAL-G files. The deviation is larger for extrapolations further away from the validity range.

2 *OLP 7.0 Caveat:* The FCS calibration for P3, C100 and C200 before revolution 94 is less well sampled with standard calibration observations, than after revolution 94. Therefore, the quality of the FCS calibration of observations before revolution 94 can be poorer as compared to observations taken later in the mission. This also applies for the FCS flat-field calibration for the C100 and C200 detectors.

For OLP 8.4 the FCS calibration files were derived once more, now based on the final complete data set of calibration measurements acquired during the mission. Furthermore, the generation of the calibration curves included the flux dependent signal linearization. Consequently revised limits resulted. Table 2.1 lists the limits used for OLP V7.0 and OLP V8.4.
The limits for the validity of the FCS ranges are included in the headers of the relevant FCS calibration files. Only a warning is written to the product file headers indicating the limit violation and possible degradation in calibration. To derive responsivities for the full range of electrical FCS powers used in the AOTs the lower and upper ends of the calibrated ranges were extrapolated using a model of the FCS (grey body).
Therefore, both OLP V7.0 caveats remain for OLP Version 8.4:

Caveat 1: A poorer calibration accuracy can be expected for observations for which the headers of the PHT data products indicate that the FCS power settings were outside the validity range given in the header of the P*FCSPOW*.FITS CAL-G files. The deviation is larger for extrapolations further away from the validity range.

Due to a change in the illumination characteristics of the long wavelength section of the FCS in the beginning of revolution 94, the FCS power files for the FIR detectors P3, C100, and C200 are time dependent. Before revolution 94 the coverage of the calibration curves by standard sources is less good than for the rest of the mission. This affects only a small number of Routine Phase observations (from rev. 79 to rev. 93):

Caveat 2: The FCS calibration for P3, C100 and C200 before revolution 94 is less well sampled with standard calibration observations, than after revolution 94. Therefore, the quality of the FCS calibration of observations before revolution 94 can be poorer as compared to observations taken later in the mission. This also applies for the FCS flat-field calibration for the C100 and C200 detectors.

Table 2.1 compares the valid ranges of the main FCS, FCS1, for OLP V7.0 and OLP V8.4 (in mW of electrical FCS power). In general the ranges remain more or less the same, except for filters P_11.3, C_60, C_90, C_100, C_105 and C_160 for which in the case of after revolution 94 measurements a considerable extension of the valid range could be achieved. Note that strictly speaking for PHT-P the power range is associated with the corresponding standard aperture (cf. Sect. 2.2 for a table of the standard apertures per PHT-P filter and additional caveat).

Table 2.1: Validity Ranges of FCS Tables (for FCS1 only). The validity range is given by the calibrated electrical heating power range (in mW) for each filter.

	up to revolution 93				**after revolution 93**			
	OLP V7.0		**OLP V8.4**		**OLP V7.0**		**OLP V8.4**	
Filter	**min**	**max**	**min**	**max**	**min**	**max**	**min**	**max**
P_3.29	17.48	50.00	17.48	50.00	17.48	50.00	17.48	50.00
P_3.6	11.29	50.01	9.49	50.01	11.29	50.01	9.49	50.01
P_4.85	13.30	35.34	15.01	35.34	13.30	35.34	15.01	35.34
P_7.3	7.48	22.13	7.48	22.13	7.48	22.13	7.48	22.13
P_7.7	8.59	24.41	8.59	24.41	8.59	24.41	8.59	24.41
P_10	4.47	11.49	5.45	11.49	4.47	11.49	5.45	11.49
P_11.3	4.81	8.92	4.81	11.78	4.81	8.92	4.81	11.78
P_11.5	3.50	9.49	3.73	9.68	3.50	9.49	3.73	9.68
P_12.8	4.00	7.63	3.65	7.63	4.00	7.63	3.65	7.63
P_16	2.66	6.58	2.66	6.58	2.66	6.58	2.66	6.58
P_20	1.72	4.00	1.72	4.00	1.72	4.00	1.72	4.00
P_25	1.40	3.61	1.40	3.61	1.40	3.61	1.40	3.61
P_60	1.34	2.98	1.05	2.98	0.42	2.13	0.42	2.13
P_100	0.42	1.84	0.42	1.84	0.27	1.84	0.27	1.84
C_50	1.93	4.23	1.03	4.23	0.59	4.36	0.59	5.27
C_60	1.23	3.88	1.09	3.88	0.77	3.05	0.39	6.39
C_70	0.75	4.03	0.74	4.03	0.43	3.15	0.43	3.15
C_90	0.54	1.93	0.46	1.93	0.29	1.94	0.29	4.40
C_100	0.46	2.03	0.46	2.03	0.20	1.75	0.20	3.79
C_105	0.40	2.22	0.40	2.22	0.20	3.09	0.20	5.84
C_120	0.31	1.86	0.31	1.86	0.24	3.47	0.24	3.47
C_135	0.27	1.34	0.27	1.34	0.17	2.66	0.17	2.60
C_160	0.22	1.16	0.22	1.16	0.13	1.62	0.07	2.45
C_180	0.27	1.90	0.27	1.90	0.18	2.91	0.12	2.88
C_200	0.22	0.81	0.22	0.81	0.13	5.78	0.16	5.78

2.2 Inhomogeneous FCS Illumination of PHT-P Apertures

The illumination of the both the PHT-P apertures and the PHT-C arrays by the internal Fine Calibration Source (FCS) is not flat. As a result the illumination of the detector does not scale with the area of the aperture. This effect is corrected for in the case of PHT-C by the so-called illumination matrix (PC1ILLUM and PC2ILLUM cal-G files). Currently, for PHT-P linearity with the aperture area is assumed and the corresponding PHT-P CAL-G

files (PP1FCSAP, PP2FCSAP and PP3FCSAP) only contain correction factors of 1 (i.e. they do not imply any correction).

Table 2.2: ISOPHOT Standard Calibration Apertures

Filter	**Standard Aperture**
P_3.29	23"
P_3.6	23"
P_4.85	23"
P_7.3	23"
P_7.7	23"
P_10	52"
P_11.3	52"
P_11.5	52"
P_12.8	52"
P_16	52"
P_20	79"
P_25	79"
P_60	180"
P_100	180"

Therefore the following caveat remains in place:

Caveat 3: In case the FCS calibration of an observation is performed in a non-standard aperture of this filter (cf. Table 1) strong deviations (factor $\simeq 2$) of the correct responsivity and thus the derived fluxes can occur. The deviations are strongest for the usage of the largest apertures in combination with P1 filters.

2.3 Non-geometric Aperture Beam Size Scaling

By evaluation of multi-aperture measurements on flat backgrounds it has been found that in some filters strong non-linear behaviour w.r.t. the geometrical aperture area occurs (in particular for the largest apertures, ≥ 120", of the 11.5 micron filter). This means, that, if observations are performed in apertures deviating strongly from the ones used in calibration (cf. Table 2.2), deviations from the correct flux can occur. This is especially of importance for multi-aperture measurements, because often background measurements are performed in different (larger) apertures than the related source observations and are scaled to the corresponding on-source aperture size.
The extended source calibration and the correction for non-geometric beam size effects of ISOPHOT-P is not yet finalized. Currently, the s/w uses the geometrical beam sizes only. Therefore the following caveat still applies:

Caveat 4: If observations are performed in apertures, which are different in diameter from the ones used in standard calibration, deviations from the correct flux calibration can occur. This implies especially for extended source or background observations using the largest apertures with P1 and P2.

2.4 Non-linearity of Detector Responsivity with Flux

It has been a major calibration project for OLP V8.4 to characterize the non-linearity of the detector systems with incident flux. New calibration files PP1SLINR, PP2SLINR, PP3SLINR, PC1SLINR, PC2SLINR have been established which provide a linearization of the detector signals so that the responsivity becomes homogeneous for the full applicable flux range.

With the successful implementation of this correction, the OLP 7.0 caveat:

1 *OLP 7.0 Caveat* Measurements with inband powers far away ($\geq$ factor 10) from the ones used for the related FCS measurement(s) have poorer calibration accuracy.

is no longer applicable for OLP version 8.4. Note however, that the linearity calibration is only valid for certain signal ranges. Table 2.3 lists the lower and upper signal limits as given in the headers of the calibration files PP1SLINR, PP2SLINR, PP3SLINR, PC1SLINR, PC2SLINR. The polynomial approximations to the non-linearity curves are not extrapolated beyond the calibrated signal ranges but are kept at the level of the boundary. In different filters different relative signal ranges may be covered so that in some cases with signals at the boundaries of the calibrated ranges some unsteadiness may be introduced.

Table 2.3: Calibrated Signal Ranges of Non-linearity Correction Tables

Detector	**Filter**	**Lower Limit** [V/s]	**Upper Limit** [V/s]
P1	3.3	0.000	55.4
P1	3.6	0.000	166.1
P1	4.8	0.000	126.8
P1	7.3	0.000	95.5
P1	7.7	0.000	27.1
P1	10.0	0.000	23.5
P1	11.3	0.000	2.9
P1	12.0	0.021	35.7
P1	12.8	0.031	11.4
P1	15.0	0.019	3.7
P2	20.0	0.075	9.5
P2	25.0	0.100	10.9
P3	60.0	0.248	56.3
P3	100.0	0.267	68.1
C100	60.0	0.000	60.1
C100	65.0	0.000	48.5
C100	80.0	0.117	32.2
C100	90.0	0.000	47.5
C100	100.0	0.000	39.0
C100	105.0	0.000	35.7
C200	120.0	0.000	32.3
C200	150.0	0.000	35.6
C200	170.0	0.000	36.8
C200	180.0	0.000	22.6
C200	200.0	0.000	9.4

2.5 Detector Signal Transients

PHT OLP does not use physical (Fouks) or empirical (exponential, signal jump) signal transient correction functions, as they are available in the PIA, because those require still a highly interactive mode. Currently OLP detects detector transients by statistical trend analysis methods and discards parts of a measurement found to be affected by drifts. This method works reasonably well, if a given measurement reaches stability, i.e. for bright sources and for very long observations. The condition that stability is achieved is that the variation of the signals during the considered time interval is less than 5%. Then the signals within the stability period are used to derive the final signal per chopper plateau. In case this criterium is not met, OLP uses the weighted mean of the last 8 signals.

Caveat 5: The transient correction only works satisfactory for measurements longer than the detector transient time constant at a given illumination. The transients are very often the limiting factor for the achieved accuracy. Measurements flagged by the OLP software as *"plateau data affected by residual drift"* can show strong deviations (residual drift is greater than 5%) from the correct result.

Note: The quality of an observation, w.r.t. drift and other criteria is coded into the SPD field **PxxSFLAG** where xx identifies the detectors as follows: C1, C2, P1, P2, P3, SS and SL. The flags are given for each chopper plateau individually and are defined in the OLP include file SPP_PIX_FLAGS_PAR.INC. The following table gives an overview:

Table 2.4: Quality flags for PHT SPD Data

Flag	Description
0	normal
1	calibration measurement saturated
2	part of plateau data affected by drifts
3	all ramps on plateau rejected
4	plateau data affected by residual drift
5	zero standard deviation
7	zero signal for plateau

2.6 Long Term Detector Drifts

For single pointing measurements with one FCS measurement per detector no attempt is made by PHT OLP software to correct for long term detector responsivity drifts, i.e. stability of the detector responsivity during the execution time of an AOT is assumed. For raster pointing observations and sparse maps OLP does a linear interpolation with time of the responsivity values derived from the two bracketing FCS measurements. Detailed investigation of PHT-C maps has shown that the detector long term drift is not linear, but very often shows an exponential behaviour due to switch-on effects. Therefore, models of the detector behaviour or baseline fits would be required for optimum results.

Caveat 6: PHT OLP does not correct (in case of single pointings) or correct only with a linear interpolation (in case of maps) for long term detector drifts within an AOT.

2.7 Error Calculation and Propagation

Uncertainties provided by OLP 8.4 are still pure statistical errors from signal evaluation, as for OLP V7.0. In order to assess all other uncertainties it is necessary to refer to the related documentation on PHT calibration in combination with the OLP products. (cf. documents ISO Data User Manual (IDUM) [2] and ISOPHOT Error Budgets [3]).

Caveat 7: The PHT OLP software does only provide an uncertainty from the statistical signal evaluation. It does not give any estimates of the systematic uncertainties of all performed calibration steps. Therefore, OLP 8.4 uncertainties are **minimal** errors. It is essential to refer to special documentation which provide an overview of the uncertainties introduced step by step. These depend on the exact observing conditions and evaluation steps which may even not be completed inside OLP (e.g. background subtraction in maps or from independent staring measurements).

2.8 Missing Measurements and Chopper Correction

For OLP 7.0 the following caveat had been imposed on the data products:

1 *OLP 7.0 Caveat:* In case there are measurements missing from an AOT there may be a mismatch between the chopper correction keywords and the related filter number.

With the revision of the chopped signal correction in OLP 8.4 the reading of the chopper corrections from the SPD header has been removed. Consequently, the caveat is no longer applicable.

2.9 Limitations in Use of PHT Color Correction Factors

With the OLP V7.0 and CAL-G V4.0 for the first time CAL-G files with color correction factors for several different SEDs were provided. These color correction factors are not applied by PHT OLP, but can be applied inside PIA. They have been calculated from the bandpass transmission files currently available, which have typically about 300 data points equally spaced in wavelength. Two different interpolation and integration methods have been used to derive the color correction factors and they give equal results except for the cases where steep Wien branches are convolved with the bandpass transmission numbers. Furthermore, the bandpass transmission files used are centred on the main throughput range. All wavelengths for which the transmission was below 10^{-4} have been excluded. Taking into account the latest available data sets of all transmission components (filter transmission, field lens transmission, blocking material transmission, spectral detector responses) the bandpass transmission of some filters (in particular P1 filters) need some update and refinement, because they show minor credible transmission peaks outside the main range. In case of extreme source SEDs these "leaks" can make a significant contribution to the resulting inband power and hence alter the corresponding color correction factor considerably.
For CALG V5.4 there was no re-determination of color correction factors. Therefore, the following caveats still apply for CAL-G V5.4 color correction factors:

Caveat 8: For the establishment of the color correction factors provided by CAL-G Version 5.4 not yet final PHT filter bandpass data including a wide wavelength range outside the nominal bandpass have been used. For some filters and in the case of extremely rising or falling SEDs this can mean an underestimate by out-of-band contributions. Color correction factors above 2 should be considered as less accurate and factors above 4 only as an indication of the order of the correction, as they clearly depend on the integration and interpolation method used. This applies in particular for SEDs of cold sources in combination with the P1 filters which fall onto the steep Wien branch of these SEDs. In these cases it is recommended to contact the ISO Data Centres for the most recent bandpass transmission and establish the color correction factor yourself.

With CAL-G V5.4 the relative spectral system responses of all ISOPHOT-P and -C bandpasses are provided in the two new CAL-G files PPFILTRAN.FITS and PCFILTRAN.FITS. This enables observers to calculate color correction factors for any SED shape not covered by the dedicated color correction CAL-G files.

2.10 Empirical PPSF Correction Factors for Array Centered C200 Photometry

For OLP 7.0 the following caveat had been imposed on the data products:

1 *OLP 7.0 Caveat:* The correction factors for the filters C_180 and C_200 appear to be too large by 20 to 30%. Photometric fluxes derived for both filters in array centered mode should be corrected towards larger values by this percentage (as the uncorrected flux value is divided by the PPSF factor).

For OLP 8.4 the empirical factors have been redetermined from a larger calibration data set. For comparison we list theoretical and the empirical ones for OLP V7.0 and OLP V8.4 in Table 2.5:

Table 2.5: PPSF Factors for Array Centered C200 Photometry. Factors apply to the whole array, i.e. the sum of all 4 pixels.

C200 Filter	**theoretical PPSF**	**empirical PPSF OLP V7.0**	**empirical PPSF OLP V8.4**
C_120	0.814	0.574	0.498 ± 0.028
C_135	0.846	0.668	0.568 ± 0.029
C_160	0.733	0.708	0.528 ± 0.021
C_180	0.818	0.972	0.612 ± 0.046
C_200	0.655	1.054	0.693 ± 0.020

The new values are smaller than the old ones for all filters and confirm two findings:

1 the strong deviation from the theoretical values for the shorter wavelengths.

2 the strong correction for the C_180 and C_200 values with regard to the OLP V7.0 values in the direction as predicted by the OLP V7.0 caveat.

Scientific validation of the OLP 8.4 products has demonstrated that this caveat is no longer applicable.

2.11 Incomplete Raster Map Appearance in Case of Zero Signal Flag

A new caveat from OLP 8.4 Scientific Validation comes from the investigation of PHT-P raster maps:

Caveat 9: In case the total flux on the detector is very small, resulting in close to zero or even negative signals at the end of the DERIVE_SPD processing stage, OLP sets the "zero signal flag" for the corresponding plateaux times and does not continue to process these data sections in DERIVE_AAR (cf. description of SPD product types, coding of pixel status flag PPxSFLAG; a listing of the quality flags is given in Table 2.4). This leads then to incomplete appearing map products PGAI. The most likely cases are for the short wavelength filters of PHT-P1, where the sky background (Zodiacal Light) shows a minimum, in particular in combination with small aperture sizes.

2.12 Application of Point Spread Function Fraction Factors to AAR Data Products

It should be noted that:

Caveat 10: The point spread function fraction correction factors are applied to all data products associated to point source photometry, like PPAP and PCAP, regardless whether a background subtraction was performed or not. For staring mode observations without background subtration this has to be accounted for when subtracting the separate background measurement.

The background measurement can be either a point source photometry (in Jy), of type PPAP or PCAP, too:

$F_{src+back} = F_{on} / f_{psf}$
$F_{back} = F_{off} / f_{psf}$
$\rightarrow F_{src} = F_{src+back} - F_{back} = (F_{on} - F_{off}) / f_{psf}$

or an extended source measurement of type PPAE or PCAE (in MJy sr^{-1}; for the conversion of in-band power to surface brightness, cf. chapter 8.4.10 in [2]):

$F_{src+back} = F_{on} / f_{psf}$
$B_{back} = (F_{off_pix} / ((1-\varepsilon^2) \cdot \Omega)$
$\rightarrow F_{src} = F_{src+back} - F_{back} = (F_{on} - n_{pix} \cdot (B_{back} \cdot (1-\varepsilon^2) \cdot \Omega)) / f_{psf}$

F_{on}, F_{off}, F_{off_pix} are fluxes in the aperture uncorrected for point source function effects (the latter one for one single pixel of the array). B_{back} is the surface brightness of the background.

Please note the following definitions with regard to application of f_{psf}-factors to header keywords :

1) For PPAP and PPAE:
   $f_{psf} = f_{psf}^{aperture}$
   $n_{pix} = 1$

2) For PCAP and PCAE staring modes:
   total flux of the array is used!
   $f_{psf} = f_{psf}^{array}$
   converted flux from surface brightness has to be multiplied with number of pixels, because the solid angle Ω is defined per pixel!
   $n_{pix} = 9$ for C100, $n_{pix} = 4$ for C200

3) For C100 PCAP and PCAE chopped mode (PHT22):
   $f_{psf} = f_{psf}^{pixel}$
   because only the central pixel is used!
   $n_{pix} = 1$
   Note that f_{psf}^{array} is applied to the data fields PCAPSRCE for consistency with the staring mode!

4) For C200 PCAP and PCAE chopped mode (PHT22):
   $f_{psf} = f_{psf}^{array}$
   $n_{pix} = 4$

2.13 Failure of Chopped Signal Pattern Generator in Case of Data Reduction

With OLP 8.4 a signal pattern of the chopped measurement is generated for a more robust determination of the difference signal. This pattern consists of 4 points each for the on-source and the off-source cycle, regardless of how many ramps per chopper plateau are actually performed (however, the minimum number of ramps is four per chopper plateau).

Caveat 11: In case of the data reduction factor being greater than 1 (i.e. for bright sources with very fast read-outs) the generation of the chopped signal pattern fails due to a timing jitter. The pattern will be zero and the resulting flux will be zero, too.

73 chopped photometry TDTs with a total of 113 measurements having a data reduction factor of at least 2 are affected. Solutions will be worked out for future OLP versions. In case a zero flux value is encountered for a chopped measurement, the pattern keyword PDlPmLn (l = filter number, m = pixel number, l = logical ramp number) in the SPD product should be checked for zero values.

2.14 Residual Flat-field Structures in PHT22 Raster Maps

As part of the scientific validation of PHT22 raster maps for OLP V8.4 the flat-field accuracies for maps having a wide range of selected raster parameters, with and without pixel overlap, and a wide range of sky background brightness have been assessed. It is found that in case of no pixel overlap flat field accuracies both for C100 and C200 are in general worse than 8 % (standard deviation of the mean sky bakground versus mean sky background). This limit is due to systematic flat-field residuals of the arrays and can be recognized as systematically repeated patterns in most of the maps. In addition, for C100 maps, temporal variations of these flat-field structures are found. This is linked to non-linear detector drifts as flagged in Sect. 2.6. Therefore, for OLP 8.4 the following caveat is imposed on mapping products PGAI:

Caveat 12: Systematic flat-field residuals in maps with no pixel overlap which account to between 10 and 20 % as well as temporal variations of the flat-field in case of C100 maps limit the ability of faint source detections and photometry on low sky background levels.

Chapter 3

Prerequisites for OLP Scientific Validation

The scientific validation of the PHT pipeline follows the guidelines as out-lined in the e-mail by the ISO Project Scientist Martin Kessler, "Scope of OLP Scientific Validation - IDT AI #8/16" from 18-JUL-1995. The major goals of the scientific validation process according to this note are to:

- confirm that the applied processing has had the expected effect(s) on the data;
- establish that sufficient processing has been applied to the data so that the products are usable by the observer;
- demonstrate that the processing is reliable, stable and repeatable;
- establish the level of accuracy of the calibration;
- document any known caveats or concerns with the processing and/or calibration;
- demonstrate that, with the aid of the relevant ISO Data Users Manual (IDUM), Observers can further process products to a publish-able form.

The scientific validation process is restricted to PHT Standard Processed Data (SPD) and Auto-Analysis Products. Edited Raw Data (ERD) were declared scientifically valid for data products generated with OLP version 4.0 or higher, during the "OLP V4.0 AND BEYOND REVIEW MEETING" on the 24th of April 1996. Therefore, all tests outlined here assume the correctness of all ERD data.
All test data sets were processed with the IDC test pipeline version 8.4beta. Re-processing with a delta version of 8.4beta at RAL was performed as necessary in order to validate OLP modules which have been improved during the validation process.

Chapter 4

Overview of Results from SVP1

During the first period of the PHT OLP 8.4 Scientific Validation the following results were achieved:

- SCREW-380, the dedicated spectral response function for chopped PHT-S measurements, is correctly implemented and yields considerable calibration improvement.
- SPR-2705, the recognition of variable aperture size in PHT-P raster maps, is correctly implemented.
- SPR-2894, improved point spread function factors for the PHT-C arrays, failed correct implementation. This lead to submission of SPR-2970, however PHT-C photometry could be evaluated by correcting the products with the correct point spread function factors.
- The validation of the chopped photometry, covered by the SCREW-382 implementation, was restricted during this period to the technical check-out of the individual processing steps via 1:1 comparison to the prototype in PIA. Several SPRs to improve the OLP processing were issued, see Table 4.1 below.

By the end of SVP1 the following software problem reports for updates had been recorded:

Table 4.1: Problems found during OLP 8.4 Scientific Validation Period 1

Problem	**CI**	**SPR**
Wrong corrected output signals in CALG P%%SLINR	CALG	2953
Wrong array PSF factors in CALG PCPSF	CALG	2970
FCS-Power-Curves Off near Validity Limits	CALG	2979
Incorrect signal patterns for chopped mode	OLP	2980
Zero uncertainty in chopped mode Cal A record	OLP	2981
Pattern missing in Cal A header	OLP	2982
Floating underflow error in PHT AA for chopped mode	OLP	2983
Regression problem with installation of CALG file PC1SLINR.FITS	CALG	2985
MV53 errors writing PC1S product	OLP	2986
Incomplete SPD header for product PC1S35602204.FITS	OLP	2997
Surface brightness display range in the extreme case of one map pixel	BPG_PHT	2975
Distorted maps on PHT postcards	BPG_PHT	2984

SPR-2953 could still be corrected before the actual start of SVP1.

Chapter 5

Revalidation Tests during SVP1

5.1 Upgrade of PHT-S Spectral Response Function for Extended Sources

An overview of the test cases is outlined in Ref. [4], chapter 3.1.1.

5.1.1 References to Calibration Analysis and Software Change Documentation

- calibration report:
  - ISOPHOT Footprints and Near-Field Straylight: S - Re-analysis of cross scans to extract measured footprint and associated parameters[5]
- Software Problem Report: SPR 2793

5.1.2 Summary of Results

Please refer to Sect. 7.1 for a summary of results.

5.1.3 ISOPHOT-S Spectroscopy of the Extended Reflection Nebula NGC 7023

- authors: K. Wilke, U. Klaas
- date: 14-June-1999
- SVP period 1

Motivation

NGC 7023, a bright reflection nebula, is a prototype object with regard to exhibiting pronounced PAH features. The extended source has been observed from the ground and been mapped by ISOCAM-CVF.

Method

We compare the ISOPHOT-S extended source spectrum in $W/m^2/\mu m/sr$ with the groundbased spectrum by Sellgren et al. [6], fig. 1 therein, and the ISOCAM-CVF spectrum by Cesarsky et al. [7], fig. 5 therein, both converted to the above unit. We compare the absolute levels in the continuum and in the features and the relative strength of the features. It should be noted that no background subtraction was performed for the ISOPHOT-S measurement, while the groundbased and KAO measurements were performed in chopped mode with a chopper throw of 120arcsec E-W direction. The ISOCAM-CVF spectrum is also not background subtracted.

Results

Fig. 5.1 shows the OLP 7.0 browse product and for comparison fig. 5.2 the new OLP 8.4 beta1 product. It can be seen that the absolute flux level was shifted down by the scaling of the PHT-S solid angle as predicyted by SPR-2793. Furthermore the size of the error bars is reduced now, providing only the uncertainties due to signal evaluation, closing SPR 2844.
Fig. 5.3 shows the comparison between the ISOPHOT-S spectrum and the groundbased 4 to 13 micron spectrum by Sellgren et al. 1985. The used beam sizes are comparable, though the groundbased spectroscopy was done with several instruments with beam sizes between 10 and 27 arcsec. It should also be noted that the pointings are slightly offset from each other (HD 200775 position: RA = 21:01:36.9, DEC = +68:09:48; ISO NGC 7023 pointing: RA = 21:01:31.8, DEC = +68:10:23; see caption of Fig. 5.3 for offet values). The 6.2, 7.7, and 11.3 μm features are stronger with ISOPHOT-S, while the 3.3 μm feature is stronger in the groundbased measurement. The 8.6 μm feature is barely detected by the groundbased measurement. ISOPHOT-S has the better resolution with regard to the width of the features. The continuum level at 10 μm is identical. The relative strength of the feature and the continuum is compiled in Table 5.1.
Fig. 5.4 shows the comparison between the ISOPHOT-S spectrum and the ISOCAM-CVF spectrum obtained at RA = 21:01:00, DEC =+67:56:58 (1950) (peak of 16 μm emission; 2000 coordinates: RA = 21:01:37, DEC = +68:09:52 = approximate position of HD 200775). It is not clear from the paper which sampling aperture was used to obtain the average spectrum. The centre of the area is outside the ISOPHOT-S aperture. The relative strength of the 6.2 and 7.7 μm features are the same for both spectra, though the ISOCAM-CVF shows 22 % smaller peak levels. The 11.3 μm feature is 33 % weaker in the ISOCAM spectrum. The strength of the 8.6 μm feature is comparable as well as the continuum levels at 7 and 10 μm. Also the width of the features is the same in both spectra. The relative strength of the feature and the continuum is compiled in Table 5.1.

Conclusions

The investigation of the NGC 7023 spectrum (TDT 42300402) has shown that

1) The new correction factors for the extended PHT-S solid angle are correctly implemented and give the right scaling.

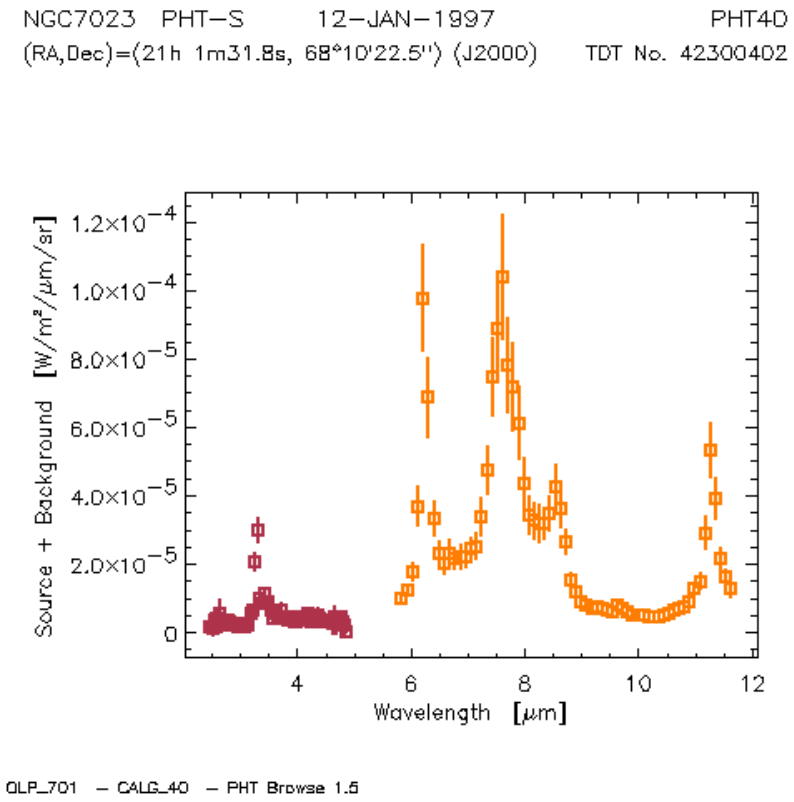

Figure 5.1: Browse product of the OLP 7.0 AAP for TDT42300402.

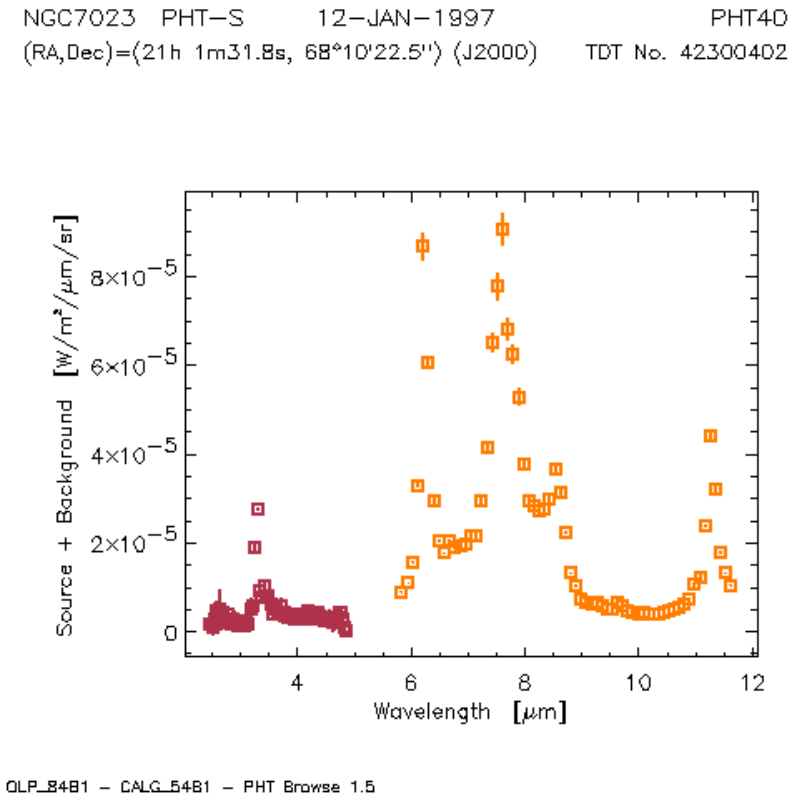

Figure 5.2: Browse product of the OLP 8.4 beta1 AAP for TDT42300402.

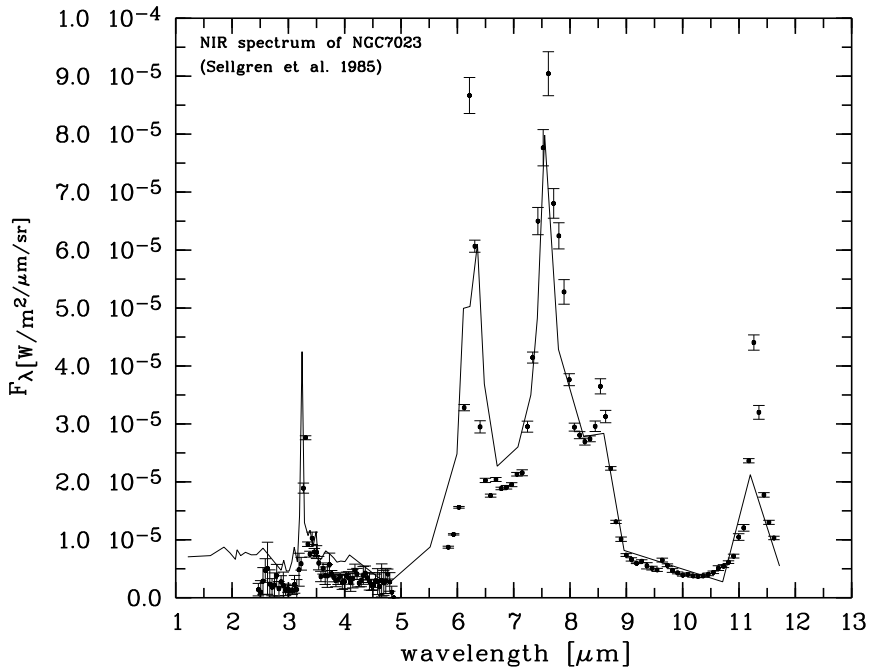

Figure 5.3: Comparison of the ISOPHOT-S spectrum of NGC 7023 with the spectrum obtained by Sellgren et al. 1985 using the KPNO, IRTF and KAO facilities (figure 1 therein). Beam sizes ranged from 10 to 27" (table 1 therein). The telescope pointings were 30" W and 20" N of HD 200775, while the pointing for the ISOPHOT observations were 28" W and 35" N of HD 200775.

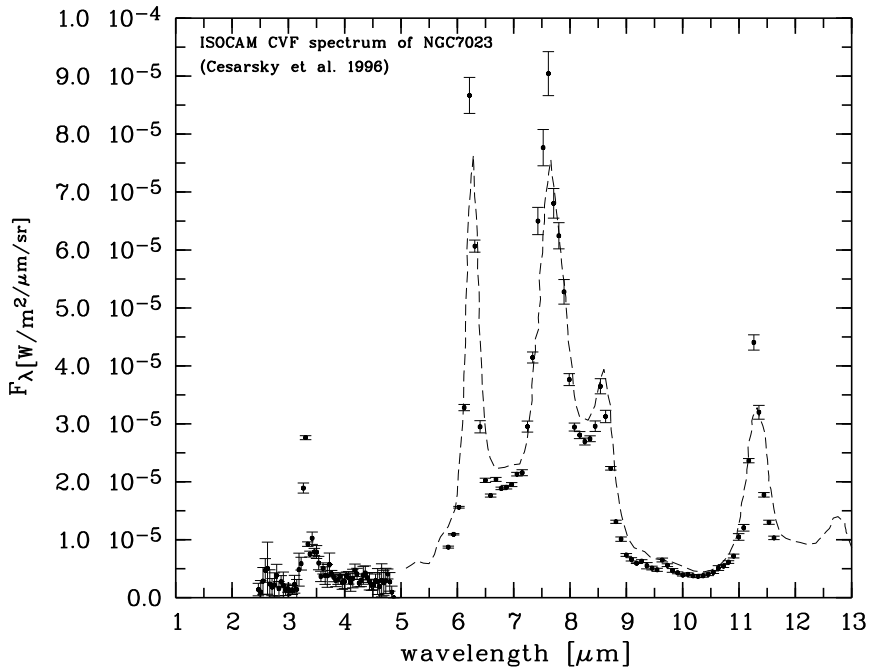

Figure 5.4: Comparison of the ISOPHOT-S spectrum of NGC 7023 with the spectrum obtained by Cesarsky et al. 1996 using ISOCAM-CVF (figure 5 therein). The size of the sampling aperture is not specified in the paper. The spectrum is integrated on a position close to HD 200775, which is 31" S and 29" E of the ISOPHOT-S position, i.e. outside the ISOPHOT-S aperture.

Table 5.1: Comparison of continuum and feature peak flux levels of NGC 7023 from PHT-S (OLP V8.4b1), groundbased $4 - 13$ μm spectroscopy (Sellgren et al. 1985) and CAM CVF (Cesarsky et al. 1996).

wavelength	**PHT-S**	**groundbased**	**CAM CVF**
[μm]	[10^{-5} W m^2 μm^{-1} sr^{-1}]		
3.3 (feature)	2.8	4.2	–
6.2 (feature)	8.5	6.0	7.5
7.7 (feature)	9.0	8.0	7.5
10 (continuum)	0.5	0.5	0.5
11.3 (feature)	4.5	2.0	3.0

2) Given the fact that different pointings on the nebula for the reference measurements, as well as different aperture sizes were used, the agreement in the absolute levels, line widths and line strength is quite remarkable.

5.2 Dedicated Spectral Response Function for Chopped PHT-S Measurements

An overview of the test cases is outlined in Ref. [4], chapter 3.1.2.

5.2.1 References to Calibration Analysis and Software Change Documentation

- calibration report:
  - Calibration of ISOPHOT-S Chopped Measurements [9]
- Software Change Request: SCREW 380

5.2.2 Summary of Results

- Algorithms and CALG files are correctly implemented.
- The new spectral response function and the first order correction proportional to the flux jump provide considerable improvement with regard to the default staring spectral response function.
- Comparison with groundbased spectroscopy suggests that absolute accuracies in the order of 10 % and relative accuracies in the order of 10 % are achieved down to flux levels of 10^{-13} W m^{-2} μm^{-1} for SS and 10^{-14} W m^{-2} μm^{-1} for SL.

5.2.3 Consistency Check of Chopped PHT-S Relative Spectral Response Function on Calibration Stars

- authors: K. Wilke, U. Klaas
- date: 18-June-1999
- SVP period 1

Motivation

We process measurements of two calibration stars (HR 6817 and HR 6847) which were used to establish the Relative Spectral Response Function (RSRF) for chopped PHT-S measurements and check whether the input model SED is reproduced. Both calibration stars were measured both in rectangular chopped and triangular chopped mode. This allows to assess the consistency of the processing of the two chopper modes.

Method

We compare the results with the flux models by Hammersley et al. 1998 [11].

Results

In Figs. 5.5 and 5.6 we compare the OLP V7.0 and OLP V8.4 browse products for HR 6817 with each other.We notice the following:

- The spectral shape of the OLP V8.4 product looks smoother.
- The flux of the OLP V8.4 product is higher showing that the new RSRF accounts for the signal losses due to chopping.

In Figs. 5.7 to 5.10 we perform an individual comparison with the flux model. The resulting spectra follow the model very closely demonstrating the consistent implementation of the correction. At the fainter flux end, in particular for HR 6847 the triangular chopped mode gives somewhat more stable results.

Conclusions

- The new Relative Spectral Response Function for chopped PHT-S measurements gives a very good reproduction of the stellar flux models. It can be expected that the overall accuracy of the mode is considerably improved with regard to the usage of the standard spectral response function derived from staring measurements.
- Rectangular and triangular chopped modes give consistent results.

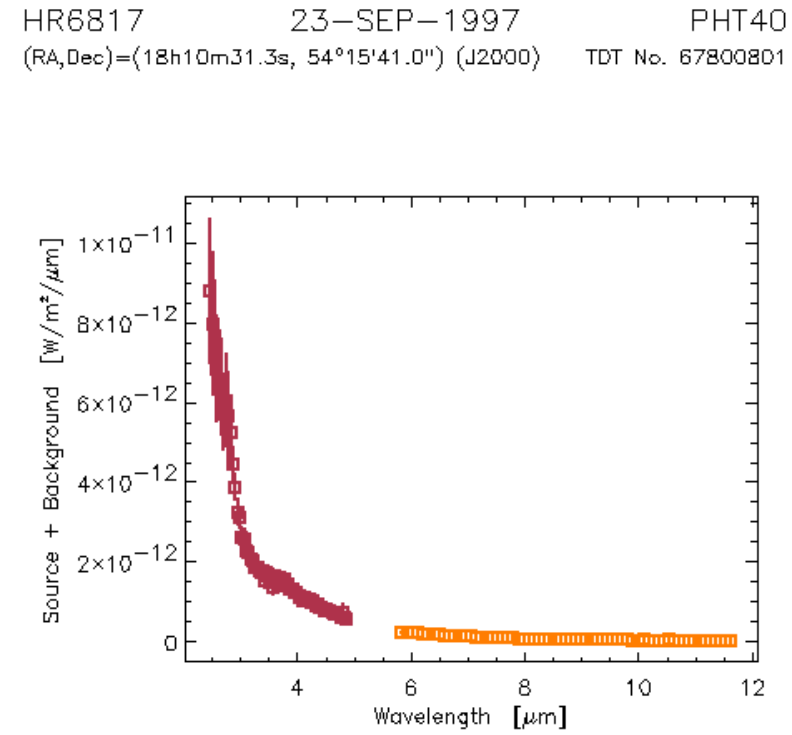

Figure 5.5: Browse product of the OLP 7.0 AAP for TDT67800801.

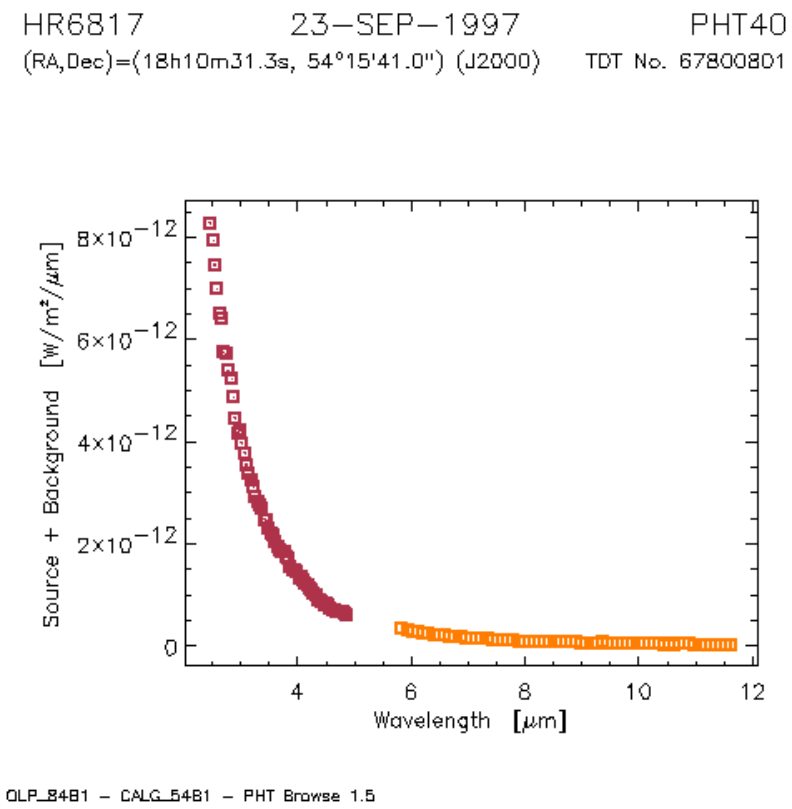

Figure 5.6: Browse product of the OLP 8.4 beta1 AAP for TDT67800801.

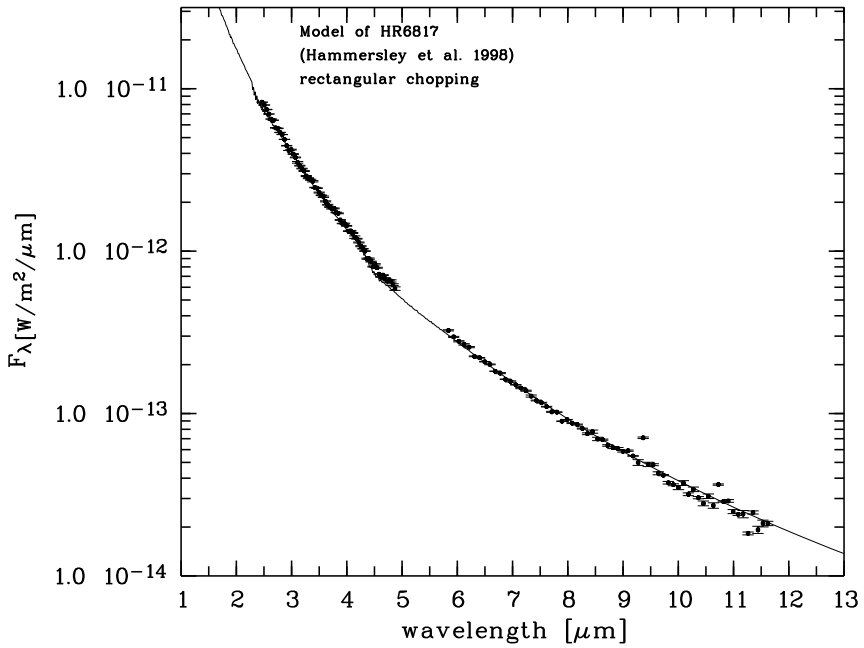

Figure 5.7: Comparison of the spectrum of HR 6817 obtained in PHT-S rectangular chopped mode with the flux model by Hammersley et al. 1998.

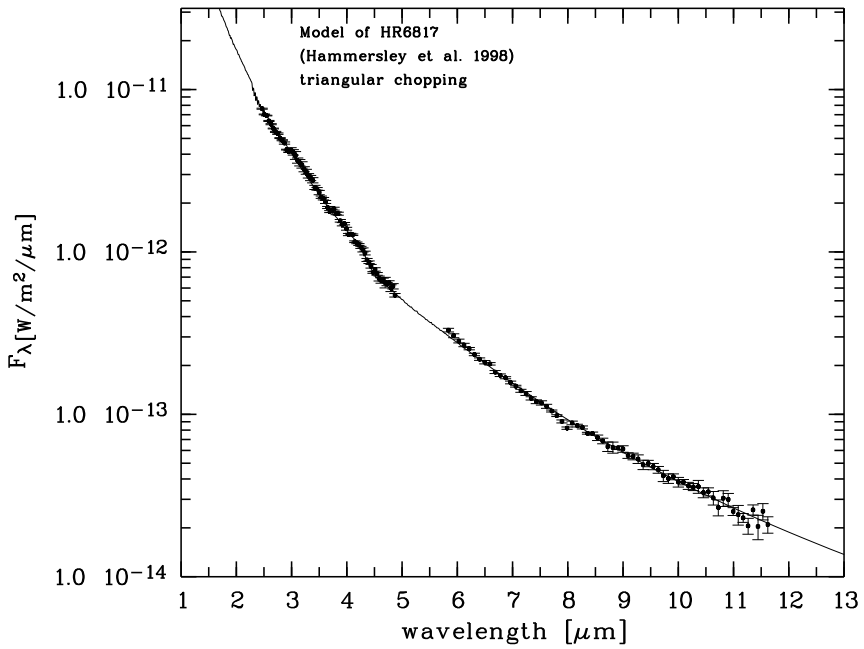

Figure 5.8: Comparison of the spectrum of HR 6817 obtained in PHT-S triangular chopped mode with the flux model by Hammersley et al. 1998.

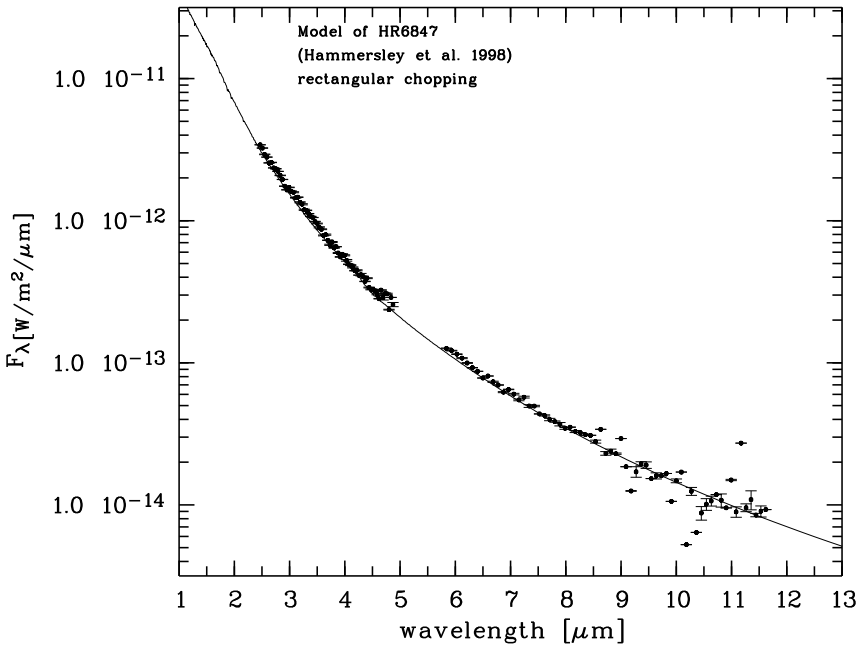

Figure 5.9: Comparison of the spectrum of HR 6847 obtained in PHT-S rectangular chopped mode with the flux model by Hammersley et al. 1998.

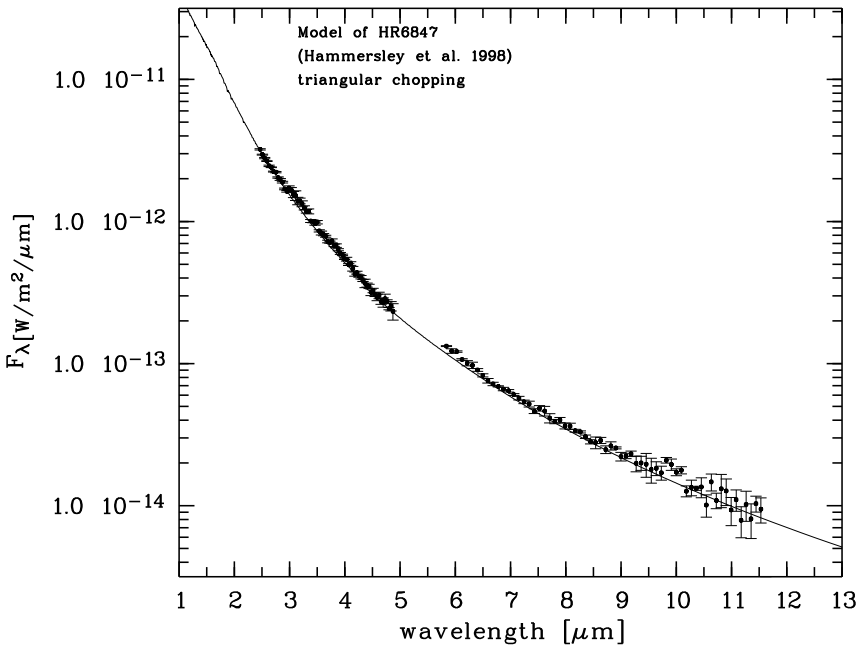

Figure 5.10: Comparison of the spectrum of HR 6847 obtained in PHT-S triangular chopped mode with the flux model by Hammersley et al. 1998.

5.2.4 MIR Spectra of Galaxies from Chopped PHT-S Measurements

- authors: K. Wilke, U. Klaas
- date: 16-June-1999
- SVP period 1

Motivation

There is a set of chopped PHT-S measurements on galaxies 10^{-14} to 10^{-12} W/m^2/μm. These galaxies have different SED shapes than the standard stars from which the chopped PHT-S spectral response function was derived. There is groundbased $8-13$ micron spectroscopy available (cf. Ref. [8]). We selected a range of galaxies from featureless continuum to spectra with PAH features and strong 10 μm silicon absorption.

Method

We compare the absolute fluxes and relative shapes of the ISOPHOT-S spectra with the groundbased spectroscopy. Note that we compare an aperture size of 24x24 arcsec^2 for ISOPHOT-S with 5 arcsec aperture size of the groundbased measurements.

Results

In Figs. 5.11 and 5.12 we do a qualitative comparison between the OLP 7.0 and OLP 8.4b1 products for the brightest source using the browse product representation. The following differences can be noticed:

1) The peculiar "absorption feature" at around 3.3 μm has disappeared in the OLP 8.4 version. This is due to the different signal transient behaviour of the shortest SS pixels in staring and chopped mode.

2) The SS and SL parts fit better together in the OLP 8.4 version. The 6 to 8 μm flux level was underestimated by the staring spectral response function.

3) Overall the flux level is higher in the OLP 8.4 version accounting for the signal losses in chopped measurements.

4) The uncertainties of the OLP 8.4 product are smaller, as only the signal uncertainties are guiven now, according to SPR 2844.

In Figs. 5.13 to 5.18 we display the ISOPHOT-S spectra compared to the groundbased $8-13$ micron spectroscopy. Despite the fact that quite different aperture sizes were used, there is in most cases a very good correspondence of the ISOPHOT-S spectrum and the groundbased spectrum, showing that the emission is dominated by the nuclei of the galaxies. Examples for higher fluxes from the ISOPHOT-S measurement are NGC 1068 and NGC 4151 which have both extended activity areas. The higher groundbased flux for 3C 273 could be due to variability, for NGC 5253 the reason is unclear.
The comparison includes nearly featureless spectra (e.g. NGC 4151, Mkn 463, NGC 1275, 3C 273), spectra with strong dust features in emission (e.g. NGC 4102, Mkn 331) and spectra with strong silicon absorption features (e.g. NGC 6240, Arp 220). NGC 5253 shows in both spectra a strong emission line, which is very likely due to its narrow width the [SIV10.4] line. The reproducibility of the measurement mode with regard to absolute flux level and shape of features for faint sources is demonstrated by the repeated spectrum of Mkn 331.

Conclusions

- For 16 galaxy spectra we find a remarkable good correspondence with $8-13$ micron groundbased spectroscopy with regard to absolute flux level and the relative shape, including occurrence of emission and absorption features and lines. Deviations for some objects can be explained by beam size effects or variability of the object.

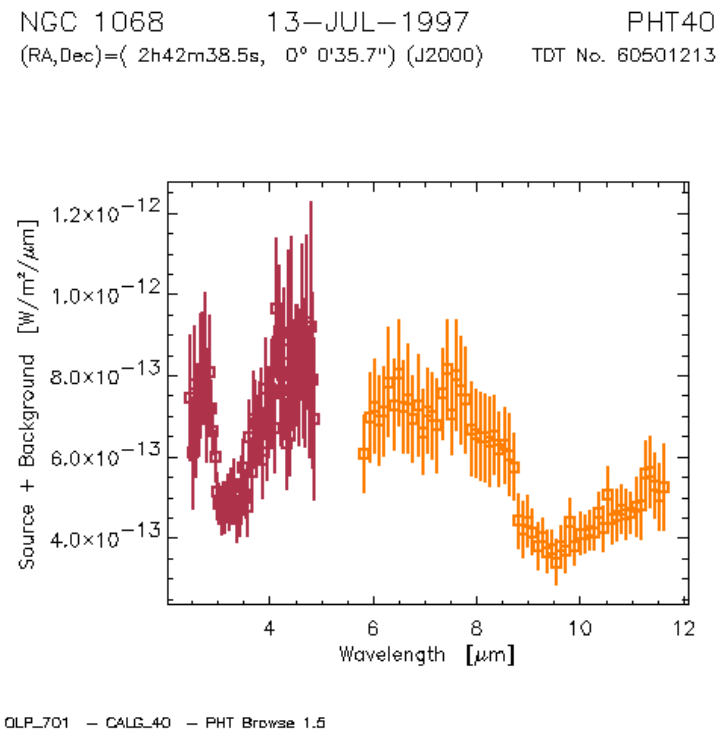

Figure 5.11: Browse product of the OLP 7.0 AAP for TDT60501213.

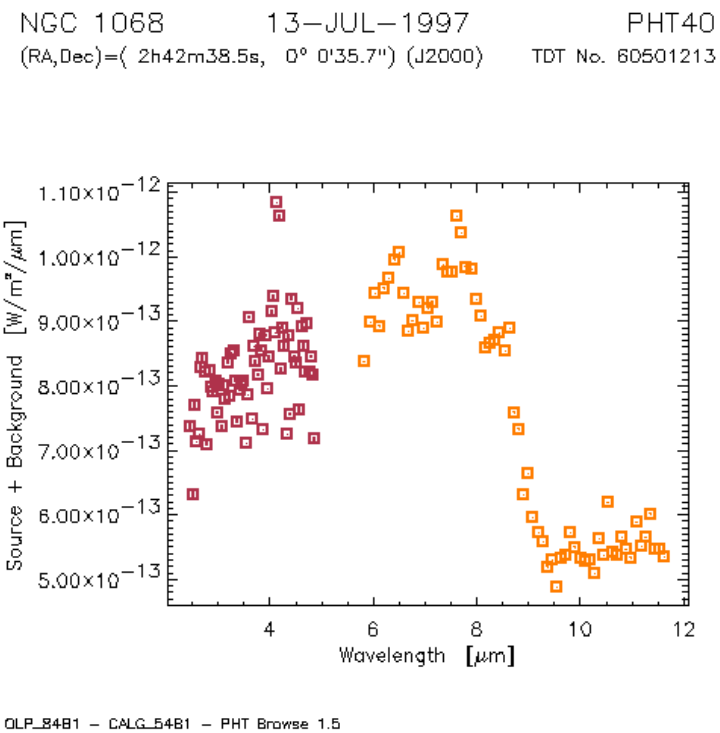

Figure 5.12: Browse product of the OLP 8.4 beta1 AAP for TDT60501213.

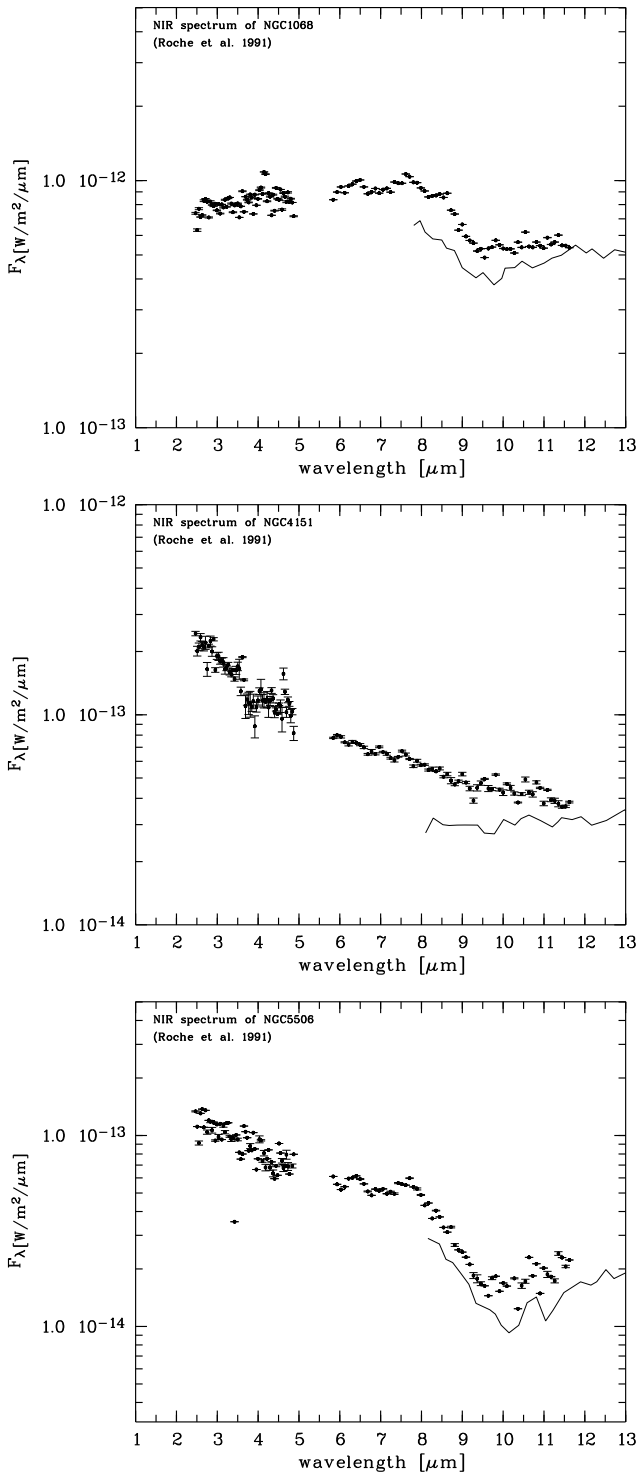

Figure 5.13: Comparison of ISOPHOT-S spectra of the 3 galaxies NGC 1068, NGC 4151 and NGC 5506 obtained in chopped mode (dots) with groundbased 8 – 13 micron spectroscopy (solid line).

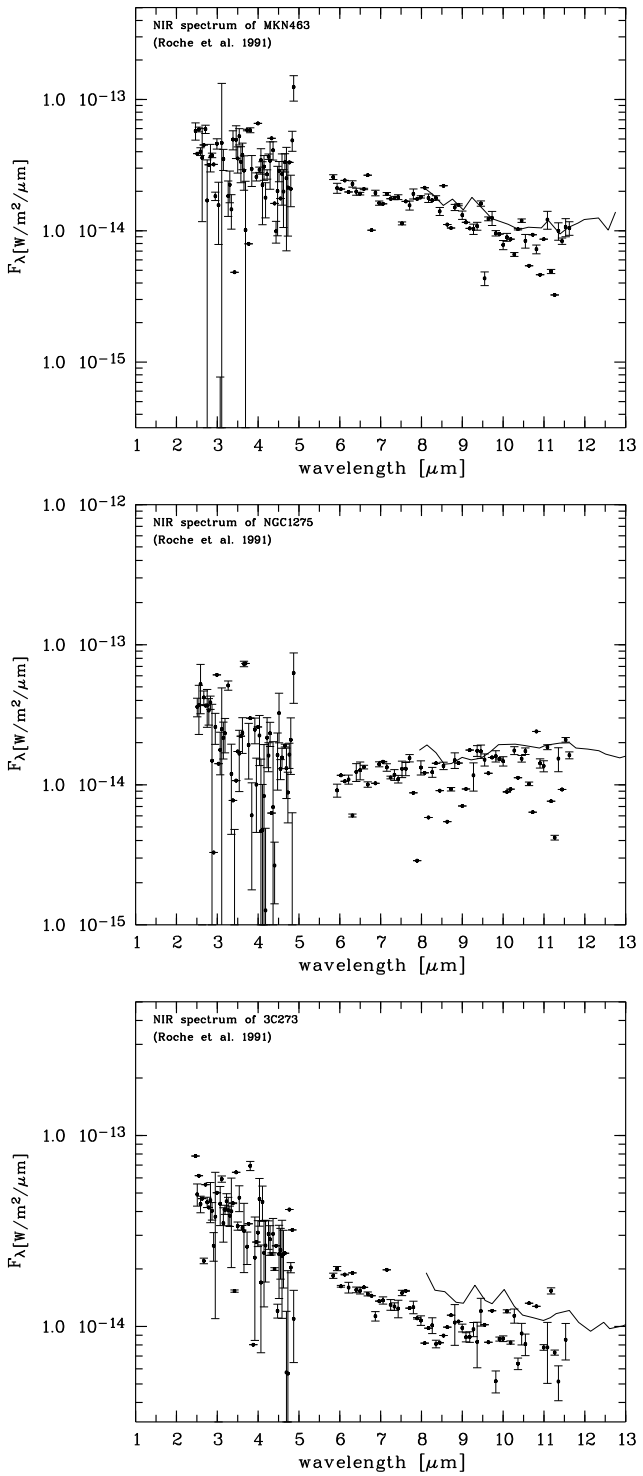

Figure 5.14: Comparison of ISOPHOT-S spectra of the 3 galaxies Mkn 463, NGC 1275 and 3C273 obtained in chopped mode (dots) with groundbased $8-13$ micron spectroscopy (solid line).

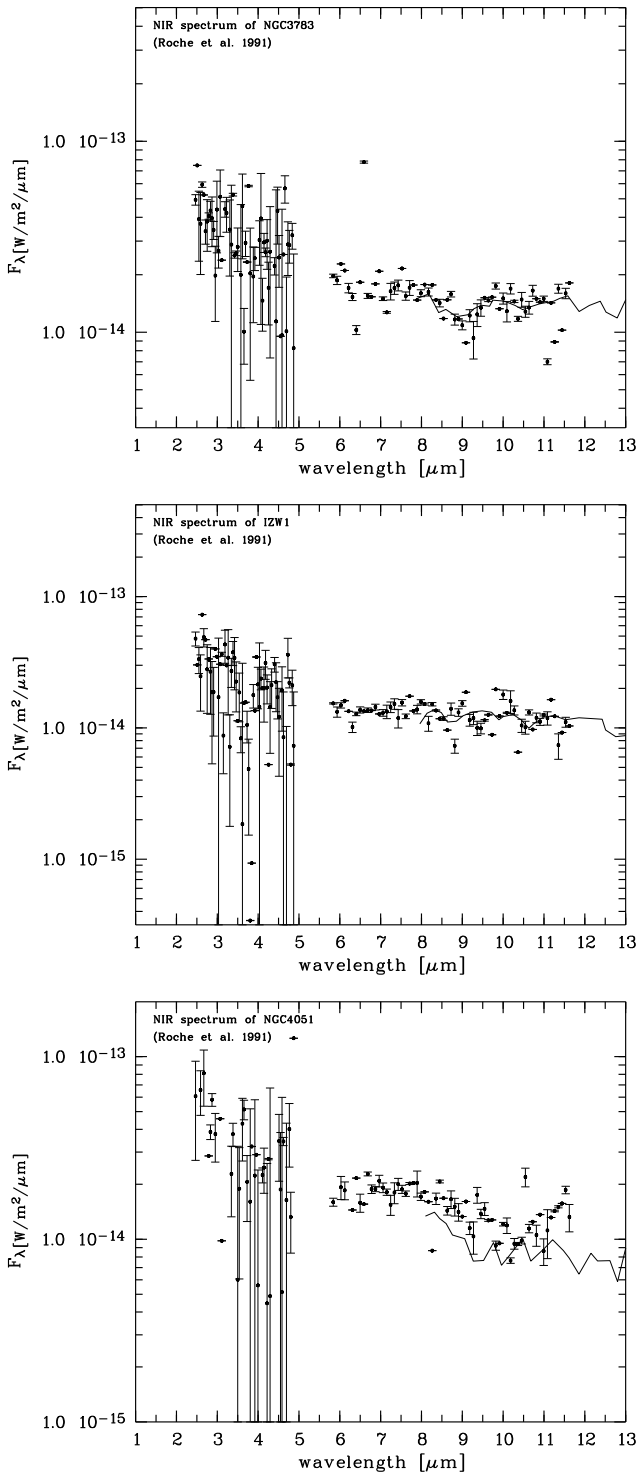

Figure 5.15: Comparison of ISOPHOT-S spectra of the 3 galaxies NGC 3783, IZw1 and NGC 4051 obtained in chopped mode (dots) with groundbased $8 - 13$ micron spectroscopy (solid line).

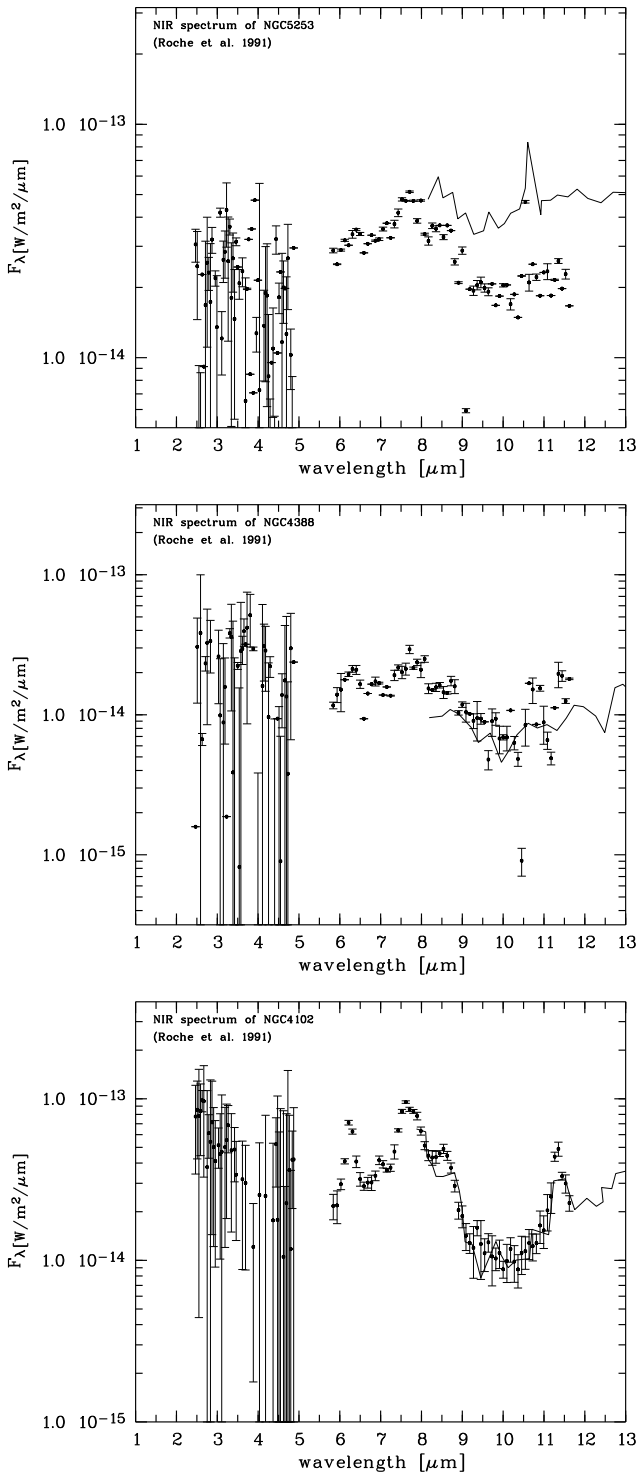

Figure 5.16: Comparison of ISOPHOT-S spectra of the 3 galaxies NGC 5253, NGC 4388 and NGC 4102 obtained in chopped mode (dots) with groundbased 8 – 13 micron spectroscopy (solid line).

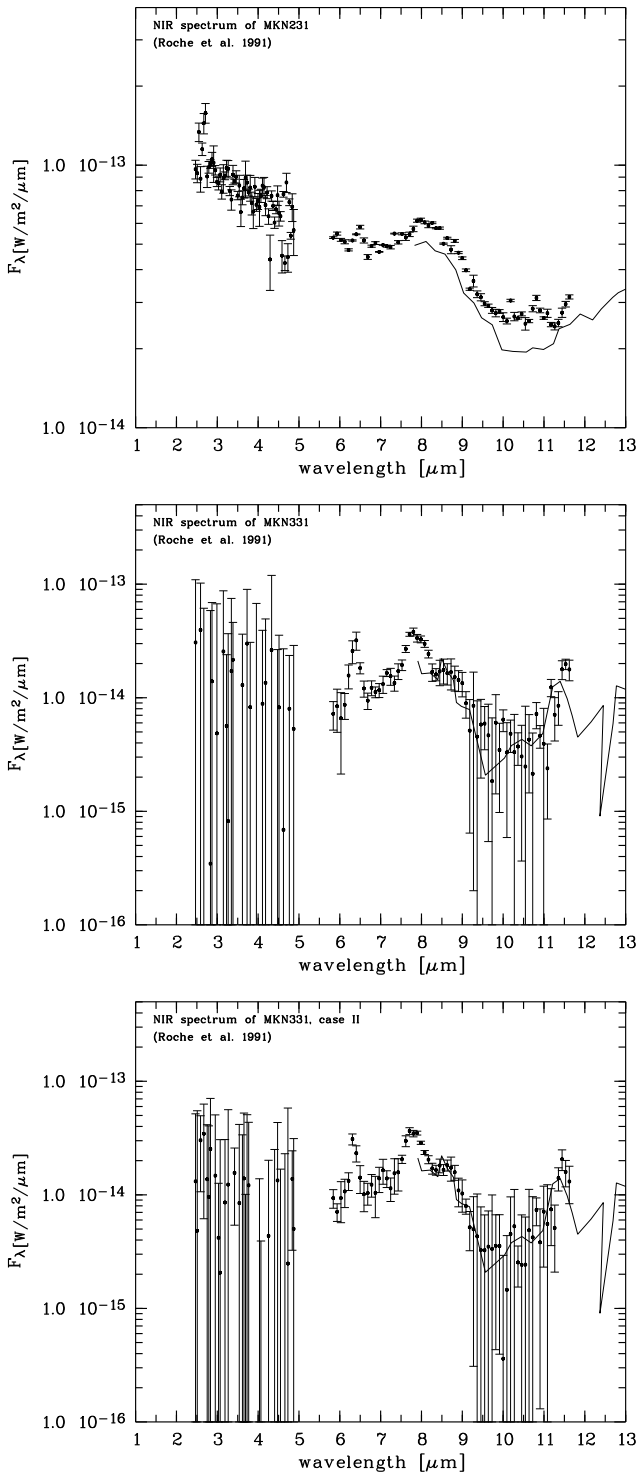

Figure 5.17: Comparison of ISOPHOT-S spectra of the 2 galaxies Mkn 231 and Mkn 331 (two spectra) obtained in chopped mode (dots) with groundbased $8-13$ micron spectroscopy (solid line).

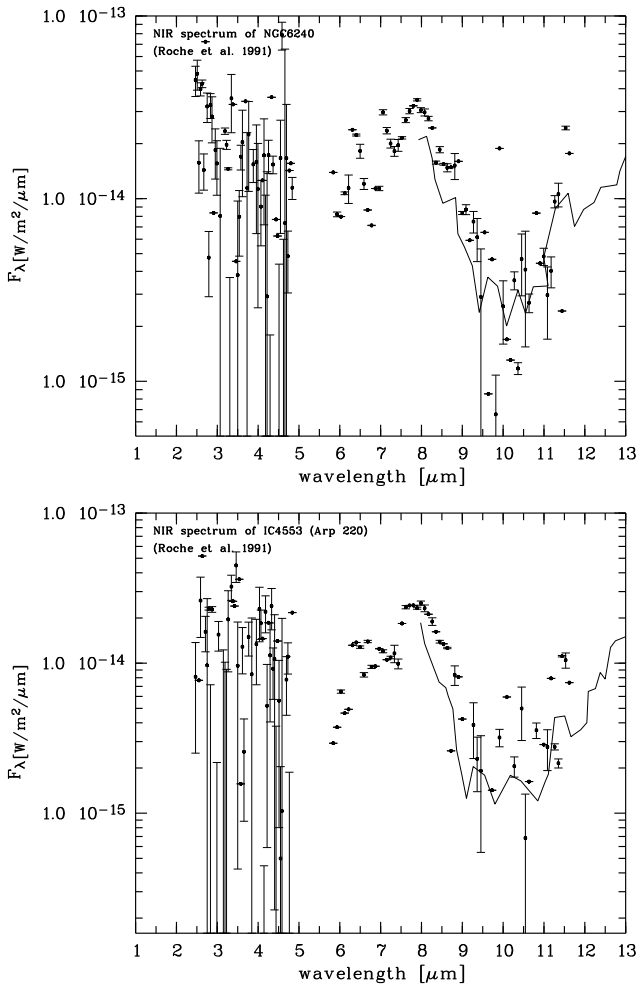

Figure 5.18: Comparison of ISOPHOT-S spectra of the 2 galaxies NGC 6240 and Arp220 obtained in chopped mode (dots) with groundbased $8-13$ micron spectroscopy (solid line).

- The comparison with the OLP 7.0 data product indicates that the new spectral response function for chopped measurements brings a considerable improvement in absolute and relative accuracy.

5.2.5 MIR Spectra of a Symbiotic Star and a Nova from Chopped PHT-S Measurements

- authors: K. Wilke, U. Klaas
- date: 22-June-1999
- SVP period 1

Motivation

In order to to increase the variety of object types for which PHT-S spectra are checked we included the spectrum of a symbiotic star, AG Peg, and the spectrum of a Nova, Nova Her91, in our test case list. For both targets groundbased 8 - 13 micron spectroscopy is available (cf. Refs. [12] and [13], respectively). The comparison for the Nova is of qualitative nature, as changes in the SED between the epoch of the groundbased measurement (1991, 67 days after the eruption) and the epoch of the ISOPHOT-S measurement (1996) are quite likely.

Method

We compare the absolute fluxes and relative shapes of the ISOPHOT-S spectra with the groundbased spectroscopy. Note that we compare an aperture size of 24x24 arcsec^2 for ISOPHOT-S with 5 arcsec aperture size of the groundbased measurements.

Results

In Fig. 5.19 we display the ISOPHOT-S spectrum of AG Peg compared to the groundbased spectroscopy. There is perfect agreement between both spectra, both in absolute level and in relative shape.
In Fig. 5.20 we display the ISOPHOT-S spectrum of Nova Her91 compared to the groundbased spectroscopy. While in 1991 the Nova showed a flux in the order of $1 - 2\ 10^{-13}$ W m^{-2} μm^{-1} in 1997, its brightness has dropped by two decades in flux in 1996. The scatter of the data points in the ISOPHOT-S spectrum is quite high, suggesting that the measurement is close to the detection limit in both channels.

Conclusions

- For the star AG Peg there is perfect agreement between the ISOPHOT-S spectrum and the ground-based $8 - 13$ micron spectroscopy showing the good performance of the new spectral response function for chopped measurements.
- The spectrum of Nova Her91 demonstrates the detection limit of the automatic processing. Beside the fact that the source is variable to allow comparison with the groundbased spectrum taken shortly after the Nova outburst, it is too faint to get a reasonable spectrum - the scatter in the data points at flux levels of 10^{-14} W m^{-2} μm^{-1} in the SS range and 10^{-15} W m^{-2} μm^{-1} in the SL range is relatively high.

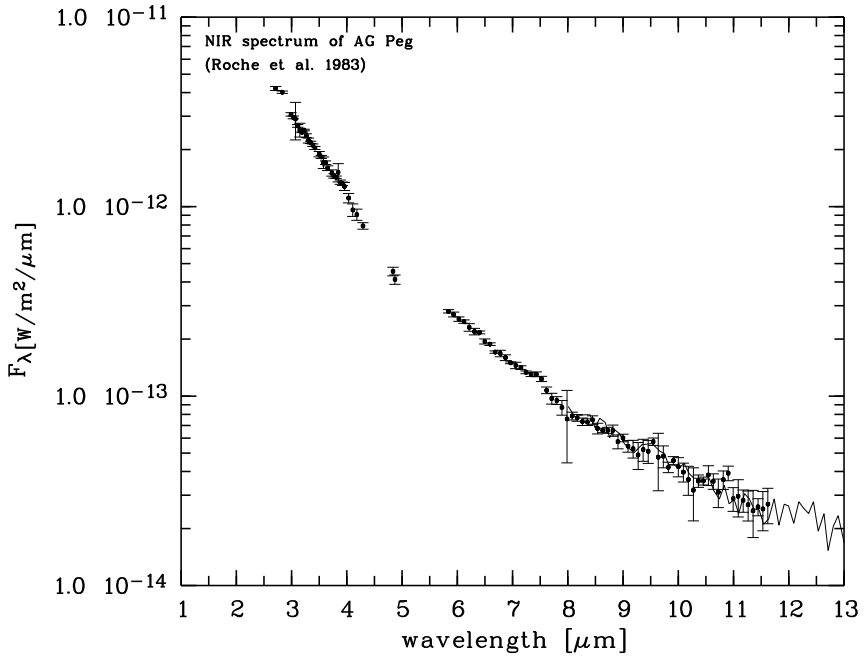

Figure 5.19: Comparison of the spectrum of the symbiotic star AG Peg obtained in PHT-S triangular chopped mode with the groundbased 8 – 13 micron spectroscopy by Roche et al. 1983.

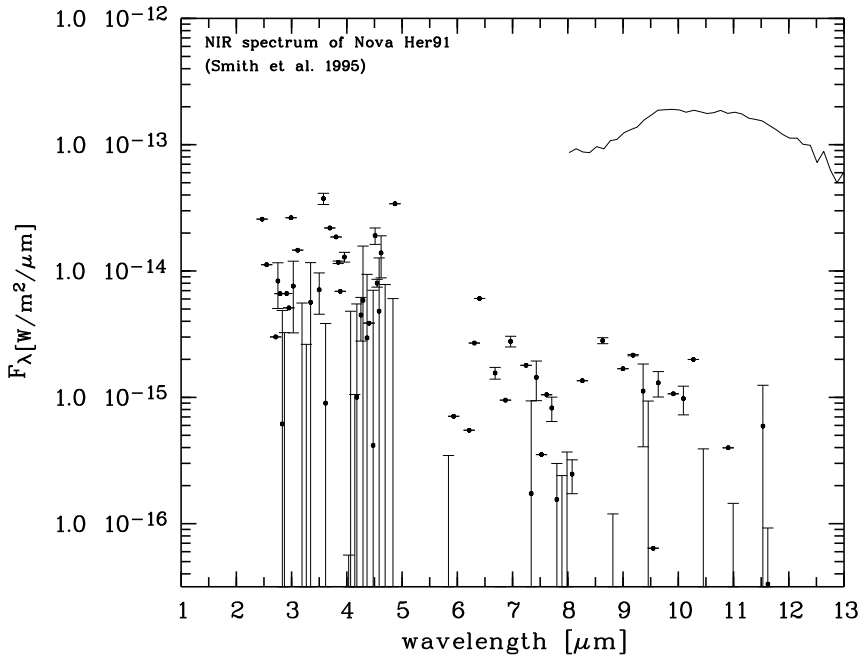

Figure 5.20: Comparison of the spectrum of Nova Her91 obtained in PHT-S rectangular chopped mode in 1996 with the groundbased 8 – 13 micron spectroscopy by Smith et al. 1995, obtained in 1991, 67 days after its maximum.

5.3 Verification of Recognition of Varying Aperture Sizes in Multi-filter Raster Maps

An overview of the test cases is outlined in Ref. [4], chapter 3.1.3.

5.3.1 References to Calibration Analysis and Software Change Documentation

- Software Problem Report: SPR-2705

5.3.2 Summary of Results

- The OLP software recognizes now the different aperture sizes used in some rasters.
- SCREW-378 is correctly implemented for PHT-P PGAI image products.
- The SPR-2705 fix is correctly implemented. Any incompleteness of the displayed PHT-P raster maps occurs for short wavelength filters and rather small aperture size on background positions where practically no flux falls onto the detector and the resulting signals are set to zero and are not processed to fluxes. An OLP caveat was formulated (cf. Sect. 2.11.)
- The Browse Product Postcard generation software cannot handle properly the display of the extreme case of only one single flux value → SPR-2975 was submitted to include treatment of this specific case.

5.3.3 Examination of Browse Products of Test Cases

- authors: U. Klaas, P. Richards, M. Radovich
- date: 25-June-1999
- SVP period 1

Motivation

The correct implementation of SPR-2705 should now lead to raster map images which reflect the different aperture sizes used for the individual filters.

Method

We compare the browse product postcards of OLP V7.0 and OLP V8.4b1. If necessary we check the AAP product for its values.

Results

1) TDT56602102

This is a 3x2 multi-filter nodding on the calibration star HD172323. The measurement was performed with the following filter-aperture combinations:

I) 7.7 μm with 23 arcsec aperture

II) 10 μm with 52 arcsec aperture

The raster step size was 60 arcsec.
Comparison of Figs. 5.21 and 5.22 shows that the different aperture sizes are now recognized and displayed in the correct scaling.

2) TDT51301125

This is a 3x1 multi-filter raster map with the following filter-aperture combinations:

I) 3.6 μm with 13.8 arcsec aperture

II) 4.8 μm with 18 arcsec aperture

III) 12 and 15 μm with 52 arcsec aperture

The raster step size was 55 arcsec.
Comparison of Figs. 5.23 and 5.24 shows that the different aperture sizes are now recognized and displayed in the correct scaling. However, at 3.6 μm no raster map can be recognized at all and at 4.8 μm only 2 out of 3 raster points can be recognized. Further investigation of the OLP SPD and AAR products reveals the following:

- In the SPD product zero signal flags are set (PPxSFLAG = 7, see sections 12.3.2 and 12.3.12 in [2])

```
PP1SFLAG from PP1S51301125.FITS
3.6um:   7   0   7
4.8um:   0   4   7
12um:    0   2   0
15um:    2   2   2
```

- From the AAR header one can see that the central pixel has an associated flux, but maximum and minimum surface brightness are identical due to the fact that there is only one single valid map pixel left:

```
FILTER1 = 'P1_3P6_UM'          / Filter
APERTR1 = '13.8" = 0.60mm'     / Aperture used
LAMBDA1 =          3.60000E-06 / Central Wavelength of filter (m)
EXBRGT1 =          8.99733E+01 / Expected brightness
SBRMAX1 =          2.40261E+01 / Maximum brightness(MJy/sr)
SBRMIN1 =          2.40261E+01 / Minimum brightness(MJy/sr)
```

The setting of the zero signal flag means that there is no further processing in DERIVE_AAR and hence no flux value will be produced for the corresponding raster point. The reason for the setting of the flag is quite obvious. The selected filters and the small apertures mean that practically no flux from the sky background reaches the detector and hence the resulting output signals are very small or even negative. The Browse Product postcard software should display this central pixel, but obviously fails to get the right scaling due to the lack of a non identical minimum and maximum values → SPR-2975 was submitted. We include a caveat in the OLP caveat list that products can look incomplete, in case the zero signal flag is set as a consequence of extremely small or negative signals.

3) TDT29000208

This is a 3x1 multi-filter raster map with the following filter-aperture combinations:

I) 3.6 μm with 13.8 arcsec aperture

II) 4.8 μm with 18 arcsec aperture

III) 12 and 15 μm with 52 arcsec aperture

The raster step size was 55 arcsec.
Comparison of Figs. 5.25 and 5.26 shows that the different aperture sizes are now recognized and displayed in the correct scaling. However, at 3.6 and at 4.8 μm no raster map can be recognized at all. Further investigation of the OLP SPD and AAR products reveals the following:

- In the SPD product zero signal flags are set (PPxSFLAG = 7, see sections 12.3.2 and 12.3.12 in [2])

```
PP1SFLAG from PP1S29000208.FITS
3.6um    7   0   7
4.8um    7   0   7
12um     0   2   0
15um     2   2   2
```

- From the AAR header one can see that the central pixel has an associated flux, but maximum and minimum surface brightness are identical due to the fact that there is only one single valid map pixel left:

```
FILTER1 = 'P1_3P6_UM'          / Filter
APERTR1 = '13.8" = 0.60mm'     / Aperture used
LAMBDA1 =          3.60000E-06 / Central Wavelength of filter (m)
EXBRGT1 =          8.99733E+01 / Expected brightness
SBRMAX1 =          2.90012E+01 / Maximum brightness(MJy/sr)
SBRMIN1 =          2.90012E+01 / Minimum brightness(MJy/sr)
FILTER2 = 'P1_4P85_UM'         / Filter
APERTR2 = '18" = 0.77mm'       / Aperture used
LAMBDA2 =          4.80000E-06 / Central Wavelength of filter (m)
EXBRGT2 =          6.64375E+01 / Expected brightness
SBRMAX2 =          8.94814E+01 / Maximum brightness(MJy/sr)
SBRMIN2 =          8.94814E+01 / Minimum brightness(MJy/sr)
```

It is therefore the same finding as for the previous test case TDT513001125.

4) TDT10300901

This is a 3x3 multi-filter raster map with the following filter-aperture combinations:

I) 3.6 μm with 13.8 arcsec aperture

II) 4.8 μm with 18 arcsec aperture

III) 12 μm with 52 arcsec aperture

The raster step size was 50 arcsec in both axes.
Comparison of Figs. 5.27 and 5.28 shows that the different aperture sizes are now recognized and displayed in the correct scaling. However, at 3.6 μm the raster map looks incomplete with 4 raster points missing. Further investigation of the OLP SPD and AAR products reveals the following:

- In the SPD product zero signal flags are set (PPxSFLAG = 7, see sections 12.3.2 and 12.3.12 in [2])

```
PP1SFLAG from PP1S10300901.FITS
3.6um    0   0   7   2   0   0   7   7   7
4.8um    2   0   0   0   2   0   0   0   0
12um     2   2   2   2   2   2   2   0   2
```

This shows that indeed 4 raster points are supressed for the 3.6 μm map, as no reliable signal could be determined.

Conclusions

- SPR-2705 is correctly implemented and OLP recognizes now different apertures applied during PHT-P rasters.
- SCREW-378 providing the minimum and maximum surface brightness keywords for PGAI image products was found to be correctly implemented for PHT-P.
- Due to extremely low sky surface brightness in some short wavelength PHT-P1 filters used in combination with rather small apertures the resulting signals are close to zero or even negative, so that OLP sets the zero signal flag in the SPD product and these raster points are not processed any further in DERIVE_AAR. In extreme cases that can result that only the on-source measurement is different from zero and the resulting raster map consists of one single valid point. In this case the Browse Product software for Postcard generation cannot handle properly the scaling of the surface brightness range → SPR-2975 was submitted. The consequences of the "zero signal flag setting" on the resulting data products leading to the appearence of incomplete maps is therefore documented in the follwoing caveat:

A new caveat from OLP 8.4 Scientific Validation comes from the investigation of PHT-P raster maps:
In case the total flux on the detector is very small resulting in close to zero or even negative signals at the end of the DERIVE_SPD processing stage OLP, sets the "zero signal flag" for the corresponding plateaux times and does not continue to process these data sections in DERIVE_AAR (cf. description of SPD product types, coding of pixel status flag PPxSFLAG). This leads then to incomplete appearing map products PGAI. The most likely cases are the short wavelength filters of PHT-P1, where the sky background (Zodiacal Light) shows a minimum, in combination with small aperture sizes.

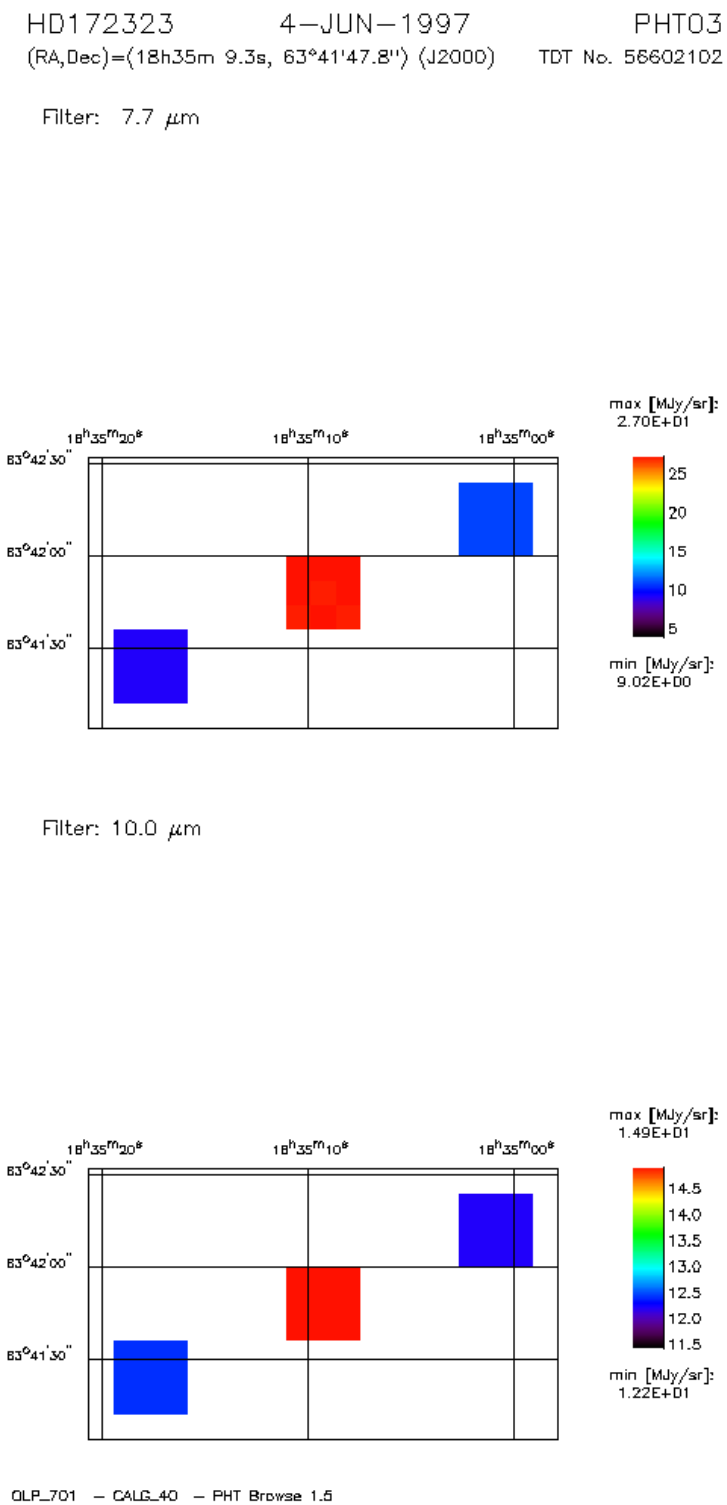

Figure 5.21: Browse product of the OLP 7.0 AAP for TDT56602102.

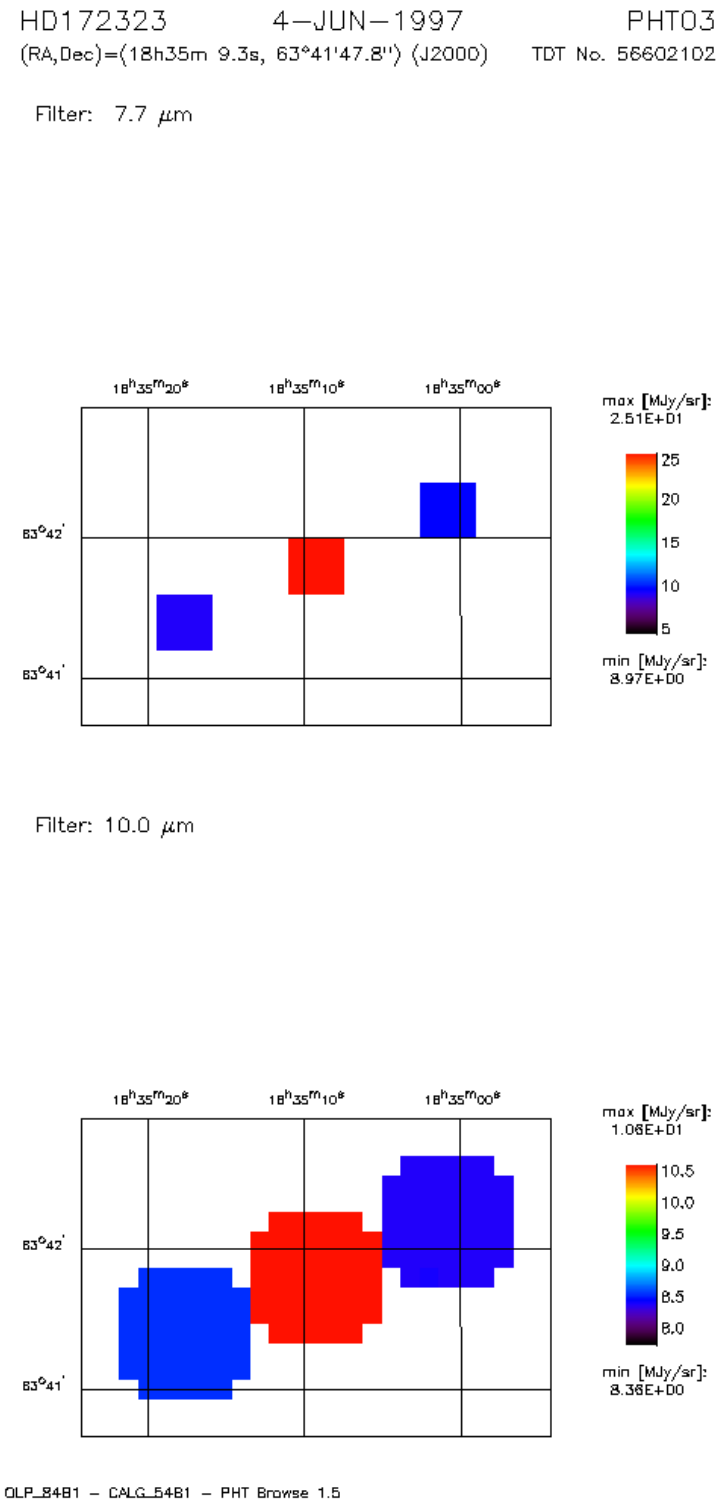

Figure 5.22: Browse product of the OLP 8.4 beta1 AAP for TDT56602102.

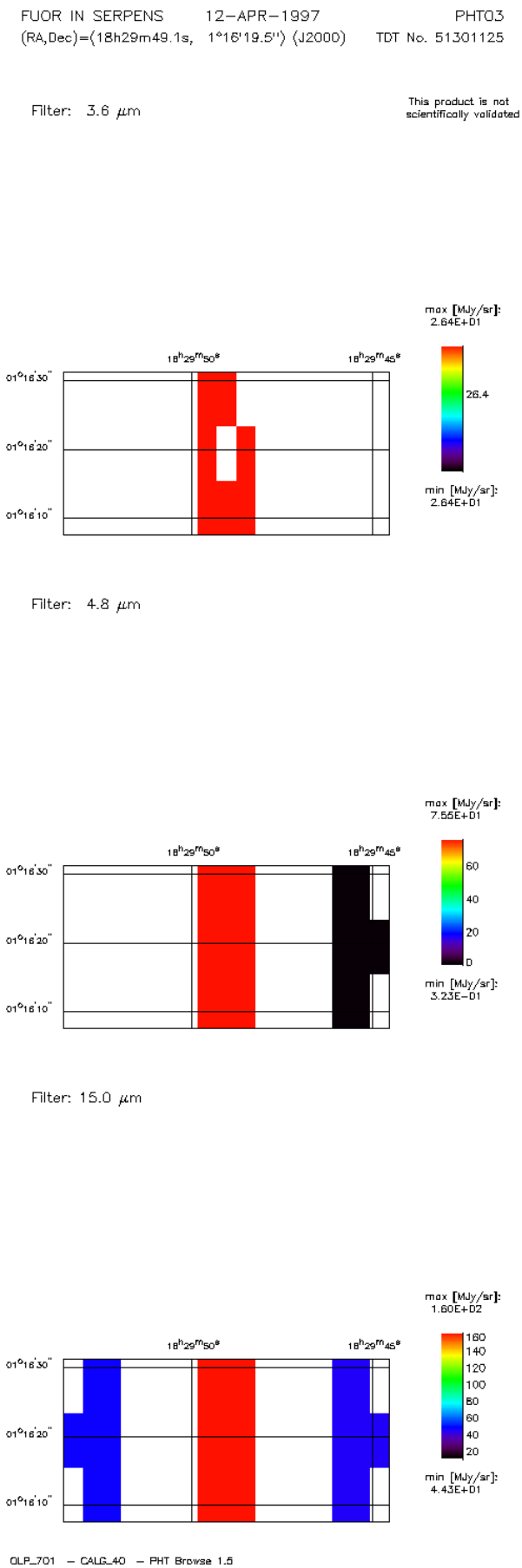

Figure 5.23: Browse product of the OLP 7.0 AAP for TDT51301125.

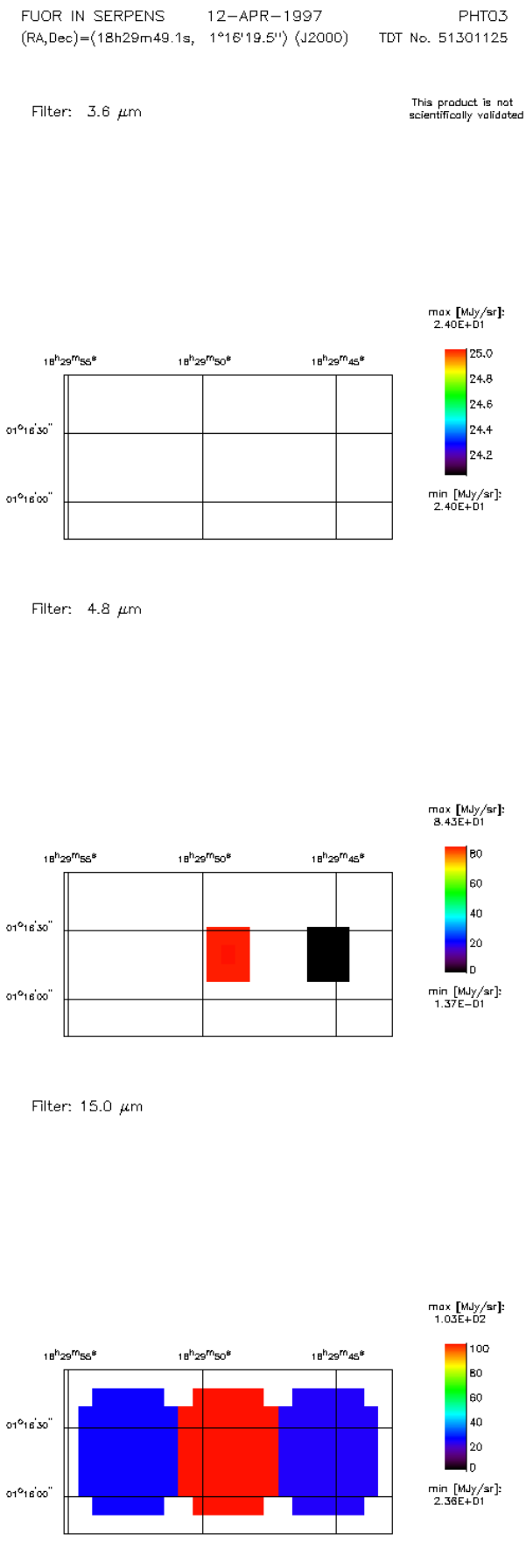

Figure 5.24: Browse product of the OLP 8.4 beta1 AAP for TDT51301125.

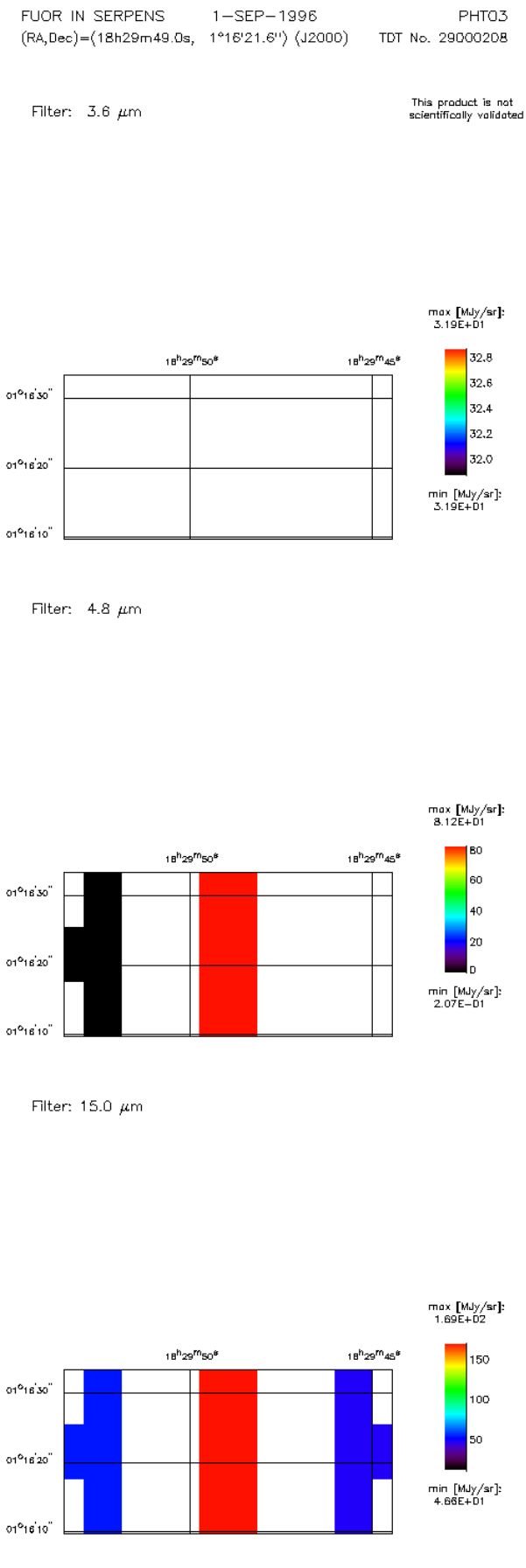

Figure 5.25: Browse product of the OLP 7.0 AAP for TDT29000208.

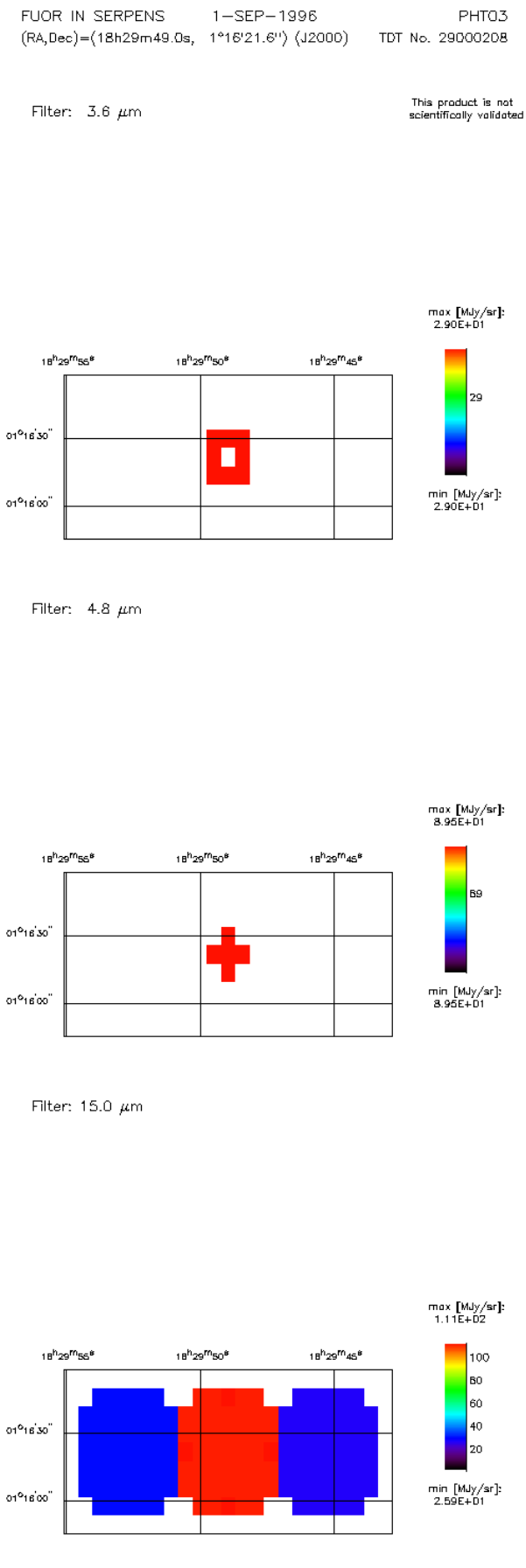

Figure 5.26: Browse product of the OLP 8.4 beta1 AAP for TDT29000208.

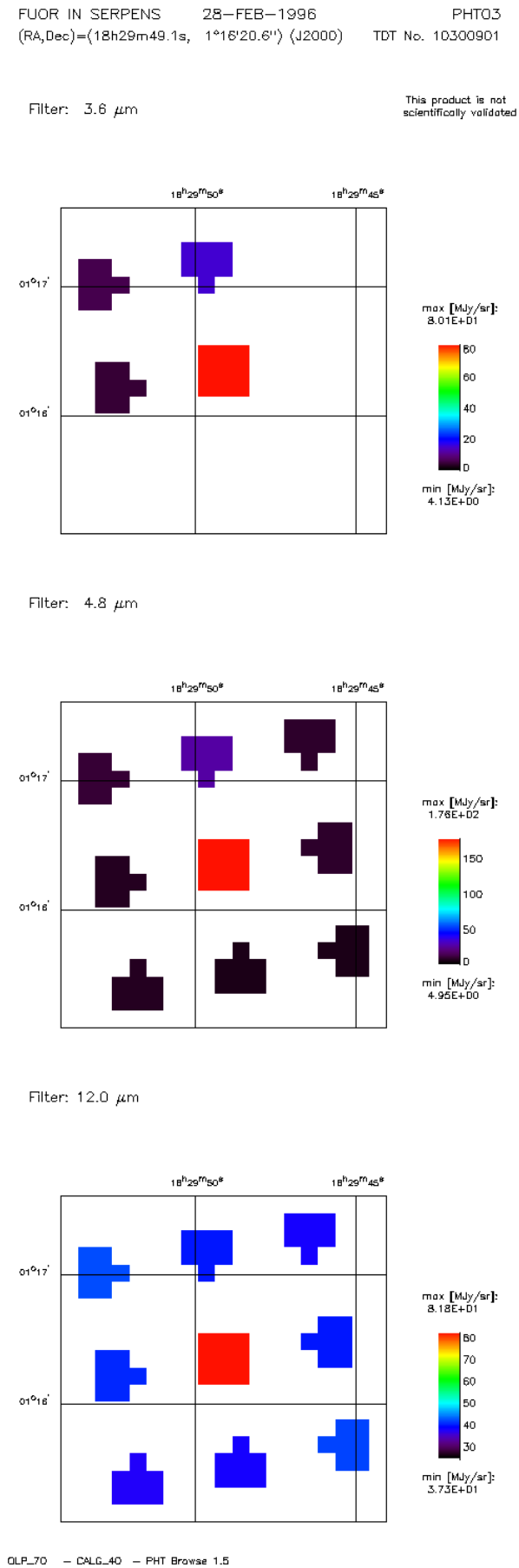

Figure 5.27: Browse product of the OLP 7.0 AAP for TDT10300901.

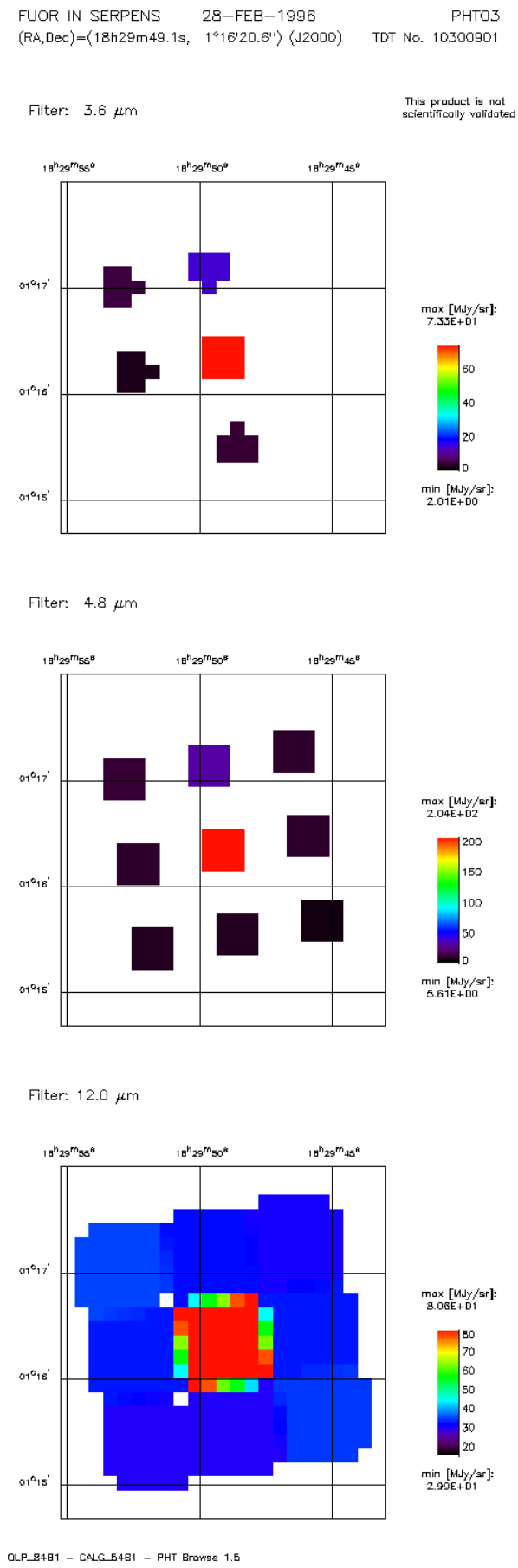

Figure 5.28: Browse product of the OLP 8.4 beta1 AAP for TDT10300901.

5.4 Revalidation of Staring Mode Photometry

An overview of the test cases is outlined in Ref. [4], chapter 3.2, with those cases foreseen for verification of implementations w.r.t. SCREWs 366, 367 and 368.

5.4.1 References to Calibration Analysis and Software Change Documentation

- calibration reports:
  - Linearization of ISOPHOT-P and -C detector signals in OLP8 [30]
  - Point Spread Function Fractions related to the ISOPHOT C100 and C200 Arrays [10]
- Software Change Requests: SCREWs 366, 367, 368
- Software Problem Reports: SPR 2894

5.4.2 Summary of Results

- This section reflects the status of the OLP 8.4 staring mode photometry performance after scientific validation period 1 obtained with the highest priority test cases. Three different deficiencies with Cal-G file implementations, documented in the SPRs 2970, 2979, and 2985 (cf. Sect. 4) were found, which prohibited a calibration accuracy assessment at this stage. The reader is therefore referred to Sect. 7.3 for a final assessment of calibration accuracies for staring mode photometry, which covers also more test cases.

5.4.3 General Re-validation of PHT03 and PHT22 Staring Mode: The SED of α Bootes (HR 5340)

- authors: M. Radovich, U. Klaas
- date: 18-June-1999
- SVP period 1

Motivation

TDTs 45200201(background, PHT-P), 45200202(α Boo, PHT-P), 45200203(background, PHT-C), 45200204(α Boo, PHT-C) is one of the key OLP V7.0 validation cases [1]. The staring mode AOTs PHT-03 and PHT-22 use all available PHT filters (but the 3.6 and 4.85 μm filters had to be excluded from the analysis, because the source saturates the measurement) on a stellar (declining) SED. α Bootes is one of the most important stellar PHT calibration standards and there are detailed models available from M. Cohen (composite spectrum from 1 to 35 μm and extrapolations to 300 μm). This test case is very suitable for a test of both the absolute calibration and the relative filter-to-filter calibration. It should be noted that this multi-filter measurement was not used for the establishment of the FCS calibration curve. During the OLP 7.0 validation the establishment of reliable C200 photometry failed due to a by far too strong background subtraction. Therefore, this "on-off" observation with independent FCS calibration for on-source and off-source measurement is considered an excellent test case for the linearization correction introduced by SCREW 366.

Method

We compare the background subtracted, color corrected flux values of both OLP V7.0 and OLP V8.4b1 results against the model prediction.

Results

In the following Tab. 5.2 we compare the photometry from part 1 of the evaluation log section with the model. We estimate the absolute photometric accuracy per detector assembly for this target as the deviation from the model flux in the filter in which the FCS calibration was done, and the relative filter-to-filter accuracy as the peak-to-peak variation of the other filters around this offset. Note that for P1 the FCS calibration was actually done in the 3.6 μm filter, but for this filter the sky measurement is heavily saturated. The photometric accuracies are presented in Tab. 5.3. Fig. 5.29 shows the PHT photometric data points in comparison to the model and IRAS photometry (color corrected) from 3.3 to 200 μm for OLP 7.0 and OLP 8.4b1, respectively.
During the OLP 7 validation [1] no reliable C200 photometry could be achieved. It showed a negative photometric bias with a relative underestimate of the total source plus background flux versus the individually calibrated background flux. What can be seen from the OLP 8.4b1 results is that now reasonable photometry is achieved out to 170 μm, only the two longest wavelength filters show again the fall-off, but less drastic, only by approximately 30 %. It should be noted that for this simple on-off measurement the exact determination of the background may be critical. In Table 5.4 the source-to-background contrast (background flux in Jy is calculated according to the following formula: $F(Jy)_{back} = 1/f_{psf} * I(MJy/sr) * (1 - \varepsilon^2) * Omega * n_{pix}$). At 105 μm the source flux is comparable with the background flux (1:0.72). From 120 to 200 μm the background becomes more and more dominant (from 1.9:1 to 5.1:1). While in the previous OLP 7 version staring off/on photometry became unreliable for source-to-background ratios below 1:1.3 (0.75) the flux dependent linearity correction brings this now down to source fluxes as faint as 1:4 (0.25).
Part 2 of the evaluation log section and Fig. 5.30 provide the surface brightness photometry of the background position and the comparison with COBE. From Table 5.5 it can be seen that the consistency with COBE has improved to within 10 % for 60 and 100 μm where the COBE photometry has very small uncertainties. For 150 and 200 μm one has to have in mind that COBE photometry has an higher uncertainty itself and seeing the trend of the ISOPHOT background fluxes the COBE 240 μm point is expected to lie at a lower level than the ISOPHOT 200 μm point.

Table 5.2: Consistency check of photometric results with HR 5340 model

Filter	**consistency w.r.t. model OLP V7.0** [%]	**consistency w.r.t. model OLP V8.4b1** [%]
3.3	+8.6	+0.0
7.3	+14.9	+8.5
7.7	+13.6	+4.4
10	+11.0	-6.0
11.3	-3.3	+0.5
12	+24.1	+7.4
12 IRAS	+10.1	+10.1
12.8	+6.9	-12.2
16	-7.5	+17.4
20	-0.1	+1.4
25	+4.5	+7.3
25 IRAS	-2.3	-2.3
60 PHT-P	+9.9	-11.5
60 PHT-C	+0.2	+14.7
60 IRAS	-6.6	-6.6
65	-2.0	+2.6
80	+7.6	-5.2
90	-3.7	-0.9
100 PHT-P	+29.3	-9.3
100 PHT-C	-0.04	-18.0
100 IRAS	-3.6	-3.6
105	-4.3	-21.9
120	-27.8	-11.4
150	-41.9	-8.8
170	-53.6	-7.0
180	-78.4	-34.9
200	-78.8	-33.6

Table 5.3: Absolute and relative calibration accuracies per detector achieved for HR 5340 observation with OLP V8.4b1

detector	**absolute accuracy** [%]	**relative accuracy** [%]
P1	< 1 at 3.3 μm	17
P2	< 2 at 20 μm	6
P3	12 at 60 μm	3
C100	< 1 at 90 μm	20
C200	7 at 170 μm	30

Conclusions

- For the flux levels covered by α Boo and its background the flux dependent signal linearization appears to work properly. This seems to be the explanation that now C200 multi-filter photometry becomes possible.
- The new C200 array PSF factors for centering the source on the array appear to work properly, too.
- PHT photometry gives a good representation of the SED from 3.3 to 170 μm.

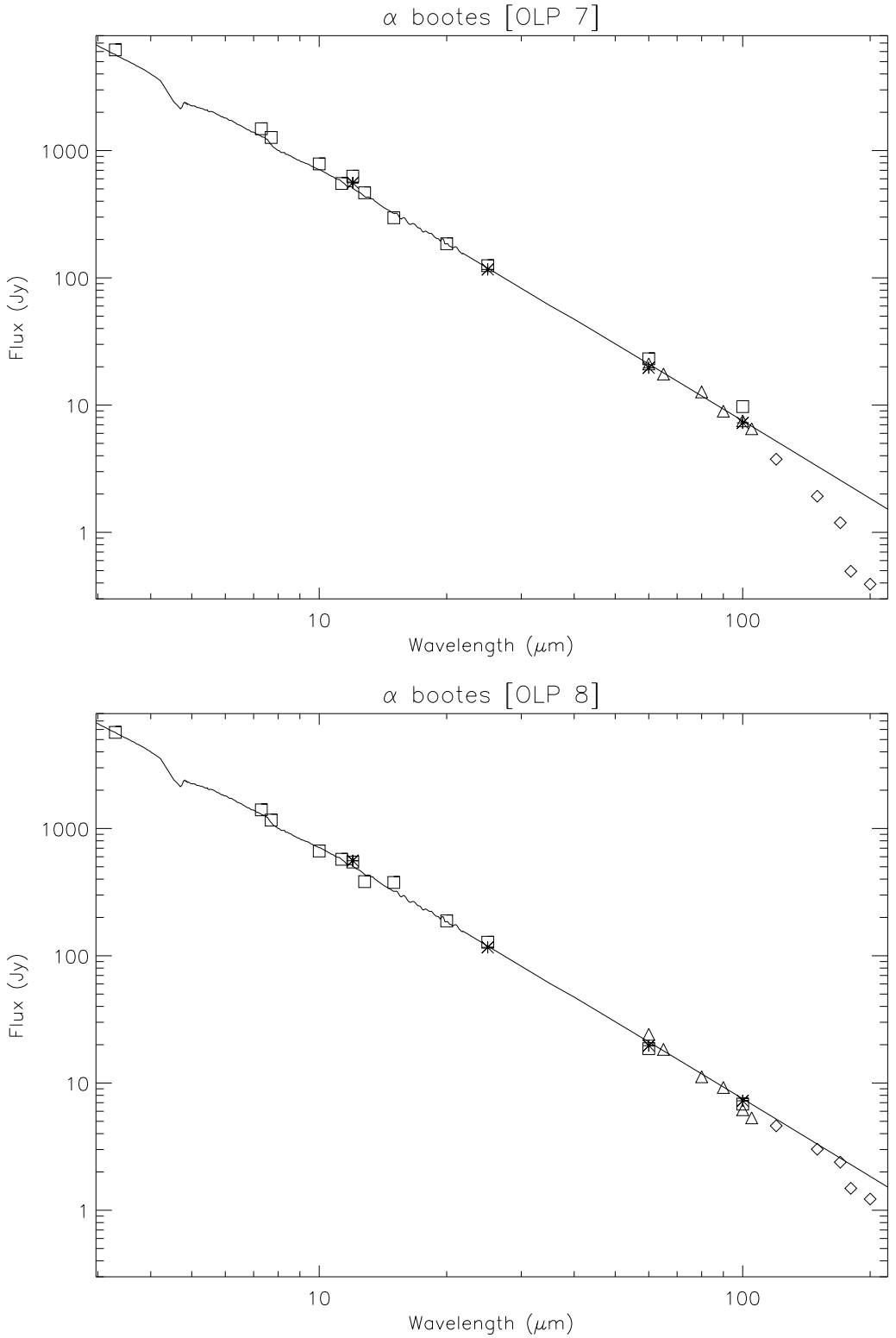

Figure 5.29: Comparison of PHT-P and PHT-C photometry, using the full ISOPHOT filter set, with the composite spectrum and out to 300 μm extrapolated SED of α Boo (HR 5340) provided by M. Cohen and with IRAS photometry for OLP 7.0 (upper panel) and OLP 8.4b1 (lower panel). All photometric points are color corrected for a 4000 K BB. The meaning of the symbols is the following: solid line: model, asterisk: IRAS, square: PHT-P (P03 AOT), triangle: C100 (P22 AOT), diamond: C200 (P22 AOT).

Table 5.4: Source-to-background contrast for α Bootes in FIR filters. The expected source flux is the model flux, the background flux is from the background measurement converted to Jy as decribed in the text.

λ_c [μm]	**background flux** [Jy]	**expected source flux** [Jy]	**source-to-backgr. contrast**
105	4.89	6.81	1.39 (1:0.72)
120	11.50	5.20	0.45 (1:2.2)
150	10.85	3.31	0.31 (1:3.2)
170	11.27	2.57	0.23 (1:4.4)
180	8.78	2.29	0.26 (1:3.9)
200	7.56	1.85	0.24 (1:4.2)

- For P1 and P2 the absolute and relative calibration accuracies are very similar for OLP 8.4b1 and OLP 7.0. For P3 the relative accuracy could be improvedto better than 10 %. For C100 the relative filter-to-filter accuracy is somewhat degraded, the photometric data points are located on an oblique line w.r.t. the model flux line. For C200 absolute and relative filter-to-filter accuracies could be determined for the first time, giving 10 % absolute accuracy and approximately 30 % relative filter-to-filter accuracy for all C200 filters used, but due to a systematic bias (see below). The relative filter-to-filter accuracy is better than 5 % for the filters shortward of 170 μm.
- With regard to OLP V7.0 the C200 multi-filter photometry is drastically improved. Proper background subtraction is still crucial for the two longest wavelengths at 180 and 200 μm which give a too low flux by approximately 30 %. This occurs for source-to-background ratios below 1:4 (0.25).
- For 60 and 100 μm the consistency with COBE annual map photometry is now within 10%. For the longer wavelengths (150 and 200 μm) the results need not necessarily to match within the same accuracy. Here COBE photometry itself has higher uncertainties and the central wavelengths of the ISOPHOT and COBE bands are different, so that the relative shape of the background SED has some impact. Furthermore, one has always to be careful comparing single pointing ISOPHOT photometry (with a 3 arcmin beam) with COBE photometry (with a 42 arcmin beam) due to structure in the background.

Table 5.5: Consistency check of α Boo background position surface brightness results with COBE/DIRBE annual maps.

wavelength μm	**consistency w.r.t. COBE OLP V7.0** [%]	**consistency w.r.t. COBE OLP V8.4b1** [%]
60	+20.0	+7.9
100	+29.5	-9.8
150	-19.8	-19.0
200	+41.4	+33.5

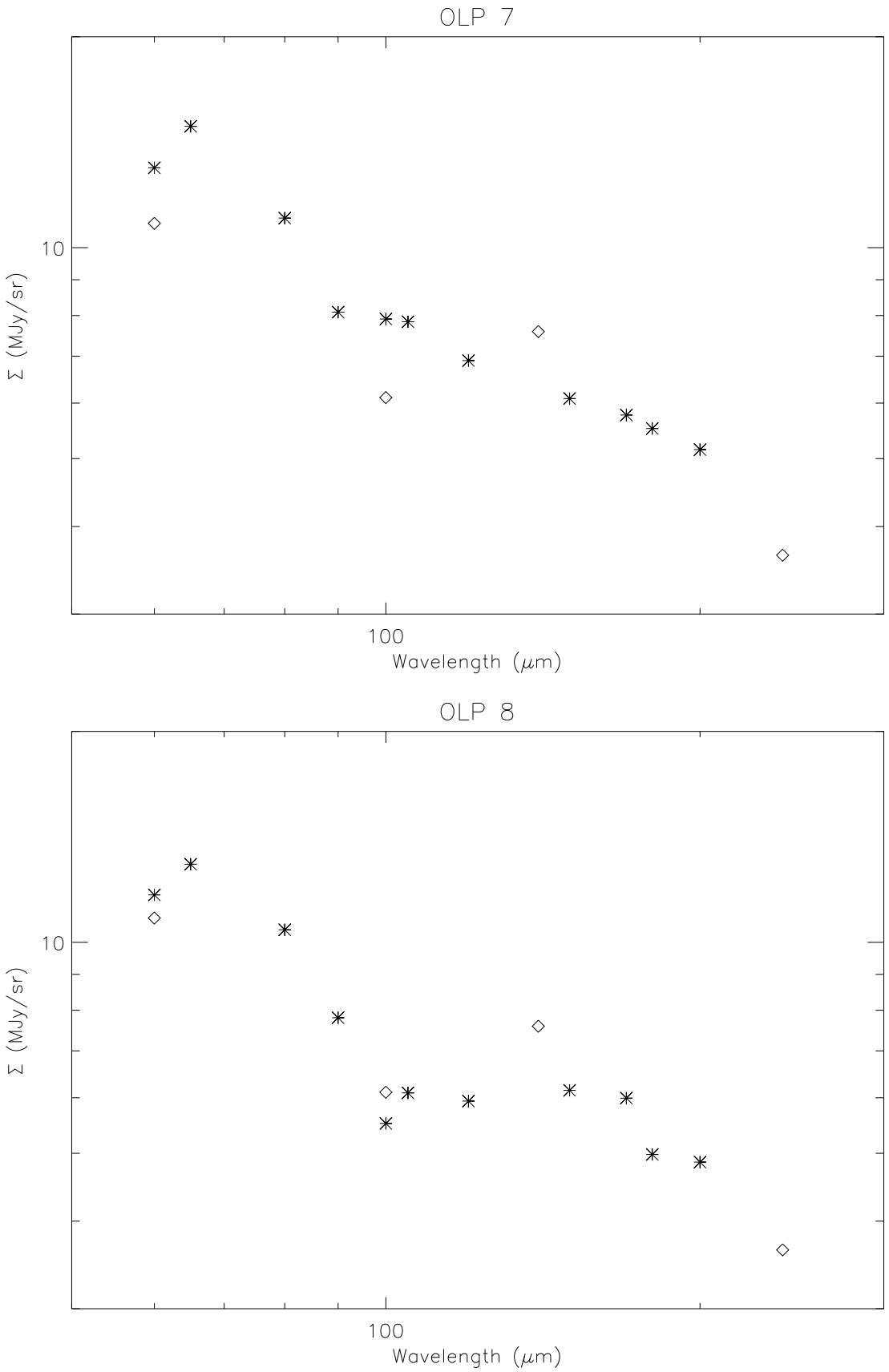

Figure 5.30: Comparison of OLP V7.0 and OLP V8.4b1 surface brightness (asterisk) with COBE annual map fluxes (diamond).

Evaluation Log

1) Point source photometry for Alpha Bootes (TDTs 45200201, 45200202, 45200203, and 45200204) in comparison with IRAS and Cohen model. Fluxes are in Jy.

PHT-P: ppap45200202 (src+back)
ppae45200201 (back)

PHT-C: pcap45200204 (src+back)
pcae45200203 (back)

color correction: black body, T=4000
model: Cohen
fluxes in Jy

Det	cwl [um]	OLP 7 [Jy]	OLP 8 [Jy]	IRAS [Jy]	Model [Jy]	% OLP 7 [(OLP-model)/model]	% OLP 8
P1	3.3	6185.493	5695.854		5695.470	8.60	0.01
P1	7.3	1483.791	1400.773		1291.496	14.89	8.46
P1	7.7	1267.990	1165.112		1116.581	13.56	4.35
P1	10.0	785.882	665.884		708.004	11.00	-5.95
P1	11.3	551.459	572.895		570.349	-3.31	0.45
P1	12.0	629.450	545.015	558.500	507.360	24.06	7.42
P1	12.8	465.644	382.347		435.541	6.91	-12.21
P1	15.0	296.661	376.618		320.700	-7.50	17.44
P2	20.0	185.297	187.989		185.467	-0.09	1.36
P2	25.0	124.560	127.784	116.400	119.146	4.54	7.25
P3	60.0	23.110	18.614	19.650	21.030	9.89	-11.49
C1	60.0	21.063	24.120	19.650	21.030	0.16	14.69
C1	65.0	17.549	18.370		17.910	-2.02	2.57
C1	80.0	12.695	11.187		11.800	7.59	-5.19
C1	90.0	8.957	9.221		9.303	-3.72	-0.89
P3	100.0	9.724	6.825	7.250	7.521	29.29	-9.25
C1	100.0	7.518	6.166	7.250	7.521	-0.04	-18.02
C1	105.0	6.521	5.322		6.814	-4.30	-21.90
C2	120.0	3.756	4.607		5.201	-27.78	-11.42
C2	150.0	1.922	3.018		3.310	-41.92	-8.83
C2	170.0	1.191	2.387		2.568	-53.63	-7.03
C2	180.0	0.494	1.487		2.286	-78.38	-34.94
C2	200.0	0.391	1.225		1.845	-78.79	-33.59

2) surface brightness photometry of Alpha Bootes background (TDT 45200203)

Cwl [um]	OLP 7.0 [MJy sr^-1]	OLP 8.4 [MJy sr^-1]	COBE [MJy sr^-1]
60.0	13.00	11.69	10.83
65.0	14.90	12.93	
80.0	11.02	10.42	
90.0	8.09	7.81	
100.0	7.91	5.51	6.11
105.0	7.84	6.10	
120.0	6.90	5.94	
150.0	6.09	6.15	7.59 (140um)
170.0	5.77	5.99	
180.0	5.52	4.98	
200.0	5.15	4.86	3.64 (240um)

5.4.4 General Re-validation of Multi-filter Staring Mode (PHT03/PHT22) and Absolute Photometry (PHT05/PHT25): The SED of γ Draconis (HR 6705)

- authors: M. Radovich, U. Klaas
- date: 01-July-1999
- SVP period 1

Motivation

The star γ Draconis (HR 6705) is one of the most important calibration stars for ISOPHOT. Also several AOT commissioning observations were performed on this star. The set of observations comprises multi-filter photometry, TDTs 35602101 (background, PHT-P), 35602102 (γ Dra, PHT-P), 35602203, 39802002 (background PHT-C), 35602204, 39802003 (γ Dra, PHT-C), absolute photometry, TDTs 35300301...35300306 (PHT-P) and 35300308...35300312 (PHT-C), multi-filter PHT-C100 photometry with different reset interval settings, cf. [4] for more details. It is one of the key OLP V7.0 validation cases [1]. The staring mode AOTs PHT-03 and PHT-22 use all available PHT filters out to 200 μm complementing the α Bootes observations towards the fainter flux end. There are detailed models available from M. Cohen (composite spectrum from 1 to 35 μm and extrapolations to 300 μm). This test case is very suitable for a test of both the absolute calibration and the relative filter-to-filter calibration.

Method

We compare the background subtracted, color corrected flux values of both OLP V7.0 and OLP V8.4b1 results against the model prediction.

Results

In the following Tab. 5.6 we compare the photometry from part 1 of the evaluation log section with the model. We estimate the absolute photometric accuracy per detector assembly for this target as the deviation from the model flux in the filter in which the FCS calibration was done, and the relative filter-to-filter accuracy as the peak-to-peak variation of the other filters around this offset. Figs. 5.31 and 5.32 show the PHT photometric data points in comparison to the model and IRAS photometry (color corrected) for OLP 7.0 and OLP 8.4b1, respectively. The photometry for C100 and C200 is already corrected for the failure of upgrade of the PSF fractions for the arrays (SPR-2970).
The photometric accuracies are presented in Tab. 5.7. We notice excessive flux by 50 % and more in the C100 range for the OLP V8.4b1, both in the multi-filter and absolute mode. This systematic deviation points to a processing or calibration problem. In part 1 of the evaluation log section we have compiled the flux contributions from the individual pixels including a comparison of the official OLP V8.4b1 test case (processed in VILSPA), with PIA and processing with the RAL OLP V8.4b1 pipeline. While the central pixel has the same flux value for the VILSPA OLP V8.4b1 and the PIA case, the surrounding pixels have systematically higher fluxes for the VILSPA OLP V8.4b1 leading to the excess flux. Using the central pixel alone, the fluxes are quite consistenet with the model. The RAL OLP V8.4b1 does not show the excess fluxes in the off-centre pixels on-source. Investigation of this problem led to the finding that following SPR-2953 not the correct CALG file PC1SLINR (cf. SPR-2953 analysis) was integrated in the VILSPA OLP V8.4b1, but the one of the initial delivery. This file has completely different scalings (at least for some signal ranges) than the correct one. This regression problem is documented in SPR-2985. This means that all quantitative photometry with C100 can be unreliable for the OLP V8.4b1, including background measurements.
We also noted that in the data products PCAP35602204.FITS, PCAP39802003.FITS, the PHT-C on-source measurements, the keyword SBACK (= source+background flux) is zero. This should not be the case. The official OLP 7.0 data products do not show this behaviour, which points towards another regression problem. We checked the headers of these files and also the ones for the corresponding background measurements, PCAE35602203.FITS

Table 5.6: Consistency check of photometric results with HR 6705 model

Filter	**mode**	**consistency w.r.t. model OLP V7.0** [%]	**consistency w.r.t. model OLP V8.4b1** [%]
3.3	multf	3.08	-3.23
3.6	multf	10.07	8.39
4.8	multf	16.10	11.93
7.3	multf	4.92	-2.83
7.7	multf	11.82	6.48
10.0	multf	-17.38	-15.43
11.3	multf	6.18	15.16
12.0	multf	-5.06	-14.92
12.0	abs	-6.71	-10.86
12.0 IRAS		-7.5	-7.5
12.8	multf	-13.68	-6.84
15.0	multf	36.37	64.13
20.0	multf	-2.89	-2.85
25.0	multf	5.79	2.32
25.0	abs	-7.13	-5.92
25.0 IRAS		7.1	7.1
60.0 PHT-P	multf	-7.41	14.70
60.0 PHT-P	abs	-0.27	5.88
60.0 PHT-C	multf	-6.57	56.14
60.0 PHT-C(a)	abs	28.17	54.34
60.0 PHT-C(b)	abs	33.48	49.03
60.0 IRAS		-0.8	-0.8
65.0	multf	55.35	59.78
80.0	multf	31.94	60.03
90.0	multf	27.10	91.34
100.0 (PHT-P)	multf	-39.89	5.85
100.0 (PHT-C)	multf	16.28	51.97
100.0 IRAS		+0.4	+0.4
105.0	multf	-31.27	9.86
120.0	multf	-86.12	-81.11
150.0	multf	-86.17	-80.01
170.0	multf	-154.91	-159.50
170.0	abs	-29.05	-7.21
180.0	multf	-262.53	-311.14
200.0	multf	-139.78	-143.50

and PCAE39802002.FITS, see below. It comes out that also the keyword SBBRT is zero, i.e. both point source (PCAP) and extended source (PCAE) products are affected. In contrary, P25 AAP products (e.g. PCAP35300309.FITS (C100), PCAP35300312.FITS (C200), PCAE35300308.FITS (C100), PCAE35300311.FITS (C200)) do not show this behaviour.
For completeness, we also checked the headers of the related SPD products. No anomaly was found, except for product PC1S35602204.FITS which did not contain the keywords TRS1Sm ... RU2PnFm (cf. chapter 12.3.1.2 in [2]). It turned out that the measurement was interrupted due to a R/T problem, with only 3 out of 6 sky measurements executed and a missing FCS measurement. Therefore the processing goes a special way, using default responsivities, which are clearly indicated, however the production of the mentioned keyword list is prohibited → SPR-2997 was submitted.

```
PCAP35602204.FITS (P22)

FILTER1 = 'C100_105_UM'         / Filter
```

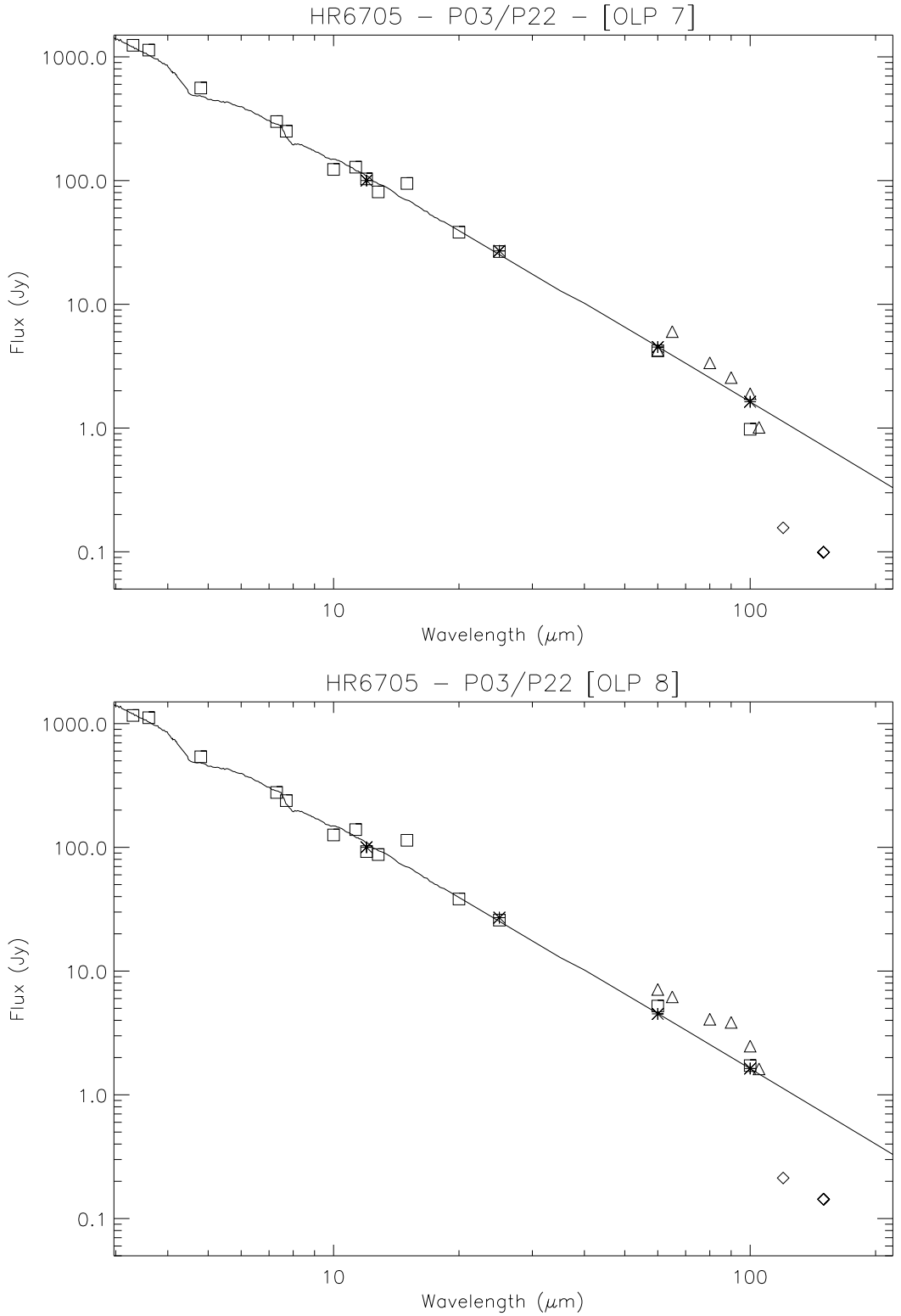

Figure 5.31: Comparison of PHT-P and PHT-C multi-filter photometry (P03/P22), using the full ISOPHOT filter set, with the composite spectrum and out to 300 μm extrapolated SED of γ Dra (HR 6705) provided by M. Cohen and with IRAS photometry for OLP 7.0 (upper panel) and OLP 8.4b1 (lower panel). All photometric points are color corrected for a 4000 K BB. The meaning of the symbols is the following: solid line: model, asterisk: IRAS, square: PHT-P (P03 AOT), triangle: C100 (P22 AOT), diamond: C200 (P22 AOT).

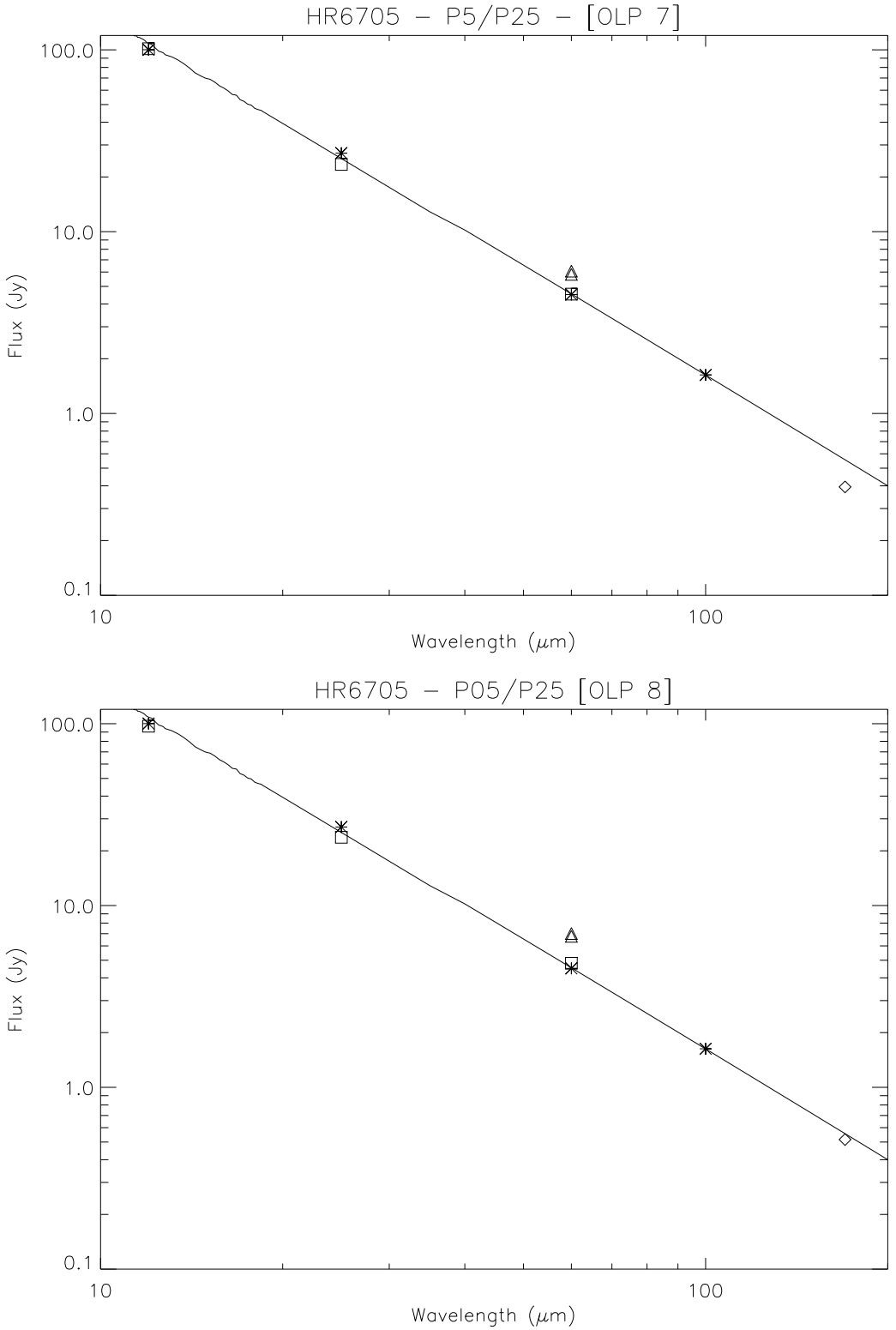

Figure 5.32: Comparison of PHT-P and PHT-C absolute photometry (P05/P25), with the composite spectrum and out to 300 μm extrapolated SED of γ Dra (HR 6705) provided by M. Cohen and with IRAS photometry for OLP 7.0 (upper panel) and OLP 8.4b1 (lower panel). All photometric points are color corrected for a 4000 K BB. The meaning of the symbols is the following: solid line: model, asterisk: IRAS, square: PHT-P (P05 AOT), triangle: C100 (P25 AOT), diamond: C200 (P25 AOT).

```
LAMBDA1 =          1.05000E-04 / Central Wavelength of filter (m)
EXFLUX1 =          1.50000E+00 / Expected source flux (Jy)
UNCFLX1 =          4.00000E-01 / Unc. in expected flux (Jy)
MXBACK1 =          4.49997E+00 / Max expected background (MJy/ster)
SBACK1  =          0.00000E+00 / Flux density (source + background)(Jy)
SBACKU1 =          0.00000E+00 / Unc. in flux (source + background)(Jy)
BACK1   =          0.00000E+00 / Measured background (MJy/ster)
FILTER2 = 'C100_50_UM'         / Filter
LAMBDA2 =          6.50000E-05 / Central Wavelength of filter (m)
EXFLUX2 =          1.60000E+00 / Expected source flux (Jy)
UNCFLX2 =          4.00000E-01 / Unc. in expected flux (Jy)
MXBACK2 =          4.49997E+00 / Max expected background (MJy/ster)
SBACK2  =          0.00000E+00 / Flux density (source + background)(Jy)
SBACKU2 =          0.00000E+00 / Unc. in flux (source + background)(Jy)
BACK2   =          0.00000E+00 / Measured background (MJy/ster)
FILTER3 = 'C100_90_UM'         / Filter
LAMBDA3 =          9.00000E-05 / Central Wavelength of filter (m)
EXFLUX3 =          5.00000E+00 / Expected source flux (Jy)
UNCFLX3 =          1.00000E+00 / Unc. in expected flux (Jy)
MXBACK3 =          8.00000E+00 / Max expected background (MJy/ster)
SBACK3  =          0.00000E+00 / Flux density (source + background)(Jy)
SBACKU3 =          0.00000E+00 / Unc. in flux (source + background)(Jy)
BACK3   =          0.00000E+00 / Measured background (MJy/ster)
FILTER4 = 'C200_200_UM'        / Filter
LAMBDA4 =          2.00000E-04 / Central Wavelength of filter (m)
EXFLUX4 =          4.00000E-01 / Expected source flux (Jy)
UNCFLX4 =          1.00000E-01 / Unc. in expected flux (Jy)
MXBACK4 =          7.10003E+00 / Max expected background (MJy/ster)
SBACK4  =          0.00000E+00 / Flux density (source + background)(Jy)
SBACKU4 =          0.00000E+00 / Unc. in flux (source + background)(Jy)
BACK4   =          0.00000E+00 / Measured background (MJy/ster)
FILTER5 = 'C200_120_UM'        / Filter
LAMBDA5 =          1.20000E-04 / Central Wavelength of filter (m)
EXFLUX5 =          1.20000E+00 / Expected source flux (Jy)
UNCFLX5 =          2.99999E-01 / Unc. in expected flux (Jy)
MXBACK5 =          5.00000E+00 / Max expected background (MJy/ster)
SBACK5  =          0.00000E+00 / Flux density (source + background)(Jy)
SBACKU5 =          0.00000E+00 / Unc. in flux (source + background)(Jy)
BACK5   =          0.00000E+00 / Measured background (MJy/ster)
FILTER6 = 'C200_180_UM'        / Filter
LAMBDA6 =          1.80000E-04 / Central Wavelength of filter (m)
EXFLUX6 =          5.00000E-01 / Expected source flux (Jy)
UNCFLX6 =          2.00000E-01 / Unc. in expected flux (Jy)
MXBACK6 =          6.49995E+00 / Max expected background (MJy/ster)
SBACK6  =          0.00000E+00 / Flux density (source + background)(Jy)
SBACKU6 =          0.00000E+00 / Unc. in flux (source + background)(Jy)
BACK6   =          0.00000E+00 / Measured background (MJy/ster)
FILTER7 = 'C200_135_UM'        / Filter
LAMBDA7 =          1.50000E-04 / Central Wavelength of filter (m)
EXFLUX7 =          1.00000E+00 / Expected source flux (Jy)
UNCFLX7 =          2.00000E-01 / Unc. in expected flux (Jy)
MXBACK7 =          5.49997E+00 / Max expected background (MJy/ster)
SBACK7  =          0.00000E+00 / Flux density (source + background)(Jy)
SBACKU7 =          0.00000E+00 / Unc. in flux (source + background)(Jy)
BACK7   =          0.00000E+00 / Measured background (MJy/ster)
FILTER8 = 'C200_160_UM'        / Filter
LAMBDA8 =          1.70000E-04 / Central Wavelength of filter (m)
EXFLUX8 =          5.99998E-01 / Expected source flux (Jy)
UNCFLX8 =          2.00000E-01 / Unc. in expected flux (Jy)
MXBACK8 =          5.99998E+00 / Max expected background (MJy/ster)
SBACK8  =          0.00000E+00 / Flux density (source + background)(Jy)
SBACKU8 =          0.00000E+00 / Unc. in flux (source + background)(Jy)
BACK8   =          0.00000E+00 / Measured background (MJy/ster)
END
```

PCAP39802003.FITS (P22)

```
FILTER1 = 'C100_105_UM'         / Filter
LAMBDA1 =          1.05000E-04 / Central Wavelength of filter (m)
EXFLUX1 =          1.50000E+00 / Expected source flux (Jy)
UNCFLX1 =          5.00000E-01 / Unc. in expected flux (Jy)
MXBACK1 =          8.00000E+00 / Max expected background (MJy/ster)
SBACK1  =          0.00000E+00 / Flux density (source + background)(Jy)
SBACKU1 =          0.00000E+00 / Unc. in flux (source + background)(Jy)
BACK1   =          0.00000E+00 / Measured background (MJy/ster)
FILTER2 = 'C100_100_UM'         / Filter
LAMBDA2 =          1.00000E-04 / Central Wavelength of filter (m)
EXFLUX2 =          1.50000E+00 / Expected source flux (Jy)
UNCFLX2 =          5.00000E-01 / Unc. in expected flux (Jy)
MXBACK2 =          8.00000E+00 / Max expected background (MJy/ster)
SBACK2  =          0.00000E+00 / Flux density (source + background)(Jy)
SBACKU2 =          0.00000E+00 / Unc. in flux (source + background)(Jy)
BACK2   =          0.00000E+00 / Measured background (MJy/ster)
FILTER3 = 'C100_70_UM'          / Filter
LAMBDA3 =          8.00000E-05 / Central Wavelength of filter (m)
EXFLUX3 =          3.50002E+00 / Expected source flux (Jy)
UNCFLX3 =          1.00000E+00 / Unc. in expected flux (Jy)
MXBACK3 =          8.00000E+00 / Max expected background (MJy/ster)
SBACK3  =          0.00000E+00 / Flux density (source + background)(Jy)
SBACKU3 =          0.00000E+00 / Unc. in flux (source + background)(Jy)
BACK3   =          0.00000E+00 / Measured background (MJy/ster)
FILTER4 = 'C100_50_UM'          / Filter
LAMBDA4 =          6.50000E-05 / Central Wavelength of filter (m)
EXFLUX4 =          5.99998E+00 / Expected source flux (Jy)
UNCFLX4 =          2.00000E+00 / Unc. in expected flux (Jy)
MXBACK4 =          8.00000E+00 / Max expected background (MJy/ster)
SBACK4  =          0.00000E+00 / Flux density (source + background)(Jy)
SBACKU4 =          0.00000E+00 / Unc. in flux (source + background)(Jy)
BACK4   =          0.00000E+00 / Measured background (MJy/ster)
FILTER5 = 'C100_90_UM'          / Filter
LAMBDA5 =          9.00000E-05 / Central Wavelength of filter (m)
EXFLUX5 =          2.00000E+00 / Expected source flux (Jy)
UNCFLX5 =          1.00000E+00 / Unc. in expected flux (Jy)
MXBACK5 =          8.00000E+00 / Max expected background (MJy/ster)
SBACK5  =          0.00000E+00 / Flux density (source + background)(Jy)
SBACKU5 =          0.00000E+00 / Unc. in flux (source + background)(Jy)
BACK5   =          0.00000E+00 / Measured background (MJy/ster)
FILTER6 = 'C100_60_UM'          / Filter
LAMBDA6 =          6.00000E-05 / Central Wavelength of filter (m)
EXFLUX6 =          5.00000E+00 / Expected source flux (Jy)
UNCFLX6 =          2.00000E+00 / Unc. in expected flux (Jy)
MXBACK6 =          8.00000E+00 / Max expected background (MJy/ster)
SBACK6  =          0.00000E+00 / Flux density (source + background)(Jy)
SBACKU6 =          0.00000E+00 / Unc. in flux (source + background)(Jy)
BACK6   =          0.00000E+00 / Measured background (MJy/ster)
END
```

PCAP35300309.FITS (P25)

```
FILTER1 = 'C100_60_UM'          / Filter
LAMBDA1 =          6.00000E-05 / Central Wavelength of filter (m)
EXFLUX1 =          4.49997E+00 / Expected source flux (Jy)
UNCFLX1 =          5.00000E-01 / Unc. in expected flux (Jy)
MXBACK1 =          6.29999E+00 / Max expected background (MJy/ster)
SBACK1  =          1.03256E+01 / Flux density (source + background)(Jy)
SBACKU1 =          2.05494E-01 / Unc. in flux (source + background)(Jy)
BACK1   =          0.00000E+00 / Measured background (MJy/ster)
```

```
END


PCAE35602203.FITS (P22)

FILTER1 = 'C100_105_UM'        / Filter
LAMBDA1 =          1.05000E-04 / Central Wavelength of filter (m)
EXFLUX1 =          4.49997E+00 / Expected source brightness (MJy/ster)
UNCFLX1 =          4.49997E+00 / Unc. in expected brightness (MJy/ster)
MXBACK1 =          1.00000E-07 / Max expected background (MJy/ster)
SBBRT1  =          0.00000E+00 / Brightness (source + background)(MJy/ster)
SBBRTU1 =          0.00000E+00 / Unc. brightness (source + background)(MJy/ster)
BACK1   =          0.00000E+00 / Measured background (MJy/ster)
FILTER2 = 'C100_70_UM'         / Filter
LAMBDA2 =          8.00000E-05 / Central Wavelength of filter (m)
EXFLUX2 =          5.49997E+00 / Expected source brightness (MJy/ster)
UNCFLX2 =          5.49997E+00 / Unc. in expected brightness (MJy/ster)
MXBACK2 =          1.00000E-07 / Max expected background (MJy/ster)
SBBRT2  =          0.00000E+00 / Brightness (source + background)(MJy/ster)
SBBRTU2 =          0.00000E+00 / Unc. brightness (source + background)(MJy/ster)
BACK2   =          0.00000E+00 / Measured background (MJy/ster)
FILTER3 = 'C100_50_UM'         / Filter
LAMBDA3 =          6.50000E-05 / Central Wavelength of filter (m)
EXFLUX3 =          8.00000E+00 / Expected source brightness (MJy/ster)
UNCFLX3 =          8.00000E+00 / Unc. in expected brightness (MJy/ster)
MXBACK3 =          1.00000E-07 / Max expected background (MJy/ster)
SBBRT3  =          0.00000E+00 / Brightness (source + background)(MJy/ster)
SBBRTU3 =          0.00000E+00 / Unc. brightness (source + background)(MJy/ster)
BACK3   =          0.00000E+00 / Measured background (MJy/ster)
FILTER4 = 'C100_60_UM'         / Filter
LAMBDA4 =          6.00000E-05 / Central Wavelength of filter (m)
EXFLUX4 =          6.29999E+00 / Expected source brightness (MJy/ster)
UNCFLX4 =          6.29999E+00 / Unc. in expected brightness (MJy/ster)
MXBACK4 =          1.00000E-07 / Max expected background (MJy/ster)
SBBRT4  =          0.00000E+00 / Brightness (source + background)(MJy/ster)
SBBRTU4 =          0.00000E+00 / Unc. brightness (source + background)(MJy/ster)
BACK4   =          0.00000E+00 / Measured background (MJy/ster)
FILTER5 = 'C100_100_UM'        / Filter
LAMBDA5 =          1.00000E-04 / Central Wavelength of filter (m)
EXFLUX5 =          4.49997E+00 / Expected source brightness (MJy/ster)
UNCFLX5 =          4.49997E+00 / Unc. in expected brightness (MJy/ster)
MXBACK5 =          1.00000E-07 / Max expected background (MJy/ster)
SBBRT5  =          0.00000E+00 / Brightness (source + background)(MJy/ster)
SBBRTU5 =          0.00000E+00 / Unc. brightness (source + background)(MJy/ster)
BACK5   =          0.00000E+00 / Measured background (MJy/ster)
FILTER6 = 'C100_90_UM'         / Filter
LAMBDA6 =          9.00000E-05 / Central Wavelength of filter (m)
EXFLUX6 =          5.00000E+00 / Expected source brightness (MJy/ster)
UNCFLX6 =          5.00000E+00 / Unc. in expected brightness (MJy/ster)
MXBACK6 =          1.00000E-07 / Max expected background (MJy/ster)
SBBRT6  =          0.00000E+00 / Brightness (source + background)(MJy/ster)
SBBRTU6 =          0.00000E+00 / Unc. brightness (source + background)(MJy/ster)
BACK6   =          0.00000E+00 / Measured background (MJy/ster)
FILTER7 = 'C200_200_UM'        / Filter
LAMBDA7 =          2.00000E-04 / Central Wavelength of filter (m)
EXFLUX7 =          7.10003E+00 / Expected source brightness (MJy/ster)
UNCFLX7 =          7.10003E+00 / Unc. in expected brightness (MJy/ster)
MXBACK7 =          1.00000E-07 / Max expected background (MJy/ster)
SBBRT7  =          0.00000E+00 / Brightness (source + background)(MJy/ster)
SBBRTU7 =          0.00000E+00 / Unc. brightness (source + background)(MJy/ster)
BACK7   =          0.00000E+00 / Measured background (MJy/ster)
FILTER8 = 'C200_120_UM'        / Filter
LAMBDA8 =          1.20000E-04 / Central Wavelength of filter (m)
EXFLUX8 =          5.00000E+00 / Expected source brightness (MJy/ster)
```

```
UNCFLX8 =          5.00000E+00 / Unc. in expected brightness (MJy/ster)
MXBACK8 =          1.00000E-07 / Max expected background (MJy/ster)
SBBRT8  =          0.00000E+00 / Brightness (source + background)(MJy/ster)
SBBRTU8 =          0.00000E+00 / Unc. brightness (source + background)(MJy/ster)
BACK8   =          0.00000E+00 / Measured background (MJy/ster)
FILTER9 = 'C200_180_UM'        / Filter
LAMBDA9 =          1.80000E-04 / Central Wavelength of filter (m)
EXFLUX9 =          6.49995E+00 / Expected source brightness (MJy/ster)
UNCFLX9 =          6.49995E+00 / Unc. in expected brightness (MJy/ster)
MXBACK9 =          1.00000E-07 / Max expected background (MJy/ster)
SBBRT9  =          0.00000E+00 / Brightness (source + background)(MJy/ster)
SBBRTU9 =          0.00000E+00 / Unc. brightness (source + background)(MJy/ster)
BACK9   =          0.00000E+00 / Measured background (MJy/ster)
FILTER10= 'C200_135_UM'        / Filter
LAMBDA10=          1.50000E-04 / Central Wavelength of filter (m)
EXFLUX10=          5.49997E+00 / Expected source brightness (MJy/ster)
UNCFLX10=          5.49997E+00 / Unc. in expected brightness (MJy/ster)
MXBACK10=          1.00000E-07 / Max expected background (MJy/ster)
SBBRT10 =          0.00000E+00 / Brightness (source + background)(MJy/ster)
SBBRTU10=          0.00000E+00 / Unc. brightness (source + background)(MJy/ster)
BACK10  =          0.00000E+00 / Measured background (MJy/ster)
FILTER11= 'C200_160_UM'        / Filter
LAMBDA11=          1.70000E-04 / Central Wavelength of filter (m)
EXFLUX11=          5.99998E+00 / Expected source brightness (MJy/ster)
UNCFLX11=          5.99998E+00 / Unc. in expected brightness (MJy/ster)
MXBACK11=          1.00000E-07 / Max expected background (MJy/ster)
SBBRT11 =          0.00000E+00 / Brightness (source + background)(MJy/ster)
SBBRTU11=          0.00000E+00 / Unc. brightness (source + background)(MJy/ster)
BACK11  =          0.00000E+00 / Measured background (MJy/ster)
END
```

PCAE39802002.FITS (P22)

```
FILTER1 = 'C100_50_UM'         / Filter
LAMBDA1 =          6.50000E-05 / Central Wavelength of filter (m)
EXFLUX1 =          8.00000E+00 / Expected source brightness (MJy/ster)
UNCFLX1 =          8.00000E+00 / Unc. in expected brightness (MJy/ster)
MXBACK1 =          1.00000E+00 / Max expected background (MJy/ster)
SBBRT1  =          0.00000E+00 / Brightness (source + background)(MJy/ster)
SBBRTU1 =          0.00000E+00 / Unc. brightness (source + background)(MJy/ster)
BACK1   =          0.00000E+00 / Measured background (MJy/ster)
FILTER2 = 'C100_105_UM'        / Filter
LAMBDA2 =          1.05000E-04 / Central Wavelength of filter (m)
EXFLUX2 =          8.00000E+00 / Expected source brightness (MJy/ster)
UNCFLX2 =          8.00000E+00 / Unc. in expected brightness (MJy/ster)
MXBACK2 =          1.00000E+00 / Max expected background (MJy/ster)
SBBRT2  =          0.00000E+00 / Brightness (source + background)(MJy/ster)
SBBRTU2 =          0.00000E+00 / Unc. brightness (source + background)(MJy/ster)
BACK2   =          0.00000E+00 / Measured background (MJy/ster)
FILTER3 = 'C100_60_UM'         / Filter
LAMBDA3 =          6.00000E-05 / Central Wavelength of filter (m)
EXFLUX3 =          8.00000E+00 / Expected source brightness (MJy/ster)
UNCFLX3 =          8.00000E+00 / Unc. in expected brightness (MJy/ster)
MXBACK3 =          1.00000E+00 / Max expected background (MJy/ster)
SBBRT3  =          0.00000E+00 / Brightness (source + background)(MJy/ster)
SBBRTU3 =          0.00000E+00 / Unc. brightness (source + background)(MJy/ster)
BACK3   =          0.00000E+00 / Measured background (MJy/ster)
FILTER4 = 'C100_70_UM'         / Filter
LAMBDA4 =          8.00000E-05 / Central Wavelength of filter (m)
EXFLUX4 =          8.00000E+00 / Expected source brightness (MJy/ster)
UNCFLX4 =          8.00000E+00 / Unc. in expected brightness (MJy/ster)
MXBACK4 =          1.00000E+00 / Max expected background (MJy/ster)
SBBRT4  =          0.00000E+00 / Brightness (source + background)(MJy/ster)
```

```
SBBRTU4 =          0.00000E+00 / Unc. brightness (source + background)(MJy/ster)
BACK4   =          0.00000E+00 / Measured background (MJy/ster)
FILTER5 = 'C100_100_UM'        / Filter
LAMBDA5 =          1.00000E-04 / Central Wavelength of filter (m)
EXFLUX5 =          8.00000E+00 / Expected source brightness (MJy/ster)
UNCFLX5 =          8.00000E+00 / Unc. in expected brightness (MJy/ster)
MXBACK5 =          1.00000E+00 / Max expected background (MJy/ster)
SBBRT5  =          0.00000E+00 / Brightness (source + background)(MJy/ster)
SBBRTU5 =          0.00000E+00 / Unc. brightness (source + background)(MJy/ster)
BACK5   =          0.00000E+00 / Measured background (MJy/ster)
FILTER6 = 'C100_90_UM'         / Filter
LAMBDA6 =          9.00000E-05 / Central Wavelength of filter (m)
EXFLUX6 =          8.00000E+00 / Expected source brightness (MJy/ster)
UNCFLX6 =          8.00000E+00 / Unc. in expected brightness (MJy/ster)
MXBACK6 =          1.00000E+00 / Max expected background (MJy/ster)
SBBRT6  =          0.00000E+00 / Brightness (source + background)(MJy/ster)
SBBRTU6 =          0.00000E+00 / Unc. brightness (source + background)(MJy/ster)
BACK6   =          0.00000E+00 / Measured background (MJy/ster)
END


PCAE35300308.FITS (P25)

FILTER1 = 'C100_60_UM'         / Filter
LAMBDA1 =          6.00000E-05 / Central Wavelength of filter (m)
EXFLUX1 =          6.29999E+00 / Expected source brightness (MJy/ster)
UNCFLX1 =          2.99999E+00 / Unc. in expected brightness (MJy/ster)
MXBACK1 =          1.00000E-07 / Max expected background (MJy/ster)
SBBRT1  =          5.71115E+00 / Brightness (source + background)(MJy/ster)
SBBRTU1 =          1.09085E-01 / Unc. brightness (source + background)(MJy/ster)
BACK1   =          0.00000E+00 / Measured background (MJy/ster)
END
```

Table 5.7: Absolute and relative calibration accuracies per detector achieved for HR 6705 observation with OLP V8.4b1

detector	**mode**	**absolute accuracy** [%]	**relative accuracy** [%]
P1	multf	8 at 3.6 μm	25
P1	abs	11 at 12 μm	n/a
P2	multf	$<$ 3 at 20 μm	5
P2	abs	6 at 25 μm	n/a
P3	multf	15 at 60 μm	10
P3	abs	6 at 60 μm	n/a
C100	multf	55 at 60 μm	35
C100	abs	55 at 60 μm	n/a
C200	abs	8 at 170 μm	n/a

Part 4 of the evaluation log section and Fig. 5.33 provide the surface brightness photometry of the background position and the comparison with COBE. From Table 5.8 it can be seen that the internal consistency of the measurements from the two revolutions 356 and 398, in particular at 60 μm, has improved. The consistency with COBE cannot be investigated in more detail, as the faulty calibration file may also affect the background measurements. This has to await period 2, when the corrections will be in place.

Table 5.8: Consistency check of γ Dra background position surface brightness results with COBE/DIRBE annual maps.

wavelength μm	**consistency w.r.t. COBE OLP V7.0** [%]	**consistency w.r.t. COBE OLP V8.4b1** [%]
60 (rev 356)	-16.3	-16.9
60 (rev 398)	+15.4	+2.6
100 (rev 356)	-2.0	-40.3
100 (rev 398)	+20.2	-22.2
150 (rev 356)	-31.9	-35.2
200 (rev 356)	+24.2	+1.0

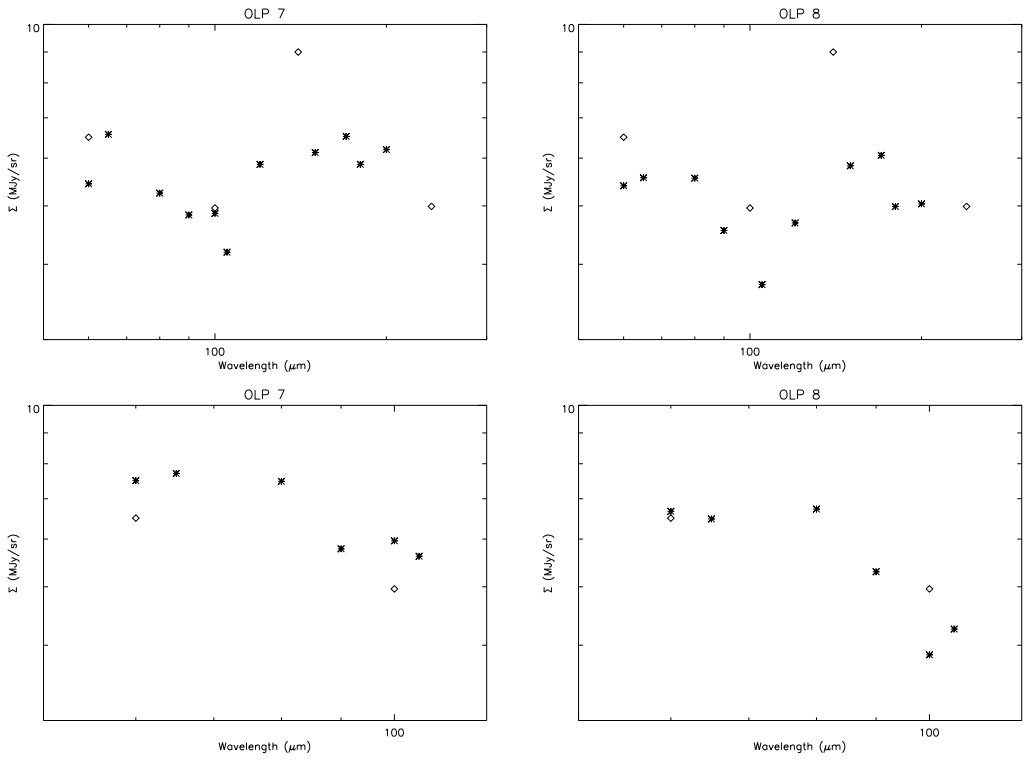

Figure 5.33: Comparison of OLP V7.0 and OLP V8.4b1 surface brightness (asterisk) with COBE annual map fluxes (diamond): TDT35602203 upper left and right panel, TDT39802002 lower left and right panel.

Conclusions

- The SCREW-366, 367 implementation works for PHT-P. While for P1 no improvement in calibration accuracy can be noted, the relative filter-to-filter accuracy is still on the 20 – 25 % level, P2 absolute and relative photometry has slightly improved, and P3 relative photometry has considerably improved.
- Both multi-filter and absolute photometry with C100 show flux excesses of greater than 50 % with regard to the model. This could be traced back to a wrong CALG file PC1SLINR.FITS in the system as documented by SPR-2985. The photometric accuracy has to be re-assessed after the correction during SVP2.
- Staring "on-off" multi-filter photometry with C200 shows still a significant flux deficiency of or even negative source fluxes, while absolute photometry is now accurate

within 10 % for this source.

- We find a kind of regression problem in so far, as the flux keyword both for point and extended source fluxes are zero for P22 AOTs, while for P25 AOTs they are nominal.
- The self-consistency of surface brightness values from the background position and its consistency with COBE photometry looks in general improved, however final quantitative assessment will only be possible after SVP2, after fix of SPR-2985.

Evaluation Log

```
1) P03 and P22 multi-filter photometry

PHT-P: ppap35602102 (src+back)  FCS: 15, 20, 60 um
       ppae35602101 (back)      FCS: 3.3, 20, 100 um

PHT-C1: pcap39802003 (src+back)   FCS: 60 um
        pcae39802002 (back)       FCS: 90 um

PHT-C2: pcap35602204 (src+back)   FCS: 170 um
        pcae35602203 (back)       FCS: 170 um


color correction: black body, T=4000
model: Cohen

Det   cwl    OLP 7      OLP 8      IRAS     Model     % OLP 7    % OLP 8
P1    3.3  1240.160   1164.273           1203.159      3.08      -3.23
P1    3.6  1134.352   1117.075           1030.575     10.07       8.39
P1    4.8   559.957    539.840            482.322     16.10      11.93
P1    7.3   299.980    277.822            285.925      4.92      -2.83
P1    7.7   250.549    238.588            224.074     11.82       6.48
P1   10.0   123.116    126.034            149.024    -17.38     -15.43
P1   11.3   128.291    139.136            120.822      6.18      15.16
P1   12.0   103.215     92.502   100.160   108.718     -5.06     -14.92
P1   12.8    81.039     87.453             93.877    -13.68      -6.84
P1   15.0    94.790    114.088             69.510     36.37      64.13
P2   20.0    38.248     38.263             39.387     -2.89      -2.85
P2   25.0    26.691     25.813    27.030   25.229      5.79       2.32
P3   60.0     4.208      5.213     4.510    4.545     -7.41      14.70
C1   60.0     4.246      7.097*    4.510    4.545     -6.57      56.14
C1   65.0     6.015      6.187              3.872     55.35      59.78
C1   80.0     3.365      4.081              2.550     31.94      60.03
C1   90.0     2.557      3.850**            2.012     27.10      91.34
P3  100.0     0.978      1.722     1.630    1.627    -39.89       5.85
C1  100.0     1.892      2.473     1.630    1.627     16.28      51.97
C1  105.0     1.013      1.619              1.474    -31.27       9.86
C2  120.0     0.156      0.213              1.126    -86.12     -81.11
C2  150.0     0.099      0.143              0.717    -86.17     -80.01
C2  170.0    -0.305     -0.331              0.556   -154.91    -159.50
C2  180.0    -0.805     -1.046              0.495   -262.53    -311.14
C2  200.0    -0.159     -0.174              0.400   -139.78    -143.50

* PIA gives 5.55 Jy
**PIA gives 2.80 Jy
  fluxes per pixel from PIA and OLP (after psf correction) for C1_90

  src+bkg    0.664822     0.687095     0.708221     0.588886      2.03199
  PIA        0.711567     0.530075     0.561871     0.559210

  src+bkg    0.786159     0.849696     0.842278     0.615346      2.02128
  OLP VILSPA 0.725610     0.767552     0.776841     0.686698

  src+bkg    0.5869655    0.5983763    0.6007107    0.5061610     1.786139
  OLP RAL    0.6003410    0.4554087    0.4917087    0.4757688

  bkg        0.409097     0.437912     0.449970     0.472092      0.441043
  PIA        0.454834     0.361066     0.429965     0.335595

  bkg        0.390477     0.416690     0.423756     0.451608      0.391607
  OLP VILSPA 0.442522     0.354471     0.388784     0.345748

  bkg        0.3681233    0.3978464    0.4124589    0.4266492     0.3884707
```

```
  OLP RAL    0.4067865    0.3482770    0.3762138    0.3235113


(total(src+bkg)-total(bkg))/cc:      3.85 (OLP)  2.80 (PIA)
(sb(p5)-b(p5))*psf_arr/psf_pix/cc  : 1.82 (OLP)  1.78 (PIA)


2) P05 and P25 absolute photometry


PHT-P1: ppap35300302 (src+back)
        ppae35300301 (back)

PHT-P2: ppap35300304 (src+back)
        ppae35300303 (back)

PHT-P3: ppap35300306 (src+back)
        ppae35300305 (back)

PHT-C1: pcap35300309 (src+back$^a$)
        pcap35300310 (src+back$^b$)
        pcae35300308 (back)

PHT-C2: pcap35300312 (src+back)
        pcae35300311 (back)

color correction: black body, T=4000
model: Cohen

Det     cwl   OLP 7    OLP 8      IRAS     Model    % OLP 7   % OLP 8
P1     12.0  101.421   96.917   100.160   108.718    -6.71    -10.86
P2     25.0   23.431   23.736    27.030    25.229    -7.13     -5.92
P3     60.0    4.533    4.812     4.510     4.545    -0.27      5.88
C1(a) 60.0    5.825    7.015     4.510     4.545    28.17     54.34
C1(b) 60.0    6.067    6.774     4.510     4.545    33.48     49.03
C2    170.0   0.395    0.516               0.556   -29.05     -7.21


3) Photometry for different reset interval settings


PHT-C: pcap67100802 (src+back)   FCS: 90 um
       pcap67100801 (back)       FCS: 90 um

PHT-C: pcap67100911 (src+back)   FCS: 90 um
       pcap67100910 (back)       FCS: 90 um



color correction: black body, T= 4000
model: Cohen

Det    cwl   OLP 7   OLP 8    IRAS    Model    % OLP 7    % OLP 8
                     PCAP67100802
C1    90.0   1.858   1.696            2.012     -7.66     -15.72
C1   100.0   2.185   1.143   1.630    1.627     34.31     -29.73
C1   105.0   1.716   2.047            1.474     16.40      38.88
                     PCAP67100911
C1    90.0   1.600   2.087            2.012    -20.48       3.75
C1   100.0   2.139   1.183   1.630    1.627     31.49     -27.27
C1   105.0   1.110   1.195            1.474    -24.72     -18.94


4) Surface brightness on background positions
```

Gamma Dra

TDT 39802002

Cwl [um]	OLP 7.0 [MJy sr^-1]	OLP 8.4 [MJy sr^-1]	COBE [MJy sr^-1]
60.0	7.50	6.67	6.50
65.0	7.71	6.48	
80.0	7.48	6.73	
90.0	5.78	5.29	
100.0	5.96	3.86	4.96
105.0	5.62	4.25	

TDT 35602203

Cwl [um]	OLP 7.0 [MJy sr^-1]	OLP 8.4 [MJy sr^-1]	COBE [MJy sr^-1]
60.0	5.44	5.40	6.50
65.0	6.57	5.57	
80.0	5.25	5.56	
90.0	4.83	4.55	
100.0	4.86	2.96	4.96
105.0	4.19	3.70	
120.0	5.86	4.68	
150.0	6.13	5.83	9.00 (140um)
170.0	6.52	6.06	
180.0	5.86	4.99	
200.0	6.20	5.04	4.99 (240um)

5.4.5 General Re-validation of PHT03 and PHT05 Staring Mode: The SED of Sirius (HR 2491)

- authors: M. Radovich, U. Klaas
- date: 08-July-1999
- SVP period 1

Motivation

Beside Vega (HR 7001), Sirius is the main primary stellar standard with a model provided by M. Cohen (1-300 μm, R = 4000 up to 35 μm, delivered 12-Jan-1996). Therefore, a dedicated cross-calibration program was performed on this star using absolute photometry complemented by multi-filter photometry out to 25 μm.

Method

We compare the background subtracted, color corrected flux values of both OLP V7.0 and OLP V8.4b1 results against the model prediction.

Results

In the following Tab. 5.9 we compare the photometry from part 1 of the evaluation log section with the model. We estimate the absolute photometric accuracy per detector assembly for this target as the deviation from the model flux in the filter in which the FCS calibration was done, and the relative filter-to-filter accuracy as the peak-to-peak variation of the other filters around this offset. Two multi-filter sequences were performed, one from 3.3 to 12 μm with absolute calibration at 3.3 μm, and the other one from 11.3 to 15 μm with absolute calibration at 12.8 μm. The photometric accuracies are presented in Tab. 5.10. Fig. 5.34 shows the PHT photometric data points in comparison to the model and IRAS photometry (color corrected) for OLP 7.0 and OLP 8.4b1, respectively.

Table 5.9: Consistency check of photometric results with Sirius model

Filter	**mode**	**consistency w.r.t. model OLP V7.0** [%]	**consistency w.r.t. model OLP V8.4b1** [%]
3.3	multf	8.70	10.88
3.3	abs	1.05	3.87
7.7	multf	1.35	4.01
11.3	multf	-6.22	17.11
12.0	multf	14.72	11.56
12.0	abs	7.25	2.12
12.8	multf	-3.81	15.52
15.0	multf	-10.27	16.06
25.0	abs	20.32	12.48

Conclusions

- For P1, the absolute photometry gives more accurate fluxes than the multi-filter photometry. The absolute accuracies achieved for the absolute mode are better than 5 %.
- The long wavelength multi-filter sequence from 11.3 to 15 μm shows in general some flux excess with regard to the model. The absolute photomteric accuracy for the multi-filter mode is around 15 %. The relative filter-to-filter calibration is slightly improved w.r.t. OLP V7.0, being better than 7 %.
- The absolute PHT-P2 photometry is improved to better than 15 %.

Table 5.10: Absolute and relative calibration accuracies per detector achieved for HR 5340 observation with OLP V8.4b1

detector	**mode**	**absolute accuracy** [%]	**relative accuracy** [%]
P1	multf	11 at 3.3 μm	7
P1	abs	4 at 3.3 μm	n/a
P1	abs	2 at 12.0 μm	n/a
P1	multf	16 at 12.8 μm	2
P2	abs	13 at 25 μm	n/a

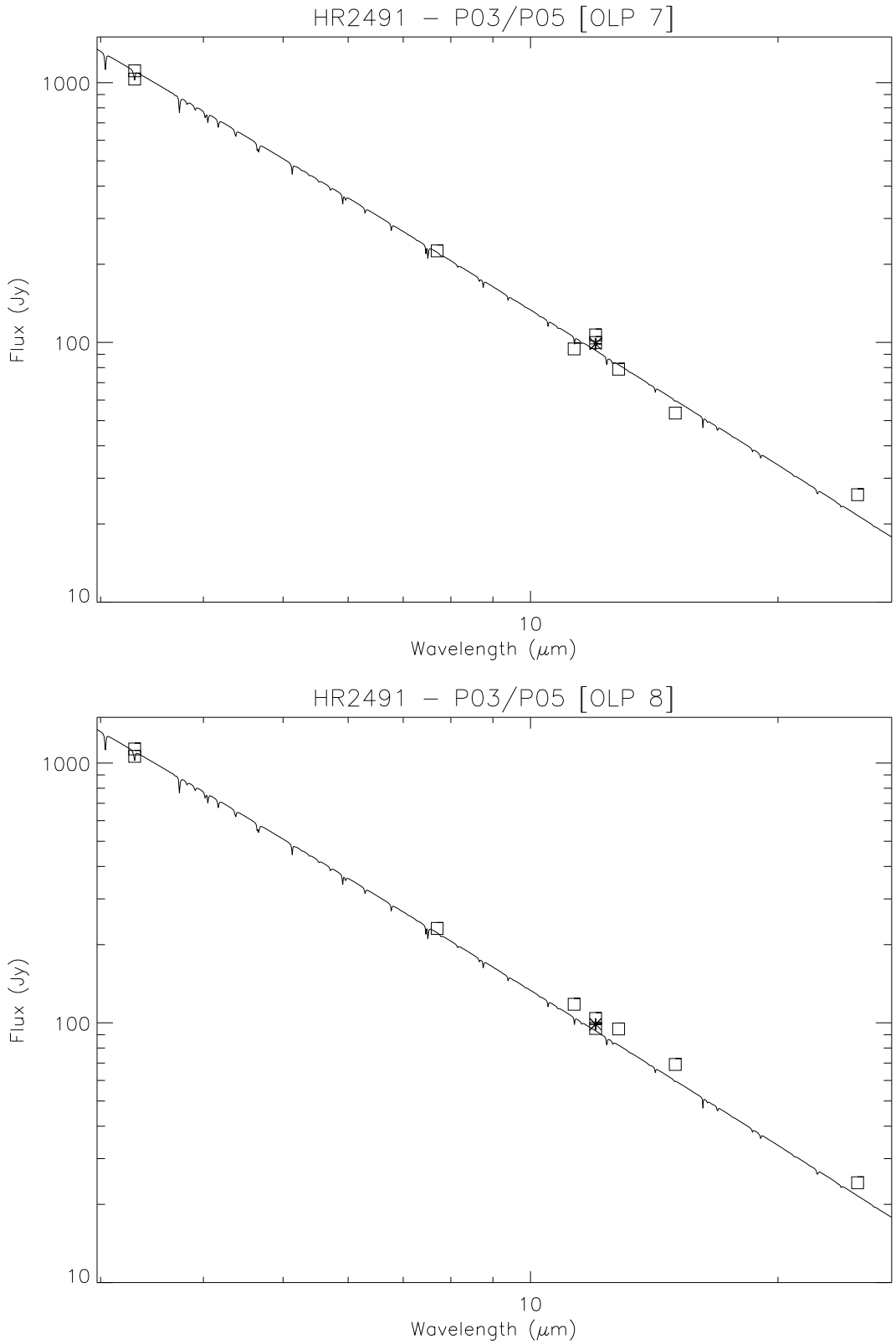

Figure 5.34: Comparison of PHT-P absolute and multi-filter photometry with the composite spectrum of Sirius (HR 2491) provided by M. Cohen and with IRAS photometry for OLP 7.0 (upper panel) and OLP 8.4b1 (lower panel). All photometric points are color corrected for a 10000 K BB. The meaning of the symbols is the following: solid line: model, asterisk: IRAS, square: PHT-P (P03 and P05 AOTs).

Evaluation Log

```
1) P03 multi-filter and P05 absolute photometry

PHT-P1: ppap70705302 (src+back)   multi-filter P03, FCS: 3.3 um
PHT-P1: ppap70705301 (src+back)   multi-filter P03, FCS: 12.8 um
PHT-P1: ppap70705310 (src+back)   absolute P05
PHT-P1: ppap70705313 (src+back)   absolute P05
PHT-P2: ppap70705707 (src+back)   absolute P05


color correction: black body, T=10 000 K
model: Cohen
fluxes in Jy

Det    cwl     OLP 7      OLP 8       IRAS     Model     % OLP 7      % OLP 8
ppap70705302
P1     3.3    1110.840   1133.059             1021.900     8.70         10.88
P1     7.7     225.038    230.947              222.038     1.35          4.01
P1    12.0     106.866    103.930    98.690     93.157    14.72         11.56
ppap70705301
P1    11.3      94.395    117.881              100.654    -6.22         17.11
P1    12.8      78.875     94.729               82.001    -3.81         15.52
P1    15.0      53.447     69.134               59.566   -10.27         16.06
ppap70705310
P1     3.3    1032.600   1061.453             1021.900     1.05          3.87
ppap70705313
P1    12.0      99.908     95.136    98.690     93.157     7.25          2.12
ppap70705707
P2    25.0      25.919     24.229               21.541    20.32         12.48
```

5.4.6 General Re-validation of PHT03 Staring Mode: Photometric Reproducibility Aspects in the Case of the SED of Vega (HR 7001)

- authors: M. Radovich, U. Klaas
- date: 09-July-1999
- SVP period 1

Motivation

We investigate here the photometric accuracy of PHT-P multi-filter aperture photometry for an observation of Vega from a general observer program which was repeated several times as part of a variability monitoring project. From 3.3 to 100 μm it used the typical exposure time of 32 s per filter and non-standard apertures. The absolute calibration via the FCS of the on-source measurement was performed in the 3.6, 20, and 100 μm filter, respectively. The absolute calibration of the off-source measurement was performed in the 7.3, 25, and 100 μm filter, respectively. We selected 3 measurements out of this program from rev. 85 (TDT 08500106; before rev. 94 FCS change!), rev. 558 (TDT 55800419) and rev. 865 (TDT 86500706). The used apertures w.r.t. the standard apertures for point source calibration are listed in the following Table 5.11:

Table 5.11: Apertures used in the Vega variability monitoring program versus standard apertures

filter	**program aperture** ["]	**standard aperture** ["]
P1_3P29_UM	18	23
P1_3P6_UM	18	23
P1_4P85_UM	18	23
P1_7P3_UM	18	23
P1_10_UM	18	52
P1_11P5_UM	18	52
P1_12P8_UM	18	52
P1_16P0_UM	18	52
P2_20_UM	52	79
P2_25_UM	52	79
P3_60_UM	120	180
P3_100_UM	120	180

Method

Vega is one of the primary photometric stellar standards. However, due to its IR excess, the photospheric models, e.g. by Cohen, are valid only out to approximately 15 μm. Beyond 15 μm we solely compare with the available IRAS photometry.
The color correction was dependent on the relative contribution by the stellar photosphere and the IR disc, and hence on the wavelength. We followed the description as given in Ref.[14]:

- from 3.3 to 16 μm the SED behaves like a 10000 K Black Body,
- from 60 to 100 μm the SED behaves like an 80 K modified BB, $\varepsilon \propto \nu$
- from 20 to 25 μm the SED is a mixture of a 10000 K BB and an 80 K modified BB with a ratio 2:1.

Results

In parts 1 to 3 of the evaluation log section we give the background subtracted and color corrected photometry for the three epochs. For illustration the resulting SEDs are plotted in Figs. 5.35 to 5.37. In Table 5.12 we compare these fluxes against Cohen's Vega model up to 20 μm and against IRAS beyond 20 μm and inter-compare the OLP 7.0 and OLP 8.4b1 results. In Table 5.13 we list for the OLP 8.4b1 results the absolute and relative filter-to-filter calibration accuracies for the three revolutions. In Table 5.14 we compare the relative shapes of the SED measured for the three revolutions and processed with OLP 8.4. The corresponding analysis for the OLP 7.0 results are presented in [1] Sect. 5.18.3.
From 3.6 to 10 μm the photometry agrees to within 20 %, for most cases to within 10 % with the model. The 12 μm point appears always too low by at least 25 %. The relative shape of the SED between 12.8 and 15 μm looks now okay, implying that part of the huge 15 μm excess observed for OLP V7.0 can be explained by the non-linearity with flux. Whether the full discrepancy between measurement and model at 12.8 and 15 μm can be explained by signal transients (which certainly play a role at 15 μm because of the relatively short exposre time of 32 s) remains to be investigated. The source is fainter than the three previous stars α Boo, γ Dra and Sirius. The 25 μm photometry is now more consistent with IRAS than for OLP V7.0 (within 20 to 30 %). The P3 photometry is in good agreement with IRAS (within 20 %).

Table 5.12: Consistency check of photometric results with Vega model and IRAS photometry for the three epochs on revs. 085, 558, and 865 for OLP V7.0 and OLP V8.4b1, respectively.

filter	**ref.**	**consistency w.r.t. model or IRAS**					
		OLP V7.0			**OLP V8.4b1**		
		rev. 085 [%]	**rev. 558** [%]	**rev. 865** [%]	**rev. 085** [%]	**rev. 558** [%]	**rev. 865** [%]
3.3	model	-10.6	+4.1	+0.8	-9.7	+4.6	+1.7
3.6	model	-5.5	+9.9	+10.2	-6.7	+8.3	+8.8
4.8	model	+3.4	+18.6	+18.2	+2.5	+17.5	+17.2
7.3	model	-1.8	+11.9	+12.2	-5.3	+7.7	+8.2
10	model	-20.5	+4.7	-13.7	-15.0	+12.1	-8.2
12	model	-34.6	-20.2	-30.6	-31.7	-18.7	-26.9
12	IRAS	-38.4	-24.8	-34.6	-35.7	-23.5	-31.2
12.8	model	+12.2	+55.8	+24.9	+44.9	+96.8	+60.7
15	model	+60.8	+111	+80.7	+45.7	+98.4	+62.0
20	model	+49.2	+40.8	+41.9	+36.8	+41.9	+38.6
25	IRAS	+38.2	+31.6	+31.9	+20.2	+20.4	+21.3
60	IRAS	+9.1	-0.4	+20.0	+22.9	-4.0	+17.1
100	IRAS	+5.2	-4.5	+6.3	+10.6	-7.6	+4.6

The absolute photometry for P1 in the 3.6 μm filter is as accurate as 10 %. Up to 10 μm a relative filter-to-filter calibration of better than 15 % is verified. As mentioned above the strong offsets in the relative filter-to-filter calibration for the filters between 12 and 15 μm can be explained to some extent by signal transients. An absolute calibration accuracy for P2 can not easily be determined, as at 20 μm the star starts to show its IR excess, hence the model is no longer an accurate flux reference and at 25 μm only a relative filter calibration is available. Absolute P3 photometry at 100 μm agrees with IRAS to within 10 % yielding a relative-filter-to-filter calibration between 100 and 60 μm of 15 %.
The relative shape of the SED is reproduced in the three measurements within 10 % for fluxes out to 25 μm, at 60 and 100 μm within 20 %. The fluxes, even those affected by signal transients vary relative by 15 % (1 σ) at most.

Conclusions

- PHT-P photometry with the minimum recommended exposure time of 32 s and in non-standard apertures yields about ± 10% absolute accuracy for P1 and P3. The

Table 5.13: Consistency check of absolute and relative photometric results with Vega model and IRAS photometry for the three epochs on revs. 085, 558, and 865 for OLP V8.4b1 only. The values in each second column per revolution give the offset relative to the FCS calibration filter.

filter	**ref.**	**consistency w.r.t. model or IRAS**					
		rev. 085 [%]		**rev. 558** [%]		**rev. 865** [%]	
3.3	model	-9.7	-3.0	+4.6	-3.7	+1.7	-7.1
3.6	model	-6.7	0.00	+8.3	0.00	+8.8	0.00
4.8	model	+2.5	+9.2	+17.5	+9.2	+17.2	+8.4
7.3	model	-5.3	+1.4	+7.7	-0.6	+8.2	-0.6
10	model	-15.0	-8.3	+12.1	+3.8	-8.2	-17.0
12	model	-31.7	-25.0	-18.7	-27.0	-26.9	-35.7
12	IRAS	-35.7	–	-23.5	–	-31.2	–
12.8	model	+44.9	+51.6	+96.8	+88.5	+60.7	+51.9
15	model	+45.7	+52.4	+98.4	+90.1	+62.0	+53.2
20	model	+36.8	0.00	+41.9	0.00	+38.6	0.00
25	IRAS	+20.2	–	+20.4	–	+21.3	–
60	IRAS	+22.9	+12.3	-4.0	+3.6	+17.1	+12.5
100	IRAS	+10.6	0.00	-7.6	0.00	+4.6	0.00

Table 5.14: Normalized fluxes w.r.t. flux in the 3.3 μm filter and relative variation (1 σ) of the flux for the revolutions 085, 558, and 865.

Filter	**normalized flux**			**relative variation of SED shape** [%]	**relative variation of flux** [%]
	rev. 085	**rev. 558**	**rev. 865**		
3.3	1.0000	1.0000	1.0000	–	7.6
3.6	0.9448	0.9472	0.9791	2.0	8.5
4.8	0.6102	0.6040	0.6201	1.3	7.7
7.3	0.2536	0.2487	0.2574	1.7	7.4
10	0.1237	0.1408	0.1187	9.1	14.7
12	0.0696	0.0715	0.0661	4.0	8.8
12.8	0.1300	0.1524	0.1281	9.9	15.9
15	0.0954	0.1121	0.0942	10.0	16.0
20	0.0511	0.0439	0.0457	8.0	0.6
25	0.0416	0.0360	0.0373	7.7	0.5
60	0.0326	0.0219	0.0276	19.6	12.7
100	0.0267	0.0193	0.0224	16.3	9.0

relative filter-to-filter calibration is better than 15 % for P1 and better than 10 % for P3.

- The P2 accuracy is difficult to estimate for the selected target, due to an unknown mixture of highly different temperature components which involve different ratios of color correction factors for ISOPHOT and the reference photometry, however there is now better agreement with IRAS photometry (better than 25 %).
- The accuracy in several filters of this measurement sequence appears to be currently limited by the accuracy of the signal evaluation due to signal transients, however, we notice the change in the relative shape of the SED between 12.8 and 15 μm, probably due to the new linearity correction.

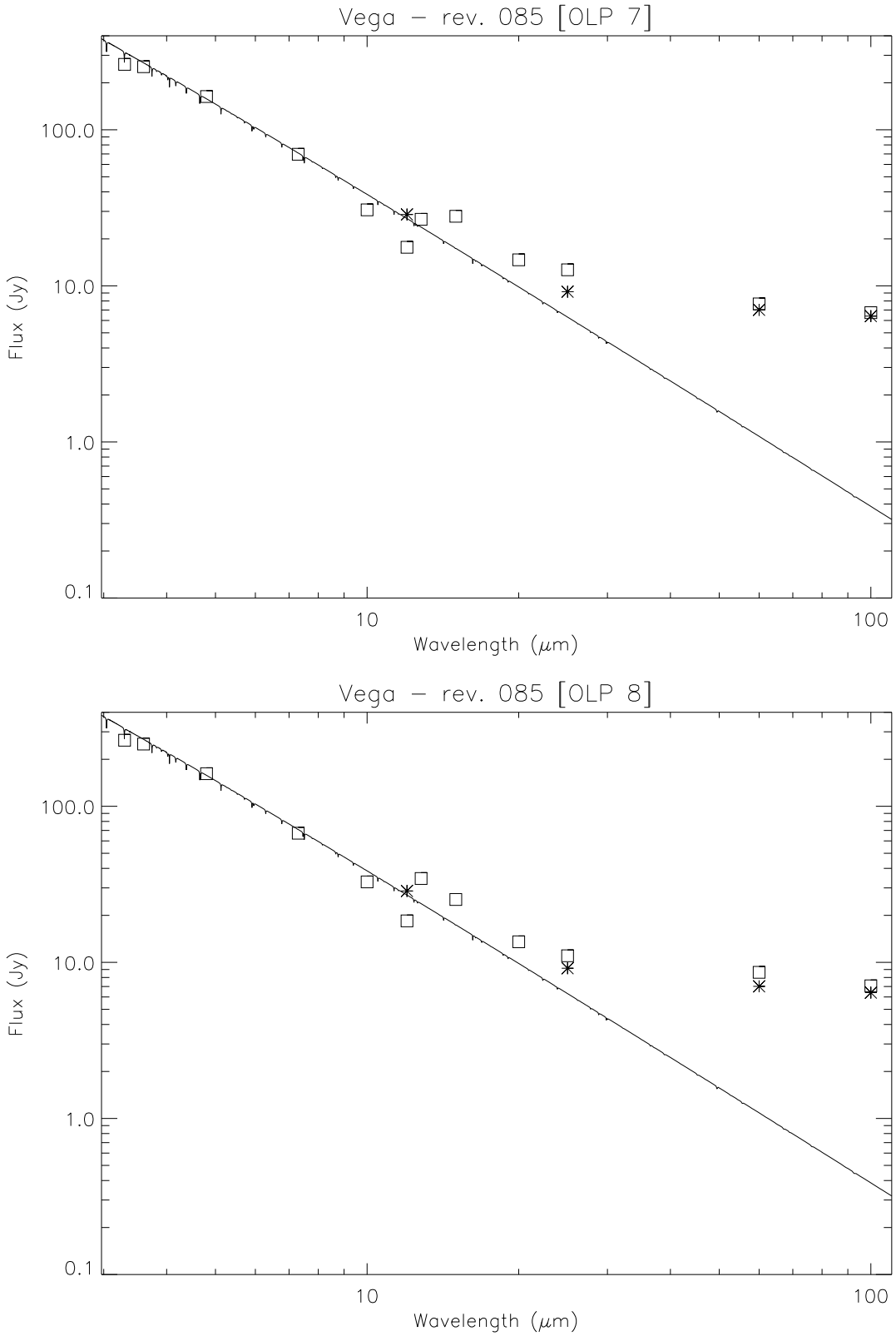

Figure 5.35: Comparison of PHT-P multi-filter photometry of Vega (HR 7001) on revolution 085 with the composite spectrum provided by M. Cohen out to 15 μm and with IRAS photometry beyond 15 μm for OLP 7.0 (upper panel) and OLP 8.4b1 (lower panel). A description of the applied color correction factors is given in the text. The meaning of the symbols is the following: solid line: model, asterisk: IRAS, square: PHT-P.

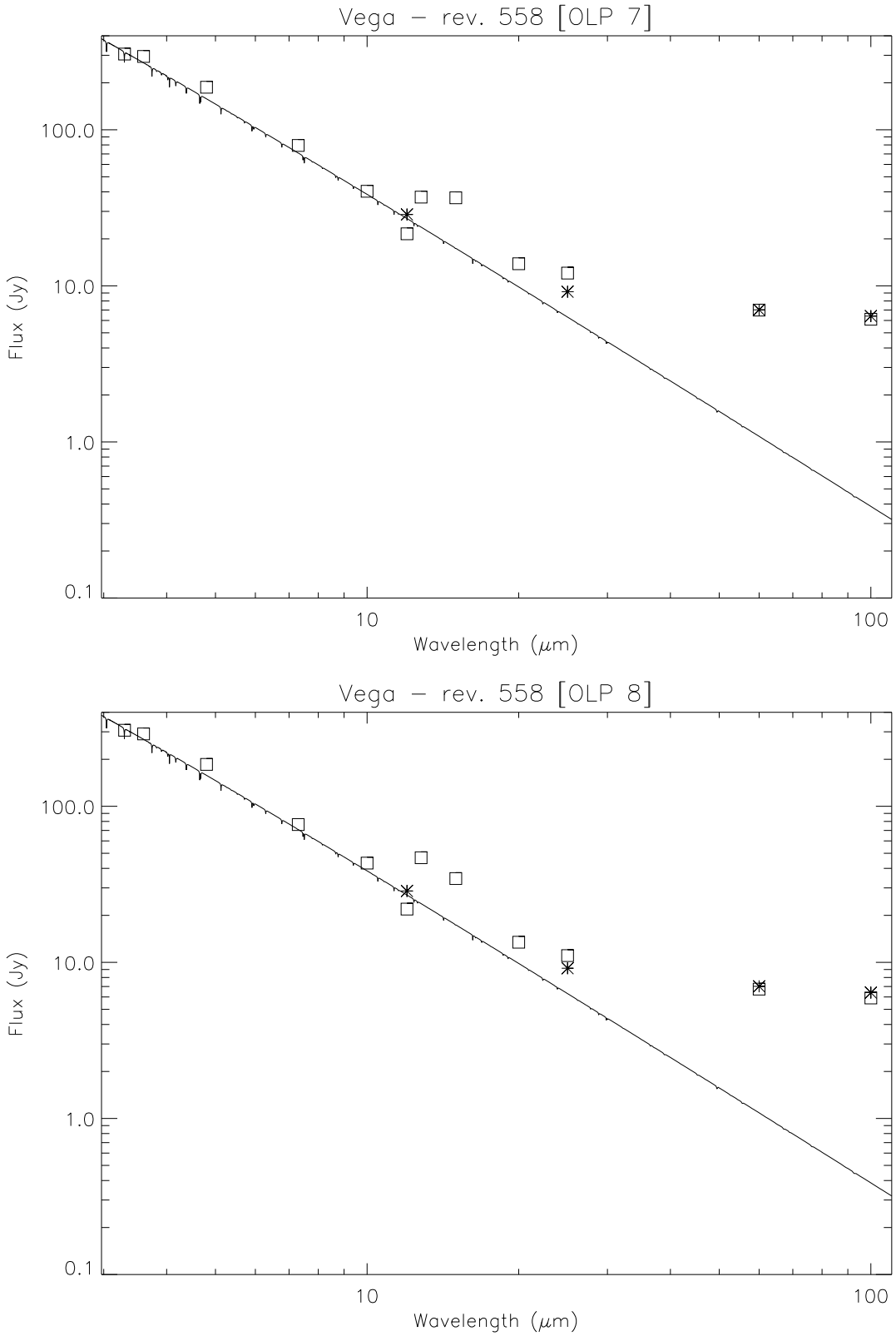

Figure 5.36: Comparison of PHT-P multi-filter photometry of Vega (HR 7001) on revolution 558 with the composite spectrum provided by M. Cohen out to 15 μm and with IRAS photometry beyond 15 μm for OLP 7.0 (upper panel) and OLP 8.4b1 (lower panel). A description of the applied color correction factors is given in the text. The meaning of the symbols is the following: solid line: model, asterisk: IRAS, square: PHT-P.

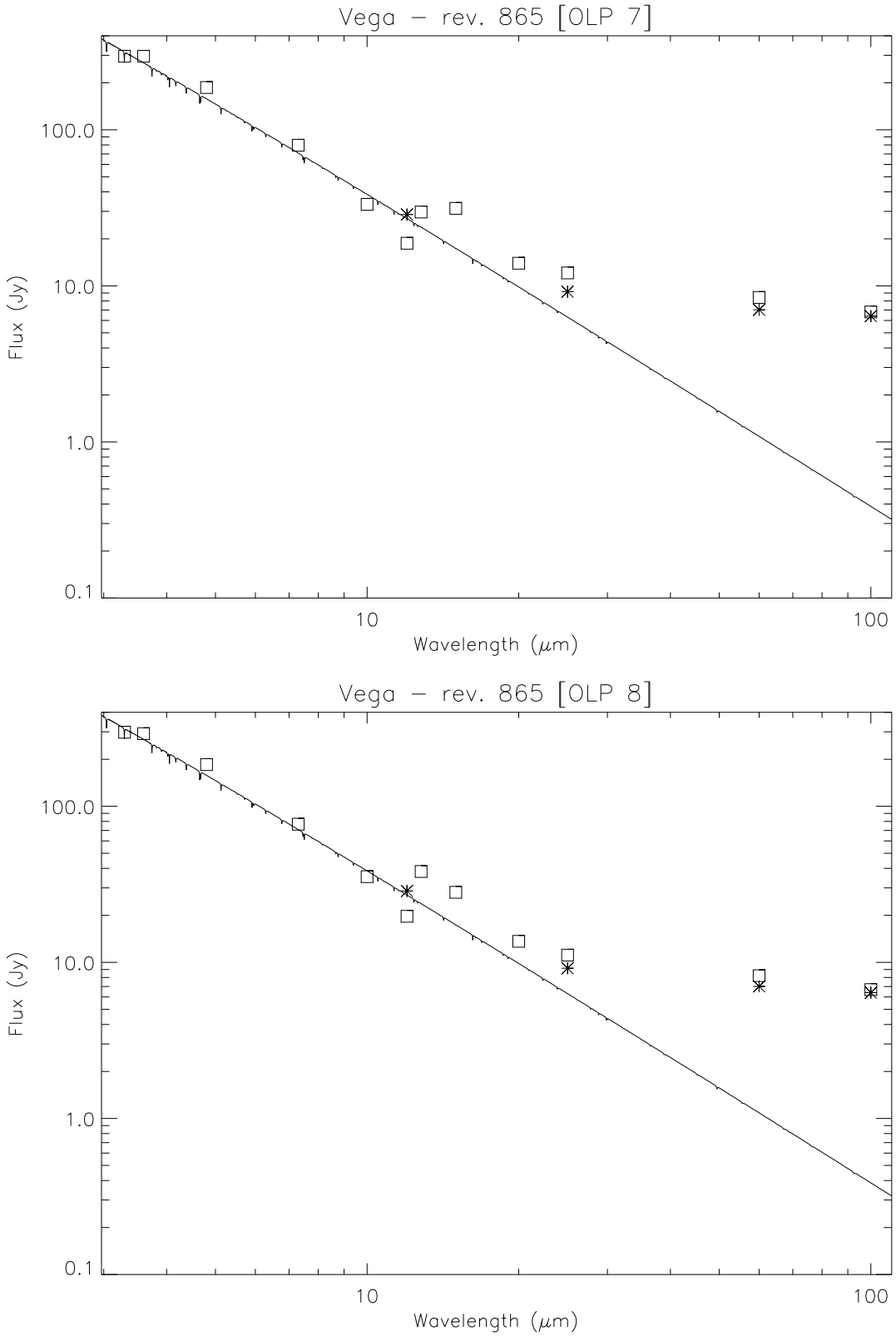

Figure 5.37: Comparison of PHT-P multi-filter photometry of Vega (HR 7001) on revolution 865 with the composite spectrum provided by M. Cohen out to 15 μm and with IRAS photometry beyond 15 μm for OLP 7.0 (upper panel) and OLP 8.4b1 (lower panel). A description of the applied color correction factors is given in the text. The meaning of the symbols is the following: solid line: model, asterisk: IRAS, square: PHT-P.

Evaluation Log

```
1) Vega PHT-P aperture photometry from 3.3 to 100 um on revolution 085

Measurements:
PHT-P: ppap08500106 (src+back)  FCS = 3.6, 20, 100 um
       ppap08500105 (back)      FCS = 7.3, 25, 100 um

 Colour correction: see text for wavelength dependent color correction
                    application

 Model: Cohen

Fluxes are in Jy.

Det   cwl   OLP 7     OLP 8     IRAS    Model      % OLP 7    % OLP 8
     [um]   [Jy]      [Jy]      [Jy]    [Jy]      [(OLP-model)/model]
P1    3.3  262.363   264.984           293.430     -10.59       -9.69
P1    3.6  253.543   250.345           268.410      -5.54       -6.73
P1    4.8  163.215   161.700           157.795       3.44        2.47
P1    7.3   69.658    67.198            70.934      -1.80       -5.27
P1   10.0   30.682    32.769            38.570     -20.45      -15.04
P1   12.0   17.659    18.441   28.660   26.997     -34.59      -31.69
P1   12.8   26.679    34.451            23.779      12.20       44.88
P1   15.0   27.904    25.284            17.356      60.78       45.68
P2   20.0   14.680    13.547             9.838      49.22       37.71
P2   25.0   12.674    11.024    9.170    6.301     101.15       74.97
P3   60.0    7.662     8.629    7.020    1.087     605.10      694.11
P3  100.0    6.733     7.075    6.400    0.387    1641.99     1730.52


2) Vega PHT-P aperture photometry from 3.3 to 100 um on revolution 558

Measurements:
PHT-P: ppap55800420 (src+back)  FCS = 3.6, 20, 100 um
       ppap55800419 (back)      FCS = 7.3, 25, 100 um

 Colour correction: black bodysee text for color correction

 Model: Cohen


Det   cwl   OLP 7     OLP 8     IRAS    Model      % OLP 7    % OLP 8
     [um]   [Jy]      [Jy]      [Jy]    [Jy]      [(OLP-model)/model]
P1    3.3  305.492   306.993           293.430       4.11        4.62
P1    3.6  294.957   290.779           268.410       9.89        8.33
P1    4.8  187.203   185.415           157.795      18.64       17.50
P1    7.3   79.368    76.357            70.934      11.89        7.65
P1   10.0   40.371    43.227            38.570       4.67       12.07
P1   12.0   21.543    21.938   28.660   26.997     -20.20      -18.74
P1   12.8   37.035    46.791            23.779      55.75       96.78
P1   15.0   36.645    34.429            17.356     111.14       98.37
P2   20.0   13.851    13.462             9.838      40.80       36.84
P2   25.0   12.072    11.047    9.170    6.301      91.61       75.33
P3   60.0    6.990     6.737    7.020    1.087     543.30      520.05
P3  100.0    6.110     5.911    6.400    0.387    1480.91     1429.35


3) Vega PHT-P aperture photometry from 3.3 to 100 um on revolution 865


Measurements:
PHT-P: ppap86500706 (src+back)  FCS = 3.6, 20, 100 um
       ppap86500705 (back)      FCS = 7.3, 25, 100 um
```

Colour correction: black bodysee text for color correction

Model: Cohen

Det	cwl [um]	OLP 7 [Jy]	OLP 8 [Jy]	IRAS [Jy]	Model [Jy]	% OLP 7 [(OLP-model)/model]	% OLP 8
P1	3.3	295.786	298.270		293.430	0.80	1.65
P1	3.6	295.808	292.034		268.410	10.21	8.80
P1	4.8	186.549	184.949		157.795	18.22	17.21
P1	7.3	79.606	76.780		70.934	12.23	8.24
P1	10.0	33.282	35.400		38.570	-13.71	-8.22
P1	12.0	18.742	19.727	28.660	26.997	-30.58	-26.93
P1	12.8	29.700	38.202		23.779	24.90	60.66
P1	15.0	31.365	28.111		17.356	80.72	61.97
P2	20.0	13.963	13.636		9.838	41.94	38.61
P2	25.0	12.096	11.125	9.170	6.301	91.99	76.57
P3	60.0	8.425	8.218	7.020	1.087	675.32	656.33
P3	100.0	6.802	6.691	6.400	0.387	1659.85	1631.10

5.4.7 General Re-validation of PHT03 and PHT22 Staring Mode: The SED of Arp 220

- authors: M. Radovich, U. Klaas
- date: 10-July-1999
- SVP period 1

Motivation

TDTs 47600413(background, PHT-P), 47600414(Arp 220, PHT-P), 47600415(background, PHT-C), 47600416(Arp 220, PHT-C) is one of the key OLP V7.0 validation cases [1]. The staring mode AOTs PHT-03 and PHT-22 in all PHT filters measure a galaxy SED which is steeply rising between 10 and 60 μm and gradually declining beyond 100 μm, hence has a very different shape than a stellar atmosphere SED. It can therefore be used for a check of the robustness of the relative filter-to-filter calibration and the color correction factors applied to modified Black Bodies in the temperature range 50 – 120 K. Arp 220 is significantly bright over the full wavelength range from 3.3 to 200 μm. Its photometric properties are discussed in detail in "Infrared spectral energy distributions of the interacting galaxies Arp 244, NGC 6240 and Arp 220" [15].

Method

We compare the background subtracted flux values of both OLP V7.0 and OLP V8.4b1 results against the IRAS photometry and a model fit based on the OLP V6.x calibration.

Results

Fig. 5.38 shows the derived SED for Arp 220. The model fit from [15] is plotted as a guide line to easier recognize the changes w.r.t. OLP V7.0. Note that this fit cannot serve as reference photometry.
We have color corrected the photometry w.r.t. modified blackbodies with emissivities $\propto \lambda^{-1}$ for the 12.8 to 200 μm range (for details, see part 2 of the evaluation log section. This color corrected SED are shown in Fig. 5.39.
We notice the following results:

- C200 photometry looks very good now. The SED in the C200 range is very smooth (note in comparison with the uncorrected photometry the importance of color correction) and the model is in fair agreement with the SED. Linearization and point spread fraction corrections for the C200 array centred photometry seem to be correctly implemented.
- C100 photometry fits at the long wavelength side, but is off at the short wavelength side, inm particular for the 60 μm point. This could be traced back to the use of a wrong CALG file (cf. SPR-2985).
- The P3 photometry is now more consistent with IRAS, the model and shows a smooth transition to the C200 range.
- The small shoulder in the 12 to 25 μm range also visible in the OLP V7.0 data is now gone. This may well be okay, however the 16 μm point appears to be too low. The 11.3 μ point appears to be more realistic now, as it should not be severly affected by absorption as the 10 μm point.
- From the PHT-S spectrum in Sect. 5.2.4 we calculate a flux density in the narrow band filters at 7.7 and 11.3 μm of 0.5 and 0.42 Jy, respectively. The PHT-P fluxes are smaller.

In Fig. 5.40 we plot the derived multi-filter surface brightness values in comparison with COBE photometry. Though not yet scientifically validated we note a very good agreement between PHT-P surface brightness values and COBE photometry, in particular the transition between P1 and P2 range is much smoother now, the only points which sticks a bit off is

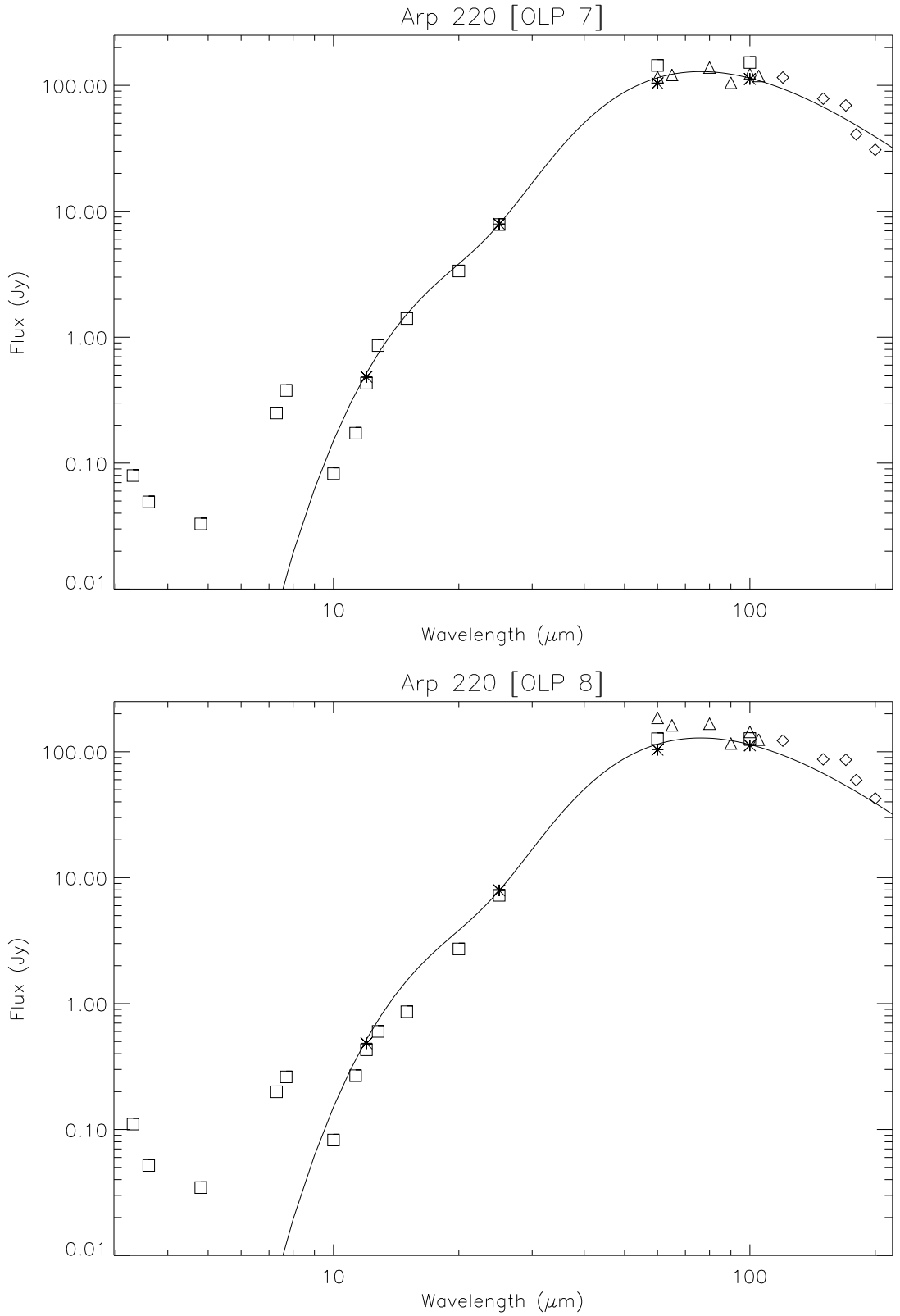

Figure 5.38: Comparison of PHT-P absolute and multi-filter photometry with the composite spectrum of Sirius (HR 2491) provided by M. Cohen and with IRAS photometry for OLP 7.0 (upper panel) and OLP 8.4b1 (lower panel). All photometric points are color corrected for a 10000 K BB. The meaning of the symbols is the following: solid line: model, asterisk: IRAS, square: PHT-P (P03 and P05 AOTs).

the 11.3 μm point (the 3.3 μm point has to be excluded from the discussion, because a fair photometry on the background in this narrow band filter cannot be performed with the selected aperture). Also the C200 surface brightness photometry looks well matched with COBE/DIRBE, for C100 surface brightness we cannoty judge due to the CALG file problem (SPR-2985). The P3 surface brightness values are too low, but have been improved with regard to OLP V7.0.

Conclusions

- We do not perform calibration accuracy assessment here due to the C100 CALG file problem (SPR-2985). Confer to the final assessment in Sect. 7.3.7.
- The C200 photometric points show a smooth distribution after color correction with a modified black body of 47 K. The upgraded point spread function fraction factors for array centred photometry appear to work very well and also the relative filter-to-filter corrections.
- The PHT-P3 photometry looks improved and is now much more consistent with IRAS and the C200 photometry.
- The P1 and P2 photometry looks reasonable. The indication of a deficiency of some 40 % of the flux in the narrow band filters at 7.7 and 11.3 μm versus PHT-S spectroscopy needs more detailed investigation summing the PHT-S fluxes over the narrow band filter bandpass.
- Surface brightness photometry looks very good for this test case, even for the non-validated PHT-P photometry.

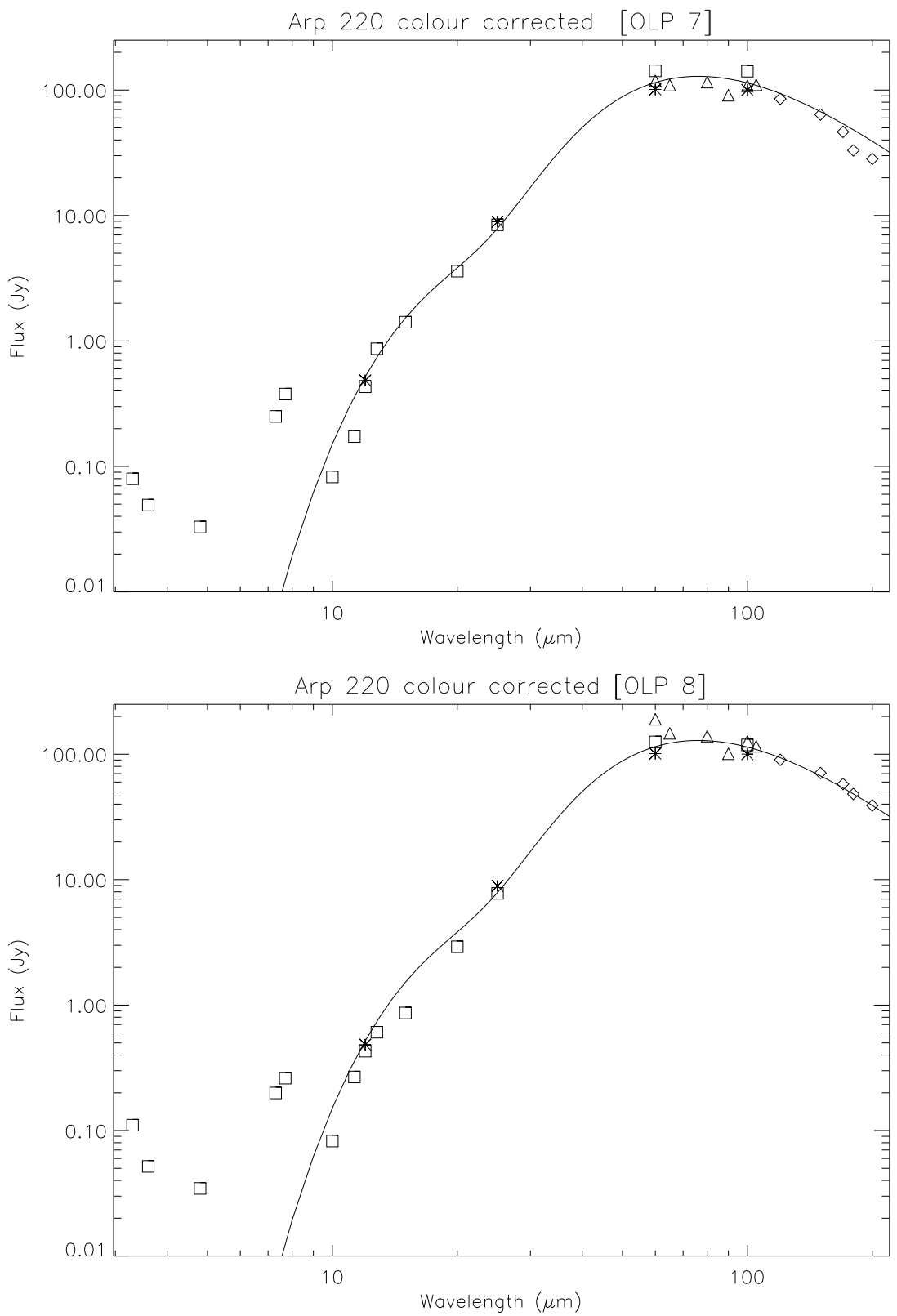

Figure 5.39: Comparison of PHT-P and PHT-C photometry, using the full ISOPHOT filter set, with IRAS photometry and the model fit as described in [8]. Note that this model fit only serves as a guide for the eye to recognize more easily the changes between the two versions. It is not an absolute photometric reference. No color correction has been applied. The meaning of the symbols is the following: solid line: model, asterisk: IRAS, square: PHT-P (P03 AOT), triangle: C100 (P22 AOT), diamond: C200 (P22 AOT).

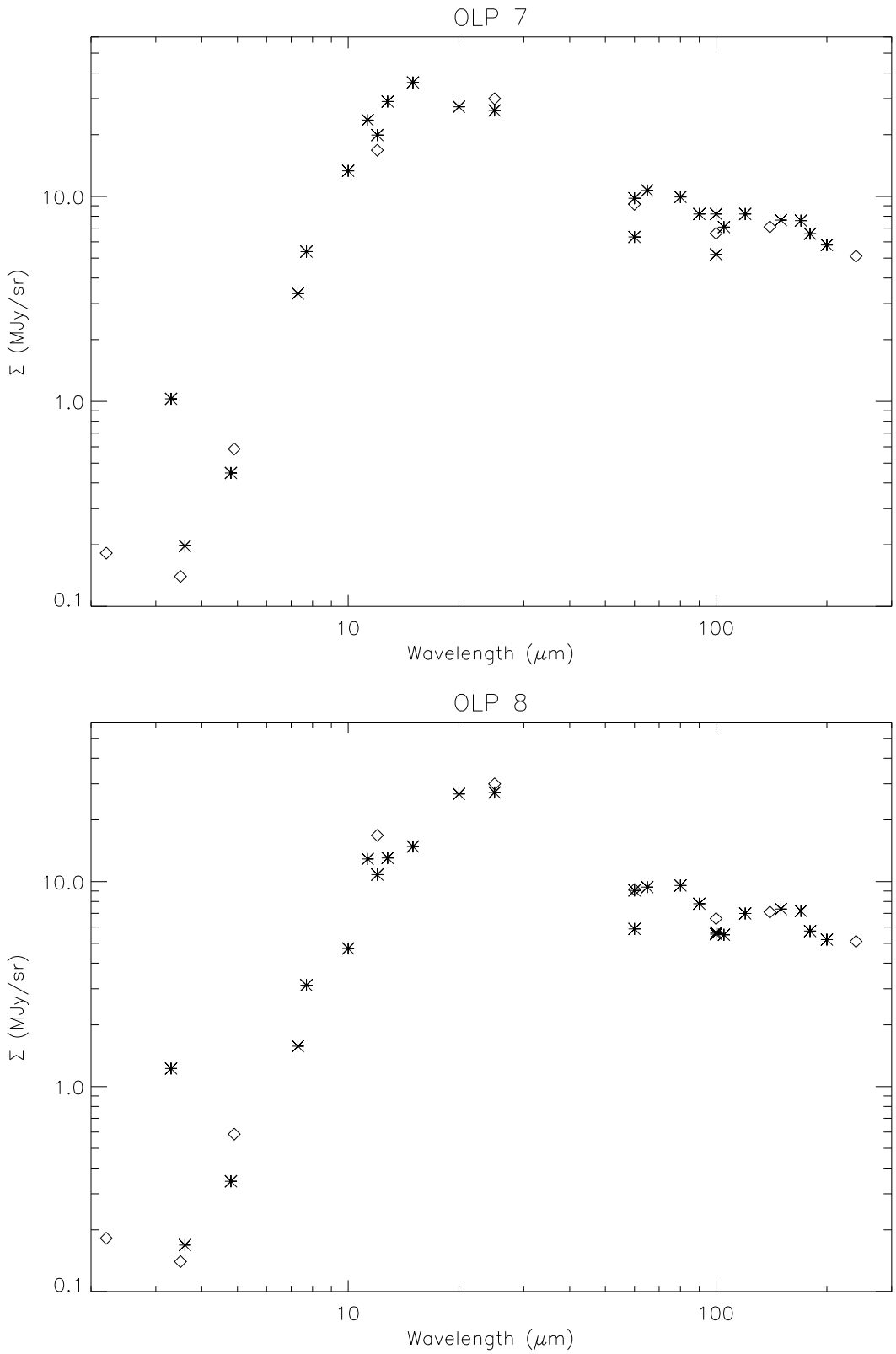

Figure 5.40: Comparison of PHT surface brightness photometry with COBE, both for OLP 7.0 and OLP 8.4b1. Asterisk: PHT-P and PHT-C photometry, diamond: COBE.

Evaluation Log

```
1) point source photometry of Arp 220 (not colour corrected)

PHT-P: ppap47600414 (src+back)   FCS: 3.3, 25, 100 um
       ppae47600413 (back)       FCS: 3.3, 20, 100 um

PHT-C: pcap47600416 (src+back)   FCS: 90, 170 um
       pcae47600415 (back)       FCS: 90, 170 um

fluxes are in Jy

Det   cwl     OLP 7     OLP 8     IRAS
P1    3.3     0.080     0.110
P1    3.6     0.049     0.052
P1    4.8     0.033     0.035
P1    7.3     0.250     0.199
P1    7.7     0.377     0.262
P1   10.0     0.082     0.082
P1   11.3     0.173     0.268
P1   12.0     0.431     0.430     0.484
P1   12.8     0.858     0.601
P1   15.0     1.407     0.862
P2   20.0     3.355     2.717
P2   25.0     7.850     7.242     7.920
P3   60.0   143.959   126.857   103.800
C1   60.0   116.112   185.894   103.800
C1   65.0   120.954   162.072
C1   80.0   138.594   166.944
C1   90.0   104.753   116.268
P3  100.0   151.866   127.363   112.400
C1  100.0   122.924   143.675   112.400
C1  105.0   118.729   124.742
C2  120.0   115.413   122.571
C2  150.0    78.419    87.091
C2  170.0    69.316    86.342
C2  180.0    40.852    59.597
C2  200.0    30.786    42.555


2) point source photometry of Arp 220 (colour corrected from 10 to 200 um)

PHT-P: ppap47600414 (src+back)   FCS: 3.3, 25, 100 um
       ppae47600413 (back)       FCS: 3.3, 20, 100 um

PHT-C: pcap47600416 (src+back)   FCS: 90, 170 um
       pcae47600415 (back)       FCS: 90, 170 um

Model: $\nu$ (B$_\nu$(50 K) + B$_\nu$(120 K))

fluxes are in Jy

Det   cwl     OLP 7     OLP 8     IRAS       Model
P1    3.3     0.080     0.110
P1    3.6     0.049     0.052
P1    4.8     0.033     0.035
P1    7.3     0.250     0.199
P1    7.7     0.377     0.262
P1   10.0     0.082     0.082
P1   11.3     0.173     0.268
P1   12.0     0.431     0.430
P1   12.8     0.867     0.608              0.746
P1   15.0     1.413     0.865              1.525
P2   20.0     3.604     2.918              3.827
```

P2	25.0	8.431	7.779	8.909	7.902
P3	60.0	142.252	125.353	101.200	114.880
C1	60.0	118.602	189.882	101.200	114.880
C1	65.0	109.362	146.539		122.541
C1	80.0	115.591	139.236		128.115
C1	90.0	90.853	100.840		122.723
P3	100.0	141.402	118.588	100.180	113.981
C1	100.0	108.113	126.363	100.180	113.981
C1	105.0	110.036	115.609		109.033
C2	120.0	85.113	90.392		93.777
C2	150.0	63.807	70.863		67.225
C2	170.0	46.458	57.870		53.793
C2	180.0	33.052	48.218		48.236
C2	200.0	28.244	39.041		39.038

3) Surface brightness photometry of Arp 220 background

cwl	OLP7 (MJy/sr)	OLP8 (MJy/sr)	COBE (MJy/sr)
3.3	1.02953	1.23	
3.6	0.197192	0.17	0.140 (3.5 mu)
4.8	0.447629	0.35	0.586 (4.9 mu)
7.3	3.35605	1.57	
7.7	5.37823	3.12	
10.0	13.3312	4.72	
11.3	23.5819	12.89	
12.0	19.9237	10.81	16.812
12.8	29.0355	13.04	
15.0	35.9734	14.83	
20.0	27.3773	26.76	
25.0	26.2661	27.21	29.992
60.0	6.33876	5.88	9.152
100.0	5.21377	5.63	6.602
TDT 47600415			
60.0	9.79199	9.05	9.152
65.0	10.6884	9.40	
80.0	9.93851	9.57	
90.0	8.21081	7.80	
100.0	7.08431	5.55	6.602
105.0	7.08431	5.50	
120.0	8.21167	6.99	
150.0	7.66279	7.34	7.104 (140 mu)
170.0	7.61650	7.19	
180.0	6.5757	5.55	
200.0	5.78939	5.21	5.111 (240 mu)

Chapter 6

Overview of Results from SVP2

During the first period of the PHT OLP 8.4 Scientific Validation the following results were achieved:

- More test cases of extended source ISOPHOT-S spectroscopy shows good agreement in absolute level and relative shape with reference spectroscopy.
- More test cases of chopped ISOPHOT-S point source spectroscopy show the very good calibration accuracy of this mode now.
- The new signal linearization correction is correcly implemented. While in many cases improvements can be seen, a few limitations and shortcomings may have been noticed which will be investigated and finetuned.
- Staring mode photometry was further consolidated, in particular P3 photometry performance was considerably improved.
- Aperture photometry from P22 raster maps yields photometric accuracies in the order of 30 to 40 %.

By the end of SVP2 the following software problem reports for updates had been recorded:

Table 6.1: Problems found during OLP 8.4 Scientific Validation Period 2

Problem	**CI**	**SPR**
Zero values in keywords of PCAP and PCAE products for AOT P22	OLP	3006
Negative uncertainty in PHT-C SPD products	OLP	3010
Scaling of the ISOPHOT default responsivity CalG files	CALG	3025
Pixel 5 instead of array averages for PHT-C100 AAR	OLP	3026
Timing problems for sawtooth chopped mode	OLP	3027
Zero RPIDs for chopped observations	OLP	3028
Asymmetry in high-contrast chopped measurements	OLP	3029
Wrong color correction factors in Cal G files PCCMBBONE and PCCMBBTWO	CALG	3179

The problem of keywords with zero values had already been noted during SVP1, see Sect. 5.4.4 for details. We confirmed with this version that the problem was not gone with the new implementation and that it affects all PCAP and PCAE products related to PHT22 AOTs:

```
all PCAP test products, check of keyword SBACK

/archive/OLP8test-II/All/PCAP06903806.FITS  P39   ST  SBACK NE 0
/archive/OLP8test-II/All/PCAP06903808.FITS  P39   ST  SBACK NE 0
/archive/OLP8test-II/All/PCAP25202511.FITS  P38   ST  SBACK NE 0
```

```
/archive/OLP8test-II/All/PCAP25202513.FITS  P38   ST  SBACK NE 0
/archive/OLP8test-II/All/PCAP35300309.FITS  P25   ST  SBACK NE 0
/archive/OLP8test-II/All/PCAP35300310.FITS  P25   ST  SBACK NE 0
/archive/OLP8test-II/All/PCAP35300312.FITS  P25   ST  SBACK NE 0
/archive/OLP8test-II/All/PCAP35602204.FITS  P22   ST  SBACK = 0
/archive/OLP8test-II/All/PCAP39200303.FITS  P37   ST  SBACK NE 0
/archive/OLP8test-II/All/PCAP39200304.FITS  P38   ST  SBACK NE 0
/archive/OLP8test-II/All/PCAP39200305.FITS  P38   ST  SBACK NE 0
/archive/OLP8test-II/All/PCAP39200306.FITS  P38   ST  SBACK NE 0
/archive/OLP8test-II/All/PCAP39200307.FITS  P38   ST  SBACK NE 0
/archive/OLP8test-II/All/PCAP39200308.FITS  P38   ST  SBACK NE 0
/archive/OLP8test-II/All/PCAP39200309.FITS  P38   ST  SBACK NE 0
/archive/OLP8test-II/All/PCAP39200310.FITS  P38   ST  SBACK NE 0
/archive/OLP8test-II/All/PCAP39200311.FITS  P38   ST  SBACK NE 0
/archive/OLP8test-II/All/PCAP39200312.FITS  P39   ST  SBACK NE 0
/archive/OLP8test-II/All/PCAP39802003.FITS  P22   ST  SBACK = 0
/archive/OLP8test-II/All/PCAP45200204.FITS  P22   ST  SBACK = 0
/archive/OLP8test-II/All/PCAP47600416.FITS  P22   ST  SBACK = 0
/archive/OLP8test-II/All/PCAP55204703.FITS  P25   ST  SBACK NE 0
/archive/OLP8test-II/All/PCAP55204907.FITS  P25   ST  SBACK NE 0
/archive/OLP8test-II/All/PCAP57901303.FITS  P25   ST  SBACK NE 0
/archive/OLP8test-II/All/PCAP57901707.FITS  P25   ST  SBACK NE 0
/archive/OLP8test-II/All/PCAP57902111.FITS  P25   ST  SBACK NE 0
/archive/OLP8test-II/All/PCAP59402203.FITS  P25   ST  SBACK NE 0
/archive/OLP8test-II/All/PCAP59402607.FITS  P25   ST  SBACK NE 0
/archive/OLP8test-II/All/PCAP62900720.FITS  P22   ST  SBACK = 0
/archive/OLP8test-II/All/PCAP62900721.FITS  P22   ST  SBACK = 0
/archive/OLP8test-II/All/PCAP65002002.FITS  P25   ST  SBACK NE 0
/archive/OLP8test-II/All/PCAP65002305.FITS  P25   ST  SBACK NE 0
/archive/OLP8test-II/All/PCAP65002608.FITS  P25   ST  SBACK NE 0
/archive/OLP8test-II/All/PCAP67100801.FITS  P22   ST  SBACK = 0
/archive/OLP8test-II/All/PCAP67100802.FITS  P22   ST  SBACK = 0
/archive/OLP8test-II/All/PCAP67100910.FITS  P22   ST  SBACK = 0
/archive/OLP8test-II/All/PCAP67100911.FITS  P22   ST  SBACK = 0

all PCAE test products, check of keyword SBBRT

/archive/OLP8test-II/All/PCAE06903805.FITS  P37   ST  SBBRT NE 0
/archive/OLP8test-II/All/PCAE06903807.FITS  P37   ST  SBBRT NE 0
/archive/OLP8test-II/All/PCAE25202509.FITS  P37   ST  SBBRT NE 0
/archive/OLP8test-II/All/PCAE25202510.FITS  P38   ST  SBBRT NE 0
/archive/OLP8test-II/All/PCAE25202512.FITS  P38   ST  SBBRT NE 0
/archive/OLP8test-II/All/PCAE25202514.FITS  P39   ST  SBBRT NE 0
/archive/OLP8test-II/All/PCAE35300307.FITS  P25   ST  SBBRT NE 0
/archive/OLP8test-II/All/PCAE35300308.FITS  P25   ST  SBBRT NE 0
/archive/OLP8test-II/All/PCAE35300311.FITS  P25   ST  SBBRT NE 0
/archive/OLP8test-II/All/PCAE35602203.FITS  P22   ST  SBBRT = 0
/archive/OLP8test-II/All/PCAE39802002.FITS  P22   ST  SBBRT = 0
/archive/OLP8test-II/All/PCAE45200203.FITS  P22   ST  SBBRT = 0
/archive/OLP8test-II/All/PCAE47600415.FITS  P22   ST  SBBRT = 0
/archive/OLP8test-II/All/PCAE55204702.FITS  P25   ST  SBBRT NE 0
/archive/OLP8test-II/All/PCAE55204906.FITS  P25   ST  SBBRT NE 0
/archive/OLP8test-II/All/PCAE57901302.FITS  P25   ST  SBBRT NE 0
/archive/OLP8test-II/All/PCAE57901606.FITS  P25   ST  SBBRT NE 0
/archive/OLP8test-II/All/PCAE57902010.FITS  P25   ST  SBBRT NE 0
/archive/OLP8test-II/All/PCAE59402102.FITS  P25   ST  SBBRT NE 0
/archive/OLP8test-II/All/PCAE59402506.FITS  P25   ST  SBBRT NE 0
```

The keyword problem was fixed and the fix confirmed with OLP V8.6.
The error in calculating the color correction factors for modified black bodies was discovered late, but could still be taken into account for Version 2.0 of this report by applying the correct factors to the OLP V8 results; OLP V7 results remained unchanged, hence are wrong for modified BB SEDs.

Chapter 7

Revalidation Tests during SVP2

7.1 Upgrade of PHT-S Spectral Response Function for Extended Sources

An overview of the test cases is outlined in Ref. [4], chapter 3.1.1.

7.1.1 References to Calibration Analysis and Software Change Documentation

- calibration report:
  - ISOPHOT Footprints and Near-Field Straylight: S - Re-analysis of cross scans to extract measured footprint and associated parameters[5]
- Software Problem Report: SPR 2793

7.1.2 Summary of Results

- The test cases of this section and of Sect. 5.1 demonstrate that the absolute flux levels are consistent with reference photometry (COBE/DIRBE) and spectroscopy.
- Some inconsitencies in the relative shapes may be removed by the introduction of the dynamic response calibration, being capable to cope with transient effects, with OLP V9.0.

7.1.3 ISOPHOT-S Spectroscopy of the Extended HII Region M17

- authors: K. Wilke, U. Klaas
- date: 28-July-1999
- SVP period 2

Motivation

M17, a bright HII region in combination with a Molecular Cloud, is a good example exhibiting pronounced PAH features in combination with narrow ionic lines. The extended source has been observed at several positions with ISO-SWS and been mapped by ISOCAM-CVF.

Method

We compare the ISOPHOT-S extended source spectrum in $W/m^2/\mu m/sr$ with the ISO-SWS spectrum by Verstraete et al. [16], fig. 2 therein, and the ISOCAM-CVF spectra by Cesarsky et al. [17], fig. 2 therein, both converted to the above unit. It has to be emphasized that the position of the ISOPHOT-S spectrum does not coincide either with one of the positions along the scan as presenetd by Verstrate et al. nor with the three spectra displayed from the CAM-CVF map by Cesarsky et al. The position of the ISOPHOT-S spectrum lies somewhat south of the scan performed with SWS and south-east of the connecting line between positions 1 and 3 of the CAM-CVF spectra. It should, however, be possible to construct the spectrum from the CAM-CVF map at the ISOPHOT-S position. Therefore, the comparison of abolute levels and also relative feature strength is rather limited in such a complex object as M17 and we will restrict our analysis to qualitative comparison. It should be noted that no background subtraction was performed for the ISOPHOT-S measurement, as is the case for the other spectra.

Results

Fig. 7.1 shows the comparison of the ISOPHOT-S spectrum with the HII-region spectrum obtained with SWS. In the ISOPHOT-S spectrum the PAH features are much more pronounced relative to the continuum and there seems to be some silicate absorption at $9.7\,\mu m$ which is not seen in the SWS spectrum. We note the existence of the narrow forbidden lines of [ArII]7.0, [ArIII]9.0 and [SIV]10.5 as a signature of the HII region. The narrow ionic lines become much clearer visible in the continuum subtracted SWS spectrum (Fig. 7.2).
Fig. 7.3 shows the comparison with the CAM-CVF spectrum on an HII-region like area. Again in the ISOPHOT-S spectrum the PAH features are more pronounced and the absorption trough at $9.7\,\mu m$ is not seen in the CVF spectrum. The forbidden lines show up in the CVF spectrum as somewhat broader features due to the smaller spectral resolution. The ultra-compact HII-region (Fig. 7.4) is much brighter and all features are washed out in the CVF spectrum. This CAM position is farthest away from the ISOPHOT-S position.
Fig. 7.5 compares the ISOPHOT-S spectrum with the SWS spectrum of the Molecular Cloud position. This SWS position is also relative far away (to the west into the MC) from the ISOPHOT position. While now the relative strength of the PAH features resemble better, the SWS spectrum does not show any narrow lines any more and is much weaker in total flux.
The closest correspondence of the ISOPHOT-S spectrum is with the CVF spectrum of the molecular cloud position, cf. Fig. 7.6.

Conclusions

- A quantitative analysis of the ISOPHOT-S spectrum of the extended nebula M17 was not possible due to different pointings of the published spectra.
- A quite good correspondence in absolute level and relative line shape with a CAM-CVF spectrum at the closest position argues for a reasonable calibration of both spectra.
- This comparison can be improved, as the CAM-CVF map contains the ISOPHOT-S position and a CAM-CVF spectrum for this specific pointing can be generated.

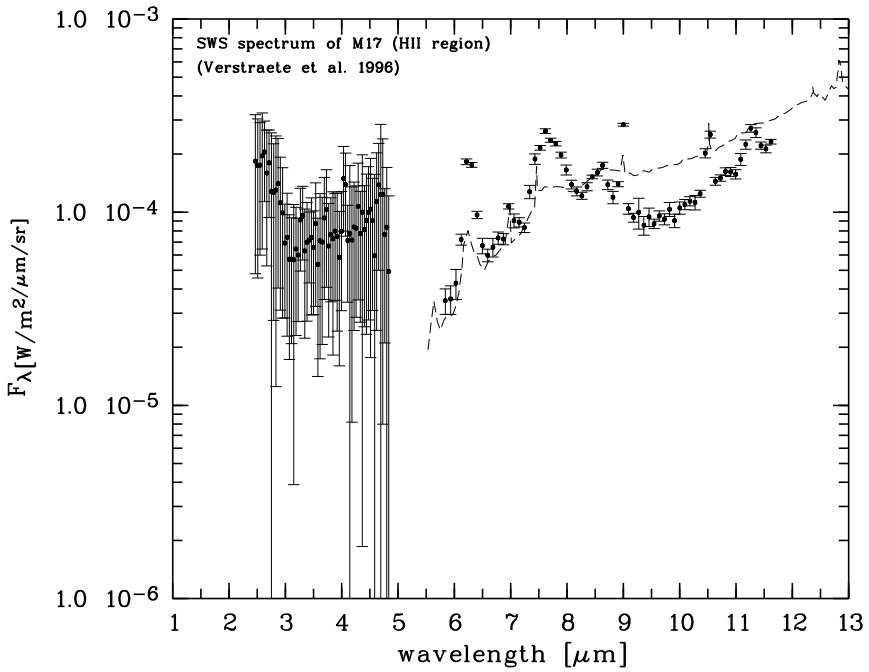

Figure 7.1: Comparison of the ISOPHOT-S spectrum of M17 with the HII region spectrum obtained by Verstraete et al. 1996 (figure 2a therein).

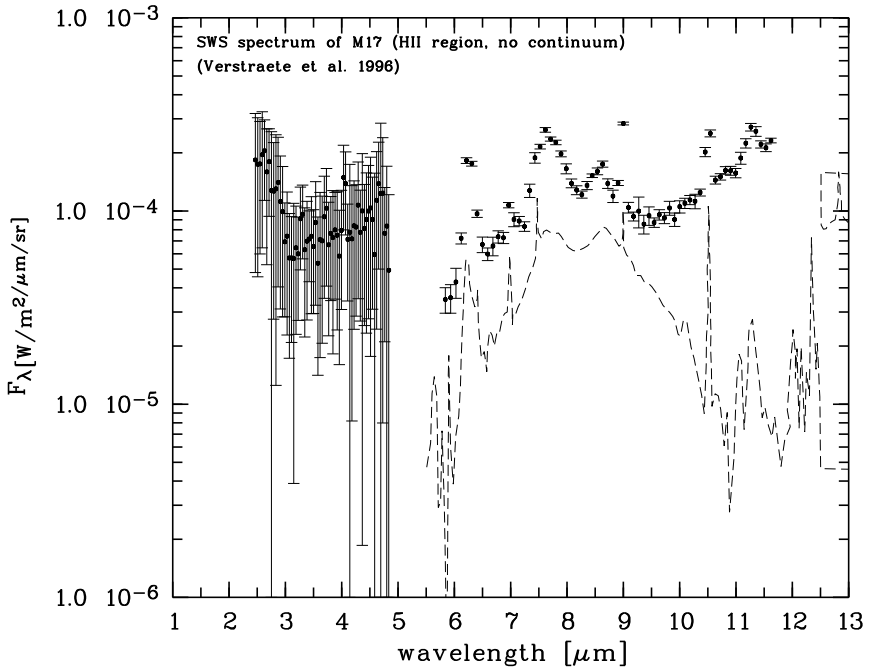

Figure 7.2: Comparison of the ISOPHOT-S spectrum of M17 with the HII region spectrum with no continuum presented by Verstraete et al. 1996 (figure 2b therein).

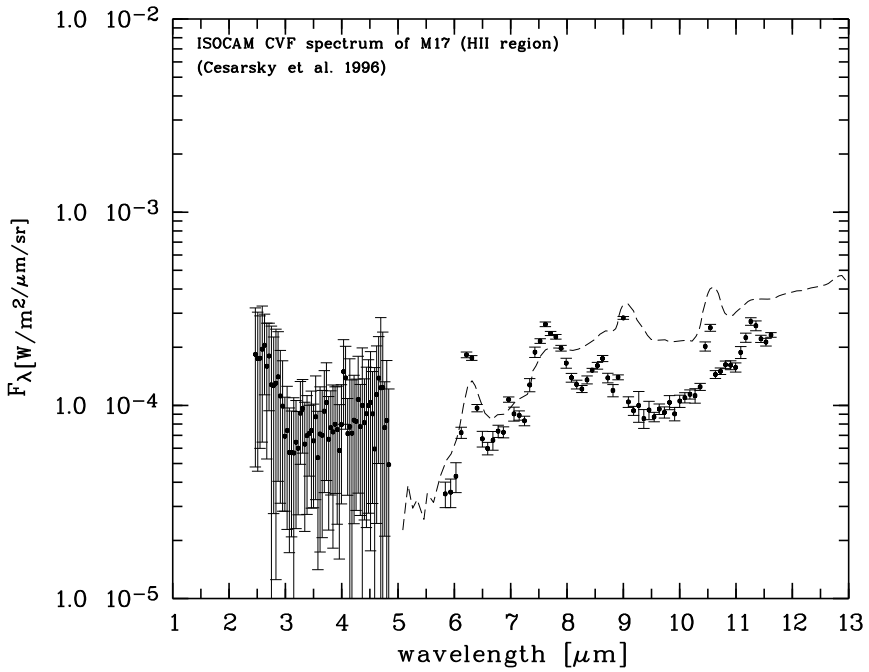

Figure 7.3: Comparison of the ISOPHOT-S spectrum of M17 with the HII region spectrum obtained by Cesarsky et al. 1996 on position 1 (figure 2 therein).

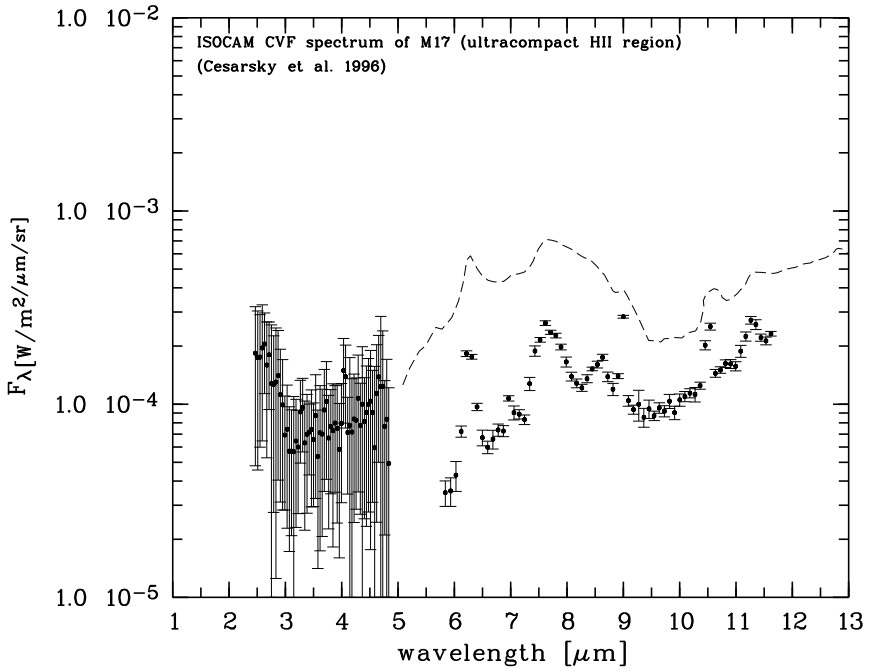

Figure 7.4: Comparison of the ISOPHOT-S spectrum of M17 with the ultra-compact HII region spectrum obtained by Cesarsky et al. 1996 on position 2 (figure 2 therein).

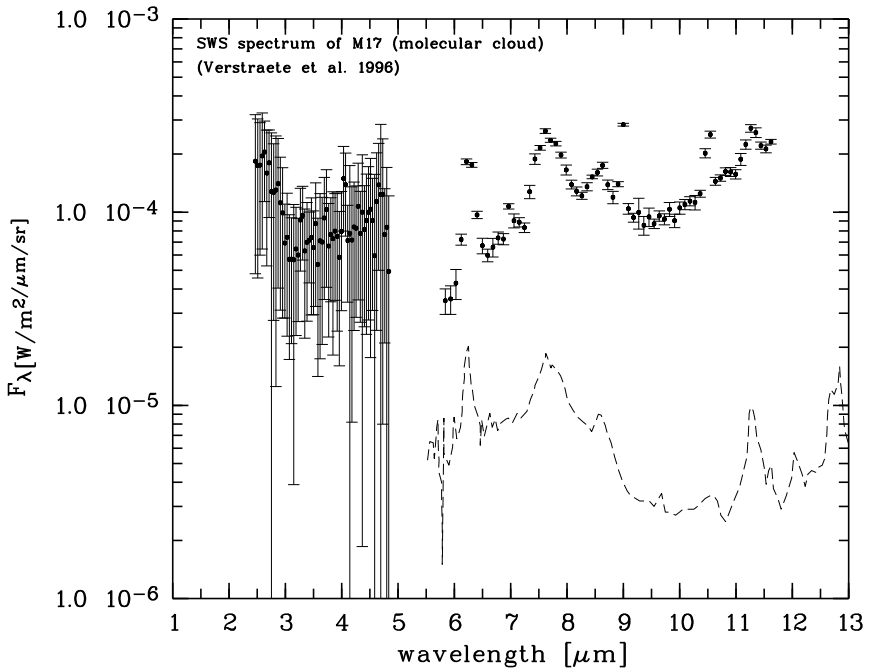

Figure 7.5: Comparison of the ISOPHOT-S spectrum of M17 with the Molecular Cloud spectrum obtained by Verstraete et al. 1996 (figure 2d therein).

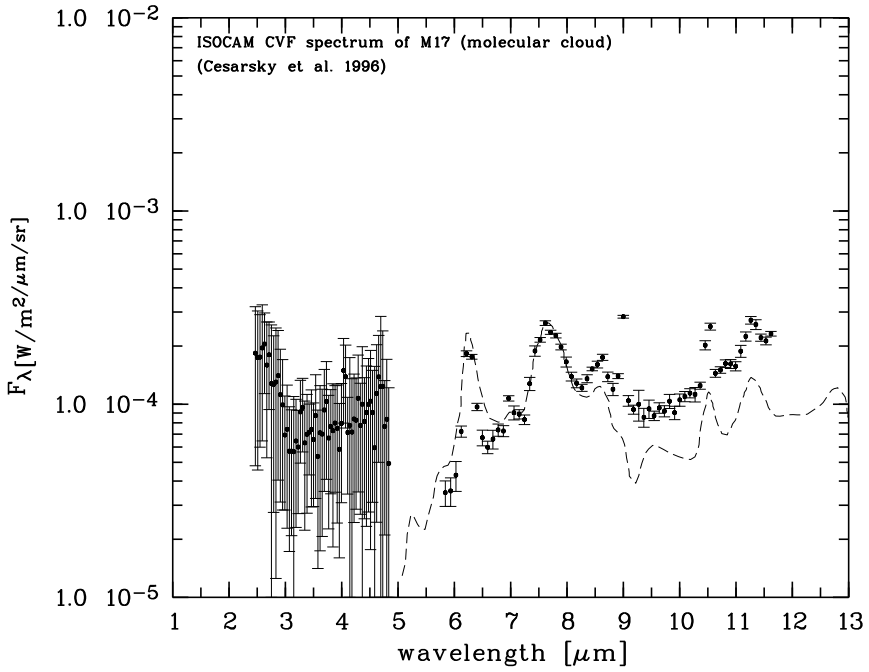

Figure 7.6: Comparison of the ISOPHOT-S spectrum of M17 with the Molecular Cloud spectrum obtained by Cesarsky et al. 1996 on position 3 (figure 2 therein).

7.1.4 Absolute Surface Brightness Spectrum of the Zodiacal Light

- authors: K. Wilke, U. Klaas
- date: 29-July-1999
- SVP period 2

Motivation

The plain Zodiacal Light background can be compared to COBE/DIRBE absolute photometry, as there should be no impact by the very different beam sizes.

Method

We compare the ISOPHOT-S extended source spectrum of the Zodiacal Light from a position in the ecliptic plain at an ecliptic longitude of 66 degrees against the COBE/DIRBE photometry from annnual maps.

Results

Fig. 7.7 shows the ISOPHOT-S spectrum (this time without error bars). For the short wavelength channel the detection limit is reached and the extremely low flux in the cosmological window is not measurable with the comparably small aperture of ISOPHOT-S. The long wavelength channel shows well detected flux over the full wavelength range. This is a measurement of one of the faintest sources ($4\ 10^{-7}\,\mathrm{W\,m^{-2}\,\mu m^{-1}\,sr^{-1}}$ at $5.8\,\mu$m corresponds to $4.5\,\mathrm{MJy\,sr^{-1}}$) performed with ISOPHOT-S. We see that the ISOPHOT-S spectrum fits nicely between the COBE/DIRBE photometric data points at 4.9 and $12\,\mu$m.

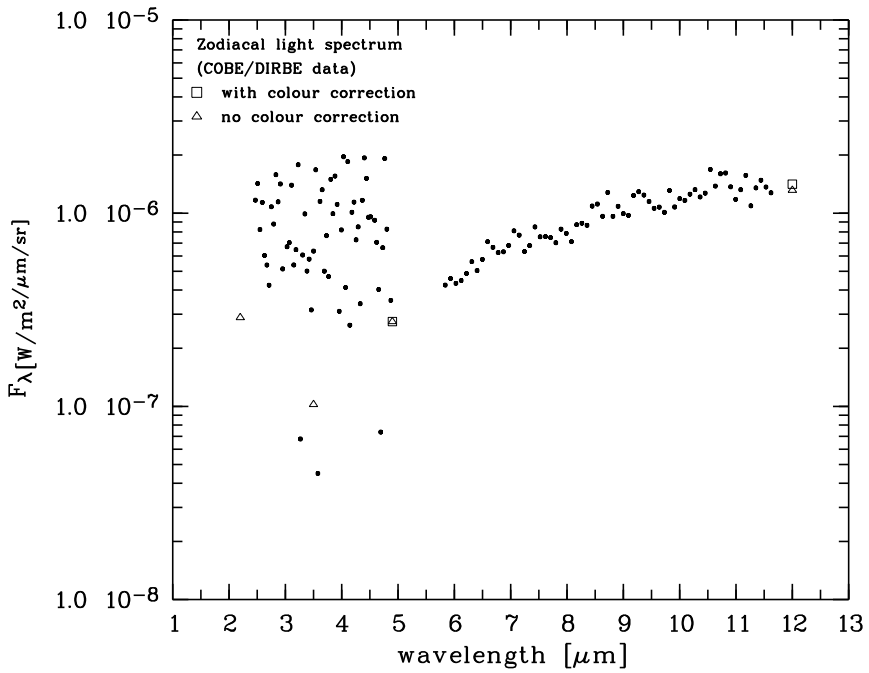

Figure 7.7: Comparison of the ISOPHOT-S spectrum of the Zodiacal Light on a position in the ecliptic plane at minimum ecliptic longitude (close to ISO Sun constraint) with COBE/DIRBE photometry. For colur correction of the COBE/DIRBE data points a 260 K BB has been assumed.

Conclusions

- The absolute level and relative shape of an ISOPHOT-S spectrum of the Zodiacal Light agrees very well with COBE/DIRBE photometry at 4.9 and $12\,mu$m.

- The abolute calibration is accurate for this very low surface brightness level ($4\ 10^{-7}\,\mathrm{W\,m^{-2}\,\mu m^{-1}\,sr^{-1}}$ at $5.8\,\mu\mathrm{m}$ corresponds to $4.5\,\mathrm{MJy\,sr^{-1}}$)

7.1.5 Diffuse Emission of the Galactic Disk

- authors: K. Wilke, U. Klaas
- date: 03-August-1999
- SVP period 2

Motivation

As part of the Central Program spectrophotometry of the UIR bands was performed at various positions along the Galactic plane [23]. Also with IRTS/MIRS spectra of the UIR bands in the diffuse Galactic light were taken [24].

Method

We compare the ISOPHOT-S extended source spectrum of the diffuse Galactic light at the position l = 45 deg and b = 0 deg with the IRTS/MIRS result at l = 50 deg (Fig. 1b in [24]).

Results

Fig. 7.8 shows the result of this comparison. There is a good agreement in absolute level with the b = 0 deg IRTS/MIRS spectrum with regard to the UIR bands at 6.2 and 7.7 μm. The IRTS spectrum indicates the presence of a silicate absorption feature which is not confirmed by any of the four ISOPHOT-S spectra. Whether this is a calibration issue or could be due to change of the physical properties within 5 deg of the Galactic plane needs further investigation.

Conclusions

- For the diffuse Galactic UIR band emission good consistency with IRTS/MIRS is found for the absolute level of the extended source spectrum for the 6 - 9 μm range.
- Beyond 9 μm the IRTS spectrum shows a silicate absorption feature which is not reproduced by none of the four ISOPHOT-S spectra. Whether this is a calibration issue or could be due to change of the physical properties within 5 deg of the Galactic plane needs further investigation.

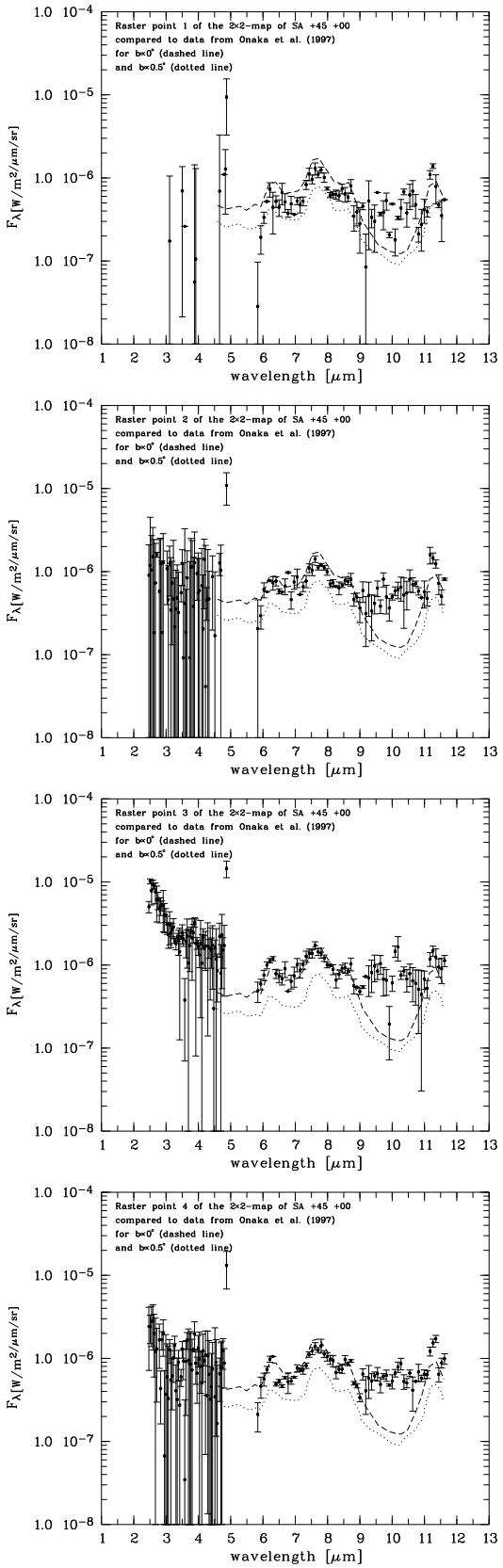

Figure 7.8: Comparison of the ISOPHOT-S spectrum of the diffuse Galactic light at the position l = 45 deg and b = 0 deg from 4 raster positions of a 2x2 raster, with 24 arcesc separation between the raster points (corresponding to the aperture size of ISOPHOT-S), with IRTS/MIRS spectrum for l = 50 deg, b = 0 deg and b = 0.5 deg.

7.2 Dedicated Spectral Response Function for Chopped PHT-S Measurements

An overview of the test cases is outlined in Ref. [4], chapter 3.1.2.

7.2.1 References to Calibration Analysis and Software Change Documentation

- calibration report:
  - Calibration of ISOPHOT-S Chopped Measurements [9]
- Software Change Request: SCREW 380

7.2.2 Summary of Results

- The additional test cases from SVP2 confirm the good absolute and relative accuracy derived from SVP1 test cases (cf. Sect. 5.2).

7.2.3 MIR Spectra of the Stars HD 23763, HR 7428 and HD 23441 from Chopped PHT-S Measurements

- authors: K. Wilke, U. Klaas
- date: 30-July-1999
- SVP period 2

Motivation

We found three star in the data base with similar spectral type as standard star but different brightness. It is therefore possible to test absolute and relative accuracy of the new ISOPHOT-S chopped calibration on differen brightness levels than standard stars used to establish the calibration. The properties of the three stars are compiled in Table 7.1:

Table 7.1: Properties of stars used for verification of chopped ISOPHOT-S spectra

Name	**Spectral Type**	**Apparent Brightness** (mag)	**Comment**	**Reference Star**	**Spectral Type**	**Apparent Brightness** (mag)
HD 23763	A1V	m_k = 6.567		Sirius (HR 2491)	A1V	m_k = -1.39
HR 7428	K2II-III+A0V	m_v = 6.37	RS CVn binary	HR 6688	K2III	m_v = 3.747
(HD 184398)	Sp(IR) K2II-III Ca-					
HD 23441	A0Vn	m_v = 6.43	Pleiades 859	Vega (HR 7001)	A0V	m_v = 0.033

For a reference of the spectral types of HR 7428, cf. [20], and of HD 23441, cf. [22]. HR 7428 has an IRAS 12 μm flux of 1.82 Jy, cf. [21] (=1.26 Jy for T=4000 K BB).

Method

Scale the model spectra of Sirius, HR 6688 and Vega according to the apparent brightness ratio in the K or V band. Compare the absolute fluxes and relative shapes of the ISOPHOT-S spectra with the scaled model spectra.

Results

Figs. 7.9 to 7.11 show the comparison of the measurement with the scaled model predictions. Below $6\,10^{-15}$ W m^{-2} μm^{-1} the scatter of the data points becomes very high. Above this flux level the agreement of measurement and model prediction is very good. For HR 7428 the match of the spectral classification with the spectrum of the reference star is least good, and here we see a systematic offset. Whether this is related to calibration accuracy, accuracy of the apparent brightness ratio or systematic flux difference of the slightly different spectral types remains open. Its 12 μm flux of 1.26 Jy corresponds to $2.63\,10^{-14}$ W m^{-2} μm^{-1} which fits very well with the extrapolation of the ISOPHOT-S spectrum.

Conclusions

- We find a very good agreement between ISOPHOT-S chopped measurement spectra and model SEDs of stars with known spectral type and apparent V or K magnitude above flux levels of $6\,10^{-15}$ W m^{-2} μm^{-1} (corresponding to 130 mJy at 8 μm).
- From this test case set we can conclude that the new chopped spectral response function also works for staring mode.
- With the assumption that the offset between the HR 7428 spectrum and the model prediction is totally accounted for by a calibration uncertainty, then the absolute calibration accuracy is still better than 10,%. The relative shape of the spectra indicates a relative accuracy which is much better than 10 % for these stars.

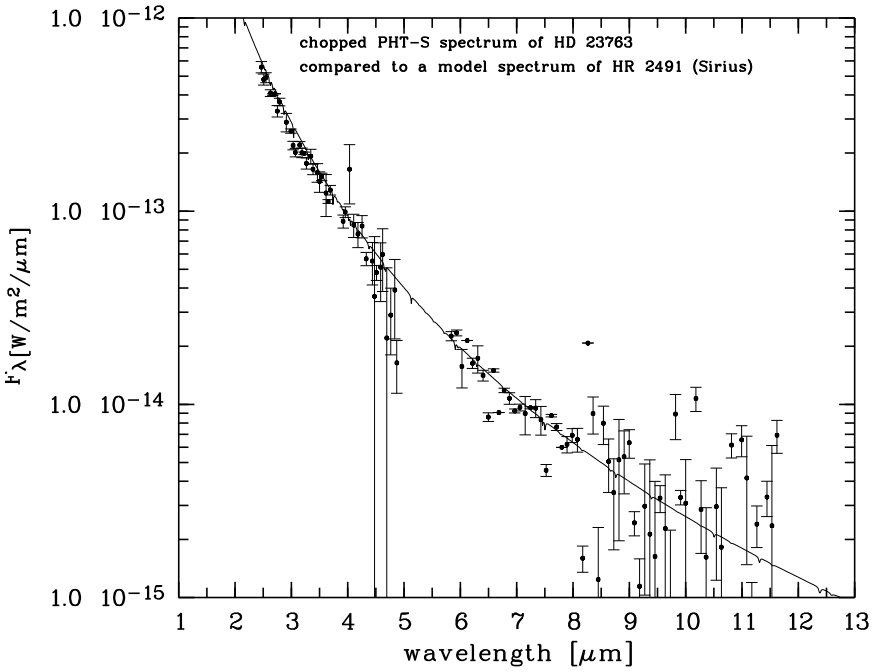

Figure 7.9: Comparison of the spectrum of the A1V star HD 23763 obtained in PHT-S sawtooth chopped mode with the model of Sirius scaled with the K-magnitude ratio of (6.567 mag / -1.39 mag).

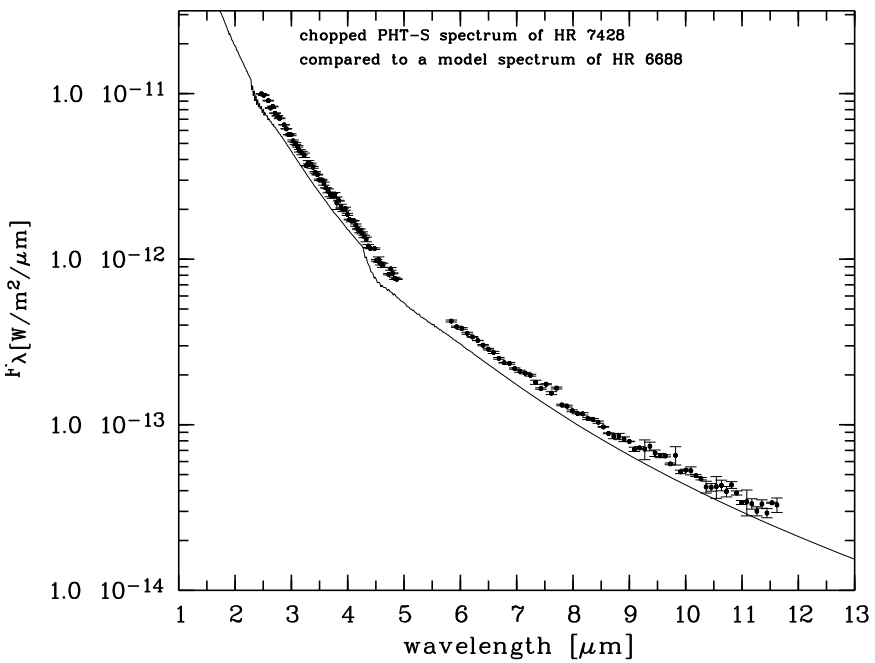

Figure 7.10: Comparison of the spectrum of the RS CVn binary HR 7428 (spectral type: K2II-III+A0V) obtained in PHT-S rectangular chopped mode with the model of HR 6688 (spectral type: K2III) scaled with the V-magnitude ratio of (6.37 mag / 3.747 mag).

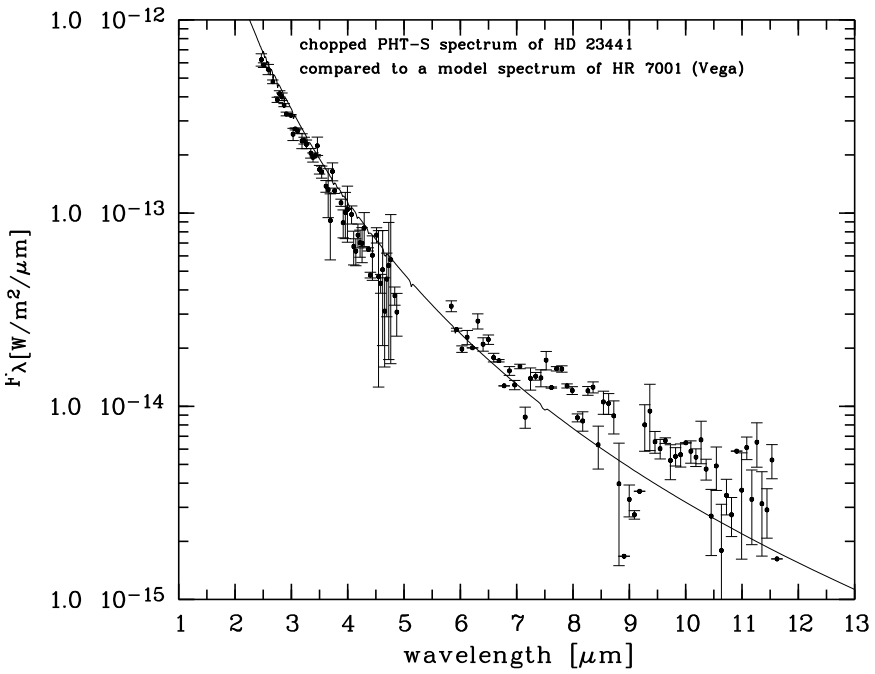

Figure 7.11: Comparison of the spectrum of the A0Vn star HD 23441 obtained in PHT-S sawtooth chopped mode with the model of Vega scaled with the V-magnitude ratio of (6.43 mag / 0.033 mag).

7.3 Revalidation of Staring Mode Photometry

An overview of the test cases is outlined in Ref. [4], chapter 3.2, with those cases foreseen for verification of implementations w.r.t. SCREWs 366, 367 and 368.

7.3.1 References to Calibration Analysis and Software Change Documentation

- calibration reports:
  - Linearization of ISOPHOT-P and -C detector signals in OLP8 [30]
  - Point Spread Function Fractions Related to the ISOPHOT C100 and C200 Arrays [10]
- Software Change Requests: SCREWs 366, 367, 368
- Software Problem Reports: SPR 2894, 2970, 2979, 2985

7.3.2 Summary of Results

- The major and most risky change with regard to staring mode photometry upgrades, the flux dependent signal linearization, was successfully implemented. Improved faint source flux determination in on-off measurements is put down to this calibration upgrade.
- C200 array centred photometry uses now the right and even improved point spread function correction factors.
- Improved performance in absolute and relative calibration accuracy is found, in particular for P1, P3, and C200 detectors.

7.3.3 General Re-validation of PHT03 and PHT22 Staring Mode: The SED of α Bootes (HR 5340) - Final Assessment

- authors: M. Radovich, U. Klaas
- date: 21-July-1999
- SVP period 2

Motivation

This is the final calibration accuracy assessment and a repetition of the assessment performed for SVP1, cf. Sect. 5.4.3 to check for changes.
TDTs 45200201(background, PHT-P), 45200202(α Boo, PHT-P), 45200203(background, PHT-C), 45200204(α Boo, PHT-C) is one of the key OLP V7.0 validation cases [1]. The staring mode AOTs PHT-03 and PHT-22 use all available PHT filters (but the 3.6 and 4.85 μm filters had to be excluded from the analysis, because the source saturates the measurement) on a stellar (declining) SED. α Bootes is one of the most important stellar PHT calibration standards and there are detailed models available from M. Cohen (composite spectrum from 1 to 35 μm and extrapolations to 300 μm). This test case is very suitable for a test of both the absolute calibration and the relative filter-to-filter calibration. It should be noted that this multi-filter measurement was not used for the establishment of the FCS calibration curve. During the OLP 7.0 validation the establishment of reliable C200 photometry failed due to a by far too strong background subtraction. Therefore, this "on-off" observation with independent FCS calibration for on-source and off-source measurement is considered an excellent test case for the linearization correction introduced by SCREW 366.

Method

We compare the background subtracted, color corrected flux values of both OLP V7.0 and OLP V8.4b3 results against the model prediction.

Results

In the following Tab. 7.2 we compare the photometry from part 1 of the evaluation log section with the model. We estimate the absolute photometric accuracy per detector assembly for this target as the deviation from the model flux in the filter in which the FCS calibration was done, and the relative filter-to-filter accuracy as the peak-to-peak variation of the other filters around this offset. Note that for P1 the FCS calibration was actually done in the 3.6 μm filter, but for this filter the sky measurement is heavily saturated. The photometric accuracies are presented in Tab. 7.3. Fig. 7.12 shows the PHT photometric data points in comparison to the model and IRAS photometry (color corrected) from 3.3 to 200 μm for OLP 7.0 and OLP 8.4b3, respectively.
During the OLP 7 validation [1] no reliable C200 photometry could be achieved. It showed a negative photometric bias with a relative underestimate of the total source plus background flux versus the individually calibrated background flux. What can be seen from the OLP 8.4b3 results is that now reasonable photometry is achieved out to 170 μm, only the two longest wavelength filters show again the fall-off, but less drastic, only by approximately 30 %. It should be noted that for this simple on-off measurement the exact determination of the background may be critical. In Table 7.4 the source-to-background contrast (background flux in Jy is calculated according to the following formula: $F(Jy)_{back} = 1/f_{psf}$ * I(MJy/sr) * (1 - ε^2) * Omega * n_{pix}). At 105 μm the source flux is comparable with the background flux (1:0.93). From 120 to 200 μm the background becomes more and more dominant (from 1.9:1 to 5.1:1). While in the previous OLP 7 version staring off/on photometry became unreliable for source-to-background ratios below 1:1.3 (0.75) the flux dependent linearity correction brings this now down to source fluxes as faint as 1:4 (0.25).
Part 2 of the evaluation log section and Fig. 7.13 provide the surface brightness photometry of the background position and the comparison with COBE. From Table 7.5 it can be seen that the consistency with COBE has improved to within 10 % for 60 μm where the COBE photometry has very small uncertainties, but for 100 μm the consistency has degraded to 40 %. For 150 and 200 μm one has to have in mind that COBE photometry has an higher

Table 7.2: Consistency check of photometric results with HR 5340 model

Filter	**consistency w.r.t. model OLP V7.0** [%]	**consistency w.r.t. model OLP V8.4b3** [%]
3.3	+8.6	+0.0
7.3	+14.9	+8.5
7.7	+13.6	+4.4
10	+11.0	-6.0
11.3	-3.3	+0.5
12	+24.1	+7.4
12 IRAS	+10.1	+10.1
12.8	+6.9	-12.2
16	-7.5	+17.4
20	-0.1	+1.4
25	+4.5	+7.3
25 IRAS	-2.3	-2.3
60 PHT-P	+9.9	-11.5
60 PHT-C	+0.2	+3.4
60 IRAS	-6.6	-6.6
65	-2.0	+2.7
80	+7.6	+5.0
90	-3.7	-1.9
100 PHT-P	+29.3	-9.3
100 PHT-C	-0.04	-4.8
100 IRAS	-3.6	-3.6
105	-4.3	-11.4
120	-27.8	-11.4
150	-41.9	-8.8
170	-53.6	-7.0
180	-78.4	-34.9
200	-78.8	-33.6

Table 7.3: Absolute and relative calibration accuracies per detector achieved for HR 5340 observation with OLP V8.4b3

detector	**absolute accuracy** [%]	**relative accuracy** [%]
P1	< 1 at 3.3 μm	17
P2	< 2 at 20 μm	6
P3	12 at 60 μm	3
C100	< 2 at 90 μm	10
C200	7 at 170 μm	30
		< 5 for $\lambda <$170 μm

uncertainty itself and seeing the trend of the ISOPHOT background fluxes the COBE 240 μm point is expected to lie at a lower level than the ISOPHOT 200 μm point.

Conclusions

- For the flux levels covered by α Boo and its background the flux dependent signal linearization appears to work properly. This seems to be the explanation that now C200 multi-filter photometry becomes possible.

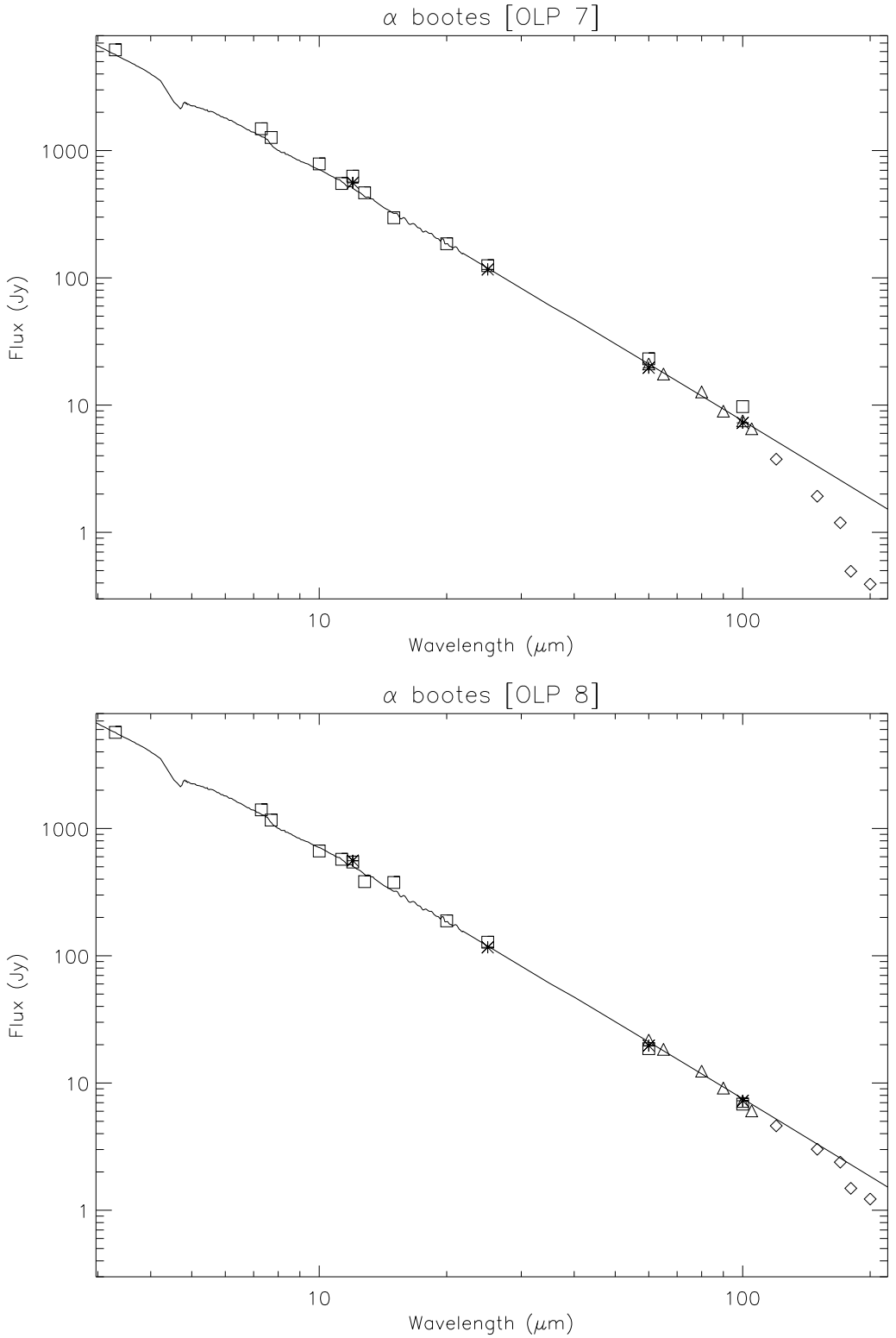

Figure 7.12: Comparison of PHT-P and PHT-C photometry, using the full ISOPHOT filter set, with the composite spectrum and out to 300 μm extrapolated SED of α Boo (HR 5340) provided by M. Cohen and with IRAS photometry for OLP 7.0 (upper panel) and OLP 8.4b3 (lower panel). All photometric points are color corrected for a 4000 K BB. The meaning of the symbols is the following: solid line: model, asterisk: IRAS, square: PHT-P (P03 AOT), triangle: C100 (P22 AOT), diamond: C200 (P22 AOT).

Table 7.4: Source-to-background contrast for α Bootes in FIR filters. The expected source flux is the model flux, the background flux is from the background measurement converted to Jy as decribed in the text.

λ_c [μm]	**background flux** [Jy]	**expected source flux** [Jy]	**source-to-backgr. contrast**
60	8.02	21.03	2.62 (1:0.38)
65	10.87	17.91	1.65 (1:0.61)
80	7.24	11.80	1.63 (1:0.61)
90	5.29	9.30	1.76 (1:0.57)
100	6.43	7.52	1.17 (1:0.85)
105	6.37	6.81	1.07 (1:0.93)
120	11.50	5.20	0.45 (1:2.2)
150	10.85	3.31	0.31 (1:3.2)
170	11.27	2.57	0.23 (1:4.4)
180	8.78	2.29	0.26 (1:3.9)
200	7.56	1.85	0.24 (1:4.2)

- The new C200 array PSF factors for centering the source on the array appear to work properly, too.
- PHT photometry gives a good representation of the SED from 3.3 to 170 μm.
- For P1 and P2 the absolute and relative calibration accuracies are very similar for OLP 8.4b3 and OLP 7.0. For P3 the relative accuracy could be improved to better than 10 %. The degradance of the C100 relative filter-to-filter accuracy found during SVP1 is explained by the use of the wrong CALG file (SPR-2985). The relative C100 filter-to-filter calibration achieved with version 8.4b3 is as good as OLP 7.0. For C200 absolute and relative filter-to-filter accuracies could be determined for the first time, giving 10 % absolute accuracy and approximately 30 % relative filter-to-filter accuracy for all C200 filters used, but due to a systematic bias (see below). The relative filter-to-filter accuracy is better than 5 % for the filters shortward of 170 μm.
- With regard to OLP V7.0 the C200 multi-filter photometry is drastically improved. Proper background subtraction is still crucial for the two longest wavelengths at 180 and 200 μm which give a too low flux by approximately 30 %. This occurs for source-to-background ratios below 1:4 (0.25).
- For 60 and 100 μm the consistency with COBE annual map photometry is now within 10%. For 100 μm is now less good (from 30% to 40%. Overall, the distribution looks more scattered than the one from OLP 7.0 and also the one from OLP 8.4b1. In particular the 65 μm point sticks out drastically. This should be followed up, on the

Table 7.5: Consistency check of α Boo background position surface brightness results with COBE/DIRBE annual maps.

wavelength μm	**consistency w.r.t. COBE OLP V7.0** [%]	**consistency w.r.t. COBE OLP V8.4b3** [%]
60	+20.0	+10.5
100	+29.5	+38.8
150	-19.8	-19.0
200	+41.4	+33.5

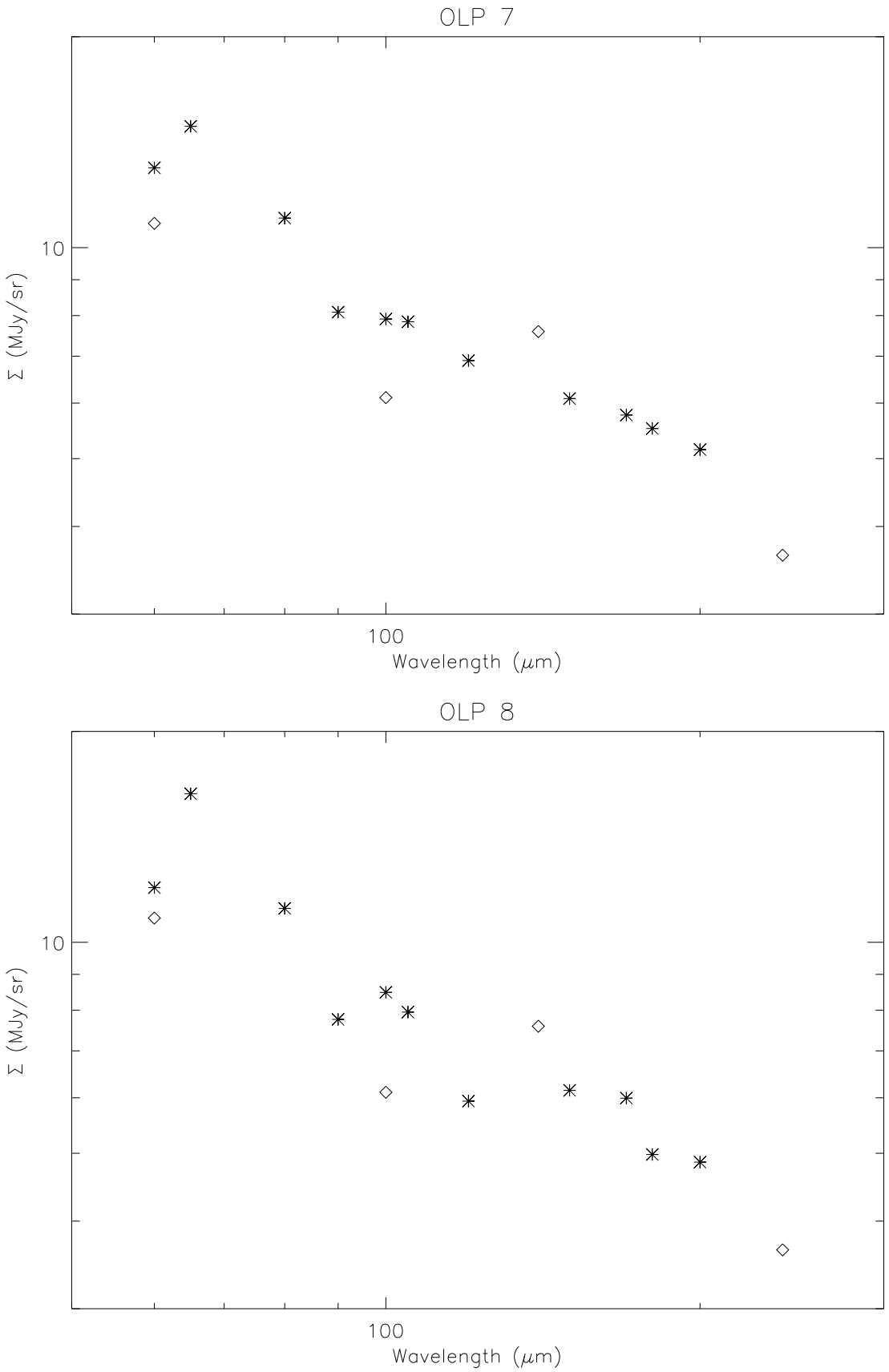

Figure 7.13: Comparison of OLP V7.0 and OLP V8.4b3 surface brightness (asterisk) with COBE annual map fluxes (diamond).

other hand it should be noted that the individual points have not been color corrected. For the longer wavelengths (150 and 200 μm) the results need not necessarily to match within the same accuracy. Here COBE photometry itself has higher uncertainties and the central wavelengths of the ISOPHOT and COBE bands are different, so that the relative shape of the background SED has some impact. Furthermore, one has always to be careful comparing single pointing ISOPHOT photometry (with a 3 arcmin beam) with COBE photometry (with a 42 arcmin beam) due to structure in the background.

Evaluation Log

1) Point source photometry for Alpha Bootes (TDTs 45200201, 45200202, 45200203, and 45200204) in comparison with IRAS and Cohen model. Fluxes are in Jy.

PHT-P: ppap45200202 (src+back)
ppae45200201 (back)

PHT-C: pcap45200204 (src+back)
pcae45200203 (back)

color correction: black body, T=4000
model: Cohen

Det	cwl [um]	OLP 7 [Jy]	OLP 8 [Jy]	IRAS [Jy]	Model [Jy]	% OLP 7 [(OLP-model)/model]	% OLP 8
P1	3.3	6185.493	5695.854		5695.470	8.60	0.01
P1	7.3	1483.791	1400.773		1291.496	14.89	8.46
P1	7.7	1267.990	1165.112		1116.581	13.56	4.35
P1	10.0	785.882	665.884		708.004	11.00	-5.95
P1	11.3	551.459	572.895		570.349	-3.31	0.45
P1	12.0	629.450	545.015	558.500	507.360	24.06	7.42
P1	12.8	465.644	382.347		435.541	6.91	-12.21
P1	15.0	296.661	376.618		320.700	-7.50	17.44
P2	20.0	185.297	187.989		185.467	-0.09	1.36
P2	25.0	124.560	127.784	116.400	119.146	4.54	7.25
P3	60.0	23.110	18.614	19.650	21.030	9.89	-11.49
C1	60.0	21.063	21.747	19.650	21.030	0.16	3.41
C1	65.0	17.549	18.395		17.910	-2.02	2.71
C1	80.0	12.695	12.390		11.800	7.59	5.00
C1	90.0	8.957	9.127		9.303	-3.72	-1.90
P3	100.0	9.724	6.825	7.250	7.521	29.29	-9.25
C1	100.0	7.518	7.160	7.250	7.521	-0.04	-4.80
C1	105.0	6.521	6.036		6.814	-4.30	-11.42
C2	120.0	3.756	4.607		5.201	-27.78	-11.42
C2	150.0	1.922	3.018		3.310	-41.92	-8.83
C2	170.0	1.191	2.387		2.568	-53.63	-7.03
C2	180.0	0.494	1.487		2.286	-78.38	-34.94
C2	200.0	0.391	1.225		1.845	-78.79	-33.59

2) surface brightness photometry of Alpha Bootes background (TDT 45200203)

Cwl [um]	OLP 7.0 [MJy sr^-1]	OLP 8.4 [MJy sr^-1]	COBE [MJy sr^-1]
60.0	13.00	11.97	10.83
65.0	14.90	16.29	
80.0	11.02	11.18	
90.0	8.09	7.76	
100.0	7.91	8.48	6.11
105.0	7.84	7.95	
120.0	6.90	5.94	
150.0	6.09	6.15	7.59 (140um)
170.0	5.77	5.99	
180.0	5.52	4.98	
200.0	5.15	4.86	3.64 (240um)

7.3.4 General Re-validation of Multi-filter Staring Mode (PHT03/PHT22) and Absolute Photometry (PHT05/PHT25): The SED of γ Draconis (HR 6705) - Final Assessment

- authors: M. Radovich, U. Klaas
- date: 23-July-1999
- SVP period 2

Motivation

This is the final calibration accuracy assessment and a repetition of the assessment performed for SVP1, cf. Sect. 5.4.4 to check for changes.
The star γ Draconis (HR 6705) is one of the most important calibration stars for ISOPHOT. Also several AOT commissioning observations were performed on this star. The set of observations comprises multi-filter photometry, TDTs 35602101 (background, PHT-P), 35602102 (γ Dra, PHT-P), 35602203, 39802002 (background PHT-C), 35602204, 39802003 (γ Dra, PHT-C), absolute photometry, TDTs 35300301...35300306 (PHT-P) and 35300308...35300312 (PHT-C), multi-filter PHT-C100 photometry with different reset interval settings, cf. [4] for more details. It is one of the key OLP V7.0 validation cases [1]. The staring mode AOTs PHT-03 and PHT-22 use all available PHT filters out to 200 μm complementing the α Bootes observations towards the fainter flux end. There are detailed models available from M. Cohen (composite spectrum from 1 to 35 μm and extrapolations to 300 μm). This test case is very suitable for a test of both the absolute calibration and the relative filter-to-filter calibration.

Method

We compare the background subtracted, color corrected flux values of both OLP V7.0 and OLP V8.4b3 results against the model prediction.

Results

In the following Tab. 7.6 we compare the photometry from part 1 of the evaluation log section with the model. We estimate the absolute photometric accuracy per detector assembly for this target as the deviation from the model flux in the filter in which the FCS calibration was done, and the relative filter-to-filter accuracy as the peak-to-peak variation of the other filters around this offset. Figs. 7.14 and 7.15 show the PHT photometric data points in comparison to the model and IRAS photometry (color corrected) for OLP 7.0 and OLP 8.4b3, respectively. While the absolute photometry as shown in Fig. 7.15 looks excellent now we notice some features in the multi-filter photometry of Fig. 7.14 which needs individual follow-up:

- The 15 μm flux shows a high excess of 65 % with regard to the model. This could be due to an initial signal transient as the multi-filter sequence was started with this filter. For the establishment of the relative filter-to-filter calibration accuracy this value will not be taken into account. Indeed a repeated measurement in the 15 and 3.6 μm filter with twice the exposure time in the 15 μm filter shows the same absolute accuracy at 3.6 μm and a relative filter-to-filter accuracy of 15 %.
- The C100 filters are systematically too high by 20 to 40 %, except the 105 μm filter which is significantly too low. Again, this filter was the first filter in the multi-filter sequence performed on rev. 398. It is hard to believe the the flux deficiency in the 105 μm filter is due to background features, since the adjacent 100 μm filter does not show this problem. Also cirrus confusion is very likely to be ruled out, as for the off position the well selected calibration measurement offset was chosen. Another indicator that the too low flux comes from the signal processing is given below in the investigation of measurements varying the reset interval time. The relative shape of the SED as given by the measurements from 60 μm to 100 μm looks improved. In the investigation of the systematic offset, it should be checked whether signal transients in the FCS measurement could be responsible for this.

- All C200 fluxes are too low and from 170 μm onwards are even negative. The excellent absolute photometry performance at 170 μm seems to rule out a problem with the photometric calibration.

Table 7.6: Consistency check of photometric results with HR 6705 model

Filter	**mode**	**consistency w.r.t. model OLP V7.0** [%]	**consistency w.r.t. model OLP V8.4b3** [%]
3.3	multf	3.08	-3.23
3.6	multf	10.07	8.39
3.6	multf 2	–	8.62
4.8	multf	16.10	11.93
7.3	multf	4.92	-2.83
7.7	multf	11.82	6.48
10.0	multf	-17.38	-15.43
11.3	multf	6.18	15.16
12.0	multf	-5.06	-14.92
12.0	abs	-6.71	-10.86
12.0 IRAS		-7.5	-7.5
12.8	multf	-13.68	-6.84
15.0	multf	36.37	64.13
15.0	multf 2	–	21.36
20.0	multf	-2.89	-2.85
25.0	multf	5.79	2.32
25.0	abs	-7.13	-7.09
25.0 IRAS		7.1	7.1
60.0 PHT-P	multf	-7.41	14.70
60.0 PHT-P	abs	-0.27	5.88
60.0 PHT-C	multf	-6.57	17.89
60.0 PHT-C(a)	abs	28.17	14.43
60.0 PHT-C(b)	abs	33.48	8.71
60.0 IRAS		-0.8	-0.8
65.0	multf	55.35	43.76
80.0	multf	31.94	30.54
90.0	multf	27.10	32.28
100.0 (PHT-P)	multf	-39.89	5.85
100.0 (PHT-C)	multf	16.28	22.85
100.0 IRAS		+0.4	+0.4
105.0	multf	-31.27	-53.69
120.0	multf	-86.12	-81.11
150.0	multf	-86.17	-80.01
170.0	multf	-154.91	-159.50
170.0	abs	-29.05	-7.21
180.0	multf	-262.53	-311.14
200.0	multf	-139.78	-143.50

As for α Bootes we performed source-to-background contrast calculation (background flux in Jy is calculated according to the following formula: $F(Jy)_{back} = 1/f_{psf}$ * I(MJy/sr) * (1 - ε^2) * Omega * n_{pix}) which is given in Table 7.7. While for all C100 filters the source fluxes are above the critical contrast ratio of 1:4 (0.25) for C200 they are clearly below with contrasts between 1:8 and 1:20. The only case which argues against the contrast as the only limiting factor for accurate source flux determination is the absolute photometry measurement which gives excellent results. However here the applied measurement times are much longer.
Part 3 of the evaluation log and Fig. 7.16 provide an analysis of C100 multi-filter measurements from 90 μm to 105 μm and varying the reset interval by a factor of 2. (The off pointing

Table 7.7: Source-to-background contrast for γ Draconis in FIR filters. The expected source flux is the model flux, the background flux is from the background measurement converted to Jy as decribed in the text.

λ_c [μm]	**background flux** [Jy]	**expected source flux** [Jy]	**source-to-backgr. contrast**
60.0	4.14	4.55	1.10 (1:0.91)
65.0	5.36	3.87	0.72 (1:1.39)
80.0	3.74	2.55	0.68 (1:1.47)
90.0	3.55	2.01	0.57 (1:1.75)
100.0	4.19	1.63	0.39 (1:2.56)
105.0	4.03	1.47	0.37 (1:2.70)
120.0	9.07	1.13	0.12 (1:8.33)
150.0	10.28	0.72	0.07 (1:14.3)
170.0	11.40	0.56	0.05 (1:20.0)
180.0	8.79	0.50	0.06 (1:16.7)
200.0	7.84	0.40	0.05 (1:20.0)

position is different from the one used on rev. 398). While TDT 67100802 is close to the set-up used in the multi-filter measurement TDT 39800203 above, TDT 67100911 uses a factor of 2 faster reset interval. It can be seen that for both measurements the 105 μnm flux value does not show the huge flux deficiency as noticed above, in contrary for TDT 67100802 the flux is by 80 % higher than the model prediction. This points to the fact that the signal evaluation may be problematic in some of the measurements. TDT 67100911 gives the best absolute and relative calibration accuracy for C100 on this target with 15 % absolute and 10 % relative. This could be a consequence of the long measurement times (512 s per filter). The photometric accuracies are presented in Tab. 7.8. The excessive flux by 50 % and more in the C100 range noted for the OLP V8.4b1, both in the multi-filter and absolute mode is gone. The 15 μm and 105 μm results from the multi-filter measurements on revs. 356 and 398 have not been taken into account. Also the C200 multi-filter measurements from rev. 356 could not be used to establish quantitative numbers.

Table 7.8: Absolute and relative calibration accuracies per detector achieved for HR 6705 observation with OLP V8.4b3

detector	**mode**	**absolute accuracy** [%]	**relative accuracy** [%]
P1	multf	8 at 3.6 μm	25
P1	abs	11 at 12 μm	n/a
P2	multf	$<$ 3 at 20 μm	5
P2	abs	7 at 25 μm	n/a
P3	multf	15 at 60 μm	10
P3	abs	6 at 60 μm	n/a
C100	multf	18 at 60 μm	25
C100	multf	15 at 90 μm	25
C100	abs	15 at 60 μm	n/a
C200	abs	8 at 170 μm	n/a

Part 4 of the evaluation log section and Fig. 7.17 provide the surface brightness photometry of the background position and the comparison with COBE. From Table 7.9 it can be seen that at 60 μm the internal consistency of the measurements from the two revolutions 356 and 398 and the consistency with COBE has improved. At 100 μm the ISOPHOT fluxes are systematically higher with an average consistency to COBE of 20 %. We notice a similar behaviour for the background of α Boo, cf. Table 7.5. Also, relative to the adjacent filters,

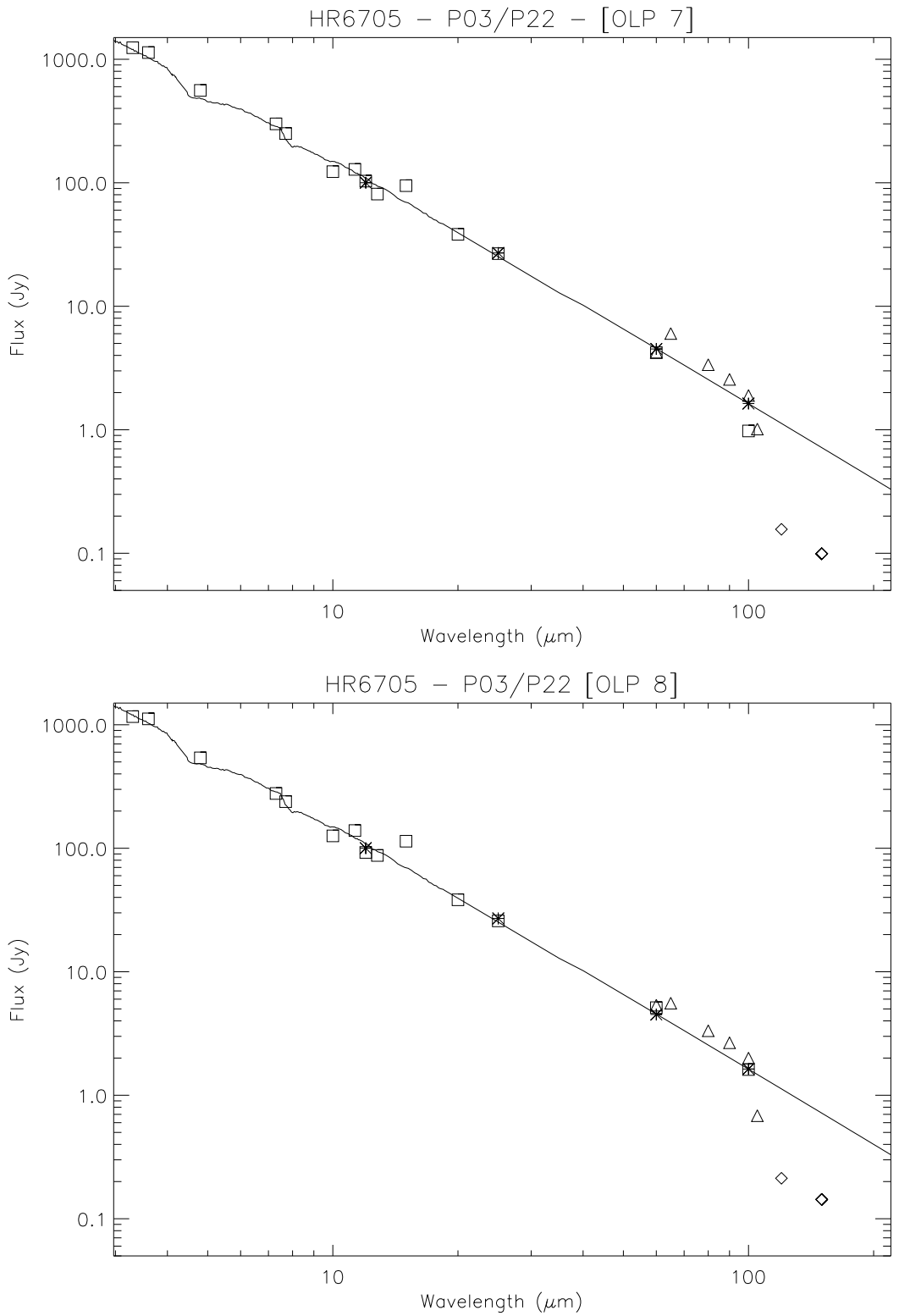

Figure 7.14: Comparison of PHT-P and PHT-C multi-filter photometry (P03/P22), using the full ISOPHOT filter set, with the composite spectrum and out to 300 μm extrapolated SED of γ Dra (HR 6705) provided by M. Cohen and with IRAS photometry for OLP 7.0 (upper panel) and OLP 8.4b3 (lower panel). All photometric points are color corrected for a 4000 K BB. The meaning of the symbols is the following: solid line: model, asterisk: IRAS, square: PHT-P (P03 AOT), triangle: C100 (P22 AOT), diamond: C200 (P22 AOT).

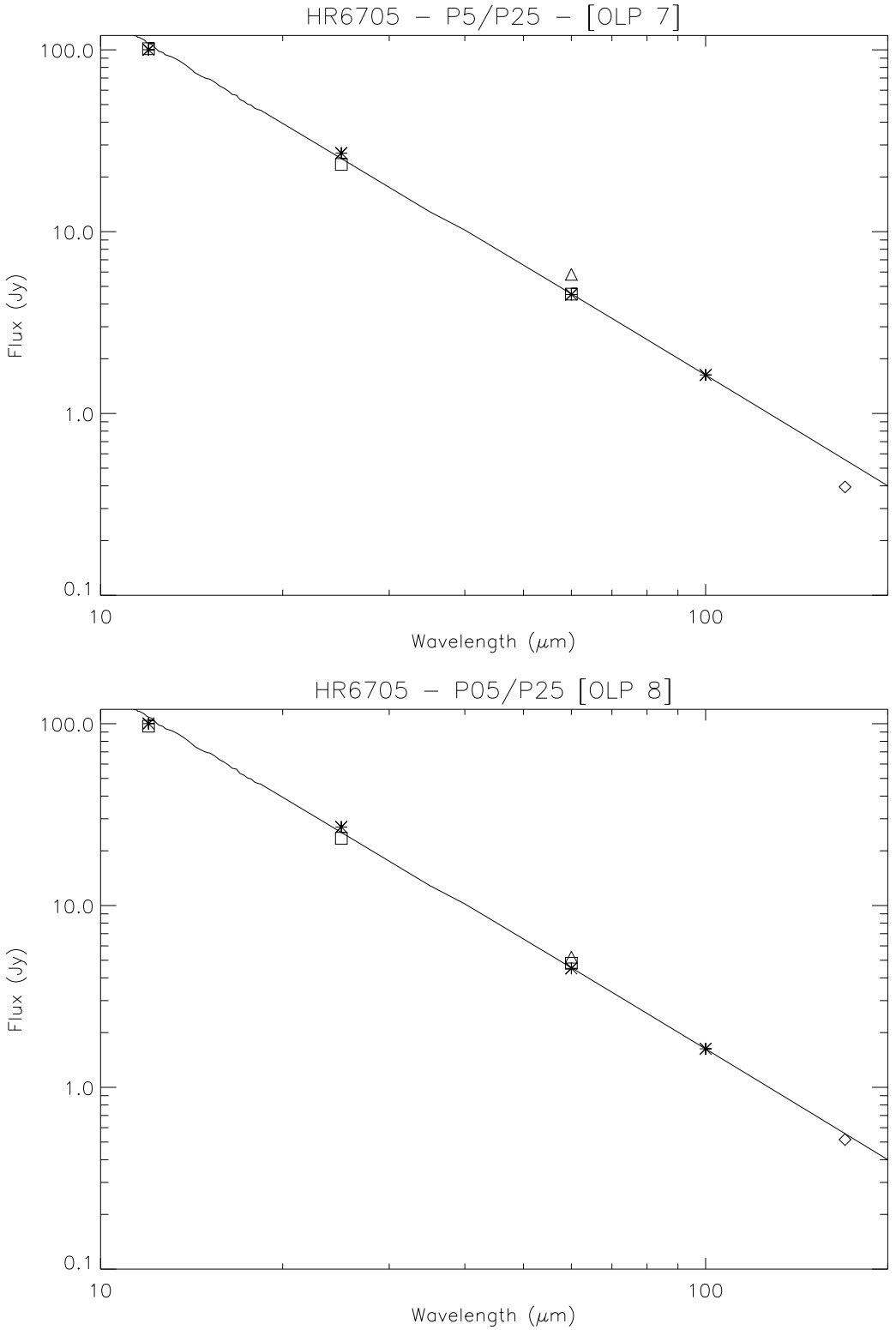

Figure 7.15: Comparison of PHT-P and PHT-C absolute photometry (P05/P25), with the composite spectrum and out to 300 μm extrapolated SED of γ Dra (HR 6705) provided by M. Cohen and with IRAS photometry for OLP 7.0 (upper panel) and OLP 8.4b3 (lower panel). All photometric points are color corrected for a 4000 K BB. The meaning of the symbols is the following: solid line: model, asterisk: IRAS, square: PHT-P (P05 AOT), triangle: C100 (P25 AOT), diamond: C200 (P25 AOT).

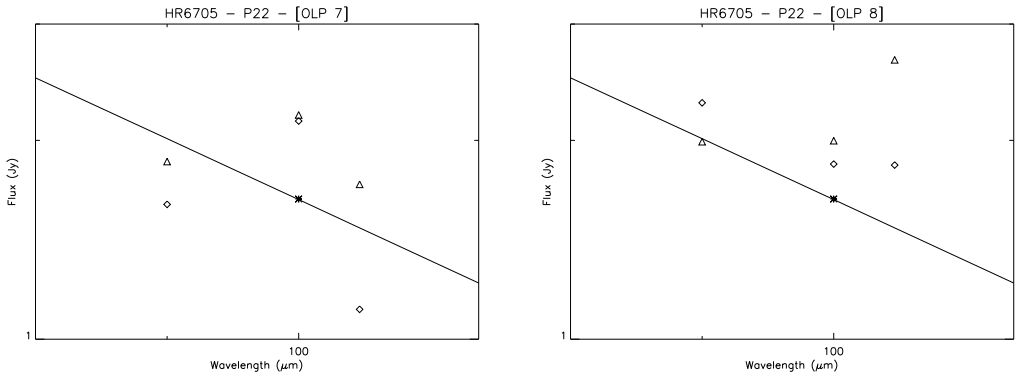

Figure 7.16: Comparison of PHT-C100 multi-filter photometry (P22), with the composite spectrum and out to 300 μm extrapolated SED of γ Dra (HR 6705) provided by M. Cohen and with IRAS photometry for OLP 7.0 (left panel) and OLP 8.4b3 (right panel). All photometric points are color corrected for a 4000 K BB. The meaning of the symbols is the following: solid line: model, asterisk: IRAS, triangle: C100 (TDT 67100802, reset interval length comparable to standard set-up for source), diamond: C100 (TDT 67100911, reset interval shorter by a factor of 2 than standard set-up).

the 100 μm value sticks out a bit. A significant outlier seems to be the 65 μm point, which was already seen for the α Bootes background. Overall, the resulting background SEDs look more scattered than for OLP 7.0, however no color correction has been performed.

Table 7.9: Consistency check of γ Dra background position surface brightness results with COBE/DIRBE annual maps.

wavelength μm	**consistency w.r.t. COBE OLP V7.0** [%]	**consistency w.r.t. COBE OLP V8.4b3** [%]
60 (rev 356)	-16.3	-4.9
60 (rev 398)	+15.4	+10.5
100 (rev 356)	-2.0	+11.5
100 (rev 398)	+20.2	+32.9
150 (rev 356)	-31.9	-35.2
200 (rev 356)	+24.2	+1.0

Conclusions

- The SCREW-366, 367 implementation works for PHT-P. While for P1 no improvement in calibration accuracy can be noted, the relative filter-to-filter accuracy is still on the 20 – 25 % level, P2 absolute and relative photometry has slightly improved, and P3 relative photometry has considerably improved.
- The SCREW-366 implementation also works for C100. There is no gain in absolute photometric accuracy with regard to OLP 7.0, however a relative filter-to-filter accuracy of 25 % could be established now. The fluxes show a positive offset with regard to the model. Whether this is a consequence of the signal linearization calibration or of the signal evalutaion of the FCS measurement will have to be established. The strong flux deficiency found in the 105 μm filter of the main multi-filter sequence cannot be attributed to photometric calibration deficiencies but is rather likely affected by signal transients, as could be shown by other multi-filter sequences using this filter.
- Staring "on-off" multi-filter photometry with C200 shows still a significant flux defi-

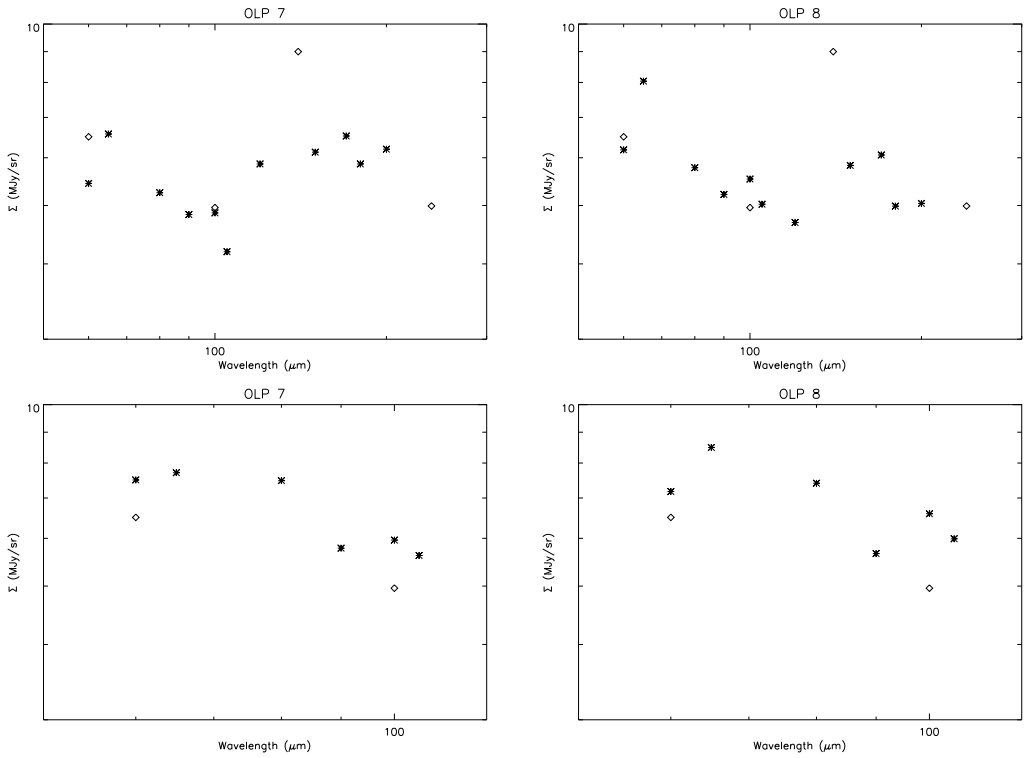

Figure 7.17: Comparison of OLP V7.0 and OLP V8.4b3 surface brightness (asterisk) with COBE annual map fluxes (diamond): TDT35602203 upper left and right panel, TDT39802002 lower left and right panel.

ciency of or even negative source fluxes, while absolute photometry is now accurate within 10 % for this source. The most likely reason for this deficiency appears to be the relatively short measurement times in combination with a rather low source to background contrast (< 1:8).

- The impression of the accuracy achieved for the surface brightness values is mixed. On the one hand there is considerably better agreement with COBE at 60 μm. On the other hand the data points show a somewhat larger scatter, in particular the 65 μm data point and somewhat less the 100 μm data point stick systematically out, what was already found for the α Bootes background. This is responsible for a somewhat worse consistency with COBE at 100 μm.

Evaluation Log

```
1) P03 and P22 multi-filter photometry

PHT-P: ppap35602102 (src+back)  FCS: 3.6, 20, 60 um
       ppae35602101 (back)      FCS: 12, 20, 100 um
       ppap39801901 (src+back)  FCS: 3.6 (3.6 and 15 um filter only)

PHT-C1: pcap39802003 (src+back)   FCS: 60 um
        pcae39802002 (back)       FCS: 90 um

PHT-C2: pcap35602204 (src+back)   FCS: 170 um
        pcae35602203 (back)       FCS: 170 um


color correction: black body, T=4000
model: Cohen

Det   cwl    OLP 7      OLP 8      IRAS     Model     % OLP 7    % OLP 8
P1    3.3  1240.160   1164.273           1203.159      3.08      -3.23
P1    3.6  1134.352   1117.075           1030.575     10.07       8.39
P1    3.6             1119.439           1030.575                 8.62 (TDT 39801901)
P1    4.8   559.957    539.840            482.322     16.10      11.93
P1    7.3   299.980    277.822            285.925      4.92      -2.83
P1    7.7   250.549    238.588            224.074     11.82       6.48
P1   10.0   123.116    126.034            149.024    -17.38     -15.43
P1   11.3   128.291    139.136            120.822      6.18      15.16
P1   12.0   103.215     92.502   100.160   108.718     -5.06     -14.92
P1   12.8    81.039     87.453             93.877    -13.68      -6.84
P1   15.0    94.790    114.088             69.510     36.37      64.13
P1   15.0               84.356             69.510                21.36 (TDT 39801901)
P2   20.0    38.248     38.263             39.387     -2.89      -2.85
P2   25.0    26.691     25.813    27.030   25.229      5.79       2.32
P3   60.0     4.208      5.213     4.510    4.545     -7.41      14.70
C1   60.0     4.246      5.358     4.510    4.545     -6.57      17.89
C1   65.0     6.015      5.567              3.872     55.35      43.76
C1   80.0     3.365      3.329              2.550     31.94      30.54
C1   90.0     2.557      2.662              2.012     27.10      32.28
P3  100.0     0.978      1.722     1.630    1.627    -39.89       5.85
C1  100.0     1.892      1.999     1.630    1.627     16.28      22.85
C1  105.0     1.013      0.683              1.474    -31.27     -53.69
C2  120.0     0.156      0.213              1.126    -86.12     -81.11
C2  150.0     0.099      0.143              0.717    -86.17     -80.01
C2  170.0    -0.305     -0.331              0.556   -154.91    -159.50
C2  180.0    -0.805     -1.046              0.495   -262.53    -311.14
C2  200.0    -0.159     -0.174              0.400   -139.78    -143.50


2) P05 and P25 absolute photometry


PHT-P1: ppap35300302 (src+back)
        ppae35300301 (back)

PHT-P2: ppap35300304 (src+back)
        ppae35300303 (back)

PHT-P3: ppap35300306 (src+back)
        ppae35300305 (back)

PHT-C1: pcap35300309 (src+back$^a$)
        pcap35300310 (src+back$^b$)
        pcae35300308 (back)
```

PHT-C2: pcap35300312 (src+back)
        pcae35300311 (back)

color correction: black body, T=4000
model: Cohen

Det	cwl	OLP 7	OLP 8	IRAS	Model	% OLP 7	% OLP 8
P1	12.0	101.421	96.917	100.160	108.718	-6.71	-10.86
P2	25.0	23.431	23.440	27.030	25.229	-7.13	-7.09
P3	60.0	4.533	4.812	4.510	4.545	-0.27	5.88
C1(a)	60.0	5.825	5.201	4.510	4.545	28.17	14.43
C1(b)	60.0	6.067	4.941	4.510	4.545	33.48	8.71
C2	170.0	0.395	0.516		0.556	-29.05	-7.21

3) Photometry for different reset interval settings

PHT-C: pcap67100802 (src+back) FCS: 90 um
       pcap67100801 (back)   FCS: 90 um

PHT-C: pcap67100911 (src+back) FCS: 90 um
       pcap67100910 (back)   FCS: 90 um

color correction: black body, T= 4000
model: Cohen

Det	cwl	OLP 7	OLP 8	IRAS	Model	% OLP 7	% OLP 8
			PCAP67100802				
C1	90.0	1.858	1.991		2.012	-7.66	-1.06
C1	100.0	2.185	1.998	1.630	1.627	34.31	22.78
C1	105.0	1.716	2.648		1.474	16.40	79.67
			PCAP67100911				
C1	90.0	1.600	2.280		2.012	-20.48	13.31
C1	100.0	2.139	1.841	1.630	1.627	31.49	13.18
C1	105.0	1.110	1.835		1.474	-24.72	24.49

4) Surface brightness on background positions

Gamma Dra

TDT 39802002

Cwl [um]	OLP 7.0 [MJy sr^-1]	OLP 8.4 [MJy sr^-1]	COBE [MJy sr^-1]
60.0	7.50	7.18	6.50
65.0	7.71	8.49	
80.0	7.48	7.41	
90.0	5.78	5.66	
100.0	5.96	6.59	4.96
105.0	5.62	5.99	

TDT 35602203

Cwl [um]	OLP 7.0 [MJy sr^-1]	OLP 8.4 [MJy sr^-1]	COBE [MJy sr^-1]
60.0	5.44	6.18	6.50
65.0	6.57	8.04	
80.0	5.25	5.78	
90.0	4.83	5.22	

100.0	4.86	5.53	4.96
105.0	4.19	5.02	
120.0	5.86	4.68	
150.0	6.13	5.83	9.00 (140um)
170.0	6.52	6.06	
180.0	5.86	4.99	
200.0	6.20	5.04	4.99 (240um)

7.3.5 General Re-validation of PHT03 and PHT05 Staring Mode: The SED of Sirius (HR 2491) - Final Assessment

- authors: M. Radovich, U. Klaas
- date: 22-July-1999
- SVP period 2

Motivation

This is the final calibration acxcuracy assessment and a repetiition of the assessment performed for SVP1, cf. Sect. 5.4.5.
Beside Vega (HR 7001), Sirius is the main primary stellar standard with a model provided by M. Cohen (1-300 μm, R = 4000 up to 35 μm, delivered 12-Jan-1996). Therefore, a dedicated cross-calibration program was performed on this star using absolute photometry complemented by multi-filter photometry out to 25 μm.

Method

We compare the background subtracted, color corrected flux values of both OLP V7.0 and OLP V8.4b3 results against the model prediction.

Results

In the following Tab. 7.10 we compare the photometry from part 1 of the evaluation log section with the model. We estimate the absolute photometric accuracy per detector assembly for this target as the deviation from the model flux in the filter in which the FCS calibration was done, and the relative filter-to-filter accuracy as the peak-to-peak variation of the other filters around this offset. Two multi-filter sequences were performed, one from 3.3 to 12 μm with absolute calibration at 3.3 μm, and the other one from 11.3 to 15 μm with absolute calibration at 12.8 μm. The photometric accuracies are presented in Tab. 7.11. Fig. 7.18 shows the PHT photometric data points in comparison to the model and IRAS photometry (color corrected) for OLP 7.0 and OLP 8.4b3, respectively.

Table 7.10: Consistency check of photometric results with Sirius model

Filter	**mode**	**consistency w.r.t. model OLP V7.0** [%]	**consistency w.r.t. model OLP V8.4b3** [%]
3.3	multf	8.70	10.88
3.3	abs	1.05	3.87
7.7	multf	1.35	4.01
11.3	multf	-6.22	17.11
12.0	multf	14.72	11.56
12.0	abs	7.25	2.12
12.8	multf	-3.81	15.52
15.0	multf	-10.27	16.06
25.0	abs	20.32	12.48

Conclusions

- The results of the OLP 8.4b1 version are fully reproduced and confirmed by the OLP 8.4b3 version.
- For P1, the absolute photometry gives more accurate fluxes than the multi-filter photometry. The absolute accuracies achieved for the absolute mode are better than 5 %.

Table 7.11: Absolute and relative calibration accuracies per detector achieved for HR 5340 observation with OLP V8.4b3

detector	**mode**	**absolute accuracy** [%]	**relative accuracy** [%]
P1	multf	11 at 3.3 μm	7
P1	abs	4 at 3.3 μm	n/a
P1	abs	2 at 12.0 μm	n/a
P1	multf	16 at 12.8 μm	2
P2	abs	13 at 25 μm	n/a

- The long wavelength multi-filter sequence from 11.3 to 15 μm shows in general some flux excess with regard to the model. The absolute photomteric accuracy for the multi-filter mode is around 15 %. The relative filter-to-filter calibration is slightly improved w.r.t. OLP V7.0, being better than 7 %.
- The absolute PHT-P2 photometry is improved to better than 15 %.

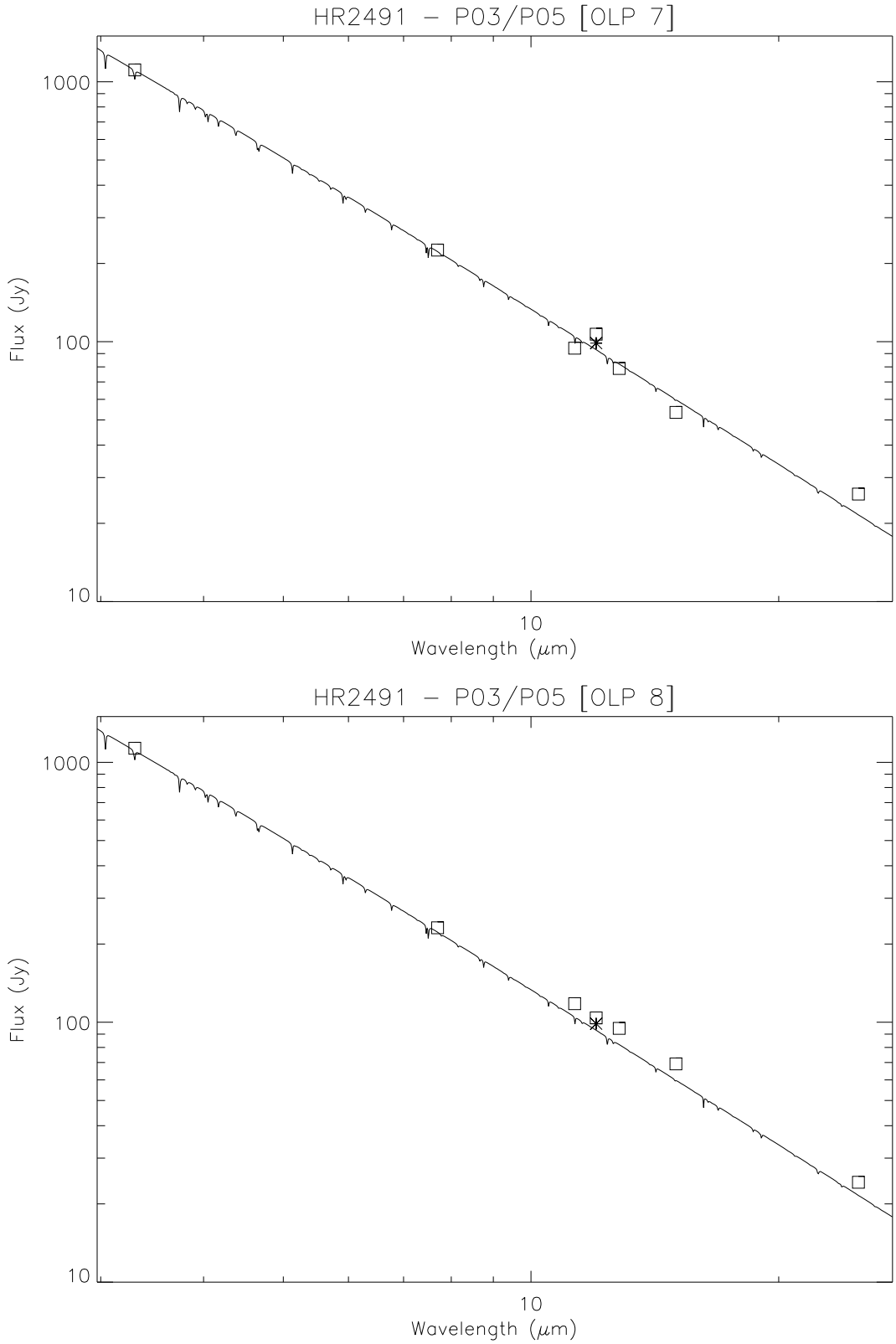

Figure 7.18: Comparison of PHT-P absolute and multi-filter photometry with the composite spectrum of Sirius (HR 2491) provided by M. Cohen and with IRAS photometry for OLP 7.0 (upper panel) and OLP 8.4b3 (lower panel). All photometric points are color corrected for a 10000 K BB. The meaning of the symbols is the following: solid line: model, asterisk: IRAS, square: PHT-P (P03 and P05 AOTs).

Evaluation Log

```
1) P03 multi-filter and P05 absolute photometry

PHT-P1: ppap70705302 (src+back)   multi-filter P03, FCS: 3.3 um
PHT-P1: ppap70705301 (src+back)   multi-filter P03, FCS: 12.8 um
PHT-P1: ppap70705310 (src+back)   absolute P05
PHT-P1: ppap70705313 (src+back)   absolute P05
PHT-P2: ppap70705707 (src+back)   absolute P05


color correction: black body, T=10 000 K
model: Cohen
fluxes in Jy

Det    cwl     OLP 7      OLP 8       IRAS     Model     % OLP 7      % OLP 8
ppap70705302
P1     3.3    1110.840   1133.059             1021.900     8.70         10.88
P1     7.7     225.038    230.947              222.038     1.35          4.01
P1    12.0     106.866    103.930    98.690     93.157    14.72         11.56
ppap70705301
P1    11.3      94.395    117.881              100.654    -6.22         17.11
P1    12.8      78.875     94.729               82.001    -3.81         15.52
P1    15.0      53.447     69.134               59.566   -10.27         16.06
ppap70705310
P1     3.3    1032.600   1061.453             1021.900     1.05          3.87
ppap70705313
P1    12.0     99.908     95.136    98.690     93.157     7.25          2.12
ppap70705707
P2    25.0     25.919     24.229               21.541    20.32         12.48
```

7.3.6 General Re-validation of PHT03 Staring Mode: Photometric Reproducibility Aspects in the Case of the SED of Vega (HR 7001)- Final Assessment

- authors: M. Radovich, U. Klaas
- date: 27-July-1999
  revised version on 09-March-2000 to correct OLP 8 results for wrong modified BB color correction (SPR-3179)
- SVP period 2

Motivation

This is the final calibration accuracy assessment and a repetition of the assessment performed fro SVP1, cf. Sect. 5.4.6 to check for changes.
We investigate here the photometric accuracy of PHT-P multi-filter aperture photometry for an observation of Vega from a general observer program which was repeated several times as part of a variability monitoring project. From 3.3 to 100 μm it used the typical exposure time of 32 s per filter and non-standard apertures. The absolute calibration via the FCS of the on-source measurement was performed in the 3.6, 20, and 100 μm filter, respectively. The absolute calibration of the off-source measurement was performed in the 7.3, 25, and 100 μm filter, respectively. We selected 3 measurements out of this program from rev. 85 (TDT 08500106; before rev. 94 FCS change!), rev. 558 (TDT 55800419) and rev. 865 (TDT 86500706). The used apertures w.r.t. the standard apertures for point source calibration are listed in the following Table 7.12:

Table 7.12: Apertures used in the Vega variability monitoring program versus standard apertures

filter	**program aperture** ["]	**standard aperture** ["]
P1_3P29_UM	18	23
P1_3P6_UM	18	23
P1_4P85_UM	18	23
P1_7P3_UM	18	23
P1_10_UM	18	52
P1_11P5_UM	18	52
P1_12P8_UM	18	52
P1_16P0_UM	18	52
P2_20_UM	52	79
P2_25_UM	52	79
P3_60_UM	120	180
P3_100_UM	120	180

Method

Vega is one of the primary photometric stellar standards. However, due to its IR excess, the photospheric models, e.g. by Cohen, are valid only out to approximately 15 μm. Beyond 15 μm we solely compare with the available IRAS photometry.
The color correction was dependent on the relative contribution by the stellar photosphere and the IR disc, and hence on the wavelength. We followed the description as given in Ref.[14]:

- from 3.3 to 16 μm the SED behaves like a 10000 K Black Body,
- from 60 to 100 μm the SED behaves like an 80 K modified BB, $\varepsilon \propto \nu$

- from 20 to 25 μm the SED is a mixture of a 10000 K BB and an 80 K modified BB with a ratio 2:1.

Note that results in this report have been corrected for wrong color correction factors applied previously for modified black bodies, but this only for IRAS and OLP 8 fluxes, OLP 7 fluxes remain as they were presented in [1].

Results

In parts 1 to 3 of the evaluation log section we give the background subtracted and color corrected photometry for the three epochs. We notice that with regard to OLP V8.4b1 there are slight changes in the fluxes, namely

- for rev. 085 in all P1 and P3 filters
- for rev. 558 in all P2 and P3 filters
- for rev. 865 in all P2 and P3 filters

This is very likely a consequence of modifications to the FCS power files according to SPR-2979. Therefore we redo the quantitative analysis here.
For illustration the resulting SEDs are plotted in Figs. 7.19 to 7.21. In Table 7.13 we compare these fluxes against Cohen's Vega model up to 20 μm and against IRAS beyond 20 μm and inter-compare the OLP 7.0 and OLP 8.4b3 results. In Table 7.14 we list for the OLP 8.4b3 results the absolute and relative filter-to-filter calibration accuracies for the three revolutions. In Table 7.15 we compare the relative shapes of the SED measured for the three revolutions and processed with OLP 8.4. The corresponding analysis for the OLP 7.0 results are presented in [1] Sect. 5.18.3.
From 3.6 to 10 μm the photometry agrees to within 20 %, for most cases to within 10 % with the model. The 12 μm point appears always too low by at least 25 %. The relative shape of the SED between 12.8 and 15 μm looks now okay, implying that part of the huge 15 μm excess observed for OLP V7.0 can be explained by the non-linearity with flux. Whether the full discrepancy between measurement and model at 12.8 and 15 μm can be explained by signal transients (which certainly play a role at 15 μm because of the relatively short exposre time of 32 s) remains to be investigated. The source is fainter than the three previous stars α Boo, γ Dra and Sirius. With the correct color correction (both for ISO and IRAS) the 25 μm photometry is now more consistent with IRAS than for OLP V7.0 (however, for the OLP V7.0 fluxes the color correction is wrong!). The ISO fluxes are about 18 % higher than the IRAS fluxes, but this with a reproducibility of 0.6 %! The P3 photometry gives always lower fluxes than IRAS, for revolution 85 and 865 60 and 100 μm fluxes are lower by 10-15 %, however for revolution 558 they are lower by 20-30 %. The f_{60}/f_{100} ratio is 1.22 for the two first revolutions, while it is 1.13 for the latter revolution. Whether this is an indication of a variability in the FIR (the 25 μm fluxes remain constant) is not subject of this report.
The absolute photometry for P1 in the 3.6 μm filter is as accurate as 10 %. Up to 10 μm a relative filter-to-filter calibration of better than 10 % is verified. As mentioned above the strong offsets in the relative filter-to-filter calibration for the filters between 12 and 15 μm can be explained to some extent by signal transients. An absolute calibration accuracy for P2 can not easily be determined, as at 20 μm the star starts to show its IR excess, hence the model is no longer an accurate flux reference. At 25 μm only a relative filter calibration is available, however the f_{20}/f_{25} ratio is 1.103 $\pm$ 0.003. As already mentioned above, the ISO 25 μm flux is higher than the IRAS flux by 17.6 $\pm$ 0.7 %. Whether this reproducible flux difference has a physical origin cannot be decided here. The reproducibility of the 60 to 100 μm flux calibration appears to be better than 7 %. Again, as in the 25 μm case, there are systematic flux differences with regard to IRAS with the ISO fluxes always being lower. The issue is however, more complex, since the ISO observations on rev. 558 are systematically lower than the ones on revs. 85 and 865. Whether this is an indication of variability in the FIR is outside the scope of this report.
The relative shape of the SED is reproduced in the three measurements within 10 % for fluxes out to 25 μm, at 60 and 100 μm they are systematically different for rev. 558 (15-20 % lower than on revs. 85 and 865; in terms of reproducibility this gives a variation of the SED shape by 10 %). The fluxes, even those affected by signal transients vary relative by 15 % (1 σ) at most.

Table 7.13: Consistency check of photometric results with Vega model and IRAS photometry for the three epochs on revs. 085, 558, and 865 for OLP V7.0 and OLP V8.4b3, respectively.

filter	**ref.**	**consistency w.r.t. model or IRAS**					
		OLP V7.0			**OLP V8.4b3**		
		rev. 085 [%]	**rev. 558** [%]	**rev. 865** [%]	**rev. 085** [%]	**rev. 558** [%]	**rev. 865** [%]
3.3	model	-10.6	+4.1	+0.8	-9.7	+4.6	+1.7
3.6	model	-5.5	+9.9	+10.2	-6.7	+8.3	+8.8
4.8	model	+3.4	+18.6	+18.2	+2.5	+17.5	+17.2
7.3	model	-1.8	+11.9	+12.2	-5.3	+7.7	+8.2
10	model	-20.5	+4.7	-13.7	-15.1	+12.1	-8.2
12	model	-34.6	-20.2	-30.6	-31.7	-18.7	-26.9
12	IRAS	-38.3	-24.8	-34.6	-35.7	-23.4	-31.1
12.8	model	+12.2	+55.8	+24.9	+44.8	+96.8	+60.7
15	model	+60.8	+111	+80.7	+45.4	+98.4	+62.0
20	model	+49.2	+40.8	+41.9	+31.7	+29.9	+31.5
25	IRAS	+27.5	+21.5	+21.7	+18.2	+16.9	+17.6
60	IRAS	-16.0	-23.4	-7.6	-10.3	-28.7	-12.9
100	IRAS	-9.1	-17.5	-8.1	-9.5	-22.4	-12.1

Table 7.14: Consistency check of absolute and relative photometric results with Vega model and IRAS photometry for the three epochs on revs. 085, 558, and 865 for OLP V8.4b3 only. The values in each second column per revolution give the offset relative to the FCS calibration filter.

filter	**ref.**	**consistency w.r.t. model or IRAS**					
		rev. 085 [%]		**rev. 558** [%]		**rev. 865** [%]	
3.3	model	-9.7	-3.0	+4.6	-3.7	+1.7	-7.1
3.6	model	-6.7	0.00	+8.3	0.00	+8.8	0.00
4.8	model	+2.5	+9.2	+17.5	+9.2	+17.2	+8.4
7.3	model	-5.3	+1.4	+7.7	-0.6	+8.2	-0.6
10	model	-15.1	-8.4	+12.1	+3.8	-8.2	-17.0
12	model	-31.7	-25.0	-18.7	-27.0	-26.9	-35.7
12	IRAS	-35.7	–	-23.4	–	-31.1	–
12.8	model	+44.8	+51.5	+96.8	+88.5	+60.7	+51.9
15	model	+45.4	+52.1	+98.4	+90.1	+62.0	+53.2
20	model	+31.7	0.00	+29.9	0.00	+31.5	0.00
25	IRAS	+18.2	–	+16.9	–	+17.6	–
60	IRAS	-10.3	-0.8	-28.7	-6.3	-12.9	-0.8
100	IRAS	-9.5	0.00	-22.4	0.00	-12.1	0.00

Conclusions

- PHT-P photometry with the minimum recommended exposure time of 32 s and in non-standard apertures yields about ± 10% absolute accuracy for P1. The relative filter-to-filter calibration is better than 10 % for P1, P2, and P3. For P1 this is restricted to filters shortward of 10 μm. It will have to be investigated what is the reason for the negative offset of the 12 μm point and the positive offset of the 12.8 and 15 μm points. Signal transients may play an important role.

- No significant difference between the P3 measurements performed before revolution 94 and after can be noted. In the contrary, the measurements from rev. 85 and 865

Table 7.15: Normalized fluxes w.r.t. flux in the 3.3 μm filter and relative variation (1 σ) of the flux for the revolutions 085, 558, and 865.

Filter	**normalized flux**			**relative variation of SED shape** [%]	**relative variation of flux** [%]
	rev. 085	**rev. 558**	**rev. 865**		
3.3	1.0000	1.0000	1.0000	–	7.6
3.6	0.9448	0.9472	0.9791	2.0	8.5
4.8	0.6102	0.6040	0.6201	1.3	7.7
7.3	0.2536	0.2487	0.2574	1.7	7.4
10	0.1236	0.1408	0.1187	9.1	14.7
12	0.0695	0.0715	0.0661	4.0	8.8
12.8	0.1299	0.1524	0.1281	9.9	15.9
15	0.0953	0.1121	0.0942	10.0	16.0
20	0.0489	0.0416	0.0434	8.5	0.8
25	0.0443	0.0378	0.0392	8.5	0.6
60	0.0309	0.0212	0.0266	18.5	12.0
100	0.0253	0.0187	0.0218	15.1	8.0

are very consistent, while the one from rev. 558 seems to be systematically different. Whether this is an indication of intrinsic source variation is out of scope of this report. This finding is interpreted, that calibration is properly taking care of the change in the FCS illumination at rev. 94 and that the time dependent CALG files are working fine for this case.

- The P2 accuracy is difficult to estimate for the selected target, due to an unknown mixture of highly different temperature components which involve different ratios of color correction factors for ISOPHOT and the reference photometry. The ISOPHOT fluxes are always higher than the IRAS flux by 17.5 % with a reproducibility of 0.6 %. Also the 20 μm / 25 μm color is very reproducible.

- The accuracy in several filters of this measurement sequence appears to be currently limited by the accuracy of the signal evaluation due to signal transients, however, we notice the change in the relative shape of the SED between 12.8 and 15 μm, probably due to the new linearity correction.

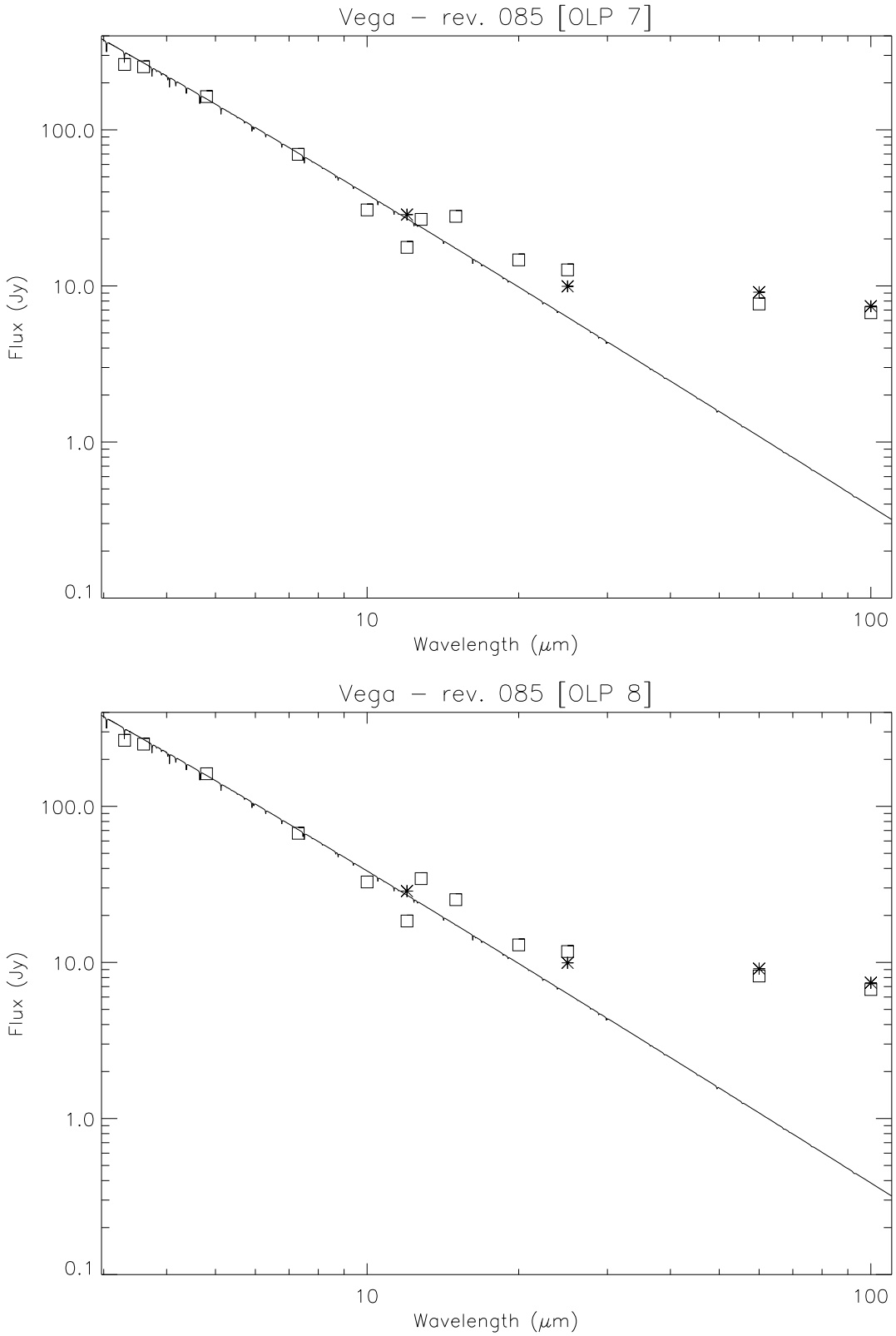

Figure 7.19: Comparison of PHT-P multi-filter photometry of Vega (HR 7001) on revolution 085 with the composite spectrum provided by M. Cohen out to 15 μm and with IRAS photometry beyond 15 μm for OLP 7.0 (upper panel) and OLP 8.4b3 (lower panel). A description of the applied color correction factors is given in the text (**note** that IRAS and OLP V8 results are correctly color corrected, while OLP V7 results were kept as presented in the validation report for OLP V7.0). The meaning of the symbols is the following: solid line: model, asterisk: IRAS, square: PHT-P.

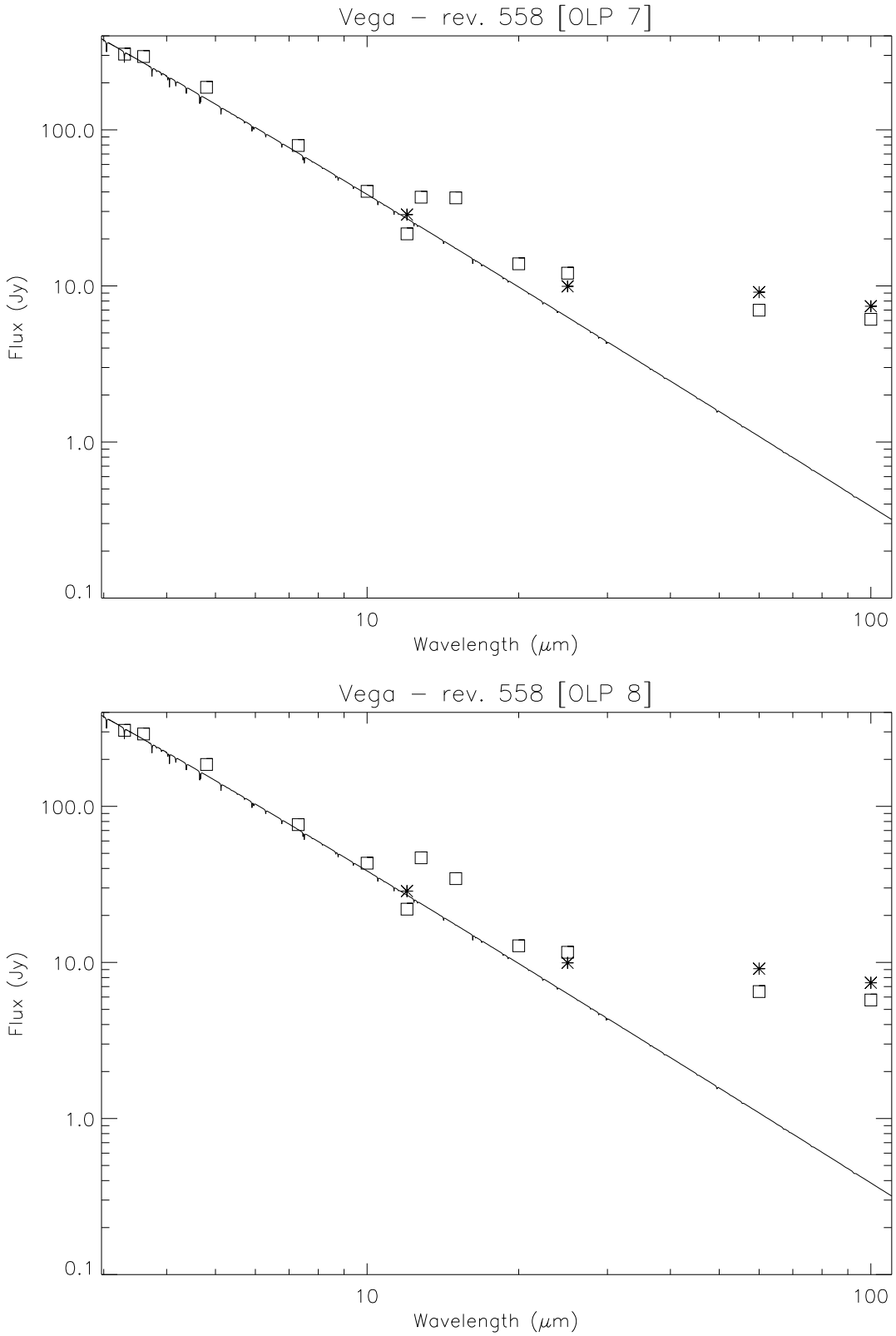

Figure 7.20: Comparison of PHT-P multi-filter photometry of Vega (HR 7001) on revolution 558 with the composite spectrum provided by M. Cohen out to 15 μm and with IRAS photometry beyond 15 μm for OLP 7.0 (upper panel) and OLP 8.4b3 (lower panel). A description of the applied color correction factors is given in the text (**note** that IRAS and OLP V8 results are correctly color corrected, while OLP V7 results were kept as presented in the validation report for OLP V7.0). The meaning of the symbols is the following: solid line: model, asterisk: IRAS, square: PHT-P.

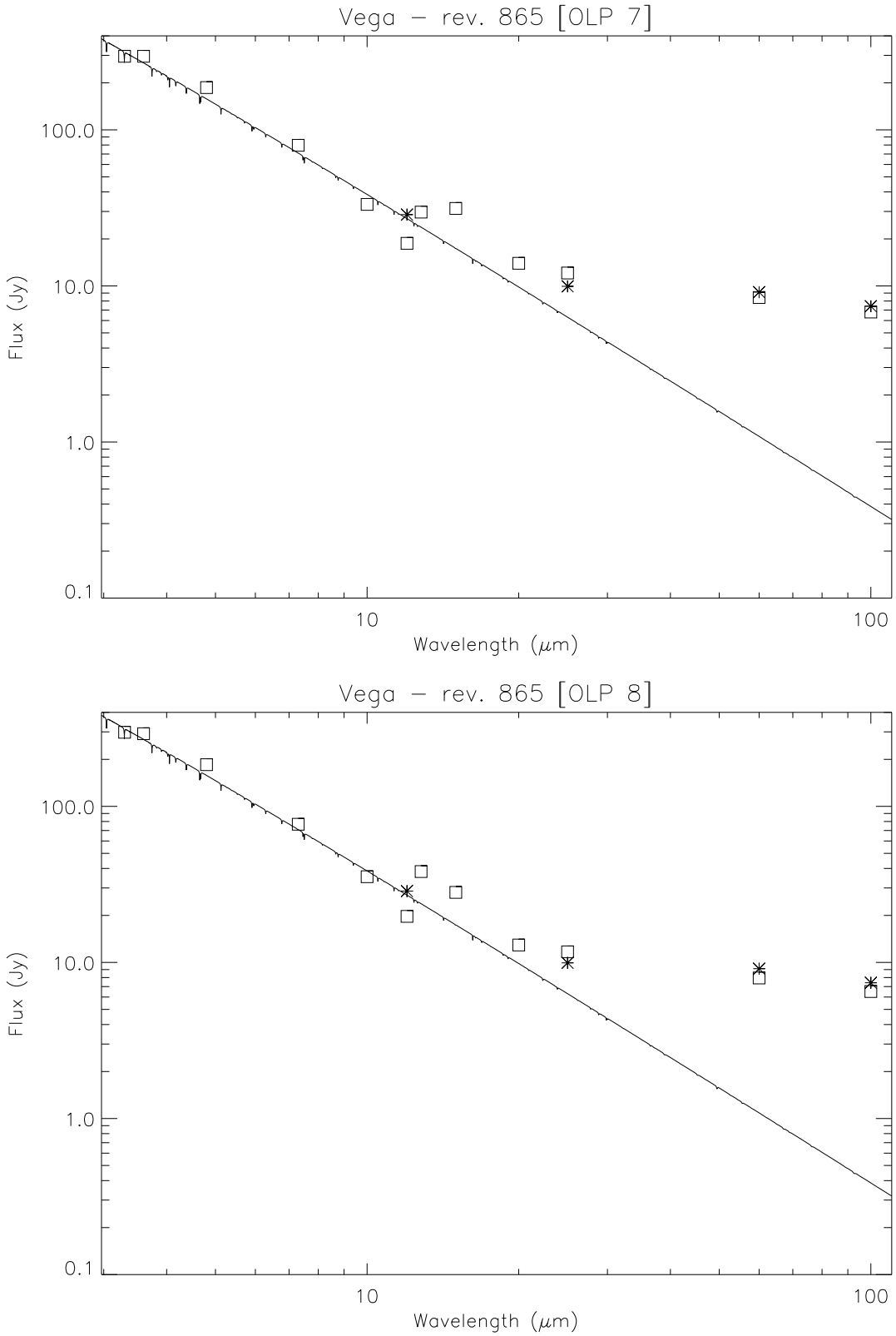

Figure 7.21: Comparison of PHT-P multi-filter photometry of Vega (HR 7001) on revolution 865 with the composite spectrum provided by M. Cohen out to 15 μm and with IRAS photometry beyond 15 μm for OLP 7.0 (upper panel) and OLP 8.4b3 (lower panel). A description of the applied color correction factors is given in the text (**note** that IRAS and OLP V8 results are correctly color corrected, while OLP V7 results were kept as presented in the validation report for OLP V7.0). The meaning of the symbols is the following: solid line: model, asterisk: IRAS, square: PHT-P.

Evaluation Log

1) Vega PHT-P aperture photometry from 3.3 to 100 um on revolution 085

Measurements:
PHT-P: ppap08500106 (src+back) FCS = 3.6, 20, 100 um
       ppap08500105 (back)   FCS = 7.3, 25, 100 um

 Colour correction: see text for wavelength dependent color correction
                    application

 Model: Cohen

Fluxes are in Jy.

Det	cwl [um]	OLP 7 [Jy]	OLP 8 [Jy]	IRAS [Jy]	Model [Jy]	% OLP 7 [(OLP-model)/model]	% OLP 8
P1	3.3	262.363	264.977		293.430	-10.59	-9.70
P1	3.6	253.543	250.343		268.410	-5.54	-6.73
P1	4.8	163.215	161.699		157.795	3.44	2.47
P1	7.3	69.658	67.196		70.934	-1.80	-5.27
P1	10.0	30.682	32.763		38.570	-20.45	-15.06
P1	12.0	17.659	18.429	28.640	26.997	-34.59	-31.74
P1	12.8	26.679	34.425		23.779	12.20	44.77
P1	15.0	27.904	25.240		17.356	60.78	45.43
P2	20.0	14.680	12.951		9.838	49.22	31.65
P2	25.0	12.674	11.742	9.938	6.301	101.15	86.36
P3	60.0	7.662	8.182	9.121	1.087	605.10	652.97
P3	100.0	6.733	6.706	7.408	0.387	1641.99	1634.99

2) Vega PHT-P aperture photometry from 3.3 to 100 um on revolution 558

Measurements:
PHT-P: ppap55800420 (src+back) FCS = 3.6, 20, 100 um
       ppap55800419 (back)   FCS = 7.3, 25, 100 um

 Colour correction: black bodysee text for color correction

 Model: Cohen

Det	cwl [um]	OLP 7 [Jy]	OLP 8 [Jy]	IRAS [Jy]	Model [Jy]	% OLP 7 [(OLP-model)/model]	% OLP 8
P1	3.3	305.492	306.993		293.430	4.11	4.62
P1	3.6	294.957	290.779		268.410	9.89	8.33
P1	4.8	187.203	185.415		157.795	18.64	17.50
P1	7.3	79.368	76.357		70.934	11.89	7.65
P1	10.0	40.371	43.227		38.570	4.67	12.07
P1	12.0	21.543	21.938	28.640	26.997	-20.20	-18.74
P1	12.8	37.035	46.791		23.779	55.75	96.78
P1	15.0	36.645	34.429		17.356	111.14	98.37
P2	20.0	13.851	12.775		9.838	40.80	29.86
P2	25.0	12.072	11.613	9.938	6.301	91.61	84.31
P3	60.0	6.990	6.507	9.121	1.087	543.30	498.84
P3	100.0	6.110	5.745	7.408	0.387	1480.91	1386.31

3) Vega PHT-P aperture photometry from 3.3 to 100 um on revolution 865

Measurements:
PHT-P: ppap86500706 (src+back) FCS = 3.6, 20, 100 um
       ppap86500705 (back)   FCS = 7.3, 25, 100 um

Colour correction: black bodysee text for color correction

Model: Cohen

Det	cwl [um]	OLP 7 [Jy]	OLP 8 [Jy]	IRAS [Jy]	Model [Jy]	% OLP 7 [(OLP-model)/model]	% OLP 8
P1	3.3	295.786	298.270		293.430	0.80	1.65
P1	3.6	295.808	292.034		268.410	10.21	8.80
P1	4.8	186.549	184.949		157.795	18.22	17.21
P1	7.3	79.606	76.780		70.934	12.23	8.24
P1	10.0	33.282	35.400		38.570	-13.71	-8.22
P1	12.0	18.742	19.727	28.640	26.997	-30.58	-26.93
P1	12.8	29.700	38.202		23.779	24.90	60.66
P1	15.0	31.365	28.111		17.356	80.72	61.97
P2	20.0	13.963	12.934		9.838	41.94	31.48
P2	25.0	12.096	11.689	9.938	6.301	91.99	85.52
P3	60.0	8.425	7.947	9.121	1.087	675.32	631.38
P3	100.0	6.802	6.511	7.408	0.387	1659.85	1584.59

7.3.7 General Re-validation of PHT03 and PHT22 Staring Mode: The SED of Arp 220 - Final Assessment

- authors: M. Radovich, U. Klaas
- date: 26-July-1999
  revised version on 07-March-2000 to correct OLP 8 results for wrong modified BB color correction (SPR-3179)
- SVP period 2

Motivation

This is the final calibration assessment and a repetition of the assessment performed for SVP1, cf. Sect. 5.4.7 to check for changes.
TDTs 47600413(background, PHT-P), 47600414(Arp 220, PHT-P), 47600415(background, PHT-C), 47600416(Arp 220, PHT-C) is one of the key OLP V7.0 validation cases [1]. The staring mode AOTs PHT-03 and PHT-22 in all PHT filters measure a galaxy SED which is steeply rising between 10 and 60 μm and gradually declining beyond 100 μm, hence has a very different shape than a stellar atmosphere SED. It can therefore be used for a check of the robustness of the relative filter-to-filter calibration and the color correction factors applied to modified Black Bodies in the temperature range 50 – 120 K. Arp 220 is significantly bright over the full wavelength range from 3.3 to 200 μm. Its photometric properties are discussed in detail in "Infrared spectral energy distributions of the interacting galaxies Arp 244, NGC 6240 and Arp 220" [15].

Method

We compare the background subtracted flux values of both OLP V7.0 and OLP V8.4b3 results against the IRAS photometry and a model fit based on the OLP V6.x calibration.

Results

Fig. 7.22 shows the derived SED for Arp 220. The model fit from [15] is plotted as a guide line to easier recognize the changes w.r.t. OLP V7.0. Note that this fit cannot serve as reference photometry.
We have color corrected the photometry w.r.t. modified blackbodies with emissivities $\propto \lambda^{-1}$ for the 12.8 to 200 μm range (for details, see part 2 of the evaluation log section. This color corrected SED are shown in Fig. 7.23. Note, that the color correction is only correct for the OLP 8 result, the OLP 7 result has wrong color correction factors applied (as documented in SPR-3179) but was kept as presented in [1].
We notice the following results:

- C200 photometry looks quite good now, fluxes are a bit higher than indicated by the model. The SED in the C200 range is very smooth with some remaining flux excess of the 170 μm point (note in comparison with the uncorrected photometry the importance of color correction). Linearization and point spread fraction corrections for the C200 array centred photometry seem to be correctly implemented.
- The distribution of the C100 photometric points looks rather smooth and displays a flat shape of the SED over 40 μm. The color correction straightens the shape, however the remaining dip of up to 25 % at 80 μm with regard to the model is hardly believable. At 100 μm the flux is quite close to the IRAS one (within 6 %). The reason for this dip has to be investigated. It may be related to the fact that the source is quite bright and signals may exceed the upper limit of the calibrated range of the linearity correction.
- The P3 photometry is now more consistent with IRAS, the model and the C100 photometry and shows a smooth transition to the C200 range. Fluxes are still about 15 % too high with regard to IRAS and the model.
- The small shoulder in the 12 to 25 μm range also visible in the OLP V7.0 data is now gone. This may well be okay, however the 16 μm point appears to be too low. The

11.3 μ point appears to be more realistic now, as it should not be severly affected by absorption as the 10 μm point.

- From the PHT-S spectrum in Sect. 5.2.4 we calculate a flux density in the narrow band filters at 7.7 and 11.3 μm of 0.5 and 0.42 Jy, respectively. The PHT-P fluxes are smaller.

In Fig. 7.24 we plot the derived multi-filter surface brightness values in comparison with COBE photometry. Though not yet scientifically validated we note a very good agreement between PHT-P surface brightness values and COBE photometry, in particular the transition between P1 and P2 range is much smoother now, the only points which sticks a bit off is the 11.3 μm point (the 3.3 μm point has to be excluded from the discussion, because a fair photometry on the background in this narrow band filter cannot be performed with the selected aperture). Also the C100 and C200 surface brightness photometry looks well matched with COBE/DIRBE, again as in the previous test cases we notice the excess at 65 and 100 μm. The P3 surface brightness values are too low, but have been improved with regard to OLP V7.0.

Conclusions

- We find a good consistency with IRAS photometry (-11 % at 12 μm, -11 % at 25 μm, +17 % (P3) and -15 % (C100) at 60 μm, +15 % (P3) and -6 % (C100) at 100 μm.
- The C200 photometric points show a relatively smooth distribution after color correction with a modified black body of 47 K. The upgraded point spread function fraction factors for array centred photometry appear to work very well and also the relative filter-to-filter corrections.
- The C100 photometric points lie too low by up to 25 %. In particular the dip at 80 μm is hardly believable and needs further investigation. This may be related to the upper limits of the calibrated ranges of the C100 signal linearity corrections.
- The PHT-P3 photometry looks improved, and is now much more consistent with IRAS and the C200 photometry.
- The P1 and P2 photometry looks reasonable. The indication of a deficiency of some 40 % of the flux in the narrow band filters at 7.7 and 11.3 μm versus PHT-S spectroscopy needs more detailed investigation summing the PHT-S fluxes over the narrow band filter bandpass.
- Surface brightness photometry looks very good for this test case, even for the non-validated PHT-P photometry. We confirm with this test case the systematic positive excess of surface brightness flux at 65 and 100 μm.

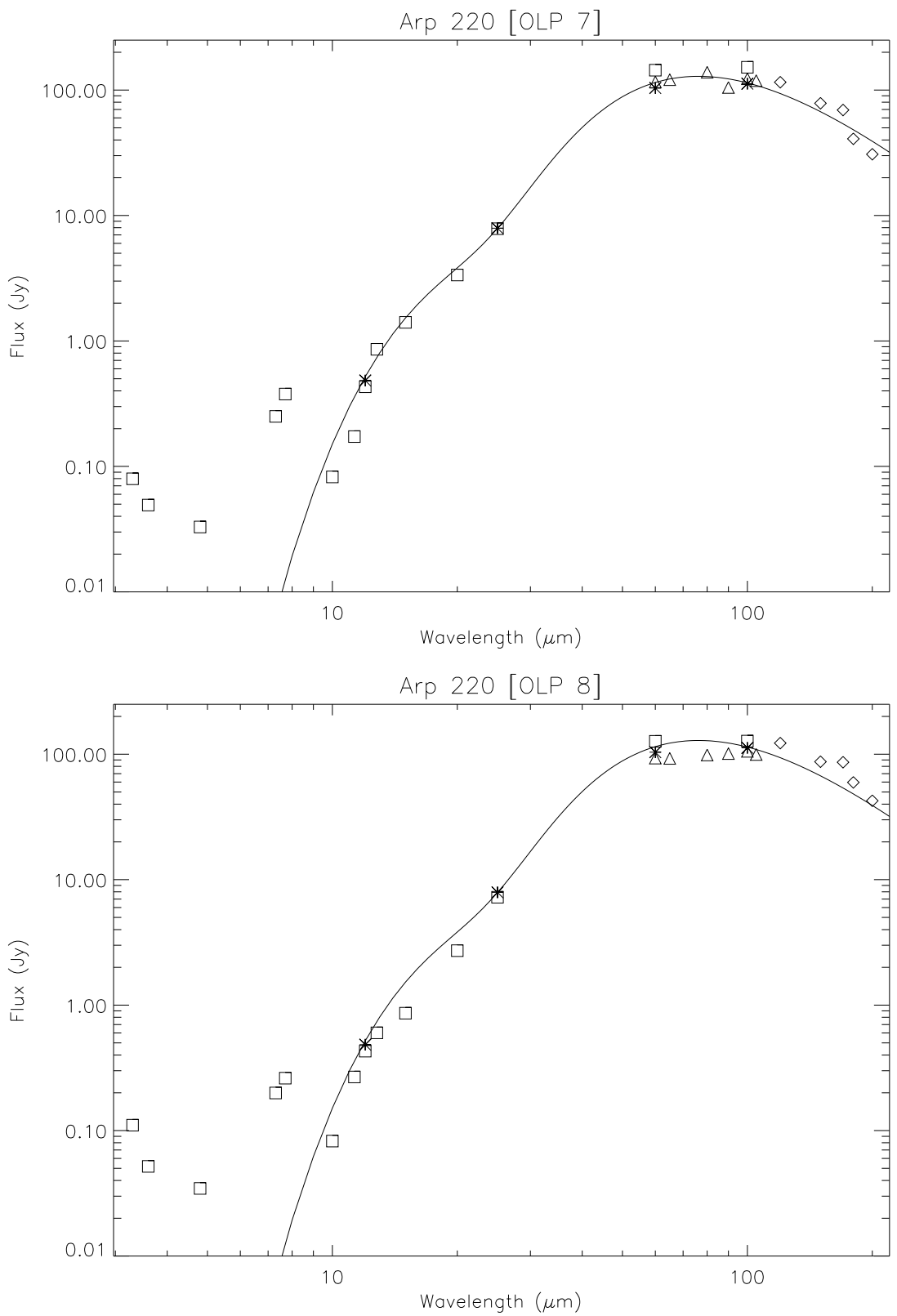

Figure 7.22: Comparison of PHT-P and PHT-C photometry, using the full ISOPHOT filter set, with IRAS photometry and the model fit as described in [8]. Note that this model fit only serves as a guide for the eye to recognize more easily the changes between the two versions. It is not an absolute photometric reference. No color correction has been applied. The meaning of the symbols is the following: solid line: model, asterisk: IRAS, square: PHT-P (P03 AOT), triangle: C100 (P22 AOT), diamond: C200 (P22 AOT).

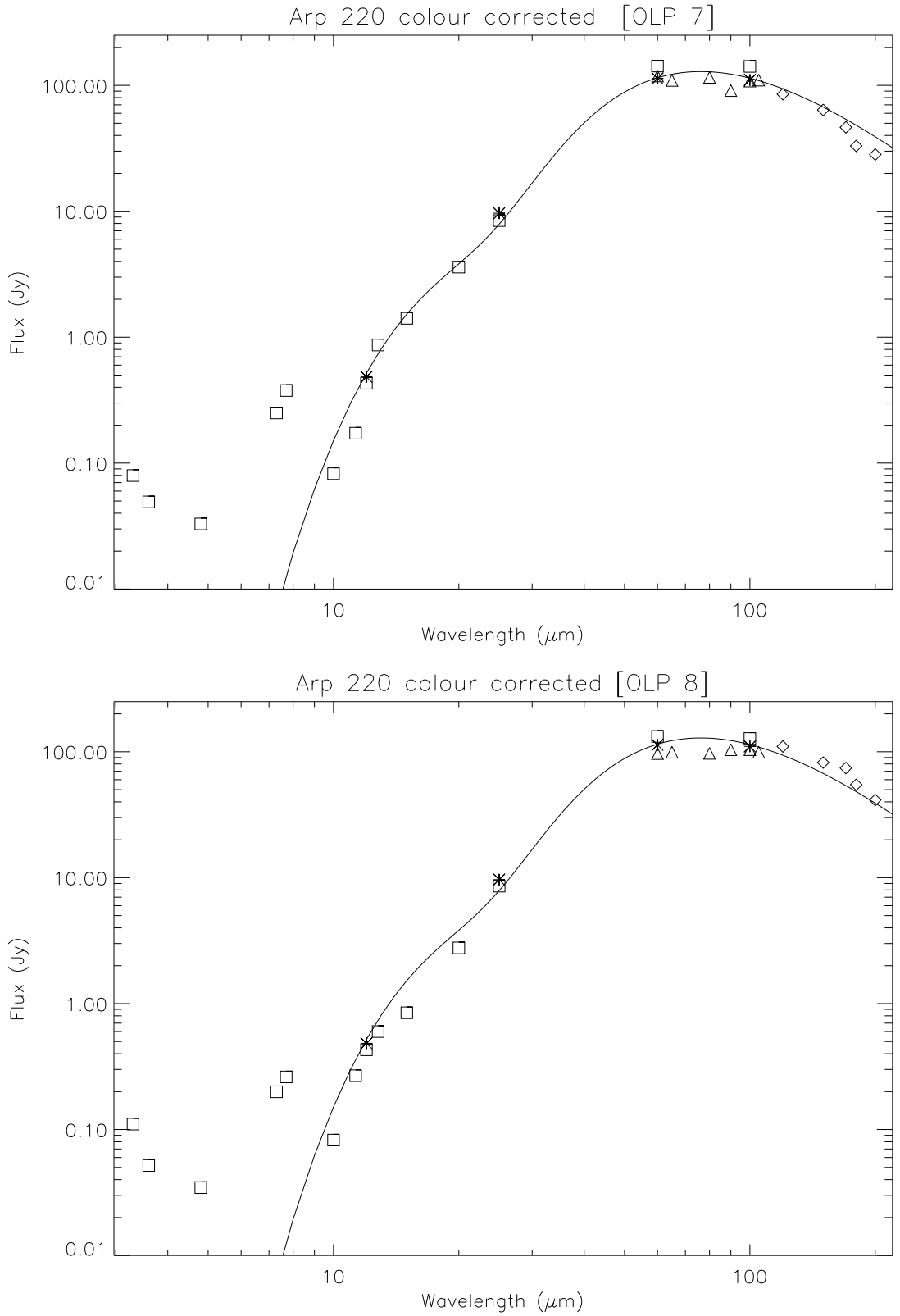

Figure 7.23: Comparison of PHT-P and PHT-C photometry, using the full ISOPHOT filter set, with IRAS photometry and the model fit as described in [8]. Note that this model fit only serves as a guide for the eye to recognize more easily the changes between the two versions. It is not an absolute photometric reference. Color correction according to the model parameters, modified BBs $\propto \lambda^{-1}$ with T1 = 120 K and T2 = 47 K, has been applied (**note:** for OLP 7 wrong factors were used). The meaning of the symbols is the following: solid line: model, asterisk: IRAS, square: PHT-P (P03 AOT), triangle: C100 (P22 AOT), diamond: C200 (P22 AOT).

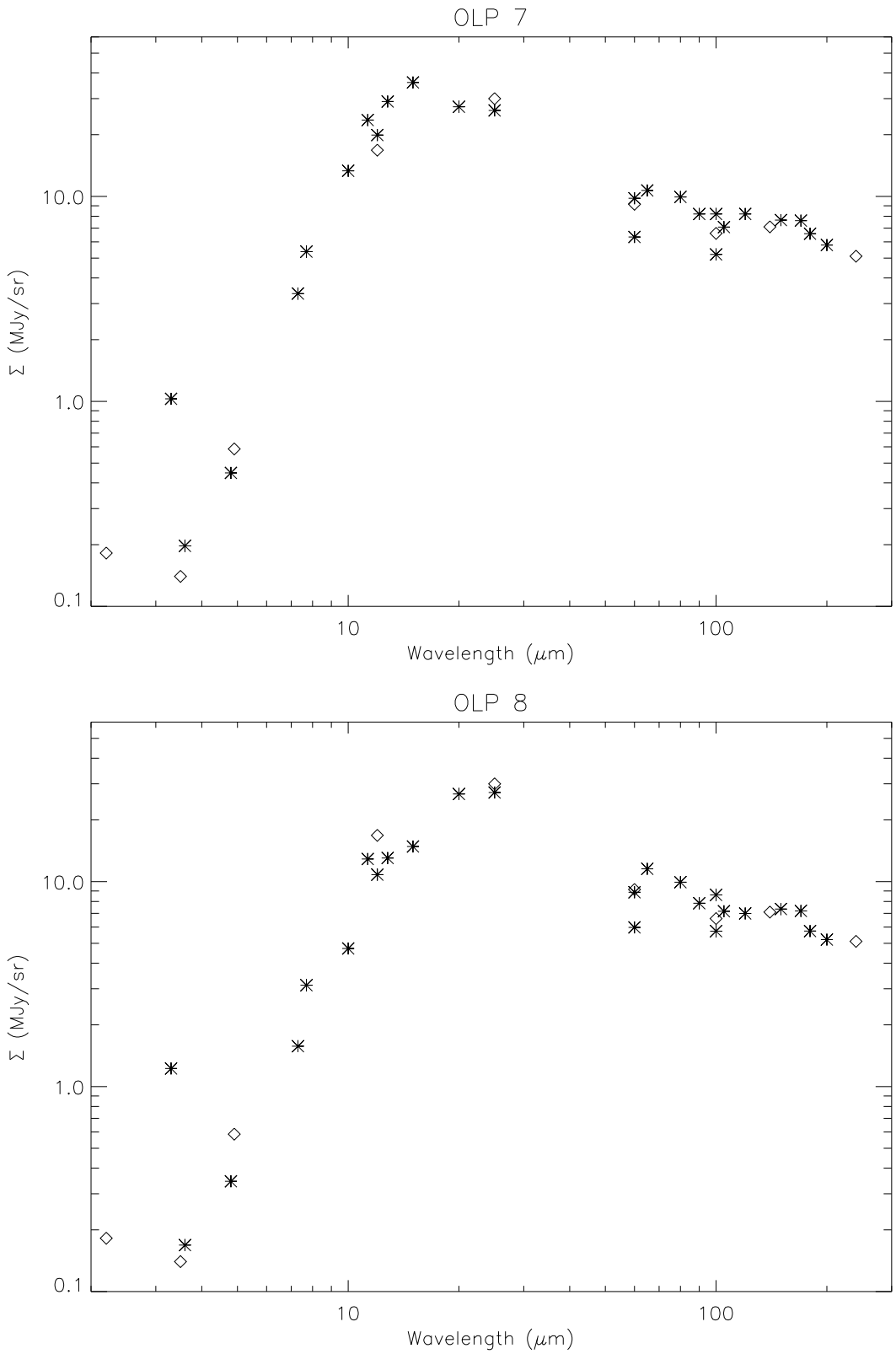

Figure 7.24: Comparison of PHT surface brightness photometry with COBE, both for OLP 7.0 and OLP 8.4b3. Asterisk: PHT-P and PHT-C photometry, diamond: COBE.

Evaluation Log

```
1) point source photometry of Arp 220 (not colour corrected)

Measurements:
PHT-P: ppap47600414 (src+back)   FCS = 3.3, 25, 100 um
       ppae47600413 (back)       FCS = 3.3, 20, 100 um
PHT-C: pcap47600416 (src+back)   FCS = 90, 170 um
       pcae47600415 (back)       FCS = 90, 170 um

 Model: Sum of 2 modified bb, em. $\propto \lambda^{-1}$, T1=120 K, T2 = 47 K

fluxes are in Jy

Det   cwl    OLP 7     OLP 8     IRAS       Model     Delta(OLP 7) Delta(OLP 8)
P1    3.3     0.080     0.110                0.000         --           --
P1    3.6     0.049     0.052                0.000         --           --
P1    4.8     0.033     0.035                0.000         --           --
P1    7.3     0.250     0.199                0.009         --           --
P1    7.7     0.377     0.262                0.015         --           --
P1   10.0     0.082     0.082                0.151       -45.40       -45.43
P1   11.3     0.173     0.268                0.367       -52.83       -27.05
P1   12.0     0.431     0.430     0.484      0.519       -16.99       -17.26
P1   12.8     0.858     0.601                0.746        14.94       -19.44
P1   15.0     1.407     0.862                1.525        -7.72       -43.48
P2   20.0     3.355     2.717                3.827       -12.33       -29.02
P2   25.0     7.850     7.242     7.920      7.902        -0.66        -8.35
P3   60.0   143.959   126.798   103.800    114.880        25.31        10.37
C1   60.0   116.112    93.042   103.800    114.880         1.07       -19.01
C1   65.0   120.954    92.523              122.541        -1.29       -24.50
C1   80.0   138.594    98.543              128.115         8.18       -23.08
C1   90.0   104.753   101.134              122.723       -14.64       -17.59
P3  100.0   151.866   127.305   112.400    113.981        33.24        11.69
C1  100.0   122.924   105.380   112.400    113.981         7.85        -7.55
C1  105.0   118.729    99.406              109.033         8.89        -8.83
C2  120.0   115.413   122.571               93.777        23.07        30.70
C2  150.0    78.419    87.091               67.225        16.65        29.55
C2  170.0    69.316    86.342               53.793        28.86        60.51
C2  180.0    40.852    59.597               48.236       -15.31        23.56
C2  200.0    30.786    42.555               39.038       -21.14         9.01


2) point source photometry of Arp 220 (colour corrected from 10 to 200 um)

Measurements:
PHT-P: ppap47600414 (src+back)   FCS = 3.3, 25, 100 um
       ppae47600413 (back)       FCS = 3.3, 20, 100 um
PHT-C: pcap47600416 (src+back)   FCS = 90, 170 um
       pcae47600415 (back)       FCS = 90, 170 um

 Model: Sum of 2 modified bb, em. $\propto \lambda^{-1}$, T1=120 K, T2 = 47 K

fluxes are in Jy

Det   cwl    OLP 7     OLP 8     IRAS       Model     Delta(OLP 7) Delta(OLP 8)
P1    3.3     0.080     0.110                0.000         --           --
P1    3.6     0.049     0.052                0.000         --           --
P1    4.8     0.033     0.035                0.000         --           --
P1    7.3     0.250     0.199                0.009         --           --
P1    7.7     0.377     0.262                0.015         --           --
P1   10.0     0.082     0.082                0.151       -45.40       -45.43
P1   11.3     0.173     0.268                0.367       -52.83       -27.05
P1   12.0     0.431     0.430     0.484      0.519       -16.99       -17.26
P1   12.8     0.867     0.600                0.746        16.21       -19.60
```

P1	15.0	1.413	0.846		1.525	-7.35	-44.54
P2	20.0	3.604	2.769		3.827	-5.84	-27.64
P2	25.0	8.431	8.570	9.647	7.902	-6.71	8.46
P3	60.0	142.252	132.357	113.300	114.880	23.83	15.21
C1	60.0	118.602	96.717	113.300	114.880	3.24	-15.81
C1	65.0	109.362	99.273		122.541	-10.75	-18.99
C1	80.0	115.591	97.087		128.115	-9.78	-24.22
C1	90.0	90.853	103.727		122.723	-25.97	-15.48
P3	100.0	141.402	127.432	110.400	113.981	24.06	11.80
C1	100.0	108.113	103.925	110.400	113.981	-5.15	-8.82
C1	105.0	110.036	99.109		109.033	0.92	-9.10
C2	120.0	85.113	110.127		93.777	-9.24	17.43
C2	150.0	63.807	82.084		67.225	-5.08	22.10
C2	170.0	46.458	74.241		53.793	-13.64	38.01
C2	180.0	33.052	54.727		48.236	-31.48	13.46
C2	200.0	28.244	41.395		39.038	-27.65	6.04

3) Surface brightness photometry of Arp 220 background

cwl	OLP7 (MJy/sr)	OLP8 (MJy/sr)	& COBE (MJy/sr)
3.3	1.03	1.23	
3.6	0.20	0.17	
4.8	0.45	0.35	
7.3	3.36	1.57	
7.7	5.38	3.12	
10.0	13.33	4.72	
11.3	23.58	12.89	
12.0	19.92	10.81	16.81
12.8	29.04	13.04	
15.0	35.97	14.83	
20.0	27.38	26.76	
25.0	26.27	27.21	29.99
60.0	6.34	5.98	9.15
100.0	5.21	5.73	6.60
60.0	9.79	8.87	9.15
65.0	10.69	11.54	
80.0	9.94	9.93	
90.0	8.21	7.84	
100.0	8.21	8.61	6.60
105.0	7.08	7.17	
120.0	8.21	6.99	
150.0	7.66	7.34	7.10
170.0	7.62	7.19	
180.0	6.58	5.74	
200.0	5.79	5.21	5.11

7.3.8 Re-validation of C200 Absolute Photometry: The SEDs of Ceres and Uranus - Final Assessment

- authors: M. Radovich, U. Klaas
- date: 30-July-1999
- SVP period 2

Motivation

When performing the analysis of absolute C200 photometry test cases during OLP V7.0 scientific validation we noticed flux deficiencies in the order of 30 % with regard to the references for the long wavelength bands, in particular for 180 and 200 μm. This could be traced back to a poor array point spread function factor. For OLP 8.4 these factors were re-calibrated, see Sect. 7.3.1 for the calibration reference. We repeat the analysis here in order to check the new C200 array centered photometry point spread function correction factors.

Method

We compare the background subtracted, color corrected flux values of both OLP V7.0 and OLP V8.4b3 results against the model prediction by Lagerros for Ceres and Abbas for Uranus.

Results

Fig. 7.25 shows the results for ceres and Fig. 7.26 the results for Uranus, respectively. In Table 7.16 we have compiled the consistency check w.r.t. the model predictions. For all C200 filters an absolute photometric accuracy of 10 % is now achieved.

Table 7.16: Consistency check of C200 absolute photometry results with model predictions

Filter/ Object	**mode**	**consistency w.r.t. model OLP V7.0** [%]	**consistency w.r.t. model OLP V8.4b3** [%]
120.0 / Ceres	abs	-1.22	6.10
150.0 / Ceres	abs	-5.06	-0.94
170.0 / Ceres	abs	-11.52	8.53
180.0 / Ceres	abs	-27.59	-3.96
200.0 / Ceres	abs	-39.38	-11.80
120.0 / Uranus	abs	1.42	-7.55
200.0 / Uranus	abs	-27.27	-10.11

Conclusions

- The point spread function factors for C200 array centred photometry were successfully upgraded.
- For both Uranus (500 - 900 Jy) and Ceres (40 -1 20 Jy) C200 absolute photometry is now as accurate as 10 % over the full C200 wavelength range.

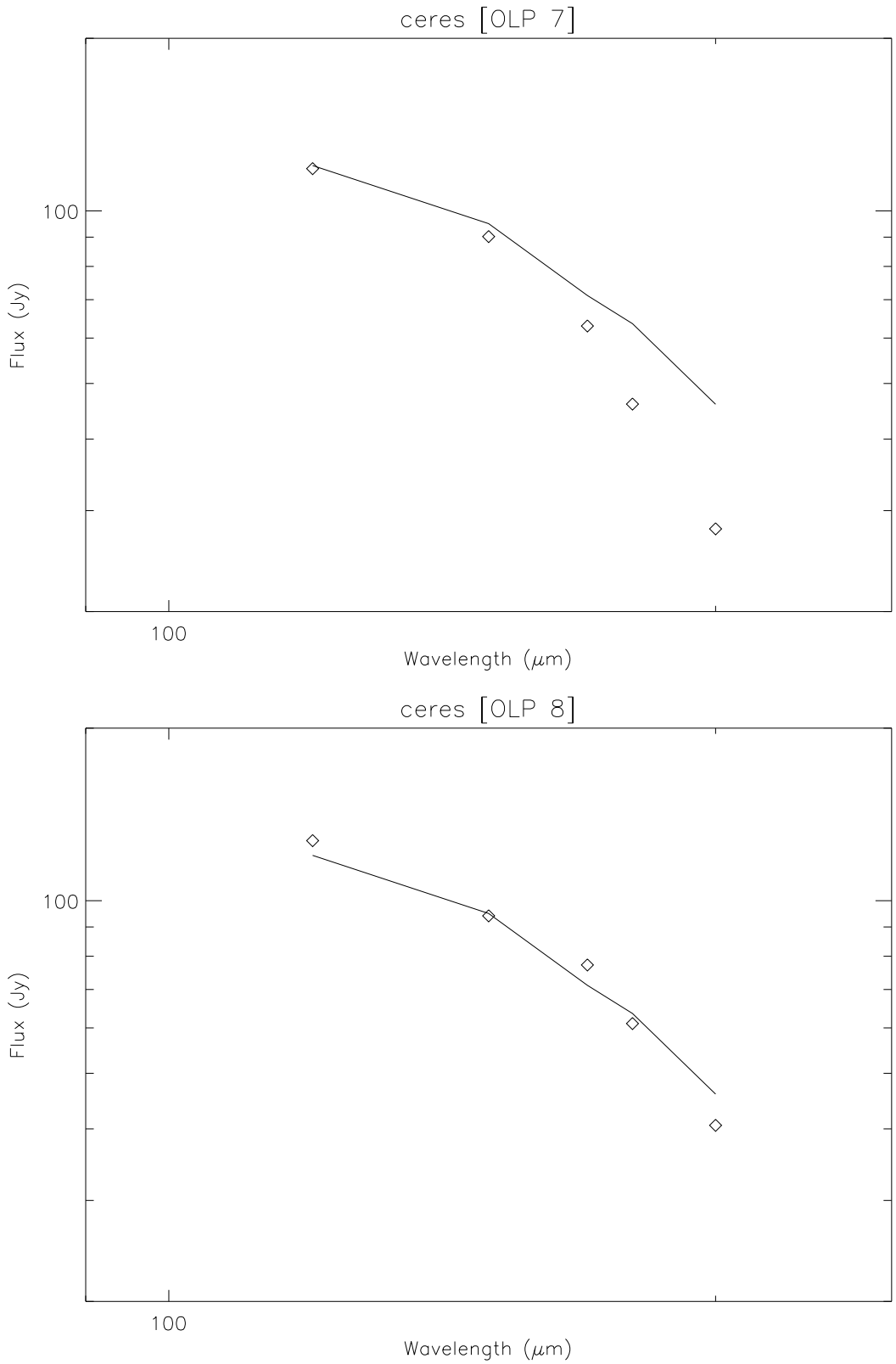

Figure 7.25: Comparison of C200 photometry of Ceres with the model thermophysical model by Lagerros for OLP 7.0 (upper panel) and OLP 8.4b3 (lower panel). All photometric points are color corrected for a 240 K BB. The meaning of the symbols is the following: solid line: Lagerros model, diamond: PHT-C200 (P25 AOT).

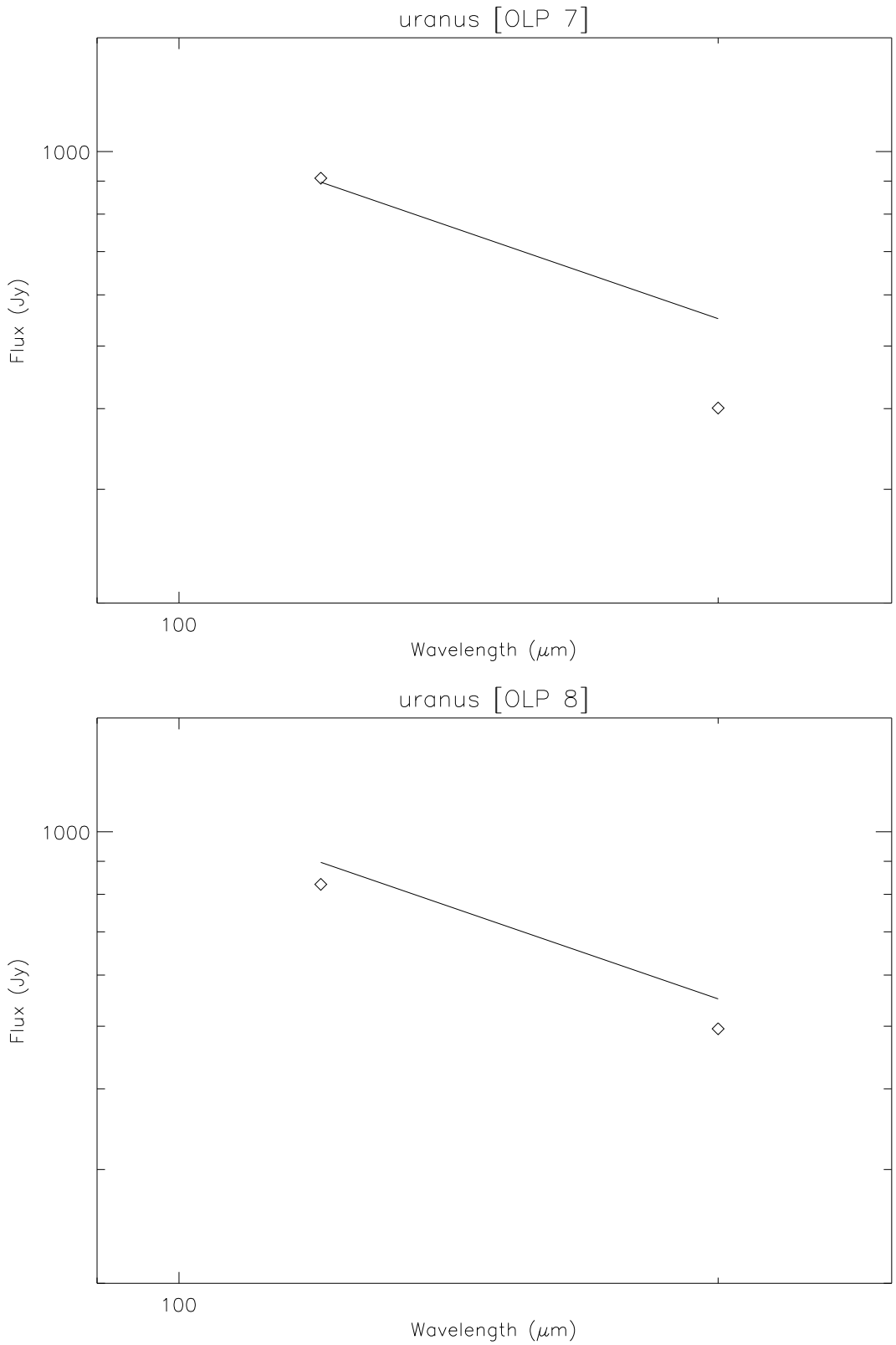

Figure 7.26: Comparison of C200 photometry of Uranus with the model provided by Abbas for OLP 7.0 (upper panel) and OLP 8.4b3 (lower panel). All photometric points are color corrected for a 60 K BB. The meaning of the symbols is the following: solid line: Abbas model, diamond: PHT-C200 (P25 AOT).

Evaluation Log

```
1) Absolute C200 Photometry of Ceres

PHT-C (120 um): pcap57901707 (src+back)
                pcae57901606 (back)
PHT-C (170 um): pcap57902111 (src+back)
                pcae57902010 (back)
PHT-C (200 um): pcap57901303 (src+back)
                pcae57901302 (back)
PHT-C (150 um): pcap59402607 (src+back)
                pcae59402506 (back)
PHT-C (180 um): pcap59402203 (src+back)
                pcae59402102 (back)

 Colour correction: black body, T = 240 K

 Model: Lagerros

Det   cwl    OLP 7    OLP 8    Model   % OLP 7   % OLP 8
C2   120.0  118.500  127.281  119.960   -1.22      6.10
C2   150.0   90.190   94.105   95.000   -5.06     -0.94
C2   170.0   62.980   77.252   71.180  -11.52      8.53
C2   180.0   46.030   61.055   63.570  -27.59     -3.96
C2   200.0   27.880   40.563   45.990  -39.38    -11.80


2) Absolute C200 Photometry of Uranus

PHT-C (120 um): pcap55204907 (src+back)
                pcae55204906 (back)
PHT-C (200 um): pcap55204703 (src+back)
                pcae55204702 (back)

 Colour correction: black body, T = 60

 Model: Abbas

Det   cwl    OLP 7    OLP 8    Model   % OLP 7   % OLP 8
C2   120.0  909.403  829.006  896.660    1.42     -7.55
C2   200.0  400.814  495.406  551.130  -27.27    -10.11
```

7.3.9 General Re-validation of Point Source Photometry from PHT03 and PHT22 Nodding Mode

- authors: M. Radovich, U. Klaas
- date: 02-August-1999
  revised version on 07-March-2000 to corect OLP 8 results for wrong modified BB color correction (SPR-3179)
- SVP period 2

Motivation

We have selected nodding observations as staring reference measurements for the chopped photometry validation. These observations, for which a large subset is performed on standard stars, are also used to verify the proper re-validation of the nodding mode itself.

Method

For all nodding observations with known reference fluxes we determine the consistency and derive absolute calibration numbers (as each nodding observation has two FCS calibration per filter, no relative filter-to-filter calibration values can be established from this assessment).

Results

Table 7.17 lists the derived source fluxes from the mapping products PGAI and compares, where available, against reference fluxes. For ISOPHOT-P the surface brightness values of the map product was converted into Jy using the conversion formula as given in [2], Sect. 8.4.10.1, equation 8.18. For ISOPHOT-C an aperture photometry on the array area of the on-source pointing, comprising the total object was performed. The resulting area in number of image pixels was converted into the number of true detector pixels. For conversion into Jy the above conversion formula was applied. The backgrounds were derived from the off-positions in the same way.
For P1 we get inconclusive results. There is a large scatter in the accuracies between 1 and 50 %. The case PGAI78300902 was already noticed during OLP V7.0 validation (cf. chapter 6.6 in [1]). Some calibration offset may be explained by the use of non-standard apertures, in particular with the short wavelength filters. In the case of TDT 78300902 signal transients may play an important role, as the source-to-background contrast is quite high, and actually the accuracy becomes much better the fainter the source flux, in particular, when the source flux drops below 3 Jy.
For P2 we find in the 3 to 6 Jy range a systematic excess in flux for ISOPHOT-model. This excess in the order of 25 to 30 % could indicate a calibration issue. For all measurements larger apertures than the standard aperture (79 arcsec) were used: either 120 or 180 arcsec. For OLP V7.0 the fluxes were found to be the same as the reference flux or up to 25 % too low (cf. Sections 6.6 and 6.8 of [1]. For the fainter fluxes below 1 Jy two test cases point to a better calibration accuracy in the order of 10 %. However, both were performed in the standard aperture.
The P3 nodding observations are absolutely calibrated with an accuracy of 10 % for the full covered flux range from 0.5 to 20 Jy.
The C100 absolute calibration in the flux range 0.5 to 4 Jy is within 25 The fainter source with a flux of 0.2 Jy shows the negative deficiency as found for several staring on-off measurements. The sum of all array pixels gives in three cases a more accurate result than the one from the central pixel 5 alone.
For C200 there is only one measurement with an absolute reference. It is for the star γ Dra. The achieved calibration accuracy is consistent with the calibration accuarcy achieved for absolute photometry on this source (cf. Sect. 7.3.4).

Table 7.17: Consistency check of OLP 8.4b3 nodding photometry results with reference fluxes. In case of C100 some fluxes have been obtained in a twofold way: using all pixels of the array or only pixel 5 (p5).

OLP product name	**target name**	**filter** (μm)	**flux** (Jy)	**color correction for spectrum**	**reference flux** (Jy)	**consistency w.r.t. reference** (%)
P1 detector						
PGAI51800417	PG1700+518	7.3	0.059	–	–	–
PGAI51800417	PG1700+518	12	0.041	–	–	–
PGAI74800701	HD172323	12	0.037	BB T=5720 K	0.064	-42.3
PGAI74801107	HR5986	12	2.192	BB T=6080 K	2.216	-1.1
PGAI78300902	HR6817	3.3	51.181	BB T=5000 K	10.216	+400
PGAI78301108	HR6817	3.6	13.151	BB T=5000 K	8.780	+49.8
PGAI78301006	HR6817	7.3	2.391	BB T=5000 K	2.358	+1.4
PGAI82501011	HR6847	3.6	4.409	BB T=5700 K	3.06	+44.1
P2 detector						
PGAI51800418	PG1700+518	25	0.272		–	–
PGAI74800609	HR7310	25	4.128	BB T=4850 K	3.403	+21.3
PGAI74800902	HR5986	25	0.561	BB T=6080 K	0.518	+8.3
PGAI76901901	HR6132	20	7.401	BB T=5000 K	5.909	+25.2
PGAI76902010	HR6132	20	7.051	BB T=5000 K	5.909	+19.3
PGAI76902105	HR6132	25	4.993	BB T=5000 K	3.803	+31.3
PGAI76902215	HR6132	25	5.853	BB T=5000 K	3.803	+53.9
PGAI81101704	IR03068-5346	20	0.120	mBBnu2 T=140 K	–	–
PGAI81101704	IR03068-5346	25	0.155	mBBnu2 T=140 K	0.176 (IRAS)	-11.9
P3 detector						
PGAI74800203	HR7310	60	0.658	BB T=4850 K	0.586	+12.3
PGAI79002002	HR617	60	2.143	BB T=4000 K	2.325	-7.8
PGAI79002002	HR617	100	0.898	BB T=4000 K	0.831	+8.1
PGAI86101305	HR1457	60	18.878	BB T=4000 K	19.12	-1.3
PGAI86101201	HR1457	100	5.058	BB T=4000 K	6.842	-26.1
C100 detector						
PGAI70705605	Sirius	60 (p5)	4.491	BB T=10000 K	3.680	+22.0
PGAI70705605	Sirius	60	4.103	BB T=10000 K	3.680	+11.5
PGAI74800504	HR7310	60	0.737	BB T=4850 K	0.586	+25.8
PGAI74800504	HR7310	100	0.117	BB T=4850 K	0.208	-43.8
PGAI81101907	IR03068-5346	60 (p5)	3.988	mBBnu2 T=40 K	3.822 (IRAS)	+4.3
PGAI81101907	IR03068-5346	60	3.585	mBBnu2 T=40 K	3.822 (IRAS)	-6.2
PGAI81101907	IR03068-5346	100 (p5)	4.280	mBBnu2 T=40 K	3.862 (IRAS)	+12.0
PGAI81101907	IR03068-5346	100	3.799	mBBnu2 T=40 K	3.862 (IRAS)	-1.6
C200 detector						
PGAI74801211	HR6705	170	0.524	BB T=4000 K	0.5563	-5.8
PGAI81102009	IR03068-5346	120	2.915	mBBnu2 T=40 K	–	–
PGAI81102009	IR03068-5346	200	1.121	mBBnu2 T=40 K	–	–

Conclusions

- The P1 test cases give inconclusive results about the absolute calibration accuracy of nodding mode measurements. A range from very accurate measurements ($\sim 1\,\%$) up to very high discrepancies (+400 %) can be found. There seems, however, to be the trend that for lower source-to-background contrasts the accuracy increases drastically and that signal transient effects and measurements in non-standard apertures can cause these high discrepancies. This needs to be followed up in more detail in the calibration project of the ISOPHOT-P aperture calibration.

- For P2 there is a range of test cases in the 3 to 6 Jy range for which ISOPHOT fluxes show a systematic excess of 25 to 30 % over the reference flux. All measurements were performed in large apertures (120 or 180 arcsec versus 79 arcsec of the standard

apertures). Preliminary calibrations of P2 aperture sequences indicate variations of 20 % of the flux per aperture area. Again, this needs to be followed up in more detail in the calibration project of the ISOPHOT-P aperture calibration. For fainter sources measured in the standard aperture calibration consistency with the reference of better than 10 % are achieved.

- The P3 test cases yield good and excellent results with an absolute accuracy of 10 % for the full covered flux range from 0.5 to 20 Jy. The relatively bad photometric accuracy obtained for HR 1457 (α Tau) at 100 μm could be caused by cirrus confusion, as the Taurus region has a relatively bright cirrus background.
- The C100 absolute calibration in the flux range 0.5 to 4 Jy is within 25 The fainter source with a flux of 0.2 Jy shows the negative deficiency as found for several staring on-off measurements. The sum of all array pixels gives in two out of three cases a more accurate result than the one from the central pixel 5 alone.
- In the case of C200 only one test case allows the derivation of an absolute accuracy. It is consistent with the absolute photometry result of the source γ Dra (HR 6705).

7.3.10 General Re-validation of Point Source Photometry from PHT22 Mini-Maps

- authors: M. Radovich, U. Klaas
- date: 03-August-1999
- SVP period 2

Motivation

We have selected mini-map observations as staring reference measurements for the chopped photometry validation. These observations, for which a large subset is performed on stars, are also used to verify the proper re-validation of the mini-map mode itself.

Method

For all mini-map observations with known reference fluxes we determine the consistency and derive absolute calibration numbers (as each mini-map observation has two FCS calibration per filter, no relative filter-to-filter calibration values can be established from this assessment).

Results

Table 7.18 lists the derived source fluxes from the mapping products PGAI and compares, where available, against reference fluxes. Aperture photometry on the map area of the source, comprising the total object was performed. As the maps have a fine image grid with image pixels smaller than the physical detector pixels, the number of image pixels was converted into the number of true detector pixels. For conversion into Jy the conversion formula as given in [2], Sect. 8.4.10.1, equation 8.18 was used.
For C100 there are several targets which were mainly selected for comparison with chopped photometry on the same target. They could have an infrared excess, hence the reference flux which is calculated by extrapolating the photospheric emission to longer wavelengths has to be considered as a lower limit; indeed the fluxes from the mini-maps are always higher. We do not consider these cases for derivation of absolute accuracies of mini-maps. For C100 the only test cases for determination of absolute accuracies in this table are the measurements of Sirius and HR 7310. The achieved accuracies are not good with respect to the results achieved for absolute photometry and nodding mode. They are only in the order of 30 to 40 %. Also for C200 the accuracy is of the same order, from the brightest source (Uranus) to the faintest source (HR 6705). These results look worse than the ones achieved fro OLP V7.0, however a spot check of one measurement with the method used now for OLP 8.0 revealed that the evalutaion results performed for OLP V7.0 validation could be incorrect: For the 60 μm Sirius measurement (PGAI70705603) a color corrected flux of 5.236 Jy was found, while previously [1] a value of 3.189 Jy was quoted. The consistency with the Sirius model flux would therefore be +42.3 % instead of -13.3 % for the OLP V7.0 product versus +32.0 % for the OLP V8.4b3 product, which would in fact have improved the calibration.
Therefore we declare all results of this chapter as preliminary, pending verification by an independent evaluation.
What could be the reason for the current performance data of mini-map photometry. There are several items, like flat-field accuracy, background variations as well as an unsufficient size of the map for background determination. Another issue may be the array filling factors which are corrected for in the case of single pointings. All these items have to be analysed in greater depth. One way to cross-check the map photometry with single pointing photometry is to inspect the related data products of type PCAS.
In Table 7.19 we provide the variation of the background fluxes taken at several points of the mini-map and the source-to-background contrast. From this table we can see the following:

- The background variations and the source-to-background contrast do not alone determine the final photometric accuracy. This can be seen from the cases Sirius 100 μm versus HR 7310 100 μm, the scatter in fluxes for HR 6705 (however background field rotated with time!), or the two Uranus observations.

Table 7.18: Consistency check of OLP 8.4b3 mini-map photometry results with reference fluxes. Percentages marked by (*) could be influenced by a possible IR excess and no proper color correction as well as an unreliable reference flux. IR excess means that the source has definitely no pure photospheric continuum and is not useful for establishment of absolute accuracy values. HD 172167 = HR 7001 = Vega.

OLP product name	**target name**	**filter** (μm)	**flux** (Jy)	**color correction for spectrum**	**reference flux** (Jy)	**consistency w.r.t. reference** (%)
C100 detector						
PGAI61001139	HD 142373	60	0.088	BB T=10000 K	0.064 (*)	+37.5 (*)
PGAI61001236	HD 128167	60	0.370	BB T=10000 K	0.048 (*)	–
PGAI61002158	HD 203280	60	0.278	BB T=10000 K	0.243 (*)	+14.4 (*)
PGAI64700880	HD 139664	60	1.298	BB T=10000 K	0.045 (*)	–
PGAI69100108	HD 12311	60	0.180	BB T=10000 K	0.178 (*)	+1.1
PGAI69301251	HD 185395	60	0.158	BB T=10000 K	0.051 (*)	–
PGAI69500449	HD 185144	60	0.194	BB T=10000 K	0.096 (*)	–
PGAI69700102	HD 1581	60	0.201	BB T=10000 K	0.094 (*)	–
PGAI70705603	Sirius	60	4.856	BB T=10000 K	3.680	+32.0
PGAI70705604	Sirius	100	1.011	BB T=10000 K	1.302	-22.3
PGAI71500582	HD 172167	60	8.661	BB T=10000 K	1.170 (*)	–
PGAI71800269	HD 216956	60	9.188	BB T=10000 K	0.605 (*)	–
PGAI72300260	HD 203608	60	0.327	BB T=10000 K	0.080 (*)	–
PGAI72400584	HD 187642	60	1.470	BB T=10000 K	1.050 (*)	+40.0 (*)
PGAI74800404	HR 7310	100	0.348	BB T=4852 K	0.208	+67.3
PGAI75701121	HD 10700	60	0.792	BB T=10000 K	0.253 (*)	–
C200 detector						
PGAI55204704	Uranus	200	383.785	BB T=60 K	551.130	-30.0
PGAI55204908	Uranus	120	837.772	BB T=60 K	896.660	-6.6
PGAI55206105	HR6705	170	0.298	BB T=4000 K	0.566	-47.4
PGAI57903105	HR6705	170	0.329	BB T=4000 K	0.566	-41.9
PGAI57901808	Ceres	120	92.644	BB T=240 K	119.960	-22.8
PGAI59402708	Ceres	150	95.291	BB T=240 K	95.000	+0.3
PGAI57902212	Ceres	170	43.267	BB T=240 K	71.180	-39.2
PGAI59402304	Ceres	180	73.217	BB T=240 K	63.570	+15.2
PGAI57901404	Ceres	200	29.928	BB T=240 K	45.990	-34.9
PGAI59403105	HR6705	170	0.203	BB T=4000 K	0.566	-64.1
PGAI65001005	HR6705	170	0.146	BB T=4000 K	0.566	-74.2
PGAI65002103	HR1654	150	-0.095	BB T=4000 K	0.254	–
PGAI65002406	HR1654	170	-0.058	BB T=4000 K	0.197	–
PGAI65002709	HR1654	120	0.285	BB T=4000 K	0.399	-28.6
PGAI83200605	HR6705	170	0.301	BB T=4000 K	0.566	-46.8

- For the brighter source Ceres there seems to be some relationship between the background variation and the finally achieved accuracy. The two filters with the smallest variations show the highest accuracy. They have also similar source-to-background contrasts, while in the other 3 filters source flux is "somehow lost" with regard to the background. We also notice that the measurements in the two "good filters" were taken on an another revolution than the measurements of the three "bad ones". Different background conditions (moving source) or detector stability criteria may play a role.

- For HR 1654 the background surface brightness is higher than the on-source surface brightness in two filters, hence yielding non-detections.

Table 7.19: Homogeneity of background and source-to-background contrast in mini-maps of standards.

OLP product name	**target name**	**filter** (μm)	**flux** (Jy)	**σ(bkg) / av(bkg)*100** (%)	**F(src)/F(bkg)**
C100 detector					
PGAI70705603	Sirius OLP7	60	5.236	7.95	1.39
PGAI70705603	Sirius	60	4.856	7.59	1.38
PGAI70705604	Sirius	100	1.011	4.89	1.05
PGAI74800404	HR7310	100	0.348	2.43	1.05
C200 detector					
PGAI55204704	Uranus	200	383.785	4.92	2.57
PGAI55204908	Uranus	120	837.772	26.36	*****
PGAI57901808	Ceres	120	92.644	21.29	2.69
PGAI59402708	Ceres	150	95.291	2.80	4.48
PGAI57902212	Ceres	170	43.267	17.01	1.88
PGAI59402304	Ceres	180	73.217	9.16	4.75
PGAI57901404	Ceres	200	29.928	18.73	1.84
PGAI55206105	HR6705	170	0.298	10.14	1.02
PGAI57903105	HR6705	170	0.329	10.75	1.03
PGAI59403105	HR6705	170	0.203	11.48	1.02
PGAI65001005	HR6705	170	0.146	12.99	1.01
PGAI83200605	HR6705	170	0.301	7.44	1.03
PGAI65002103	HR1654	150	-0.095	4.01	0.99
PGAI65002406	HR1654	170	-0.058	4.79	0.99
PGAI65002709	HR1654	120	0.285	6.51	1.03

Conclusions

- Aperture of photometry of point sources in mini-maps yields an accuracy of 30 to 40 % for both PHT-C arrays.
- The reason for the worse performance than absolute photometry and nodding mode photometry needs more detailed investigations.

Chapter 8

Validation of the Chopped Point Source Photometry during SVP2

8.1 Revalidation of Chopped Photometry Test Cases from OLP 7.0 Validation Program

An overview of the test cases is outlined in Ref. [4], chapter 4.1.

8.1.1 References to Calibration Analysis and Software Change Documentation

- calibration reports:
  - Analysis of Chopped ISOPHOT Measurements [19]
- Software Change Requests: SCREW 382
- Software Problem Reports: SPR 2980, 2981, 2982, 2983

8.1.2 Summary of Results

- With regard to OLP V7.0 an improvement of the chopped photometry performance is noted, in particular for C100.
- The achieved general calibration accuracies, in particular for faint sources, for which this mode is preferentially used, are not yet sufficient to declare this mode scientifically valid.

8.1.3 Validation of PHT03 and PHT22 Chopped Mode: The SED of IRAS 03068-5346

- authors: M. Radovich, U. Klaas
- date: 06-August-1999
  revised version on 09-March-2000 to correct OLP8 results for wrong modified BB color correction (SPR-3179)
- SVP period 2

Motivation

Like for validation of staring mode observations The measurements on the IR galaxy IRAS 03068-5346 were designed to check out the processing of multi-filter chopped mode for all PHT-P and PHT-C filters. For reference photometry in nodding mode was taken for some filters (cf. Sect. 7.3.9) and IRAS photometry is available.

Method

We compare the background subtracted flux values of both OLP V7.0 and OLP V8.4b3 results against the IRAS photometry and the ISOPHOT nodding mode photometry.

Results

Fig. 8.1 shows the derived SED for IRAS 03068-5346. In comparison to OLP V7.0 we notice that C100 chopped photometry is now much more consistent with IRAS (with the old correction method, the correction was too strong) and also P3 photometry has improved. Fluxes are in general too low by 20 %.
For more details on consistency, also with the ISOPHOT staring modes, we have compiled in Table 8.1 the measurements in filters which have a corresponding measurement with IRAS or PHT nodding.
The P1 measurements are for quite faint flux level. There is no signal correction performed and the actual response used for OLP V8.4b3 gives a somewhat worse result than the OLP V7.0 default calibration. However, the signals are quite small, so that the result may not be so meaningful, but should be followed-up to figure out whether in this case the detection limit is reached or some improvement is still possible.
For P2 the absolute calibration of the 25 μm filter looked better for the OLP V7.0 version, however, the relative calibration between 20 and 25 μm is the same in both versions. The same arguments as for P1 may apply here.
For the brighter source fluxes measured with P3, C100 and C200 there is a clear improvement by the OLP V8.4b3 version. The fluxes from chopped photometry are consistent with IRAS and PHT nodding to within 25 %. In particular the too strong flux corrections seen for C100 in OLP V7.0 is gone now.
Fig. 8.2 shows the derived sky background SED at the position of IRAS 03068-5346 (not color corrected). Actually, here results from OLP V8.6b1 were used which include the fixes for SPRs 3006 and 3029. In comparison to OLP V7.0 one can see that the SED is much smoother now and also matches with COBE/DIRBE photometry to within 50 % for practically all filters (the strong outlier is the C_65 filter measurement). It resembles the measured SEDs from staring mode observations, like seen in Fig. 7.24. Quantitative numbers with regard to the consistency are given in Table 8.2.

Conclusions

- The flux levels for P1 and P2 detectors appear too faint to draw quantitative conclusions without further detailed interactive analysis for the reason of the relatively strong flux discrepancies with regard to IRAS and PHT nodding mode.
- For the brighter flux levels above 1 Jy in the 60 to 200 μm range the new chopper correction in OLP 8.4b3 shows more accurate and homogeneous results. Consistency with IRAS and PHT nodding mode is within 25 %

Table 8.1: Consistency check of chopped photometric results with ISOPHOT nodding observations or IRAS.

Filter	**reference**	**consistency w.r.t. reference**	
		OLP V7.0 [%]	**OLP V8.4b3** [%]
12.0	IRAS	-80.0	-97.3
20.0	PHT nodding	+95.0	+47.5
25.0	PHT nodding	-6.5	-58.7
25.0	IRAS	-17.6	-63.6
60.0 (P3)	IRAS	+38.9	-24.1
60.0 (C100)	PHT nodding	+69.0	-22.6
60.0 (C100)	IRAS	+76.3	-19.2
100.0 (P3)	IRAS	+5.3	-22.0
100.0 (C100)	PHT nodding	+41.4	-11.3
100.0 (C100)	IRAS	+56.7	-1.7
120.0	PHT nodding	+17.5	-16.5
200.0	PHT nodding	-39.0	-30.5

Table 8.2: Consistency check of γ Dra background position surface brightness results with COBE/DIRBE annual maps.

wavelength μm	**consistency w.r.t. COBE OLP V7.0** [%]	**consistency w.r.t. COBE OLP V8.4b3** [%]
12 (P1)	+102	-30.4
25 (P2)	+44.3	+12.8
60 (P3)	+8.7	-46.3
60 (C100)	+121	-40.3
100 (P3)	+57.1	+11.4
100 (C100)	+163	+45.5
150	-4.0	-6.5
200	-48.8	-20.9

- Although the new OLP 8 signal loss correction for chopped measurements is mainly designed to get the differential (source) fluxes correct, the implemented corrections for the absolute background level bring considerable improvement versus OLP V7.

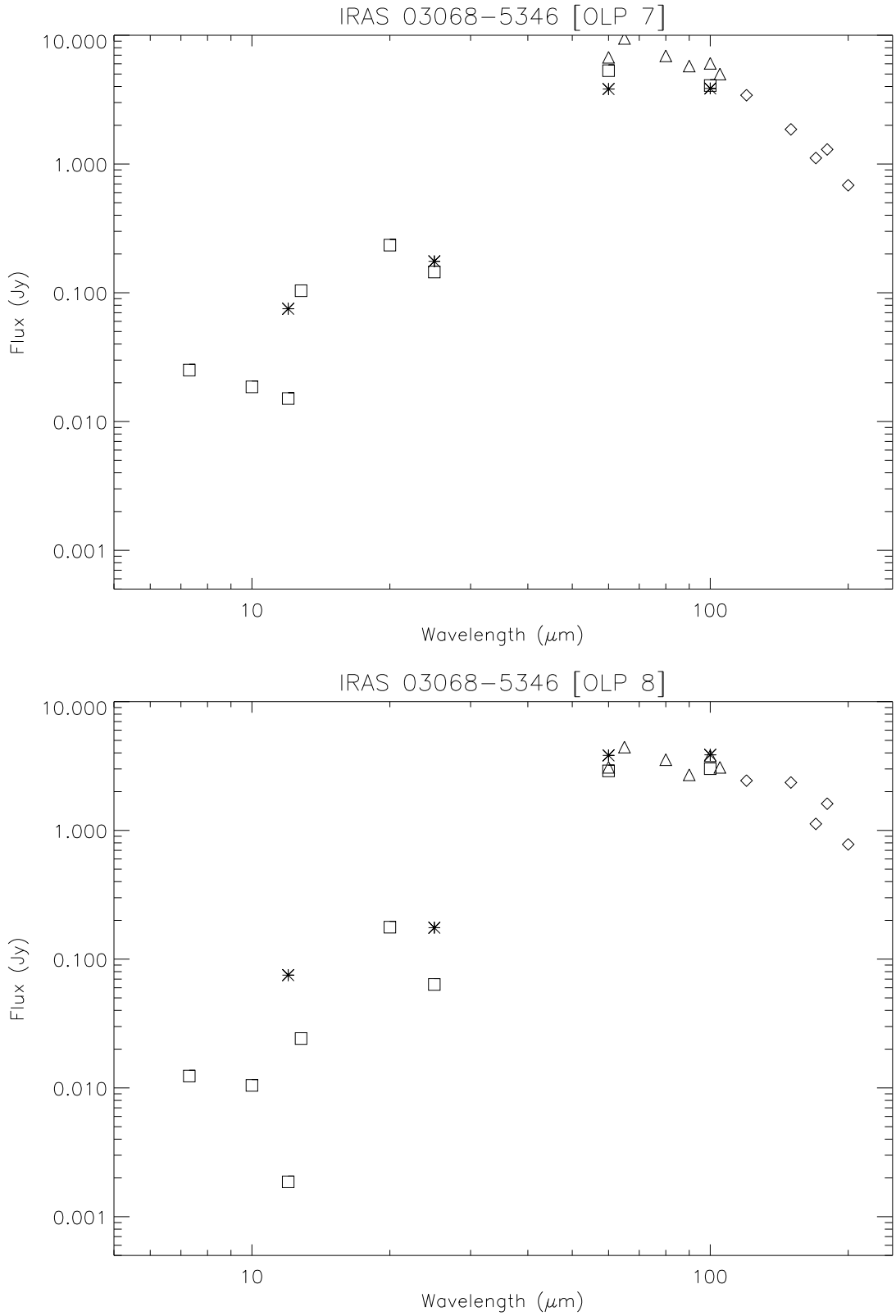

Figure 8.1: Comparison of PHT-P and PHT-C chopped photometry, using the full ISOPHOT filter set, with IRAS photometry. Color correction has been applied (modified BBs $\propto \lambda^{-2}$ with T1 = 140 K and T2 = 40 K). The meaning of the symbols is the following: asterisk: IRAS, square: PHT-P (P03 AOT), triangle: C100 (P22 AOT), diamond: C200 (P22 AOT).

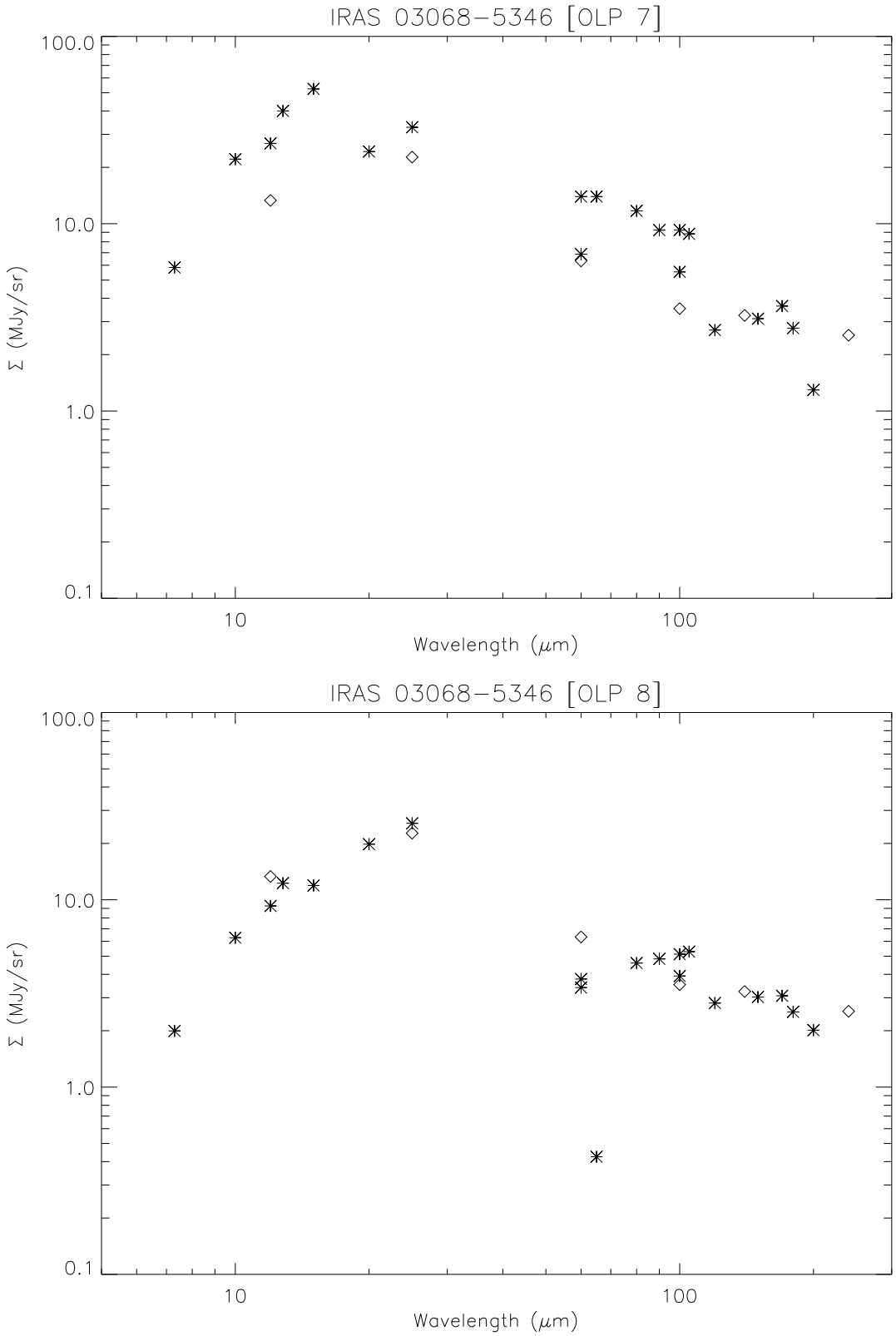

Figure 8.2: Comparison of surface brightness from chopped PHT photometry of the background beam for IRAS 03068-5346 with COBE, both for OLP 7.0 and OLP 8.6b1. Asterisk: PHT-P and PHT-C photometry, diamond: COBE.

Evaluation Log

```
1) Chopped Point Source Photometry

Measurements:
PHT-P1: ppap81101701:  FCS =  12 um
PHT-P2: ppap81101701:  FCS =  25 um
PHT-P3: ppap81101802:  FCS = 100 um
PHT-C1: pcap81101906:  FCS =  90 um
PHT-C2: pcap81102008:  FCS = 170 um

 Colour correction: mod. bb, em.=2, T =   140(P1, P2)   40(P3, C1, C2)

fluxes are in Jy

Det   cwl   OLP 7    OLP 8   IRAS
P1    7.3   0.025    0.012
P1   10.0   0.019    0.010
P1   12.0   0.015    0.002   0.075
P1   12.8   0.104    0.024
P1   15.0  -0.015    0.000
P2   20.0   0.234    0.177
P2   25.0   0.145    0.064   0.176
P3   60.0   5.307    2.899   3.822
C1   60.0   6.739    3.088   3.822
C1   65.0   9.443    4.434
C1   80.0   6.914    3.540
C1   90.0   5.766    2.701
P3  100.0   4.068    3.014   3.862
C1  100.0   6.050    3.797   3.862
C1  105.0   4.994    3.085
C2  120.0   3.425    2.434
C2  150.0   1.859    2.355
C2  170.0   1.113    1.124
C2  180.0   1.298    1.613
C2  200.0   0.684    0.779

TDT: ppap54502911 (OLP 8 only)
P1   10.0           -0.005
P1   12.0            0.036
P1   15.0            0.016
P2   25.0           -0.080


2) Background photometry from off-source beam

fluxes are in MJr/sr

Det   cwl   OLP7     OLP8    COBE
P1    7.3   5.84     2.00
P1   10.0  22.11     6.27
P1   12.0  26.85     9.27   13.32
P1   12.8  40.01    12.26
P1   15.0  52.45    11.92
P2   20.0  24.28    19.81
P2   25.0  32.74    25.60   22.69
P3   60.0   6.88     3.40    6.33
C1   60.0  13.96     3.78    6.33
C1   65.0  13.96     0.42
C1   80.0  11.70     4.59
C1   90.0   9.24     4.84
P3  100.0   5.53     3.92    3.52
C1  100.0   9.25     5.12    3.52
C1  105.0   8.83     5.29
```

```
C2  120.0   2.71     2.81
C2  150.0   3.11     3.03    3.24
C2  170.0   3.63     3.07
C2  180.0   2.77     2.52
C2  200.0   1.30     2.01    2.54
```

8.1.4 Validation of PHT03 and PHT22 Chopped Mode: The FIR Excess SED of Vega

- authors: M. Radovich, U. Klaas
- data: 08-October-1999
  revised version on 10-March-2000 to correct OLP8 results for wrong modified BB color correction (SPR-3179)
- SVP period 2

Motivation

We investigate here observations of a general observer's program for which photometry using Interactive Analysis has been published, cf. Ref. [14]. In addition, IRAS photometry at 25, 60, and 100 μm is available.

Method

We compare the color corrected source flux values of both OLP V7.0 and OLP V8.4b3 with model fluxes, IRAS photometry and the photometry derived in [14] (called HWK photometry in the following).
The color correction was dependent on the relative contribution by the stellar photosphere and the IR disc, and hence on the wavelength. We followed the description as given in Ref.[14]:

- from 60 to 100 μm the SED behaves like an 80 K modified BB, $\varepsilon \propto \nu$
- from 20 to 25 μm the SED is a mixture of a 10000 K BB and an 80 K modified BB with a ratio 2:1.

Results

In the evaluation log we provide a comparison of the various photometric results and in Fig. 8.3 we plot the ISOPHOT OLP V8.4b3 photometry versus the photospheric model and the IRAS photometry.
For the 25 μm filter we notice that the ISOPHOT flux is just on the photosperic model prediction (-5.5 %) and underestimates the total flux, including the IR excess, as determined with IRAS by 40 % and as determined by HWK by 44 %. It is not consistent either with the results from staring mode photometry obtained on rev. 85 presented in Sect. 7.3.6, which gives even 11.7 Jy.
The 90 μm flux derived from measurement PCAP08900789 is zero. This is because of the failure of the chopped signal pattern generator for the read-out set-up selected for this measurement (reset interval = 1/16 s, data reduction factor = 2), cf. Caveat in Sect. 2.13.
While for OLP V7.0 the 60 μm flux derived from TDT 10601101 was, after applying the correct color correction factors, consistent with the IRAS flux (+5 %), it is now lower by 45 %. The 60 μm flux derived from TDT 08900789 is too low with regard to the IRAS value, too (-36 %). The ISOPHOT fluxes, being derived with two different FCS calibration files (TDT 08900789 with pre-rev 94 calibration and TDT 10601101 with post-rev. 94 calibration) correspond to within $\pm$ 8 %. With the staring mode ISOPHOT observations performed on Rev. 85 (cf. Sect. 7.3.6) the correspondence is not so good either, because this gives only a 10 % lower flux than IRAS. The fluxes at longer C100 wavelengths, 80 and 100 μm, derived from measurement 10601101 show a strange fall-off with regard to IRAS photometry and the C200 data points. A quite similar behaviour was found for OLP V7.0. With this version 8.4, which uses only the central pixel for derivation of the flux, some flux loss may be explained, if the cold disc emission of Vega is extended, however, at 60 μm HWK derived a Gaussian width of only 22 arcsec from high resolution scans, and the OLP V7.0 photometry determined the flux from the full array.
The 120 μm photometric point looks to be much more consistent with the IRAS photometry. In general the derived fluxes are higher than HWK derived. At 150μm the internal consistency of the chopped photometry is $\pm$ 7 %. While the 08900790 photometry indicates

a steep fall-off of the SED beyond 100 μm the 10601101 photometry yields a much flatter SED and the 200 μm point appears considerably too high.

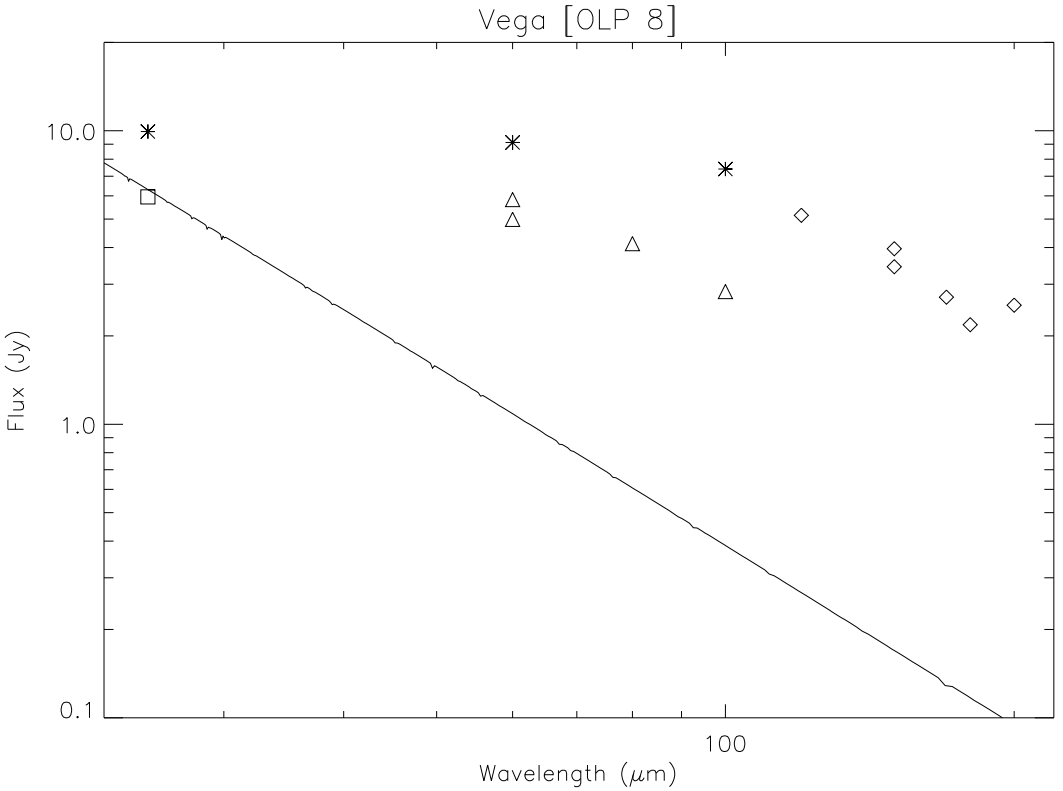

Figure 8.3: Comparison of PHT-P and PHT-C chopped photometry with the photospheric model of Vega by M. Cohen and with IRAS photometry. Color correction has been applied according to the description in the method section. The meaning of the symbols is the following: solid line: photospheric model, asterisk: IRAS, square: PHT-P (P03 AOT), triangle: C100 (P22 AOT), diamond: C200 (P22 AOT).

Conclusions

- The P2 chopped photometry underestimates the flux by at least 40 %, indicating that signal loss factors have to be determined for P2, too.
- The C100 chopped photometry yields now in general considerably lower fluxes than IRAS and shows in particular a strange and not understood fall-off towards longer wavelengths.
- There is a strong flux discrepancy in the SED between the ISOPHOT 100 μm and 120 μm fluxes, the latter one being more consistent with IRAS 100 μm photometry.
- The 90 μm zero flux of TDT 08900789 can be explained by a general chopped photometry caveat (cf. Sect. 2.13).
- No accuracy numbers have been derived for this example due to the uncertainty in the SED and hence the application of correct color correction factors.

Evaluation Log

```
Measurements:
PHT-P: ppap08900788    FCS = 25 um
PHT-C: pcap08900789    FCS = 90 um
       pcap08900790    FCS = 150 um
       pcap10601101    FCS = 60, 170 um

 Model: Cohen

 Color correction: see section Method for wavelength dependent color correction
                   application

 fluxes are in Jy

Det   cwl   OLP 7   OLP 8   IRAS   Model  HWK photom.
TDT 08900788
P2   25.0  10.081   5.951  9.938   6.301    10.58
TDT 08900789
C1   60.0    --     5.828  9.121   1.087    8.677
C1   90.0    --     0.000          0.478
TDT 08900790
C2  150.0    --     3.441          0.169    2.853
C2  180.0    --     2.184          0.117
TDT 10601101
C1   60.0   9.570   4.991  9.121   1.087    8.677
C1   80.0   7.440   4.125          0.607    6.845
C1  100.0   5.175   2.832  7.408   0.387    5.112
C2  120.0   6.948   5.150          0.267    3.650
C2  150.0   4.508   3.962          0.169    2.853
C2  170.0   3.181   2.711          0.129    1.722
C2  200.0   1.544   2.544          0.094    1.234
```

8.1.5 Comparison of Chopped and Staring Mode Photometry of Standard Stars from the Empirical Signal Correction Calibration Program

- authors: M. Radovich, U. Klaas
- date: 15-September-1999
- SVP period 2

Motivation

A large calibration program had been set up to establish the empirical signal loss correction factors in chopped measurements from a comparison of chopped and nodding/staring photometry in the same instrumental set-up, on the same source and on the same revolution (as one block of measurements, to minimize differences in detector responsivities.) We have selected a few of these measurements to verify the end product of the chopped photometric calibration, as produced by OLP. This does not only include the signal correction, but also the signal derivation itself and the flux calibration using the chopped FCS measurement. We have selected test cases with more than one filter per detector in order to see the relative wavelength behaviour of the correction.

Method

All targets are standard stars for which flux models are available. In all cases ISOPHOT reference photometry, either in simple staring mode or in nodding technique are available. This allows to determine the absolute accuracy w.r.t. the model and in case of a discrepancy to cross-check how the consolidated staring mode photometry behaves.

Results

In Fig. 8.4 we show the results for the P1 test case, 3.3 to 7.3 μm fluxes of the star HR 6817. Considerable improvement with regard to OLP V7.0 is recognizeable. The exception is the 3.3 μm point which is off by a factor of 7. This behaves, however, now consistent with the result of the nodding mode measurement. Since both modes have an own FCS measurement at 3.3 mum this suggests that the FCS calibration is off by a factor $5-7$ for the flux range of 10 Jy. In fact, the SPD data product gives a responsivity value of RS1P1F1 = 0.152163 A/W, a factor of 8 less than the default responsivity. For the other filters, the gain with regard to OLP V7.0 must be attributed to the usage of the actual responsivity (in combination with the linearity correction) instead of the default responsivity, since no signal correction is applied for P1.
In Fig. 8.5 we show the results for the P2 test case, 20 and 25 μm fluxes of the star HR 6132. There is no improvement, as the OLP V7.0 calibration gave already very good results. Since there is no signal correction applied for P2, for this test case default responsivity (OLP V7.0) and actual responsivity (OLP V8.4b3) give equivalent results. In Table 8.3 we present the results of a second test case with a larger aperture (180 arcsec instead of 120 arcsec, the standard aperture size for P2 is 79 arcsec). Here the accuracies are less good. They give an overestimate of the flux by about 30 %. The comparison with the corresponding nodding mode test cases shows that for the 120 arcsec aperture the fluxes are underestimated by 20 %, though in this case they are closer to the model prediction. For the 180 arcsec aperture there is no consistent picture at all.
In Fig. 8.6 we show the results for the P3 test case, 60 and 100 μm fluxes of the star HR 1457. The overall accuracy is in the order of 20 %. Chopped and nodding mode results are consistent. The flux underestimate, in particular at 100 μm which is also true for the IRAS flux, may be indicative of a weak cirrus confusion in this sky area (HR 1457 = α Tau).
In Table 8.3 we present the results for the C100 test case, 90, 100 and 105 μm fluxes of the star HR 6705 for two different chopper frequencies. With regard to OLP V7.0 a drastic improvement in the photometric accuracy can be noted. The correction for the faster chopper frequency is better than for the slower one. Nevertheless, there is still a considerable flux excess of 50 % found for the majority of the cases. It should be noted, however, that the C100 staring observations also show a positive flux excess of 20 - 30 % (with the exception

of the fluxes in the 105 μm filter which do not fit together at all) which has to be subtracted to get the residual error in the chopped signal correction.
In Fig. 8.7 we show the results for the C200 test case, 120 and 180 μm fluxes of the star HR 5340. The overall accuracy with regard to OLP V7.0 has been improved with an accuracy of better than 25 %. Chopped photometry results and staring mode on-off measurements give consistent results. This suggests that the accuracy improvement at 180 μm is linked to the non-linearity correction.

Conclusions

- For P1 there is a considerable improvement of the chopped photometry accuracy, except for the 3.3 μm filter. The achieved accuracies are better than 10 % for the test case HR 6817. Since there is no signal loss correction for P1, the improvement must be attributed to the usage of the actual responsivities derived from the FCS measurements instead of default responsivities. The considerably too high flux at 3.3 μm is consistent with the finding in the nodding mode. Since both modes have a FCS calibration in this filter suggests that the FCS1 calibration for the 3.3 μm filter is off by a factor of $5 - 7$ for the flux range 10 Jy, as indicated by the low derived actual responsivity RS1P1F1 = 0.152163 / Responsivity (A/W).

- For P2 accuracies of better than 40 % are found. There is a dependence on the selected aperture size. The measurement with an aperture size closer to the standard aperture gives the more accurate results (better than 15 %).

- For P3 accuracies of better than 20 % are found. The fluxes are in general underestimated and at 100 μm they may suffer from a weak cirrus confusion.

- For C100 we find a considerable improvement of the flux accuracies with a significantly reduced positive flux excess. Yet the residual flux excess is still in the order of 50 % for the majority of measurements. It has, however, to be noted, that the staring mode test cases also show a positive flux excess of $20 - 30$ % for this source. For the measurements with higher chopper frequencies better accuracies are achieved than for the lower frequencies.

- For C200 accuracies of better than 25 % are found. The fluxes are smaller than the model fluxes, similar as found for staring on-off measurements, so that the signal non-linearity may be the limiting factor of accuracy here.

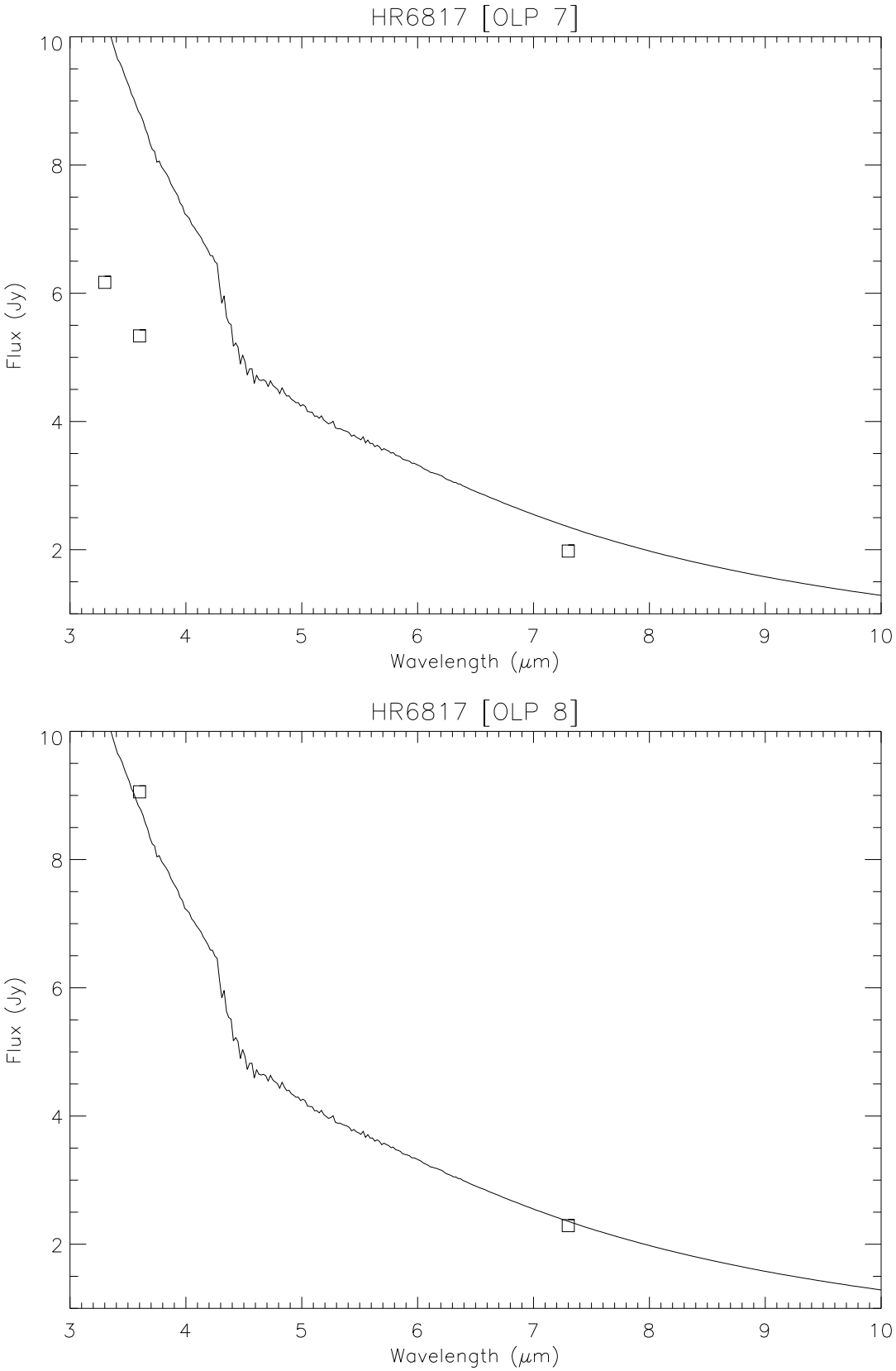

Figure 8.4: Comparison of PHT-P1 chopped photometry with the model spectrum of HR 6817, provided by P. Hammersley, for OLP 7.0 (upper panel) and OLP 8.4b3 (lower panel). All photometric points are color corrected for a 5000 K BB. The meaning of the symbols is the following: solid line: model, square: PHT-P1.

Table 8.3: Consistency check of chopped and staring photometric results of standard stars with models from Hammersley and Cohen. Staring mode results are discussed in sections 7.3.9, 7.3.4 and 7.3.3, respectively. Chopper frequencies refer to a pair of on-source and off-source plateaux, also for triangular mode to allow easy comparison of the chopper plateau dwell times ($1/2 \cdot f_{chop}$).

Filter	**Mode**	**Exposure Time** (s)	**consistency w.r.t. reference photometry**		
			chopped mode		**staring mode**
			OLP V7.0 (%)	**OLP V8.4b3** (%)	**OLP V8.4b3** (%)
P1 detector, HR 6817					
3.3	f_{chop} = 0.0313 Hz triangular chop	512	-39.8	+587	+400
3.6	f_{chop} = 0.0625 Hz triangular chop	512	-39.4	+2.8	+49.8
7.3	f_{chop} = 0.125 Hz triangular chop	512	-16.1	-2.9	+1.4
P2 detector, HR 6132					
20.0	f_{chop} = 0.0625 Hz triangular, 120" aper.	256	+4.7	+1.8	+25.2
20.0	f_{chop} = 0.0625 Hz triangular, 180" aper.	256	+13.8	+23.7	-19.3
25.0	f_{chop} = 0.0625 Hz triangiular, 120" aper.	256	-1.2	+11.0	+31.3
25.0	f_{chop} = 0.0625 Hz triangular, 180" aper	256	+13.7	+42.7	+53.9
P3 detector, HR 1457					
60.0	f_{chop} = 0.5 Hz triangular chop	512	+13.0	-13.3	-1.3
100.0	f_{chop} = 0.25 Hz triangular chop	512	+2.8	-19.7	-26.1
C100 detector, HR 6705					
90.0	f_{chop} = 0.25 Hz rectangular chop	512	+82.4	+56.4	+32.3
90.0	f_{chop} = 0.5 Hz rectangular chop	512	+34.0	+6.8	+32.3
100.0	f_{chop} = 0.125 Hz rectangular chop	512	+101	+90.7	+22.9
100.0	f_{chop} = 0.25 Hz rectangular chop	512	+36.1	+28.2	+22.9
105.0	f_{chop} = 0.0625 Hz rectangular chop	512	+84.1	+47.0	-53.7
105.0	f_{chop} = 0.125 Hz rectangular chop	512	+88.7	+51.9	-53.7
C200 detector, HR 5340					
120.0	f_{chop} = 0.0313 Hz rectangular chop	512	+3.0	-6.0	-11.4
180.0	f_{chop} = 0.0625 Hz rectangular chop	512	-43.4	-25.8	-34.9

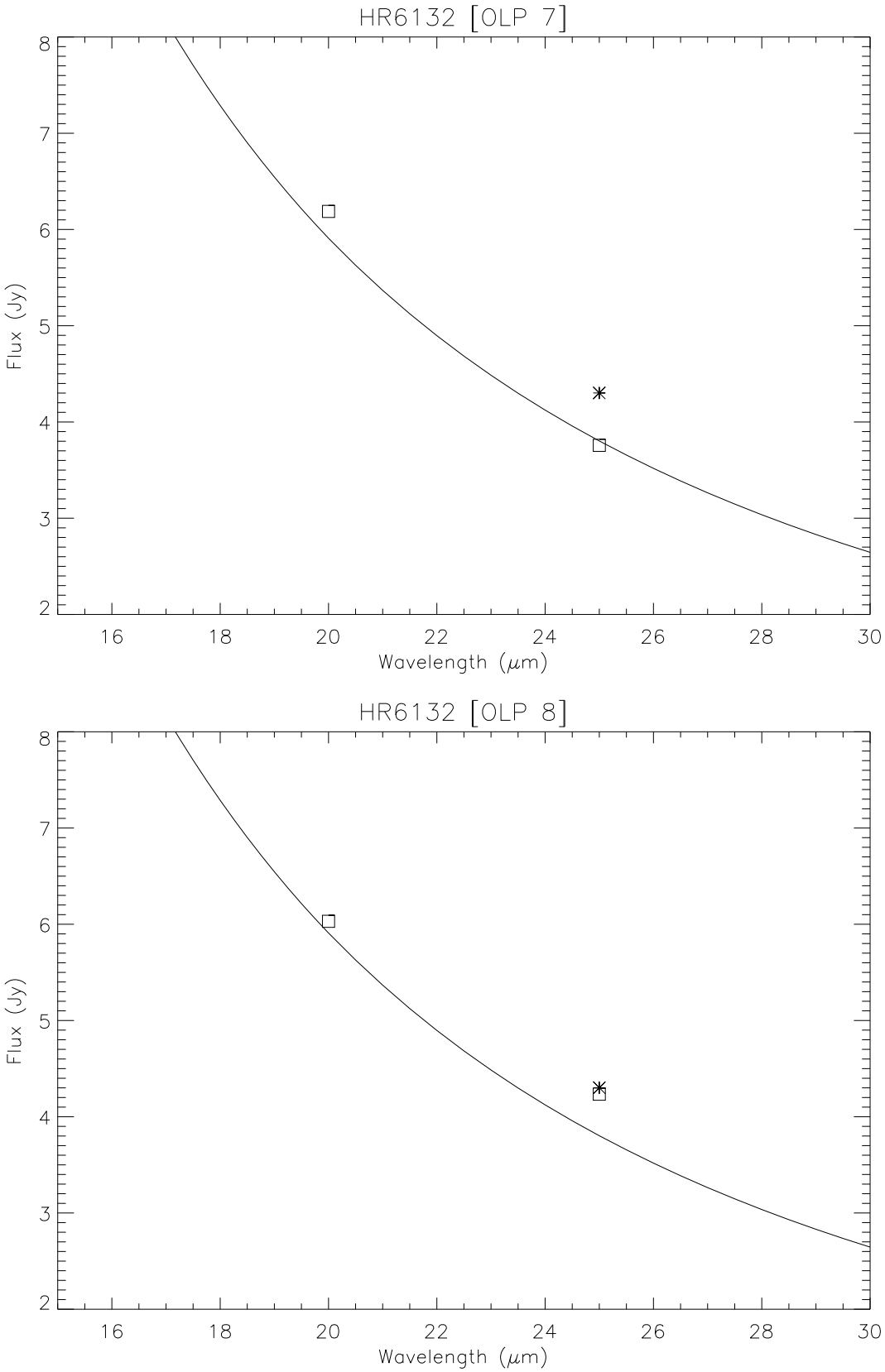

Figure 8.5: Comparison of PHT-P2 chopped photometry with the model spectrum of HR 6132, provided by P. Hammersley, for OLP 7.0 (upper panel) and OLP 8.4b3 (lower panel). All photometric points are color corrected for a 5000 K BB. The meaning of the symbols is the following: solid line: model, square: PHT-P2, asterisk: IRAS. Only the results with the 120 arcsec aperture are shown.

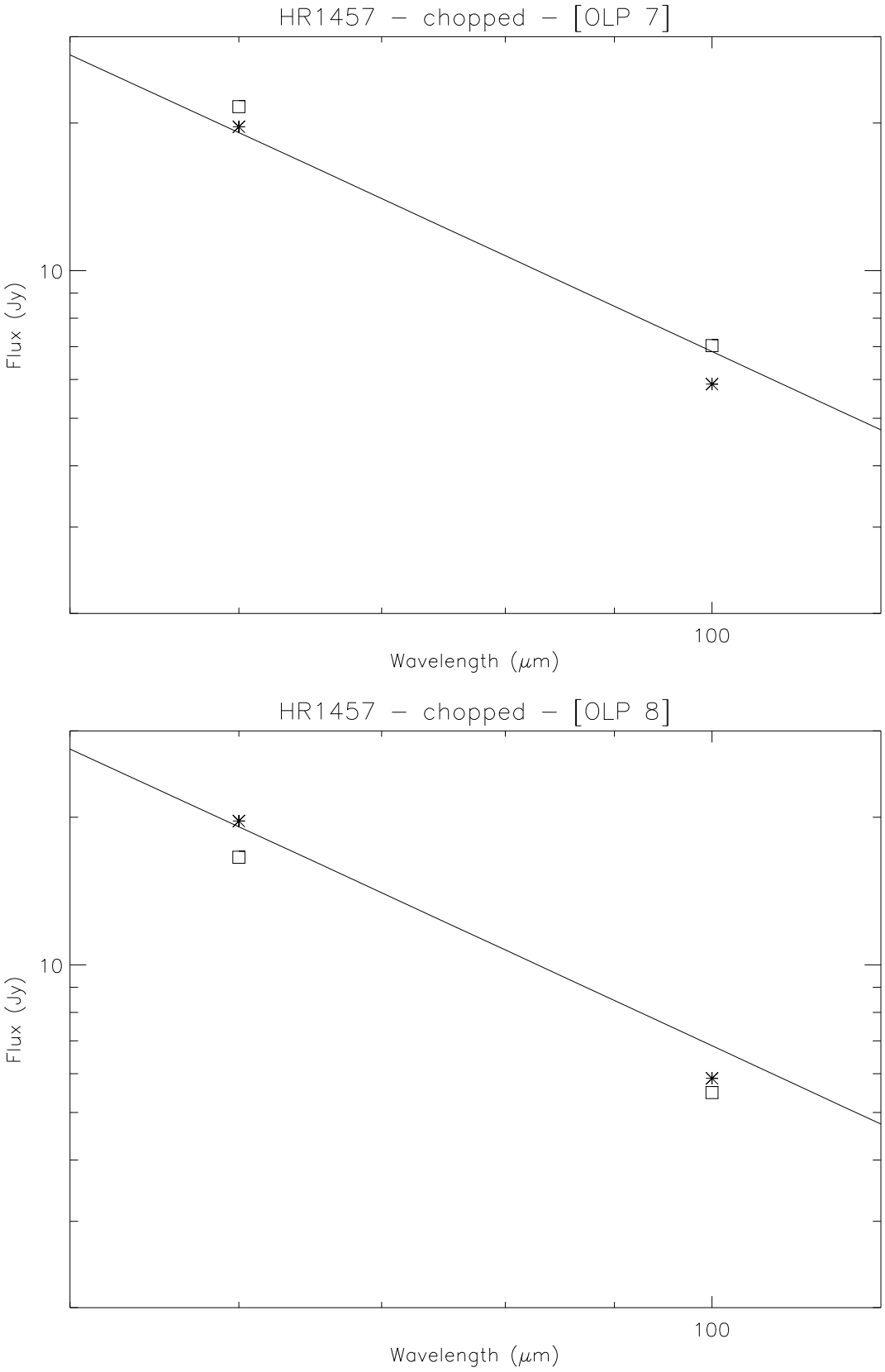

Figure 8.6: Comparison of PHT-P3 chopped photometry with the model spectrum of HR 1457, provided by M. Cohen, for OLP 7.0 (upper panel) and OLP 8.4b3 (lower panel). All photometric points are color corrected for a 4000 K BB. The meaning of the symbols is the following: solid line: model, square: PHT-P3, asterisk: IRAS.

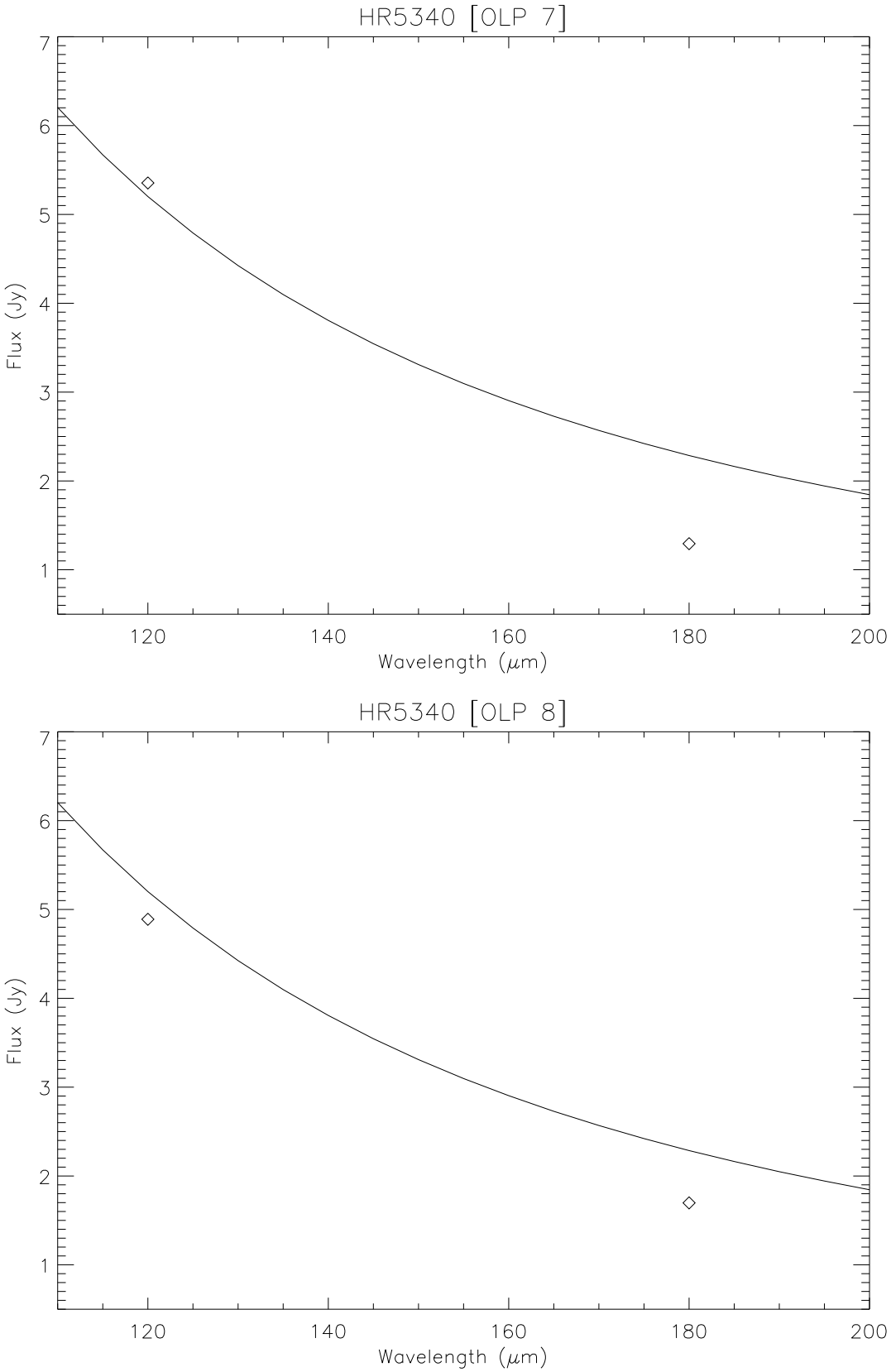

Figure 8.7: Comparison of PHT-C200 chopped photometry with the model spectrum of HR 5340, provided by M. Cohen, for OLP 7.0 (upper panel) and OLP 8.4b3 (lower panel). All photometric points are color corrected for a 4000 K BB. The meaning of the symbols is the following: solid line: model, diamond: PHT-C200.

Evaluation Log

```
1) HR 6817 chopped photometry

Measurements:
PHT-P1: ppap78300901
PHT-P1: ppap78301005
PHT-P1: ppap78301107

 Colour correction: black body, T =  5000

 Model: Hammersley

 fluxes are in Jy

Det   cwl  OLP 7   OLP 8   Model
P1    3.3  6.171  70.438  10.251
P1    3.6  5.335   9.057   8.809
P1    7.3  1.979   2.290   2.358

2) HR 6132 chopped photometry

Measurements:
PHT-P2:  ppap76901902
PHT-P2a: ppap76902011
PHT-P2:  ppap76902106
PHT-P2a: ppap76902216

 Colour correction: black body, T =  5000

 Model: Hammersley

 fluxes are in Jy

Det   cwl  OLP 7   OLP 8    IRAS   Model
P2   20.0  6.188   6.014           5.909
P2a  20.0  6.722   7.308           5.909
P2   25.0  3.757   4.222   4.301   3.803
P2a  25.0  4.324   5.425   4.301   3.803

3) HR 1457 chopped photometry

Measurements:
PHT-P3 : ppap86101202
PHT-P3 : ppap86101306

 Colour correction: black body, T =  4000

 Model: Cohen

 fluxes are in Jy

Det   cwl  OLP 7   OLP 8    IRAS   Model
P3   60.0 21.603  16.578  19.650  19.120
P3  100.0  7.033   5.492   5.870   6.842

4) HR 6705 chopped photometry

Measurements:
PHT-C1 (a): pcap67100803   FCS =  90 um
PHT-C1 (b): pcap67100912   FCS =  90 um

 Colour correction: black body, T =  4000
```

```
 Model: Cohen

Det   cwl  OLP 7   OLP 8    IRAS   Model
C1   90.0  3.669   3.148           2.012
C1  100.0  3.277   3.103   1.630   1.627
C1  105.0  2.714   2.166           1.474
C1b  90.0  2.695   2.149           2.012
C1b 100.0  2.215   2.086   1.630   1.627
C1b 105.0  2.781   2.239           1.474

5) HR 5340 chopped photometry

Measurements:
PHT-C2: pcap62900722   FCS = 120 um

 Colour correction: black body, T =  4000

 Model: Cohen

 fluxes are in Jy

Det   cwl  OLP 7   OLP 8   Model
C2  120.0  5.354   4.889   5.201
C2  180.0  1.294   1.697   2.286
```

8.1.6 OLP Chopped and Staring Mode Photometric Results for the Faint Point Source Detection Limit Program

- authors: U. Klaas, M. Radovich
- Date: 26-November-1999
- SVP period 2

Motivation

In order to determine the optimal observing strategies for faint point sources a dedicated engineering program had been performed. This resulted in recommendations for the most sensitive and photometrically accurate faint source observation modes [27]. This program was largely done using AOTs so that the resulting OLP fluxes can be checked for their accuracies.

Method

Both chopped and staring (sparse map, nodding mode was not yet available at that time) mode OLP 7 and OLP 8 results are compared with each other. All targets are faint standard stars for which M. Cohen has provided extensions of the SED out to 300 μm, so that comparison with the model prediction is possible. All observations had been evaluated interactively for an assessment report [28] using PIA V5.5. In the following table we list the results as they were presented in this assessment report:

Filter	Target	Obs. mode	t(meas) (on-source)	PHT flux [mJy]	S/N	Bgd [MJy/sr]	Flux [mJy]	Detlimit [mJy]
P_60	HR5981	staring	256 s	146 +- 17	8.6	5.5	130	15.1
P_60	HR5981	TriChop	256 s	85 +- 11*	7.7	4.6	130	16.9*
P_60	HR5981	raster	256 s	152 +- 12	12.7	5.3	130	10.2
C_60	HR5981	staring	256 s	104 +- 10	10.3	6.9	130	12.6
C_60	HR5981	TriChop	256 s	39 +- 9	4.5	6.8	130	29.0
C_60	HR5981	raster	256 s	104 +- 10	10.3	8.6	130	12.6
C_60	HR5981	P32	256 s	74 +- 11	6.7	8.6	130	19.3
C_90	IRC+60228	staring	256 s	87 +- 7	12.8	4.7	75	5.9
C_90	IRC+60228	TriChop	128 s	20 +- 12	1.6	4.5	75	46.8
C_90	IRC+60228	raster	256 s	48 +- 7	6.9	5.3	75	10.9
C_90	IRC+60228	P32	256 s	49 +- 10	5.1	5.8	75	14.7
C_90	SAO248381	staring	256 s	80 +- 9	9.0	5.7	79	8.8
C_90	SAO248381	chopping	128 s	32 +- 5	6.3	5.1	79	12.6
C_90	SAO248381	staring	256 s	73 +- 19	3.9	5.6	79	20.3

In April 1997 the sparse map staring sequence gave the most accurate photometric results. Chopped and PHT32 mode gave in general always too low fluxes which was explained with the signal losses due to the chopper signal modulation.
Note, that in this report we do not address the mapping observations done in raster or PHT32 mode.

Results

In the evaluation log we give the detailed results of the sparse map and chopped photometry evaluation. For the sparse map evaluation it was checked whether there was a systematic gradient between background position 1 and 2. This turned out to be not the case for all 4 measurements. Therefore the measurements from both background positions were averaged (simple average). Also all repeated on-source measurements were averaged before the background subtraction was performed.

The sparse map measurement with P3 on HR 5981 is a 3.5 σ detection taking into account the combined scatter of on-source and off-source measurements. The resulting consistency with the model is 20 %. With regard to OLP 7 this is a slight improvement. The chopped measurement gives a too low flux, by a factor of 2. The OLP 7 flux was a factor of 3 too high.
The sparse map measurement with C100 on HR 5981 is a 1.5 σ detection taking into account the combined scatter of on-source and off-source measurements. The resulting consistency with the model is only 90 %. With regard to OLP 7 this looks like a degradation, the 20 % increase in flux may be accounted to the linearization. The chopped measurement gives a very good consistency with the model. In comparison, OLP 7 yielded a non-detection.
The sparse map measurement with C100 on SAO 248381 is a 1.5 σ detection taking into account the combined scatter of on-source and off-source measurements. The resulting consistency with the model is 30 %. For OLP 7 a non-detection resulted for the same evaluation technique of the sparse map. The chopped measurement gives a very good consistency with the model. In comparison OLP 7 gave a too high flux, by a factor of 4.
The sparse map measurement with C100 on IRC+60228 is a 2 σ detection taking into account the combined scatter of on-source and off-source measurements. The resulting flux is a factor of 3 too high. The OLP 7 was by 50 % too high. The chopped measurement gives a too high flux, too, confirming a more general behaviour found for other sources of this brightness range. The OLP 7 was a factor of 5 too high.

Conclusions

- For PHT-P3 the one test case gives the following conclusion: The sparse map accuracy is slightly improved. The chopped photometry yields a more realistic flux range, though now the resulting flux is 50 % too low.

- For PHT-C100 sparse maps one sees a very good reproducibility of the on-source and off-source measurements, the scatter is only a few percent (1-4 % in most cases). However, the source flux is in the order of 2 to 10 % of the total flux, so that the resulting S/N ratios are 1.5 to 5. This imposes an extra uncertainty on the photometric flux values.

- OLP 8.4 PHT-C100 sparse map fluxes are consistently higher than the OLP 7.0 ones. This appears to be a consequence of the signal linearity correction. The resulting fluxes are always higher than the reference flux. This could indicate that the linearity correction is too strong in this range, however, the scatter is quite large, so that the reulsting calibration accuracies are certainly not determined by the linearity correction.

- The chopped C100 photometry is considerably improved. All three sources are detected (for OLP V7 the detection of one failed). For 2 sources excellent consistency with the reference flux is achieved. For the 3rd source the flux is too high by a fcator of 2, however, considerably lowered with regard to the OLP V7 result.

Evaluation Log

```
1) HR 5981 (K5III) with PHT-P at 60 um

OLP 8 evaluation:

a) sparse map

TDT number    flux      pointing
39200516    0.3446 Jy   bg 1 (dummy) only short sky exposure (neglected here)
39200517    0.4637 Jy   bg 1
39200518    0.6214 Jy   star
39200519    0.3998 Jy   bg 2
39200520    0.6278 Jy   star
39200521    0.4199 Jy   bg 1
39200522    0.6630 Jy   star
39200523    0.4968 Jy   bg 2
39200524    0.6113 Jy   star
39200525    0.5040 Jy   bg 1

star clearly detected against both background pointings!

     <bg 1>    <bg 2>       <star>
     0.4637    0.3998       0.6214
     0.4199    0.4968       0.6278
     0.5040                 0.6630
                            0.6113
        no gradient
        recognizable
        bg 1 = bg 2

        0.4568              0.6309
      +-0.0461 (1 sig)    +-0.0225 (1 sig)
        10% rel.            4% rel.

diff:      0.1741 Jy
cc:        1.132
cc flux:   0.1538 Jy
model:     0.130  Jy
delta %:   +18.3

b) chopped photometry (from OFRP 8.6)

TDT number   flux
39200626   0.0638 Jy

cc:        1.132
cc flux:   0.0564 Jy
model:     0.130  Jy
delta %:   -56.6

c) OLP 7 comparison

   sparse map:

   color correction already applied (see OLP 7 report)

     <bg 1>    <bg 2>       <star>
     0.400     0.371        0.570
     0.382     0.452        0.575
     0.457                  0.604
                            0.556
        no gradient
        recognizable
```

```
        bg 1 = bg 2

        0.412               0.576
      +-0.040 (1 sig)     +-0.020
        10% rel.            3% rel.

diff:      0.164 Jy
model:     0.130 Jy
delta %:   +26.2

   chopped photometry:

   color correction already applied (see OLP 7 report)

flux:      0.392 Jy
model:     0.130 Jy
delta %:   +202%


2) HR 5981 (K5III) with PHT-C at 60 um

OLP 8 evaluation:

a) sparse map

TDT number    flux      pointing
39200303    4.1861 Jy   bg 1 (dummy) only short sky exposure (neglected here)
39200304    5.5611 Jy   bg 1
39200305    5.8738 Jy   src
39200306    5.5561 Jy   bg 2
39200307    5.7376 Jy   src
39200308    5.7194 Jy   bg1
39200309    5.8550 Jy   src
39200310    5.3445 Jy   bg 2
39200311    5.6013 Jy   src
39200312    5.3404 Jy   bg 1

star clearly detected against both background pointings!

     <bg 1>    <bg 2>       <star>
     5.5611    5.5561       5.8738
     5.7194    5.3445       5.7376
     5.3404                 5.8550
                            5.6013
        no gradient
        recognizable
        bg 1 = bg 2

        5.5043              5.7669
      +-0.1617 (1 sig)    +-0.1258 (1 sig)
        3% rel.             2% rel.

diff:      0.2626 Jy
cc:        1.060
cc flux:   0.2478 Jy
model:     0.130  Jy
delta %:   +90.6

b) chopped photometry (from OFRP 8.6)

TDT number   flux
39200413   0.1454 Jy

cc:        1.060
```

```
cc flux:   0.1372 Jy
model:     0.130  Jy
delta %:   +5.5

c) OLP 7 comparison

   sparse map:

   color correction already applied (see OLP 7 report)

     <bg 1>    <bg 2>       <star>
     4.530     4.517        4.801
     4.663     4.377        4.693
     4.387                  4.737
                            4.575
        no gradient
        recognizable
        bg 1 = bg 2

        4.495               4.702
      +-0.118 (1 sig)     +-0.095
        3% rel.             2% rel.

diff:      0.207 Jy
model:     0.130 Jy
delta %:   +59.2

   chopped photometry:

   color correction already applied (see OLP 7 report)

flux:     -0.137 Jy  --> not detected
model:     0.130 Jy
delta %:    --


3) SAO 248381 (HD 8810, HR 420) (K5III) with PHT-C at 90 um

OLP 8 evaluation:

a) sparse map (from OFRP OLP 8.6)

TDT number    flux           pointing
25000702    4.6797 MJysr^-1  bg 1 (dummy) only short sky exposure (neglected here)
25000703    5.6483 MJysr^-1  bg 1
25000704    3.9139 Jy        src
25000705    5.3907 MJysr^-1  bg 2
25000706    3.8534           src
25000707    5.4608 MJysr^-1  bg 1


     <bg 1>    <bg 2>   bg(Jy)    <star>
     5.6483    5.3907   3.750     3.9139
     5.4608                       3.8534

        no gradient
        recognizable
        bg 1 = bg 2

        5.4999 MJysr^-1           3.8837
      +-0.1332 (1 sig)          +-0.0428 (1 sig)
        2% rel.                   1% rel.

diff:      0.1337 Jy
```

```
cc:        1.164
cc flux:   0.1149 Jy
model:     0.088  Jy
delta %:   +30.6

b) chopped photometry (from OFRP 8.6)

TDT number   flux
25000801   0.0879 Jy

cc:        1.164
cc flux:   0.0755 Jy
model:     0.088  Jy
delta %:   -14.2

c) OLP 7 comparison

   sparse map:

   color correction already applied (see OLP 7 report)

     <bg 1>    <bg 2>       <star>
     3.561     3.473        3.563
     3.475                  3.450
        no gradient
        recognizable
        bg 1 = bg 2

        3.503               3.507
      +-0.050 (1 sig)     +-0.080
        1.5% rel.           2% rel.

diff:      0.004 Jy  --> not detected
model:     0.088 Jy
delta %:   -95.4

   chopped photometry:

   color correction already applied (see OLP 7 report)

flux:      0.353 Jy
model:     0.088 Jy
delta %:   +301


4) IRC+60228 (K5III) with PHT-C at 90 um

OLP 8 evaluation:

a) sparse map (from OFRP OLP 8.6)

TDT number    flux           pointing
25202509    3.0873 MJysr^-1  bg 1 (dummy) only short sky exposure (neglected here)
25202510    4.8162 MJysr^-1  bg 1
25202511    3.4848 Jy        src
25202512    4.4999 MJysr^-1  bg 2
25202513    3.3449           src
25202514    4.5711 MJysr^-1  bg 1


     <bg 1>    <bg 2>   bg(Jy)    <star>
     4.8162    4.4999   3.1562    3.4848
     4.5711                       3.3449
```

```
        no gradient
        recognizable
        bg 1 = bg 2

        4.6291 MJysr^-1           3.4149
      +-0.1659 (1 sig)          +-0.0989 (1 sig)
        4% rel.                   3% rel.

diff:      0.2587 Jy
cc:        1.164
cc flux:   0.2222 Jy
model:     0.084  Jy
delta %:   +165

b) chopped photometry (from OFRP 8.6)

TDT number   flux
25202409   0.2140 Jy

cc:        1.164
cc flux:   0.1838 Jy
model:     0.084  Jy
delta %:   +119

c) OLP 7 comparison

   sparse map:

   color correction already applied (see OLP 7 report)

     <bg 1>    <bg 2>       <star>
     3.053     2.977        3.129
     2.849                  3.042
        no gradient
        recognizable
        bg 1 = bg 2

        2.960               3.086
      +-0.103 (1 sig)     +-0.062
        3.5% rel.           2% rel.

diff:      0.126 Jy
model:     0.084 Jy
delta %:   +50.0

   chopped photometry:

   color correction already applied (see OLP 7 report)

flux:      0.407 Jy
model:     0.084 Jy
delta %:   +385
```

8.1.7 Comparison of Chopped and Staring Mode Photometry of Stars Observed by the MFAINT and CFAINT Programs

- authors: M. Radovich, U. Klaas
- date: 08-October-1999
- SVP period 2

Motivation

The faint stars observed repeatedly by the monitoring program MFAINT have also been observed several times in chopped mode by the program CFAINT. MFAINT used the most recommended observation modes (nodding for P1, P2, and P3 and mini-map for C100 and C200). We compare here the results of the measurement set performed on revolution 748.

Method

Both colour corrected nodding and chopped photometry are compared with each other and against the model predictions by Cohen or Hammersley. We compare also the flux values of OLP V7.0 and OLP V8.4b3.

Results

In Table 8.4 we list the relative consistency of the chopped photometry with the models.
With P1, the measurement of the faint star HD 172323 shows a deficit in flux - the same amount is found for the nodding measurement. The accuracy for OLP V7.0 had been better.
The brighter star HR 5986 shows good photometric accuracy for both chopped and nodding mode, which is improved with regard to OLP V7.0.
For P2 the chopped photometric results give a very good accuracy in the flux range 0.5 - 3.5 Jy, so that this flux range stands out with regard to the otherwise worse P2 accuracy of 40 %.
For P3 there is a slight degradance found for the test case HR 7310.
The C100 test case shows remarkable improvement with regard to OLP V7.0. Obviously in this flux range the flux dependent signal correction factor brings a big improvement over the average factor used in the OLP V7.0 correction, see Fig. 8.8 for an illustration.
The C200 test case shows a negative flux result. This may be explained by an insufficient chopper offset (vignetting) correction. This result manifests that below 1 Jy the OLP V8.4 C200 chopped photomery calibration is not yet working.

Conclusions

- For P1 the test cases confirm an accurate behaviour above 1 Jy. The fainter source is at the very faint end with accuracies of about 50 %. Remarkable is the good agreement with the nodding mode result. Since this measurement is from a monitoring program more measurements should be checked whether there is a systematic behaviour.
- For P2 the test cases give very good accuracies in the order of 10 % in contrary to an accuracy of only 40 % found in the flux ranges around the range 0.5 - 3.5 Jy considered here. It could be a consequence of the missing signal correction, which may not be essential for the 0.5 - 3.5 Jy range.
- For P3 the accuracy has slightly degraded with regard to OLP V7.0. Here the nodding photometry gives a more accurate result.
- For the C100 test case a remarkable improvement can be seen. In the considered flux range 0.2 - 0.6 Jy the additional dependence of the signal correction factor on the flux difference seems to be responsible for the good improvement, while the source is still bright enough for not suffering from the insufficient chopper offset correction seen for flux levels below.

Table 8.4: Consistency check of chopped and staring photometric results of standard stars with models from Hammersley and Cohen. Nodding mode results are discussed in sections 7.3.9. Chopper frequencies refer to a pair of on-source and off-source plateaux, also for triangular mode to allow easy comparison of the chopper plateau dwell times ($1/2 \cdot f_{chop}$).

Filter	**Source**	**Mode**	**Expo. Time** (s)	**consistency w.r.t. reference photometry**		
				chopped mode		**nodding mode**
				OLP V7.0 (%)	**OLP V8.4b3** (%)	**OLP V8.4b3** (%)
12.0	HD 172323	$f_{chop} = 0.0156$ Hz triangular chop	512	-3.1	-44.7	-42.3
12.0	HR 5986	$f_{chop} = 0.0313$ Hz triangular chop	128	-30.2	-9.9	-1.1
25.0	HR 5986	$f_{chop} = 0.0156$ Hz triangular chop	256	44.2	-9.7	8.3
25.0	HR 7310	$f_{chop} = 0.0313$ Hz triangular chop	128	5.3	6.9	21.3
60.0 (P3)	HR 7310	$f_{chop} = 0.125$ Hz rectangular chop	512	16.0	-32.5	12.3
60.0 (C100)	HR 7310	$f_{chop} = 0.0625$ Hz triangular chop	256	110	0.9	25.8
100.0 (C100)	HR 7310	$f_{chop} = 0.0625$ Hz triangular chop	256	125	9.0	-43.8
170.0	HR 6705	$f_{chop} = 0.0625$ Hz rectangular chop	128	-62.3	-101	-5.8

- For C200 the general trend is confirmed that for the faint flux levels (below 1 Jy) negative fluxes are derived which may be explained by an insufficient chopper offset (vignetting) corection.

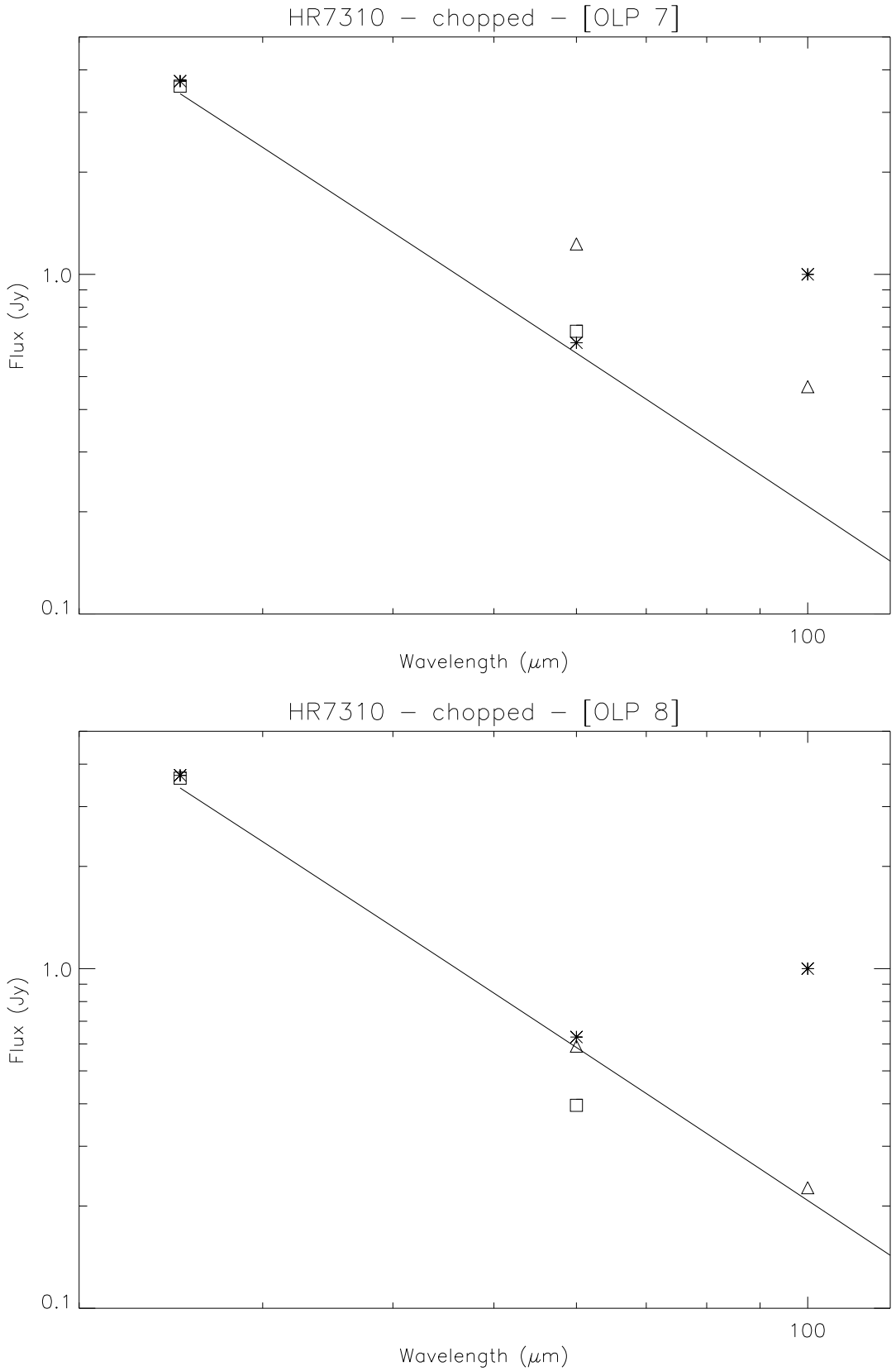

Figure 8.8: Comparison of PHT-P2, -P3 and -C100 chopped photometry with the model spectrum of HR 7310, provided by M. Cohen, for OLP 7.0 (upper panel) and OLP 8.4b3 (lower panel). All photometric points are color corrected for a 4850 K BB. The meaning of the symbols is the following: solid line: model, asterisk: IRAS (100 μm: upper limit), square: PHT-P, triangle: PHT-C100.

Evaluation Log

```
1) HR 7310

Measurements:
PHT-P2 : ppap74800610   FCS = 25 um
PHT-P3 : ppap74800303   FCS = 60 um
PHT-C1 : pcap74800505   FCS = 60 um

 Colour correction: black body, T =  4852 K

 Model: Cohen

 fluxes are in Jy

Det   cwl   OLP 7   OLP 8    IRAS   Model   OLP 8 nodding
P2   25.0   3.583   3.637   3.707   3.403      4.128
P3   60.0   0.680   0.396   0.629   0.586      0.658
C1   60.0   1.229   0.591   0.629   0.586      0.737
C1  100.0   0.467   0.226   1.000:  0.208      0.117


2) HD 172323

Measurements:
PHT-P1 : ppap74800801

 Colour correction: black body, T =  5719 K

 Model: Hammersley

 fluxes are in Jy

Det   cwl   OLP 7   OLP 8    IRAS   Model   OLP 8 nodding
P1   12.0   0.062   0.035     --    0.064      0.037


3) HR 5986

Measurements:
PHT-P1 : ppap74801108
PHT-P2 : ppap74801002

 Colour correction: black body, T =  6084 K

 Model: Hammersley

 fluxes are in Jy

Det   cwl   OLP 7   OLP 8    IRAS   Model   OLP 8 nodding
P1   12.0   1.546   1.997   2.362   2.216      2.192
P2   25.0   0.747   0.468   0.589   0.518      0.561


4) HR 6705

Measurements:
PHT-C200 : pcap74801212

 Colour correction: black body, T =  4000 K

 Model: Cohen

 fluxes are in Jy
```

Det	cwl	OLP 7	OLP 8	IRAS	Model	OLP 8 nodding
C2	170.0	0.210	-0.009	--	0.556	0.524

8.2 Validation of Additional Chopped Photometry Test Cases for OLP 8.4 Validation Program

An overview of the test cases is outlined in Ref. [4], chapters 4.2 and 4.3.

8.2.1 References to Calibration Analysis and Software Change Documentation

- calibration reports:
  - Analysis of Chopped ISOPHOT Measurements [19]
- Software Change Requests: SCREW 382
- Software Problem Reports: SPR 2980, 2981, 2982, 2983

8.2.2 Summary of Results

- The results of additional test cases for assessment of the calibration accuracy of chopped PHT-P and PHT-C photometry confirm the impression obtained by the assessment of test cases from the OLP 7.0 validation program (cf. Sect. 8.1).
- The calibration accuracies, which are in general not better than $40 - 50\,\%$, are not yet sufficient to declare the chopped photometry scientifically valid.
- Deficiencies appear to be in the following areas:
  a) Not yet fully established signal correction factors for the P2 detector.
  b) Not yet fully established or implemented chopper offset corrections, mainly affecting faint source photometry.

8.2.3 Validation of PHT03 and PHT22 Chopped Mode Photometry by Comparison with Staring Mode References on Other Revolutions

- authors: M. Radovich, U. Klaas
- date: 29-October-1999
- SVP period 2

Motivation

In order to increase our data base of comparison of chopped photometry with stellar flux models and with staring mode photometry we have searched the guest observer data base for chopped observations with staring counterparts. We could identify several star measurements which had been performed in chopped mode at 60 and 90 μm and were repeated later in mini-map mode at 60 μm. Furthermore, several chopped measurements of stars at 25 μm were found, for which IRAS FSC fluxes are available. It should be noted that these observations were performed to search for IR excesses, so that the listed model fluxes (related to the photospheric emission) may not be appropriate and therefore this sample is not fully suited for derivation of chopped photometry accuracy. It allows however a statistical assessment of the performance of the chopped photometry corrections for P2 and C100 over a larger flux scale.

Method

Compare the chopped photometry fluxes with model fluxes (caveat for photospheric emission only; no modelling of IR excesses!) and with staring mode or IRAS photometry to judge the large scale correction behaviour of the chopper frequency and signal jump dependent signal correction.

Results

In the evaluation log we give the chopped photometry results compared with model fluxes (at 90 μm and beyond Rayleigh Jeans extrapolated from 60 μm fluxes) as well as available IRAS photometry (at 25 μm) and PHT-C mini-map photometry.
In Fig. 8.9 we plot the chopped photometry results versus the model predictions. At 25 μm there are 5 stars with fluxes between 150 mJy and 25 Jy. We note the excess of the chopped photometry for one star. However, also the IRAS FSC photometry in Fig. 8.10 shows the same amount of excess w.r.t. the model so that this is a true excess. For the remmaining four stars there is a quite good correspondence between IRAS FSC and model fluxes so that we can use the model fluxes as absolute reference for these four stars.
The 60 μm fluxes in Fig. 8.9 chop some scatter around the unit line, whereas in Fig. 8.10 the fluxes are always on or above the unit line. This may be interpreted that the sample shows some tendency for IR excess at 60 μm. For the four stars which have consistent fluxes between model and mini-map within 40 % we perform an accuracy determination. The derived accuracies for the chopped photometry are very good, better than 20 %. Astonishingly, the measurement of the faintest source with a predicted flux below 100 mJy does not show the huge flux excess as found for the stars of same brightness in chapter 8.2.4. This may be linked to the four times faster chopper frequency in this case which may have a more accurately determined zero point chopper offset correction.
The comparison between chopped photometry and mini-map photometry at 60 μm, shown in Fig. 8.11, shows that in the 100 to 300 mJy range some significant flux loss is still existing for chopped photometry. The two cases with the largest deviations 54801898 and 17902205 were performed relatively late during the revolution (the latter one before re-curing during handover was introduced). Two other cases with relatively low chopped flux values, 08900295 and 10902817 have only 16 s FCS measurement times. However, 16 s FCS measurement time does not degrade the measurement accuracy in general, at least for the somewhat brighter sources (e.g. 08900314 and 13001002). There are three pairs of measurements on the same source. HD 10700 was re-measured within a short time yielding a repeatibility of $\pm$ 5 %. The other two pairs are considerably less well consistent, however, for HD 1581 the significantly

fainter flux is derived for a measurement late in the revolution (17902205, see above) and for HD 185144 the fainter flux is derived for a measurement with a 16 s FCS measurement (08900295, see above).

Table 8.5: Consistency check of chopped P2 and C100 photometric results of stars with their model predictions. Chopper frequencies refer to a pair of on-source and off-source plateaux, also for triangular mode to allow easy comparison of the chopper plateau dwell times (1/2 · f_{chop}).

target	λ (μm)	**Mode**	**Expo. Time** (s)	**OLP V8.4b3 flux** (Jy)	**Model flux** (Jy)	**consistency w.r.t. model OLP V8.4b3** (%)
HD 48915	25.0	f_{chop} = 0.1250 Hz triangular chop	256	22.049	26.300	-16.16
HD 185144	25.0	f_{chop} = 0.0313 Hz triangular chop	256	0.491	0.546	-10.07
HD 185395	25.0	f_{chop} = 0.0313 Hz triangular chop	256	0.170	0.287	-40.77
HD 207129	25.0	f_{chop} = 0.0313 Hz triangular chop	256	0.265	0.162	+63.58
HD 187642	60.0	f_{chop} = 0.2500 Hz triangular chop	256	1.072	1.050	+2.10
HD 203280	60.0	f_{chop} = 0.1250 Hz triangular chop	256	0.269	0.243	+10.70
HD 12311	60.0	f_{chop} = 0.0625 Hz triangular chop	256	0.169	0.178	-5.06
HD 142373	60.0	f_{chop} = 0.0625 Hz triangular chop	256	0.074	0.064	+15.63

Conclusions

- For 25 μm chopped photometry we find a quite good consistency with model fluxes for flux levels above 0.2 Jy. The measurements of this investigation confirm a trend of flux underestimate, which may be due to the to be revised assumption that P2 measurements do not show any flux loss.
- 25 μm staring on - off photometry below 300 mJy has to be revisited, since both staring reference test cases resulted in a significant underestimate of the flux, which was not observed for the chopped measurements.
- 60 μm chopped photometry accuracies have to be treated with some care for this sample, since the sources may show an IR excess, so that the reference photospheric model flux may not be applicable. Accuracies better than 20 % were derived for the examples for which a quite good consistency (better than 40 %) exists betwen model fluxes and mini-map photometry.
- The flux excess for chopped measurements below 200 mJy may strongly depend on the chopper frequency, since the sample considered here contained one source which did not confirm the general trend. The chopper frequency selected for this measurement was 4 times faster than the one in the affected measurements.
- For some test cases significant flux losses of chopped photometry w.r.t. mini-map photometry was found. Reasons may be space weather impact and short (16 s) FCS measurement times.

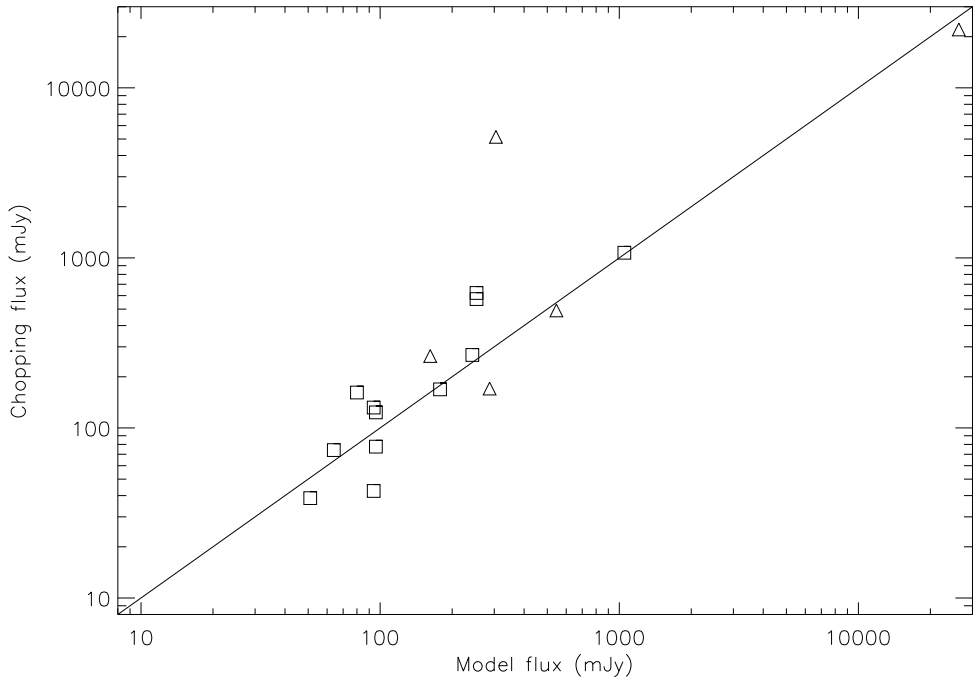

Figure 8.9: Comparison of PHT-P2 and -C100 chopped photometry with the photospheric model fluxes of stars. All photometric points are color corrected for a 10000 K BB. The meaning of the symbols is the following: solid line: flux equality chopped photometry and model, triangle: PHT-P2 25 μm fluxes, square: PHT-C100 60 μm fluxes.

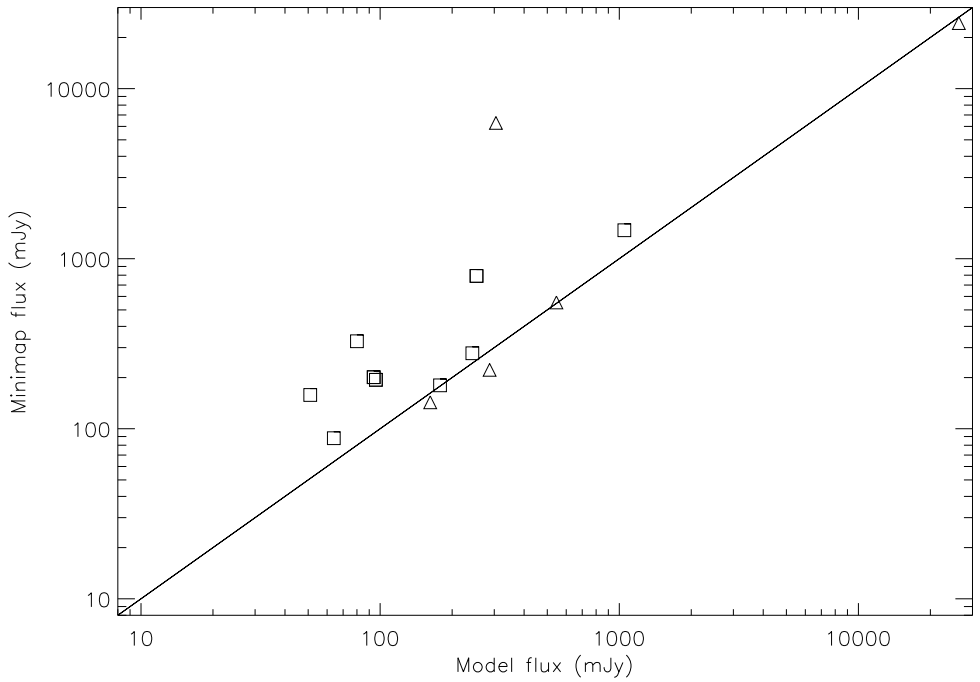

Figure 8.10: Comparison of IRAS FSC and PHT-C100 mini-map photometry with the photospheric model fluxes of stars. All photometric points are color corrected for a 10000 K BB. The meaning of the symbols is the following: solid line: flux equality IRAS/ISOPHOT photometry and model, triangle: IRAS FSC 25 μm fluxes, square: PHT-C100 60 μm mini-map fluxes.

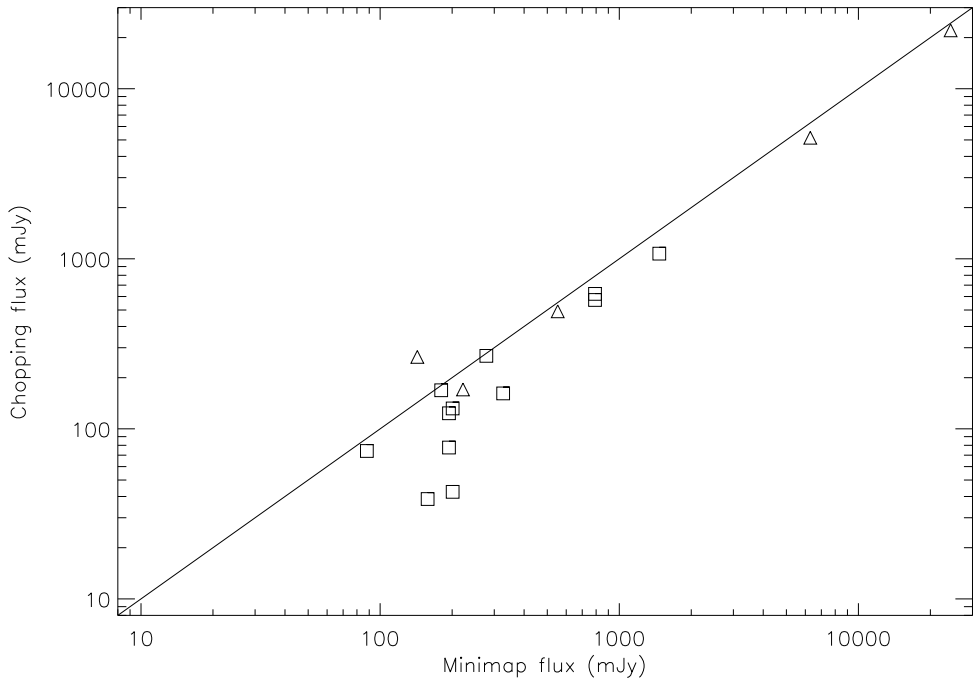

Figure 8.11: Comparison of PHT-P2 and -C100 chopped photometry with IRAS FSC 25 μm photometry and PHT C100 minimap photometry of stars. All photometric points are color corrected for a 10000 K BB. The meaning of the symbols is the following: solid line: flux equality chopped photometry and IRAS FSC/ISOPHOT mini-map photometry, triangle: 25 μm fluxes, square: 60 μm fluxes.

Evaluation Log

1) Chopped Photometry

Fluxes are in mJy
model values are expectations from photospheric model extrapolations
(kindly provided by R. Laureijs)
Reference values flag:
i: data from IRAS FSC;
e: extrapolated values from 60 um with Rayleigh Jeans (not valid for
excess sources in map case)
m: mini-map photometry from chapter 7.3.10
o: on - off (for P2 staring observations)

A color correction for a blackbody with T=10 000 K was applied

TDT	Name	cwl	chop	model	map	flag
70201079	HD 39060	25	5151.114	305.000	6290.000	i
	(HR 2020 - Beta Pic)				6377.900	o
13500819	HD 207129	25	264.889	162.000	143.000	i
					72.8	o
28801094	HD 185144	25	491.030	546.000	553.000	i
54801897	HD 185395	25	170.426	287.000	222.000	i
	(HR 7469)				32.500	o
72301710	HD 48915	25	22049.867	26300.000	24300.000	i
	(HR 2491 - Sirius)				20498.400	o
08900314	HD 203280	60	268.652	243.000	278.000	m
08900314	HD 203280	90	198.876	48.000	123.556	m,e
09000156	HD 139664	90	984.354	8.889	576.889	m,e
09101386	HD 166620	60	57.923	24.000	mini-map not processed	
09101386	HD 166620	90	52.560	4.741	--	
36901486	HD 166620	60	20.870	24.000	mini-map not processed	
36901486	HD 166620	90	16.846	4.741	--	
16402729	HD 216956	60	0.000	605.000	9188.000	m
16402729	HD 216956	90	0.000	119.506	4083.556	m,e
17902323	HD 12311	60	168.643	178.000	180.000	m
17902323	HD 12311	90	103.232	35.160	80.000	m,e
17902205	HD 1581	60	42.622	94.000	201.000	m
17902205	HD 1581	90	22.746	18.568	89.333	m,e
85900105	HD 1581	60	131.780	94.000	201.000	m
85900105	HD 1581	90	131.876	18.568	89.333	m,e
08900295	HD 185144	60	77.644	96.000	194.000	m
08900295	HD 185144	90	96.220	18.963	86.222	m,e
28801095	HD 185144	60	123.484	96.000	194.000	m
28801095	HD 185144	90	122.365	18.963	86.222	m,e
10902817	HD 203608	60	161.598	80.000	327.000	m
10902817	HD 203608	90	120.038	15.803	145.333	m,e
13001002	HD 187642	60	1072.280	1050.000	1470.000	m
13001002	HD 187642	90	723.783	207.408	653.333	m,e
39301217	HD 10700	60	621.714	253.000	792.000	m
39301217	HD 10700	90	414.233	49.975	352.000	m,e
39301181	HD 10700	60	572.841	253.000	792.000	m
39301181	HD 10700	80	250.564	80.050	445.500	m,e
39301181	HD 10700	100	511.583	32.789	285.120	m,e
39301181	HD 10700	120	225.962	15.812	198.000	m,e
39301181	HD 10700	150	24.920	6.477	126.720	m,e
39301181	HD 10700	170	97.590	3.926	98.657	m,e
39301181	HD 10700	200	-43.996	2.049	71.280	m,e
28100659	HD 142373	60	74.112	64.000	88.000	m
28100659	HD 142373	90	27.660	12.642	39.111	m,e
54801898	HD 185395	60	38.664	51.000	158.000	m
54801898	HD 185395	90	30.164	10.074	70.222	m,e

2) P2 on - off photometry

Fluxes are in mJy
model values are expectations from photospheric model extrapolations
(kindly provided by R. Laureijs)

A color correction for a blackbody with T=10 000 K was applied

TDT	Name	cc Flux	model	% (OLP8-model)/model
70705707 - 70705711	HD 48915 (HR 2491, Sirius)	20498.4	26300.0	-22.06
76602301 - 76602302	HD 39060 (HR 2020, Beta Pic)	6377.9	--	IR excess
71300502 - 71300501	HD 185395 (HR 7469)	32.5	287.0	-88.68
55302203 - 55302202	HD 207129	72.8	162.0	-55.06

8.2.4 Validation of PHT03 and PHT22 Chopped Mode Photometry: Fluxes and SEDs of Known Stars

- authors: M. Radovich, U. Klaas
- date: 10-September-1999
- SVP period 2

Motivation

In addition to the sources which had staring mode reference measurements and reference fluxes we selected from the data base measurements of stars which have model predictions.

Method

We compare the background subtracted and color corrected flux values of both OLP 8.4b3 against the model fluxes.

Results

In Tables 8.6 and 8.7 we list the results for the PHT03 and PHT22 AOTs respectively. For P1 there are only two test cases with somehow diverging results from the same observation. In the case of P2, 25 μm filter, there seems to be some systematic that the flux is underestimated by 30 % except for one case. Currently there is no signal correction for P2 applied. An investigation of a possible dependence of the signal loss on the chopper plateau will have to be performed. The two P3 test cases give satisfying results, however, they are restricted to source fluxes above 1 Jy. In the case of C100 only one brighter source is available which gives satifying results, too. All other sources are very faint, with expected fluxes below 100 mJy. For those we observe a considerable positive excess for the ISOPHOT fluxes. A very likely reason is a non-adequate vignetting correction which is the zero line correction of the chopper signal loss correction files. Indications for this have been recently found in calibration analysis. Therefore, the current calibration method does not work properly for sources below 300 mJy. For C200 the test cases give only non-detections due to too short on-source integration times.

Conclusions

- For P1 there are not enough test cases from this sample to come to a conclusive result. The accuracy is expected to be in the order of 40 % like for the other detectors, see below.
- For P2 ISOPHOT fluxes are underestimated by 30-40 % in all except one case. The achieved calibration accuracy is in the order of 40 %.
- For P3 calibration accuracies of better than 40 % are acheived for fluxes above 1 Jy
- For C100 there is one bright source with a flux above 4 Jy for which an accuracy of 40 % is achieved. All other sources have expected source fluxes below 100 mJy and the ISOPHOT fluxes are considerably higher. The reason for that might be a non-adequate vignetting correction (as zero point calibration in the signal loss correction files).
- For C200 there is no test case with a positive source detection. With selected 128 s on-source integration time, the 1 σ sensitivity limit in the 170 μm filter is 64 mJy under best conditions. The expected source fluxes are close to this limit which is in nearly all cases dominated by sky noise.

Table 8.6: Consistency check of chopped PHT03 photometric results of stars with their model predictions. Chopper frequencies refer to a pair of on-source and off-source plateaux, also for triangular mode to allow easy comparison of the chopper plateau dwell times (1/2 · f_{chop}).

target	λ (μm)	**Mode**	**Expo. Time** (s)	**OLP V8.4b3 flux** (Jy)	**Model flux** (Jy)	**consistency w.r.t. model OLP V8.4b3** (%)
BS 5062	7.3	f_{chop} = 0.0156 Hz rectangular chop	64	2.665	2.559	+4.14
	12.0	f_{chop} = 0.0156 Hz rectangular chop	64	1.461	0.972	+50.38
	25.0	f_{chop} = 0.0156 Hz rectangular chop	64	0.152	0.227	-32.86
HR 5447	25.0	f_{chop} = 0.0156 Hz rectangular chop	256	0.222	0.256	-13.38
HR 5914	25.0	f_{chop} = 0.0156 Hz rectangular chop	256	0.192	0.381	-49.54
HR 7557	25.0	f_{chop} = 0.0156 Hz rectangular chop	256	3.499	5.268	-33.59
HR 4983	25.0	f_{chop} = 0.0156 Hz rectangular chop	256	0.584	0.455	+28.35
BS 6056	60.0	f_{chop} = 0.0156 Hz rectangular chop	64	4.460	4.222	+5.64
	100.0	f_{chop} = 0.0156 Hz rectangular chop	64	2.081	1.520	+36.91
BS 7001	60.0	f_{chop} = 0.0156 Hz rectangular chop	64	6.813	7.020	-2.95
	100.0	f_{chop} = 0.0156 Hz rectangular chop	64	7.173	6.400	+12.08

Table 8.7: Consistency check of chopped PHT22 photometric results of stars with their model predictions. Chopper frequencies refer to a pair of on-source and off-source plateaux, also for triangular mode to allow easy comparison of the chopper plateau dwell times (1/2 · f_{chop}).

target	λ (μm)	**Mode**	**Expo. Time** (s)	**OLP V8.4b3 flux** (Jy)	**Model flux** (Jy)	**consistency w.r.t. model OLP V8.4b3** (%)
BS 5062	60.0	f_{chop} = 0.0156 Hz rectangular chop	128	0.101	0.039	+161
	90.0	f_{chop} = 0.0156 Hz rectangular chop	64	0.131	0.017	+668
	60.0	f_{chop} = 0.0156 Hz rectangular chop	512	0.155	0.039	+301
	100.0	f_{chop} = 0.0156 Hz rectangular chop	256	0.070	0.014	+407
HR 5304	60.0	f_{chop} = 0.0156 Hz rectangular chop	256	0.080	0.043	+86.75
	100.0	f_{chop} = 0.0156 Hz rectangular chop	256	0.083	0.015	+446
HR 5986	60.0	f_{chop} = 0.0156 Hz rectangular chop	256	0.145	0.089	+62.76
	100.0	f_{chop} = 0.0156 Hz rectangular chop	256	0.073	0.032	+132
HR 7180	90.0	f_{chop} = 0.0156 Hz rectangular chop	256	0.179	0.067	+169
	170.0	f_{chop} = 0.0156 Hz rectangular chop	256	-2.053	0.018	–
HR 7557	150.0	f_{chop} = 0.0156 Hz rectangular chop	256	-1.136	0.141	–
	180.0	f_{chop} = 0.0156 Hz rectangular chop	256	-1.082	0.092	–
HR 8775	60.0	f_{chop} = 0.0156 Hz rectangular chop	256	9.477	11.519	-17.72
	100.0	f_{chop} = 0.0156 Hz rectangular chop	256	5.872	4.121	+42.47

Evaluation Log

```
1) BS 5062

Measurements:
PHT-P: ppap19500982    FCS = 7.3, 25 um
PHT-C: pcap19500983    FCS = 90 um
       pcap20200943    FCS = 60 um

 Color correction: bb, T =  8087

 Model: Hammersley

 fluxes are in Jy

Det   cwl   OLP 8.4b3  OLP 8.4   Model
P1    7.3    2.665      2.517    2.559
P1   12.0    1.461      1.380    0.972
P2   25.0    0.152      0.153    0.227
C1   60.0    0.101      0.088    0.039
C1   90.0    0.131      0.114    0.017
C1   60.0    0.155      0.153    0.039
C1  100.0    0.070      0.069    0.014

2) HR 5304

Measurements:
PHT-C: PCAP24602245    FCS = 60 um

 Colour correction: black body, T =  6143

 Model: Cohen

 fluxes are in Jy

Det   cwl    OLP 8   Model
C1   60.0    0.080   0.043
C1  100.0    0.083   0.015

3) HR 5447

Measurements:
PHT-P: PPAP26900346    FCS = 25 um

 Colour correction: black body, T =  6687

 Model: Cohen

 fluxes are in Jy

Det   cwl    OLP 8   Model
P2   25.0    0.222   0.256

4) HR 5914

Measurements:
PHT-P: PPAP28100658    FCS = 25 um

 Colour correction: black body, T =  5676

 Model: Cohen

 fluxes are in Jy
```

```
Det   cwl    OLP 8   Model
P2   25.0    0.192   0.381

5) HR 5986

Measurements:
PHT-C: PCAP27702221    FCS = 60 um

 Colour correction: black body, T =  6084

 Model: Cohen

 fluxes are in Jy

Det   cwl    OLP 8  Model
C1   60.0    0.145  0.089
C1  100.0    0.073  0.032

6) HR 7180

Measurements:
PHT-C: PCAP11104817    FCS = 90 um, 170um

 Colour correction: black body, T =  4601

 Model: Cohen

 fluxes are in Jy

Det   cwl    OLP 8  Model
C1   90.0    0.179  0.067
C2  170.0   -2.053  0.018

7) HR 7557

Measurements:
PHT-P: ppap13001001    FCS = 25 um
PHT-C: pcap13001003    FCS = 150 um

 Colour correction: black body, T =  7596

 Model: Hammersley

 fluxes are in Jy

Det   cwl    OLP 8  Model
P2    25.0   3.499  5.268
C2   150.0  -1.136  0.141
C2   180.0  -1.082  0.092

8) HR 8775

Measurements:
PHT-C: PCAP20601741    FCS = 60 um

 Colour correction: black body, T =  3595

 Model: Cohen

 fluxes are in Jy

Det   cwl    OLP 8   Model
C1   60.0    9.477  11.519
C1  100.0    5.872   4.121
```

```
9) HR 4983

Measurements:
PHT-P: PPAP21501031   FCS = 25 um

 Colour correction: black body, T =  5895

 Model: Hammersley

 fluxes are in Jy

Det   cwl    OLP 8   Model
P2   25.0    0.584   0.455

10) BS 6056

Measurements:
PHT-P: PPAP08201229   FCS = 100 um

 Colour correction: black body, T =  3700

 Model: Cohen (Rayleigh Jeans extrapolation from 30 um flux = 16.889 Jy)

 fluxes are in Jy

Det   cwl    OLP 8   Model
P3   60.0    4.460   4.222
P3  100.0    2.081   1.520

11) BS 7001 (HR 7001 = Vega)

Measurements:
PHT-P: PPAP08500241   FCS = 100 um

 Colour correction: modified bb. em. propto lambda^{-1}, T = 80

 fluxes are in Jy

Det   cwl    OLP 8   IRAS
P3   60.0    6.813   7.020
P3  100.0    7.173   6.400
```

Chapter 9

Validation of the ISOPHOT-C mapping mode PHT22 during SVP2

9.1 Verification of Flux Conservation in P22 Raster Maps

An overview of the test cases is outlined in Ref. [4], chapter 5.2.

9.1.1 References to Calibration Analysis and Software Change Documentation

- calibration reports:
  - ISOPHOT Data User Manual [2], chapter 8.5 (Mapping)
- Software Change Requests: none
- Software Problem Reports: none

9.1.2 Summary of Results

- Point source photometry performed on maps with different raster step size gives an internal consistency of ± 15 % fpr both C100 and C200 maps.
- Together with the derived absolute accuracy for minimaps (Sect. 7.3.10) point source photometry from P22 raster maps can be declared scientifically valid with an accuracy of 30 %.

9.1.3 Verification of Flux Conservation for Different Raster Step Sizes

- authors: M. Radovich, U. Klaas
- date: 04-August-1999
  revised version on 10-March-2000 to correct OLP 8 results for wrong modified BB color correction (SPR-3179)
- SVP period 2

Motivation

There are some targets for which P22 raster maps were repeated with different raster step sizes. These maps provide a good opportunity whether to check whether integral aperture photometry gives identical results for the mapping products of type PGAI.

Method

We determine the consistency between the background subtracted source fluxes for the maps with different raster step sizes. If available we compare against a reference flux to establish the absolute photometric accuracy of the map products.

Results

In Table 9.1 we list the photometric results for a point source covered by two maps with different raster step size. The parameters of the raster map are given, too. For C200 it appears, as if the finer step size (always corresponding to half a pixel) gives a higher flux.

Table 9.1: Results from comparison of sets of P22 raster maps with different raster step size.

OLP product name	**target name**	**filter** (μm)	**raster parameters** **MxN**	**dMxdN** (arcsec)	**flux** (Jy)	**color correction for spectrum**
C100 detector						
PGAI85201502	BD+31 643	60	11 x 11	69 x 69	325.757	–
PGAI85201603	BD+31 643	60	9 x 9	15 x 15	319.498	–
PGAI86401601	HR 1457	100	9 x 3	69 x 69	5.464	BB T=4000 K
PGAI86401602	HR 1457	100	7 x 7	15 x 15	7.189	BB T=4000 K
C200 detector						
PGAI62402306	HR 2020	170	2 x 2	90 x 90	2.389	mBBnu1 T=85 K
PGAI70201081	HR 2020	170	3 x 3	46 x 46	3.187	mBBnu1 T=85 K
PGAI63801301	NGC 6543	170	4 x 4	92 x 92	20.884	–
PGAI63801303	NGC 6543	170	10 x 10	46 x 46	28.817	–
PGAI72600404	NGC 6503	170	4 x 4	92 x 92	42.828	–
PGAI72600406	NGC 6503	170	10 x 10	46 x 46	47.932	–
PGAI72600507	IC 1228	170	4 x 4	92 x 92	8.421	–
PGAI72600509	IC 1228	170	10 x 10	46 x 46	14.236	–

In Table 9.2 we derive the internal consistency of the point source photometry from the pair of maps as the ratio of half the flux difference over the average flux. An unbiased comparison with reference photometry is only possible for α Tau (HR 1457) with regard to the model extrapolation performed by Cohen. Here it looks as if the finer grid provides the more accurate photometry. The internal consistency for a pair of maps is on average $\pm$ 15 % for both C100 and C200 maps.

Conclusions

- For C100 the flux of a point source is conserved with an accuracy of $\pm$ 15 % for different raster step size.

Table 9.2: Consistency check of point source photometry derived from sets of P22 raster maps with different raster step size and comparison with reference photometry. Internal consistency is derived as the ratio of half of the difference in flux over the average flux for a pair of maps. For C200 reference photometry is from interactive processing on the same set of data (*).

target name	**filter** (μm)	**flux** (Jy)	**internal consistency** (%)	**reference flux** (Jy)	**consistency w.r.t. reference flux** (%)
C100 detector					
BD+31 643	60	325.757	+1.0	–	–
BD+31 643	60	319.498	-1.0	–	–
HR 1457	100	5.464	-13.6	6.842	-20.1
HR 1457	100	7.189	+13.6	6.842	+5.1
C200 detector					
HR 2020	170	2.389	-14.3	2.5 (*)[25]	–
HR 2020	170	3.187	+14.3	2.5 (*)[25]	–
NGC 6543	170	20.884	-16.0	24 (*)	–
NGC 6543	170	28.817	+16.0	24 (*)	–
NGC 6503	170	42.828	-5.6	45 (*)	–
NGC 6503	170	47.932	+5.6	45 (*)	–
IC 1228	170	8.421	-25.7	7 (*)	–
IC 1228	170	14.236	+25.7	7 (*)	–

- For α Tau (HR 1457) the absolute calibration accuracy at 100 μm is found to be 20 %.
- For C200 the flux of a point source is conserved with an accuracy of $\pm$ 15 % for different raster step size.

9.2 Determination of Flat-Field Accuracies

An overview of the test cases is outlined in Ref. [4], chapter 5.1.

9.2.1 References to Calibration Analysis and Software Change Documentation

- calibration reports:
  - none
- Software Change Requests: none
- Software Problem Reports: none

9.2.2 Summary of Results

- For C100 maps flat-field accuracies between 3.5 and 20 % were found. Maps with pixel overlap have typically 4 to 12 % accuracy, maps without any pixel overlap between 8 and 20 % accuracy.
- For C200 maps flat-field accuracies between 3 and 15 % were found. Maps with pixel overlap have typically 3 to 5 % accuracy, maps without any pixel overlap between 7 and 15 % accuracy.
- In most cases the flat field accuracy is limited by systematic array flat field residuals which can be recognized as systematic patterns.
- The relative low flat-field accuracies in case of no pixel overlap and temporal variations of the flat field structure for C100 mean a restriction in determining faint sources out of the maps. This is a caveat in the release of the P22 raster mode as "scientifically validated".

9.2.3 Flat-field Accuracies of C100 Maps

- authors: U. Klaas
- date: 10-January-2000
- SVP period 2

Motivation

As part of the scientific validation of staring raster maps the current flat-field accuracy is determined. At the moment the flat-field correction is performed as part of the FCS calibration taking into account the actual response of the individual pixels to the illumination by the FCS and interpolating between the two bracketing FCS measurements. This cannot correct for non-linear temporal detector drifts. The flat-field correction has to take into account a non-homogenous FCS illumination over the array (FCS illumination matrix). This is averaged and odes not take into account possible systematic effects with heating power of the FCS. The responsivity matrix of the array is determined by rastering point source standards which are centered on each pixel, so that the bulk of the intensity is collected inside the central area of the pixel. For a flat sky, when the full pixel area and its spatial sensitivity is essential, there may be systematic variations due to slightly different solid angles among the pixels. There may be systematic additive offsets among the pixels as indicated by statistical flat-field assessment. Therefore, it is expected, that for faint surface brightness systematic flat-field effects should be seen much stronger than in for bright surface brightness. Also the raster step size and final oversampling is expected to play a role, since several pixels are averaged or not.

Method

We use the SKYVIEW program to determine the areas for the flat-field accuracy measurement on the preselected maps. The areas are defined drawing a polygon (rectangle). Afterwards a statistics on the defined area is performed determining the mean and standard deviation of the surface brightness. The flat-field accuracy is defined as the ratio of the standard deviation and the mean. It is checked that the minimum flux value is not undefined (equivalent to -1).

Results

In Table 9.3 we present the results of the analysis covering maps in 3 out of the 6 C100 filters, raster parameters in the range from no pixel overlap up to steps of 0.75 of the pixel size and a wide range of surface brightness values. In most cases with pixel overlap steps of 1.5 of a pixel, i.e. a displacement by half of the array had been selected. The detailed evaluation providing the coordinates of the selected background fields as well as brightness maxima and minima is given in the evaluation log section. The description of systematic flat field structures in Table 9.3 is somehow subjective and depends also on the dynamic range of the map.
The listed flat-field accuracy is the standard deviation of the mean flux derived for the background field. Some slight impact by real background structures cannot be excluded. In general the achieved flat-field accuracy is $< \pm 20\,\%$. There is no dependence on the selected filter found.
Usually for the same raster parameters maps with higher surface brightness values show a somewhat better flat field accuracy, however, there is no clear correlation. The flat field accuracy is improved by pixel overlap in both dimensions, then flat field accuracies as good as 3.5 % are found; usually they lie in the range 4 to 12 %.
This behaviour confirms that the current flat-field accuracy is limited by systematic instrumental flat-field residuals imposed by the FCS measurements. In the evaluation log, for two maps with no pixel overlap the surface brightness has been measured individually for series of pixel nonaplets. Systematic patterns showing repeatedly the array flat-field can be recognized. The scatter of the average brightness per pixel is in general considerably smaller than the scatter of the average of the nine pixels. The relative flat-field residuals, normalized to the mean brightness value, have been established, too. They are different for

the different filters and they do not coincide for one filter; they seem to be highly dependent on the actual illumination of the pair of the FCS measurements. In Fig. 9.1 an example each for a map with strong and variable flat-field residuals and for a map with only marginal flat-field residuals is presented.
In contrary to C200 (cf. Section 9.2.4), several C100 maps show variability of the flat field structure with time. This means that both the absolute level can change due to drifts and a certain pattern can stand out in part of the map. The latter behaviour may be due to spiking of individual pixels. This is clearly a non-linear and variable effect which cannot be removed by a static flat-field.

Table 9.3: C100 flat-field accuracies for various filters, raster parameters and surface brightnesses.

OLP product name	**filter** (μm)	**raster parameters MxN**	**dMxdN** (arcsec)	**over sampling**	**aligned with S/C-Y**	**surface brightness** (MJy sr^{-1})	**flat-field accuracy** (%)	**systematic ff structure**
PGAI19002101	60	5x5	135x135	N	Y	6.8	19.6	strong
PGAI08900102	60	7x7	130x130	N	Y	9.5	14.6	strong
PGAI85001219	60	3x3	120x120	(Y)	Y	18.9	15.5	marginal
PGAI29902250	60	5x5	110x110	(Y)	Y	9.8	10.5	recognizable
PGAI30301380	60	5x5	110x110	(Y)	Y	40.7	7.4	recognizable
PGAI68300807	60	19x19	92x92	Y	Y	21.0	11.7	strong
PGAI84403913	60	10x10	69x69	Y	Y	23.7	5.7	recognizable
PGAI69801101	60	9x12	69x69	Y	Y	104.4	4.2	recognizable
PGAI70401550	60	9x11	37x35	Y	N	10.0	5.0	none
PGAI35100809	90	12x12	135x135	N	Y	5.1	9.6	recognizable
PGAI58200903	90	9x9	135x135	N	Y	7.8	41.0	strong
PGAI19201091	90	10x20	130x130	N	Y	4.7	20.3 9-33	strong / variable
PGAI86901244	90	9x9	130x130	N	Y	5.2	12.6	strong
PGAI41502788	90	12x12	130x130	N	Y	8.2	7.7 5-9	recognizable / variable
PGAI09000606	90	5x5	130x130	N	Y	11.9	13.4	strong
PGAI08901904	90	3x3	130x130	N	Y	15.5	16.5	strong
PGAI40100614	90	13x19	138x92	Y	Y	13.7	6.4	recognizable
PGAI87001338	90	9x18	130x65	Y	Y	5.3	13.8 7-20	recognizable / variable
PGAI16701405	90	11x21	130x65	Y	Y	15.4	8.1	recognizable
PGAI57501902	90	8x8	92x92	Y	Y	12.1 $\pm$3%	5.8 4-6	recognizable / variable
PGAI52700514	90	5x10	90x90	Y	N	4.4	4.6	recognizable
PGAI60002009	90	16x16	87x87	Y	Y	6.4	5.4	recognizable
PGAI50000124	90	20x20	75x138	Y	Y	4.7 4.4-5.8	13.2 7-14	recognizable variable
PGAI50100273	90	20x20	75x130	Y	Y	5.6	6.1	recognizable
PGAI20701079	90	5x5	75x75	Y	N	22.0	3.3	marginal
PGAI20800709	90	18x18	69x69	Y	Y	5.8	3.4	marginal
PGAI86800640	90	18x9	65x130	Y	Y	5.4	5.8	recognizable
PGAI10101158	100	7x7	135x135	N	Y	27.5	13.8	strong
PGAI79401149	100	4x4	135x135	N	Y	44.7	8.0	recognizable
PGAI31000626	100	7x7	135x135	N	Y	136.9	7.7	marginal
PGAI44900714	100	20x20	135x135	N	Y	116.6	13.3[a]	marginal
PGAI15601578	100	7x10	135x92	Y	Y	12.6	18.0	strong
PGAI27600420	100	7x10	135x90	Y	Y	14.2	9.8	recognizable
PGAI71901220	100	10x14	135x90	Y	Y	16.1	4.4	recognizable
PGAI33401134	100	5x7	135x90	Y	Y	27.9	10.3	marginal
PGAI79401149	100	3x3	69x69	Y	Y	43.7	7.4	recognizable

[a] contamination by sources?

Conclusions

- In general the achieved flat-field accuracy of C100 maps is better than $\pm 20\,\%$ (standard deviation of the mean background flux).
- There is some trend that with increasing absolute surface brightness better flat-field accuracies are found.
- The flat-field accuracy is limited by systematic instrumental flat-field residuals of the C100 array.
- The flat-field accuracy is significantly improved when there is overlap of individual pixels. Then the flat-field residuals are averaged out. The best results are observed, if the raster step size is less equal than half of the array size in both directions resulting in half a pixel displacement in the center of the map; then accuracies between 3.5 and 12 % are achieved.
- The flat-field residuals can be time dependent and only show up in part of the map.

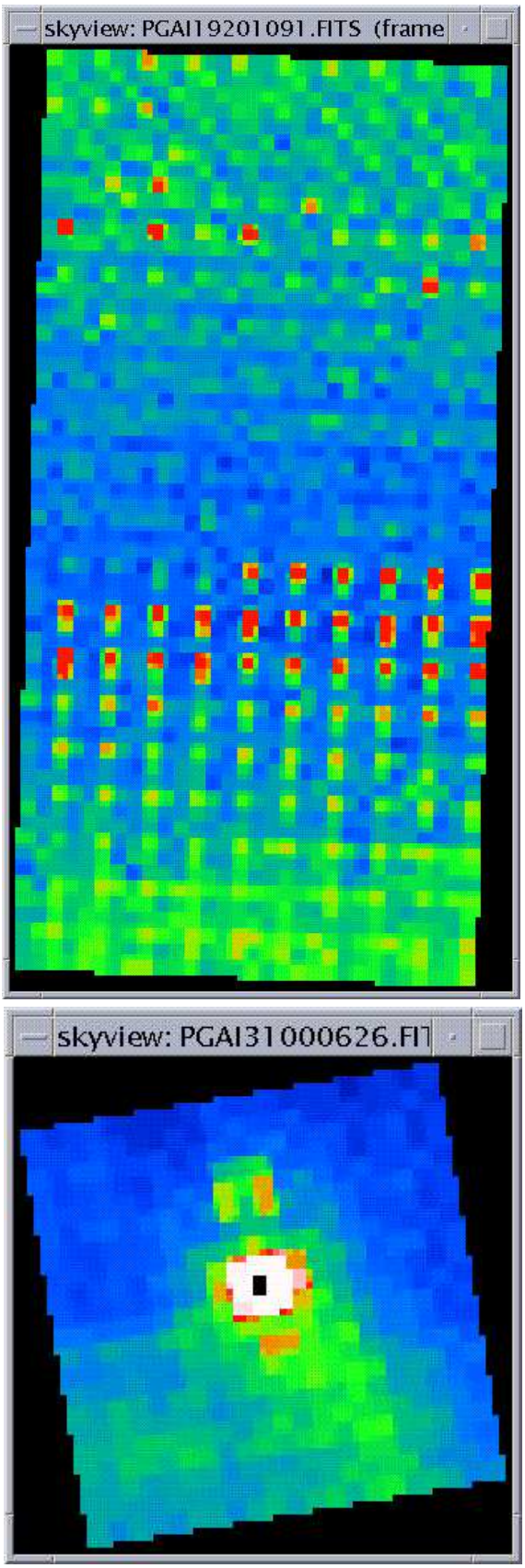

Figure 9.1: Example of a map with strong flat-field residual showing a strong pattern which is time dependent (only visible for part of the map, upper panel) and example of a map with hardly visible flat field residuals due to pixel overlap and high dynamic range of the map (lower panel). The average flat field accuracy is 20 % (between 9 and 33 %) for the upper map and 8 % for the lower map.

Evaluation Log

```
PGAI19002101.FITS  NGC104
======================================================================

Maximum 9.97286    at RA = 0h23m48.60s  Dec = -72d03m06.2s
Minimum 4.50572    at RA = 0h23m25.72s  Dec = -72d07m21.2s

Mean    6.79813
st dev  1.33155
                                  Flux units MJY/SR

Flux integral      3.20484e-05   MJY
Inside 4.7143e-06 Steradian area
(890 pixels)

Centroid                            RA = 0h24m03.59s  Dec = -72d04m56.1s


Flux weighted centroid              RA = 0h24m02.61s  Dec = -72d04m53.2s

vertex# 1  at RA = 0h25m13.16s  Dec = -72d05m05.6s

vertex# 2  at RA = 0h23m48.50s  Dec = -72d10m06.6s

vertex# 3  at RA = 0h22m53.29s  Dec = -72d04m35.5s

vertex# 4  at RA = 0h24m21.03s  Dec = -71d59m51.1s

internal systematic flat-field structures of array (regular pattern generated by
the nine pixels; note: pixel numbering is arbitrary and needs not to comply
with official numbering scheme):

1) 4.60554 MJY/SR   at RA = 0h25m42.51s  Dec = -72d05m49.9s
2) 5.34038 MJY/SR   at RA = 0h25m36.04s  Dec = -72d06m20.1s
3) 4.29180 MJY/SR   at RA = 0h25m26.30s  Dec = -72d06m50.4s
4) 5.21397 MJY/SR   at RA = 0h25m35.94s  Dec = -72d05m05.0s
5) 6.53606 MJY/SR   at RA = 0h25m26.21s  Dec = -72d05m35.3s
6) 6.80156 MJY/SR   at RA = 0h25m19.74s  Dec = -72d06m05.5s
7) 8.21534 MJY/SR   at RA = 0h25m29.39s  Dec = -72d04m35.2s
8) 6.29640 MJY/SR   at RA = 0h25m22.92s  Dec = -72d05m05.4s
9) 9.19739 MJY/SR   at RA = 0h25m13.19s  Dec = -72d05m35.6s

1) 5.80694 MJY/SR   at RA = 0h25m26.08s  Dec = -72d03m50.2s
2) 5.64577 MJY/SR   at RA = 0h25m16.37s  Dec = -72d04m20.5s
3) 5.49381 MJY/SR   at RA = 0h25m09.89s  Dec = -72d04m50.7s
4) 6.03175 MJY/SR   at RA = 0h25m19.55s  Dec = -72d03m20.4s
5) 8.91280 MJY/SR   at RA = 0h25m09.84s  Dec = -72d03m50.6s
6) 5.57568 MJY/SR   at RA = 0h25m03.36s  Dec = -72d04m20.8s
7) 8.99669 MJY/SR   at RA = 0h25m09.78s  Dec = -72d02m50.6s
8) 7.44171 MJY/SR   at RA = 0h25m03.31s  Dec = -72d03m20.7s
9) 7.08873 MJY/SR   at RA = 0h24m56.84s  Dec = -72d03m50.9s

1) 5.49750 MJY/SR   at RA = 0h25m06.49s  Dec = -72d02m05.6s
2) 5.77732 MJY/SR   at RA = 0h24m56.79s  Dec = -72d02m50.8s
3) 5.83948 MJY/SR   at RA = 0h24m50.31s  Dec = -72d03m05.9s
4) 3.90636 MJY/SR   at RA = 0h24m59.97s  Dec = -72d01m35.7s
5) 6.89637 MJY/SR   at RA = 0h24m50.26s  Dec = -72d02m05.9s
6) 5.76108 MJY/SR   at RA = 0h24m43.79s  Dec = -72d02m36.0s
7) 8.45424 MJY/SR   at RA = 0h24m53.47s  Dec = -72d01m05.8s
8) 7.17111 MJY/SR   at RA = 0h24m47.00s  Dec = -72d01m35.9s
9) 7.83310 MJY/SR   at RA = 0h24m37.29s  Dec = -72d02m06.0s

1) 3.76105 MJY/SR   at RA = 0h24m46.95s  Dec = -72d00m20.8s
```

```
2) 5.31484 MJY/SR   at RA = 0h24m37.25s  Dec = -72d00m51.0s
3) 4.83424 MJY/SR   at RA = 0h24m30.78s  Dec = -72d01m21.1s
4) 4.45056 MJY/SR   at RA = 0h24m43.70s  Dec = -71d59m50.9s
5) 6.34356 MJY/SR   at RA = 0h24m34.00s  Dec = -72d00m21.0s
6) 5.35473 MJY/SR   at RA = 0h24m24.29s  Dec = -72d00m51.1s
7) 7.98678 MJY/SR   at RA = 0h24m37.20s  Dec = -71d59m05.9s
8) 5.62887 MJY/SR   at RA = 0h24m27.51s  Dec = -71d59m51.0s
9) 7.53287 MJY/SR   at RA = 0h24m21.03s  Dec = -72d00m06.1s

1) 2.89824 MJY/SR   at RA = 0h24m27.48s  Dec = -71d58m36.0s
2) 5.76113 MJY/SR   at RA = 0h24m21.02s  Dec = -71d59m06.0s
3) 5.43898 MJY/SR   at RA = 0h24m14.55s  Dec = -71d59m36.1s
4) 3.92299 MJY/SR   at RA = 0h24m24.24s  Dec = -71d58m06.0s
5) 7.50781 MJY/SR   at RA = 0h24m14.54s  Dec = -71d58m36.0s
6) 4.84559 MJY/SR   at RA = 0h24m08.07s  Dec = -71d59m06.1s
7) 7.99219 MJY/SR   at RA = 0h24m17.76s  Dec = -71d57m21.0s
8) 7.41715 MJY/SR   at RA = 0h24m08.07s  Dec = -71d57m51.0s
9) 7.18301 MJY/SR   at RA = 0h24m01.60s  Dec = -71d58m21.0s

1) 4.67900 MJY/SR   at RA = 0h25m19.82s  Dec = -72d07m20.6s
2) 5.80907 MJY/SR   at RA = 0h25m13.33s  Dec = -72d07m50.7s
3) 5.86554 MJY/SR   at RA = 0h25m03.56s  Dec = -72d08m06.0s
4) 4.24799 MJY/SR   at RA = 0h25m13.25s  Dec = -72d06m35.7s
5) 8.07217 MJY/SR   at RA = 0h25m03.51s  Dec = -72d07m05.9s
6) 6.93526 MJY/SR   at RA = 0h24m57.01s  Dec = -72d07m36.0s
7) 7.87661 MJY/SR   at RA = 0h25m06.71s  Dec = -72d06m05.8s
8) 6.77315 MJY/SR   at RA = 0h24m56.97s  Dec = -72d06m36.0s
9) 8.01552 MJY/SR   at RA = 0h24m50.47s  Dec = -72d07m06.1s

1) 5.56768 MJY/SR   at RA = 0h25m00.16s  Dec = -72d05m20.9s
2) 6.10872 MJY/SR   at RA = 0h24m50.42s  Dec = -72d05m51.1s
3) 5.85618 MJY/SR   at RA = 0h24m43.92s  Dec = -72d06m21.2s
4) 6.11765 MJY/SR   at RA = 0h24m53.63s  Dec = -72d04m51.0s
5) 8.22792 MJY/SR   at RA = 0h24m47.14s  Dec = -72d05m21.1s
6) 6.05295 MJY/SR   at RA = 0h24m37.40s  Dec = -72d05m51.2s
7) 8.69375 MJY/SR   at RA = 0h24m47.11s  Dec = -72d04m21.0s
8) 6.41778 MJY/SR   at RA = 0h24m40.61s  Dec = -72d04m36.1s
9) 8.84593 MJY/SR   at RA = 0h24m34.12s  Dec = -72d05m06.2s

1) 5.48239 MJY/SR   at RA = 0h24m40.58s  Dec = -72d03m36.1s
2) 5.44808 MJY/SR   at RA = 0h24m34.09s  Dec = -72d04m06.2s
3) 4.80574 MJY/SR   at RA = 0h24m27.60s  Dec = -72d04m36.3s
4) 5.25720 MJY/SR   at RA = 0h24m37.32s  Dec = -72d03m06.1s
5) 7.97455 MJY/SR   at RA = 0h24m27.58s  Dec = -72d03m36.2s
6) 5.86130 MJY/SR   at RA = 0h24m21.09s  Dec = -72d03m51.3s
7) 8.68441 MJY/SR   at RA = 0h24m30.80s  Dec = -72d02m21.1s
8) 6.67089 MJY/SR   at RA = 0h24m21.07s  Dec = -72d02m51.2s
9) 9.96623 MJY/SR   at RA = 0h24m14.58s  Dec = -72d03m21.3s

1) 6.34572 MJY/SR   at RA = 0h24m24.30s  Dec = -72d01m51.1s
2) 5.80325 MJY/SR   at RA = 0h24m14.57s  Dec = -72d02m21.2s
3) 5.74330 MJY/SR   at RA = 0h24m08.09s  Dec = -72d02m51.3s
4) 5.49379 MJY/SR   at RA = 0h24m17.81s  Dec = -72d01m21.2s
5) 7.52183 MJY/SR   at RA = 0h24m11.33s  Dec = -72d01m51.2s
6) 5.63096 MJY/SR   at RA = 0h24m01.59s  Dec = -72d02m21.2s
7) 8.14499 MJY/SR   at RA = 0h24m14.56s  Dec = -72d00m36.1s
8) 7.06682 MJY/SR   at RA = 0h24m04.84s  Dec = -72d01m06.2s
9) 8.41206 MJY/SR   at RA = 0h23m58.35s  Dec = -72d01m36.2s

1) 5.27846 MJY/SR   at RA = 0h24m08.08s  Dec = -72d00m06.1s
2) 5.75729 MJY/SR   at RA = 0h23m58.36s  Dec = -72d00m36.1s
3) 6.05852 MJY/SR   at RA = 0h23m51.87s  Dec = -72d00m51.1s
4) 4.89793 MJY/SR   at RA = 0h24m01.60s  Dec = -71d59m21.1s
5) 8.47089 MJY/SR   at RA = 0h23m51.88s  Dec = -72d00m06.1s
```

```
6) 5.25859 MJY/SR   at RA = 0h23m45.40s  Dec = -72d00m21.1s
7) 8.94270 MJY/SR   at RA = 0h23m55.13s  Dec = -71d58m51.0s
8) 7.30589 MJY/SR   at RA = 0h23m45.42s  Dec = -71d59m21.0s
9) 9.21311 MJY/SR   at RA = 0h23m38.93s  Dec = -71d59m51.0s

1) 5.17682 MJY/SR   at RA = 0h24m53.80s  Dec = -72d08m36.1s
2) 6.50530 MJY/SR   at RA = 0h24m47.29s  Dec = -72d09m06.3s
3) 6.42817 MJY/SR   at RA = 0h24m37.51s  Dec = -72d09m36.4s
4) 5.01829 MJY/SR   at RA = 0h24m50.50s  Dec = -72d07m51.2s
5) 10.8561 MJY/SR   at RA = 0h24m40.73s  Dec = -72d08m21.3s
6) 5.80946 MJY/SR   at RA = 0h24m30.95s  Dec = -72d08m51.4s
7) 8.93843 MJY/SR   at RA = 0h24m40.70s  Dec = -72d07m21.3s
8) 5.68733 MJY/SR   at RA = 0h24m34.19s  Dec = -72d07m51.4s
9) 8.18557 MJY/SR   at RA = 0h24m27.68s  Dec = -72d08m21.4s

1) 5.67266 MJY/SR   at RA = 0h24m37.43s  Dec = -72d06m51.3s
2) 5.47847 MJY/SR   at RA = 0h24m27.66s  Dec = -72d07m21.4s
3) 5.57308 MJY/SR   at RA = 0h24m21.14s  Dec = -72d07m36.4s
4) 5.92716 MJY/SR   at RA = 0h24m30.89s  Dec = -72d06m06.3s
5) 7.04094 MJY/SR   at RA = 0h24m21.13s  Dec = -72d06m36.4s
6) 7.14187 MJY/SR   at RA = 0h24m14.62s  Dec = -72d07m06.4s
7) 9.74621 MJY/SR   at RA = 0h24m24.37s  Dec = -72d05m36.3s
8) 7.79594 MJY/SR   at RA = 0h24m14.61s  Dec = -72d06m06.4s
9) 8.24155 MJY/SR   at RA = 0h24m08.10s  Dec = -72d06m36.4s

1) 5.89203 MJY/SR   at RA = 0h24m17.85s  Dec = -72d05m06.3s
2) 6.91624 MJY/SR   at RA = 0h24m11.35s  Dec = -72d05m36.4s
3) 5.09008 MJY/SR   at RA = 0h24m04.84s  Dec = -72d05m51.4s
4) 6.80120 MJY/SR   at RA = 0h24m14.59s  Dec = -72d04m21.3s
5) 9.00171 MJY/SR   at RA = 0h24m04.84s  Dec = -72d04m51.3s
6) 5.72473 MJY/SR   at RA = 0h23m58.33s  Dec = -72d05m21.4s
7) 7.80591 MJY/SR   at RA = 0h24m08.09s  Dec = -72d03m51.3s
8) 7.66978 MJY/SR   at RA = 0h23m58.34s  Dec = -72d04m21.3s
9) 7.39138 MJY/SR   at RA = 0h23m51.83s  Dec = -72d04m36.3s

1) 5.74635 MJY/SR   at RA = 0h24m01.59s  Dec = -72d03m21.3s
2) 7.06195 MJY/SR   at RA = 0h23m55.09s  Dec = -72d03m51.3s
3) 5.86903 MJY/SR   at RA = 0h23m45.33s  Dec = -72d04m06.3s
4) 5.15242 MJY/SR   at RA = 0h23m58.35s  Dec = -72d02m36.2s
5) 9.97286 MJY/SR   at RA = 0h23m48.60s  Dec = -72d03m06.2s
6) 5.38932 MJY/SR   at RA = 0h23m38.85s  Dec = -72d03m36.2s
7) 9.61305 MJY/SR   at RA = 0h23m48.62s  Dec = -72d01m51.2s
8) 7.94073 MJY/SR   at RA = 0h23m38.87s  Dec = -72d02m36.1s
9) 9.17559 MJY/SR   at RA = 0h23m32.37s  Dec = -72d02m51.1s

1) 6.14097 MJY/SR   at RA = 0h23m45.38s  Dec = -72d01m21.1s
2) 6.42050 MJY/SR   at RA = 0h23m35.64s  Dec = -72d01m51.1s
3) 5.52751 MJY/SR   at RA = 0h23m25.89s  Dec = -72d02m21.0s
4) 5.66578 MJY/SR   at RA = 0h23m38.91s  Dec = -72d00m51.0s
5) 7.70745 MJY/SR   at RA = 0h23m29.17s  Dec = -72d01m21.0s
6) 5.44765 MJY/SR   at RA = 0h23m22.67s  Dec = -72d01m50.9s
7) 9.46134 MJY/SR   at RA = 0h23m32.45s  Dec = -72d00m06.0s
8) 7.45092 MJY/SR   at RA = 0h23m22.71s  Dec = -72d00m35.9s
9) 9.01813 MJY/SR   at RA = 0h23m12.97s  Dec = -72d01m05.7s

1) 6.06542 MJY/SR   at RA = 0h24m30.98s  Dec = -72d10m06.5s
2) 4.98309 MJY/SR   at RA = 0h24m24.45s  Dec = -72d10m21.6s
3) 6.15734 MJY/SR   at RA = 0h24m17.92s  Dec = -72d10m51.6s
4) 6.44101 MJY/SR   at RA = 0h24m24.43s  Dec = -72d09m21.5s
5) 7.42767 MJY/SR   at RA = 0h24m17.91s  Dec = -72d09m51.6s
6) 5.83495 MJY/SR   at RA = 0h24m11.38s  Dec = -72d10m21.6s
7) 8.84285 MJY/SR   at RA = 0h24m21.16s  Dec = -72d08m51.5s
8) 6.29069 MJY/SR   at RA = 0h24m11.37s  Dec = -72d09m06.5s
9) 8.64246 MJY/SR   at RA = 0h24m04.84s  Dec = -72d09m36.6s
```

```
1) 5.59790 MJY/SR   at RA = 0h24m14.63s  Dec = -72d08m06.5s
2) 7.23512 MJY/SR   at RA = 0h24m04.84s  Dec = -72d08m36.5s
3) 4.81985 MJY/SR   at RA = 0h23m58.31s  Dec = -72d09m06.5s
4) 5.61154 MJY/SR   at RA = 0h24m08.10s  Dec = -72d07m21.5s
5) 7.58000 MJY/SR   at RA = 0h23m58.31s  Dec = -72d08m06.5s
6) 6.99850 MJY/SR   at RA = 0h23m51.79s  Dec = -72d08m21.5s
7) 8.43411 MJY/SR   at RA = 0h24m04.84s  Dec = -72d06m51.4s
8) 5.90322 MJY/SR   at RA = 0h23m51.80s  Dec = -72d07m21.4s
9) 7.89205 MJY/SR   at RA = 0h23m45.26s  Dec = -72d08m06.4s

1) 5.34972 MJY/SR   at RA = 0h23m58.32s  Dec = -72d06m21.4s
2) 4.56732 MJY/SR   at RA = 0h23m48.55s  Dec = -72d06m51.4s
3) 7.23084 MJY/SR   at RA = 0h23m38.76s  Dec = -72d07m21.4s
4) 5.28804 MJY/SR   at RA = 0h23m51.82s  Dec = -72d05m51.4s
5) 9.55375 MJY/SR   at RA = 0h23m42.04s  Dec = -72d06m21.3s
6) 6.71401 MJY/SR   at RA = 0h23m35.52s  Dec = -72d06m36.3s
7) 8.86093 MJY/SR   at RA = 0h23m45.32s  Dec = -72d05m06.3s
8) 5.87987 MJY/SR   at RA = 0h23m35.54s  Dec = -72d05m36.2s
9) 8.51304 MJY/SR   at RA = 0h23m29.02s  Dec = -72d06m06.2s

1) 5.85940 MJY/SR   at RA = 0h23m38.82s  Dec = -72d04m36.2s
2) 6.50510 MJY/SR   at RA = 0h23m32.30s  Dec = -72d05m06.2s
3) 5.42935 MJY/SR   at RA = 0h23m22.53s  Dec = -72d05m21.1s
4) 6.11554 MJY/SR   at RA = 0h23m32.33s  Dec = -72d04m06.1s
5) 7.85926 MJY/SR   at RA = 0h23m25.81s  Dec = -72d04m36.1s
6) 6.16368 MJY/SR   at RA = 0h23m16.05s  Dec = -72d04m51.0s
7) 9.62945 MJY/SR   at RA = 0h23m25.86s  Dec = -72d03m21.0s
8) 4.80288 MJY/SR   at RA = 0h23m19.34s  Dec = -72d03m51.0s
9) 7.99182 MJY/SR   at RA = 0h23m09.57s  Dec = -72d04m20.8s

1) 6.00113 MJY/SR   at RA = 0h23m19.39s  Dec = -72d02m35.9s
2) 5.73325 MJY/SR   at RA = 0h23m12.86s  Dec = -72d03m20.8s
3) 7.45170 MJY/SR   at RA = 0h23m03.09s  Dec = -72d03m50.7s
4) 5.31417 MJY/SR   at RA = 0h23m16.17s  Dec = -72d02m05.8s
5) 9.29619 MJY/SR   at RA = 0h23m06.41s  Dec = -72d02m35.7s
6) 5.76938 MJY/SR   at RA = 0h22m59.89s  Dec = -72d03m05.6s
7) 8.67268 MJY/SR   at RA = 0h23m09.70s  Dec = -72d01m35.7s
8) 5.79052 MJY/SR   at RA = 0h22m59.94s  Dec = -72d02m05.5s
9) 7.46892 MJY/SR   at RA = 0h22m53.44s  Dec = -72d02m20.4s

1) 4.41314 MJY/SR   at RA = 0h24m08.11s  Dec = -72d11m21.7s
2) 6.29101 MJY/SR   at RA = 0h24m01.56s  Dec = -72d11m51.7s
3) 5.66373 MJY/SR   at RA = 0h23m55.01s  Dec = -72d12m21.7s
4) 4.41435 MJY/SR   at RA = 0h24m01.57s  Dec = -72d10m36.6s
5) 10.0777 MJY/SR   at RA = 0h23m55.02s  Dec = -72d11m21.6s
6) 6.35720 MJY/SR   at RA = 0h23m45.20s  Dec = -72d11m36.6s
7) 9.16132 MJY/SR   at RA = 0h23m58.30s  Dec = -72d10m06.6s
8) 5.49339 MJY/SR   at RA = 0h23m48.49s  Dec = -72d10m21.6s
9) 7.44483 MJY/SR   at RA = 0h23m38.67s  Dec = -72d11m06.5s

1) 6.16146 MJY/SR   at RA = 0h23m48.50s  Dec = -72d09m36.5s
2) 6.34759 MJY/SR   at RA = 0h23m41.97s  Dec = -72d09m51.5s
3) 4.81174 MJY/SR   at RA = 0h23m32.14s  Dec = -72d10m36.5s
4) 5.14001 MJY/SR   at RA = 0h23m45.25s  Dec = -72d08m51.5s
5) 7.87689 MJY/SR   at RA = 0h23m35.44s  Dec = -72d09m21.4s
6) 5.33711 MJY/SR   at RA = 0h23m28.90s  Dec = -72d09m51.4s
7) 9.27130 MJY/SR   at RA = 0h23m38.73s  Dec = -72d08m21.4s
8) 6.00578 MJY/SR   at RA = 0h23m28.93s  Dec = -72d08m51.3s
9) 7.68688 MJY/SR   at RA = 0h23m22.38s  Dec = -72d09m21.3s

1) 5.36112 MJY/SR   at RA = 0h23m32.22s  Dec = -72d07m51.3s
2) 5.74665 MJY/SR   at RA = 0h23m25.68s  Dec = -72d08m21.3s
3) 5.77823 MJY/SR   at RA = 0h23m15.88s  Dec = -72d08m36.1s
```

```
4) 4.50572 MJY/SR   at RA = 0h23m25.73s  Dec = -72d07m06.2s
5) 10.6868 MJY/SR   at RA = 0h23m19.18s  Dec = -72d07m51.2s
6) 5.61379 MJY/SR   at RA = 0h23m09.38s  Dec = -72d08m06.0s
7) 9.84510 MJY/SR   at RA = 0h23m19.23s  Dec = -72d06m36.1s
8) 6.62793 MJY/SR   at RA = 0h23m12.69s  Dec = -72d07m06.0s
9) 7.65561 MJY/SR   at RA = 0h23m02.90s  Dec = -72d07m20.9s

1) 5.18853 MJY/SR   at RA = 0h23m12.75s  Dec = -72d05m51.0s
2) 5.98867 MJY/SR   at RA = 0h23m06.21s  Dec = -72d06m20.9s
3) 5.74151 MJY/SR   at RA = 0h22m56.41s  Dec = -72d06m50.7s
4) 5.86193 MJY/SR   at RA = 0h23m06.26s  Dec = -72d05m20.8s
5) 8.92766 MJY/SR   at RA = 0h22m59.72s  Dec = -72d05m50.7s
6) 5.53973 MJY/SR   at RA = 0h22m53.18s  Dec = -72d06m20.6s
7) 9.82820 MJY/SR   at RA = 0h23m03.04s  Dec = -72d04m50.7s
8) 6.88009 MJY/SR   at RA = 0h22m53.26s  Dec = -72d05m05.5s
9) 7.46742 MJY/SR   at RA = 0h22m46.70s  Dec = -72d05m50.4s

1) 5.16938 MJY/SR   at RA = 0h22m56.58s  Dec = -72d04m05.6s
2) 6.97390 MJY/SR   at RA = 0h22m46.79s  Dec = -72d04m35.4s
3) 6.46758 MJY/SR   at RA = 0h22m40.25s  Dec = -72d05m05.2s
4) 6.33551 MJY/SR   at RA = 0h22m53.36s  Dec = -72d03m35.5s
5) 8.50877 MJY/SR   at RA = 0h22m43.57s  Dec = -72d04m05.3s
6) 6.31336 MJY/SR   at RA = 0h22m33.78s  Dec = -72d04m35.0s
7) 8.87823 MJY/SR   at RA = 0h22m46.91s  Dec = -72d02m50.3s
8) 6.35209 MJY/SR   at RA = 0h22m37.13s  Dec = -72d03m20.0s
9) 7.72160 MJY/SR   at RA = 0h22m27.34s  Dec = -72d03m49.8s

average:
1) 5.356   MJY/SR +- 0.791 MJY/SR        0.801
2) 5.980   MJY/SR +- 0.658 MJY/SR        0.894
3) 5.690   MJY/SR +- 0.727 MJY/SR        0.851
4) 5.325   MJY/SR +- 0.786 MJY/SR        0.800
5) 8.353   MJY/SR +- 1.223 MJY/SR        1.249
6) 5.929   MJY/SR +- 0.606 MJY/SR        0.886
7) 8.839   MJY/SR +- 0.628 MJY/SR        1.321
8) 6.590   MJY/SR +- 0.820 MJY/SR        0.985
9) 8.151   MJY/SR +- 0.752 MJY/SR        1.218

mean of all 9: 6.690 MJY/SR +- 1.381 MJY/SR

flat-field accuracy of map determined by internal flat-field of array

====================================================================
====================================================================

PGAI08900102.FITS  A2256
====================================================================

Maximum 14.0582    at RA = 17h04m09.44s  Dec =  78d42m10.2s
Minimum 5.30239    at RA = 17h02m42.60s  Dec =  78d41m25.8s

Mean    9.50401
st dev  1.38601
                                    Flux units MJY/SR

Flux integral      9.72615e-05   MJY
Inside 1.02337e-05 Steradian area
(1932 pixels)

Centroid                            RA = 17h02m52.51s  Dec =  78d43m00.4s


Flux weighted centroid              RA = 17h02m54.08s  Dec =  78d42m59.7s
```

```
vertex# 1  at RA = 17h05m16.69s  Dec =  78d46m08.9s

vertex# 2  at RA = 17h03m58.62s  Dec =  78d35m55.1s

vertex# 3  at RA = 17h00m30.28s  Dec =  78d39m38.6s

vertex# 4  at RA = 17h01m45.61s  Dec =  78d50m10.8s

=====================================================================
=====================================================================

PGAI85001219.FITS  S88
=====================================================================

Maximum 24.3729    at RA = 5h13m22.21s  Dec = -69d33m08.4s
Minimum 12.4853    at RA = 5h13m36.53s  Dec = -69d33m08.5s

Mean    18.8788
st dev  2.92006
                                  Flux units MJY/SR

Flux integral      2.09e-05   MJY
Inside 1.10707e-06 Steradian area
(209 pixels)

Centroid                            RA = 5h13m36.52s  Dec = -69d31m38.4s


Flux weighted centroid              RA = 5h13m35.22s  Dec = -69d31m38.0s

vertex# 1  at RA = 5h13m59.38s  Dec = -69d30m08.2s

vertex# 2  at RA = 5h13m13.66s  Dec = -69d29m38.2s

vertex# 3  at RA = 5h13m13.61s  Dec = -69d33m08.4s

vertex# 4  at RA = 5h13m59.46s  Dec = -69d33m38.3s

=====================================================================
=====================================================================

PGAI29902250.FITS  C5239
=====================================================================

Maximum 12.1211    at RA = 21h23m59.08s  Dec = -69d39m31.2s
Minimum 7.86627    at RA = 21h24m24.99s  Dec = -69d39m31.2s

Mean    9.78903
st dev  1.02593
                                  Flux units MJY/SR

Flux integral      1.41038e-05   MJY
Inside 1.44077e-06 Steradian area
(272 pixels)

Centroid                            RA = 21h24m36.15s  Dec = -69d41m03.3s


Flux weighted centroid              RA = 21h24m35.75s  Dec = -69d41m03.6s

vertex# 1  at RA = 21h25m11.25s  Dec = -69d44m00.9s

vertex# 2  at RA = 21h23m50.43s  Dec = -69d40m01.2s
```

```
vertex# 3  at RA = 21h24m01.98s  Dec = -69d38m01.1s

vertex# 4  at RA = 21h25m22.72s  Dec = -69d42m15.6s

=====================================================================
=====================================================================

PGAI30301380.FITS  C4121
=====================================================================

Maximum 48.1638    at RA = 18h50m05.55s  Dec = -7d58m09.5s
Minimum 35.1226    at RA = 18h50m09.59s  Dec = -7d51m24.1s

Mean    40.7279
st dev  3.00834
                                  Flux units MJY/SR

Flux integral      4.14209e-05   MJY
Inside 1.01702e-06 Steradian area
(192 pixels)

Centroid                            RA = 18h50m07.06s  Dec = -7d54m31.8s


Flux weighted centroid              RA = 18h50m07.04s  Dec = -7d54m35.2s

vertex# 1  at RA = 18h50m10.60s  Dec = -7d58m39.5s

vertex# 2  at RA = 18h50m03.53s  Dec = -7d58m39.5s

vertex# 3  at RA = 18h50m03.53s  Dec = -7d50m24.1s

vertex# 4  at RA = 18h50m10.60s  Dec = -7d50m24.1s

=====================================================================
=====================================================================

PGAI68300807.FITS  TMC-2
=====================================================================

Maximum 34.6925    at RA = 4h32m17.73s  Dec =  24d47m34.2s
Minimum 16.2874    at RA = 4h32m05.64s  Dec =  24d40m03.7s

Mean    21.0417
st dev  2.4651
                                  Flux units MJY/SR

Flux integral      0.000886305   MJY
Inside 4.21214e-05 Steradian area
(7952 pixels)

Centroid                            RA = 4h32m38.21s  Dec =  24d41m09.9s


Flux weighted centroid              RA = 4h32m38.72s  Dec =  24d41m13.4s

vertex# 1  at RA = 4h33m43.61s  Dec =  24d34m17.9s

vertex# 2  at RA = 4h31m45.89s  Dec =  24d29m47.9s

vertex# 3  at RA = 4h31m33.63s  Dec =  24d48m03.4s

vertex# 4  at RA = 4h33m29.42s  Dec =  24d52m34.1s
```

```
====================================================================
====================================================================

PGAI84403913.FITS  B209
====================================================================

Maximum 27.5279    at RA = 4h14m26.67s  Dec =  28d12m01.8s
Minimum 20.6054    at RA = 4h14m44.85s  Dec =  28d14m31.8s

Mean    23.6652
st dev  1.34192
                                  Flux units MJY/SR

Flux integral      6.94459e-05   MJY
Inside 2.93452e-06 Steradian area
(554 pixels)

Centroid                            RA = 4h14m37.46s  Dec =  28d11m01.7s


Flux weighted centroid              RA = 4h14m37.43s  Dec =  28d11m00.2s

vertex# 1  at RA = 4h14m51.64s  Dec =  28d08m01.4s

vertex# 2  at RA = 4h14m30.08s  Dec =  28d07m01.5s

vertex# 3  at RA = 4h14m23.27s  Dec =  28d14m01.9s

vertex# 4  at RA = 4h14m44.85s  Dec =  28d15m01.8s

====================================================================
====================================================================

PGAI69801101.FITS  SGR 1814-14
====================================================================

Maximum 118.75    at RA = 18h14m16.75s  Dec = -13d55m29.6s
Minimum 93.092    at RA = 18h14m12.62s  Dec = -14d00m44.8s

Mean    104.387
st dev  4.37017
                                  Flux units MJY/SR

Flux integral      0.000357195   MJY
Inside 3.42184e-06 Steradian area
(646 pixels)

Centroid                            RA = 18h14m21.39s  Dec = -13d58m29.7s


Flux weighted centroid              RA = 18h14m21.43s  Dec = -13d58m27.4s

vertex# 1  at RA = 18h14m32.22s  Dec = -13d54m44.6s

vertex# 2  at RA = 18h14m34.28s  Dec = -14d01m44.9s

vertex# 3  at RA = 18h14m10.56s  Dec = -14d02m14.9s

vertex# 4  at RA = 18h14m08.50s  Dec = -13d55m14.6s

====================================================================
====================================================================

PGAI70401550.FITS  Cha N
```

```
=====================================================================

Maximum 11.5284    at RA = 11h10m44.25s  Dec = -76d33m34.8s
Minimum 9.25209    at RA = 11h10m31.24s  Dec = -76d30m34.7s

Mean    9.99313
st dev  0.502066
                                    Flux units MJY/SR

Flux integral      7.72825e-06   MJY
Inside 7.73356e-07 Steradian area
(146 pixels)

Centroid                              RA = 11h10m43.33s  Dec = -76d31m29.2s


Flux weighted centroid                RA = 11h10m43.16s  Dec = -76d31m31.1s

vertex# 1  at RA = 11h10m52.60s  Dec = -76d29m04.5s

vertex# 2  at RA = 11h10m05.50s  Dec = -76d31m34.9s

vertex# 3  at RA = 11h10m44.26s  Dec = -76d33m49.8s

vertex# 4  at RA = 11h11m14.26s  Dec = -76d32m04.3s

=====================================================================
=====================================================================

PGAI35100809.FITS  M03
=====================================================================

Maximum 8.24613    at RA = 13h37m15.24s  Dec =  70d27m51.9s
Minimum 3.34379    at RA = 13h36m12.39s  Dec =  70d39m38.2s

Mean    5.08959
st dev  0.487789
                                    Flux units MJY/SR

Flux integral      0.000219368   MJY
Inside 4.31014e-05 Steradian area
(8137 pixels)

Centroid                              RA = 13h36m12.39s  Dec =  70d34m52.9s


Flux weighted centroid                RA = 13h36m12.43s  Dec =  70d34m51.1s

vertex# 1  at RA = 13h38m53.80s  Dec =  70d26m18.0s

vertex# 2  at RA = 13h34m31.17s  Dec =  70d21m20.5s

vertex# 3  at RA = 13h33m28.70s  Dec =  70d43m18.8s

vertex# 4  at RA = 13h37m55.89s  Dec =  70d48m21.8s

=====================================================================
=====================================================================

PGAI58200903.FITS  KBM2
=====================================================================

Maximum 15.2402    at RA = 1h13m56.14s  Dec =  5d30m53.3s
Minimum 2.42464    at RA = 1h13m31.00s  Dec =  5d32m23.3s
```

```
Mean    7.84667
st dev  3.21516
                                    Flux units MJY/SR

Flux integral      4.07738e-05   MJY
Inside 5.19632e-06 Steradian area
(981 pixels)

Centroid                              RA = 1h13m43.93s  Dec =  5d31m30.6s


Flux weighted centroid                RA = 1h13m43.93s  Dec =  5d31m27.7s

vertex# 1  at RA = 1h14m06.20s  Dec =  5d30m08.3s

vertex# 2  at RA = 1h13m32.01s  Dec =  5d26m38.1s

vertex# 3  at RA = 1h13m21.95s  Dec =  5d32m53.3s

vertex# 4  at RA = 1h13m55.14s  Dec =  5d36m23.6s

internal systematic flat-field structures of array (regular pattern generated by
the nine pixels; note: pixel numbering is arbitrary and needs not to comply
with official numbering scheme):

1) 5.97496 MJY/SR   at RA = 1h13m42.06s  Dec =  5d37m08.6s
2) 6.01222 MJY/SR   at RA = 1h13m39.05s  Dec =  5d36m53.6s
3) 13.4267 MJY/SR   at RA = 1h13m37.03s  Dec =  5d36m23.5s
4) 2.77970 MJY/SR   at RA = 1h13m43.07s  Dec =  5d36m23.6s
5) 4.68999 MJY/SR   at RA = 1h13m40.05s  Dec =  5d36m08.5s
6) 9.74893 MJY/SR   at RA = 1h13m38.04s  Dec =  5d35m53.5s
7) 4.53163 MJY/SR   at RA = 1h13m44.07s  Dec =  5d35m38.5s
8) 7.65885 MJY/SR   at RA = 1h13m42.06s  Dec =  5d35m23.5s
9) 10.5778 MJY/SR   at RA = 1h13m39.05s  Dec =  5d35m08.5s

1) 6.08981 MJY/SR   at RA = 1h13m46.09s  Dec =  5d34m53.5s
2) 6.06531 MJY/SR   at RA = 1h13m43.07s  Dec =  5d34m38.5s
3) 13.8076 MJY/SR   at RA = 1h13m41.06s  Dec =  5d34m23.5s
4) 2.80396 MJY/SR   at RA = 1h13m47.09s  Dec =  5d34m08.5s
5) 4.69676 MJY/SR   at RA = 1h13m44.07s  Dec =  5d34m08.5s
6) 9.58539 MJY/SR   at RA = 1h13m42.06s  Dec =  5d33m38.4s
7) 4.67179 MJY/SR   at RA = 1h13m48.10s  Dec =  5d33m23.4s
8) 7.42789 MJY/SR   at RA = 1h13m45.08s  Dec =  5d33m08.4s
9) 10.1176 MJY/SR   at RA = 1h13m43.07s  Dec =  5d32m53.4s

1) 6.28038 MJY/SR   at RA = 1h13m49.10s  Dec =  5d32m53.4s
2) 6.32724 MJY/SR   at RA = 1h13m47.09s  Dec =  5d32m38.4s
3) 14.1678 MJY/SR   at RA = 1h13m44.08s  Dec =  5d32m23.4s
4) 2.73665 MJY/SR   at RA = 1h13m50.11s  Dec =  5d32m08.4s
5) 5.04147 MJY/SR   at RA = 1h13m48.10s  Dec =  5d31m53.4s
6) 10.2914 MJY/SR   at RA = 1h13m45.08s  Dec =  5d31m38.3s
7) 5.01923 MJY/SR   at RA = 1h13m52.12s  Dec =  5d31m23.3s
8) 7.91696 MJY/SR   at RA = 1h13m49.10s  Dec =  5d31m08.3s
9) 11.4382 MJY/SR   at RA = 1h13m46.09s  Dec =  5d30m53.3s

1) 6.80776 MJY/SR   at RA = 1h13m53.13s  Dec =  5d30m53.3s
2) 6.77049 MJY/SR   at RA = 1h13m51.11s  Dec =  5d30m38.3s
3) 15.0245 MJY/SR   at RA = 1h13m47.09s  Dec =  5d30m23.3s
4) 3.25720 MJY/SR   at RA = 1h13m54.13s  Dec =  5d30m08.3s
5) 5.59153 MJY/SR   at RA = 1h13m51.11s  Dec =  5d29m53.3s
6) 10.8609 MJY/SR   at RA = 1h13m48.10s  Dec =  5d29m23.2s
7) 5.29208 MJY/SR   at RA = 1h13m55.14s  Dec =  5d29m23.2s
8) 9.03159 MJY/SR   at RA = 1h13m52.12s  Dec =  5d29m08.2s
```

```
9) 11.7576 MJY/SR   at RA = 1h13m50.11s  Dec =  5d28m53.2s

1) 5.95311 MJY/SR   at RA = 1h13m34.02s  Dec =  5d36m08.5s
2) 6.31246 MJY/SR   at RA = 1h13m31.00s  Dec =  5d35m53.5s
3) 13.2793 MJY/SR   at RA = 1h13m28.99s  Dec =  5d35m38.5s
4) 2.85124 MJY/SR   at RA = 1h13m35.02s  Dec =  5d35m23.5s
5) 4.80445 MJY/SR   at RA = 1h13m32.01s  Dec =  5d35m08.5s
6) 9.49191 MJY/SR   at RA = 1h13m30.00s  Dec =  5d34m53.4s
7) 4.35238 MJY/SR   at RA = 1h13m36.03s  Dec =  5d34m53.5s
8) 7.55090 MJY/SR   at RA = 1h13m34.02s  Dec =  5d34m23.4s
9) 10.6512 MJY/SR   at RA = 1h13m31.00s  Dec =  5d34m23.4s

1) 5.79211 MJY/SR   at RA = 1h13m37.04s  Dec =  5d34m08.4s
2) 6.22614 MJY/SR   at RA = 1h13m35.02s  Dec =  5d33m53.4s
3) 14.2226 MJY/SR   at RA = 1h13m32.01s  Dec =  5d33m38.4s
4) 2.96611 MJY/SR   at RA = 1h13m38.04s  Dec =  5d33m23.4s
5) 4.69542 MJY/SR   at RA = 1h13m36.03s  Dec =  5d33m08.4s
6) 9.62649 MJY/SR   at RA = 1h13m33.01s  Dec =  5d32m53.4s
7) 4.44828 MJY/SR   at RA = 1h13m40.05s  Dec =  5d32m38.4s
8) 7.71511 MJY/SR   at RA = 1h13m37.04s  Dec =  5d32m23.4s
9) 10.7540 MJY/SR   at RA = 1h13m34.02s  Dec =  5d32m08.3s

1) 5.89657 MJY/SR   at RA = 1h13m41.06s  Dec =  5d31m53.3s
2) 6.24599 MJY/SR   at RA = 1h13m39.05s  Dec =  5d31m38.3s
3) 13.7993 MJY/SR   at RA = 1h13m36.03s  Dec =  5d31m23.3s
4) 2.88547 MJY/SR   at RA = 1h13m42.07s  Dec =  5d31m08.3s
5) 4.58280 MJY/SR   at RA = 1h13m39.05s  Dec =  5d31m08.3s
6) 9.77353 MJY/SR   at RA = 1h13m37.04s  Dec =  5d30m38.3s
7) 4.13740 MJY/SR   at RA = 1h13m43.07s  Dec =  5d30m38.3s
8) 7.48206 MJY/SR   at RA = 1h13m41.06s  Dec =  5d30m23.3s
9) 11.3896 MJY/SR   at RA = 1h13m38.04s  Dec =  5d30m08.2s

1) 6.06865 MJY/SR   at RA = 1h13m44.08s  Dec =  5d29m53.2s
2) 6.07612 MJY/SR   at RA = 1h13m42.07s  Dec =  5d29m38.2s
3) 14.9825 MJY/SR   at RA = 1h13m39.05s  Dec =  5d29m23.2s
4) 3.02933 MJY/SR   at RA = 1h13m45.08s  Dec =  5d29m08.2s
5) 5.11063 MJY/SR   at RA = 1h13m42.07s  Dec =  5d28m53.2s
6) 10.4065 MJY/SR   at RA = 1h13m40.06s  Dec =  5d28m23.2s
7) 4.84770 MJY/SR   at RA = 1h13m46.09s  Dec =  5d28m23.2s
8) 8.05544 MJY/SR   at RA = 1h13m44.08s  Dec =  5d28m23.2s
9) 11.1738 MJY/SR   at RA = 1h13m42.07s  Dec =  5d27m53.1s

1) 5.06270 MJY/SR   at RA = 1h13m25.97s  Dec =  5d35m08.4s
2) 5.41435 MJY/SR   at RA = 1h13m22.96s  Dec =  5d34m53.4s
3) 13.4077 MJY/SR   at RA = 1h13m19.94s  Dec =  5d34m38.4s
4) 2.42658 MJY/SR   at RA = 1h13m26.98s  Dec =  5d34m23.4s
5) 4.30773 MJY/SR   at RA = 1h13m23.96s  Dec =  5d34m23.4s
6) 9.08478 MJY/SR   at RA = 1h13m21.95s  Dec =  5d33m53.4s
7) 3.83798 MJY/SR   at RA = 1h13m27.99s  Dec =  5d33m53.4s
8) 6.67943 MJY/SR   at RA = 1h13m25.98s  Dec =  5d33m38.4s
9) 10.0937 MJY/SR   at RA = 1h13m22.96s  Dec =  5d33m23.4s

1) 5.05817 MJY/SR   at RA = 1h13m28.99s  Dec =  5d33m08.4s
2) 5.52109 MJY/SR   at RA = 1h13m26.98s  Dec =  5d32m53.3s
3) 13.8151 MJY/SR   at RA = 1h13m23.97s  Dec =  5d32m38.3s
4) 2.42464 MJY/SR   at RA = 1h13m30.00s  Dec =  5d32m23.3s
5) 4.49960 MJY/SR   at RA = 1h13m27.99s  Dec =  5d32m08.3s
6) 8.92530 MJY/SR   at RA = 1h13m24.97s  Dec =  5d31m53.3s
7) 3.95463 MJY/SR   at RA = 1h13m31.00s  Dec =  5d31m38.3s
8) 6.85504 MJY/SR   at RA = 1h13m27.99s  Dec =  5d31m23.3s
9) 10.1586 MJY/SR   at RA = 1h13m25.98s  Dec =  5d31m08.3s

1) 5.44524 MJY/SR   at RA = 1h13m33.02s  Dec =  5d31m08.3s
2) 5.57358 MJY/SR   at RA = 1h13m30.00s  Dec =  5d30m53.3s
```

```
3) 14.3995 MJY/SR   at RA = 1h13m26.98s  Dec =  5d30m38.2s
4) 2.55597 MJY/SR   at RA = 1h13m34.02s  Dec =  5d30m23.2s
5) 4.58621 MJY/SR   at RA = 1h13m31.01s  Dec =  5d30m08.2s
6) 9.83430 MJY/SR   at RA = 1h13m27.99s  Dec =  5d29m53.2s
7) 4.18213 MJY/SR   at RA = 1h13m35.03s  Dec =  5d29m53.2s
8) 7.16359 MJY/SR   at RA = 1h13m32.01s  Dec =  5d29m38.2s
9) 10.8578 MJY/SR   at RA = 1h13m30.00s  Dec =  5d29m08.2s

1) 5.76564 MJY/SR   at RA = 1h13m36.03s  Dec =  5d29m08.2s
2) 6.10711 MJY/SR   at RA = 1h13m34.02s  Dec =  5d28m53.2s
3) 14.8578 MJY/SR   at RA = 1h13m31.01s  Dec =  5d28m23.1s
4) 2.84233 MJY/SR   at RA = 1h13m37.04s  Dec =  5d28m23.2s
5) 4.91872 MJY/SR   at RA = 1h13m34.02s  Dec =  5d28m08.1s
6) 10.3575 MJY/SR   at RA = 1h13m32.01s  Dec =  5d27m38.1s
7) 4.73128 MJY/SR   at RA = 1h13m38.05s  Dec =  5d27m38.1s
8) 8.19714 MJY/SR   at RA = 1h13m36.04s  Dec =  5d27m23.1s
9) 11.7081 MJY/SR   at RA = 1h13m33.02s  Dec =  5d27m08.1s

1) 5.03305 MJY/SR   at RA = 1h13m16.92s  Dec =  5d34m23.4s
2) 5.64184 MJY/SR   at RA = 1h13m14.91s  Dec =  5d34m08.3s
3) 13.5895 MJY/SR   at RA = 1h13m11.90s  Dec =  5d33m38.3s
4) 2.52962 MJY/SR   at RA = 1h13m17.93s  Dec =  5d33m38.3s
5) 4.50648 MJY/SR   at RA = 1h13m15.92s  Dec =  5d33m23.3s
6) 10.0788 MJY/SR   at RA = 1h13m12.90s  Dec =  5d32m53.3s
7) 3.98008 MJY/SR   at RA = 1h13m19.94s  Dec =  5d32m53.3s
8) 6.83458 MJY/SR   at RA = 1h13m16.93s  Dec =  5d32m38.3s
9) 10.8387 MJY/SR   at RA = 1h13m13.91s  Dec =  5d32m23.3s

1) 5.23499 MJY/SR   at RA = 1h13m20.95s  Dec =  5d32m08.3s
2) 5.56619 MJY/SR   at RA = 1h13m17.93s  Dec =  5d31m53.3s
3) 14.2320 MJY/SR   at RA = 1h13m14.92s  Dec =  5d31m38.2s
4) 2.38168 MJY/SR   at RA = 1h13m21.96s  Dec =  5d31m38.3s
5) 4.45912 MJY/SR   at RA = 1h13m18.94s  Dec =  5d31m23.2s
6) 10.3153 MJY/SR   at RA = 1h13m15.92s  Dec =  5d30m53.2s
7) 3.95396 MJY/SR   at RA = 1h13m22.96s  Dec =  5d30m53.2s
8) 7.08447 MJY/SR   at RA = 1h13m19.95s  Dec =  5d30m38.2s
9) 11.0360 MJY/SR   at RA = 1h13m16.93s  Dec =  5d30m23.2s

1) 5.10775 MJY/SR   at RA = 1h13m23.97s  Dec =  5d30m08.2s
2) 5.69876 MJY/SR   at RA = 1h13m21.96s  Dec =  5d29m53.2s
3) 14.5683 MJY/SR   at RA = 1h13m18.94s  Dec =  5d29m38.2s
4) 2.33644 MJY/SR   at RA = 1h13m24.97s  Dec =  5d29m38.2s
5) 4.43296 MJY/SR   at RA = 1h13m22.96s  Dec =  5d29m23.2s
6) 9.85111 MJY/SR   at RA = 1h13m19.95s  Dec =  5d28m53.1s
7) 3.65524 MJY/SR   at RA = 1h13m26.99s  Dec =  5d28m53.2s
8) 7.13806 MJY/SR   at RA = 1h13m23.97s  Dec =  5d28m38.1s
9) 11.1730 MJY/SR   at RA = 1h13m20.95s  Dec =  5d28m08.1s

1) 5.44912 MJY/SR   at RA = 1h13m26.99s  Dec =  5d28m08.1s
2) 5.93859 MJY/SR   at RA = 1h13m24.98s  Dec =  5d27m53.1s
3) 15.1658 MJY/SR   at RA = 1h13m21.96s  Dec =  5d27m23.1s
4) 2.63437 MJY/SR   at RA = 1h13m29.00s  Dec =  5d27m23.1s
5) 4.74702 MJY/SR   at RA = 1h13m25.98s  Dec =  5d27m08.1s
6) 10.4148 MJY/SR   at RA = 1h13m23.97s  Dec =  5d26m53.0s
7) 4.11359 MJY/SR   at RA = 1h13m30.00s  Dec =  5d26m53.1s
8) 7.87606 MJY/SR   at RA = 1h13m27.99s  Dec =  5d26m38.0s
9) 12.3825 MJY/SR   at RA = 1h13m23.97s  Dec =  5d26m08.0s

average:
1) 5.688   MJY/SR +- 0.516 MJY/SR        0.775
2) 5.968   MJY/SR +- 0.372 MJY/SR        0.813
3) 14.17   MJY/SR +- 0.618 MJY/SR        1.929
4) 2.715   MJY/SR +- 0.261 MJY/SR        0.370
5) 4.729   MJY/SR +- 0.318 MJY/SR        0.644
```

```
6) 9.915   MJY/SR +- 0.517 MJY/SR        1.350
7) 4.356   MJY/SR +- 0.462 MJY/SR        0.593
8) 7.541   MJY/SR +- 0.603 MJY/SR        1.027
9) 11.01   MJY/SR +- 0.638 MJY/SR        1.499

mean of all 9: 7.344 MJY/SR +- 3.683 MJY/SR

flat-field accuracy of map determined by internal flat-field of array

================================================================
================================================================

PGAI19201091.FITS  N1_5B
========================================================

best part:
----------

Maximum 5.47091    at RA = 16h09m38.95s  Dec =  54d35m04.4s
Minimum 3.20904    at RA = 16h10m13.48s  Dec =  54d33m04.4s

Mean    4.17649
st dev  0.367685
                                  Flux units MJY/SR

Flux integral      6.22091e-05   MJY
Inside 1.48951e-05 Steradian area
(2812 pixels)

Centroid                            RA = 16h10m01.73s  Dec =  54d33m45.8s


Flux weighted centroid              RA = 16h10m01.89s  Dec =  54d33m51.1s

vertex# 1  at RA = 16h11m06.87s  Dec =  54d29m18.1s

vertex# 2  at RA = 16h08m55.94s  Dec =  54d28m48.1s

vertex# 3  at RA = 16h08m55.69s  Dec =  54d38m03.6s

vertex# 4  at RA = 16h11m05.40s  Dec =  54d38m48.6s


worst part:
-----------

Maximum 12.5949    at RA = 16h09m20.08s  Dec =  54d27m33.7s
Minimum 2.98937    at RA = 16h09m40.74s  Dec =  54d27m49.1s

Mean    4.71402
st dev  1.54275
                                  Flux units MJY/SR

Flux integral      6.50718e-05   MJY
Inside 1.38039e-05 Steradian area
(2606 pixels)

Centroid                            RA = 16h10m01.50s  Dec =  54d24m06.8s


Flux weighted centroid              RA = 16h10m01.09s  Dec =  54d24m08.4s

vertex# 1  at RA = 16h11m05.13s  Dec =  54d28m48.2s
```

```
vertex# 2  at RA = 16h08m55.96s  Dec =  54d28m03.1s

vertex# 3  at RA = 16h08m57.91s  Dec =  54d19m17.7s

vertex# 4  at RA = 16h11m08.35s  Dec =  54d20m17.7s


average:
--------

Maximum 13.0318    at RA = 16h11m03.80s  Dec =  54d44m04.0s
Minimum 2.98937    at RA = 16h09m40.74s  Dec =  54d27m49.1s

Mean    4.72401
st dev  0.964179
                                  Flux units MJY/SR

Flux integral      0.000307681   MJY
Inside 6.51314e-05 Steradian area
(12296 pixels)

Centroid                            RA = 16h10m01.47s  Dec =  54d30m53.1s


Flux weighted centroid              RA = 16h10m01.53s  Dec =  54d30m44.0s

vertex# 1  at RA = 16h11m11.52s  Dec =  54d11m17.1s

vertex# 2  at RA = 16h11m03.99s  Dec =  54d51m19.3s

vertex# 3  at RA = 16h08m50.15s  Dec =  54d50m18.9s

vertex# 4  at RA = 16h08m59.84s  Dec =  54d10m32.4s

====================================================================
====================================================================

PGAI86901244.FITS  S2_C90_D
====================================================================

Maximum 7.79182    at RA = 5h02m03.52s  Dec = -30d28m21.5s
Minimum 3.8544    at RA = 5h02m40.69s  Dec = -30d31m36.6s

Mean    5.1707
st dev  0.649643
                                  Flux units MJY/SR

Flux integral      7.06363e-05   MJY
Inside 1.36609e-05 Steradian area
(2579 pixels)

Centroid                            RA = 5h02m24.22s  Dec = -30d34m26.1s


Flux weighted centroid              RA = 5h02m23.51s  Dec = -30d34m21.9s

vertex# 1  at RA = 5h02m50.03s  Dec = -30d41m52.0s

vertex# 2  at RA = 5h01m42.56s  Dec = -30d37m06.6s

vertex# 3  at RA = 5h02m00.04s  Dec = -30d26m51.4s

vertex# 4  at RA = 5h03m05.09s  Dec = -30d31m51.3s
```

```
====================================================================
====================================================================

PGAI41502788.FITS  Sculptor
====================================================================

best:
-----

Maximum 9.04908    at RA = 0h23m29.72s  Dec = -30d09m44.6s
Minimum 6.57762    at RA = 0h23m42.44s  Dec = -30d08m59.3s

Mean    7.8742
st dev  0.379763
                                  Flux units MJY/SR

Flux integral      8.40443e-05   MJY
Inside 1.06734e-05 Steradian area
(2015 pixels)

Centroid                            RA = 0h23m24.32s  Dec = -30d04m14.3s


Flux weighted centroid              RA = 0h23m24.25s  Dec = -30d04m15.9s

vertex# 1  at RA = 0h23m49.43s  Dec = -30d13m29.3s

vertex# 2  at RA = 0h23m22.80s  Dec = -30d15m00.0s

vertex# 3  at RA = 0h22m58.44s  Dec = -29d55m14.3s

vertex# 4  at RA = 0h23m27.30s  Dec = -29d53m43.9s


worst:
------

Maximum 12.162    at RA = 0h22m12.17s  Dec = -30d07m44.6s
Minimum 6.4858    at RA = 0h22m14.50s  Dec = -30d05m14.6s

Mean    8.41419
st dev  0.734978
                                  Flux units MJY/SR

Flux integral      9.19918e-05   MJY
Inside 1.09329e-05 Steradian area
(2064 pixels)

Centroid                            RA = 0h22m21.06s  Dec = -30d08m28.9s


Flux weighted centroid              RA = 0h22m21.02s  Dec = -30d08m27.7s

vertex# 1  at RA = 0h22m48.05s  Dec = -30d17m15.4s

vertex# 2  at RA = 0h22m19.06s  Dec = -30d18m45.3s

vertex# 3  at RA = 0h21m53.73s  Dec = -29d59m58.9s

vertex# 4  at RA = 0h22m23.78s  Dec = -29d58m14.3s


average:
--------
```

```
Maximum 12.162    at RA = 0h22m12.17s  Dec = -30d07m44.6s
Minimum 6.4858    at RA = 0h22m14.50s  Dec = -30d05m14.6s

Mean    8.1619
st dev  0.625301
                                  Flux units MJY/SR

Flux integral      0.000271937   MJY
Inside 3.33179e-05 Steradian area
(6290 pixels)

Centroid                            RA = 0h22m50.59s  Dec = -30d06m45.0s


Flux weighted centroid              RA = 0h22m49.90s  Dec = -30d06m45.8s

vertex# 1  at RA = 0h23m45.96s  Dec = -30d13m44.4s

vertex# 2  at RA = 0h22m19.06s  Dec = -30d19m00.3s

vertex# 3  at RA = 0h21m53.73s  Dec = -29d59m58.9s

vertex# 4  at RA = 0h23m23.84s  Dec = -29d54m29.0s

=====================================================================
=====================================================================

PGAI09000606.FITS  HYDRA 33
=====================================================================

Maximum 16.0106    at RA = 13h15m04.89s  Dec = -42d39m13.5s
Minimum 8.3139    at RA = 13h14m49.93s  Dec = -42d37m58.4s

Mean    11.891
st dev  1.59287
                                  Flux units MJY/SR

Flux integral      6.85921e-05   MJY
Inside 5.76839e-06 Steradian area
(1089 pixels)

Centroid                            RA = 13h15m02.00s  Dec = -42d36m46.0s


Flux weighted centroid              RA = 13h15m02.35s  Dec = -42d36m51.2s

vertex# 1  at RA = 13h15m33.45s  Dec = -42d36m13.1s

vertex# 2  at RA = 13h15m06.26s  Dec = -42d42m43.7s

vertex# 3  at RA = 13h14m30.89s  Dec = -42d36m58.1s

vertex# 4  at RA = 13h14m56.74s  Dec = -42d30m58.1s

=====================================================================
=====================================================================

PGAI08901904.FITS  HYDRA 34
=========================================================

Maximum 22.2889    at RA = 13h25m00.71s  Dec = -20d14m51.7s
Minimum 11.5585    at RA = 13h25m09.24s  Dec = -20d14m21.7s
```

```
Mean    15.504
st dev  2.55836
                                  Flux units MJY/SR

Flux integral      2.36517e-05   MJY
Inside 1.52553e-06 Steradian area
(288 pixels)

Centroid                            RA = 13h25m07.64s  Dec = -20d13m44.2s


Flux weighted centroid              RA = 13h25m07.50s  Dec = -20d13m48.3s

vertex# 1  at RA = 13h25m19.91s  Dec = -20d12m51.6s

vertex# 2  at RA = 13h25m11.38s  Dec = -20d16m36.8s

vertex# 3  at RA = 13h24m55.38s  Dec = -20d14m36.7s

vertex# 4  at RA = 13h25m03.91s  Dec = -20d10m51.5s

====================================================================
====================================================================

PGAI40100614.FITS  North_1
====================================================================

Maximum 16.4489    at RA = 20h33m44.56s  Dec =  65d06m48.2s
Minimum 10.8369    at RA = 20h32m42.72s  Dec =  65d12m19.2s

Mean    13.7358
st dev  0.889263
                                  Flux units MJY/SR

Flux integral      8.73824e-05   MJY
Inside 6.36165e-06 Steradian area
(1201 pixels)

Centroid                            RA = 20h32m58.56s  Dec =  65d07m40.0s


Flux weighted centroid              RA = 20h32m58.61s  Dec =  65d07m36.2s

vertex# 1  at RA = 20h33m56.52s  Dec =  65d08m17.9s

vertex# 2  at RA = 20h33m08.81s  Dec =  65d01m33.6s

vertex# 3  at RA = 20h32m02.30s  Dec =  65d06m48.5s

vertex# 4  at RA = 20h32m45.10s  Dec =  65d13m49.3s


Maximum 16.6936    at RA = 20h31m13.90s  Dec =  65d21m17.9s
Minimum 11.5691    at RA = 20h31m39.94s  Dec =  65d30m04.2s

Mean    13.7444
st dev  0.860085
                                  Flux units MJY/SR

Flux integral      0.000142403   MJY
Inside 1.03609e-05 Steradian area
(1956 pixels)

Centroid                            RA = 20h31m49.33s  Dec =  65d29m06.6s
```

```
Flux weighted centroid                RA = 20h31m49.04s  Dec =  65d29m02.0s

vertex# 1  at RA = 20h33m04.46s  Dec =  65d34m20.2s

vertex# 2  at RA = 20h31m25.99s  Dec =  65d19m33.2s

vertex# 3  at RA = 20h30m35.30s  Dec =  65d23m46.3s

vertex# 4  at RA = 20h32m11.13s  Dec =  65d38m35.2s

======================================================================
======================================================================

PGAI87001338.FITS  S2_C90_A
======================================================================

best:
-----

Maximum 6.12786    at RA = 5h03m03.51s  Dec = -30d34m29.6s
Minimum 3.97784    at RA = 5h03m12.79s  Dec = -30d32m14.3s

Mean    4.86964
st dev  0.344659
                                  Flux units MJY/SR

Flux integral      3.62667e-05   MJY
Inside 7.44753e-06 Steradian area
(1406 pixels)

Centroid                            RA = 5h02m53.20s  Dec = -30d38m22.1s


Flux weighted centroid                RA = 5h02m53.11s  Dec = -30d38m22.9s

vertex# 1  at RA = 5h03m17.43s  Dec = -30d31m14.1s

vertex# 2  at RA = 5h02m53.11s  Dec = -30d47m00.3s

vertex# 3  at RA = 5h02m28.64s  Dec = -30d45m15.4s

vertex# 4  at RA = 5h02m54.18s  Dec = -30d29m44.5s


worst:
------

Maximum 16.2234    at RA = 5h01m38.59s  Dec = -30d41m59.8s
Minimum 4.31434    at RA = 5h01m46.77s  Dec = -30d37m59.8s

Mean    5.76668
st dev  1.15262
                                  Flux units MJY/SR

Flux integral      4.76211e-05   MJY
Inside 8.25796e-06 Steradian area
(1559 pixels)

Centroid                            RA = 5h02m01.73s  Dec = -30d35m28.5s


Flux weighted centroid                RA = 5h02m01.26s  Dec = -30d35m32.6s
```

```
vertex# 1  at RA = 5h02m03.03s  Dec = -30d44m00.3s

vertex# 2  at RA = 5h01m36.27s  Dec = -30d41m59.7s

vertex# 3  at RA = 5h01m59.61s  Dec = -30d26m59.4s

vertex# 4  at RA = 5h02m27.47s  Dec = -30d28m59.7s


average:
--------

Maximum 11.0642    at RA = 5h01m53.75s  Dec = -30d35m59.8s
Minimum 4.05274    at RA = 5h02m57.74s  Dec = -30d42m30.0s

Mean    5.25767
st dev  0.725777
                                  Flux units MJY/SR

Flux integral      0.000114601   MJY
Inside 2.1797e-05 Steradian area
(4115 pixels)

Centroid                            RA = 5h02m26.17s  Dec = -30d36m59.7s


Flux weighted centroid              RA = 5h02m24.77s  Dec = -30d36m52.5s

vertex# 1  at RA = 5h02m51.94s  Dec = -30d47m00.3s

vertex# 2  at RA = 5h01m37.43s  Dec = -30d41m14.7s

vertex# 3  at RA = 5h01m59.61s  Dec = -30d26m59.4s

vertex# 4  at RA = 5h03m15.12s  Dec = -30d32m44.2s

================================================================
================================================================

PGAI16701405.FITS  Helix
================================================================

Maximum 18.5875    at RA = 22h29m56.43s  Dec = -20d40m10.8s
Minimum 11.7965    at RA = 22h30m01.77s  Dec = -20d36m10.6s

Mean    15.2265
st dev  1.28542
                                  Flux units MJY/SR

Flux integral      2.5648e-05   MJY
Inside 1.68443e-06 Steradian area
(318 pixels)

Centroid                            RA = 22h30m00.71s  Dec = -20d38m48.2s


Flux weighted centroid              RA = 22h30m00.73s  Dec = -20d38m53.1s

vertex# 1  at RA = 22h30m12.48s  Dec = -20d41m10.7s

vertex# 2  at RA = 22h30m00.71s  Dec = -20d42m25.9s

vertex# 3  at RA = 22h29m48.94s  Dec = -20d36m25.7s
```

```
vertex# 4  at RA = 22h30m00.70s  Dec = -20d35m10.6s


Maximum 18.4172    at RA = 22h29m16.80s  Dec = -21d01m11.8s
Minimum 13.2138    at RA = 22h29m09.30s  Dec = -21d01m26.7s

Mean    15.5207
st dev  1.19622
                                  Flux units MJY/SR

Flux integral      2.09642e-05   MJY
Inside 1.35073e-06 Steradian area
(255 pixels)

Centroid                            RA = 22h29m15.73s  Dec = -21d01m56.8s


Flux weighted centroid              RA = 22h29m15.70s  Dec = -21d01m55.2s

vertex# 1  at RA = 22h29m15.74s  Dec = -20d58m41.7s

vertex# 2  at RA = 22h29m26.45s  Dec = -21d03m57.0s

vertex# 3  at RA = 22h29m15.72s  Dec = -21d05m12.0s

vertex# 4  at RA = 22h29m05.01s  Dec = -20d59m56.6s

================================================================
================================================================

PGAI57501902.FITS  0016+16
================================================================

best:
-----

Maximum 12.4754    at RA = 0h18m18.98s  Dec =  16d23m24.1s
Minimum 10.4837    at RA = 0h18m25.24s  Dec =  16d19m54.0s

Mean    11.6675
st dev  0.457002
                                  Flux units MJY/SR

Flux integral      2.69458e-05   MJY
Inside 2.30948e-06 Steradian area
(436 pixels)

Centroid                            RA = 0h18m17.94s  Dec =  16d23m46.7s


Flux weighted centroid              RA = 0h18m17.92s  Dec =  16d23m47.9s

vertex# 1  at RA = 0h18m30.46s  Dec =  16d19m54.0s

vertex# 2  at RA = 0h18m18.99s  Dec =  16d18m53.9s

vertex# 3  at RA = 0h18m05.41s  Dec =  16d27m39.3s

vertex# 4  at RA = 0h18m16.89s  Dec =  16d28m39.4s


worst:
------
```

```
Maximum 14.8464    at RA = 0h18m47.15s  Dec =  16d27m24.3s
Minimum 10.9846    at RA = 0h18m47.15s  Dec =  16d23m24.2s

Mean    12.5186
st dev  0.683687
                                  Flux units MJY/SR

Flux integral      4.57543e-05   MJY
Inside 3.6549e-06 Steradian area
(690 pixels)

Centroid                            RA = 0h18m40.59s  Dec =  16d26m46.2s


Flux weighted centroid              RA = 0h18m40.56s  Dec =  16d26m48.7s

vertex# 1  at RA = 0h18m56.54s  Dec =  16d23m09.1s

vertex# 2  at RA = 0h18m38.80s  Dec =  16d21m39.1s

vertex# 3  at RA = 0h18m24.19s  Dec =  16d30m09.5s

vertex# 4  at RA = 0h18m42.98s  Dec =  16d31m54.6s


average:
--------

Maximum 14.8464    at RA = 0h18m47.15s  Dec =  16d27m24.3s
Minimum 10.4837    at RA = 0h18m25.24s  Dec =  16d19m54.0s

Mean    12.1271
st dev  0.698301
                                  Flux units MJY/SR

Flux integral      0.000100595   MJY
Inside 8.29504e-06 Steradian area
(1566 pixels)

Centroid                            RA = 0h18m32.74s  Dec =  16d25m10.2s


Flux weighted centroid              RA = 0h18m32.98s  Dec =  16d25m14.3s

vertex# 1  at RA = 0h18m59.66s  Dec =  16d22m39.0s

vertex# 2  at RA = 0h18m18.99s  Dec =  16d18m53.9s

vertex# 3  at RA = 0h18m05.41s  Dec =  16d27m39.3s

vertex# 4  at RA = 0h18m47.16s  Dec =  16d31m24.5s

================================================================
================================================================

PGAI52700514.FITS  NGC5907N
================================================================

Maximum 5.10056    at RA = 15h14m50.85s  Dec =  56d30m58.0s
Minimum 3.61179    at RA = 15h15m12.64s  Dec =  56d26m13.0s

Mean    4.373
st dev  0.202188
```

```
                                    Flux units MJY/SR

Flux integral      2.26772e-05   MJY
Inside 5.18573e-06 Steradian area
(979 pixels)

Centroid                              RA = 15h15m13.26s  Dec =  56d30m34.5s


Flux weighted centroid                RA = 15h15m13.09s  Dec =  56d30m36.6s

vertex# 1  at RA = 15h15m50.69s  Dec =  56d28m57.9s

vertex# 2  at RA = 15h15m12.64s  Dec =  56d24m42.9s

vertex# 3  at RA = 15h14m34.49s  Dec =  56d32m27.8s

vertex# 4  at RA = 15h15m16.23s  Dec =  56d36m13.5s

======================================================================
======================================================================

PGAI60002009.FITS  SMC HI c12
======================================================================

Maximum 7.48885    at RA = 0h41m57.37s  Dec = -74d11m57.8s
Minimum 5.70107    at RA = 0h41m12.20s  Dec = -74d18m26.4s

Mean    6.40072
st dev  0.342903
                                    Flux units MJY/SR

Flux integral      5.70272e-05   MJY
Inside 8.90949e-06 Steradian area
(1682 pixels)

Centroid                              RA = 0h41m57.18s  Dec = -74d13m35.4s


Flux weighted centroid                RA = 0h41m57.35s  Dec = -74d13m33.6s

vertex# 1  at RA = 0h42m51.95s  Dec = -74d20m59.6s

vertex# 2  at RA = 0h41m00.66s  Dec = -74d20m55.9s

vertex# 3  at RA = 0h41m03.23s  Dec = -74d06m10.3s

vertex# 4  at RA = 0h42m52.84s  Dec = -74d06m13.9s

======================================================================
======================================================================

PGAI50000124.FITS  N2_2
======================================================================

best:
-----

Maximum 5.63858    at RA = 16h33m59.77s  Dec =  40d53m12.7s
Minimum 2.83099    at RA = 16h35m20.42s  Dec =  40d46m26.5s

Mean    4.36568
st dev  0.309266
                                    Flux units MJY/SR
```

```
Flux integral      0.00011308   MJY
Inside 2.59021e-05 Steradian area
(4890 pixels)

Centroid                              RA = 16h34m42.78s  Dec =  40d49m24.9s


Flux weighted centroid                RA = 16h34m42.55s  Dec =  40d49m28.0s

vertex# 1  at RA = 16h35m38.81s  Dec =  40d40m55.5s

vertex# 2  at RA = 16h34m36.76s  Dec =  40d35m56.9s

vertex# 3  at RA = 16h33m46.50s  Dec =  40d57m42.8s

vertex# 4  at RA = 16h34m48.83s  Dec =  41d02m58.1s


worst:
------

Maximum 9.15391    at RA = 16h35m47.05s  Dec =  40d55m25.8s
Minimum 3.53608    at RA = 16h35m21.92s  Dec =  40d57m26.9s

Mean    5.76709
st dev  0.790456
                                    Flux units MJY/SR

Flux integral      8.9628e-05   MJY
Inside 1.55413e-05 Steradian area
(2934 pixels)

Centroid                              RA = 16h35m42.15s  Dec =  40d54m28.0s


Flux weighted centroid                RA = 16h35m43.36s  Dec =  40d54m12.8s

vertex# 1  at RA = 16h36m26.45s  Dec =  40d45m08.0s

vertex# 2  at RA = 16h35m49.39s  Dec =  40d41m55.1s

vertex# 3  at RA = 16h34m58.13s  Dec =  41d03m42.9s

vertex# 4  at RA = 16h35m34.03s  Dec =  41d07m11.9s


average:
--------

Maximum 9.15391    at RA = 16h35m47.05s  Dec =  40d55m25.8s
Minimum 2.83099    at RA = 16h35m20.42s  Dec =  40d46m26.5s

Mean    4.71589
st dev  0.624552
                                    Flux units MJY/SR

Flux integral      0.000370077   MJY
Inside 7.84745e-05 Steradian area
(14815 pixels)

Centroid                              RA = 16h34m18.56s  Dec =  40d47m20.1s
```

```
Flux weighted centroid               RA = 16h34m20.93s  Dec =  40d47m31.6s

vertex# 1  at RA = 16h36m18.51s  Dec =  40d44m38.5s

vertex# 2  at RA = 16h33m11.21s  Dec =  40d28m25.5s

vertex# 3  at RA = 16h32m17.94s  Dec =  40d49m53.8s

vertex# 4  at RA = 16h35m27.37s  Dec =  41d06m12.2s

================================================================
================================================================

PGAI50100273.FITS  N2_5
================================================================

Maximum 6.54501    at RA = 16h37m31.11s  Dec =  41d56m46.1s
Minimum 3.78583    at RA = 16h37m21.61s  Dec =  42d00m15.9s

Mean    5.4547
st dev  0.340588
                                  Flux units MJY/SR

Flux integral      7.91389e-05   MJY
Inside 1.45084e-05 Steradian area
(2739 pixels)

Centroid                           RA = 16h37m30.61s  Dec =  41d57m14.1s


Flux weighted centroid               RA = 16h37m30.69s  Dec =  41d57m17.2s

vertex# 1  at RA = 16h38m11.52s  Dec =  41d51m47.1s

vertex# 2  at RA = 16h37m25.94s  Dec =  41d46m45.4s

vertex# 3  at RA = 16h36m47.85s  Dec =  42d03m14.1s

vertex# 4  at RA = 16h37m39.00s  Dec =  42d07m01.9s


Maximum 6.90576    at RA = 16h39m05.33s  Dec =  42d04m03.0s
Minimum 4.21136    at RA = 16h38m47.81s  Dec =  41d51m02.4s

Mean    5.77505
st dev  0.347232
                                  Flux units MJY/SR

Flux integral      0.000101131   MJY
Inside 1.75118e-05 Steradian area
(3306 pixels)

Centroid                           RA = 16h38m47.81s  Dec =  42d01m13.3s


Flux weighted centroid               RA = 16h38m47.80s  Dec =  42d01m15.2s

vertex# 1  at RA = 16h39m34.86s  Dec =  41d53m17.0s

vertex# 2  at RA = 16h38m46.47s  Dec =  41d49m17.4s

vertex# 3  at RA = 16h38m01.91s  Dec =  42d09m32.8s

vertex# 4  at RA = 16h38m46.46s  Dec =  42d13m18.5s
```

```
====================================================================
====================================================================

PGAI20701079.FITS  GF9-I6
====================================================================

Maximum 23.955    at RA = 20h48m15.37s  Dec =  60d02m43.5s
Minimum 20.5525    at RA = 20h48m19.43s  Dec =  60d06m58.7s

Mean    21.9537
st dev  0.716328
                                    Flux units MJY/SR

Flux integral      1.06985e-05   MJY
Inside 4.8732e-07 Steradian area
(92 pixels)

Centroid                              RA = 20h48m16.39s  Dec =  60d04m13.6s


Flux weighted centroid                RA = 20h48m16.38s  Dec =  60d04m12.0s

vertex# 1  at RA = 20h48m21.37s  Dec =  60d01m13.4s

vertex# 2  at RA = 20h48m11.35s  Dec =  60d01m13.5s

vertex# 3  at RA = 20h48m11.40s  Dec =  60d07m13.8s

vertex# 4  at RA = 20h48m21.44s  Dec =  60d07m13.7s

====================================================================
====================================================================

PGAI20800709.FITS  LHE1
====================================================================

Maximum 6.63432    at RA = 10h50m59.79s  Dec =  57d41m18.0s
Minimum 5.17508    at RA = 10h50m18.63s  Dec =  57d39m32.6s

Mean    5.76273
st dev  0.187992
                                    Flux units MJY/SR

Flux integral      4.12392e-05   MJY
Inside 7.1562e-06 Steradian area
(1351 pixels)

Centroid                              RA = 10h51m11.15s  Dec =  57d39m31.2s


Flux weighted centroid                RA = 10h51m11.26s  Dec =  57d39m31.5s

vertex# 1  at RA = 10h52m03.29s  Dec =  57d36m01.7s

vertex# 2  at RA = 10h50m14.93s  Dec =  57d37m17.4s

vertex# 3  at RA = 10h50m16.69s  Dec =  57d43m02.7s

vertex# 4  at RA = 10h52m10.95s  Dec =  57d41m31.7s


Maximum 6.58177    at RA = 10h49m45.38s  Dec =  57d26m16.1s
Minimum 5.02566    at RA = 10h50m00.21s  Dec =  57d28m16.6s
```

```
Mean    5.77395
st dev  0.20993
                                  Flux units MJY/SR

Flux integral      3.37958e-05   MJY
Inside 5.85314e-06 Steradian area
(1105 pixels)

Centroid                            RA = 10h50m08.48s  Dec =  57d29m45.5s


Flux weighted centroid              RA = 10h50m08.44s  Dec =  57d29m45.5s

vertex# 1  at RA = 10h50m35.50s  Dec =  57d35m32.6s

vertex# 2  at RA = 10h50m24.47s  Dec =  57d23m31.9s

vertex# 3  at RA = 10h49m39.88s  Dec =  57d24m15.8s

vertex# 4  at RA = 10h49m54.41s  Dec =  57d36m01.8s

================================================================
================================================================

PGAI86800640.FITS  S2_C90_B
================================================================

Maximum 6.31604    at RA = 5h02m43.12s  Dec = -30d29m38.6s
Minimum 4.35471    at RA = 5h02m46.62s  Dec = -30d33m38.8s

Mean    5.43723
st dev  0.314041
                                  Flux units MJY/SR

Flux integral      3.55978e-05   MJY
Inside 6.54704e-06 Steradian area
(1236 pixels)

Centroid                            RA = 5h02m47.09s  Dec = -30d35m08.6s


Flux weighted centroid              RA = 5h02m46.90s  Dec = -30d35m09.2s

vertex# 1  at RA = 5h03m09.84s  Dec = -30d30m38.3s

vertex# 2  at RA = 5h02m54.80s  Dec = -30d41m39.1s

vertex# 3  at RA = 5h02m24.54s  Dec = -30d39m24.2s

vertex# 4  at RA = 5h02m38.47s  Dec = -30d28m53.6s

================================================================
================================================================

PGAI10101158.FITS  L134_C100
================================================================

Maximum 34.0971    at RA = 15h53m26.10s  Dec = -4d29m50.4s
Minimum 18.9697    at RA = 15h53m24.10s  Dec = -4d24m35.1s

Mean    27.4709
st dev  3.78377
                                  Flux units MJY/SR
```

```
Flux integral      9.25459e-05   MJY
Inside 3.36887e-06 Steradian area
(636 pixels)

Centroid                              RA = 15h53m31.42s  Dec = -4d27m48.1s


Flux weighted centroid                RA = 15h53m31.57s  Dec = -4d27m54.8s

vertex# 1  at RA = 15h53m45.17s  Dec = -4d24m50.1s

vertex# 2  at RA = 15h53m41.16s  Dec = -4d31m35.5s

vertex# 3  at RA = 15h53m17.07s  Dec = -4d30m35.4s

vertex# 4  at RA = 15h53m22.09s  Dec = -4d24m05.1s

=====================================================================
=====================================================================

PGAI79401149.FITS  L1166
=====================================================================

Maximum 52.7776    at RA = 22h05m36.96s  Dec =  59d32m02.9s
Minimum 37.0624    at RA = 22h05m05.36s  Dec =  59d33m47.9s

Mean    44.7403
st dev  3.57047
                                   Flux units MJY/SR

Flux integral      0.000113754   MJY
Inside 2.54254e-06 Steradian area
(480 pixels)

Centroid                              RA = 22h05m22.91s  Dec =  59d33m15.3s


Flux weighted centroid                RA = 22h05m23.18s  Dec =  59d33m14.1s

vertex# 1  at RA = 22h05m50.81s  Dec =  59d35m02.9s

vertex# 2  at RA = 22h05m25.11s  Dec =  59d29m02.8s

vertex# 3  at RA = 22h04m55.51s  Dec =  59d31m32.7s

vertex# 4  at RA = 22h05m19.18s  Dec =  59d37m18.1s

=====================================================================
=====================================================================

PGAI31000626.FITS  Rho_Oph_16
=====================================================================

Maximum 169.433    at RA = 16h32m39.89s  Dec = -24d28m33.8s
Minimum 110.434    at RA = 16h32m42.08s  Dec = -24d23m03.5s

Mean    138.608
st dev  10.5371
                                   Flux units MJY/SR

Flux integral      0.00026725   MJY
Inside 1.92809e-06 Steradian area
(364 pixels)
```

```
Centroid                              RA = 16h32m48.13s  Dec = -24d26m03.6s


Flux weighted centroid                RA = 16h32m48.03s  Dec = -24d26m06.7s

vertex# 1  at RA = 16h32m37.69s  Dec = -24d28m48.8s

vertex# 2  at RA = 16h32m42.08s  Dec = -24d22m48.5s

vertex# 3  at RA = 16h32m58.56s  Dec = -24d23m18.3s

vertex# 4  at RA = 16h32m54.19s  Dec = -24d29m18.7s

================================================================
================================================================

PGAI44900714.FITS  Rho_Oph_Ma
================================================================

Maximum 160.699    at RA = 16h28m38.77s  Dec = -24d13m08.7s
Minimum 81.5964    at RA = 16h29m28.09s  Dec = -24d08m06.9s

Mean    116.592
st dev  15.5143
                                   Flux units MJY/SR

Flux integral      0.000883761   MJY
Inside 7.57995e-06 Steradian area
(1431 pixels)

Centroid                              RA = 16h28m57.69s  Dec = -24d10m30.2s


Flux weighted centroid                RA = 16h28m56.33s  Dec = -24d10m34.0s

vertex# 1  at RA = 16h29m29.18s  Dec = -24d08m06.9s

vertex# 2  at RA = 16h28m32.15s  Dec = -24d06m08.5s

vertex# 3  at RA = 16h28m26.70s  Dec = -24d12m53.9s

vertex# 4  at RA = 16h29m22.69s  Dec = -24d14m52.5s

================================================================
================================================================

PGAI15601578.FITS  OPT_IR4
================================================================

Maximum 18.2121    at RA = 18h11m57.86s  Dec =  44d32m37.7s
Minimum 7.47226    at RA = 18h12m09.11s  Dec =  44d35m22.8s

Mean    12.633
st dev  2.2791
                                   Flux units MJY/SR

Flux integral      4.65738e-05   MJY
Inside 3.68669e-06 Steradian area
(696 pixels)

Centroid                              RA = 18h12m10.54s  Dec =  44d31m17.2s
```

```
Flux weighted centroid                RA = 18h12m10.13s  Dec =  44d31m10.3s

vertex# 1  at RA = 18h12m34.31s  Dec =  44d28m21.9s

vertex# 2  at RA = 18h12m10.45s  Dec =  44d26m07.3s

vertex# 3  at RA = 18h11m46.63s  Dec =  44d34m22.9s

vertex# 4  at RA = 18h12m10.52s  Dec =  44d36m22.8s

================================================================
================================================================

PGAI27600420.FITS  TPN
================================================================

Maximum 18.0274    at RA = 12h46m01.68s  Dec = -78d41m52.3s
Minimum 11.7086    at RA = 12h47m09.23s  Dec = -78d47m51.2s

Mean    14.223
st dev  1.39753
                                  Flux units MJY/SR

Flux integral      5.64288e-05   MJY
Inside 3.96742e-06 Steradian area
(749 pixels)

Centroid                          RA = 12h46m21.23s  Dec = -78d46m03.3s


Flux weighted centroid                RA = 12h46m21.33s  Dec = -78d46m01.9s

vertex# 1  at RA = 12h48m06.03s  Dec = -78d48m19.3s

vertex# 2  at RA = 12h47m04.79s  Dec = -78d51m36.5s

vertex# 3  at RA = 12h44m34.81s  Dec = -78d43m37.8s

vertex# 4  at RA = 12h45m41.17s  Dec = -78d40m37.4s

================================================================
================================================================

PGAI71901220.FITS  DC 303.8
================================================================

Maximum 17.9858    at RA = 13h05m40.39s  Dec = -76d50m45.4s
Minimum 14.5493    at RA = 13h05m31.82s  Dec = -76d48m45.1s

Mean    16.102
st dev  0.705822
                                  Flux units MJY/SR

Flux integral      4.1793e-05   MJY
Inside 2.59551e-06 Steradian area
(490 pixels)

Centroid                          RA = 13h06m11.10s  Dec = -76d51m53.5s


Flux weighted centroid                RA = 13h06m11.33s  Dec = -76d51m53.3s

vertex# 1  at RA = 13h06m50.68s  Dec = -76d55m16.4s
```

```
vertex# 2  at RA = 13h05m00.50s  Dec = -76d52m44.5s

vertex# 3  at RA = 13h05m31.85s  Dec = -76d48m30.1s

vertex# 4  at RA = 13h07m21.54s  Dec = -76d51m01.2s

=====================================================================
=====================================================================

PGAI33401134.FITS  RCRA
=====================================================================

Maximum 36.6005    at RA = 19h02m35.82s  Dec = -36d52m46.9s
Minimum 20.4721    at RA = 19h03m03.31s  Dec = -36d49m16.3s

Mean    27.8933
st dev  2.87882
                                  Flux units MJY/SR

Flux integral      9.79579e-05   MJY
Inside 3.51189e-06 Steradian area
(663 pixels)

Centroid                            RA = 19h02m47.85s  Dec = -36d50m57.8s


Flux weighted centroid              RA = 19h02m47.52s  Dec = -36d51m03.0s

vertex# 1  at RA = 19h03m03.29s  Dec = -36d47m31.2s

vertex# 2  at RA = 19h03m04.61s  Dec = -36d54m01.5s

vertex# 3  at RA = 19h02m32.07s  Dec = -36d54m17.0s

vertex# 4  at RA = 19h02m30.80s  Dec = -36d48m01.7s

=====================================================================
=====================================================================

PGAI79401149.FITS  IRAS22024+7
=====================================================================

Maximum 52.1026    at RA = 22h05m21.16s  Dec =  59d33m18.0s
Minimum 36.8087    at RA = 22h05m03.38s  Dec =  59d33m47.9s

Mean    43.6764
st dev  3.22953
                                  Flux units MJY/SR

Flux integral      0.000106653   MJY
Inside 2.4419e-06 Steradian area
(461 pixels)

Centroid                            RA = 22h05m15.29s  Dec =  59d34m35.7s


Flux weighted centroid              RA = 22h05m15.29s  Dec =  59d34m33.9s

vertex# 1  at RA = 22h05m42.92s  Dec =  59d36m33.0s

vertex# 2  at RA = 22h05m17.22s  Dec =  59d30m32.8s

vertex# 3  at RA = 22h04m47.60s  Dec =  59d32m47.6s
```

```
vertex# 4  at RA = 22h05m13.23s  Dec =  59d38m33.2s

=====================================================================
=====================================================================
```

9.2.4 Flat-field Accuracies of C200 Maps

- authors: U. Klaas
- date: 05-January-2000
- SVP period 2

Motivation

As part of the scientific validation of staring raster maps the current flat-field accuracy is determined. At the moment the flat-field correction is performed as part of the FCS calibration taking into account the actual response of the individual pixels to the illumination by the FCS and interpolating between the two bracketing FCS measurements. This cannot correct for non-linear temporal detector drifts. The flat-field correction has to take into account a non-homogenous FCS illumination over the array (FCS illumination matrix). This is averaged and odes not take into account possible systematic effects with heating power of the FCS. The responsivity matrix of the array is determined by rastering point source standards which are centered on each pixel, so that the bulk of the intensity is collected inside the central area of the pixel. For a flat sky, when the full pixel area and its spatial sensitivity is essential, there may be systematic variations due to slightly different solid angles among the pixels. There may be systematic additive offsets among the pixels as indicated by statistical flat-field assessment. Therefore, it is expected, that for faint surface brightness systematic flat-field effects should be seen much stronger than in for bright surface brightness. Also the raster step size and final oversampling is expected to play a role, since several pixels are averaged or not.

Method

We use the SKYVIEW program to determine the areas for the flat-field accuracy measurement on the preselected maps. The areas are defined drawing a polygon (rectangle). Afterwards a statistics on the defined area is performed determining the mean and standard deviation of the surface brightness. The flat-field accuracy is defined as the ratio of the standard deviation and the mean. It is checked that the minimum flux value is not undefined (equivalent to -1).

Results

In Table 9.4 we present the results of the analysis covering maps in 4 out of the 5 C200 filters, raster parameters in the range from no pixel overlap up to steps of 1/2 of the pixel size and a wide range of surface brightness values. The detailed evaluation providing the coordinates of the selected background fields as well as brightness maxima and minima is given in the evaluation log section. The description of systematic flat field structures in Table 9.4 is somehow subjective and depends also on the dynamic range of the map.
The listed flat-field accuracy is the standard deviation of the mean flux derived for the background field. Some slight impact by real background structures cannot be excluded. In general the achieved flat-field accuracy is $< \pm$ 15 %. There are some cases, in particular for low surface brightness and no pixel overlap for which the accuracy is only $< \pm$ 25 %. There is no dependence on the selected filter found.
For higher surface brightness and no pixel overlap the flat-field accuracy tends to improve. This may point to the fact that part of the flat-field residual is of additive nature. There is a considerably stronger improvement of the flat-field accuracy in case of good pixel overlap; flat-field accuracies as good as 3 % are achieved. In case of different raster steps in scan and cross-scan direction the resulting flat-field accuracy depends on the combination of pixel oversampling with the flat-field residual pattern (in one direction one maximum and minimum each may be averaged out, while in the other direction maxima and minima are averaged respectively leaving a significant flat-field residual). Examples are PGAI15601577 on the one hand and PGAI40900802 and PGAI28001303 on the other hand in Table 9.4.
This behaviour confirms that the current flat-field accuracy is limited by systematic instrumental flat-field residuals. In the evaluation log, for several maps with no pixel overlap the

surface brightness has been measured individually for series of pixel quadruplets. Systematic patterns showing repeatedly the array flat-field can be recognized. The scatter of the average brightness per pixel is in general considerably smaller than the scatter of the average of the four pixels. The relative flat-field residuals, normalized to the mean brightness value, have been established, too: For a certain filter they are reproduced, however with a scatter of 3 to 4% for an individual pixel, the flat-field residuals are different for the different filters (for the 170 and 180 μm filters they look more or less identical). In Fig. 9.2 an example each for a map with strong flat-field residuals and for a map with the best hitherto achieved flat-field accuracy is presented.
For one map a jump in the flat-field behaviour is observed when passing a bright object. This may be related to different memory behaviour of the individual pixels (different transient time constants). This is clearly a non-linear effect which cannot be removed by a static flat-field.

Table 9.4: C200 flat-field accuracies for various filters, raster parameters and surface brightnesses.

OLP product name	**filter** (μm)	**raster parameters MxN**	**dMxdN** (arcsec)	**over sampling**	**aligned with S/C-Y**	**surface brightness** (MJy sr^{-1})	**flat-field accuracy** (%)	**systematic ff structure**
PGAI56200110	150	32x4	180x180	N	N	3.4	8.6	strong
PGAI56201814	150	20x4	92x92	Y	N	22.2	4.8	marginal
PGAI08900103	170	5x5	180x180	N	Y	5.1	10.8	strong
PGAI25601309	170	7x4	180x180	N	N	10.4	7.6	strong
PGAI79400434	170	13x13	96x96	Y	Y	3.1	4.0	marginal
PGAI59300101	170	19x19	92x92	Y	Y	3.3	3.1	marginal
PGAI19800208	170	27x14	46x92	Y	Y	3.1	2.4	marginal
PGAI21001305	170	27x14	46x92	Y	Y	3.4	3.2	marginal
PGAI79900733	170	12x5	46x92	Y	Y	5.3	2.8	marginal
PGAI33600108	180	12x4	180x180	N	N	2.7	13.0	strong
PGAI33600705	180	12x4	180x180	N	N	4.7	6.1	strong
PGAI35100907	180	9x9	180x180	N	Y	4.1	12.5	strong
PGAI16701206	180	8x16	180x90	Y	Y	9.2	4.3[b]	marginal
						11.4	21.8[b]	recognizable
PGAI52700412	180	5x10	90x90	Y	N	3.0	3.9	marginal
PGAI85001037	180	15x15	90x90	Y	N	7.4	3.1	marginal
PGAI78200101	200	23x23	180x180	N	Y	2.3	22.3	strong
PGAI36803005	200	10x10	180x180	N	Y	14.8	10.0	recognizable
PGAI39602313	200	10x10	180x180	N	Y	29.1	9.5	recognizable
PGAI26101401	200	13x13	180x180	N	Y	37.6	7.0	recognizable
PGAI33401133	200	8x8	180x180	N	Y	40.0	11.4	marginal
						51.3	14.3	
PGAI86101801	200	14x6	180x180	N	N	158.0	11.0	recognizable
PGAI15601577	200	5x10	180x90	Y	Y	8.6	16.3	recognizable
PGAI33300559	200	10x20	180x90	Y	Y	18.4	7.6	marginal
PGAI10101157	200	5x10	180x90	Y	Y	49.3	6.4	marginal
PGAI31000625	200	5x10	180x90	Y	Y	180.2	4.5	marginal
PGAI26701013	200	15x30	180x90	Y	Y	184.2	14.2[a]	marginal
PGAI40900802	200	11x6	90x180	Y	Y	6.6	3.6	recognizable
PGAI28001303	200	11x6	90x180	Y	Y	10.0	5.1	recognizable

[a] contamination by sources?

[b] degradance due to memory effect after passage of bright source?

Conclusions

- In general the achieved flat-field accuracy of C200 maps is better than $\pm$ 15 % (standard deviation of the mean background flux).

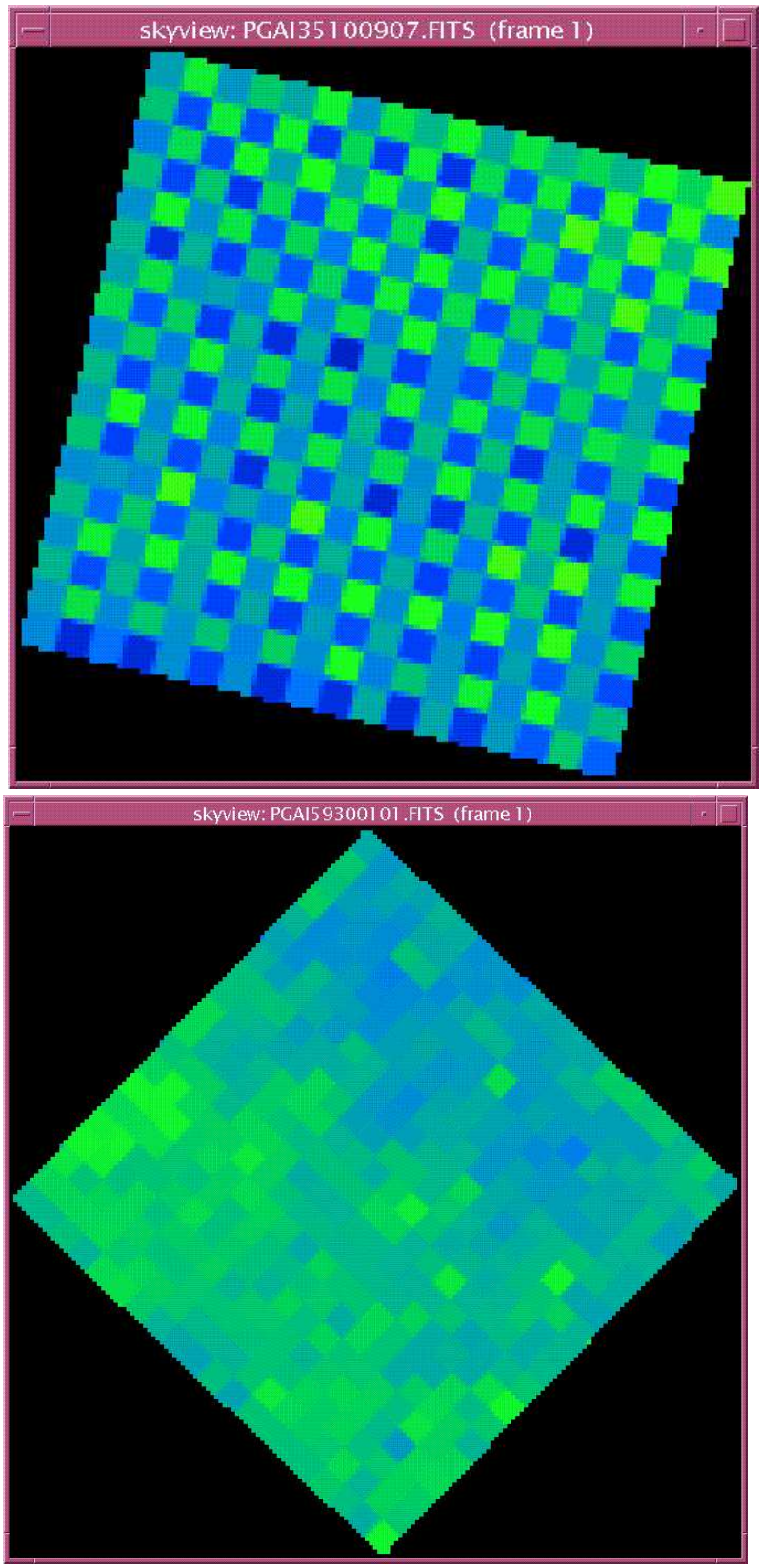

Figure 9.2: Example of a map with strong flat-field residual showing the systematic and repeated pattern of the 2x2 pixels (upper panel) and example of a map with one of the best flat-field accuracies due to proper oversampling for which no systematic pattern is recognizable (lower panel).

- A slight dependence on the absolute surface brightness is found with better flat-field accuracies for higher surface brightness.
- The flat-field accuracy is limited by systematic instrumental flat-field residuals of the C200 array. These are filter dependent.
- The flat-field accuracy is significantly improved when there is overlap of individual pixels. Then the flat-field residuals are averaged out. The best results are observed, if the raster step size is less equal than the pixel size in both directions; then accuracies between 3 and 5 % are achieved.

Evaluation Log

```
PGAI56200110.FITS  NGP_Dark
=========================================================

Maximum 4.21543    at RA = 13h42m19.74s  Dec =  40d22m43.0s
Minimum 2.68907    at RA = 13h42m11.54s  Dec =  40d35m13.1s

Mean    3.35577
st dev  0.28701
                                    Flux units MJY/SR

Flux integral      9.74981e-05   MJY
Inside 2.90538e-05 Steradian area
(5485 pixels)

Centroid                              RA = 13h42m36.94s  Dec =  40d25m56.6s


Flux weighted centroid                RA = 13h42m37.18s  Dec =  40d25m48.8s

vertex# 1  at RA = 13h44m04.82s  Dec =  40d16m15.1s

vertex# 2  at RA = 13h43m32.06s  Dec =  40d09m44.7s

vertex# 3  at RA = 13h41m08.28s  Dec =  40d35m23.6s

vertex# 4  at RA = 13h41m43.65s  Dec =  40d41m56.7s

internal systematic flat-field structures of array (regular pattern generated by
the four pixels):

1) 3.13280 MJY/SR   at RA = 13h41m38.44s  Dec =  40d39m41.2s
2) 3.58631 MJY/SR   at RA = 13h41m31.87s  Dec =  40d38m55.7s
3) 3.25492 MJY/SR   at RA = 13h41m37.20s  Dec =  40d37m26.0s
4) 3.53003 MJY/SR   at RA = 13h41m42.44s  Dec =  40d38m26.4s

1) 3.10623 MJY/SR   at RA = 13h41m26.63s  Dec =  40d37m55.2s
2) 3.45087 MJY/SR   at RA = 13h41m21.41s  Dec =  40d36m39.8s
3) 3.07876 MJY/SR   at RA = 13h41m26.72s  Dec =  40d35m40.1s
4) 3.54733 MJY/SR   at RA = 13h41m31.95s  Dec =  40d36m40.6s

1) 3.03352 MJY/SR   at RA = 13h41m50.38s  Dec =  40d37m42.0s
2) 3.36532 MJY/SR   at RA = 13h41m43.81s  Dec =  40d36m56.5s
3) 2.90186 MJY/SR   at RA = 13h41m47.80s  Dec =  40d35m41.7s
4) 3.40641 MJY/SR   at RA = 13h41m54.36s  Dec =  40d36m42.2s

1) 2.92988 MJY/SR   at RA = 13h41m37.26s  Dec =  40d35m40.9s
2) 3.66690 MJY/SR   at RA = 13h41m32.02s  Dec =  40d34m40.5s
3) 3.08189 MJY/SR   at RA = 13h41m37.32s  Dec =  40d33m55.9s
4) 3.45890 MJY/SR   at RA = 13h41m43.89s  Dec =  40d34m26.4s

1) 2.94722 MJY/SR   at RA = 13h42m00.99s  Dec =  40d35m27.5s
2) 3.43102 MJY/SR   at RA = 13h41m54.42s  Dec =  40d34m42.1s
3) 2.98492 MJY/SR   at RA = 13h42m01.04s  Dec =  40d33m27.4s
4) 3.43218 MJY/SR   at RA = 13h42m04.97s  Dec =  40d34m27.7s

1) 2.87506 MJY/SR   at RA = 13h41m49.18s  Dec =  40d33m41.7s
2) 3.45252 MJY/SR   at RA = 13h41m43.95s  Dec =  40d32m26.3s
3) 3.14094 MJY/SR   at RA = 13h41m49.25s  Dec =  40d31m26.6s
4) 3.63712 MJY/SR   at RA = 13h41m55.80s  Dec =  40d32m42.1s

1) 3.09856 MJY/SR   at RA = 13h42m12.90s  Dec =  40d33m28.1s
```

```
2) 3.58101 MJY/SR   at RA = 13h42m06.34s  Dec =  40d32m27.7s
3) 3.05534 MJY/SR   at RA = 13h42m11.63s  Dec =  40d31m28.0s
4) 3.43870 MJY/SR   at RA = 13h42m18.19s  Dec =  40d32m28.4s

1) 3.02963 MJY/SR   at RA = 13h42m01.10s  Dec =  40d31m27.4s
2) 3.66303 MJY/SR   at RA = 13h41m54.55s  Dec =  40d30m26.9s
3) 3.39318 MJY/SR   at RA = 13h41m59.84s  Dec =  40d29m27.2s
4) 3.53053 MJY/SR   at RA = 13h42m06.39s  Dec =  40d30m27.6s

1) 3.01270 MJY/SR   at RA = 13h42m24.80s  Dec =  40d31m28.7s
2) 3.57712 MJY/SR   at RA = 13h42m18.24s  Dec =  40d30m13.3s
3) 3.01112 MJY/SR   at RA = 13h42m23.52s  Dec =  40d29m43.5s
4) 3.69070 MJY/SR   at RA = 13h42m28.77s  Dec =  40d30m28.8s

1) 3.01447 MJY/SR   at RA = 13h42m34.05s  Dec =  40d29m29.0s
2) 3.57480 MJY/SR   at RA = 13h42m30.13s  Dec =  40d28m28.8s
3) 3.19962 MJY/SR   at RA = 13h42m35.41s  Dec =  40d27m29.0s
4) 3.65147 MJY/SR   at RA = 13h42m41.97s  Dec =  40d28m29.3s

1) 3.16268 MJY/SR   at RA = 13h42m23.58s  Dec =  40d27m13.4s
2) 3.79051 MJY/SR   at RA = 13h42m18.34s  Dec =  40d26m13.1s
3) 3.10726 MJY/SR   at RA = 13h42m23.62s  Dec =  40d25m28.3s
4) 3.56747 MJY/SR   at RA = 13h42m31.48s  Dec =  40d26m28.7s

1) 3.32404 MJY/SR   at RA = 13h42m35.45s  Dec =  40d25m13.8s
2) 3.53988 MJY/SR   at RA = 13h42m30.21s  Dec =  40d24m13.6s
3) 3.15331 MJY/SR   at RA = 13h42m35.49s  Dec =  40d23m13.8s
4) 3.47816 MJY/SR   at RA = 13h42m40.73s  Dec =  40d24m14.0s

1) 3.04626 MJY/SR   at RA = 13h42m57.80s  Dec =  40d25m29.7s
2) 3.30200 MJY/SR   at RA = 13h42m52.56s  Dec =  40d24m14.4s
3) 2.95844 MJY/SR   at RA = 13h42m56.51s  Dec =  40d23m14.5s
4) 3.53993 MJY/SR   at RA = 13h43m03.07s  Dec =  40d24m14.8s

1) 3.16658 MJY/SR   at RA = 13h42m47.31s  Dec =  40d23m29.2s
2) 3.64429 MJY/SR   at RA = 13h42m40.76s  Dec =  40d22m13.9s
3) 3.26869 MJY/SR   at RA = 13h42m46.04s  Dec =  40d21m14.1s
4) 3.65240 MJY/SR   at RA = 13h42m52.59s  Dec =  40d22m14.4s

1) 2.91674 MJY/SR   at RA = 13h43m08.34s  Dec =  40d23m14.9s
2) 3.39982 MJY/SR   at RA = 13h43m01.79s  Dec =  40d21m59.6s
3) 3.01832 MJY/SR   at RA = 13h43m08.36s  Dec =  40d21m14.8s
4) 3.55830 MJY/SR   at RA = 13h43m14.92s  Dec =  40d22m15.0s

1) 3.07724 MJY/SR   at RA = 13h42m57.86s  Dec =  40d20m59.5s
2) 3.99443 MJY/SR   at RA = 13h42m52.62s  Dec =  40d19m59.3s
3) 3.13600 MJY/SR   at RA = 13h42m57.89s  Dec =  40d18m59.4s
4) 3.56129 MJY/SR   at RA = 13h43m03.12s  Dec =  40d19m59.6s

1) 3.32120 MJY/SR   at RA = 13h43m20.18s  Dec =  40d21m30.0s
2) 3.50914 MJY/SR   at RA = 13h43m14.94s  Dec =  40d19m59.9s
3) 3.07879 MJY/SR   at RA = 13h43m20.20s  Dec =  40d19m14.9s
4) 3.74368 MJY/SR   at RA = 13h43m26.76s  Dec =  40d20m00.1s

1) 3.08039 MJY/SR   at RA = 13h43m09.70s  Dec =  40d19m14.7s
2) 3.56126 MJY/SR   at RA = 13h43m03.15s  Dec =  40d17m59.5s
3) 3.23127 MJY/SR   at RA = 13h43m08.41s  Dec =  40d16m59.6s
4) 3.69183 MJY/SR   at RA = 13h43m16.27s  Dec =  40d17m59.8s

1) 3.16965 MJY/SR   at RA = 13h43m32.01s  Dec =  40d19m00.1s
2) 3.22463 MJY/SR   at RA = 13h43m26.77s  Dec =  40d18m00.0s
3) 3.16437 MJY/SR   at RA = 13h43m32.02s  Dec =  40d17m00.0s
4) 3.57093 MJY/SR   at RA = 13h43m37.27s  Dec =  40d18m00.1s
```

```
1) 3.13639 MJY/SR   at RA = 13h43m20.22s  Dec =  40d16m59.8s
2) 3.71728 MJY/SR   at RA = 13h43m13.67s  Dec =  40d15m59.6s
3) 3.36463 MJY/SR   at RA = 13h43m20.24s  Dec =  40d14m44.7s
4) 3.86862 MJY/SR   at RA = 13h43m26.78s  Dec =  40d15m59.9s

1) 3.21046 MJY/SR   at RA = 13h43m43.83s  Dec =  40d16m45.1s
2) 3.70199 MJY/SR   at RA = 13h43m37.28s  Dec =  40d15m45.0s
3) 3.35910 MJY/SR   at RA = 13h43m42.53s  Dec =  40d14m45.0s
4) 3.65764 MJY/SR   at RA = 13h43m49.08s  Dec =  40d15m45.1s

1) 3.12246 MJY/SR   at RA = 13h43m32.04s  Dec =  40d14m44.9s
2) 3.70133 MJY/SR   at RA = 13h43m26.80s  Dec =  40d13m59.8s
3) 3.14664 MJY/SR   at RA = 13h43m32.05s  Dec =  40d12m44.8s
4) 4.04606 MJY/SR   at RA = 13h43m38.60s  Dec =  40d13m59.9s

average:
1) 3.08701 MJY/SR +- 0.11718 MJY/SR       0.92181
2) 3.56525 MJY/SR +- 0.17219 MJY/SR       1.06462
3) 3.14043 MJY/SR +- 0.13261 MJY/SR       0.93776
4) 3.60271 MJY/SR +- 0.14897 MJY/SR       1.07581

mean of all 4: 3.34885 MJY/SR +- 0.27281 MJY/SR

flat-field accuracy of map determined by internal flat-field of array
================================================================
================================================================

PGAI56201814.FITS  Combipht
================================================================

Maximum 25.018    at RA = 2h18m23.10s  Dec =  87d47m00.2s
Minimum 19.764    at RA = 2h07m21.92s  Dec =  87d42m35.2s

Mean    22.1639
st dev  1.0736
                                  Flux units MJY/SR

Flux integral      9.39209e-05   MJY
Inside 4.23757e-06 Steradian area
(800 pixels)

Centroid                            RA = 2h13m23.91s  Dec =  87d43m53.3s


Flux weighted centroid              RA = 2h13m34.61s  Dec =  87d43m54.7s

vertex# 1  at RA = 2h22m49.77s  Dec =  87d42m30.3s

vertex# 2  at RA = 2h20m36.48s  Dec =  87d47m24.0s

vertex# 3  at RA = 2h03m39.45s  Dec =  87d44m53.2s

vertex# 4  at RA = 2h06m26.20s  Dec =  87d40m21.0s

================================================================
================================================================

PGAI08900103.FITS  A2256
================================================================

Maximum 5.87526    at RA = 17h03m54.05s  Dec =  78d38m55.6s
Minimum 4.25031    at RA = 17h02m02.18s  Dec =  78d38m55.7s

Mean    5.09206
```

```
st dev  0.55184
                                    Flux units MJY/SR

Flux integral      1.73972e-05   MJY
Inside 3.41654e-06 Steradian area
(645 pixels)

Centroid                              RA = 17h03m15.24s  Dec =  78d39m21.2s


Flux weighted centroid                RA = 17h03m15.76s  Dec =  78d39m23.0s

vertex# 1  at RA = 17h04m45.22s  Dec =  78d40m54.8s

vertex# 2  at RA = 17h03m58.80s  Dec =  78d35m25.4s

vertex# 3  at RA = 17h01m47.02s  Dec =  78d37m55.5s

vertex# 4  at RA = 17h02m27.45s  Dec =  78d43m11.1s

internal systematic flat-field structures of array (regular pattern generated by
the four pixels):

1) 4.25608 MJY/SR   at RA = 17h03m53.81s  Dec =  78d36m10.5s
2) 5.28070 MJY/SR   at RA = 17h04m04.06s  Dec =  78d37m25.4s
3) 4.89502 MJY/SR   at RA = 17h03m38.74s  Dec =  78d38m10.7s
4) 5.66876 MJY/SR   at RA = 17h03m28.51s  Dec =  78d36m40.8s

1) 4.36038 MJY/SR   at RA = 17h04m14.39s  Dec =  78d38m55.3s
2) 5.80712 MJY/SR   at RA = 17h04m24.76s  Dec =  78d40m25.2s
3) 4.92329 MJY/SR   at RA = 17h03m59.32s  Dec =  78d40m55.6s
4) 5.87526 MJY/SR   at RA = 17h03m48.98s  Dec =  78d39m10.7s

1) 4.64260 MJY/SR   at RA = 17h04m40.24s  Dec =  78d41m39.9s
2) 6.27512 MJY/SR   at RA = 17h04m50.70s  Dec =  78d43m09.8s
3) 5.09514 MJY/SR   at RA = 17h04m20.07s  Dec =  78d43m40.4s
4) 6.26599 MJY/SR   at RA = 17h04m04.53s  Dec =  78d41m55.6s

1) 4.74757 MJY/SR   at RA = 17h05m01.22s  Dec =  78d44m39.6s
2) 6.55624 MJY/SR   at RA = 17h05m11.78s  Dec =  78d46m09.3s
3) 5.50695 MJY/SR   at RA = 17h04m40.98s  Dec =  78d46m25.2s
4) 6.41414 MJY/SR   at RA = 17h04m30.52s  Dec =  78d45m10.3s

1) 4.47913 MJY/SR   at RA = 17h02m58.10s  Dec =  78d37m10.9s
2) 5.46561 MJY/SR   at RA = 17h03m08.27s  Dec =  78d38m26.0s
3) 4.52894 MJY/SR   at RA = 17h02m42.86s  Dec =  78d39m11.0s
4) 5.76976 MJY/SR   at RA = 17h02m27.65s  Dec =  78d37m40.9s

1) 4.35806 MJY/SR   at RA = 17h03m13.41s  Dec =  78d40m11.0s
2) 5.63271 MJY/SR   at RA = 17h03m28.77s  Dec =  78d41m41.0s
3) 4.80190 MJY/SR   at RA = 17h02m58.14s  Dec =  78d41m56.1s
4) 5.86096 MJY/SR   at RA = 17h02m47.93s  Dec =  78d40m26.1s

1) 4.54868 MJY/SR   at RA = 17h03m39.04s  Dec =  78d42m41.0s
2) 5.78803 MJY/SR   at RA = 17h03m49.39s  Dec =  78d44m10.9s
3) 5.08683 MJY/SR   at RA = 17h03m23.80s  Dec =  78d44m41.2s
4) 6.15961 MJY/SR   at RA = 17h03m08.38s  Dec =  78d43m11.2s

1) 4.59958 MJY/SR   at RA = 17h03m59.79s  Dec =  78d45m40.9s
2) 6.28168 MJY/SR   at RA = 17h04m15.37s  Dec =  78d47m10.7s
3) 5.53024 MJY/SR   at RA = 17h03m44.51s  Dec =  78d47m26.1s
4) 6.91349 MJY/SR   at RA = 17h03m34.14s  Dec =  78d46m11.2s

1) 4.25031 MJY/SR   at RA = 17h02m02.26s  Dec =  78d37m55.7s
```

```
2) 5.38384 MJY/SR   at RA = 17h02m12.31s  Dec =  78d39m40.9s
3) 4.77103 MJY/SR   at RA = 17h01m41.69s  Dec =  78d40m25.5s
4) 5.89523 MJY/SR   at RA = 17h01m31.70s  Dec =  78d38m40.3s

1) 4.29923 MJY/SR   at RA = 17h02m22.42s  Dec =  78d41m11.0s
2) 5.62712 MJY/SR   at RA = 17h02m37.70s  Dec =  78d42m26.1s
3) 4.86777 MJY/SR   at RA = 17h02m07.00s  Dec =  78d42m56.0s
4) 6.01035 MJY/SR   at RA = 17h01m51.77s  Dec =  78d41m40.7s

1) 4.32340 MJY/SR   at RA = 17h01m01.09s  Dec =  78d39m24.7s
2) 6.15230 MJY/SR   at RA = 17h01m11.04s  Dec =  78d40m55.0s
3) 5.00994 MJY/SR   at RA = 17h00m50.55s  Dec =  78d41m24.6s
4) 5.92227 MJY/SR   at RA = 17h00m30.45s  Dec =  78d39m53.9s

1) 4.76080 MJY/SR   at RA = 17h01m21.10s  Dec =  78d41m55.3s
2) 6.11528 MJY/SR   at RA = 17h01m36.23s  Dec =  78d43m40.6s
3) 5.41895 MJY/SR   at RA = 17h01m05.47s  Dec =  78d43m55.0s
4) 6.38285 MJY/SR   at RA = 17h00m55.44s  Dec =  78d42m39.7s

average:
1) 4.46882 MJY/SR +- 0.18676 MJY/SR       0.83281
2) 5.86381 MJY/SR +- 0.40643 MJY/SR       1.09278
3) 5.03633 MJY/SR +- 0.31079 MJY/SR       0.93857
4) 6.09489 MJY/SR +- 0.35103 MJY/SR       1.13584

mean of all 4: 5.36596 MJY/SR +- 0.75116 MJY/SR

flat-field accuracy of map determined by internal flat-field of array
=====================================================================
=====================================================================

PGAI25601309.FITS  W Hya s-c
=====================================================================

Maximum 11.6324    at RA = 13h49m33.84s  Dec = -28d33m16.2s
Minimum 8.97955    at RA = 13h49m48.65s  Dec = -28d32m16.2s

Mean    10.2362
st dev  0.847185
                                  Flux units MJY/SR

Flux integral      1.60493e-05   MJY
Inside 1.5679e-06 Steradian area
(296 pixels)

Centroid                            RA = 13h49m44.09s  Dec = -28d32m23.7s


Flux weighted centroid              RA = 13h49m43.87s  Dec = -28d32m24.8s

vertex# 1  at RA = 13h50m05.74s  Dec = -28d33m16.1s

vertex# 2  at RA = 13h49m22.44s  Dec = -28d33m31.2s

vertex# 3  at RA = 13h49m22.45s  Dec = -28d31m31.1s

vertex# 4  at RA = 13h50m04.59s  Dec = -28d31m16.0s


Maximum 11.3861    at RA = 13h49m33.84s  Dec = -28d30m16.1s
Minimum 9.02219    at RA = 13h50m02.31s  Dec = -28d29m16.0s

Mean    10.2333
st dev  0.783557
```

```
                                  Flux units MJY/SR

Flux integral      1.32804e-05   MJY
Inside 1.29776e-06 Steradian area
(245 pixels)

Centroid                            RA = 13h49m44.09s  Dec = -28d29m31.1s


Flux weighted centroid              RA = 13h49m43.98s  Dec = -28d29m31.7s

vertex# 1  at RA = 13h50m04.59s  Dec = -28d30m16.0s

vertex# 2  at RA = 13h49m23.59s  Dec = -28d30m31.0s

vertex# 3  at RA = 13h49m23.60s  Dec = -28d28m30.9s

vertex# 4  at RA = 13h50m03.44s  Dec = -28d28m30.9s


Maximum 11.674    at RA = 13h49m33.84s  Dec = -28d27m15.9s
Minimum 9.09532    at RA = 13h50m02.30s  Dec = -28d26m15.8s

Mean    10.352
st dev  0.787151
                                  Flux units MJY/SR

Flux integral      1.34344e-05   MJY
Inside 1.29776e-06 Steradian area
(245 pixels)

Centroid                            RA = 13h49m44.09s  Dec = -28d26m30.9s


Flux weighted centroid              RA = 13h49m43.94s  Dec = -28d26m31.5s

vertex# 1  at RA = 13h50m04.58s  Dec = -28d27m15.8s

vertex# 2  at RA = 13h49m23.60s  Dec = -28d27m30.9s

vertex# 3  at RA = 13h49m23.60s  Dec = -28d25m30.8s

vertex# 4  at RA = 13h50m03.43s  Dec = -28d25m30.8s


Maximum 11.7417    at RA = 13h49m33.85s  Dec = -28d24m15.8s
Minimum 9.26011    at RA = 13h50m03.43s  Dec = -28d24m15.7s

Mean    10.6129
st dev  0.77453
                                  Flux units MJY/SR

Flux integral      1.37729e-05   MJY
Inside 1.29776e-06 Steradian area
(245 pixels)

Centroid                            RA = 13h49m44.09s  Dec = -28d23m30.8s


Flux weighted centroid              RA = 13h49m43.88s  Dec = -28d23m31.4s

vertex# 1  at RA = 13h50m04.57s  Dec = -28d24m15.7s

vertex# 2  at RA = 13h49m23.61s  Dec = -28d24m30.7s
```

```
vertex# 3  at RA = 13h49m23.61s  Dec = -28d22m30.6s

vertex# 4  at RA = 13h50m03.42s  Dec = -28d22m30.6s


Maximum 11.9556    at RA = 13h49m33.85s  Dec = -28d21m00.6s
Minimum 9.5247    at RA = 13h49m48.64s  Dec = -28d20m15.6s

Mean    10.7632
st dev  0.795997
                                    Flux units MJY/SR

Flux integral      1.19726e-05   MJY
Inside 1.11236e-06 Steradian area
(210 pixels)

Centroid                              RA = 13h49m44.09s  Dec = -28d20m23.1s


Flux weighted centroid                RA = 13h49m43.97s  Dec = -28d20m23.9s

vertex# 1  at RA = 13h50m04.56s  Dec = -28d21m15.6s

vertex# 2  at RA = 13h49m23.62s  Dec = -28d21m15.6s

vertex# 3  at RA = 13h49m23.62s  Dec = -28d19m30.5s

vertex# 4  at RA = 13h50m04.55s  Dec = -28d19m30.5s


internal systematic flat-field structures of array (regular pattern generated by
the four pixels; note: pixel numbering is arbitrary and needs not to comply
with official numbering scheme):

1) 8.97955 MJY/SR   at RA = 13h49m47.51s  Dec = -28d31m31.1s
2) 10.0509 MJY/SR   at RA = 13h49m53.20s  Dec = -28d32m01.2s
3) 9.35486 MJY/SR   at RA = 13h49m52.07s  Dec = -28d33m31.2s
4) 11.2332 MJY/SR   at RA = 13h49m45.23s  Dec = -28d33m01.2s

1) 9.09653 MJY/SR   at RA = 13h49m47.50s  Dec = -28d28m31.0s
2) 10.1007 MJY/SR   at RA = 13h49m54.34s  Dec = -28d29m01.0s
3) 9.22561 MJY/SR   at RA = 13h49m50.92s  Dec = -28d30m31.1s
4) 11.2509 MJY/SR   at RA = 13h49m45.23s  Dec = -28d29m46.1s

1) 9.34716 MJY/SR   at RA = 13h49m47.50s  Dec = -28d25m30.9s
2) 10.2894 MJY/SR   at RA = 13h49m53.19s  Dec = -28d26m00.9s
3) 9.32803 MJY/SR   at RA = 13h49m50.92s  Dec = -28d27m46.0s
4) 11.3212 MJY/SR   at RA = 13h49m45.23s  Dec = -28d27m00.9s

1) 9.58881 MJY/SR   at RA = 13h49m47.50s  Dec = -28d22m45.7s
2) 10.3289 MJY/SR   at RA = 13h49m54.33s  Dec = -28d23m00.7s
3) 9.53854 MJY/SR   at RA = 13h49m52.05s  Dec = -28d24m30.8s
4) 11.6574 MJY/SR   at RA = 13h49m45.23s  Dec = -28d23m45.8s

1) 9.52470 MJY/SR   at RA = 13h49m47.50s  Dec = -28d19m30.6s
2) 10.7017 MJY/SR   at RA = 13h49m54.32s  Dec = -28d20m00.6s
3) 9.62488 MJY/SR   at RA = 13h49m52.05s  Dec = -28d21m15.6s
4) 11.8558 MJY/SR   at RA = 13h49m45.22s  Dec = -28d21m00.6s

1) 9.12415 MJY/SR   at RA = 13h49m33.84s  Dec = -28d31m31.1s
2) 10.3311 MJY/SR   at RA = 13h49m40.67s  Dec = -28d32m01.2s
3) 9.40839 MJY/SR   at RA = 13h49m38.39s  Dec = -28d33m31.2s
4) 11.6324 MJY/SR   at RA = 13h49m31.56s  Dec = -28d32m46.2s
```

```
1) 9.19181 MJY/SR   at RA = 13h49m32.70s  Dec = -28d28m46.0s
2) 10.3434 MJY/SR   at RA = 13h49m40.67s  Dec = -28d29m01.0s
3) 9.29470 MJY/SR   at RA = 13h49m38.39s  Dec = -28d30m31.1s
4) 11.3861 MJY/SR   at RA = 13h49m31.56s  Dec = -28d29m46.0s

1) 9.36344 MJY/SR   at RA = 13h49m33.85s  Dec = -28d25m45.9s
2) 10.3937 MJY/SR   at RA = 13h49m40.67s  Dec = -28d26m00.9s
3) 9.39431 MJY/SR   at RA = 13h49m38.40s  Dec = -28d27m31.0s
4) 11.6740 MJY/SR   at RA = 13h49m31.57s  Dec = -28d26m45.9s

1) 9.67293 MJY/SR   at RA = 13h49m33.85s  Dec = -28d22m30.7s
2) 10.7985 MJY/SR   at RA = 13h49m40.68s  Dec = -28d23m00.7s
3) 9.67359 MJY/SR   at RA = 13h49m38.40s  Dec = -28d24m30.8s
4) 11.7417 MJY/SR   at RA = 13h49m31.57s  Dec = -28d24m00.8s

1) 9.52723 MJY/SR   at RA = 13h49m34.99s  Dec = -28d19m45.6s
2) 10.6953 MJY/SR   at RA = 13h49m40.68s  Dec = -28d20m00.6s
3) 9.90304 MJY/SR   at RA = 13h49m38.40s  Dec = -28d21m30.7s
4) 11.9556 MJY/SR   at RA = 13h49m31.58s  Dec = -28d20m45.6s

average:
1) 9.34163 MJY/SR +- 0.23576 MJY/SR       0.91429
2) 10.4034 MJY/SR +- 0.25246 MJY/SR       1.01820
3) 9.55382 MJY/SR +- 0.42618 MJY/SR       0.93505
4) 11.5708 MJY/SR +- 0.25673 MJY/SR       1.13246

mean of all 4: 10.2174 MJY/SR +- 1.01219 MJY/SR

flat-field accuracy of map determined by internal flat-field of array
=====================================================================
=====================================================================

PGAI79400434.FITS  N2_175_8_I
=====================================================================

Maximum 3.4252    at RA = 16h36m06.69s  Dec =  40d55m33.3s
Minimum 2.56497    at RA = 16h36m13.28s  Dec =  40d58m33.7s

Mean    3.09133
st dev  0.123946
                                    Flux units MJY/SR

Flux integral      4.91077e-05   MJY
Inside 1.58856e-05 Steradian area
(2999 pixels)

Centroid                              RA = 16h36m37.15s  Dec =  40d56m34.0s


Flux weighted centroid                RA = 16h36m36.83s  Dec =  40d56m29.5s

vertex# 1  at RA = 16h37m30.18s  Dec =  41d00m18.9s

vertex# 2  at RA = 16h36m21.34s  Dec =  40d46m03.2s

vertex# 3  at RA = 16h35m44.22s  Dec =  40d52m47.5s

vertex# 4  at RA = 16h36m53.04s  Dec =  41d07m04.5s

=====================================================================
=====================================================================

PGAI59300101.FITS  Marano 1
```

```
=====================================================================

Maximum 3.76743    at RA = 3h12m35.08s  Dec = -54d57m43.1s
Minimum 3.08038    at RA = 3h12m03.56s  Dec = -55d01m57.2s

Mean    3.32342
st dev  0.102499
                                    Flux units MJY/SR

Flux integral      5.99242e-05   MJY
Inside 1.80309e-05 Steradian area
(3404 pixels)

Centroid                              RA = 3h12m37.46s  Dec = -54d56m34.6s


Flux weighted centroid                RA = 3h12m36.94s  Dec = -54d56m38.3s

vertex# 1  at RA = 3h14m05.59s  Dec = -54d49m43.0s

vertex# 2  at RA = 3h11m45.81s  Dec = -55d08m56.7s

vertex# 3  at RA = 3h11m09.36s  Dec = -55d03m09.2s

vertex# 4  at RA = 3h13m29.10s  Dec = -54d44m13.1s

=====================================================================
=====================================================================

PGAI19800208.FITS  LHNW4
=====================================================================

Maximum 3.30238    at RA = 10h34m53.06s  Dec =  57d40m11.2s
Minimum 2.95038    at RA = 10h33m40.23s  Dec =  57d35m39.7s

Mean    3.08869
st dev  0.0739712
                                    Flux units MJY/SR

Flux integral      2.69624e-05   MJY
Inside 8.72939e-06 Steradian area
(1648 pixels)

Centroid                              RA = 10h34m21.05s  Dec =  57d36m07.7s


Flux weighted centroid                RA = 10h34m21.21s  Dec =  57d36m09.2s

vertex# 1  at RA = 10h35m08.03s  Dec =  57d39m56.2s

vertex# 2  at RA = 10h34m53.06s  Dec =  57d30m25.8s

vertex# 3  at RA = 10h33m34.75s  Dec =  57d32m24.4s

vertex# 4  at RA = 10h33m47.52s  Dec =  57d41m40.3s

=====================================================================
=====================================================================

PGAI21001305.FITS  LHNW1
=====================================================================

Maximum 3.744    at RA = 10h34m00.16s  Dec =  58d07m09.5s
Minimum 3.10788    at RA = 10h34m01.81s  Dec =  57d58m54.1s
```

```
Mean    3.44587
st dev  0.109116
                                  Flux units MJY/SR

Flux integral      5.3973e-05   MJY
Inside 1.56631e-05 Steradian area
(2957 pixels)

Centroid                            RA = 10h33m32.10s  Dec =  57d59m20.1s


Flux weighted centroid              RA = 10h33m31.88s  Dec =  57d59m23.4s

vertex# 1  at RA = 10h34m15.34s  Dec =  58d07m54.0s

vertex# 2  at RA = 10h34m10.96s  Dec =  57d50m38.4s

vertex# 3  at RA = 10h32m50.10s  Dec =  57d50m39.7s

vertex# 4  at RA = 10h32m51.94s  Dec =  58d07m40.5s

================================================================
================================================================

PGAI79900733.FITS  R Scl
================================================================

Maximum 5.53134    at RA = 1h27m01.61s  Dec = -32d35m49.2s
Minimum 4.91003    at RA = 1h26m53.30s  Dec = -32d37m49.3s

Mean    5.19748
st dev  0.167553
                                  Flux units MJY/SR

Flux integral      4.51506e-06   MJY
Inside 8.68702e-07 Steradian area
(164 pixels)

Centroid                            RA = 1h27m01.40s  Dec = -32d36m34.6s


Flux weighted centroid              RA = 1h27m01.46s  Dec = -32d36m34.1s

vertex# 1  at RA = 1h27m15.87s  Dec = -32d36m49.1s

vertex# 2  at RA = 1h26m48.54s  Dec = -32d38m04.2s

vertex# 3  at RA = 1h26m47.36s  Dec = -32d36m19.2s

vertex# 4  at RA = 1h27m13.49s  Dec = -32d35m04.1s


Maximum 5.64385    at RA = 1h27m01.61s  Dec = -32d29m03.8s
Minimum 5.12062    at RA = 1h26m46.19s  Dec = -32d28m03.8s

Mean    5.35167
st dev  0.12805
                                  Flux units MJY/SR

Flux integral      5.18761e-06   MJY
Inside 9.69344e-07 Steradian area
(183 pixels)
```

```
Centroid                              RA = 1h26m54.78s  Dec = -32d28m32.0s


Flux weighted centroid                RA = 1h26m54.84s  Dec = -32d28m32.1s

vertex# 1  at RA = 1h27m09.91s  Dec = -32d28m33.8s

vertex# 2  at RA = 1h26m41.43s  Dec = -32d30m18.8s

vertex# 3  at RA = 1h26m40.25s  Dec = -32d28m18.7s

vertex# 4  at RA = 1h27m08.72s  Dec = -32d26m48.7s

=====================================================================
=====================================================================

PGAI33600108.FITS  EBL_4
=====================================================================

Maximum 3.56157    at RA = 13h37m33.93s  Dec =  70d20m10.1s
Minimum 2.03326    at RA = 13h36m58.96s  Dec =  70d27m27.1s

Mean    2.65608
st dev  0.34642
                                   Flux units MJY/SR

Flux integral      6.21857e-05   MJY
Inside 2.34126e-05 Steradian area
(4420 pixels)

Centroid                              RA = 13h34m54.80s  Dec =  70d24m29.6s


Flux weighted centroid                RA = 13h34m55.37s  Dec =  70d24m26.3s

vertex# 1  at RA = 13h38m10.92s  Dec =  70d28m23.2s

vertex# 2  at RA = 13h38m09.57s  Dec =  70d19m52.9s

vertex# 3  at RA = 13h31m39.96s  Dec =  70d20m22.7s

vertex# 4  at RA = 13h31m41.59s  Dec =  70d28m53.3s

internal systematic flat-field structures of array (regular pattern generated by
the four pixels; note: pixel numbering is arbitrary and needs not to comply
with official numbering scheme):

1) 2.30804 MJY/SR   at RA = 13h38m04.85s  Dec =  70d27m53.6s
2) 2.74670 MJY/SR   at RA = 13h37m46.90s  Dec =  70d27m54.7s
3) 2.28065 MJY/SR   at RA = 13h37m46.69s  Dec =  70d26m24.7s
4) 3.39629 MJY/SR   at RA = 13h38m04.62s  Dec =  70d26m23.5s

1) 2.28667 MJY/SR   at RA = 13h37m28.94s  Dec =  70d27m55.7s
2) 2.52859 MJY/SR   at RA = 13h37m07.96s  Dec =  70d27m41.7s
3) 2.35831 MJY/SR   at RA = 13h37m07.86s  Dec =  70d26m41.7s
4) 3.43768 MJY/SR   at RA = 13h37m31.74s  Dec =  70d26m25.5s

1) 2.03326 MJY/SR   at RA = 13h36m53.03s  Dec =  70d27m57.4s
2) 2.54830 MJY/SR   at RA = 13h36m35.07s  Dec =  70d27m58.0s
3) 2.27689 MJY/SR   at RA = 13h36m34.95s  Dec =  70d26m28.0s
4) 3.28365 MJY/SR   at RA = 13h36m55.87s  Dec =  70d26m27.2s

1) 2.14252 MJY/SR   at RA = 13h36m14.10s  Dec =  70d27m43.7s
2) 2.54331 MJY/SR   at RA = 13h35m59.15s  Dec =  70d27m59.0s
```

```
3) 2.48189 MJY/SR   at RA = 13h35m59.09s  Dec =  70d26m44.0s
4) 3.30091 MJY/SR   at RA = 13h36m17.01s  Dec =  70d26m28.5s

1) 2.11002 MJY/SR   at RA = 13h35m44.20s  Dec =  70d28m14.3s
2) 2.61534 MJY/SR   at RA = 13h35m23.24s  Dec =  70d28m14.6s
3) 2.35147 MJY/SR   at RA = 13h35m23.21s  Dec =  70d26m44.5s
4) 3.28353 MJY/SR   at RA = 13h35m44.14s  Dec =  70d26m44.3s

1) 2.33690 MJY/SR   at RA = 13h35m05.28s  Dec =  70d28m14.7s
2) 2.75347 MJY/SR   at RA = 13h34m50.31s  Dec =  70d28m14.7s
3) 2.39564 MJY/SR   at RA = 13h34m47.32s  Dec =  70d26m44.7s
4) 3.43568 MJY/SR   at RA = 13h35m05.26s  Dec =  70d26m44.7s

1) 2.06673 MJY/SR   at RA = 13h34m32.34s  Dec =  70d28m14.6s
2) 2.63177 MJY/SR   at RA = 13h34m11.39s  Dec =  70d28m14.4s
3) 2.33331 MJY/SR   at RA = 13h34m11.44s  Dec =  70d26m44.3s
4) 3.08293 MJY/SR   at RA = 13h34m29.38s  Dec =  70d26m44.5s

1) 2.28477 MJY/SR   at RA = 13h33m53.42s  Dec =  70d28m14.1s
2) 2.67508 MJY/SR   at RA = 13h33m35.46s  Dec =  70d28m13.6s
3) 2.47373 MJY/SR   at RA = 13h33m35.54s  Dec =  70d26m58.6s
4) 3.29924 MJY/SR   at RA = 13h33m53.49s  Dec =  70d26m59.0s

1) 2.17686 MJY/SR   at RA = 13h33m20.49s  Dec =  70d28m13.2s
2) 2.68529 MJY/SR   at RA = 13h33m02.53s  Dec =  70d28m12.5s
3) 2.25269 MJY/SR   at RA = 13h32m59.66s  Dec =  70d26m57.3s
4) 3.22993 MJY/SR   at RA = 13h33m17.62s  Dec =  70d26m43.0s

1) 2.28139 MJY/SR   at RA = 13h32m41.55s  Dec =  70d28m26.6s
2) 2.81435 MJY/SR   at RA = 13h32m23.58s  Dec =  70d28m25.7s
3) 2.44803 MJY/SR   at RA = 13h32m23.77s  Dec =  70d26m55.7s
4) 3.22702 MJY/SR   at RA = 13h32m41.71s  Dec =  70d26m56.6s

1) 2.34604 MJY/SR   at RA = 13h32m05.62s  Dec =  70d28m24.7s
2) 2.82395 MJY/SR   at RA = 13h31m47.66s  Dec =  70d28m23.6s
3) 2.39820 MJY/SR   at RA = 13h31m47.89s  Dec =  70d26m53.6s
4) 3.44075 MJY/SR   at RA = 13h32m08.82s  Dec =  70d26m54.9s

1) 2.36081 MJY/SR   at RA = 13h38m01.41s  Dec =  70d24m53.7s
2) 2.82495 MJY/SR   at RA = 13h37m43.49s  Dec =  70d24m54.8s
3) 2.52583 MJY/SR   at RA = 13h37m43.29s  Dec =  70d23m24.7s
4) 3.20076 MJY/SR   at RA = 13h38m04.16s  Dec =  70d23m23.4s

1) 2.13037 MJY/SR   at RA = 13h37m28.57s  Dec =  70d24m55.6s
2) 2.63901 MJY/SR   at RA = 13h37m10.65s  Dec =  70d24m56.5s
3) 2.39310 MJY/SR   at RA = 13h37m07.51s  Dec =  70d23m26.5s
4) 3.04069 MJY/SR   at RA = 13h37m25.40s  Dec =  70d23m25.7s

1) 2.23077 MJY/SR   at RA = 13h36m55.73s  Dec =  70d24m57.1s
2) 2.83712 MJY/SR   at RA = 13h36m31.84s  Dec =  70d24m58.0s
3) 2.32071 MJY/SR   at RA = 13h36m34.71s  Dec =  70d23m27.8s
4) 3.10355 MJY/SR   at RA = 13h36m52.60s  Dec =  70d23m27.2s

1) 2.19735 MJY/SR   at RA = 13h36m19.90s  Dec =  70d24m58.4s
2) 2.68626 MJY/SR   at RA = 13h35m59.00s  Dec =  70d24m58.9s
3) 2.25192 MJY/SR   at RA = 13h35m55.95s  Dec =  70d23m43.9s
4) 3.16091 MJY/SR   at RA = 13h36m13.83s  Dec =  70d23m28.5s

1) 2.17199 MJY/SR   at RA = 13h35m41.09s  Dec =  70d25m14.2s
2) 2.81982 MJY/SR   at RA = 13h35m23.17s  Dec =  70d25m14.5s
3) 2.46040 MJY/SR   at RA = 13h35m23.14s  Dec =  70d23m44.4s
4) 3.03393 MJY/SR   at RA = 13h35m38.05s  Dec =  70d23m44.2s

1) 2.21273 MJY/SR   at RA = 13h35m05.25s  Dec =  70d25m14.6s
```

```
2) 2.59213 MJY/SR   at RA = 13h34m47.33s  Dec =  70d25m14.6s
3) 2.46250 MJY/SR   at RA = 13h34m47.35s  Dec =  70d23m44.5s
4) 3.01203 MJY/SR   at RA = 13h35m02.26s  Dec =  70d23m44.5s

1) 2.18122 MJY/SR   at RA = 13h34m29.42s  Dec =  70d24m59.5s
2) 2.58264 MJY/SR   at RA = 13h34m11.50s  Dec =  70d25m14.2s
3) 2.28227 MJY/SR   at RA = 13h34m11.55s  Dec =  70d23m44.2s
4) 3.16533 MJY/SR   at RA = 13h34m29.45s  Dec =  70d23m44.4s

1) 2.12361 MJY/SR   at RA = 13h33m53.58s  Dec =  70d25m13.9s
2) 2.76284 MJY/SR   at RA = 13h33m35.66s  Dec =  70d25m13.5s
3) 2.35620 MJY/SR   at RA = 13h33m35.76s  Dec =  70d23m43.4s
4) 3.11219 MJY/SR   at RA = 13h33m53.66s  Dec =  70d23m43.8s

1) 2.23957 MJY/SR   at RA = 13h33m20.73s  Dec =  70d25m13.0s
2) 2.67507 MJY/SR   at RA = 13h32m56.84s  Dec =  70d25m12.1s
3) 2.40575 MJY/SR   at RA = 13h32m59.97s  Dec =  70d23m42.2s
4) 3.06785 MJY/SR   at RA = 13h33m20.83s  Dec =  70d23m58.0s

1) 2.25315 MJY/SR   at RA = 13h32m41.91s  Dec =  70d25m11.5s
2) 2.94337 MJY/SR   at RA = 13h32m23.99s  Dec =  70d25m10.6s
3) 2.49829 MJY/SR   at RA = 13h32m24.18s  Dec =  70d23m40.5s
4) 3.11701 MJY/SR   at RA = 13h32m42.04s  Dec =  70d23m56.4s

1) 2.26358 MJY/SR   at RA = 13h32m06.04s  Dec =  70d25m24.6s
2) 2.80114 MJY/SR   at RA = 13h31m48.12s  Dec =  70d25m23.5s
3) 2.45566 MJY/SR   at RA = 13h31m48.35s  Dec =  70d23m53.4s
4) 3.04310 MJY/SR   at RA = 13h32m06.25s  Dec =  70d23m54.5s

1) 2.45803 MJY/SR   at RA = 13h38m03.93s  Dec =  70d21m53.4s
2) 3.02110 MJY/SR   at RA = 13h37m43.09s  Dec =  70d21m54.6s
3) 2.38548 MJY/SR   at RA = 13h37m42.88s  Dec =  70d20m24.6s
4) 3.35730 MJY/SR   at RA = 13h38m03.70s  Dec =  70d20m23.3s

1) 2.62015 MJY/SR   at RA = 13h37m25.22s  Dec =  70d21m55.6s
2) 2.97279 MJY/SR   at RA = 13h37m07.35s  Dec =  70d21m56.5s
3) 2.67502 MJY/SR   at RA = 13h37m07.21s  Dec =  70d20m41.4s
4) 3.56157 MJY/SR   at RA = 13h37m28.04s  Dec =  70d20m40.4s

1) 2.27247 MJY/SR   at RA = 13h36m49.48s  Dec =  70d21m57.2s
2) 2.85723 MJY/SR   at RA = 13h36m34.58s  Dec =  70d21m57.8s
3) 2.28069 MJY/SR   at RA = 13h36m34.48s  Dec =  70d20m42.7s
4) 3.16167 MJY/SR   at RA = 13h36m52.34s  Dec =  70d20m42.0s

1) 2.48621 MJY/SR   at RA = 13h36m16.71s  Dec =  70d21m58.3s
2) 3.02203 MJY/SR   at RA = 13h35m55.87s  Dec =  70d21m58.8s
3) 2.34035 MJY/SR   at RA = 13h35m55.80s  Dec =  70d20m43.8s
4) 3.07809 MJY/SR   at RA = 13h36m16.63s  Dec =  70d20m43.3s

1) 2.36622 MJY/SR   at RA = 13h35m40.97s  Dec =  70d21m59.1s
2) 2.79481 MJY/SR   at RA = 13h35m23.10s  Dec =  70d21m59.3s
3) 2.22293 MJY/SR   at RA = 13h35m23.07s  Dec =  70d20m44.3s
4) 3.12078 MJY/SR   at RA = 13h35m40.93s  Dec =  70d20m44.0s

1) 2.39764 MJY/SR   at RA = 13h35m05.23s  Dec =  70d21m59.4s
2) 2.81542 MJY/SR   at RA = 13h34m47.36s  Dec =  70d21m59.4s
3) 2.47019 MJY/SR   at RA = 13h34m44.39s  Dec =  70d20m44.4s
4) 3.19165 MJY/SR   at RA = 13h35m02.25s  Dec =  70d20m44.4s

1) 2.36360 MJY/SR   at RA = 13h34m29.49s  Dec =  70d21m59.3s
2) 2.87318 MJY/SR   at RA = 13h34m08.63s  Dec =  70d22m14.1s
3) 2.44889 MJY/SR   at RA = 13h34m11.66s  Dec =  70d20m44.0s
4) 3.34326 MJY/SR   at RA = 13h34m29.51s  Dec =  70d20m44.3s
```

```
1) 2.38323 MJY/SR   at RA = 13h33m50.75s  Dec =  70d22m13.7s
2) 2.84477 MJY/SR   at RA = 13h33m35.86s  Dec =  70d22m13.3s
3) 2.33119 MJY/SR   at RA = 13h33m35.94s  Dec =  70d20m58.3s
4) 3.21689 MJY/SR   at RA = 13h33m50.82s  Dec =  70d20m58.6s

1) 2.40104 MJY/SR   at RA = 13h33m17.98s  Dec =  70d22m12.8s
2) 2.85986 MJY/SR   at RA = 13h33m00.11s  Dec =  70d22m12.1s
3) 2.31494 MJY/SR   at RA = 13h33m00.23s  Dec =  70d20m57.1s
4) 3.14617 MJY/SR   at RA = 13h33m21.06s  Dec =  70d20m57.8s

1) 2.27542 MJY/SR   at RA = 13h32m42.21s  Dec =  70d22m26.4s
2) 2.81686 MJY/SR   at RA = 13h32m24.33s  Dec =  70d22m25.5s
3) 2.36828 MJY/SR   at RA = 13h32m24.52s  Dec =  70d20m55.4s
4) 2.93646 MJY/SR   at RA = 13h32m42.37s  Dec =  70d20m56.3s

1) 2.24567 MJY/SR   at RA = 13h32m06.46s  Dec =  70d22m24.5s
2) 3.01443 MJY/SR   at RA = 13h31m45.60s  Dec =  70d22m23.2s
3) 2.37120 MJY/SR   at RA = 13h31m48.81s  Dec =  70d20m53.3s
4) 3.03314 MJY/SR   at RA = 13h32m03.69s  Dec =  70d20m54.2s

average:
1) 2.27297 MJY/SR +- 0.12594 MJY/SR       0.85546
2) 2.77039 MJY/SR +- 0.14020 MJY/SR       1.04267
3) 2.38402 MJY/SR +- 0.09553 MJY/SR       0.89726
4) 3.20067 MJY/SR +- 0.14938 MJY/SR       1.20461

mean of all 4: 2.65701 MJY/SR +- 0.42049 MJY/SR

flat-field accuracy of map determined by internal flat-field of array

====================================================================
====================================================================

PGAI33600705.FITS  EBL_1
====================================================================

Maximum 5.39814    at RA = 17h49m11.61s  Dec =  69d39m26.5s
Minimum 4.10519    at RA = 17h50m29.39s  Dec =  69d43m12.3s

Mean    4.66872
st dev  0.286187
                                    Flux units MJY/SR

Flux integral      2.0798e-05   MJY
Inside 4.45474e-06 Steradian area
(841 pixels)

Centroid                              RA = 17h49m54.75s  Dec =  69d42m12.3s


Flux weighted centroid                RA = 17h49m54.11s  Dec =  69d42m10.9s

vertex# 1  at RA = 17h50m55.30s  Dec =  69d40m56.9s

vertex# 2  at RA = 17h49m17.43s  Dec =  69d37m56.6s

vertex# 3  at RA = 17h48m54.09s  Dec =  69d43m26.3s

vertex# 4  at RA = 17h50m32.33s  Dec =  69d46m27.4s


Maximum 5.41121    at RA = 17h49m43.45s  Dec =  69d31m26.7s
Minimum 4.2267    at RA = 17h51m06.57s  Dec =  69d34m56.4s
```

```
Mean    4.74548
st dev  0.291214
                                  Flux units MJY/SR

Flux integral      2.18689e-05   MJY
Inside 4.60836e-06 Steradian area
(870 pixels)

Centroid                            RA = 17h50m28.75s  Dec =  69d33m33.5s


Flux weighted centroid              RA = 17h50m28.08s  Dec =  69d33m32.6s

vertex# 1  at RA = 17h51m29.35s  Dec =  69d32m10.8s

vertex# 2  at RA = 17h49m52.07s  Dec =  69d29m11.6s

vertex# 3  at RA = 17h49m29.03s  Dec =  69d34m56.6s

vertex# 4  at RA = 17h51m03.82s  Dec =  69d37m56.6s


Maximum 5.32713    at RA = 17h50m40.48s  Dec =  69d22m56.2s
Minimum 4.23077    at RA = 17h51m40.41s  Dec =  69d26m25.2s

Mean    4.78182
st dev  0.284643
                                  Flux units MJY/SR

Flux integral      2.05166e-05   MJY
Inside 4.29054e-06 Steradian area
(810 pixels)

Centroid                            RA = 17h51m02.53s  Dec =  69d25m04.9s


Flux weighted centroid              RA = 17h51m01.98s  Dec =  69d25m05.8s

vertex# 1  at RA = 17h52m02.99s  Dec =  69d23m54.2s

vertex# 2  at RA = 17h50m26.25s  Dec =  69d20m56.3s

vertex# 3  at RA = 17h50m03.51s  Dec =  69d26m26.5s

vertex# 4  at RA = 17h51m37.74s  Dec =  69d29m10.4s
================================================================
================================================================

PGAI35100907.FITS  M03
================================================================

Maximum 5.40199    at RA = 13h34m32.42s  Dec =  70d42m21.6s
Minimum 3.00308    at RA = 13h36m30.46s  Dec =  70d36m52.9s

Mean    4.0803
st dev  0.508927
                                  Flux units MJY/SR

Flux integral      0.000198885   MJY
Inside 4.87426e-05 Steradian area
(9202 pixels)

Centroid                            RA = 13h36m13.01s  Dec =  70d34m47.3s
```

```
Flux weighted centroid                RA = 13h36m11.75s  Dec =  70d34m50.3s

vertex# 1  at RA = 13h38m02.03s  Dec =  70d49m06.5s

vertex# 2  at RA = 13h39m05.66s  Dec =  70d25m47.3s

vertex# 3  at RA = 13h34m25.29s  Dec =  70d20m20.2s

vertex# 4  at RA = 13h33m19.51s  Dec =  70d43m48.2s

internal systematic flat-field structures of array (regular pattern generated by
the four pixels; note: pixel numbering is arbitrary and needs not to comply
with official numbering scheme):

1) 3.38858 MJY/SR   at RA = 13h38m47.96s  Dec =  70d27m33.4s
2) 4.27660 MJY/SR   at RA = 13h38m29.98s  Dec =  70d27m19.3s
3) 3.85804 MJY/SR   at RA = 13h38m32.80s  Dec =  70d25m49.1s
4) 4.62089 MJY/SR   at RA = 13h38m56.77s  Dec =  70d26m17.8s

1) 3.63042 MJY/SR   at RA = 13h38m39.38s  Dec =  70d30m49.0s
2) 4.41372 MJY/SR   at RA = 13h38m24.32s  Dec =  70d30m19.7s
3) 4.04916 MJY/SR   at RA = 13h38m27.16s  Dec =  70d28m49.5s
4) 4.76225 MJY/SR   at RA = 13h38m45.19s  Dec =  70d29m18.6s

1) 3.26313 MJY/SR   at RA = 13h38m33.70s  Dec =  70d33m34.4s
2) 4.12733 MJY/SR   at RA = 13h38m15.63s  Dec =  70d33m20.2s
3) 3.86879 MJY/SR   at RA = 13h38m18.48s  Dec =  70d31m50.0s
4) 4.00743 MJY/SR   at RA = 13h38m36.53s  Dec =  70d32m04.2s

1) 3.34341 MJY/SR   at RA = 13h38m28.02s  Dec =  70d36m34.8s
2) 4.09554 MJY/SR   at RA = 13h38m06.90s  Dec =  70d36m20.7s
3) 3.88249 MJY/SR   at RA = 13h38m12.78s  Dec =  70d34m50.4s
4) 4.91057 MJY/SR   at RA = 13h38m33.87s  Dec =  70d35m04.5s

1) 3.45443 MJY/SR   at RA = 13h38m19.29s  Dec =  70d39m35.4s
2) 4.46319 MJY/SR   at RA = 13h38m01.12s  Dec =  70d39m06.1s
3) 3.78234 MJY/SR   at RA = 13h38m04.02s  Dec =  70d37m50.9s
4) 4.45035 MJY/SR   at RA = 13h38m22.15s  Dec =  70d38m05.2s

1) 3.12900 MJY/SR   at RA = 13h38m10.50s  Dec =  70d42m20.9s
2) 4.21656 MJY/SR   at RA = 13h37m55.33s  Dec =  70d42m06.4s
3) 3.92784 MJY/SR   at RA = 13h37m55.20s  Dec =  70d40m36.4s
4) 4.62444 MJY/SR   at RA = 13h38m13.37s  Dec =  70d40m50.7s

1) 3.32363 MJY/SR   at RA = 13h38m04.74s  Dec =  70d45m36.3s
2) 4.38242 MJY/SR   at RA = 13h37m46.48s  Dec =  70d45m06.9s
3) 3.93882 MJY/SR   at RA = 13h37m46.36s  Dec =  70d43m36.8s
4) 4.80515 MJY/SR   at RA = 13h38m07.61s  Dec =  70d43m51.1s

1) 3.39236 MJY/SR   at RA = 13h37m55.85s  Dec =  70d48m06.7s
2) 4.72010 MJY/SR   at RA = 13h37m37.57s  Dec =  70d47m52.3s
3) 3.35685 MJY/SR   at RA = 13h37m40.52s  Dec =  70d46m37.1s
4) 4.56560 MJY/SR   at RA = 13h37m55.72s  Dec =  70d46m36.6s

1) 3.38126 MJY/SR   at RA = 13h37m16.26s  Dec =  70d47m37.8s
2) 4.78383 MJY/SR   at RA = 13h37m04.07s  Dec =  70d47m08.0s
3) 4.05688 MJY/SR   at RA = 13h37m07.05s  Dec =  70d45m52.9s
4) 4.84361 MJY/SR   at RA = 13h37m22.25s  Dec =  70d46m07.6s

1) 3.20287 MJY/SR   at RA = 13h37m28.24s  Dec =  70d44m37.4s
2) 4.53165 MJY/SR   at RA = 13h37m10.02s  Dec =  70d44m22.8s
3) 3.51098 MJY/SR   at RA = 13h37m16.00s  Dec =  70d42m52.6s
4) 4.64727 MJY/SR   at RA = 13h37m34.22s  Dec =  70d43m22.2s
```

```
1) 3.30087 MJY/SR   at RA = 13h37m34.10s  Dec =  70d41m37.1s
2) 4.33374 MJY/SR   at RA = 13h37m18.95s  Dec =  70d41m22.5s
3) 3.85110 MJY/SR   at RA = 13h37m18.87s  Dec =  70d39m52.4s
4) 4.08406 MJY/SR   at RA = 13h37m37.04s  Dec =  70d40m21.9s

1) 3.25294 MJY/SR   at RA = 13h37m42.97s  Dec =  70d38m51.7s
2) 4.21618 MJY/SR   at RA = 13h37m24.84s  Dec =  70d38m37.2s
3) 3.98499 MJY/SR   at RA = 13h37m27.76s  Dec =  70d37m07.0s
4) 4.77196 MJY/SR   at RA = 13h37m45.88s  Dec =  70d37m21.5s

1) 3.30299 MJY/SR   at RA = 13h37m51.79s  Dec =  70d35m51.3s
2) 4.19497 MJY/SR   at RA = 13h37m33.69s  Dec =  70d35m36.8s
3) 3.79888 MJY/SR   at RA = 13h37m36.60s  Dec =  70d34m06.6s
4) 4.78218 MJY/SR   at RA = 13h37m54.67s  Dec =  70d34m21.1s

1) 3.37419 MJY/SR   at RA = 13h38m00.56s  Dec =  70d32m50.8s
2) 4.11676 MJY/SR   at RA = 13h37m42.51s  Dec =  70d32m36.4s
3) 3.77048 MJY/SR   at RA = 13h37m45.42s  Dec =  70d31m21.2s
4) 5.02065 MJY/SR   at RA = 13h38m03.42s  Dec =  70d31m20.6s

1) 3.51943 MJY/SR   at RA = 13h38m06.31s  Dec =  70d30m05.4s
2) 4.24430 MJY/SR   at RA = 13h37m48.30s  Dec =  70d29m51.1s
3) 4.10215 MJY/SR   at RA = 13h37m54.19s  Dec =  70d28m35.8s
4) 4.82761 MJY/SR   at RA = 13h38m09.19s  Dec =  70d28m50.3s

1) 3.48882 MJY/SR   at RA = 13h38m15.00s  Dec =  70d27m04.9s
2) 4.12584 MJY/SR   at RA = 13h37m57.01s  Dec =  70d26m35.6s
3) 3.94444 MJY/SR   at RA = 13h37m59.91s  Dec =  70d25m35.5s
4) 4.38219 MJY/SR   at RA = 13h38m14.85s  Dec =  70d25m34.9s

1) 3.30033 MJY/SR   at RA = 13h37m39.06s  Dec =  70d26m21.2s
2) 4.10208 MJY/SR   at RA = 13h37m21.11s  Dec =  70d26m06.7s
3) 3.78112 MJY/SR   at RA = 13h37m24.01s  Dec =  70d24m36.5s
4) 4.37196 MJY/SR   at RA = 13h37m38.95s  Dec =  70d24m51.1s

1) 3.27660 MJY/SR   at RA = 13h37m33.29s  Dec =  70d29m36.5s
2) 4.38497 MJY/SR   at RA = 13h37m15.28s  Dec =  70d29m06.9s
3) 3.92018 MJY/SR   at RA = 13h37m18.20s  Dec =  70d27m36.8s
4) 4.81852 MJY/SR   at RA = 13h37m36.17s  Dec =  70d27m51.4s

1) 3.13378 MJY/SR   at RA = 13h37m24.47s  Dec =  70d32m21.9s
2) 4.30622 MJY/SR   at RA = 13h37m06.43s  Dec =  70d32m07.3s
3) 3.78067 MJY/SR   at RA = 13h37m09.35s  Dec =  70d30m22.1s
4) 4.09244 MJY/SR   at RA = 13h37m30.38s  Dec =  70d30m51.7s

1) 3.17108 MJY/SR   at RA = 13h37m18.61s  Dec =  70d35m07.2s
2) 4.10853 MJY/SR   at RA = 13h36m57.52s  Dec =  70d34m52.5s
3) 3.88816 MJY/SR   at RA = 13h37m03.49s  Dec =  70d33m37.4s
4) 4.65959 MJY/SR   at RA = 13h37m21.53s  Dec =  70d33m37.0s

1) 3.12744 MJY/SR   at RA = 13h37m09.72s  Dec =  70d38m07.5s
2) 4.14527 MJY/SR   at RA = 13h36m48.58s  Dec =  70d37m52.8s
3) 3.85865 MJY/SR   at RA = 13h36m51.55s  Dec =  70d36m22.7s
4) 4.53107 MJY/SR   at RA = 13h37m12.67s  Dec =  70d36m52.4s

1) 3.46754 MJY/SR   at RA = 13h37m03.81s  Dec =  70d41m07.7s
2) 4.50395 MJY/SR   at RA = 13h36m42.62s  Dec =  70d40m38.0s
3) 3.83535 MJY/SR   at RA = 13h36m45.60s  Dec =  70d39m07.9s
4) 4.68887 MJY/SR   at RA = 13h37m06.77s  Dec =  70d39m37.6s

1) 3.44254 MJY/SR   at RA = 13h36m54.83s  Dec =  70d43m53.0s
2) 4.69296 MJY/SR   at RA = 13h36m33.59s  Dec =  70d43m38.2s
3) 3.74791 MJY/SR   at RA = 13h36m36.60s  Dec =  70d42m08.1s
```

```
4) 4.53008 MJY/SR   at RA = 13h36m57.81s  Dec =  70d42m37.9s

1) 3.23348 MJY/SR   at RA = 13h36m48.85s  Dec =  70d46m53.2s
2) 4.53351 MJY/SR   at RA = 13h36m27.57s  Dec =  70d46m38.4s
3) 4.06763 MJY/SR   at RA = 13h36m30.59s  Dec =  70d45m08.3s
4) 4.92035 MJY/SR   at RA = 13h36m48.81s  Dec =  70d45m23.2s

1) 3.22096 MJY/SR   at RA = 13h36m09.33s  Dec =  70d46m23.4s
2) 4.76654 MJY/SR   at RA = 13h35m51.10s  Dec =  70d45m53.3s
3) 3.92521 MJY/SR   at RA = 13h35m54.16s  Dec =  70d44m38.3s
4) 4.84655 MJY/SR   at RA = 13h36m12.37s  Dec =  70d44m53.4s

1) 3.57769 MJY/SR   at RA = 13h36m15.40s  Dec =  70d43m08.3s
2) 4.55918 MJY/SR   at RA = 13h36m00.25s  Dec =  70d43m08.3s
3) 3.86736 MJY/SR   at RA = 13h36m03.29s  Dec =  70d41m53.2s
4) 4.82737 MJY/SR   at RA = 13h36m21.45s  Dec =  70d41m53.2s

1) 3.47814 MJY/SR   at RA = 13h36m24.47s  Dec =  70d40m38.1s
2) 4.76620 MJY/SR   at RA = 13h36m06.32s  Dec =  70d40m08.1s
3) 3.87508 MJY/SR   at RA = 13h36m12.37s  Dec =  70d38m38.1s
4) 4.61030 MJY/SR   at RA = 13h36m27.47s  Dec =  70d38m53.0s

1) 3.00308 MJY/SR   at RA = 13h36m30.47s  Dec =  70d37m38.0s
2) 4.19048 MJY/SR   at RA = 13h36m12.37s  Dec =  70d37m23.0s
3) 3.80918 MJY/SR   at RA = 13h36m18.40s  Dec =  70d35m52.9s
4) 4.61453 MJY/SR   at RA = 13h36m33.46s  Dec =  70d35m52.9s

1) 3.27284 MJY/SR   at RA = 13h36m39.46s  Dec =  70d34m37.8s
2) 4.23733 MJY/SR   at RA = 13h36m21.40s  Dec =  70d34m22.9s
3) 3.98934 MJY/SR   at RA = 13h36m27.40s  Dec =  70d33m07.8s
4) 4.63994 MJY/SR   at RA = 13h36m42.43s  Dec =  70d33m22.7s

1) 3.36867 MJY/SR   at RA = 13h36m48.40s  Dec =  70d31m37.5s
2) 4.14623 MJY/SR   at RA = 13h36m30.38s  Dec =  70d31m22.7s
3) 3.76844 MJY/SR   at RA = 13h36m36.35s  Dec =  70d29m52.6s
4) 5.14255 MJY/SR   at RA = 13h36m51.35s  Dec =  70d30m07.4s

1) 3.34879 MJY/SR   at RA = 13h36m54.30s  Dec =  70d28m52.3s
2) 4.21065 MJY/SR   at RA = 13h36m39.32s  Dec =  70d28m22.5s
3) 3.80824 MJY/SR   at RA = 13h36m42.27s  Dec =  70d26m52.4s
4) 4.85027 MJY/SR   at RA = 13h36m57.24s  Dec =  70d27m22.2s

1) 3.24927 MJY/SR   at RA = 13h37m03.17s  Dec =  70d25m52.0s
2) 4.01908 MJY/SR   at RA = 13h36m45.23s  Dec =  70d25m37.3s
3) 3.87565 MJY/SR   at RA = 13h36m48.17s  Dec =  70d24m07.2s
4) 4.45006 MJY/SR   at RA = 13h37m06.09s  Dec =  70d24m21.9s

1) 3.39052 MJY/SR   at RA = 13h36m27.30s  Dec =  70d25m07.4s
2) 4.15650 MJY/SR   at RA = 13h36m12.37s  Dec =  70d24m52.4s
3) 3.80521 MJY/SR   at RA = 13h36m15.35s  Dec =  70d23m22.3s
4) 4.90311 MJY/SR   at RA = 13h36m33.24s  Dec =  70d23m22.3s

1) 3.43211 MJY/SR   at RA = 13h36m21.35s  Dec =  70d28m07.6s
2) 4.16853 MJY/SR   at RA = 13h36m00.40s  Dec =  70d27m37.5s
3) 3.89720 MJY/SR   at RA = 13h36m06.39s  Dec =  70d26m07.5s
4) 4.90970 MJY/SR   at RA = 13h36m24.33s  Dec =  70d26m22.5s

1) 3.05362 MJY/SR   at RA = 13h36m12.37s  Dec =  70d30m52.7s
2) 4.01523 MJY/SR   at RA = 13h35m57.37s  Dec =  70d30m52.7s
3) 3.74521 MJY/SR   at RA = 13h36m00.39s  Dec =  70d29m07.6s
4) 4.81302 MJY/SR   at RA = 13h36m15.37s  Dec =  70d29m37.6s

1) 3.25153 MJY/SR   at RA = 13h36m06.35s  Dec =  70d33m52.8s
2) 4.30165 MJY/SR   at RA = 13h35m48.31s  Dec =  70d33m37.7s
```

```
3) 3.90797 MJY/SR   at RA = 13h35m51.35s  Dec =  70d31m52.7s
4) 4.57167 MJY/SR   at RA = 13h36m09.37s  Dec =  70d32m07.8s

1) 3.27092 MJY/SR   at RA = 13h35m57.30s  Dec =  70d36m37.9s
2) 3.92111 MJY/SR   at RA = 13h35m39.22s  Dec =  70d36m22.8s
3) 3.92143 MJY/SR   at RA = 13h35m42.27s  Dec =  70d34m52.7s
4) 4.74640 MJY/SR   at RA = 13h36m03.34s  Dec =  70d35m07.9s

1) 3.49768 MJY/SR   at RA = 13h35m48.18s  Dec =  70d40m08.0s
2) 4.58759 MJY/SR   at RA = 13h35m33.09s  Dec =  70d39m22.8s
3) 3.94870 MJY/SR   at RA = 13h35m36.16s  Dec =  70d37m52.8s
4) 4.83939 MJY/SR   at RA = 13h35m51.24s  Dec =  70d38m08.0s

1) 3.14630 MJY/SR   at RA = 13h35m42.07s  Dec =  70d42m38.1s
2) 4.29740 MJY/SR   at RA = 13h35m26.94s  Dec =  70d42m22.9s
3) 3.92642 MJY/SR   at RA = 13h35m26.99s  Dec =  70d40m52.8s
4) 4.81058 MJY/SR   at RA = 13h35m42.11s  Dec =  70d41m08.0s

1) 3.15617 MJY/SR   at RA = 13h35m32.89s  Dec =  70d45m38.1s
2) 4.58273 MJY/SR   at RA = 13h35m17.72s  Dec =  70d45m07.9s
3) 3.76353 MJY/SR   at RA = 13h35m17.79s  Dec =  70d43m37.8s
4) 4.95588 MJY/SR   at RA = 13h35m39.00s  Dec =  70d44m08.1s

average:
1) 3.31549 MJY/SR +- 0.14272 MJY/SR       0.81963
2) 4.32367 MJY/SR +- 0.23010 MJY/SR       1.06887
3) 3.85995 MJY/SR +- 0.13528 MJY/SR       0.95423
4) 4.68126 MJY/SR +- 0.24817 MJY/SR       1.15727

mean of all 4: 4.04509 MJY/SR +- 0.59130 MJY/SR

flat-field accuracy of map determined by internal flat-field of array

====================================================================
====================================================================

PGAI16701206.FITS  Helix
====================================================================

Maximum 9.92714    at RA = 22h29m59.64s  Dec = -20d41m26.0s
Minimum 6.79387    at RA = 22h30m10.33s  Dec = -20d39m25.8s

Mean    9.19566
st dev  0.397677
                                  Flux units MJY/SR

Flux integral      1.56843e-05   MJY
Inside 1.70562e-06 Steradian area
(322 pixels)

Centroid                            RA = 22h30m02.13s  Dec = -20d39m06.9s


Flux weighted centroid              RA = 22h30m02.14s  Dec = -20d39m07.8s

vertex# 1  at RA = 22h30m14.62s  Dec = -20d41m10.8s

vertex# 2  at RA = 22h30m01.79s  Dec = -20d42m41.0s

vertex# 3  at RA = 22h29m50.01s  Dec = -20d36m55.9s

vertex# 4  at RA = 22h30m02.84s  Dec = -20d35m40.7s
```

```
Maximum 14.9668    at RA = 22h29m12.52s  Dec = -20d59m56.9s
Minimum 8.56518    at RA = 22h29m09.31s  Dec = -20d58m56.8s

Mean    11.435
st dev  2.49503
                                  Flux units MJY/SR

Flux integral      1.6657e-05   MJY
Inside 1.45666e-06 Steradian area
(275 pixels)

Centroid                            RA = 22h29m14.51s  Dec = -21d01m08.3s


Flux weighted centroid              RA = 22h29m14.83s  Dec = -21d01m15.4s

vertex# 1  at RA = 22h29m25.38s  Dec = -21d03m12.1s

vertex# 2  at RA = 22h29m13.58s  Dec = -21d04m27.1s

vertex# 3  at RA = 22h29m03.95s  Dec = -20d58m56.7s

vertex# 4  at RA = 22h29m14.67s  Dec = -20d57m41.8s

=====================================================================
=====================================================================

PGAI52700412.FITS  NGC5905N
=====================================================================

Maximum 3.33578    at RA = 15h15m18.05s  Dec =  56d35m43.5s
Minimum 2.54593    at RA = 15h15m10.82s  Dec =  56d27m13.1s

Mean    2.96958
st dev  0.11542
                                  Flux units MJY/SR

Flux integral      1.34489e-05   MJY
Inside 4.5289e-06 Steradian area
(855 pixels)

Centroid                            RA = 15h15m09.75s  Dec =  56d31m26.4s


Flux weighted centroid              RA = 15h15m09.84s  Dec =  56d31m28.7s

vertex# 1  at RA = 15h15m45.26s  Dec =  56d30m28.1s

vertex# 2  at RA = 15h15m05.39s  Dec =  56d26m13.0s

vertex# 3  at RA = 15h14m32.68s  Dec =  56d32m12.7s

vertex# 4  at RA = 15h15m16.23s  Dec =  56d36m43.6s

=====================================================================
=====================================================================

PGAI85001037.FITS  U Men
=====================================================================

Maximum 8.33505    at RA = 4h07m36.41s  Dec = -81d48m01.7s
Minimum 6.6553    at RA = 4h05m26.85s  Dec = -81d54m28.4s

Mean    7.37764
```

```
st dev  0.229365
                                    Flux units MJY/SR

Flux integral      6.88573e-05   MJY
Inside 9.33325e-06 Steradian area
(1762 pixels)

Centroid                              RA = 4h06m12.87s  Dec = -81d51m03.3s


Flux weighted centroid                RA = 4h06m13.31s  Dec = -81d51m04.0s

vertex# 1  at RA = 4h07m51.71s  Dec = -81d42m01.7s

vertex# 2  at RA = 4h07m26.19s  Dec = -82d00m17.2s

vertex# 3  at RA = 4h04m33.54s  Dec = -82d00m11.6s

vertex# 4  at RA = 4h04m58.27s  Dec = -81d42m11.6s

=====================================================================
=====================================================================

PGAI78200101.FITS  Draco main
=====================================================================

Maximum 4.6299    at RA = 16h50m20.61s  Dec =  60d28m42.5s
Minimum 1.49732    at RA = 16h50m13.92s  Dec =  60d21m12.6s

Mean    2.29145
st dev  0.511325
                                    Flux units MJY/SR

Flux integral      5.72173e-05   MJY
Inside 2.49699e-05 Steradian area
(4714 pixels)

Centroid                              RA = 16h50m09.70s  Dec =  60d20m53.9s


Flux weighted centroid                RA = 16h50m06.89s  Dec =  60d21m15.0s

vertex# 1  at RA = 16h51m42.53s  Dec =  60d17m49.1s

vertex# 2  at RA = 16h49m46.82s  Dec =  60d08m58.8s

vertex# 3  at RA = 16h48m34.85s  Dec =  60d23m32.7s

vertex# 4  at RA = 16h50m35.22s  Dec =  60d32m56.5s

internal systematic flat-field structures of array (regular pattern generated by
the four pixels; note: pixel numbering is arbitrary and needs not to comply
with official numbering scheme):

1) 2.90909 MJY/SR   at RA = 16h50m30.88s  Dec =  60d29m56.7s
2) 4.62990 MJY/SR   at RA = 16h50m20.66s  Dec =  60d29m12.5s
3) 2.39110 MJY/SR   at RA = 16h50m24.61s  Dec =  60d27m57.1s
4) 2.71339 MJY/SR   at RA = 16h50m34.83s  Dec =  60d28m41.4s

1) 2.92314 MJY/SR   at RA = 16h50m08.41s  Dec =  60d28m28.4s
2) 3.49413 MJY/SR   at RA = 16h49m58.20s  Dec =  60d27m44.0s
3) 2.28008 MJY/SR   at RA = 16h50m06.21s  Dec =  60d26m13.4s
4) 2.26975 MJY/SR   at RA = 16h50m14.38s  Dec =  60d26m57.9s
```

```
1) 2.70262 MJY/SR   at RA = 16h49m50.03s  Dec =  60d26m59.5s
2) 3.15129 MJY/SR   at RA = 16h49m39.83s  Dec =  60d26m00.1s
3) 1.82479 MJY/SR   at RA = 16h49m45.84s  Dec =  60d24m59.7s
4) 1.90655 MJY/SR   at RA = 16h49m58.06s  Dec =  60d25m43.9s

1) 2.55064 MJY/SR   at RA = 16h49m29.64s  Dec =  60d25m15.6s
2) 3.45713 MJY/SR   at RA = 16h49m17.44s  Dec =  60d24m31.2s
3) 2.04883 MJY/SR   at RA = 16h49m23.45s  Dec =  60d23m15.8s
4) 2.09406 MJY/SR   at RA = 16h49m35.66s  Dec =  60d24m15.2s

1) 2.54384 MJY/SR   at RA = 16h49m07.27s  Dec =  60d23m46.6s
2) 2.97185 MJY/SR   at RA = 16h48m55.09s  Dec =  60d23m02.0s
3) 2.28228 MJY/SR   at RA = 16h49m01.11s  Dec =  60d21m46.7s
4) 2.21934 MJY/SR   at RA = 16h49m09.24s  Dec =  60d22m31.4s

1) 2.96601 MJY/SR   at RA = 16h50m40.81s  Dec =  60d27m25.8s
2) 3.19002 MJY/SR   at RA = 16h50m30.57s  Dec =  60d26m26.6s
3) 1.82979 MJY/SR   at RA = 16h50m36.56s  Dec =  60d25m26.1s
4) 1.82800 MJY/SR   at RA = 16h50m46.77s  Dec =  60d26m10.2s

1) 2.23620 MJY/SR   at RA = 16h50m18.34s  Dec =  60d25m42.5s
2) 2.53184 MJY/SR   at RA = 16h50m08.12s  Dec =  60d24m43.2s
3) 1.95895 MJY/SR   at RA = 16h50m16.15s  Dec =  60d23m42.6s
4) 1.82429 MJY/SR   at RA = 16h50m24.31s  Dec =  60d24m27.0s

1) 2.14884 MJY/SR   at RA = 16h50m00.00s  Dec =  60d24m28.8s
2) 2.46971 MJY/SR   at RA = 16h49m49.81s  Dec =  60d23m44.4s
3) 1.95583 MJY/SR   at RA = 16h49m57.85s  Dec =  60d22m43.8s
4) 2.02741 MJY/SR   at RA = 16h50m03.94s  Dec =  60d22m58.4s

1) 2.12107 MJY/SR   at RA = 16h49m41.65s  Dec =  60d22m44.8s
2) 2.85508 MJY/SR   at RA = 16h49m29.47s  Dec =  60d22m15.5s
3) 2.22805 MJY/SR   at RA = 16h49m35.48s  Dec =  60d21m15.1s
4) 1.84999 MJY/SR   at RA = 16h49m47.66s  Dec =  60d21m44.4s

1) 2.54337 MJY/SR   at RA = 16h49m21.34s  Dec =  60d21m30.8s
2) 3.04624 MJY/SR   at RA = 16h49m11.18s  Dec =  60d20m46.3s
3) 2.06479 MJY/SR   at RA = 16h49m17.19s  Dec =  60d19m30.9s
4) 2.07697 MJY/SR   at RA = 16h49m25.31s  Dec =  60d20m15.6s

1) 1.69592 MJY/SR   at RA = 16h50m54.76s  Dec =  60d24m54.4s
2) 2.03201 MJY/SR   at RA = 16h50m42.50s  Dec =  60d23m55.5s
3) 1.58109 MJY/SR   at RA = 16h50m52.53s  Dec =  60d22m54.5s
4) 1.54516 MJY/SR   at RA = 16h51m00.69s  Dec =  60d23m23.8s

1) 1.63394 MJY/SR   at RA = 16h50m34.31s  Dec =  60d22m56.1s
2) 2.06896 MJY/SR   at RA = 16h50m24.15s  Dec =  60d22m26.9s
3) 1.96718 MJY/SR   at RA = 16h50m30.13s  Dec =  60d21m26.4s
4) 1.62069 MJY/SR   at RA = 16h50m40.29s  Dec =  60d21m55.6s

1) 1.49732 MJY/SR   at RA = 16h50m13.96s  Dec =  60d21m42.6s
2) 2.11451 MJY/SR   at RA = 16h50m01.77s  Dec =  60d20m58.5s
3) 1.91844 MJY/SR   at RA = 16h50m09.78s  Dec =  60d19m57.9s
4) 1.99763 MJY/SR   at RA = 16h50m19.93s  Dec =  60d20m27.1s

1) 1.65806 MJY/SR   at RA = 16h49m53.62s  Dec =  60d20m14.0s
2) 2.45883 MJY/SR   at RA = 16h49m39.42s  Dec =  60d19m29.8s
3) 2.02487 MJY/SR   at RA = 16h49m47.44s  Dec =  60d18m29.3s
4) 1.56433 MJY/SR   at RA = 16h49m59.62s  Dec =  60d19m13.5s

1) 1.75837 MJY/SR   at RA = 16h49m31.28s  Dec =  60d18m30.2s
2) 2.47419 MJY/SR   at RA = 16h49m21.15s  Dec =  60d18m00.7s
3) 2.23526 MJY/SR   at RA = 16h49m29.16s  Dec =  60d16m45.2s
4) 2.36175 MJY/SR   at RA = 16h49m37.28s  Dec =  60d17m29.8s
```

```
1) 1.77478 MJY/SR   at RA = 16h51m06.63s  Dec =  60d22m08.2s
2) 2.93567 MJY/SR   at RA = 16h50m56.43s  Dec =  60d21m24.1s
3) 2.11493 MJY/SR   at RA = 16h51m00.35s  Dec =  60d20m08.7s
4) 1.97095 MJY/SR   at RA = 16h51m10.54s  Dec =  60d20m52.7s

1) 1.61570 MJY/SR   at RA = 16h50m46.24s  Dec =  60d20m40.0s
2) 2.89847 MJY/SR   at RA = 16h50m34.04s  Dec =  60d19m56.0s
3) 1.94600 MJY/SR   at RA = 16h50m42.01s  Dec =  60d18m40.3s
4) 1.95511 MJY/SR   at RA = 16h50m52.19s  Dec =  60d19m24.4s

1) 1.86411 MJY/SR   at RA = 16h50m25.89s  Dec =  60d19m11.6s
2) 2.92157 MJY/SR   at RA = 16h50m13.71s  Dec =  60d18m27.5s
3) 2.03533 MJY/SR   at RA = 16h50m21.68s  Dec =  60d17m11.8s
4) 2.06207 MJY/SR   at RA = 16h50m29.82s  Dec =  60d17m56.2s

1) 1.95847 MJY/SR   at RA = 16h50m03.55s  Dec =  60d17m43.2s
2) 3.07137 MJY/SR   at RA = 16h49m55.40s  Dec =  60d16m43.7s
3) 1.88571 MJY/SR   at RA = 16h50m01.38s  Dec =  60d15m43.2s
4) 2.17404 MJY/SR   at RA = 16h50m09.53s  Dec =  60d16m42.7s

1) 1.89626 MJY/SR   at RA = 16h49m43.24s  Dec =  60d15m59.4s
2) 3.15863 MJY/SR   at RA = 16h49m31.09s  Dec =  60d15m15.0s
3) 2.25343 MJY/SR   at RA = 16h49m41.10s  Dec =  60d13m59.4s
4) 2.07491 MJY/SR   at RA = 16h49m51.25s  Dec =  60d14m58.9s

1) 1.69691 MJY/SR   at RA = 16h51m16.50s  Dec =  60d19m52.1s
2) 2.80783 MJY/SR   at RA = 16h51m06.28s  Dec =  60d18m53.0s
3) 1.73176 MJY/SR   at RA = 16h51m12.21s  Dec =  60d17m37.4s
4) 1.56504 MJY/SR   at RA = 16h51m22.39s  Dec =  60d18m21.4s

1) 1.83902 MJY/SR   at RA = 16h50m58.12s  Dec =  60d18m08.8s
2) 2.52010 MJY/SR   at RA = 16h50m47.95s  Dec =  60d17m24.7s
3) 2.13074 MJY/SR   at RA = 16h50m55.90s  Dec =  60d16m08.9s
4) 1.75777 MJY/SR   at RA = 16h51m04.05s  Dec =  60d16m53.2s

1) 1.66424 MJY/SR   at RA = 16h50m35.75s  Dec =  60d16m25.7s
2) 2.10209 MJY/SR   at RA = 16h50m25.61s  Dec =  60d15m56.5s
3) 1.82701 MJY/SR   at RA = 16h50m31.53s  Dec =  60d14m25.9s
4) 1.79650 MJY/SR   at RA = 16h50m43.70s  Dec =  60d15m09.9s

1) 1.90588 MJY/SR   at RA = 16h50m17.48s  Dec =  60d15m12.1s
2) 2.85158 MJY/SR   at RA = 16h50m07.34s  Dec =  60d14m27.8s
3) 1.86264 MJY/SR   at RA = 16h50m13.27s  Dec =  60d12m57.3s
4) 1.84461 MJY/SR   at RA = 16h50m23.41s  Dec =  60d13m41.5s

1) 1.89644 MJY/SR   at RA = 16h49m57.19s  Dec =  60d13m28.4s
2) 2.51631 MJY/SR   at RA = 16h49m47.06s  Dec =  60d12m44.0s
3) 2.13381 MJY/SR   at RA = 16h49m55.03s  Dec =  60d11m28.4s
4) 1.89280 MJY/SR   at RA = 16h50m03.12s  Dec =  60d11m57.9s

average:
1) 2.08001 MJY/SR +- 0.45945 MJY/SR       0.93595
2) 2.82917 MJY/SR +- 0.55906 MJY/SR       1.27305
3) 2.02051 MJY/SR +- 0.19494 MJY/SR       0.90918
4) 1.95972 MJY/SR +- 0.26890 MJY/SR       0.88182

mean of all 4: 2.22235 MJY/SR +- 0.40752 MJY/SR

flat-field accuracy of map determined by internal flat-field of array
=====================================================================
=====================================================================

PGAI36803005.FITS  NPC_2
```

```
=====================================================================

Maximum 18.211    at RA = 24h03m37.73s  Dec =  87d00m52.4s
Minimum 11.7994    at RA = 23h56m16.97s  Dec =  86d52m15.5s

Mean    14.7797
st dev  1.47976
                                    Flux units MJY/SR

Flux integral      0.000104671   MJY
Inside 7.08204e-06 Steradian area
(1337 pixels)

Centroid                              RA = 23h59m33.14s  Dec =  86d58m21.7s


Flux weighted centroid                RA = 23h59m36.62s  Dec =  86d58m28.3s

vertex# 1  at RA = 24h07m39.07s  Dec =  87d02m04.9s

vertex# 2  at RA = 23h58m01.07s  Dec =  86d50m55.3s

vertex# 3  at RA = 23h51m47.24s  Dec =  86d54m25.6s

vertex# 4  at RA = 24h01m13.06s  Dec =  87d05m47.7s

=====================================================================
=====================================================================

PGAI39602313.FITS  North_1
=====================================================================

Maximum 35.5631    at RA = 20h32m37.97s  Dec =  65d07m18.8s
Minimum 23.7119    at RA = 20h33m25.64s  Dec =  65d11m03.7s

Mean    29.1148
st dev  2.77995
                                    Flux units MJY/SR

Flux integral      0.000230096   MJY
Inside 7.90307e-06 Steradian area
(1492 pixels)

Centroid                              RA = 20h33m01.76s  Dec =  65d07m41.3s


Flux weighted centroid                RA = 20h33m01.48s  Dec =  65d07m40.4s

vertex# 1  at RA = 20h34m06.06s  Dec =  65d08m47.6s

vertex# 2  at RA = 20h33m04.06s  Dec =  65d00m48.5s

vertex# 3  at RA = 20h31m57.55s  Dec =  65d06m33.3s

vertex# 4  at RA = 20h32m59.44s  Dec =  65d14m34.1s

=====================================================================
=====================================================================

PGAI26101401.FITS  CHA1C
=====================================================================

Maximum 43.5023    at RA = 11h03m34.60s  Dec = -77d22m52.9s
Minimum 31.4702    at RA = 11h00m57.41s  Dec = -77d25m25.7s
```

```
Mean    37.5713
st dev  2.62688
                                  Flux units MJY/SR

Flux integral      0.000245384   MJY
Inside 6.53115e-06 Steradian area
(1233 pixels)

Centroid                            RA = 11h02m24.63s  Dec = -77d21m28.1s


Flux weighted centroid              RA = 11h02m27.21s  Dec = -77d21m27.0s

vertex# 1  at RA = 11h04m30.03s  Dec = -77d21m10.8s

vertex# 2  at RA = 11h01m14.88s  Dec = -77d27m12.5s

vertex# 3  at RA = 11h00m18.16s  Dec = -77d21m51.4s

vertex# 4  at RA = 11h03m32.50s  Dec = -77d15m37.4s

=====================================================================
=====================================================================

PGAI33401133.FITS  RCRA
=====================================================================

Maximum 54.2935    at RA = 19h02m30.81s  Dec = -36d53m01.9s
Minimum 30.8988    at RA = 19h03m07.05s  Dec = -36d48m31.1s

Mean    40.0326
st dev  4.5769
                                  Flux units MJY/SR

Flux integral      0.000114508   MJY
Inside 2.86036e-06 Steradian area
(540 pixels)

Centroid                            RA = 19h02m49.41s  Dec = -36d50m53.8s


Flux weighted centroid              RA = 19h02m48.49s  Dec = -36d50m59.1s

vertex# 1  at RA = 19h03m07.05s  Dec = -36d48m16.1s

vertex# 2  at RA = 19h03m08.35s  Dec = -36d53m01.3s

vertex# 3  at RA = 19h02m30.82s  Dec = -36d53m16.9s

vertex# 4  at RA = 19h02m29.55s  Dec = -36d49m01.7s


Maximum 62.5595    at RA = 19h01m49.45s  Dec = -37d04m47.3s
Minimum 39.6116    at RA = 19h01m26.84s  Dec = -37d07m31.9s

Mean    51.3384
st dev  7.35416
                                  Flux units MJY/SR

Flux integral      0.000118837   MJY
Inside 2.31477e-06 Steradian area
(437 pixels)
```

```
Centroid                              RA = 19h01m38.14s  Dec = -37d07m32.2s


Flux weighted centroid                RA = 19h01m38.97s  Dec = -37d07m33.0s

vertex# 1  at RA = 19h01m50.67s  Dec = -37d10m17.6s

vertex# 2  at RA = 19h01m26.80s  Dec = -37d10m32.1s

vertex# 3  at RA = 19h01m25.62s  Dec = -37d04m46.8s

vertex# 4  at RA = 19h01m49.45s  Dec = -37d04m32.3s

=====================================================================
=====================================================================

PGAI86101801.FITS  Orion MC-E
=====================================================================

Maximum 190.602    at RA = 5h36m50.17s  Dec = -5d43m44.9s
Minimum 120.787    at RA = 5h37m26.38s  Dec = -5d48m00.0s

Mean    157.98
st dev  17.415
                                   Flux units MJY/SR

Flux integral      0.00140668   MJY
Inside 8.90419e-06 Steradian area
(1681 pixels)

Centroid                              RA = 5h37m06.26s  Dec = -5d47m30.0s


Flux weighted centroid                RA = 5h37m05.63s  Dec = -5d47m22.3s

vertex# 1  at RA = 5h37m27.39s  Dec = -5d52m45.3s

vertex# 2  at RA = 5h36m45.14s  Dec = -5d52m45.3s

vertex# 3  at RA = 5h36m45.14s  Dec = -5d42m14.8s

vertex# 4  at RA = 5h37m26.38s  Dec = -5d42m14.8s

=====================================================================
=====================================================================

PGAI15601577.FITS  OPT_IR4
=====================================================================

Maximum 12.3573    at RA = 18h12m00.62s  Dec =  44d27m07.6s
Minimum 5.8506    at RA = 18h12m14.69s  Dec =  44d33m22.7s

Mean    8.58561
st dev  1.39592
                                   Flux units MJY/SR

Flux integral      3.94291e-05   MJY
Inside 4.59247e-06 Steradian area
(867 pixels)

Centroid                              RA = 18h11m59.44s  Dec =  44d32m07.1s


Flux weighted centroid                RA = 18h11m58.90s  Dec =  44d31m59.8s
```

```
vertex# 1  at RA = 18h12m03.48s  Dec =  44d37m23.1s

vertex# 2  at RA = 18h12m25.88s  Dec =  44d29m37.3s

vertex# 3  at RA = 18h11m56.41s  Dec =  44d26m37.6s

vertex# 4  at RA = 18h11m32.55s  Dec =  44d34m53.0s

internal systematic flat-field structures of array (regular pattern generated by
the four pixels; note: pixel numbering is arbitrary and needs not to comply
with official numbering scheme):

1) 8.70943 MJY/SR   at RA = 18h12m02.07s  Dec =  44d36m23.0s
2) 8.91199 MJY/SR   at RA = 18h11m53.63s  Dec =  44d35m53.1s
3) 6.61638 MJY/SR   at RA = 18h11m57.84s  Dec =  44d34m38.0s
4) 7.24202 MJY/SR   at RA = 18h12m06.28s  Dec =  44d35m07.9s

1) 9.02776 MJY/SR   at RA = 18h11m45.20s  Dec =  44d35m08.1s
2) 9.09764 MJY/SR   at RA = 18h11m39.58s  Dec =  44d34m23.0s
3) 7.47776 MJY/SR   at RA = 18h11m42.39s  Dec =  44d32m52.9s
4) 6.85380 MJY/SR   at RA = 18h11m49.41s  Dec =  44d33m53.0s

1) 8.84284 MJY/SR   at RA = 18h12m10.48s  Dec =  44d33m52.8s
2) 9.28228 MJY/SR   at RA = 18h12m02.05s  Dec =  44d33m22.9s
3) 6.94571 MJY/SR   at RA = 18h12m03.45s  Dec =  44d31m52.8s
4) 5.85925 MJY/SR   at RA = 18h12m11.87s  Dec =  44d32m22.7s

1) 10.3985 MJY/SR   at RA = 18h11m53.62s  Dec =  44d32m22.9s
2) 10.0606 MJY/SR   at RA = 18h11m46.60s  Dec =  44d31m37.9s
3) 8.67902 MJY/SR   at RA = 18h11m49.41s  Dec =  44d30m22.8s
4) 8.14129 MJY/SR   at RA = 18h11m57.83s  Dec =  44d31m07.8s

1) 7.97165 MJY/SR   at RA = 18h12m17.48s  Dec =  44d31m07.6s
2) 9.97702 MJY/SR   at RA = 18h12m09.05s  Dec =  44d30m37.7s
3) 7.75711 MJY/SR   at RA = 18h12m11.85s  Dec =  44d29m07.6s
4) 6.32838 MJY/SR   at RA = 18h12m20.27s  Dec =  44d29m52.5s

1) 11.1434 MJY/SR   at RA = 18h12m02.03s  Dec =  44d29m52.7s
2) 10.9861 MJY/SR   at RA = 18h11m55.02s  Dec =  44d29m07.7s
3) 9.31913 MJY/SR   at RA = 18h11m57.82s  Dec =  44d27m37.6s
4) 8.90728 MJY/SR   at RA = 18h12m04.83s  Dec =  44d28m22.6s

average:
1) 9.34893 MJY/SR +- 1.18211 MJY/SR       1.10794
2) 9.71927 MJY/SR +- 0.77677 MJY/SR       1.15183
3) 7.79919 MJY/SR +- 1.03120 MJY/SR       0.92428
4) 6.88495 MJY/SR +- 0.87588 MJY/SR       0.81594

mean of all 4: 8.43809 MJY/SR +- 1.32809 MJY/SR

flat-field accuracy of map determined by internal flat-field of array
pairwise coincidence of surface brightness value by averaging two pixels
in a row, but not in a column.

====================================================================
====================================================================

PGAI33300559.FITS  Cham II
====================================================================

Maximum 25.0027    at RA = 13h04m34.64s  Dec = -77d00m33.0s
Minimum 16.4171    at RA = 13h02m11.62s  Dec = -76d55m23.1s
```

```
Mean    18.4228
st dev  1.39118
                                  Flux units MJY/SR

Flux integral      0.000197902   MJY
Inside 1.07422e-05 Steradian area
(2028 pixels)

Centroid                            RA = 13h02m36.92s  Dec = -76d56m11.9s


Flux weighted centroid              RA = 13h02m35.25s  Dec = -76d56m11.4s

vertex# 1  at RA = 13h05m07.78s  Dec = -76d53m00.7s

vertex# 2  at RA = 13h04m56.97s  Dec = -77d00m46.8s

vertex# 3  at RA = 13h00m03.13s  Dec = -76d59m08.9s

vertex# 4  at RA = 13h00m16.76s  Dec = -76d51m38.6s

=====================================================================
=====================================================================

PGAI10101157.FITS  L134_C200
=====================================================================

Maximum 56.0205    at RA = 15h53m43.17s  Dec = -4d28m05.4s
Minimum 40.1661    at RA = 15h53m22.09s  Dec = -4d25m50.2s

Mean    49.3122
st dev  3.16064
                                  Flux units MJY/SR

Flux integral      0.000165343   MJY
Inside 3.35298e-06 Steradian area
(633 pixels)

Centroid                            RA = 15h53m49.34s  Dec = -4d26m55.5s


Flux weighted centroid              RA = 15h53m49.07s  Dec = -4d26m54.7s

vertex# 1  at RA = 15h54m17.30s  Dec = -4d26m35.3s

vertex# 2  at RA = 15h54m14.29s  Dec = -4d29m35.4s

vertex# 3  at RA = 15h53m21.08s  Dec = -4d27m05.3s

vertex# 4  at RA = 15h53m23.09s  Dec = -4d24m20.2s

=====================================================================
=====================================================================

PGAI31000625.FITS  Rho_Oph_16
=====================================================================

Maximum 216.366    at RA = 16h31m51.49s  Dec = -24d31m18.7s
Minimum 166.039    at RA = 16h31m51.49s  Dec = -24d29m18.6s

Mean    180.208
st dev  8.09671
                                  Flux units MJY/SR
```

```
Flux integral      0.000383731   MJY
Inside 2.12938e-06 Steradian area
(402 pixels)

Centroid                              RA = 16h31m54.25s  Dec = -24d26m48.5s


Flux weighted centroid                RA = 16h31m54.32s  Dec = -24d26m47.6s

vertex# 1  at RA = 16h32m03.61s  Dec = -24d22m33.4s

vertex# 2  at RA = 16h31m56.99s  Dec = -24d31m33.8s

vertex# 3  at RA = 16h31m44.89s  Dec = -24d31m03.6s

vertex# 4  at RA = 16h31m51.52s  Dec = -24d22m03.3s

=====================================================================
=====================================================================

PGAI26701013.FITS  Rho_Oph_Ma
=====================================================================

Maximum 246.984    at RA = 16h29m13.01s  Dec = -24d34m24.0s
Minimum 147.635    at RA = 16h29m11.80s  Dec = -24d24m23.6s

Mean    184.162
st dev  26.1232
                                   Flux units MJY/SR

Flux integral      0.00126815   MJY
Inside 6.88605e-06 Steradian area
(1300 pixels)

Centroid                              RA = 16h29m05.80s  Dec = -24d28m54.0s


Flux weighted centroid                RA = 16h29m05.25s  Dec = -24d29m08.5s

vertex# 1  at RA = 16h29m26.08s  Dec = -24d24m23.0s

vertex# 2  at RA = 16h29m19.61s  Dec = -24d34m38.8s

vertex# 3  at RA = 16h28m45.49s  Dec = -24d33m24.7s

vertex# 4  at RA = 16h28m52.00s  Dec = -24d23m09.1s

=====================================================================
=====================================================================

PGAI40900802.FITS
=====================================================================

Maximum 7.03741    at RA = 1h20m32.78s  Dec =  3d26m00.7s
Minimum 5.79304    at RA = 1h20m11.72s  Dec =  3d19m15.4s

Mean    6.59719
st dev  0.23893
                                   Flux units MJY/SR

Flux integral      6.72343e-05   MJY
Inside 1.01914e-05 Steradian area
(1924 pixels)
```

```
Centroid                              RA = 1h20m16.55s  Dec =  3d26m44.1s


Flux weighted centroid                RA = 1h20m16.66s  Dec =  3d26m45.2s

vertex# 1  at RA = 1h20m21.75s  Dec =  3d34m46.1s

vertex# 2  at RA = 1h20m43.80s  Dec =  3d22m15.5s

vertex# 3  at RA = 1h20m10.72s  Dec =  3d18m45.4s

vertex# 4  at RA = 1h19m49.66s  Dec =  3d31m15.9s

=====================================================================
=====================================================================

PGAI28001303.FITS  NGC 5128
=====================================================================

Maximum 11.3567    at RA = 13h26m08.39s  Dec = -42d57m04.8s
Minimum 8.57224    at RA = 13h26m04.27s  Dec = -42d45m04.3s

Mean    9.96032
st dev  0.5096
                                   Flux units MJY/SR

Flux integral      0.000113433   MJY
Inside 1.13885e-05 Steradian area
(2150 pixels)

Centroid                              RA = 13h26m06.33s  Dec = -42d51m04.5s


Flux weighted centroid                RA = 13h26m06.47s  Dec = -42d51m07.2s

vertex# 1  at RA = 13h26m53.44s  Dec = -42d52m18.7s

vertex# 2  at RA = 13h26m23.45s  Dec = -42d59m19.8s

vertex# 3  at RA = 13h25m19.24s  Dec = -42d49m49.1s

vertex# 4  at RA = 13h25m49.28s  Dec = -42d42m49.2s

=====================================================================
=====================================================================
```

9.3 Absolute Surface Brightness Values of P22 Maps Compared with COBE/DIRBE Photometry

We use the same test cases as for determination of the flat-field accuracy which were selected to show a range in surface brightness values (cf. [4], Section 5.1).

9.3.1 References to Calibration Analysis and Software Change Documentation

- calibration reports:
  - none
- Software Change Requests: none
- Software Problem Reports: none

9.3.2 Summary of Results

- Both for C100 and C200 a good correspondence of the ISOPHOT surface brightnesses with COBE/DIRBE photometry is found for the flux ranges 5 to 400 $\mathrm{MJy\,sr^{-1}}$ for C100 and 3 to 600 $\mathrm{MJy\,sr^{-1}}$ for C200, respectively. This consistency is better than $\pm$ 25 %.
- It has to be noted that the comparison could only be done with some remaining caveats. Therefore, no perfect agreement should be expected:
  - The areas covered by most of the ISOPHOT maps selected both for flat field and absolute surface brightness determination are considerably smaller than the beam of one COBE/DIRBE pixel. Only a few maps have comparable size with the COBE/DIRBE beam and do not suffer from the intrinsic source structure which might be extended for the ISOPHOT beam, but rather compact for the COBE/DIRBE beam. In future studies a better comparison at 60 and 100 μm can be done using the IRAS ISSA maps as a transfer. We will also check the availability of more large maps comparable in size with the COBE/DIRBE beam.
  - For a proper comparison the adequate color corrections and corrections for different wavelengths must be applied. Here the most significant case was the ISOPHOT 90 μm photometry versus the DIRBE 100 μm photometry for which we applied only a very coarse correction in order to account for a systematic flux excess at 90 μm due to the steep flux decline in the background SED between 60 and 100 μm.

9.3.3 Absolute Surface Brightness Values of C100 Maps

- authors: U. Klaas
- date: 11-January-2000
- SVP period 2

Motivation

As part of the scientific validation of staring raster maps the consistency of the absolute sky brightness with COBE/DIRBE is verified. Since the map test cases cover a wide range in flux we can extend the assessment done on staring background measurements which are currently limited in flux range. The maps offer the advantage to get a comparable solid angle coverage with the COBE/DIRBE pixels.

Method

We compare the mean surface brightness derived with the SKYVIEW program for the maps used for the flat-field assessment (see Sect. 9.2.3) with the surface brightness values in the corresponding filters or adjacent filters of COBE/DIRBE. This time we use the full maps rather than a background area in order to have the best comparable beam size with COBE/DIRBE; however in most cases the solid angles of the ISOPHOT maps are still considearbly smaller than one pixel of COBE/DIRBE. We use the COBE/DIRBE annual maps (since at the wavelengths considered the contribution by Zodiacal Light is small) and determine the fluxes for the DIRBE pixel coincident with the map area centroid. For a check of the large scale variations of the sky background we determine as well as average fluxes of a 1.5 deg circular area.

Results

In Table 9.5 we present the results of the comparison. Detailed data on the COBE/DIRBE spectra, as well as the flux assessment of the ISOPHOT maps using SKYVIEW are given in the evaluation log. It should be noted that neither colour correction with regard to a modified blackbody describing the sky background spectral energy distribution nor a wavelength correction to better match the COBE/DIRBE filter central wavelength with the ISOPHOT filter central wavelength has been performed (this may be done for a future scientific validation assesesment). Also, as already mentioned above, nearly all ISOPHOT maps are considerably smaller in area than the solid angle of one COBE/DIRBE pixel. Therefore, structures in the source or background can affect the resulting absolute flux. If a map of the test case list contained a bright compact target, this was deselected, because of the mismatch of the ISOPHOT and DIRBE beams led to uncomparable results; as expected in those cases the ISOPHOT maps gave a considerably higher average surface brightness due to the smaller area considered.
Except for the different beam sizes a comparison of the ISOPHOT/DIRBE 60 and 100 μm filters is relatively straight forward. Here in general a good agreement with better than 25 %, in particular for those maps with comparable sizes to the COBE/DIRBE beam, is found. All larger deviations can be explained by the source structure which is extended over the ISOPHOT map area, but compact inside the COBE/DIRBE beam. The largest outlier, PGAI15601578, shows a similar excess independently in the C200 range (cf. Sect. 9.3.4).
Without any correction, the ISOPHOT 90 μm filter maps seem to show a systematic positive surface brightness excess with regrad to the DIRBE 100 μm photometry. However, inspection of the COBE/DIRBE SEDs indicates a steep decline in flux between 60 and 100 μm. In fact, the 90 μm ISOPHOT values are practically always in between the 60 and 100 μm DIRBE values. Very often, the surface brightness ratio 60/100 is about 2, i.e. with a linear interpolation between 60 and 100 μm flux, the 90 μm flux is by 25% higher than the 100 μm flux due to the shape of the SED. Then, also the 90 μm map surface brightnesses are consistent with COBE/DIRBE within better than 25%. If the discrepancy between the ISOPHOT 90 μm surface brightness and the DIRBE 100 μm surface brightness is small, usually the source SED is reasonably flat between 60 and 100 μm.

Table 9.5: Consistency check of C100 map absolute surface brightness with COBE/DIRBE annual map photometry. The solid angle of one COBE/DIRBE pixel is 19.5 10^{-5} sr. No correction for the wavelength shift between ISOPHOT 90 μm and DIRBE 100 μm filters has been performed whch causes for most sky backgrounds a systematic positive excess of the 90 μm flux (see text for a quantitative estimate).

OLP product name	**filter** (μm)	**surface brightness** (MJy sr^{-1})	**solid angle** (10^{-5} sr)	**DIRBE flux** (MJy sr^{-1})	**DIRBE filter** (μm)	**solid angle** (10^{-5} sr)	**consistency** (%)
PGAI19002101	60	6.8	0.81	6.6	60	19.5	+2.2
PGAI08900102	60	9.5	1.60	6.5	60	19.5	+47
PGAI85001219	60	22.8	0.21	22.3	60	19.5	+2.2
PGAI13400214	60	39.8	0.22	39.6	60	19.5	+0.6
PGAI68300807	60	21.3	6.77	27.2	60	19.5	-22
PGAI84403913	60	23.9	1.04	24.5	60	19.5	-2.5
PGAI69801101	60	107.4	1.16	122.3	60	19.5	-12
PGAI35100809	90	5.1	5.49	3.3	100	19.5	+55
PGAI58200903	90	11.8	3.06	12.9	100	19.5	-7.9
PGAI19201091	90	4.8	7.30	3.1	100	19.5	+52
PGAI86901244	90	5.2	2.75	3.6	100	19.5	+44
PGAI41502788	90	8.1	5.10	5.7	100	19.5	+44
PGAI09000606	90	11.8	0.77	11.3	100	19.5	+4.4
PGAI08901904	90	15.1	0.23	13.6	100	19.5	+11
PGAI40100614	90	14.7	6.80	13.3	100	19.5	+10
PGAI87001338	90	5.3	2.93	3.6	100	19.5	+47
PGAI57501902	90	12.1	1.15	9.7	100	19.5	+25
PGAI52700514	90	4.4	0.85	3.7	100	19.5	+21
PGAI60002009	90	7.1	4.24	5.2	100	19.5	+37
PGAI50000124	90	4.8	8.87	3.3	100	19.5	+43
PGAI50100273	90	5.8	8.68	3.5	100	19.5	+68
PGAI20701079	90	25.6	0.33	22.8	100	19.5	+12
PGAI20800709	90	5.8	3.49	4.0	100	19.5	+46
PGAI86800640	90	5.7	2.96	3.6	100	19.5	+60
PGAI10101158	100	30.7	1.71	21.0	100	19.5	+46
PGAI79401149	100	44.2	0.51	40.6	100	19.5	+9.0
PGAI44900714	100	387.7	15.2	440.1	100	19.5	-12
PGAI15601578	100	17.4	1.82	6.1	100	19.5	+187
PGAI27600420	100	15.4	1.74	12.1	100	19.5	+27
PGAI71901220	100	18.5	3.66	16.0	100	19.5	+15
PGAI33401134	100	96.4	4.06	49.3	100	19.5	+96

Conclusions

- ISOPHOT 60 and 100 μm surface brightness values from maps obtained with different raster parameters show a consistency of better than ± 25 % with COBE/DIRBE photometry. Larger deviations for some cases can be explained by the source structure which is extended over the ISOPHOT map area, but compact with regard to the COBE/DIRBE pixel size. In the future a comparison with the IRAS/ISSA maps will be included.

- Due to a strong flux decline in the background SEDs of most areas between 60 and 100 μm ISOPHOT 90 μm surface brightness values can only be compared with COBE/DIRBE after some wavelength correction. A rough estimate using linear interpolation between 60 and 100 μm DIRBE surface brightness and taking into account that the 60 μm surface brightness is about 2 times higher than the 100 μm surface brightness yields a 90 μm surface brightness which is higher by 25%. With this correction also ISOPHOT 90 μm surface brightnesses show a consistency of better than ± 25 % with COBE/DIRBE photometry. Whether there is still a positive excess cannot be solved by this kind of study, but needs better matching area and a proper color

correction of the background SEDs.

- From the consistency in the three filters 60, 90, and 100 μm and the relative photometric accuracies of all ISOPHOT C100 filters we conclude that the consistency should also hold for the remaining ISOPHOT filters at 65, 80, and 105 μm.
- This good correspondence holds for the flux range 5 (4.5) to 400 MJy sr^{-1} and extends the verified surface brightness range covered so far by single pointing background measurements considerably. The accuracy assessment is limited to the absolute surface brightness, since each map has its individual background measurement; no statement about the relative filter-to-filter calibration accuracy can be made from this program.

Evaluation Log

```
-----------------------------------------------------

PGAI19002101.FITS  NGC 104

Centroid                              RA = 0h24m03.78s  Dec = -72d04m56.5s

DIRBE_ANNUAL,6.015750,-72.082361,0.
           1 pixel(s) will be taken
Band  Wavelength        Inu
   1     1.25      1.951+/- 0.005
   2     2.20      1.368+/- 0.003
   3     3.50      0.786+/- 0.002
   4     4.90      0.853+/- 0.006
   5    12.00     13.664+/- 0.057
   6    25.00     23.301+/- 0.056
   7    60.00      6.624+/- 0.018
   8   100.00      4.356+/- 0.021
   9   140.00      6.055+/- 1.210
  10   240.00      3.575+/- 0.677

DIRBE_ANNUAL,6.015750,-72.082361,1.5
% Compiled module: PXINCIRC.
          67 pixel(s) will be taken
Band  Wavelength        Inu
% Compiled module: MOMENT.
   1     1.25      0.282+/- 0.039
   2     2.20      0.193+/- 0.031
   3     3.50      0.142+/- 0.015
   4     4.90      0.528+/- 0.008
   5    12.00     13.492+/- 0.008
   6    25.00     23.187+/- 0.012
   7    60.00      6.675+/- 0.022
   8   100.00      4.586+/- 0.063
   9   140.00      5.462+/- 0.186
  10   240.00      3.522+/- 0.120

    Maximum 10.8927    at RA = 0h23m19.19s  Dec = -72d07m36.1s
    Minimum 4.06942    at RA = 0h24m27.49s  Dec = -71d59m06.0s

    Mean    6.77265
    st dev  1.31908
                                        Flux units MJY/SR

    Flux integral      5.49597e-05   MJY
    Inside 8.11495e-06 Steradian area
    (1532 pixels)

    Centroid                              RA = 0h24m03.78s  Dec = -72d04m56.5s


    Flux weighted centroid                RA = 0h24m03.37s  Dec = -72d05m00.4s

    vertex# 1  at RA = 0h25m32.72s  Dec = -72d05m35.2s

    vertex# 2  at RA = 0h23m51.74s  Dec = -72d11m51.7s

    vertex# 3  at RA = 0h22m33.82s  Dec = -72d04m05.0s

    vertex# 4  at RA = 0h24m17.77s  Dec = -71d58m06.0s

-----------------------------------------------------
```

```
PGAI08900102.FITS  A2256

Centroid                              RA = 17h02m54.66s  Dec =  78d42m52.2s

UIDL> DIRBE_ANNUAL,255.72775,78.7145,0.
          1 pixel(s) will be taken
Band  Wavelength        Inu
   1     1.25      0.291+/- 0.001
   2     2.20      0.205+/- 0.001
   3     3.50      0.140+/- 0.001
   4     4.90      0.452+/- 0.002
   5    12.00     12.342+/- 0.024
   6    25.00     21.567+/- 0.053
   7    60.00      6.472+/- 0.029
   8   100.00      5.103+/- 0.033
   9   140.00      7.674+/- 1.474
  10   240.00      3.669+/- 0.935
UIDL> DIRBE_ANNUAL,255.72775,78.7145,1.5
         65 pixel(s) will be taken
Band  Wavelength        Inu
   1     1.25      0.272+/- 0.010
   2     2.20      0.187+/- 0.007
   3     3.50      0.130+/- 0.004
   4     4.90      0.446+/- 0.002
   5    12.00     12.307+/- 0.007
   6    25.00     21.546+/- 0.012
   7    60.00      6.458+/- 0.009
   8   100.00      4.899+/- 0.030
   9   140.00      5.862+/- 0.228
  10   240.00      4.383+/- 0.115

    Maximum 14.0582    at RA = 17h04m09.44s  Dec =  78d42m10.2s
    Minimum 5.30239    at RA = 17h02m42.60s  Dec =  78d41m25.8s

    Mean    9.52585
    st dev  1.32535
                                       Flux units MJY/SR

    Flux integral      0.000152888   MJY
    Inside 1.60498e-05 Steradian area
    (3030 pixels)

    Centroid                              RA = 17h02m54.66s  Dec =  78d42m52.2s


    Flux weighted centroid                RA = 17h02m56.05s  Dec =  78d42m51.2s

    vertex# 1  at RA = 17h05m58.00s  Dec =  78d46m52.5s

    vertex# 2  at RA = 17h04m13.58s  Dec =  78d33m54.7s

    vertex# 3  at RA = 16h59m54.85s  Dec =  78d38m52.3s

    vertex# 4  at RA = 17h01m29.92s  Dec =  78d51m40.6s

-----------------------------------------------------

PGAI85001219.FITS  S88

Centroid                              RA = 5h13m29.74s  Dec = -69d32m27.3s

DIRBE_ANNUAL,78.373917,-69.540917,0.
          1 pixel(s) will be taken
Band  Wavelength        Inu
```

```
   1     1.25      1.359+/- 0.005
   2     2.20      1.065+/- 0.004
   3     3.50      0.624+/- 0.003
   4     4.90      0.702+/- 0.003
   5    12.00     12.251+/- 0.035
   6    25.00     21.327+/- 0.064
   7    60.00     22.342+/- 0.227
   8   100.00     37.947+/- 0.452
   9   140.00     46.021+/- 1.619
  10   240.00     24.901+/- 0.850

DIRBE_ANNUAL,78.373917,-69.540917,1.5
          68 pixel(s) will be taken
Band  Wavelength        Inu
   1     1.25      0.878+/- 0.039
   2     2.20      0.661+/- 0.031
   3     3.50      0.396+/- 0.018
   4     4.90      0.575+/- 0.010
   5    12.00     11.933+/- 0.029
   6    25.00     20.694+/- 0.051
   7    60.00     13.149+/- 0.776
   8   100.00     22.319+/- 1.441
   9   140.00     30.619+/- 1.654
  10   240.00     18.592+/- 0.865


    Maximum 125.334    at RA = 5h13m45.14s  Dec = -69d34m53.5s
    Minimum 12.4853    at RA = 5h13m36.53s  Dec = -69d33m08.5s

    Mean    22.826
    st dev  10.2898
                                        Flux units MJY/SR

    Flux integral      4.71543e-05   MJY
    Inside 2.06582e-06 Steradian area
    (390 pixels)

    Centroid                              RA = 5h13m29.74s  Dec = -69d32m27.3s


    Flux weighted centroid                RA = 5h13m28.57s  Dec = -69d32m44.5s

    vertex# 1  at RA = 5h13m59.38s  Dec = -69d30m08.2s

    vertex# 2  at RA = 5h13m56.62s  Dec = -69d35m08.4s

    vertex# 3  at RA = 5h12m59.25s  Dec = -69d34m38.4s

    vertex# 4  at RA = 5h13m02.23s  Dec = -69d29m53.2s

-----------------------------------------------------

PGAI13400214.FITS  P Cyg

Centroid                              RA = 20h17m46.88s  Dec =  38d02m09.3s

DIRBE_ANNUAL,304.445333,+38.035917,0.
           1 pixel(s) will be taken
Band  Wavelength        Inu
   1     1.25      2.526+/- 0.004
   2     2.20      2.636+/- 0.003
   3     3.50      1.757+/- 0.003
   4     4.90      1.476+/- 0.009
   5    12.00     18.138+/- 0.136
```

```
   6    25.00     28.608+/- 0.184
   7    60.00     39.575+/- 0.132
   8   100.00    119.997+/- 0.653
   9   140.00    256.482+/- 1.546
  10   240.00    192.935+/- 0.913

DIRBE_ANNUAL,304.445333,+38.035917,1.5
         69 pixel(s) will be taken
Band  Wavelength        Inu
   1     1.25      2.223+/- 0.057
   2     2.20      2.568+/- 0.105
   3     3.50      1.816+/- 0.089
   4     4.90      1.571+/- 0.057
   5    12.00     19.756+/- 0.339
   6    25.00     30.916+/- 0.710
   7    60.00     55.314+/- 5.338
   8   100.00    152.720+/- 9.478
   9   140.00    314.937+/-15.146
  10   240.00    217.917+/- 9.815

    Maximum 62.369    at RA = 20h17m46.88s  Dec =  38d02m01.8s
    Minimum 28.4691    at RA = 20h17m37.98s  Dec =  38d04m31.9s

    Mean    39.7927
    st dev  4.47357
                                      Flux units MJY/SR

    Flux integral      8.85277e-05   MJY
    Inside 2.22472e-06 Steradian area
    (420 pixels)

    Centroid                              RA = 20h17m46.88s  Dec =  38d02m09.3s


    Flux weighted centroid                RA = 20h17m46.95s  Dec =  38d02m04.9s

    vertex# 1  at RA = 20h18m00.87s  Dec =  38d04m31.9s

    vertex# 2  at RA = 20h17m59.58s  Dec =  37d59m31.6s

    vertex# 3  at RA = 20h17m32.91s  Dec =  37d59m46.6s

    vertex# 4  at RA = 20h17m32.90s  Dec =  38d04m46.9s

-----------------------------------------------------

PGAI68300807.FITS  TMC-2

Centroid                             RA = 4h32m41.90s  Dec =  24d36m14.6s

DIRBE_ANNUAL,68.174583,24.604056,0.
          1 pixel(s) will be taken
Band  Wavelength        Inu
   1     1.25      0.684+/- 0.009
   2     2.20      0.507+/- 0.006
   3     3.50      0.372+/- 0.007
   4     4.90      1.301+/- 0.040
   5    12.00     41.090+/- 0.938
   6    25.00     77.253+/- 1.468
   7    60.00     27.208+/- 0.438
   8   100.00     25.767+/- 0.177
   9   140.00     54.081+/- 1.965
  10   240.00     59.820+/- 1.358
```

```
DIRBE_ANNUAL,68.174583,24.604056,1.5
          66 pixel(s) will be taken
Band  Wavelength        Inu
   1     1.25      0.661+/- 0.010
   2     2.20      0.480+/- 0.012
   3     3.50      0.354+/- 0.008
   4     4.90      1.287+/- 0.007
   5    12.00     40.592+/- 0.124
   6    25.00     76.645+/- 0.219
   7    60.00     27.718+/- 0.103
   8   100.00     24.968+/- 0.302
   9   140.00     46.219+/- 1.020
  10   240.00     43.865+/- 1.418

    Maximum 88.9127    at RA = 4h32m17.79s  Dec =  24d29m03.4s
    Minimum 16.2874    at RA = 4h32m05.64s  Dec =  24d40m03.7s

    Mean    21.2963
    st dev  3.0293
                                       Flux units MJY/SR

    Flux integral      0.00144177   MJY
    Inside 6.77005e-05 Steradian area
    (12781 pixels)

    Centroid                              RA = 4h32m41.90s  Dec =  24d36m14.6s


    Flux weighted centroid                RA = 4h32m42.61s  Dec =  24d36m09.8s

    vertex# 1  at RA = 4h33m54.52s  Dec =  24d24m47.2s

    vertex# 2  at RA = 4h31m52.56s  Dec =  24d19m47.5s

    vertex# 3  at RA = 4h31m29.22s  Dec =  24d47m48.3s

    vertex# 4  at RA = 4h33m31.62s  Dec =  24d52m34.1s

-----------------------------------------------------

PGAI84403913.FITS  B209

Centroid                              RA = 4h14m25.87s  Dec =  28d09m00.5s

IRBE_ANNUAL,63.607792,28.150139,0.
           1 pixel(s) will be taken
Band  Wavelength        Inu
   1     1.25      0.734+/- 0.008
   2     2.20      0.582+/- 0.005
   3     3.50      0.418+/- 0.006
   4     4.90      1.296+/- 0.036
   5    12.00     38.322+/- 0.806
   6    25.00     70.615+/- 1.221
   7    60.00     24.493+/- 0.385
   8   100.00     21.844+/- 0.135
   9   140.00     48.261+/- 2.208
  10   240.00     62.471+/- 1.321

DIRBE_ANNUAL,63.607792,28.150139,1.5
          64 pixel(s) will be taken
Band  Wavelength        Inu
   1     1.25      0.643+/- 0.028
   2     2.20      0.468+/- 0.030
   3     3.50      0.334+/- 0.016
```

```
   4     4.90      1.258+/- 0.008
   5    12.00     38.322+/- 0.113
   6    25.00     71.241+/- 0.189
   7    60.00     24.564+/- 0.070
   8   100.00     20.273+/- 0.421
   9   140.00     39.253+/- 1.675
  10   240.00     40.554+/- 2.282

    Maximum 91.9213    at RA = 4h14m25.54s  Dec =  28d06m01.5s
    Minimum 17.0435    at RA = 4h14m06.26s  Dec =  28d03m31.3s

    Mean    23.8865
    st dev  4.70754
                                       Flux units MJY/SR

    Flux integral      0.000247358   MJY
    Inside 1.03556e-05 Steradian area
    (1955 pixels)

    Centroid                              RA = 4h14m25.87s  Dec =  28d09m00.5s


    Flux weighted centroid                RA = 4h14m26.23s  Dec =  28d08m58.0s

    vertex# 1  at RA = 4h14m56.16s  Dec =  28d04m46.2s

    vertex# 2  at RA = 4h14m06.26s  Dec =  28d02m31.2s

    vertex# 3  at RA = 4h13m56.01s  Dec =  28d13m16.6s

    vertex# 4  at RA = 4h14m44.85s  Dec =  28d15m31.8s

-----------------------------------------------------

PGAI69801101.FITS  SGR 1814-14

Centroid                              RA = 18h14m25.26s  Dec = -13d59m58.8s

DIRBE_ANNUAL,273.60525,-13.999667,0.
          1 pixel(s) will be taken
Band  Wavelength        Inu
   1     1.25      3.319+/- 0.020
   2     2.20      6.288+/- 0.024
   3     3.50      4.840+/- 0.017
   4     4.90      3.836+/- 0.039
   5    12.00     38.838+/- 0.862
   6    25.00     66.694+/- 1.359
   7    60.00    122.301+/- 0.792
   8   100.00    332.037+/- 1.955
   9   140.00    572.009+/- 3.146
  10   240.00    342.595+/- 1.719

DIRBE_ANNUAL,273.60525,-13.999667,1.5
         68 pixel(s) will be taken
Band  Wavelength        Inu
   1     1.25      3.655+/- 0.149
   2     2.20      6.965+/- 0.341
   3     3.50      5.510+/- 0.318
   4     4.90      4.052+/- 0.220
   5    12.00     38.625+/- 1.137
   6    25.00     67.189+/- 2.922
   7    60.00    132.423+/-18.626
   8   100.00    356.660+/-39.773
   9   140.00    588.036+/-61.223
```

```
  10   240.00    329.240+/-32.196

    Maximum 141.147    at RA = 18h14m47.70s  Dec = -14d03m59.9s
    Minimum 93.092    at RA = 18h14m12.62s  Dec = -14d00m44.8s

    Mean    107.378
    st dev  6.63006
                                       Flux units MJY/SR

    Flux integral      0.00124619   MJY
    Inside 1.16056e-05 Steradian area
    (2191 pixels)

    Centroid                              RA = 18h14m25.26s  Dec = -13d59m58.8s


    Flux weighted centroid                RA = 18h14m25.64s  Dec = -13d59m59.5s

    vertex# 1  at RA = 18h14m54.92s  Dec = -14d04m29.9s

    vertex# 2  at RA = 18h13m59.20s  Dec = -14d05m30.0s

    vertex# 3  at RA = 18h13m55.10s  Dec = -13d55m29.5s

    vertex# 4  at RA = 18h14m51.81s  Dec = -13d54m29.5s

-----------------------------------------------------

PGAI35100809.FITS  M03

Centroid                             RA = 13h36m12.60s  Dec =  70d34m49.9s

DIRBE_ANNUAL,204.0525,70.580528,0.
           1 pixel(s) will be taken
Band  Wavelength        Inu
   1     1.25      0.200+/- 0.001
   2     2.20      0.133+/- 0.001
   3     3.50      0.106+/- 0.001
   4     4.90      0.455+/- 0.003
   5    12.00     12.799+/- 0.016
   6    25.00     22.329+/- 0.026
   7    60.00      6.254+/- 0.024
   8   100.00      3.276+/- 0.023
   9   140.00      4.473+/- 1.189
  10   240.00      1.402+/- 0.679

DIRBE_ANNUAL,204.0525,70.580528,1.5
          69 pixel(s) will be taken
Band  Wavelength        Inu
   1     1.25      0.212+/- 0.011
   2     2.20      0.142+/- 0.008
   3     3.50      0.109+/- 0.004
   4     4.90      0.465+/- 0.002
   5    12.00     12.814+/- 0.012
   6    25.00     22.321+/- 0.013
   7    60.00      6.284+/- 0.005
   8   100.00      3.396+/- 0.012
   9   140.00      2.774+/- 0.154
  10   240.00      2.172+/- 0.087

    Maximum 8.24613    at RA = 13h37m15.24s  Dec =  70d27m51.9s
    Minimum 3.03483    at RA = 13h34m03.93s  Dec =  70d25m34.6s

    Mean    5.08451
```

```
    st dev  0.488322
                                        Flux units MJY/SR

    Flux integral      0.000279101   MJY
    Inside 5.48924e-05 Steradian area
    (10363 pixels)

    Centroid                              RA = 13h36m12.60s  Dec =  70d34m49.9s


    Flux weighted centroid                RA = 13h36m12.43s  Dec =  70d34m49.1s

    vertex# 1  at RA = 13h39m14.53s  Dec =  70d25m01.8s

    vertex# 2  at RA = 13h34m19.43s  Dec =  70d19m35.0s

    vertex# 3  at RA = 13h33m07.32s  Dec =  70d44m17.6s

    vertex# 4  at RA = 13h38m08.23s  Dec =  70d50m06.4s

-----------------------------------------------------

PGAI58200903.FITS  KBM2

    Centroid                              RA = 1h14m02.96s  Dec =  5d28m36.0s

DIRBE_ANNUAL,18.512333,5.476667,0.
          1 pixel(s) will be taken
Band  Wavelength        Inu
   1     1.25      0.480+/- 0.009
   2     2.20      0.318+/- 0.006
   3     3.50      0.252+/- 0.006
   4     4.90      1.177+/- 0.037
   5    12.00     39.372+/- 0.834
   6    25.00     75.663+/- 1.334
   7    60.00     25.208+/- 0.384
   8   100.00     12.856+/- 0.149
   9   140.00      4.775+/- 1.984
  10   240.00      6.728+/- 1.089

DIRBE_ANNUAL,18.512333,5.476667,1.5
         66 pixel(s) will be taken
Band  Wavelength        Inu
   1     1.25      0.496+/- 0.007
   2     2.20      0.327+/- 0.006
   3     3.50      0.249+/- 0.003
   4     4.90      1.143+/- 0.005
   5    12.00     38.475+/- 0.104
   6    25.00     74.338+/- 0.163
   7    60.00     24.756+/- 0.065
   8   100.00     12.319+/- 0.062
   9   140.00      8.271+/- 0.256
  10   240.00      4.440+/- 0.181

    Maximum 144.913    at RA = 1h13m41.07s  Dec =  5d17m22.6s
    Minimum 2.33644    at RA = 1h13m25.98s  Dec =  5d29m23.2s

    Mean    11.8402
    st dev  7.81385
                                        Flux units MJY/SR

    Flux integral      0.000361251   MJY
    Inside 3.05105e-05 Steradian area
    (5760 pixels)
```

```
    Centroid                              RA = 1h14m02.96s  Dec =  5d28m36.0s


    Flux weighted centroid                RA = 1h14m04.13s  Dec =  5d27m17.5s

    vertex# 1  at RA = 1h14m52.44s  Dec =  5d23m22.8s

    vertex# 2  at RA = 1h13m43.08s  Dec =  5d16m07.6s

    vertex# 3  at RA = 1h13m12.90s  Dec =  5d33m38.3s

    vertex# 4  at RA = 1h14m23.29s  Dec =  5d41m08.8s

-----------------------------------------------------

PGAI19201091.FITS  N1_5B

Centroid                              RA = 16h10m01.40s  Dec =  54d30m26.8s

DIRBE_ANNUAL,242.505833,54.507444,0.
          1 pixel(s) will be taken
Band  Wavelength        Inu
   1     1.25      0.233+/- 0.001
   2     2.20      0.166+/- 0.001
   3     3.50      0.115+/- 0.001
   4     4.90      0.420+/- 0.002
   5    12.00     12.120+/- 0.033
   6    25.00     21.512+/- 0.053
   7    60.00      6.172+/- 0.023
   8   100.00      3.140+/- 0.021
   9   140.00      2.179+/- 1.306
  10   240.00      1.187+/- 0.792

DIRBE_ANNUAL,242.505833,54.507444,1.5
          67 pixel(s) will be taken
Band  Wavelength        Inu
   1     1.25      0.219+/- 0.005
   2     2.20      0.149+/- 0.004
   3     3.50      0.106+/- 0.002
   4     4.90      0.414+/- 0.001
   5    12.00     12.108+/- 0.004
   6    25.00     21.519+/- 0.009
   7    60.00      6.140+/- 0.005
   8   100.00      3.188+/- 0.012
   9   140.00      3.323+/- 0.199
  10   240.00      1.892+/- 0.094

    Maximum 13.0318    at RA = 16h11m07.27s  Dec =  54d44m03.8s
    Minimum 2.98937    at RA = 16h09m40.74s  Dec =  54d27m49.1s

    Mean    4.76269
    st dev  0.973618
                                       Flux units MJY/SR

    Flux integral      0.000347841   MJY
    Inside 7.30345e-05 Steradian area
    (13788 pixels)

    Centroid                              RA = 16h10m01.40s  Dec =  54d30m26.8s


    Flux weighted centroid                RA = 16h10m01.39s  Dec =  54d30m10.9s
```

```
    vertex# 1  at RA = 16h11m16.61s  Dec =  54d09m46.9s

    vertex# 2  at RA = 16h08m56.46s  Dec =  54d09m02.2s

    vertex# 3  at RA = 16h08m44.91s  Dec =  54d51m03.8s

    vertex# 4  at RA = 16h11m07.48s  Dec =  54d51m49.2s

--------------------------------------------------

PGAI86901244.FITS  S2_C90_D

Centroid                              RA = 5h02m21.86s  Dec = -30d36m26.0s

DIRBE_ANNUAL,75.591083,-30.607222,0.
          1 pixel(s) will be taken
Band  Wavelength        Inu
   1     1.25      0.239+/- 0.002
   2     2.20      0.165+/- 0.001
   3     3.50      0.125+/- 0.001
   4     4.90      0.523+/- 0.006
   5    12.00     14.310+/- 0.103
   6    25.00     25.045+/- 0.133
   7    60.00      7.079+/- 0.028
   8   100.00      3.586+/- 0.022
   9   140.00      4.000+/- 1.567
  10   240.00      3.738+/- 0.818

DIRBE_ANNUAL,75.591083,-30.607222,1.5
         67 pixel(s) will be taken
Band  Wavelength        Inu
   1     1.25      0.247+/- 0.012
   2     2.20      0.169+/- 0.009
   3     3.50      0.128+/- 0.004
   4     4.90      0.527+/- 0.002
   5    12.00     14.270+/- 0.019
   6    25.00     25.011+/- 0.032
   7    60.00      7.084+/- 0.007
   8   100.00      3.667+/- 0.010
   9   140.00      3.274+/- 0.183
  10   240.00      2.374+/- 0.107

    Maximum 9.44088    at RA = 5h02m16.29s  Dec = -30d26m51.5s
    Minimum 3.85024    at RA = 5h01m56.56s  Dec = -30d26m06.3s

    Mean    5.17029
    st dev  0.702962
                                       Flux units MJY/SR

    Flux integral      0.000142028   MJY
    Inside 2.747e-05 Steradian area
    (5186 pixels)

    Centroid                             RA = 5h02m21.86s  Dec = -30d36m26.0s


    Flux weighted centroid               RA = 5h02m21.09s  Dec = -30d36m21.9s

    vertex# 1  at RA = 5h02m48.90s  Dec = -30d47m52.3s

    vertex# 2  at RA = 5h01m28.56s  Dec = -30d42m06.5s

    vertex# 3  at RA = 5h01m55.41s  Dec = -30d25m06.2s
```

```
    vertex# 4  at RA = 5h03m14.37s  Dec = -30d30m36.0s

--------------------------------------------------

PGAI41502788.FITS  Sculptor

Centroid                              RA = 0h22m48.05s  Dec = -30d06m29.9s

DIRBE_ANNUAL,5.700208,-30.108306,0.
          1 pixel(s) will be taken
Band  Wavelength        Inu
   1     1.25      0.847+/- 0.006
   2     2.20      0.705+/- 0.003
   3     3.50      0.434+/- 0.004
   4     4.90      0.854+/- 0.018
   5    12.00     22.080+/- 0.258
   6    25.00     39.449+/- 0.309
   7    60.00     11.528+/- 0.052
   8   100.00      5.676+/- 0.033
   9   140.00      5.608+/- 2.110
  10   240.00      2.732+/- 1.042

DIRBE_ANNUAL,5.700208,-30.108306,1.5
         68 pixel(s) will be taken
Band  Wavelength        Inu
   1     1.25      0.309+/- 0.016
   2     2.20      0.209+/- 0.014
   3     3.50      0.169+/- 0.007
   4     4.90      0.780+/- 0.004
   5    12.00     22.099+/- 0.058
   6    25.00     39.449+/- 0.099
   7    60.00     11.516+/- 0.029
   8   100.00      5.691+/- 0.025
   9   140.00      4.146+/- 0.268
  10   240.00      2.469+/- 0.171

    Maximum 12.162    at RA = 0h22m12.17s  Dec = -30d07m44.6s
    Minimum 6.4858    at RA = 0h22m14.50s  Dec = -30d05m14.6s

    Mean    8.14927
    st dev  0.665113
                                      Flux units MJY/SR

    Flux integral      0.000415736   MJY
    Inside 5.1015e-05 Steradian area
    (9631 pixels)

    Centroid                              RA = 0h22m48.05s  Dec = -30d06m29.9s


    Flux weighted centroid                RA = 0h22m47.12s  Dec = -30d06m29.9s

    vertex# 1  at RA = 0h23m58.72s  Dec = -30d14m59.1s

    vertex# 2  at RA = 0h22m08.61s  Dec = -30d21m30.2s

    vertex# 3  at RA = 0h21m37.58s  Dec = -29d57m58.3s

    vertex# 4  at RA = 0h23m27.28s  Dec = -29d51m28.8s

--------------------------------------------------

PGAI09000606.FITS  HYDRA 33
```

```
Centroid                              RA = 13h15m03.53s  Dec = -42d37m05.9s

DIRBE_ANNUAL,198.764708,-42.618306,0.
           1 pixel(s) will be taken
Band  Wavelength        Inu
   1     1.25      0.556+/- 0.007
   2     2.20      0.403+/- 0.005
   3     3.50      0.246+/- 0.003
   4     4.90      0.662+/- 0.013
   5    12.00     18.154+/- 0.235
   6    25.00     32.745+/- 0.318
   7    60.00     11.262+/- 0.081
   8   100.00     11.258+/- 0.051
   9   140.00     16.268+/- 1.707
  10   240.00      9.597+/- 0.980

DIRBE_ANNUAL,198.764708,-42.618306,1.5
          71 pixel(s) will be taken
Band  Wavelength        Inu
   1     1.25      0.528+/- 0.028
   2     2.20      0.385+/- 0.037
   3     3.50      0.246+/- 0.024
   4     4.90      0.669+/- 0.015
   5    12.00     18.429+/- 0.034
   6    25.00     33.117+/- 0.057
   7    60.00     11.266+/- 0.024
   8   100.00     11.348+/- 0.113
   9   140.00     15.557+/- 0.263
  10   240.00     10.258+/- 0.226

    Maximum 21.029    at RA = 13h14m41.76s  Dec = -42d39m58.4s
    Minimum 7.65982    at RA = 13h15m11.68s  Dec = -42d32m43.2s

    Mean    11.7606
    st dev  1.62209
                                        Flux units MJY/SR

    Flux integral      9.00792e-05   MJY
    Inside 7.65941e-06 Steradian area
    (1446 pixels)

    Centroid                              RA = 13h15m03.53s  Dec = -42d37m05.9s


    Flux weighted centroid                RA = 13h15m03.83s  Dec = -42d37m11.9s

    vertex# 1  at RA = 13h15m40.24s  Dec = -42d36m13.0s

    vertex# 2  at RA = 13h15m07.62s  Dec = -42d43m43.7s

    vertex# 3  at RA = 13h14m26.80s  Dec = -42d37m58.1s

    vertex# 4  at RA = 13h14m59.46s  Dec = -42d30m28.1s

-----------------------------------------------------

PGAI08901904.FITS  HYDRA 34

Centroid                              RA = 13h25m05.95s  Dec = -20d13m48.9s

DIRBE_ANNUAL,201.274792,-20.230250,0.
           1 pixel(s) will be taken
Band  Wavelength        Inu
   1     1.25      0.429+/- 0.007
```

```
   2     2.20      0.306+/- 0.006
   3     3.50      0.226+/- 0.006
   4     4.90      0.883+/- 0.031
   5    12.00     29.669+/- 0.690
   6    25.00     57.076+/- 1.020
   7    60.00     19.543+/- 0.268
   8   100.00     13.598+/- 0.085
   9   140.00     15.077+/- 2.424
  10   240.00      7.571+/- 1.284

DIRBE_ANNUAL,201.274792,-20.230250,1.5
          68 pixel(s) will be taken
Band  Wavelength        Inu
   1     1.25      0.431+/- 0.005
   2     2.20      0.296+/- 0.004
   3     3.50      0.220+/- 0.002
   4     4.90      0.886+/- 0.004
   5    12.00     29.378+/- 0.108
   6    25.00     55.828+/- 0.197
   7    60.00     19.203+/- 0.057
   8   100.00     13.271+/- 0.052
   9   140.00     13.002+/- 0.312
  10   240.00      8.737+/- 0.175

    Maximum 22.2889    at RA = 13h25m00.71s  Dec = -20d14m51.7s
    Minimum 11.5585    at RA = 13h25m09.24s  Dec = -20d14m21.7s

    Mean    15.1342
    st dev  2.32438
                                       Flux units MJY/SR

    Flux integral      3.42305e-05   MJY
    Inside 2.2618e-06 Steradian area
    (427 pixels)

    Centroid                              RA = 13h25m05.95s  Dec = -20d13m48.9s


    Flux weighted centroid                RA = 13h25m05.97s  Dec = -20d13m50.6s

    vertex# 1  at RA = 13h25m20.97s  Dec = -20d12m36.6s

    vertex# 2  at RA = 13h25m10.31s  Dec = -20d17m21.8s

    vertex# 3  at RA = 13h24m51.11s  Dec = -20d14m51.7s

    vertex# 4  at RA = 13h25m00.71s  Dec = -20d10m21.5s

-----------------------------------------------------

PGAI40100614.FITS  North_1

Centroid                             RA = 20h32m43.90s  Dec =  65d19m49.5s

DIRBE_ANNUAL,308.182917,65.330417,0.
           1 pixel(s) will be taken
Band  Wavelength        Inu
   1     1.25      0.624+/- 0.002
   2     2.20      0.487+/- 0.003
   3     3.50      0.297+/- 0.002
   4     4.90      0.576+/- 0.004
   5    12.00     13.359+/- 0.071
   6    25.00     22.822+/- 0.103
   7    60.00      8.065+/- 0.031
```

```
   8   100.00     13.319+/- 0.037
   9   140.00     30.829+/- 1.434
  10   240.00     29.233+/- 0.813

DIRBE_ANNUAL,308.182917,65.330417,1.5
          69 pixel(s) will be taken
Band  Wavelength        Inu
   1     1.25      0.465+/- 0.010
   2     2.20      0.344+/- 0.009
   3     3.50      0.224+/- 0.005
   4     4.90      0.540+/- 0.002
   5    12.00     13.289+/- 0.014
   6    25.00     22.663+/- 0.019
   7    60.00      8.075+/- 0.035
   8   100.00     12.744+/- 0.134
   9   140.00     24.445+/- 0.352
  10   240.00     21.688+/- 0.334

    Maximum 23.0801    at RA = 20h33m11.45s  Dec =  65d18m04.3s
    Minimum 10.1109    at RA = 20h32m30.55s  Dec =  65d37m35.3s

    Mean    14.6835
    st dev  1.7724
                                       Flux units MJY/SR

    Flux integral      0.000998357   MJY
    Inside 6.79918e-05 Steradian area
    (12836 pixels)

    Centroid                              RA = 20h32m43.90s  Dec =  65d19m49.5s


    Flux weighted centroid                RA = 20h32m40.71s  Dec =  65d19m41.6s

    vertex# 1  at RA = 20h35m52.56s  Dec =  65d23m27.5s

    vertex# 2  at RA = 20h33m18.26s  Dec =  65d00m03.4s

    vertex# 3  at RA = 20h29m36.14s  Dec =  65d15m57.0s

    vertex# 4  at RA = 20h32m08.68s  Dec =  65d39m35.2s

-----------------------------------------------------

PGAI87001338.FITS  S2_C90_A

Centroid                             RA = 5h02m23.90s  Dec = -30d36m02.9s

DIRBE_ANNUAL,75.599583,-30.600806,0.
           1 pixel(s) will be taken
Band  Wavelength        Inu
   1     1.25      0.239+/- 0.002
   2     2.20      0.165+/- 0.001
   3     3.50      0.125+/- 0.001
   4     4.90      0.523+/- 0.006
   5    12.00     14.310+/- 0.103
   6    25.00     25.045+/- 0.133
   7    60.00      7.079+/- 0.028
   8   100.00      3.586+/- 0.022
   9   140.00      4.000+/- 1.567
  10   240.00      3.738+/- 0.818

DIRBE_ANNUAL,75.599583,-30.600806,1.5
          67 pixel(s) will be taken
```

```
Band  Wavelength        Inu
   1     1.25      0.247+/- 0.012
   2     2.20      0.169+/- 0.009
   3     3.50      0.128+/- 0.004
   4     4.90      0.527+/- 0.002
   5    12.00     14.270+/- 0.019
   6    25.00     25.011+/- 0.032
   7    60.00      7.084+/- 0.007
   8   100.00      3.667+/- 0.010
   9   140.00      3.274+/- 0.183
  10   240.00      2.374+/- 0.107

    Maximum 16.2234    at RA = 5h01m38.59s  Dec = -30d41m59.8s
    Minimum 3.89408    at RA = 5h01m44.48s  Dec = -30d31m44.4s

    Mean    5.28525
    st dev  0.809375
                                       Flux units MJY/SR

    Flux integral      0.000155096   MJY
    Inside 2.93452e-05 Steradian area
    (5540 pixels)

    Centroid                              RA = 5h02m23.90s  Dec = -30d36m02.9s


    Flux weighted centroid                RA = 5h02m22.43s  Dec = -30d35m58.2s

    vertex# 1  at RA = 5h02m51.95s  Dec = -30d47m45.4s

    vertex# 2  at RA = 5h01m28.12s  Dec = -30d41m29.5s

    vertex# 3  at RA = 5h01m56.14s  Dec = -30d24m14.3s

    vertex# 4  at RA = 5h03m19.75s  Dec = -30d30m44.0s

-----------------------------------------------------

PGAI57501902.FITS  0016+16

Centroid                             RA = 0h18m33.63s  Dec =  16d25m36.6s

DIRBE_ANNUAL,4.640125,16.426833,0.
          1 pixel(s) will be taken
Band  Wavelength        Inu
   1     1.25      0.454+/- 0.006
   2     2.20      0.299+/- 0.005
   3     3.50      0.230+/- 0.005
   4     4.90      1.041+/- 0.031
   5    12.00     30.550+/- 0.611
   6    25.00     55.904+/- 0.877
   7    60.00     17.532+/- 0.225
   8   100.00      9.745+/- 0.085
   9   140.00      5.338+/- 2.150
  10   240.00      4.588+/- 1.189

DIRBE_ANNUAL,4.640125,16.426833,1.5
          70 pixel(s) will be taken
Band  Wavelength        Inu
   1     1.25      0.399+/- 0.005
   2     2.20      0.266+/- 0.003
   3     3.50      0.213+/- 0.002
   4     4.90      0.994+/- 0.003
   5    12.00     30.430+/- 0.086
```

```
   6    25.00     55.737+/- 0.163
   7    60.00     17.511+/- 0.066
   8   100.00      9.634+/- 0.039
   9   140.00      8.765+/- 0.266
  10   240.00      5.651+/- 0.152

    Maximum 14.8464    at RA = 0h18m47.15s  Dec =  16d27m24.3s
    Minimum 10.2733    at RA = 0h18m05.41s  Dec =  16d27m09.2s

    Mean    12.1408
    st dev  0.717318
                                       Flux units MJY/SR

    Flux integral      0.000139808   MJY
    Inside 1.15156e-05 Steradian area
    (2174 pixels)

    Centroid                              RA = 0h18m33.63s  Dec =  16d25m36.6s


    Flux weighted centroid                RA = 0h18m33.87s  Dec =  16d25m40.4s

    vertex# 1  at RA = 0h19m04.88s  Dec =  16d22m09.0s

    vertex# 2  at RA = 0h18m18.99s  Dec =  16d18m08.9s

    vertex# 3  at RA = 0h18m02.28s  Dec =  16d28m54.3s

    vertex# 4  at RA = 0h18m48.20s  Dec =  16d33m09.6s

-----------------------------------------------------

PGAI52700514.FITS  NGC5907N

Centroid                              RA = 15h15m22.28s  Dec =  56d28m52.5s

DIRBE_ANNUAL,228.842833,56.48125,0.
          1 pixel(s) will be taken
Band  Wavelength        Inu
   1     1.25      0.194+/- 0.001
   2     2.20      0.132+/- 0.001
   3     3.50      0.100+/- 0.001
   4     4.90      0.423+/- 0.002
   5    12.00     12.393+/- 0.023
   6    25.00     22.010+/- 0.037
   7    60.00      6.324+/- 0.023
   8   100.00      3.685+/- 0.021
   9   140.00      3.823+/- 1.287
  10   240.00      2.442+/- 0.750

DIRBE_ANNUAL,228.842833,56.48125,1.5
         67 pixel(s) will be taken
Band  Wavelength        Inu
   1     1.25      0.205+/- 0.004
   2     2.20      0.136+/- 0.003
   3     3.50      0.102+/- 0.002
   4     4.90      0.422+/- 0.001
   5    12.00     12.372+/- 0.007
   6    25.00     21.926+/- 0.011
   7    60.00      6.244+/- 0.006
   8   100.00      3.383+/- 0.014
   9   140.00      3.203+/- 0.157
  10   240.00      2.276+/- 0.075
```

```
    Maximum 12.0669    at RA = 15h15m43.37s  Dec =  56d22m27.7s
    Minimum 3.27946    at RA = 15h16m08.74s  Dec =  56d25m27.4s

    Mean    4.44318
    st dev  0.565939
                                      Flux units MJY/SR

    Flux integral      3.76566e-05   MJY
    Inside 8.47514e-06 Steradian area
    (1600 pixels)

    Centroid                             RA = 15h15m22.28s  Dec =  56d28m52.5s


    Flux weighted centroid               RA = 15h15m22.20s  Dec =  56d28m46.9s

    vertex# 1  at RA = 15h16m12.35s  Dec =  56d24m57.3s

    vertex# 2  at RA = 15h15m28.91s  Dec =  56d20m57.8s

    vertex# 3  at RA = 15h14m32.66s  Dec =  56d32m57.7s

    vertex# 4  at RA = 15h15m14.41s  Dec =  56d36m43.5s

-----------------------------------------------------

PGAI60002009.FITS

Centroid                             RA = 0h43m49.47s  Dec = -74d13m59.7s

DIRBE_ANNUAL,10.956125,-74.23325,0.
          1 pixel(s) will be taken
Band  Wavelength        Inu
   1     1.25      0.363+/- 0.002
   2     2.20      0.251+/- 0.001
   3     3.50      0.178+/- 0.001
   4     4.90      0.572+/- 0.005
   5    12.00     13.574+/- 0.042
   6    25.00     22.958+/- 0.041
   7    60.00      6.788+/- 0.016
   8   100.00      5.167+/- 0.019
   9   140.00      6.568+/- 0.999
  10   240.00      4.829+/- 0.601

DIRBE_ANNUAL,10.956125,-74.23325,1.5
         69 pixel(s) will be taken
Band  Wavelength        Inu
   1     1.25      0.428+/- 0.026
   2     2.20      0.311+/- 0.021
   3     3.50      0.207+/- 0.011
   4     4.90      0.582+/- 0.006
   5    12.00     13.523+/- 0.017
   6    25.00     22.994+/- 0.027
   7    60.00      6.680+/- 0.377
   8   100.00      5.122+/- 0.788
   9   140.00      6.957+/- 0.852
  10   240.00      4.819+/- 0.518

    Maximum 10.6302    at RA = 0h46m33.74s  Dec = -74d16m11.1s
    Minimum 5.67855    at RA = 0h41m33.58s  Dec = -74d24m12.5s

    Mean    7.06287
    st dev  0.795898
                                      Flux units MJY/SR
```

```
    Flux integral      0.000299668   MJY
    Inside 4.24287e-05 Steradian area
    (8010 pixels)

    Centroid                              RA = 0h43m49.47s  Dec = -74d13m59.7s


    Flux weighted centroid                RA = 0h43m56.32s  Dec = -74d13m55.3s

    vertex# 1  at RA = 0h46m38.99s  Dec = -74d25m11.3s

    vertex# 2  at RA = 0h40m59.90s  Dec = -74d25m11.1s

    vertex# 3  at RA = 0h41m07.47s  Dec = -74d02m40.3s

    vertex# 4  at RA = 0h46m35.14s  Dec = -74d02m40.3s

--------------------------------------------------

PGAI50000124.FITS  N2_2

Centroid                              RA = 16h34m17.46s  Dec =  40d47m35.6s

DIRBE_ANNUAL,248.57275,40.793222,0.
           1 pixel(s) will be taken
Band  Wavelength        Inu
   1     1.25      0.246+/- 0.002
   2     2.20      0.164+/- 0.001
   3     3.50      0.118+/- 0.001
   4     4.90      0.494+/- 0.006
   5    12.00     13.520+/- 0.086
   6    25.00     23.665+/- 0.100
   7    60.00      6.641+/- 0.027
   8   100.00      3.332+/- 0.020
   9   140.00      3.123+/- 1.241
  10   240.00      0.895+/- 0.721

DIRBE_ANNUAL,248.57275,40.793222,1.5
          69 pixel(s) will be taken
Band  Wavelength        Inu
   1     1.25      0.244+/- 0.445
   2     2.20      0.165+/- 0.494
   3     3.50      0.121+/- 0.275
   4     4.90      0.481+/- 0.122
   5    12.00     13.395+/- 0.043
   6    25.00     23.552+/- 0.028
   7    60.00      6.662+/- 0.008
   8   100.00      3.388+/- 0.010
   9   140.00      2.910+/- 0.165
  10   240.00      1.782+/- 0.100

    Maximum 9.15391    at RA = 16h35m47.05s  Dec =  40d55m25.8s
    Minimum 2.83099    at RA = 16h35m20.42s  Dec =  40d46m26.5s

    Mean    4.76072
    st dev  0.658141
                                       Flux units MJY/SR

    Flux integral      0.000422492   MJY
    Inside 8.87453e-05 Steradian area
    (16754 pixels)

    Centroid                              RA = 16h34m17.46s  Dec =  40d47m35.6s
```

```
    Flux weighted centroid               RA = 16h34m20.27s  Dec =  40d47m46.6s

    vertex# 1  at RA = 16h36m25.12s  Dec =  40d44m38.1s

    vertex# 2  at RA = 16h33m02.02s  Dec =  40d27m40.1s

    vertex# 3  at RA = 16h32m08.67s  Dec =  40d50m23.2s

    vertex# 4  at RA = 16h35m35.36s  Dec =  41d07m26.9s

--------------------------------------------------

PGAI50100273.FITS  N2_5

Centroid                             RA = 16h38m47.41s  Dec =  42d01m05.6s

DIRBE_ANNUAL,249.697542,42.018222,0.
          1 pixel(s) will be taken
Band  Wavelength        Inu
   1     1.25      0.278+/- 0.002
   2     2.20      0.195+/- 0.002
   3     3.50      0.135+/- 0.001
   4     4.90      0.476+/- 0.006
   5    12.00     13.216+/- 0.083
   6    25.00     23.201+/- 0.100
   7    60.00      6.557+/- 0.028
   8   100.00      3.468+/- 0.021
   9   140.00      2.002+/- 1.364
  10   240.00      3.021+/- 0.746

DIRBE_ANNUAL,249.697542,42.018222,1.5
         69 pixel(s) will be taken
Band  Wavelength        Inu
   1     1.25      0.263+/- 0.040
   2     2.20      0.181+/- 0.041
   3     3.50      0.129+/- 0.022
   4     4.90      0.479+/- 0.010
   5    12.00     13.144+/- 0.024
   6    25.00     23.189+/- 0.031
   7    60.00      6.592+/- 0.006
   8   100.00      3.421+/- 0.011
   9   140.00      3.189+/- 0.161
  10   240.00      2.013+/- 0.092

    Maximum 12.8423    at RA = 16h38m15.52s  Dec =  41d56m32.4s
    Minimum 3.71058    at RA = 16h37m56.65s  Dec =  41d59m02.1s

    Mean    5.818
    st dev  0.494335
                                       Flux units MJY/SR

    Flux integral      0.000505133   MJY
    Inside 8.68225e-05 Steradian area
    (16391 pixels)

    Centroid                             RA = 16h38m47.41s  Dec =  42d01m05.6s


    Flux weighted centroid               RA = 16h38m50.20s  Dec =  42d01m20.3s

    vertex# 1  at RA = 16h40m58.39s  Dec =  41d58m43.2s
```

```
    vertex# 2  at RA = 16h37m31.42s  Dec =  41d41m15.4s

    vertex# 3  at RA = 16h36m37.06s  Dec =  42d03m28.4s

    vertex# 4  at RA = 16h40m03.64s  Dec =  42d20m47.3s

--------------------------------------------------

PGAI20701079.FITS  GF9-I6

Centroid                              RA = 20h47m58.34s  Dec =  60d04m21.2s

DIRBE_ANNUAL,311.993083,60.072556,0.
          1 pixel(s) will be taken
Band  Wavelength        Inu
   1     1.25      0.606+/- 0.002
   2     2.20      0.478+/- 0.002
   3     3.50      0.310+/- 0.001
   4     4.90      0.621+/- 0.005
   5    12.00     14.313+/- 0.078
   6    25.00     23.911+/- 0.108
   7    60.00     10.394+/- 0.031
   8   100.00     22.779+/- 0.040
   9   140.00     52.200+/- 1.250
  10   240.00     48.678+/- 0.713

DIRBE_ANNUAL,311.993083,60.072556,1.5
         66 pixel(s) will be taken
Band  Wavelength        Inu
   1     1.25      0.638+/- 0.023
   2     2.20      0.510+/- 0.024
   3     3.50      0.338+/- 0.013
   4     4.90      0.641+/- 0.007
   5    12.00     14.243+/- 0.043
   6    25.00     23.799+/- 0.048
   7    60.00     10.339+/- 0.165
   8   100.00     21.675+/- 0.689
   9   140.00     47.408+/- 1.734
  10   240.00     41.204+/- 1.435

    Maximum 124.296    at RA = 20h47m55.33s  Dec =  60d04m13.7s
    Minimum 20.237    at RA = 20h48m21.44s  Dec =  60d06m58.7s

    Mean    25.5909
    st dev  13.177
                                       Flux units MJY/SR

    Flux integral      8.45856e-05   MJY
    Inside 3.3053e-06 Steradian area
    (624 pixels)

    Centroid                              RA = 20h47m58.34s  Dec =  60d04m21.2s


    Flux weighted centroid                RA = 20h47m57.92s  Dec =  60d04m21.0s

    vertex# 1  at RA = 20h48m21.36s  Dec =  60d00m58.4s

    vertex# 2  at RA = 20h47m33.30s  Dec =  60d00m58.4s

    vertex# 3  at RA = 20h47m33.22s  Dec =  60d07m43.7s

    vertex# 4  at RA = 20h48m23.45s  Dec =  60d07m28.7s
```

```
-----------------------------------------------------

PGAI20800709.FITS  LHE1

Centroid                              RA = 10h50m55.61s  Dec =  57d32m46.8s

DIRBE_ANNUAL,162.731708,57.546333,0.
          1 pixel(s) will be taken
Band  Wavelength        Inu
   1     1.25      0.230+/- 0.003
   2     2.20      0.161+/- 0.003
   3     3.50      0.121+/- 0.002
   4     4.90      0.522+/- 0.009
   5    12.00     15.562+/- 0.115
   6    25.00     28.267+/- 0.124
   7    60.00      8.205+/- 0.023
   8   100.00      3.954+/- 0.026
   9   140.00      3.526+/- 1.637
  10   240.00      1.836+/- 0.979

DIRBE_ANNUAL,162.731708,57.546333,1.5
         67 pixel(s) will be taken
Band  Wavelength        Inu
   1     1.25      0.260+/- 0.017
   2     2.20      0.176+/- 0.014
   3     3.50      0.130+/- 0.007
   4     4.90      0.519+/- 0.004
   5    12.00     15.597+/- 0.025
   6    25.00     28.332+/- 0.043
   7    60.00      8.212+/- 0.013
   8   100.00      3.872+/- 0.009
   9   140.00      2.921+/- 0.225
  10   240.00      1.874+/- 0.108

    Maximum 6.94697    at RA = 10h49m48.60s  Dec =  57d42m32.0s
    Minimum 4.68144    at RA = 10h52m00.99s  Dec =  57d21m46.0s

    Mean    5.76925
    st dev  0.238202
                                      Flux units MJY/SR

    Flux integral      0.000201326   MJY
    Inside 3.48964e-05 Steradian area
    (6588 pixels)

    Centroid                             RA = 10h50m55.61s  Dec =  57d32m46.8s


    Flux weighted centroid               RA = 10h50m55.33s  Dec =  57d32m49.1s

    vertex# 1  at RA = 10h52m02.84s  Dec =  57d21m31.0s

    vertex# 2  at RA = 10h49m32.46s  Dec =  57d23m45.5s

    vertex# 3  at RA = 10h49m48.56s  Dec =  57d44m02.0s

    vertex# 4  at RA = 10h52m18.44s  Dec =  57d41m46.4s

-----------------------------------------------------

PGAI86800640.FITS  S2_C90_B

Centroid                              RA = 5h02m25.47s  Dec = -30d36m22.7s
```

```
DIRBE_ANNUAL,75.606125,-30.606306,0.
           1 pixel(s) will be taken
Band  Wavelength        Inu
   1     1.25      0.239+/- 0.002
   2     2.20      0.165+/- 0.001
   3     3.50      0.125+/- 0.001
   4     4.90      0.523+/- 0.006
   5    12.00     14.310+/- 0.103
   6    25.00     25.045+/- 0.133
   7    60.00      7.079+/- 0.028
   8   100.00      3.586+/- 0.022
   9   140.00      4.000+/- 1.567
  10   240.00      3.738+/- 0.818

DIRBE_ANNUAL,75.606125,-30.606306,1.5
          67 pixel(s) will be taken
Band  Wavelength        Inu
   1     1.25      0.247+/- 0.012
   2     2.20      0.169+/- 0.009
   3     3.50      0.128+/- 0.004
   4     4.90      0.527+/- 0.002
   5    12.00     14.270+/- 0.019
   6    25.00     25.011+/- 0.032
   7    60.00      7.084+/- 0.007
   8   100.00      3.667+/- 0.010
   9   140.00      3.274+/- 0.183
  10   240.00      2.374+/- 0.107

    Maximum 9.95129    at RA = 5h02m17.57s  Dec = -30d27m08.6s
    Minimum 4.35471    at RA = 5h02m46.62s  Dec = -30d33m38.8s

    Mean    5.74624
    st dev  0.554322
                                       Flux units MJY/SR

    Flux integral      0.000169964   MJY
    Inside 2.95782e-05 Steradian area
    (5584 pixels)

    Centroid                              RA = 5h02m25.47s  Dec = -30d36m22.7s


    Flux weighted centroid                RA = 5h02m24.47s  Dec = -30d36m17.4s

    vertex# 1  at RA = 5h02m51.33s  Dec = -30d48m24.4s

    vertex# 2  at RA = 5h01m32.15s  Dec = -30d42m53.6s

    vertex# 3  at RA = 5h01m59.01s  Dec = -30d24m23.3s

    vertex# 4  at RA = 5h03m19.13s  Dec = -30d29m53.0s

-----------------------------------------------------

PGAI10101158.FITS  L134_C100

Centroid                             RA = 15h53m46.18s  Dec = -4d31m20.5s

DIRBE_ANNUAL,238.442417,-4.522361,0.
           1 pixel(s) will be taken
Band  Wavelength        Inu
   1     1.25      0.546+/- 0.006
   2     2.20      0.387+/- 0.005
   3     3.50      0.275+/- 0.005
```

```
   4     4.90      0.839+/- 0.026
   5    12.00     27.186+/- 0.518
   6    25.00     51.374+/- 0.743
   7    60.00     17.904+/- 0.179
   8   100.00     21.016+/- 0.080
   9   140.00     45.483+/- 1.921
  10   240.00     45.161+/- 1.208

DIRBE_ANNUAL,238.442417,-4.522361,1.5
          69 pixel(s) will be taken
Band  Wavelength        Inu
   1     1.25      0.472+/- 0.019
   2     2.20      0.324+/- 0.023
   3     3.50      0.246+/- 0.013
   4     4.90      0.892+/- 0.006
   5    12.00     27.865+/- 0.091
   6    25.00     51.924+/- 0.161
   7    60.00     17.780+/- 0.044
   8   100.00     16.521+/- 0.244
   9   140.00     26.370+/- 0.917
  10   240.00     21.606+/- 1.030

    Maximum 48.234    at RA = 15h53m48.19s  Dec = -4d37m35.8s
    Minimum 18.2412    at RA = 15h54m17.30s  Dec = -4d27m35.2s

    Mean    30.7034
    st dev  5.35967
                                       Flux units MJY/SR

    Flux integral      0.000525799   MJY
    Inside 1.71251e-05 Steradian area
    (3233 pixels)

    Centroid                              RA = 15h53m46.18s  Dec = -4d31m20.5s


    Flux weighted centroid                RA = 15h53m46.38s  Dec = -4d31m48.7s

    vertex# 1  at RA = 15h54m19.30s  Dec = -4d25m35.1s

    vertex# 2  at RA = 15h54m09.27s  Dec = -4d39m35.8s

    vertex# 3  at RA = 15h53m13.04s  Dec = -4d37m05.7s

    vertex# 4  at RA = 15h53m23.09s  Dec = -4d23m05.0s

-----------------------------------------------------

PGAI79401149.FITS  L1166

Centroid                             RA = 22h05m25.81s  Dec =  59d33m33.8s

DIRBE_ANNUAL,331.357542,59.559389,0.
           1 pixel(s) will be taken
Band  Wavelength        Inu
   1     1.25      1.521+/- 0.005
   2     2.20      1.645+/- 0.007
   3     3.50      1.137+/- 0.005
   4     4.90      1.159+/- 0.007
   5    12.00     16.401+/- 0.095
   6    25.00     26.611+/- 0.130
   7    60.00     17.458+/- 0.057
   8   100.00     40.598+/- 0.119
   9   140.00     86.798+/- 1.197
```

```
  10   240.00     76.104+/- 0.728

DIRBE_ANNUAL,331.357542,59.559389,1.5
          68 pixel(s) will be taken
Band  Wavelength        Inu
   1     1.25      1.245+/- 0.098
   2     2.20      1.222+/- 0.075
   3     3.50      0.824+/- 0.044
   4     4.90      0.967+/- 0.021
   5    12.00     16.346+/- 0.071
   6    25.00     26.619+/- 0.124
   7    60.00     16.748+/- 0.847
   8   100.00     42.948+/- 1.837
   9   140.00    103.221+/- 3.433
  10   240.00     91.214+/- 2.619

    Maximum 52.7776    at RA = 22h05m36.96s  Dec =  59d32m02.9s
    Minimum 36.4751    at RA = 22h04m55.51s  Dec =  59d31m47.7s

    Mean    44.2355
    st dev  3.41736
                                       Flux units MJY/SR

    Flux integral      0.000227753   MJY
    Inside 5.14865e-06 Steradian area
    (972 pixels)

    Centroid                              RA = 22h05m25.81s  Dec =  59d33m33.8s


    Flux weighted centroid                RA = 22h05m26.14s  Dec =  59d33m31.6s

    vertex# 1  at RA = 22h06m08.60s  Dec =  59d35m02.6s

    vertex# 2  at RA = 22h05m36.93s  Dec =  59d28m17.7s

    vertex# 3  at RA = 22h04m43.66s  Dec =  59d32m02.5s

    vertex# 4  at RA = 22h05m13.23s  Dec =  59d38m48.2s

-----------------------------------------------------

PGAI44900714.FITS  Rho_Oph_Ma

Centroid                             RA = 16h27m48.26s  Dec = -24d25m49.9s

DIRBE_ANNUAL,246.951083,-24.430528,0.
           1 pixel(s) will be taken
Band  Wavelength        Inu
   1     1.25      0.990+/- 0.010
   2     2.20      1.075+/- 0.010
   3     3.50      1.620+/- 0.026
   4     4.90      2.502+/- 0.048
   5    12.00     49.918+/- 0.983
   6    25.00     89.950+/- 1.516
   7    60.00    208.110+/- 4.904
   8   100.00    440.087+/- 9.461
   9   140.00    762.011+/-11.059
  10   240.00    494.475+/- 5.768

DIRBE_ANNUAL,246.951083,-24.430528,1.5
          66 pixel(s) will be taken
Band  Wavelength        Inu
   1     1.25      1.046+/- 0.032
```

```
   2     2.20      0.837+/- 0.027
   3     3.50      0.769+/- 0.051
   4     4.90      1.380+/- 0.048
   5    12.00     38.754+/- 0.563
   6    25.00     72.208+/- 0.822
   7    60.00     61.106+/- 7.618
   8   100.00    134.640+/-14.844
   9   140.00    248.798+/-21.758
  10   240.00    152.600+/-11.963

    Maximum 6141.14    at RA = 16h26m34.66s  Dec = -24d24m38.6s
    Minimum -1    at RA = 16h26m31.36s  Dec = -24d24m23.5s

    Mean    387.67
    st dev  492.398
                                       Flux units MJY/SR

    Flux integral      0.0588422   MJY
    Inside 0.000151784 Steradian area
    (28655 pixels)

    Centroid                              RA = 16h27m48.26s  Dec = -24d25m49.9s


    Flux weighted centroid                RA = 16h27m05.43s  Dec = -24d26m42.3s

    vertex# 1  at RA = 16h29m07.69s  Dec = -24d49m39.6s

    vertex# 2  at RA = 16h26m01.42s  Dec = -24d43m38.3s

    vertex# 3  at RA = 16h26m30.50s  Dec = -24d01m52.4s

    vertex# 4  at RA = 16h29m33.57s  Dec = -24d07m51.7s

-----------------------------------------------------

PGAI15601578.FITS  OPT_IR4

Centroid                             RA = 18h11m45.79s  Dec =  44d29m11.5s

DIRBE_ANNUAL,272.940792,44.486528,0.
          1 pixel(s) will be taken
Band  Wavelength        Inu
   1     1.25      0.429+/- 0.002
   2     2.20      0.297+/- 0.001
   3     3.50      0.185+/- 0.001
   4     4.90      0.525+/- 0.006
   5    12.00     13.203+/- 0.088
   6    25.00     22.915+/- 0.110
   7    60.00      6.938+/- 0.029
   8   100.00      6.062+/- 0.026
   9   140.00      6.422+/- 1.250
  10   240.00      5.853+/- 0.723

DIRBE_ANNUAL,272.940792,44.486528,1.5
          70 pixel(s) will be taken
Band  Wavelength        Inu
   1     1.25      0.338+/- 0.044
   2     2.20      0.236+/- 0.041
   3     3.50      0.160+/- 0.022
   4     4.90      0.520+/- 0.010
   5    12.00     13.227+/- 0.024
   6    25.00     22.872+/- 0.032
   7    60.00      6.815+/- 0.016
```

```
   8   100.00      5.081+/- 0.059
   9   140.00      6.148+/- 0.194
  10   240.00      4.469+/- 0.113

    Maximum 36.8875    at RA = 18h11m12.96s  Dec =  44d28m37.3s
    Minimum 7.29163    at RA = 18h12m24.53s  Dec =  44d31m52.3s

    Mean    17.3759
    st dev  5.63265
                                       Flux units MJY/SR

    Flux integral      0.000315695   MJY
    Inside 1.81686e-05 Steradian area
    (3430 pixels)

    Centroid                             RA = 18h11m45.79s  Dec =  44d29m11.5s


    Flux weighted centroid               RA = 18h11m40.41s  Dec =  44d28m32.2s

    vertex# 1  at RA = 18h12m41.28s  Dec =  44d26m06.6s

    vertex# 2  at RA = 18h11m27.04s  Dec =  44d19m22.1s

    vertex# 3  at RA = 18h10m50.46s  Dec =  44d32m06.9s

    vertex# 4  at RA = 18h12m03.51s  Dec =  44d39m08.0s

-----------------------------------------------------

PGAI27600420.FITS  TPN

Centroid                             RA = 12h44m53.62s  Dec = -78d48m32.7s

DIRBE_ANNUAL,191.223417,-78.809083,0.
          1 pixel(s) will be taken
Band  Wavelength        Inu
   1     1.25      0.495+/- 0.002
   2     2.20      0.371+/- 0.001
   3     3.50      0.238+/- 0.001
   4     4.90      0.543+/- 0.006
   5    12.00     13.189+/- 0.077
   6    25.00     22.725+/- 0.093
   7    60.00      8.005+/- 0.025
   8   100.00     12.117+/- 0.048
   9   140.00     25.119+/- 1.273
  10   240.00     23.700+/- 0.717

DIRBE_ANNUAL,191.223417,-78.809083,1.5
         68 pixel(s) will be taken
Band  Wavelength        Inu
   1     1.25      0.526+/- 0.010
   2     2.20      0.392+/- 0.011
   3     3.50      0.246+/- 0.006
   4     4.90      0.548+/- 0.003
   5    12.00     13.095+/- 0.018
   6    25.00     22.668+/- 0.023
   7    60.00      8.021+/- 0.039
   8   100.00     13.121+/- 0.306
   9   140.00     27.963+/- 0.959
  10   240.00     26.167+/- 1.166

    Maximum 20.4506    at RA = 12h44m19.24s  Dec = -78d47m37.9s
    Minimum 10.8302    at RA = 12h41m49.91s  Dec = -78d47m34.4s
```

```
    Mean    15.4067
    st dev  1.82526
                                        Flux units MJY/SR

    Flux integral      0.000268166   MJY
    Inside 1.74058e-05 Steradian area
    (3286 pixels)

    Centroid                              RA = 12h44m53.62s  Dec = -78d48m32.7s


    Flux weighted centroid                RA = 12h44m52.70s  Dec = -78d48m40.8s

    vertex# 1  at RA = 12h48m21.72s  Dec = -78d49m03.7s

    vertex# 2  at RA = 12h44m44.82s  Dec = -78d58m38.5s

    vertex# 3  at RA = 12h41m24.01s  Dec = -78d48m03.4s

    vertex# 4  at RA = 12h45m05.45s  Dec = -78d38m22.6s

-----------------------------------------------------

PGAI71901220.FITS  DC 303.8

Centroid                              RA = 13h07m02.02s  Dec = -77d01m06.2s

DIRBE_ANNUAL,196.758417,-77.018389,0.
           1 pixel(s) will be taken
Band  Wavelength        Inu
   1     1.25      1.433+/- 0.006
   2     2.20      1.808+/- 0.004
   3     3.50      1.130+/- 0.005
   4     4.90      1.013+/- 0.007
   5    12.00     13.587+/- 0.081
   6    25.00     23.208+/- 0.098
   7    60.00      8.725+/- 0.024
   8   100.00     16.021+/- 0.058
   9   140.00     35.395+/- 1.227
  10   240.00     31.551+/- 0.774

DIRBE_ANNUAL,196.758417,-77.018389,1.5
          69 pixel(s) will be taken
Band  Wavelength        Inu
   1     1.25      0.561+/- 0.029
   2     2.20      0.430+/- 0.041
   3     3.50      0.277+/- 0.024
   4     4.90      0.557+/- 0.013
   5    12.00     13.152+/- 0.020
   6    25.00     22.840+/- 0.022
   7    60.00      8.446+/- 0.041
   8   100.00     14.251+/- 0.308
   9   140.00     28.933+/- 1.171
  10   240.00     23.494+/- 1.526

    Maximum 102.275    at RA = 13h07m35.10s  Dec = -77d00m16.6s
    Minimum 13.5529    at RA = 13h07m21.98s  Dec = -77d10m47.2s

    Mean    18.4958
    st dev  4.34694
                                        Flux units MJY/SR

    Flux integral      0.000676492   MJY
```

```
    Inside 3.65755e-05 Steradian area
    (6905 pixels)

    Centroid                              RA = 13h07m02.02s  Dec = -77d01m06.2s


    Flux weighted centroid                RA = 13h07m01.71s  Dec = -77d01m09.4s

    vertex# 1  at RA = 13h11m07.39s  Dec = -76d55m54.4s

    vertex# 2  at RA = 13h08m39.14s  Dec = -77d14m46.3s

    vertex# 3  at RA = 13h02m52.92s  Dec = -77d05m54.5s

    vertex# 4  at RA = 13h05m27.58s  Dec = -76d47m30.0s

-----------------------------------------------------

PGAI33401134.FITS  RCRA

Centroid                             RA = 19h02m18.30s  Dec = -36d59m24.8s

DIRBE_ANNUAL,285.57625,-36.990222,0.
          1 pixel(s) will be taken
Band  Wavelength        Inu
   1     1.25      1.050+/- 0.012
   2     2.20      1.126+/- 0.013
   3     3.50      1.058+/- 0.012
   4     4.90      1.719+/- 0.028
   5    12.00     27.878+/- 0.504
   6    25.00     53.845+/- 0.691
   7    60.00     31.080+/- 0.340
   8   100.00     49.250+/- 0.768
   9   140.00     93.071+/- 2.599
  10   240.00     87.597+/- 1.552

DIRBE_ANNUAL,285.57625,-36.990222,1.5
         69 pixel(s) will be taken
Band  Wavelength        Inu
   1     1.25      0.923+/- 0.020
   2     2.20      0.665+/- 0.029
   3     3.50      0.411+/- 0.030
   4     4.90      0.889+/- 0.029
   5    12.00     26.239+/- 0.087
   6    25.00     49.926+/- 0.170
   7    60.00     17.395+/- 0.411
   8   100.00     14.180+/- 1.115
   9   140.00     19.452+/- 2.369
  10   240.00     14.787+/- 2.351

    Maximum 1314.93    at RA = 19h01m53.25s  Dec = -36d57m47.0s
    Minimum -1    at RA = 19h01m55.76s  Dec = -36d57m47.1s

    Mean    96.4417
    st dev  149.011
                                       Flux units MJY/SR

    Flux integral      0.00391208   MJY
    Inside 4.05641e-05 Steradian area
    (7658 pixels)

    Centroid                              RA = 19h02m18.30s  Dec = -36d59m24.8s
```

```
    Flux weighted centroid                RA = 19h01m58.78s  Dec = -36d57m09.9s

    vertex# 1  at RA = 19h03m13.56s  Dec = -37d10m17.0s

    vertex# 2  at RA = 19h01m30.56s  Dec = -37d11m47.3s

    vertex# 3  at RA = 19h01m23.30s  Dec = -36d48m31.0s

    vertex# 4  at RA = 19h03m05.79s  Dec = -36d47m01.1s

--------------------------------------------------
```

9.3.4 Absolute Surface Brightness Values of C200 Maps

- authors: U. Klaas
- date: 07-January-2000
- SVP period 2

Motivation

As part of the scientific validation of staring raster maps the consistency of the absolute sky brightness with COBE/DIRBE is verified. Since the map test cases cover a wide range in flux we can extend the assessment done on staring background measurements which are currently limited in flux range. The maps offer the advantage to get a comparable solid angle coverage with the COBE/DIRBE pixels.

Method

We compare the mean surface brightness derived with the SKYVIEW program for the maps used for the flat-field assessment (see Sect. 9.2.4) with the surface brightness values in the corresponding filters or adjacent filters of COBE/DIRBE. This time we use the full maps rather than a background area in order to have the best comparable beam size with COBE/DIRBE; however in most cases the solid angles of the ISOPHOT maps are still considearbly smaller than one pixel of COBE/DIRBE. We use the COBE/DIRBE annual maps (since at the wavelengths considered the contribution by Zodiacal Light is small) and determine the fluxes for the DIRBE pixel coincident with the map area centroid. Since the longest wavelength COBE/DIRBE filters (140 and 240 μm) have an internal uncertainty of 20 to 30 %, for a subsample of maps with low dynamic range we use as well the average fluxes of a 1.5 deg circular area, which gives a more robust photometry (this means averaging about 70 COBE/DIRBE pixels).

Results

In Table 9.6 we present the results of the comparison. Detailed data on the COBE/DIRBE spectra, as well as the flux assessment of the ISOPHOT maps using SKYVIEW are given in the evaluation log. It should be noted that neither colour correction with regard to a modified blackbody describing the sky background spectral energy distribution nor a wavelength correction to better match the COBE/DIRBE filter central wavelength with the ISOPHOT filter central wavelength has been performed (this may be done for a future scientific validation assesesment). Also, as already mentioned above, nearly all ISOPHOT maps are considerably smaller in area than the solid angle of one COBE/DIRBE pixel. Therefore, structures in the source or background can affect the resulting absolute flux. In case of a flat field the flux of the centered COBE/DIRBE pixel as well as the 3 deg cicular area average is listed to give an impression of the variation of the background (and also of the stability of the COBE/DIRBE measurement in one pixel). If the map contains a bright target and is smaller than the COBE/DIRBE pixel, then only the flux of the centered COBE/DIRBE pixel is given.
Taking into account the discrepancies in beam size and the non-correction for different central wavelengths of filters and background SEDs the general agreement is in the order of 20 to 30 %. Restricting the comparison to ISOPHOT maps with comparable solid angles with the COBE/DIRBE measurement, the consistency is confirmed to be better than 25 %. This holds for all filters and a surface brightness range between 3 (2.5) and 600 MJy sr^{-1}. Therefore, for the absolute accuracy this investigation extends the covered surface brightness range considerably beyond the one covered by the investigations performed on staring background observations (cf. Sect 7.3).
Larger deviations between the average ISOPHOT map flux and the COBE/DIRBE flux only occur for bright central sources which are compact in comparison with the COBE/DIRBE beam. In these cases the COBE/DIRBE fluxes are always less than the ISOPHOT fluxes.

Table 9.6: Consistency check of C200 map absolute surface brightness with COBE/DIRBE annual map photometry. The solid angle of one COBE/DIRBE pixel is 19.5 10^{-5} sr.

OLP product name	**filter** (μm)	**surface brightness** (MJy sr^{-1})	**solid angle** (10^{-5} sr)	**DIRBE flux** (MJy sr^{-1})	**DIRBE filter** (μm)	**solid angle** (10^{-5} sr)	**consistency** (%)
PGAI56200110	150	3.6	2.91	4.1	140	19.5	-13
PGAI56201814	150	22.2	0.42	20.9	140	19.5	+6.2
PGAI08900103	170	5.5	1.26	7.7	140	19.5	-29
PGAI79400434	170	3.2	3.15	2.2	140	19.5	+45
				2.9	140	215.3	+10
PGAI59300101	170	3.5	6.53	3.5	140	19.5	-1.4
				3.4	140	215.3	+4.2
PGAI19800208	170	3.2	3.41	5.0	140	19.5	-37
				3.3	140	215.3	-3.6
PGAI21001305	170	3.6	3.39	4.1	140	19.5	-12
				3.5	140	215.3	+3.4
PGAI79900733	170	6.0	0.50	7.0	140	19.5	-14
PGAI33600108	180	2.7	2.50	2.7	140	19.5	-2.6
				2.8	140	215.3	-4.0
PGAI33600705	180	4.7	2.55	5.7	140	19.5	-17
				5.7	140	215.3	-17
PGAI35100907	180	4.1	4.92	4.5	140	19.5	-8.2
PGAI16701206	180	15.0	4.11	12.7	140	19.5	+18
PGAI52700412	180	3.2	0.87	3.8	140	19.5	-16
				3.2	140	215.3	0
PGAI85001037	180	8.1	3.78	10.1	140	19.5	-19
				9.3	140	215.3	-13
PGAI78200101	200	6.3	28.40	5.3	240	34.45	+20
PGAI36803005	200	14.8	0.71	15.5	240	19.5	-4.5
				14.9	240	215.3	-0.9
PGAI39602213	200	36.2	6.22	29.2	240	19.5	+24
PGAI26101401	200	69.8	11.03	85.4	240	19.5	-18
PGAI33401133	200	138.6	3.89	87.6	240	19.5	+58
PGAI86101801	200	251.9	5.01	287.9	240	19.5	-13
PGAI15601577	200	11.4	1.38	5.9	240	19.5	+95
PGAI33300559	200	38.0	6.55	55.7	240	19.5	-32
PGAI10101157	200	69.7	1.41	45.2	240	19.5	+54
PGAI31000625	200	345.5	1.45	207.8	240	19.5	+66
PGAI26701013	200	593.3	15.49	494.5	240	19.5	+20
PGAI40900802	200	6.9	1.97	5.6	240	19.5	+23
PGAI28001303	200	13.0	2.00	12.8	240	19.5	+1.6

Conclusions

- The average surface brightness of ISOPHOT maps obtained with different raster parameters shows a consistency of better than ± 25 % with COBE/DIRBE 140 and 240 μm photometry. This may be improved taking into account color corrections and corrections for different central wavelengths of the ISOPHOT and COBE/DIRBE filters.
- This good correspondence is found for all the 4 considered C200 filters.
- This good correspondence holds for the flux range 3 (2.5) to 600 MJy sr^{-1} and extends the verified surface brightness range covered so far by single pointing background measurements considerably. The accuracy assessment is limited to the absolute surface brightness, since each map has its individual background measurement; no statement about the relative filter-to-filter calibration accuracy can be made from this program.

Evaluation Log

```
--------------------------------------------------

PGAI56200110.FITS  NGP_Dark

Centroid     RA = 13h42m36.94s  Dec =  40d25m56.6s

DIRBE_ANNUAL,205.653917,40.432389,0.

           1 pixel(s) will be taken
Band  Wavelength        Inu
   1     1.25      0.204+/- 0.001
   2     2.20      0.137+/- 0.001
   3     3.50      0.107+/- 0.001
   4     4.90      0.484+/- 0.006
   5    12.00     14.940+/- 0.069
   6    25.00     27.143+/- 0.063
   7    60.00      7.763+/- 0.026
   8   100.00      3.669+/- 0.025
   9   140.00      4.135+/- 1.509
  10   240.00      1.034+/- 0.877

DIRBE_ANNUAL,205.653917,40.432389,1.5

          71 pixel(s) will be taken
Band  Wavelength        Inu
   1     1.25      0.237+/- 0.043
   2     2.20      0.159+/- 0.063
   3     3.50      0.116+/- 0.041
   4     4.90      0.485+/- 0.026
   5    12.00     14.974+/- 0.020
   6    25.00     27.228+/- 0.031
   7    60.00      7.809+/- 0.012
   8   100.00      3.767+/- 0.009
   9   140.00      2.636+/- 0.189
  10   240.00      1.950+/- 0.109

flux assessment of ISOPHOT map, cf. chapter on C200 flat-field accuracy

--------------------------------------------------

PGAI56201814.FITS  Combipht

Centroid                              RA = 2h13m23.91s  Dec =  87d43m53.3s

DIRBE_ANNUAL,33.34963,87.73147,0.
           1 pixel(s) will be taken
Band  Wavelength        Inu
   1     1.25      0.273+/- 0.001
   2     2.20      0.178+/- 0.001
   3     3.50      0.136+/- 0.001
   4     4.90      0.524+/- 0.004
   5    12.00     13.840+/- 0.046
   6    25.00     23.683+/- 0.060
   7    60.00      7.518+/- 0.021
   8   100.00     10.744+/- 0.031
   9   140.00     20.919+/- 1.266
  10   240.00     23.610+/- 0.761

DIRBE_ANNUAL,33.34963,87.73147,1.5
          66 pixel(s) will be taken
Band  Wavelength        Inu
   1     1.25      0.305+/- 0.085
```

```
   2     2.20      0.210+/- 0.044
   3     3.50      0.155+/- 0.021
   4     4.90      0.534+/- 0.011
   5    12.00     13.788+/- 0.019
   6    25.00     23.554+/- 0.027
   7    60.00      7.372+/- 0.023
   8   100.00      8.757+/- 0.178
   9   140.00     17.748+/- 0.538
  10   240.00     16.824+/- 0.622

flux assessment of ISOPHOT map, cf. chapter on C200 flat-field accuracy

--------------------------------------------------

PGAI08900103.FITS  A2256

Centroid                              RA = 17h02m48.63s  Dec =  78d42m47.0s

DIRBE_ANNUAL,255.702625,78.713056,0.
          1 pixel(s) will be taken
Band  Wavelength        Inu
   1     1.25      0.291+/- 0.001
   2     2.20      0.205+/- 0.001
   3     3.50      0.140+/- 0.001
   4     4.90      0.452+/- 0.002
   5    12.00     12.342+/- 0.024
   6    25.00     21.567+/- 0.053
   7    60.00      6.472+/- 0.029
   8   100.00      5.103+/- 0.033
   9   140.00      7.674+/- 1.474
  10   240.00      3.669+/- 0.935

    Maximum 6.97234    at RA = 17h01m25.83s  Dec =  78d44m55.5s
    Minimum 4.25031    at RA = 17h02m02.18s  Dec =  78d38m55.7s

    Mean    5.45381
    st dev  0.669521
                                      Flux units MJY/SR

    Flux integral      6.85527e-05   MJY
    Inside 1.25697e-05 Steradian area
    (2373 pixels)

    Centroid                             RA = 17h02m48.63s  Dec =  78d42m47.0s


    Flux weighted centroid               RA = 17h02m48.31s  Dec =  78d42m57.2s

    vertex# 1  at RA = 17h05m32.39s  Dec =  78d46m23.7s

    vertex# 2  at RA = 17h03m58.75s  Dec =  78d34m55.4s

    vertex# 3  at RA = 17h00m05.12s  Dec =  78d39m23.1s

    vertex# 4  at RA = 17h01m35.46s  Dec =  78d50m25.9s

--------------------------------------------------

PGAI79400434.FITS  N2_175_8_I

Centroid                              RA = 16h36m55.72s  Dec =  40d53m21.3s

DIRBE_ANNUAL,249.232167,40.88925,0.
          1 pixel(s) will be taken
```

```
Band  Wavelength        Inu
   1     1.25      0.272+/- 0.001
   2     2.20      0.180+/- 0.001
   3     3.50      0.129+/- 0.001
   4     4.90      0.487+/- 0.006
   5    12.00     13.422+/- 0.084
   6    25.00     23.557+/- 0.097
   7    60.00      6.633+/- 0.027
   8   100.00      3.311+/- 0.019
   9   140.00      2.152+/- 1.219
  10   240.00      2.651+/- 0.695

DIRBE_ANNUAL,249.232167,40.88925,1.5
          69 pixel(s) will be taken
Band  Wavelength        Inu
   1     1.25      0.244+/- 0.009
   2     2.20      0.165+/- 0.008
   3     3.50      0.121+/- 0.006
   4     4.90      0.481+/- 0.002
   5    12.00     13.383+/- 0.015
   6    25.00     23.504+/- 0.023
   7    60.00      6.657+/- 0.008
   8   100.00      3.412+/- 0.010
   9   140.00      2.885+/- 0.168
  10   240.00      1.808+/- 0.094

    Maximum 7.18101    at RA = 16h37m28.79s  Dec =  40d52m03.5s
    Minimum 2.56497    at RA = 16h36m13.28s  Dec =  40d58m33.7s

    Mean    3.16228
    st dev  0.361649
                                       Flux units MJY/SR

    Flux integral      9.97156e-05   MJY
    Inside 3.15328e-05 Steradian area
    (5953 pixels)

    Centroid                             RA = 16h36m55.72s  Dec =  40d53m21.3s


    Flux weighted centroid               RA = 16h36m56.40s  Dec =  40d53m17.4s

    vertex# 1  at RA = 16h38m07.20s  Dec =  40d54m02.5s

    vertex# 2  at RA = 16h36m59.66s  Dec =  40d39m33.2s

    vertex# 3  at RA = 16h35m44.22s  Dec =  40d52m47.5s

    vertex# 4  at RA = 16h36m51.72s  Dec =  41d07m04.5s

--------------------------------------------------

PGAI59300101.FITS  Marano 1

    Centroid                             RA = 3h13m25.02s  Dec = -55d03m46.7s

DIRBE_ANNUAL,48.354250,-55.062972,0.
           1 pixel(s) will be taken
Band  Wavelength        Inu
   1     1.25      0.232+/- 0.001
   2     2.20      0.154+/- 0.001
   3     3.50      0.118+/- 0.001
   4     4.90      0.491+/- 0.003
   5    12.00     12.989+/- 0.013
```

```
   6    25.00     22.393+/- 0.020
   7    60.00      6.269+/- 0.020
   8   100.00      3.512+/- 0.019
   9   140.00      3.538+/- 1.450
  10   240.00      2.315+/- 0.766

DIRBE_ANNUAL,48.354250,-55.062972,1.5
         68 pixel(s) will be taken
Band  Wavelength        Inu
   1     1.25      0.209+/- 0.005
   2     2.20      0.143+/- 0.004
   3     3.50      0.113+/- 0.002
   4     4.90      0.496+/- 0.001
   5    12.00     13.052+/- 0.014
   6    25.00     22.389+/- 0.018
   7    60.00      6.275+/- 0.006
   8   100.00      3.593+/- 0.035
   9   140.00      3.351+/- 0.157
  10   240.00      2.492+/- 0.106

    Maximum 4.11179    at RA = 3h12m31.19s  Dec = -55d15m43.8s
    Minimum 3.08038    at RA = 3h12m03.56s  Dec = -55d01m57.2s

    Mean    3.48771
    st dev  0.164778
                                      Flux units MJY/SR

    Flux integral      0.000227769   MJY
    Inside 6.53062e-05 Steradian area
    (12329 pixels)

    Centroid                             RA = 3h13m25.02s  Dec = -55d03m46.7s


    Flux weighted centroid               RA = 3h13m26.28s  Dec = -55d03m57.3s

    vertex# 1  at RA = 3h15m41.95s  Dec = -55d03m54.3s

    vertex# 2  at RA = 3h13m22.11s  Dec = -55d23m30.0s

    vertex# 3  at RA = 3h11m07.61s  Dec = -55d03m09.1s

    vertex# 4  at RA = 3h13m29.10s  Dec = -54d44m13.1s

--------------------------------------------------

PGAI19800208.FITS  LHNW4

Centroid                            RA = 10h34m52.17s  Dec =  57d34m19.4s

DIRBE_ANNUAL,158.717375,57.572056,0.
          1 pixel(s) will be taken
Band  Wavelength        Inu
   1     1.25      0.291+/- 0.004
   2     2.20      0.186+/- 0.002
   3     3.50      0.129+/- 0.002
   4     4.90      0.530+/- 0.009
   5    12.00     15.979+/- 0.126
   6    25.00     28.999+/- 0.138
   7    60.00      8.348+/- 0.026
   8   100.00      3.861+/- 0.027
   9   140.00      5.041+/- 1.774
  10   240.00      2.267+/- 1.041
```

```
DIRBE_ANNUAL,158.717375,57.572056,1.5
          68 pixel(s) will be taken
Band  Wavelength        Inu
   1     1.25      0.255+/- 0.013
   2     2.20      0.170+/- 0.011
   3     3.50      0.126+/- 0.006
   4     4.90      0.532+/- 0.003
   5    12.00     15.901+/- 0.026
   6    25.00     28.872+/- 0.043
   7    60.00      8.359+/- 0.013
   8   100.00      3.910+/- 0.012
   9   140.00      3.312+/- 0.235
  10   240.00      1.878+/- 0.125

    Maximum 3.5731    at RA = 10h35m19.18s  Dec =  57d33m10.7s
    Minimum 2.95038    at RA = 10h33m40.23s  Dec =  57d35m39.7s

    Mean    3.18679
    st dev  0.113022
                                       Flux units MJY/SR

    Flux integral      0.000108827   MJY
    Inside 3.41495e-05 Steradian area
    (6447 pixels)

    Centroid                              RA = 10h34m52.17s  Dec =  57d34m19.4s


    Flux weighted centroid                RA = 10h34m52.73s  Dec =  57d34m20.2s

    vertex# 1  at RA = 10h36m19.22s  Dec =  57d42m09.5s

    vertex# 2  at RA = 10h35m52.46s  Dec =  57d22m24.5s

    vertex# 3  at RA = 10h33m23.79s  Dec =  57d26m38.6s

    vertex# 4  at RA = 10h33m53.02s  Dec =  57d46m10.6s

--------------------------------------------------

PGAI21001305.FITS  LHNW1

Centroid                               RA = 10h32m57.86s  Dec =  57d58m12.0s

DIRBE_ANNUAL,158.241083,57.970000,0.
           1 pixel(s) will be taken
Band  Wavelength        Inu
   1     1.25      0.218+/- 0.002
   2     2.20      0.146+/- 0.002
   3     3.50      0.115+/- 0.002
   4     4.90      0.520+/- 0.010
   5    12.00     15.790+/- 0.129
   6    25.00     28.769+/- 0.141
   7    60.00      8.309+/- 0.023
   8   100.00      3.930+/- 0.023
   9   140.00      4.069+/- 1.729
  10   240.00      0.281+/- 1.011

DIRBE_ANNUAL,158.241083,57.970000,1.5
          68 pixel(s) will be taken
Band  Wavelength        Inu
   1     1.25      0.245+/- 0.006
   2     2.20      0.163+/- 0.004
   3     3.50      0.123+/- 0.002
```

```
   4     4.90      0.529+/- 0.002
   5    12.00     15.861+/- 0.027
   6    25.00     28.848+/- 0.044
   7    60.00      8.346+/- 0.013
   8   100.00      3.914+/- 0.012
   9   140.00      3.480+/- 0.209
  10   240.00      1.835+/- 0.114

    Maximum 4.56321    at RA = 10h32m04.54s  Dec =  58d08m09.8s
    Minimum 3.09286    at RA = 10h34m12.76s  Dec =  57d48m23.2s

    Mean    3.60222
    st dev  0.235685
                                       Flux units MJY/SR

    Flux integral      0.000122117   MJY
    Inside 3.39006e-05 Steradian area
    (6400 pixels)

    Centroid                              RA = 10h32m57.86s  Dec =  57d58m12.0s


    Flux weighted centroid                RA = 10h32m55.62s  Dec =  57d58m16.8s

    vertex# 1  at RA = 10h34m15.34s  Dec =  58d07m54.0s

    vertex# 2  at RA = 10h34m12.76s  Dec =  57d48m08.2s

    vertex# 3  at RA = 10h31m40.62s  Dec =  57d48m08.1s

    vertex# 4  at RA = 10h31m43.68s  Dec =  58d08m24.2s

--------------------------------------------------

PGAI79900733.FITS  R Scl

Centroid                             RA = 1h26m58.05s  Dec = -32d32m34.0s

DIRBE_ANNUAL,21.741875,-32.542778,0.
          1 pixel(s) will be taken
Band  Wavelength        Inu
   1     1.25      1.934+/- 0.031
   2     2.20      4.144+/- 0.038
   3     3.50      2.997+/- 0.037
   4     4.90      2.249+/- 0.012
   5    12.00     19.516+/- 0.150
   6    25.00     33.683+/- 0.153
   7    60.00      9.963+/- 0.028
   8   100.00      5.584+/- 0.033
   9   140.00      7.029+/- 2.030
  10   240.00      3.658+/- 0.960

    Maximum 12.1975    at RA = 1h26m52.11s  Dec = -32d33m04.0s
    Minimum 4.55051    at RA = 1h26m43.80s  Dec = -32d34m34.1s

    Mean    6.04588
    st dev  1.68289
                                       Flux units MJY/SR

    Flux integral      3.00713e-05   MJY
    Inside 4.97385e-06 Steradian area
    (939 pixels)

    Centroid                              RA = 1h26m58.05s  Dec = -32d32m34.0s
```

```
    Flux weighted centroid               RA = 1h26m58.18s  Dec = -32d32m31.8s

    vertex# 1  at RA = 1h27m17.06s  Dec = -32d36m19.1s

    vertex# 2  at RA = 1h26m46.17s  Dec = -32d37m34.2s

    vertex# 3  at RA = 1h26m39.07s  Dec = -32d28m48.7s

    vertex# 4  at RA = 1h27m09.91s  Dec = -32d27m33.7s

-------------------------------------------------

PGAI33600108.FITS  EBL_4

Centroid                              RA = 13h34m56.29s  Dec =  70d24m29.6s

DIRBE_ANNUAL,203.734542,+70.408222,0.
          1 pixel(s) will be taken
Band  Wavelength        Inu
   1     1.25      0.230+/- 0.001
   2     2.20      0.151+/- 0.001
   3     3.50      0.112+/- 0.001
   4     4.90      0.465+/- 0.003
   5    12.00     12.825+/- 0.016
   6    25.00     22.327+/- 0.024
   7    60.00      6.238+/- 0.021
   8   100.00      3.408+/- 0.021
   9   140.00      2.725+/- 1.198
  10   240.00      3.216+/- 0.647

DIRBE_ANNUAL,203.734542,+70.408222,1.5
         66 pixel(s) will be taken
Band  Wavelength        Inu
   1     1.25      0.213+/- 0.012
   2     2.20      0.142+/- 0.009
   3     3.50      0.109+/- 0.004
   4     4.90      0.467+/- 0.002
   5    12.00     12.832+/- 0.013
   6    25.00     22.327+/- 0.014
   7    60.00      6.282+/- 0.005
   8   100.00      3.379+/- 0.013
   9   140.00      2.774+/- 0.159
  10   240.00      2.172+/- 0.090

    Maximum 3.56157    at RA = 13h37m33.89s  Dec =  70d19m55.0s
    Minimum 2.03326    at RA = 13h36m58.96s  Dec =  70d27m27.1s

    Mean    2.65662
    st dev  0.34627
                                       Flux units MJY/SR

    Flux integral      6.63497e-05   MJY
    Inside 2.49752e-05 Steradian area
    (4715 pixels)

    Centroid                              RA = 13h34m56.29s  Dec =  70d24m29.6s


    Flux weighted centroid                RA = 13h34m56.97s  Dec =  70d24m25.7s

    vertex# 1  at RA = 13h38m13.95s  Dec =  70d28m38.0s
```

```
    vertex# 2  at RA = 13h38m12.51s  Dec =  70d19m37.7s

    vertex# 3  at RA = 13h31m40.00s  Dec =  70d20m07.7s

    vertex# 4  at RA = 13h31m38.55s  Dec =  70d29m08.1s

--------------------------------------------------

PGAI33600705.FITS  EBL_1

Centroid                              RA = 17h50m12.06s  Dec =  69d37m57.1s

DIRBE_ANNUAL,267.55025,69.632528,0.
          1 pixel(s) will be taken
Band  Wavelength        Inu
   1     1.25      0.253+/- 0.002
   2     2.20      0.170+/- 0.002
   3     3.50      0.117+/- 0.001
   4     4.90      0.428+/- 0.002
   5    12.00     11.947+/- 0.031
   6    25.00     20.946+/- 0.060
   7    60.00      6.303+/- 0.027
   8   100.00      4.391+/- 0.030
   9   140.00      5.660+/- 1.500
  10   240.00      2.945+/- 0.799

DIRBE_ANNUAL,267.55025,69.632528,1.5
         69 pixel(s) will be taken
Band  Wavelength        Inu
   1     1.25      0.266+/- 0.011
   2     2.20      0.183+/- 0.007
   3     3.50      0.124+/- 0.004
   4     4.90      0.430+/- 0.002
   5    12.00     11.956+/- 0.004
   6    25.00     20.979+/- 0.008
   7    60.00      6.377+/- 0.012
   8   100.00      4.805+/- 0.045
   9   140.00      5.660+/- 0.169
  10   240.00      3.788+/- 0.105

    Maximum 5.49876    at RA = 17h48m36.42s  Dec =  69d47m56.0s
    Minimum -1    at RA = 17h50m46.34s  Dec =  69d29m26.5s

    Mean    4.68072
    st dev  0.364709
                                      Flux units MJY/SR

    Flux integral      0.00011953   MJY
    Inside 2.55367e-05 Steradian area
    (4821 pixels)

    Centroid                              RA = 17h50m12.06s  Dec =  69d37m57.1s


    Flux weighted centroid                RA = 17h50m12.34s  Dec =  69d37m46.4s

    vertex# 1  at RA = 17h52m02.99s  Dec =  69d23m54.2s

    vertex# 2  at RA = 17h50m26.25s  Dec =  69d20m41.3s

    vertex# 3  at RA = 17h48m18.67s  Dec =  69d51m55.5s

    vertex# 4  at RA = 17h49m57.49s  Dec =  69d55m12.9s
```

```
--------------------------------------------------

PGAI35100907.FITS  M03

Centroid                              RA = 13h36m12.37s  Dec =  70d34m45.4s


    Maximum 5.40199    at RA = 13h34m32.42s  Dec =  70d42m21.6s
    Minimum 3.00308    at RA = 13h36m30.46s  Dec =  70d36m52.9s

    Mean    4.07829
    st dev  0.509387
                                        Flux units MJY/SR

    Flux integral      0.000200817   MJY
    Inside 4.92406e-05 Steradian area
    (9296 pixels)

    Centroid                              RA = 13h36m12.37s  Dec =  70d34m45.4s


    Flux weighted centroid                RA = 13h36m11.04s  Dec =  70d34m48.9s

    vertex# 1  at RA = 13h38m02.03s  Dec =  70d49m06.5s

    vertex# 2  at RA = 13h39m05.63s  Dec =  70d25m32.3s

    vertex# 3  at RA = 13h34m25.29s  Dec =  70d20m20.2s

    vertex# 4  at RA = 13h33m16.48s  Dec =  70d43m48.1s

DIRBE_ANNUAL,204.051542,70.579278,0.
           1 pixel(s) will be taken
Band  Wavelength        Inu
   1     1.25      0.200+/- 0.001
   2     2.20      0.133+/- 0.001
   3     3.50      0.106+/- 0.001
   4     4.90      0.455+/- 0.003
   5    12.00     12.799+/- 0.016
   6    25.00     22.329+/- 0.026
   7    60.00      6.254+/- 0.024
   8   100.00      3.276+/- 0.023
   9   140.00      4.473+/- 1.189
  10   240.00      1.402+/- 0.679

DIRBE_ANNUAL,204.051542,70.579278,1.5
          69 pixel(s) will be taken
Band  Wavelength        Inu
   1     1.25      0.212+/- 0.011
   2     2.20      0.142+/- 0.008
   3     3.50      0.109+/- 0.004
   4     4.90      0.465+/- 0.002
   5    12.00     12.814+/- 0.012
   6    25.00     22.321+/- 0.013
   7    60.00      6.284+/- 0.005
   8   100.00      3.396+/- 0.012
   9   140.00      2.774+/- 0.154
  10   240.00      2.172+/- 0.087

--------------------------------------------------

PGAI16701206.FITS  Helix

Centroid                              RA = 22h29m37.97s  Dec = -20d50m13.4s
```

```
DIRBE_ANNUAL,337.408208,-20.837056,0.
           1 pixel(s) will be taken
Band  Wavelength        Inu
   1     1.25      0.425+/- 0.010
   2     2.20      0.314+/- 0.007
   3     3.50      0.226+/- 0.008
   4     4.90      1.046+/- 0.047
   5    12.00     33.316+/- 0.950
   6    25.00     62.722+/- 1.462
   7    60.00     20.972+/- 0.342
   8   100.00     12.635+/- 0.144
   9   140.00     12.741+/- 2.636
  10   240.00      4.345+/- 1.605

    Maximum 32.2717    at RA = 22h29m10.40s  Dec = -20d51m26.4s
    Minimum 6.79387    at RA = 22h30m10.33s  Dec = -20d39m25.8s

    Mean    15.0457
    st dev  5.33778
                                       Flux units MJY/SR

    Flux integral      0.000617808   MJY
    Inside 4.1062e-05 Steradian area
    (7752 pixels)

    Centroid                              RA = 22h29m37.97s  Dec = -20d50m13.4s


    Flux weighted centroid                RA = 22h29m36.77s  Dec = -20d50m22.0s

    vertex# 1  at RA = 22h30m41.46s  Dec = -20d54m56.0s

    vertex# 2  at RA = 22h29m13.58s  Dec = -21d04m42.1s

    vertex# 3  at RA = 22h28m34.03s  Dec = -20d45m40.5s

    vertex# 4  at RA = 22h30m02.84s  Dec = -20d35m40.7s

--------------------------------------------------

PGAI52700412.FITS  NGC5907N

Centroid                               RA = 15h15m21.38s  Dec =  56d28m59.0s

DIRBE_ANNUAL,228.839083,56.483056,0.
           1 pixel(s) will be taken
Band  Wavelength        Inu
   1     1.25      0.194+/- 0.001
   2     2.20      0.132+/- 0.001
   3     3.50      0.100+/- 0.001
   4     4.90      0.423+/- 0.002
   5    12.00     12.393+/- 0.023
   6    25.00     22.010+/- 0.037
   7    60.00      6.324+/- 0.023
   8   100.00      3.685+/- 0.021
   9   140.00      3.823+/- 1.287
  10   240.00      2.442+/- 0.750

DIRBE_ANNUAL,228.839083,56.483056,1.5
          67 pixel(s) will be taken
Band  Wavelength        Inu
   1     1.25      0.205+/- 0.004
   2     2.20      0.136+/- 0.003
```

```
   3     3.50      0.102+/- 0.002
   4     4.90      0.422+/- 0.001
   5    12.00     12.372+/- 0.007
   6    25.00     21.926+/- 0.011
   7    60.00      6.244+/- 0.006
   8   100.00      3.383+/- 0.014
   9   140.00      3.203+/- 0.157
  10   240.00      2.276+/- 0.075

    Maximum 11.8842    at RA = 15h15m39.76s  Dec =  56d22m12.8s
    Minimum 2.36455    at RA = 15h16m10.54s  Dec =  56d24m57.4s

    Mean    3.20345
    st dev  0.977672
                                      Flux units MJY/SR

    Flux integral      2.78963e-05   MJY
    Inside 8.70821e-06 Steradian area
    (1644 pixels)

    Centroid                              RA = 15h15m21.38s  Dec =  56d28m59.0s


    Flux weighted centroid                RA = 15h15m22.43s  Dec =  56d28m30.7s

    vertex# 1  at RA = 15h16m12.34s  Dec =  56d24m42.3s

    vertex# 2  at RA = 15h15m27.11s  Dec =  56d21m12.8s

    vertex# 3  at RA = 15h14m30.85s  Dec =  56d32m57.7s

    vertex# 4  at RA = 15h15m14.41s  Dec =  56d36m58.6s

--------------------------------------------------

PGAI85001037.FITS  U Men

Centroid                             RA = 4h09m39.24s  Dec = -81d51m18.0s

DIRBE_ANNUAL,62.4135,-81.855,0.
          1 pixel(s) will be taken
Band  Wavelength        Inu
   1     1.25      3.213+/- 0.051
   2     2.20      5.143+/- 0.058
   3     3.50      3.930+/- 0.040
   4     4.90      3.118+/- 0.027
   5    12.00     13.712+/- 0.044
   6    25.00     22.153+/- 0.057
   7    60.00      6.542+/- 0.021
   8   100.00      5.928+/- 0.023
   9   140.00     10.087+/- 1.377
  10   240.00      5.852+/- 0.831

DIRBE_ANNUAL,62.4135,-81.855,1.5
         69 pixel(s) will be taken
Band  Wavelength        Inu
   1     1.25      0.290+/- 0.073
   2     2.20      0.208+/- 0.122
   3     3.50      0.142+/- 0.095
   4     4.90      0.453+/- 0.067
   5    12.00     12.014+/- 0.045
   6    25.00     20.954+/- 0.035
   7    60.00      6.405+/- 0.014
   8   100.00      6.057+/- 0.066
```

```
   9   140.00      9.348+/- 0.248
  10   240.00      6.444+/- 0.130

    Maximum 11.1696    at RA = 4h09m42.77s  Dec = -81d51m03.0s
    Minimum 6.6553    at RA = 4h05m26.85s  Dec = -81d54m28.4s

    Mean    8.14607
    st dev  0.768085
                                       Flux units MJY/SR

    Flux integral      0.000308087   MJY
    Inside 3.78203e-05 Steradian area
    (7140 pixels)

    Centroid                             RA = 4h09m39.24s  Dec = -81d51m18.0s


    Flux weighted centroid               RA = 4h09m51.99s  Dec = -81d51m29.1s

    vertex# 1  at RA = 4h14m38.97s  Dec = -82d01m56.6s

    vertex# 2  at RA = 4h04m32.60s  Dec = -82d01m41.6s

    vertex# 3  at RA = 4h04m52.32s  Dec = -81d40m26.2s

    vertex# 4  at RA = 4h14m32.91s  Dec = -81d40m25.6s

--------------------------------------------------

PGAI78200101.FITS  Draco main

Centroid                            RA = 16h46m43.27s  Dec =  60d00m34.1s

DIRBE_ANNUAL,251.68029,60.00947,0.6
          11 pixel(s) will be taken
Band  Wavelength        Inu
   1     1.25      0.258+/- 0.009
   2     2.20      0.174+/- 0.008
   3     3.50      0.121+/- 0.004
   4     4.90      0.418+/- 0.002
   5    12.00     11.941+/- 0.012
   6    25.00     21.081+/- 0.018
   7    60.00      6.218+/- 0.028
   8   100.00      4.767+/- 0.206
   9   140.00      4.844+/- 0.559
  10   240.00      5.274+/- 0.466

    Maximum 22.5793    at RA = 16h47m07.86s  Dec =  60d16m02.9s
    Minimum 0.557602    at RA = 16h47m53.92s  Dec =  59d32m01.0s

    Mean    6.32057
    st dev  4.51859
                                       Flux units MJY/SR

    Flux integral      0.00179462   MJY
    Inside 0.000283933 Steradian area
    (53603 pixels)

    Centroid                             RA = 16h46m43.27s  Dec =  60d00m34.1s


    Flux weighted centroid               RA = 16h46m21.83s  Dec =  60d07m37.0s

 vertex# 1  at RA = 16h51m40.41s  Dec =  59d44m17.6s
```

```
 vertex# 2  at RA = 16h46m09.90s  Dec =  59d18m43.6s

 vertex# 3  at RA = 16h41m31.14s  Dec =  60d14m31.4s

 vertex# 4  at RA = 16h47m36.09s  Dec =  60d42m34.3s

-------------------------------------------------

PGAI36803005.FITS  NPC_2

Centroid                              RA = 23h59m33.14s  Dec =  86d58m21.7s

DIRBE_ANNUAL,359.888085,86.972694,0.
           1 pixel(s) will be taken
Band  Wavelength        Inu
   1     1.25      0.407+/- 0.002
   2     2.20      0.283+/- 0.002
   3     3.50      0.185+/- 0.001
   4     4.90      0.538+/- 0.004
   5    12.00     13.610+/- 0.044
   6    25.00     23.297+/- 0.062
   7    60.00      7.061+/- 0.023
   8   100.00      7.668+/- 0.033
   9   140.00     17.082+/- 1.265
  10   240.00     15.491+/- 0.750

DIRBE_ANNUAL,359.888085,86.972694,1.5
          71 pixel(s) will be taken
Band  Wavelength        Inu
% Compiled module: MOMENT.
   1     1.25      0.335+/- 0.032
   2     2.20      0.226+/- 0.023
   3     3.50      0.159+/- 0.011
   4     4.90      0.523+/- 0.006
   5    12.00     13.540+/- 0.014
   6    25.00     23.219+/- 0.021
   7    60.00      7.130+/- 0.011
   8   100.00      7.922+/- 0.128
   9   140.00     15.767+/- 0.407
  10   240.00     14.935+/- 0.518

-------------------------------------------------

PGAI39602313.FITS  North_1

Centroid                              RA = 20h33m01.76s  Dec =  65d07m41.3s

DIRBE_ANNUAL,308.257335,65.128139,0.
           1 pixel(s) will be taken
Band  Wavelength        Inu
   1     1.25      0.490+/- 0.002
   2     2.20      0.365+/- 0.002
   3     3.50      0.233+/- 0.001
   4     4.90      0.546+/- 0.004
   5    12.00     13.419+/- 0.069
   6    25.00     22.846+/- 0.099
   7    60.00      8.253+/- 0.035
   8   100.00     13.541+/- 0.032
   9   140.00     26.668+/- 1.488
  10   240.00     24.661+/- 0.852

DIRBE_ANNUAL,308.257335,65.128139,1.5
          63 pixel(s) will be taken
```

```
Band  Wavelength        Inu
   1     1.25      0.472+/- 0.010
   2     2.20      0.350+/- 0.010
   3     3.50      0.227+/- 0.005
   4     4.90      0.541+/- 0.002
   5    12.00     13.297+/- 0.015
   6    25.00     22.682+/- 0.020
   7    60.00      8.191+/- 0.037
   8   100.00     12.910+/- 0.146
   9   140.00     25.234+/- 0.366
  10   240.00     21.872+/- 0.357

    Maximum 65.1823    at RA = 20h33m06.66s  Dec =  65d18m19.3s
    Minimum 23.7119    at RA = 20h33m25.64s  Dec =  65d11m03.7s

    Mean    36.2005
    st dev  6.92201
                                      Flux units MJY/SR

    Flux integral      0.0022531   MJY
    Inside 6.22393e-05 Steradian area
    (11750 pixels)

    Centroid                             RA = 20h32m44.30s  Dec =  65d19m44.5s


    Flux weighted centroid               RA = 20h32m42.31s  Dec =  65d20m01.8s

 vertex# 1  at RA = 20h35m47.56s  Dec =  65d21m42.7s

 vertex# 2  at RA = 20h33m01.69s  Dec =  65d00m33.5s

 vertex# 3  at RA = 20h29m43.11s  Dec =  65d17m42.5s

 vertex# 4  at RA = 20h32m23.26s  Dec =  65d38m50.2s

DIRBE_ANNUAL,308.184585,65.329028,0.
          1 pixel(s) will be taken
Band  Wavelength        Inu
   1     1.25      0.624+/- 0.002
   2     2.20      0.487+/- 0.003
   3     3.50      0.297+/- 0.002
   4     4.90      0.576+/- 0.004
   5    12.00     13.359+/- 0.071
   6    25.00     22.822+/- 0.103
   7    60.00      8.065+/- 0.031
   8   100.00     13.319+/- 0.037
   9   140.00     30.829+/- 1.434
  10   240.00     29.233+/- 0.813

--------------------------------------------------

PGAI26101401.FITS  CHA1C

Centroid                            RA = 11h07m55.92s  Dec = -77d28m19.0s

DIRBE_ANNUAL,166.983000,-77.471944,0.
          1 pixel(s) will be taken
Band  Wavelength        Inu
   1     1.25      0.593+/- 0.002
   2     2.20      0.538+/- 0.002
   3     3.50      0.371+/- 0.002
   4     4.90      0.619+/- 0.005
   5    12.00     12.769+/- 0.068
```

```
   6    25.00     22.619+/- 0.091
   7    60.00     11.004+/- 0.028
   8   100.00     25.705+/- 0.061
   9   140.00     70.083+/- 1.402
  10   240.00     85.406+/- 0.818

    Maximum 285.028    at RA = 11h06m37.79s  Dec = -77d23m30.2s
    Minimum 31.9312    at RA = 11h00m57.55s  Dec = -77d25m10.7s

    Mean    69.8107
    st dev  26.9809
                                       Flux units MJY/SR

    Flux integral      0.00770077   MJY
    Inside 0.000110309 Steradian area
    (20825 pixels)

    Centroid                             RA = 11h07m55.92s  Dec = -77d28m19.0s


    Flux weighted centroid               RA = 11h07m54.92s  Dec = -77d29m28.2s

    vertex# 1  at RA = 11h15m36.07s  Dec = -77d34m07.1s

    vertex# 2  at RA = 11h05m56.54s  Dec = -77d53m00.7s

    vertex# 3  at RA = 11h00m22.73s  Dec = -77d21m51.9s

    vertex# 4  at RA = 11h09m47.45s  Dec = -77d03m28.5s

-------------------------------------------------

PGAI33401133.FITS  RCRA

Centroid                             RA = 19h02m17.05s  Dec = -36d59m32.2s

DIRBE_ANNUAL,285.571042,-36.992278,0.
          1 pixel(s) will be taken
Band  Wavelength        Inu
   1     1.25      1.050+/- 0.012
   2     2.20      1.126+/- 0.013
   3     3.50      1.058+/- 0.012
   4     4.90      1.719+/- 0.028
   5    12.00     27.878+/- 0.504
   6    25.00     53.845+/- 0.691
   7    60.00     31.080+/- 0.340
   8   100.00     49.250+/- 0.768
   9   140.00     93.071+/- 2.599
  10   240.00     87.597+/- 1.552

    Maximum 1205.98    at RA = 19h01m50.75s  Dec = -36d56m46.9s
    Minimum -1    at RA = 19h02m02.02s  Dec = -36d58m02.1s

    Mean    138.573
    st dev  153.802
                                       Flux units MJY/SR

    Flux integral      0.00538549   MJY
    Inside 3.88638e-05 Steradian area
    (7337 pixels)

    Centroid                             RA = 19h02m17.05s  Dec = -36d59m32.2s
```

```
    Flux weighted centroid               RA = 19h02m05.24s  Dec = -36d58m22.1s

    vertex# 1  at RA = 19h03m13.55s  Dec = -37d09m16.9s

    vertex# 2  at RA = 19h01m25.54s  Dec = -37d11m02.1s

    vertex# 3  at RA = 19h01m20.79s  Dec = -36d49m45.9s

    vertex# 4  at RA = 19h03m08.30s  Dec = -36d48m01.0s

--------------------------------------------------
PGAI86101801.FITS  Orion MC-E

    Centroid                             RA = 5h37m02.44s  Dec = -5d33m29.5s

DIRBE_ANNUAL,84.260167,-5.558194,0.
           1 pixel(s) will be taken
Band  Wavelength        Inu
   1     1.25      0.840+/- 0.024
   2     2.20      0.778+/- 0.030
   3     3.50      1.470+/- 0.064
   4     4.90      2.167+/- 0.090
   5    12.00     40.920+/- 1.408
   6    25.00    110.920+/- 5.828
   7    60.00    434.900+/-30.436
   8   100.00    506.866+/-28.039
   9   140.00    651.540+/-32.022
  10   240.00    287.916+/-11.154

    Maximum 893.762    at RA = 5h36m43.14s  Dec = -5d28m29.1s
    Minimum -1    at RA = 5h37m02.24s  Dec = -5d33m14.4s

    Mean    251.869
    st dev  127.688
                                      Flux units MJY/SR

    Flux integral      0.0126343   MJY
    Inside 5.01622e-05 Steradian area
    (9470 pixels)

    Centroid                             RA = 5h37m02.44s  Dec = -5d33m29.5s


    Flux weighted centroid               RA = 5h36m58.04s  Dec = -5d31m29.3s

    vertex# 1  at RA = 5h37m34.43s  Dec = -5d52m45.2s

    vertex# 2  at RA = 5h36m33.06s  Dec = -5d53m15.3s

    vertex# 3  at RA = 5h36m31.09s  Dec = -5d13m58.4s

    vertex# 4  at RA = 5h37m31.38s  Dec = -5d13m43.4s

--------------------------------------------------

PGAI15601577.FITS  OPT_IR4

Centroid                           RA = 18h11m45.29s  Dec =  44d29m05.3s

DIRBE_ANNUAL,272.938708,44.484806,0.
           1 pixel(s) will be taken
Band  Wavelength        Inu
   1     1.25      0.429+/- 0.002
   2     2.20      0.297+/- 0.001
```

```
   3     3.50      0.185+/- 0.001
   4     4.90      0.525+/- 0.006
   5    12.00     13.203+/- 0.088
   6    25.00     22.915+/- 0.110
   7    60.00      6.938+/- 0.029
   8   100.00      6.062+/- 0.026
   9   140.00      6.422+/- 1.250
  10   240.00      5.853+/- 0.723

    Maximum 20.4619    at RA = 18h11m14.37s  Dec =  44d25m07.3s
    Minimum 5.75163    at RA = 18h12m16.09s  Dec =  44d33m07.7s

    Mean    11.3951
    st dev  3.28776
                                       Flux units MJY/SR

    Flux integral      0.000156874   MJY
    Inside 1.37668e-05 Steradian area
    (2599 pixels)

    Centroid                              RA = 18h11m45.29s  Dec =  44d29m05.3s


    Flux weighted centroid                RA = 18h11m41.06s  Dec =  44d28m32.5s

    vertex# 1  at RA = 18h12m34.26s  Dec =  44d26m52.0s

    vertex# 2  at RA = 18h11m27.00s  Dec =  44d20m37.3s

    vertex# 3  at RA = 18h10m56.07s  Dec =  44d31m07.2s

    vertex# 4  at RA = 18h12m03.48s  Dec =  44d37m38.1s

--------------------------------------------------

PGAI33300559.FITS  Cham II

Centroid                              RA = 13h00m49.30s  Dec = -77d06m18.7s

DIRBE_ANNUAL,195.205417,-77.105194,0.
          1 pixel(s) will be taken
Band  Wavelength        Inu
   1     1.25      1.367+/- 0.014
   2     2.20      1.747+/- 0.011
   3     3.50      1.092+/- 0.011
   4     4.90      1.008+/- 0.008
   5    12.00     13.460+/- 0.080
   6    25.00     23.135+/- 0.095
   7    60.00      9.176+/- 0.026
   8   100.00     20.057+/- 0.055
   9   140.00     50.397+/- 1.253
  10   240.00     55.675+/- 0.735

    Maximum 111.708    at RA = 12h59m17.73s  Dec = -77d07m38.5s
    Minimum 16.4171    at RA = 13h02m11.62s  Dec = -76d55m23.1s

    Mean    37.997
    st dev  20.3964
                                       Flux units MJY/SR

    Flux integral      0.00248708   MJY
    Inside 6.54546e-05 Steradian area
    (12357 pixels)
```

```
    Centroid                              RA = 13h00m49.30s  Dec = -77d06m18.7s


    Flux weighted centroid                RA = 13h00m10.55s  Dec = -77d08m34.3s

    vertex# 1  at RA = 13h05m07.78s  Dec = -76d53m00.7s

    vertex# 2  at RA = 13h04m31.75s  Dec = -77d21m49.3s

    vertex# 3  at RA = 12h56m18.62s  Dec = -77d19m01.6s

    vertex# 4  at RA = 12h57m16.46s  Dec = -76d50m48.3s

--------------------------------------------------

PGAI10101157.FITS  L134_C200

Centroid                              RA = 15h53m46.08s  Dec = -4d31m23.9s

DIRBE_ANNUAL,238.442000,-4.523306,0.
          1 pixel(s) will be taken
Band  Wavelength        Inu
   1     1.25      0.546+/- 0.006
   2     2.20      0.387+/- 0.005
   3     3.50      0.275+/- 0.005
   4     4.90      0.839+/- 0.026
   5    12.00     27.186+/- 0.518
   6    25.00     51.374+/- 0.743
   7    60.00     17.904+/- 0.179
   8   100.00     21.016+/- 0.080
   9   140.00     45.483+/- 1.921
  10   240.00     45.161+/- 1.208

    Maximum 135.481    at RA = 15h53m35.13s  Dec = -4d37m05.8s
    Minimum 37.882    at RA = 15h53m28.11s  Dec = -4d24m20.2s

    Mean    69.6857
    st dev  19.5758
                                      Flux units MJY/SR

    Flux integral      0.00098888   MJY
    Inside 1.41906e-05 Steradian area
    (2679 pixels)

    Centroid                              RA = 15h53m46.08s  Dec = -4d31m23.9s


    Flux weighted centroid                RA = 15h53m44.63s  Dec = -4d32m09.2s

    vertex# 1  at RA = 15h54m17.30s  Dec = -4d26m35.3s

    vertex# 2  at RA = 15h54m08.27s  Dec = -4d38m50.9s

    vertex# 3  at RA = 15h53m15.05s  Dec = -4d36m05.7s

    vertex# 4  at RA = 15h53m23.09s  Dec = -4d24m05.2s

--------------------------------------------------

PGAI31000625.FITS  Rho_OPh_16

Centroid                              RA = 16h32m21.87s  Dec = -24d29m30.2s

DIRBE_ANNUAL,248.091125,-24.491722,0.
```

```
          1 pixel(s) will be taken
Band  Wavelength        Inu
   1     1.25      1.117+/- 0.010
   2     2.20      0.889+/- 0.008
   3     3.50      0.721+/- 0.008
   4     4.90      1.350+/- 0.043
   5    12.00     38.926+/- 0.975
   6    25.00     71.528+/- 1.482
   7    60.00     48.831+/- 0.411
   8   100.00    123.307+/- 1.182
   9   140.00    274.444+/- 3.114
  10   240.00    207.760+/- 2.173

    Maximum 1061.62    at RA = 16h32m32.18s  Dec = -24d28m48.8s
    Minimum -1    at RA = 16h32m24.49s  Dec = -24d29m03.8s

    Mean    345.479
    st dev  159.926
                                       Flux units MJY/SR

    Flux integral      0.00500868   MJY
    Inside 1.44978e-05 Steradian area
    (2737 pixels)

    Centroid                              RA = 16h32m21.87s  Dec = -24d29m30.2s


    Flux weighted centroid                RA = 16h32m23.58s  Dec = -24d29m58.0s

    vertex# 1  at RA = 16h32m56.36s  Dec = -24d24m33.3s

    vertex# 2  at RA = 16h32m47.61s  Dec = -24d36m49.0s

    vertex# 3  at RA = 16h31m47.07s  Dec = -24d34m18.8s

    vertex# 4  at RA = 16h31m55.92s  Dec = -24d22m18.3s

--------------------------------------------------

PGAI26701013.FITS  Rho_Oph_Ma

Centroid                             RA = 16h27m47.13s  Dec = -24d25m57.3s

DIRBE_ANNUAL,246.946375,-24.432583,0.
          1 pixel(s) will be taken
Band  Wavelength        Inu
   1     1.25      0.990+/- 0.010
   2     2.20      1.075+/- 0.010
   3     3.50      1.620+/- 0.026
   4     4.90      2.502+/- 0.048
   5    12.00     49.918+/- 0.983
   6    25.00     89.950+/- 1.516
   7    60.00    208.110+/- 4.904
   8   100.00    440.087+/- 9.461
   9   140.00    762.011+/-11.059
  10   240.00    494.475+/- 5.768

    Maximum 4939.35    at RA = 16h26m31.34s  Dec = -24d24m23.8s
    Minimum 140.681    at RA = 16h29m20.58s  Dec = -24d23m53.2s

    Mean    593.337
    st dev  438.383
                                       Flux units MJY/SR
```

```
    Flux integral      0.0919356   MJY
    Inside 0.000154947 Steradian area
    (29252 pixels)

    Centroid                              RA = 16h27m47.13s  Dec = -24d25m57.3s


    Flux weighted centroid                RA = 16h27m20.64s  Dec = -24d27m19.9s

    vertex# 1  at RA = 16h29m33.54s  Dec = -24d07m51.9s

    vertex# 2  at RA = 16h29m09.87s  Dec = -24d49m39.8s

    vertex# 3  at RA = 16h25m59.19s  Dec = -24d43m53.4s

    vertex# 4  at RA = 16h26m26.09s  Dec = -24d02m07.6s

--------------------------------------------------

PGAI40900802.FITS  NGC 474

Centroid                             RA = 1h20m06.80s  Dec =  3d24m57.5s

DIRBE_ANNUAL,20.028333,3.404333,0.
           1 pixel(s) will be taken
Band  Wavelength        Inu
   1     1.25      0.542+/- 0.008
   2     2.20      0.353+/- 0.005
   3     3.50      0.266+/- 0.006
   4     4.90      1.189+/- 0.036
   5    12.00     38.385+/- 0.780
   6    25.00     72.937+/- 1.237
   7    60.00     24.243+/- 0.333
   8   100.00     11.880+/- 0.130
   9   140.00      8.335+/- 1.967
  10   240.00      5.596+/- 1.012

    Maximum 17.8955    at RA = 1h19m42.65s  Dec =  3d24m15.6s
    Minimum 5.53332    at RA = 1h19m59.69s  Dec =  3d32m31.0s

    Mean    6.87223
    st dev  1.30793
                                      Flux units MJY/SR

    Flux integral      0.000135379   MJY
    Inside 1.96994e-05 Steradian area
    (3719 pixels)

    Centroid                              RA = 1h20m06.80s  Dec =  3d24m57.5s


    Flux weighted centroid                RA = 1h20m05.94s  Dec =  3d24m56.9s

    vertex# 1  at RA = 1h20m46.81s  Dec =  3d20m45.4s

    vertex# 2  at RA = 1h19m50.67s  Dec =  3d15m00.2s

    vertex# 3  at RA = 1h19m26.60s  Dec =  3d29m00.8s

    vertex# 4  at RA = 1h20m22.75s  Dec =  3d35m01.1s

--------------------------------------------------

PGAI28001303.FITS  NGC 5128
```

```
Centroid                              RA = 13h25m55.17s  Dec = -42d53m49.4s

DIRBE_ANNUAL,201.479875,-42.897056,0.
           1 pixel(s) will be taken
Band  Wavelength        Inu
   1     1.25      0.709+/- 0.005
   2     2.20      0.568+/- 0.004
   3     3.50      0.351+/- 0.003
   4     4.90      0.729+/- 0.014
   5    12.00     18.618+/- 0.233
   6    25.00     33.545+/- 0.311
   7    60.00     12.911+/- 0.087
   8   100.00     15.510+/- 0.075
   9   140.00     20.757+/- 1.817
  10   240.00     12.795+/- 1.013

    Maximum 158.105    at RA = 13h25m35.56s  Dec = -43d00m34.9s
    Minimum 9.0557    at RA = 13h25m35.63s  Dec = -42d48m19.3s

    Mean    13.0258
    st dev  11.5354
                                       Flux units MJY/SR

    Flux integral      0.000261361   MJY
    Inside 2.00649e-05 Steradian area
    (3788 pixels)

    Centroid                              RA = 13h25m55.17s  Dec = -42d53m49.4s


    Flux weighted centroid                RA = 13h25m51.51s  Dec = -42d55m13.7s

    vertex# 1  at RA = 13h26m54.81s  Dec = -42d52m33.7s

    vertex# 2  at RA = 13h26m01.57s  Dec = -43d04m35.2s

    vertex# 3  at RA = 13h24m55.96s  Dec = -42d55m03.8s

    vertex# 4  at RA = 13h25m47.91s  Dec = -42d43m04.2s

--------------------------------------------------
```

Chapter 10

Conclusions and Outlook

The Scientific Validation of the OLP 8.4 version has demonstrated and achieved the following:

- Further consolidation with improved photometric accuracy for staring mode observations, including faint source photometry.
- More detailed assessment of the photometric accuracy of absolute and multi-filter staring modes.
- Correction for non-linearity of signals due to flux dependence of detector responsivity.
- Upgraded FCS power tables from the full data set of celestial standard measurements obtained during the mission.
- Improvement of the effective solid angle of ISOPHOT-S.
- Improvement of the spectral response function for chopped PHT-S measurements resulting in considerably better absolute and relative accuracy.
- Validation of the staring PHT-C mapping mode PHT22.

The validation of chopped photometry calibration was not yet successful over a sufficiently large flux range for all ISOPHOT-P and -C detectors. However, the signal processing could be considerably improved by introducing the chopped pattern, a concept on which further improvements of the photometric calibration will built up. First refinements will be implemented for OLP 9.0, the final calibration method can, however, be only expected for OLP 10.0 (to be released in February 2001).

For the next PHT specific OLP Version 9.0, to be validated during spring 2000, the following items are confirmed for inclusion:

- Dynamic response correction for staring PHT-S measurements.
- Refinements for and validation of chopped photometry.
- Refinements in signal linearization and FCS calibration.
- Extension of data records in order to provide complementary flux information (Jy/pixel in case of extended source data product, MJy sr^{-1} in case of point source data product).

A basic schedule is outlined in the following Table 10.1.

Beside the consolidated items listed above the following items are still being considered for implementation into OLP:

- **Deglitching**
  Inclusion of the two-threshold algorithm to cope with glitch tails is being studied.

Table 10.1: Schedule for PHT OLP 9.0 Upgrades

OLP 9.0 requirements definition meeting	29-Nov-1999
Freeze of OLP 9.0 requirements	07/15-Jan-2000
Software and Cal-G file implementation (SPR fixing and new features)	Nov-1999 - Feb-2000
OLP 9.0 test plan	11-Feb-2000
OLP 9.0 software and calibration file delivery (1)	15-Feb-2000
OLP 9.0 scientific validation period I	06 - 29-Mar-2000
OLP 9.0 software and calibration file upgrades delivery (2)	29-Mar-2000
OLP 9.0 scientific validation period II	17-Apr - 05-May-2000
OLP 9.0 software and calibration file upgrades final delivery (3)	05-May-2000
Release of OLP 9.0 for On-the-fly re-processing	12-May-2000
Version 1 of ISOPHOT OLP 9.0 Scientific Validation Report	22-May-2000
Version 4.0 of ISOPHOT Calibration Accuracies (adapted to OLP 9)	June 2000

- **Impact on photometric results by a limited accuracy of the reset interval correction**
  This item will be investigated in more detail in the extension of the error propagation document [3].
- **FCS aperture correction (ISOPHOT-P)**
  This item requires a finalisation of the signal linearisation correction. It may be restricted to a correction of the 180 arcsec aperture with regard to the standard aperture in the respective filter in order to properly calibrate wide beam measurements on extended sources.
- **FCS straylight corrections for long wavelength detectors**
  This issue will be re-analysed, in particular for C200, to assess the fraction of sky background to the total heated FCS signal which would introduce a zero point offset into the FCS calibration.
- **Relative flux correction for multi-aperture measurements (ISOPHOT-P)**
  This correction accounts for non-flat beam profiles of the ISOPHOT-P apertures which are not concentric relative to each other, either. An absolute calibration of the multi-aperture sequence depends on a successful calibration of the FCS in non-standard apertures.
- **Non-linear drift removal in PHT-P nodding sequences**
  This item requires a finalisation of the signal linearisation correction. The timely evolution of the sky background signal level can then be used to fit a non-linear baseline.
- **Correction for systematic flat-field residuals**
  Dependent on the redundancy achieved by the mapping parameters (raster step size)

extra correction factors for systematic flatfield residuals can be derived from a statistical correlation method of surface brightness calibrated maps for a certain dynamic range in brightness or from flat sky background areas.

- **Non-linear drift correction in maps**
  Median filtering presents a method, which is however dependent on the background structure and may fail for an automatic processing. An extra map product with drift correction switched on may be provided.

- **Transient correction**
  A simple automatic algorithm, currently used for the special observational data base to establish the FCS calibration, may be applied. The amount of correction is limited in order to exclude excessive corrections by failed fits. This transient correction could be switched on, in case the currently implemented Man drift recognition algorithm indicated a non-stable measurement.

- **PHT32 calibration**
  This is a certain aspect of transient correction due to the fast chopper sweeps. Whether the methods developed for chopped photometry correction or a full transient modelling of the flux history will give satisfying photometry with this mode is still completely open.

Most of these issues are quite complex calibration programmes. They need detailed assessment and feasibility studies before a certain correction can eventually be implemented into the OLP. Therefore, no warranty can be given that all the items listed above will be finally available in OLP 10, which is the version foreseen to establish the ISO legacy archive. Another factor is the manpower available in all data centres working on ISOPHOT calibration issues.

Bibliography

[1] U. Klaas and M. Radovich, "Report on the PHT Scientific Validation for OLP Version 7.0", SAI/98-049/Rp, Version 2.0, 20-July-1998.

[2] R.J. Laureijs, U. Klaas, P.J. Richards and B. Schulz, "ISO Data User Manual (IDUM)", SAI/95-220/Dc, Version 4.0, October 1998

[3] R.J. Laureijs and U. Klaas, "ISOPHOT Error Budgets", SAI/98-091/Dc, Version 1.0, 21-April-1999 (DERIVE_SPD Processing Steps)

[4] U. Klaas, "Plan for the PHT Scientific (Re-)Validation of PHT OLP Version 8.4", SAI/99-002/Dc, Version 1.0, 07-May-1999

[5] U. Herbstmeier, "ISOPHOT Footprints and Near-Field Straylight: S - Re-analysis of cross scans to extract measured footprint and associated parameters", Version 1.0, PHTNDC internal calibration report, 18-March-1998

[6] K. Sellgren, L.J. Allamandola, J.D. Bregman, et al., "Emission Features in the 4-13 Micron Spectra of the Reflection Nebulae NGC 7023 and NGC 2023", ApJ 299, 416, 1985

[7] D. Cesarsky, J. Lequeux, A. Abergel, et al., "Infrared Spectrophotometry of M17 with ISOCAM", A&A 315, L305, 1996

[8] P.F. Roche, D.K. Aitken, C.H. Smith and M.J. Ward, "An Atlas of Mid-infrared Spectra of Galaxy Nuclei", MNRAS 248, 606, 1991

[9] J. Acosta-Pulido, "Calibration of ISOPHOT-S Chopped Measurements", IDC PHT Internal Calibration Report, 08-March-1999

[10] R.J. Laureijs, "Point Spread Function Fractions Related to the ISOPHOT C100 and C200 Arrays", IDC PHT Internal Calibration Report, Version 1.0, 29-June-1999

[11] P.L. Hammersley, M. Jourdain De Muizon, M.F. Kessler, P. Bouchet, R.D. Joseph, H. Habing, A. Salama, L. Metcalfe, "Infrared standards for ISO. I. A new calibration of mid infrared photometry", A&AS 128, 207, 1998

[12] P.F. Roche, D.A. Allen, D.K. Aitken, "Symbiotic stars: spectrophotometry at 3-4 and 8-13 um", MNRAS 204, 1009, 1983

[13] C.H. Smith, D.K. Aitken, P.F. Roche, C.M. Wright, "Mid-infrared spectroscopy of galactic novae", MNRAS 277, 259, 1995

[14] I. Heinrichsen, H.J. Walker, and U. Klaas, "Infrared Mapping of the Dust Disc around Vega", MNRAS 293, L78, 1998

[15] U. Klaas, M. Haas, I. Heinrichsen, B. Schulz, "Infrared spectral energy distributions of the interacting galaxies Arp 244, NGC 6240 and Arp 220", 1997, A&A 325, L21

[16] L. Verstraete, J.L. Puget, E. Falgarone, S. Drapatz, C.M. Wright, R. Timmermann, "SWS Spectroscopy of Small Grain Features across the M17-Southwest Photodissociation Front", 1996, A&A 315, L337

[17] D. Cesarsky, J. Lequeux, A. Abergel, M. Perault, E. Palazzi, S. Madden, D. Tran, "Infrared Spectrophotometry of M17 with ISOCAM", 1996, A&A 315, L309

[18] B. Schulz & S. Huth, "Explanatory Supplement for FCS Monitoring Observations", Draft 2.0, 20-June-97 and related diagrams

[19] P. Ábrahám, M. Radovich, L. Schmidtobreick, U. Klaas, T. Kranz, "Analysis of Chopped ISOPHOT Measurements", Version 1.0, PHT/MPIA Calibration Report, 24-November-1999

[20] N. Ginestet, J.M. Carquillat, C. Jaschek, "Spectral classifications in the near infrared of stars with composite spectra", 1999, A&A Supp 134, 473

[21] C.K. Mitrou, J.G. Doyle, M. Mathioudakis, E. Antonopoulou, "The emission of the RS CVn binaries in the IRAS passbands", 1996, A&A Supp 115, 61

[22] C.L. Perry, E.H. Olsen, D.L. Crawford, "A catalog of bright uvbybeta standard stars", 1987, PASP 99, 1184

[23] K. Mattila, D. Lemke, L.K. Haikala, R.J. Laureijs, A. Léger, K. Lehtinen, Ch. Leinert, and P.G. Mezger, "Spectrophotometry of UIR bands in the diffuse emission of the galactic disk", 1996, A&A 315, L353

[24] T. Onaka, and the IRTS team, "IRTS observations of the unidentified infrared bands in the diffuse Galactic light", 1997, Diffuse Infrared Radiation and the IRTS, H. Okuda, T. Matsumoto, and T.L. Roellig (eds.), ASP Conference Series, Vol. 124, 170

[25] I. Heinrichsen, H.J. Walker, U. Klaas, R.J. Sylvester, and D. Lemke, "An infrared image of the dust disc around β Pic", 1999, MNRAS 304, 589

[26] U. Klaas, J.A. Acosta–Pulido, P. Ábrahám, H.O. Castañeda, L. Cornwall, F. Garzon, P. Hammersley, I. Heinrichsen, U. Kinkel, D. Lemke, J. Schubert, and M. Wells, "ISOPHOT-S: Capabilities and Calibration", Proc. First ISO Workshop on Analytical Spectroscopy, p. 113, ESA SP-419, December 1997

[27] U. Klaas, P. Ábrahám, M. Haas, U. Herbstmeier, and R.J. Laureijs, "General ISOPHOT Observing Strategies for Faint Sources", SAI/97-013/Wb, Version 1.3, 28-February-1997

[28] P. Ábrahám, U. Klaas, M. Haas, U. Herbstmeier, M. Linden, and D. Lemke, "Detection Limit and Observing Strategy for Very Faint Point Sources: Test Observations with P3, C100, and C200", Version 2.0, PHT/MPIA Calibration Report, 29-April-1997

[29] B.T. Soifer, L. Boehmer, G. Neugebauer, D.B. Sanders, "The *IRAS* Bright Galaxy Sample. IV. Complete *IRAS* Observations", 1989 AJ 98, 766

[30] B. Schulz, Linearization of ISOPHOT-P and C detector signals in OLP8", IDC PHT Internal Calibration Report, Version 1.0, 29-Sep-1999

[31] T. Müller & J.S.V. Lagerros, "Asteroids as far-infrared photometric standards for ISOPHOT", 1998, A&A 338, 340

[32] U. Herbstmeier, P. Abraham, D. Lemke, R.J. Laureijs, U. Klaas, K. Mattila, Ch. Leinert, Ch. Surace, M. Kunkel, "Small-scale structures in the far-infrared background", 1998, A&A 332, 739

[33] C. Gabriel, M. Haas, I. Heinrichsen, and W.-M. Tai, "The ISOPHOT Interactive Analysis - PIA User's Manual", 1999 (for PIA V8.1)